Proceedings Of The Third National Seismic Conference & Workshop On Bridges & Highways

Advances in Engineering and Technology for the Seismic Safety of Bridges in the New Millennium

Sponsored By:

Federal Highway Administration
Oregon Department Of Transportation
Washington State Department Of Transportation

Organized By:

Federal Highway Administration, Western Resource Center
Multidisciplinary Center For Earthquake Engineering Research

April 28 – May 1, 2002

DoubleTree Hotel
Columbia River Complex
Portland, Oregon

This workshop and conference was sponsored by the Federal Highway Administration through a contract to the Multidisciplinary Center for Earthquake Engineering Research (MCEER). The proceedings were published by MCEER. Additional copies can be requested from MCEER Publications, University at Buffalo, State University of New York, Red Jacket Quadrangle, Buffalo, NY 14261; phone (716) 645-3391; fax: (716) 645-3399; email: *mceer@mceermail.buffalo.edu*.

Opinions, findings, conclusions and recommendations expressed in papers contained in this publication are those of the author(s) and do not necessarily reflect the views of MCEER or the Federal Highway Administration.

Proceedings of the Third National Seismic Conference and Workshop on Bridges and Highways

Advances in Engineering and Technology for the Seismic Safety of Bridges in the New Millennium

Held at
Double Tree Hotel Columbia River Complex
Portland, Oregon
April 28-May 1, 2002

Edited by
Roland Nimis
Federal Highway Administration
Western Resource Center

Michel Bruneau
Multidisciplinary Center for Earthquake Engineering Research
and the University at Buffalo

Publication Date: March 11, 2002

Sponsored by
Federal Highway Administration
Oregon Department of Transportation
Washington State Department of Transportation

Co-Sponsored by
California Department of Transportation
Mid America Earthquake Center
Multidisciplinary Center for Earthquake Engineering Research
Pacific Earthquake Engineering Research Center
Transportation Research Board

Organized by:
Federal Highway Administration, Western Resource Center
Multidisciplinary Center for Earthquake Engineering Research

Preface

Once again, I had the honor and pleasure of working with some of the best engineers in the structural and seismic fields in organizing the *National Seismic Conference & Workshop on Bridges and Highways*. This is the third conference in the series and follows the successful conferences held in San Diego, California in 1995 and in Sacramento, California in 1997. The 2002 seismic conference was organized through a lot of hard work by the Steering Committee, Technical Committee and the staff at the Multidisciplinary Center for Earthquake Engineering Research (MCEER). It was the Steering Committee's objective to focus the *3rd National Seismic Conference* on seismic events, lessons learned and design code developments that have taken place since 1997. I believe we have achieved that objective.

The Federal Highway Administration is proud to continue co-sponsoring the National Seismic Conference in order to provide a dedicated forum for the exchange of information on current national and international research and practices for seismic-resistant design and retrofit of bridges and highway systems in all seismic zones. The conference will focus on advances in engineering and technology that provide increased seismic safety of highway bridges, other highway structures, and highway systems in the new millennium. The International Forum will be conducted by invited speakers from countries that have implemented advanced earthquake design and mitigation technologies and approaches. New and innovative technologies in earthquake engineering and information on the latest research and developments affecting earthquake engineering will be displayed in the conference's Technology Show and Information Display.

Five quick years have elapsed since the second conference and many significant seismic events have occurred around the world that have taught us new lessons or reconfirmed old lessons learned from past earthquakes. Past lessons on the importance of proper detailing, adequate bearing seats and column concrete confinements have been reconfirmed over and over again by recent earthquakes. New lessons have been learned from the recent 1999 Kocaeli and Duzce earthquakes in Turkey; the 1999 Chi-Chi earthquake in Taiwan, the 2001 Nisqually earthquake near Seattle, Washington, the 2001 Gujarat earthquake in India and the 2002 Istanbul earthquake in Turkey. These major seismic events have given us a better understanding of the near-fault and ground rupture effects, as well as the behavior of structures that were designed or retrofitted using modern codes.

During the same time period, our design methodologies have undergone many changes and a new "Comprehensive Specification for the Seismic Design of Bridges" (NCHRP 12-49) has been completed by the joint-venture partnership of the Applied Technology Council (ATC) and MCEER. Based on NCHRP 12-49, sponsorship of MCEER and funding from FHWA, a set of seismic design provisions titled "Recommended LRFD Guidelines for the Seismic Design of Highway Bridges" is being developed by a team of practicing engineers and researchers. These provisions will be submitted to AASHTO for adoption as guide specifications.

Also, numerous universities and the three National Earthquake Engineering Research Centers, established by the National Science Foundation, are performing research to advance the knowledge of seismic hazards and their effects on buildings, bridges and other facilities to reduce the impacts of future earthquakes. At the same time, new shake tables and dynamic

testing facilities came online since the Second National Seismic Conference. The world renowned Charles Lee Powell Structures Laboratory at the University of California, San Diego has been expanded to a Physics High Bay Laboratory and a new Structure Response Modification Device (SMRD) has been built. This gives UCSD the capability to test very large structural specimens and large full-size seismic isolation and energy dissipation devices, such as the ones being used on the new Benicia-Martinez Bridge. The University of California, Berkeley has expanded their seismic testing laboratory and shake table at the Richmond Field Station. The University of Nevada, Reno has also expanded their facilities with the new Large-Scale Structures Laboratory equipped with three MTS shake tables.

The events and developments in the seismic field have indeed been very exciting during the past few years. It is the Steering Committee's hope that the *3rd National Seismic Conference & Workshop on Bridges and Highways* will contribute to the safety of the bridges and highway systems in the United States and abroad by presenting and helping facilitate the exchange of information on current seismic design practices.

I would like to express my appreciation to all the Steering Committee and Technical Committee members for their guidance and assistance in organizing this conference. The Technical Committee, chaired by Tom Post, did an excellent job of reviewing and ranking the numerous abstracts received.

My very special thanks go to Jim Cooper (FHWA), Jim Roberts (retired Caltrans) and Jim Gates (retired Caltrans). To Jim Cooper for planting the seed and giving me the opportunity to organize the first and subsequent conferences. To Jim Roberts for his dedication to the engineering community and for supporting the First and Second National Seismic Conferences with his time and staff while he was Chief Bridge Engineer for Caltrans. To Jim Gates for giving freely of his time and technical expertise in developing the technical programs for the First and Second National Seismic Conference. Without the support of the three Jims the First and Second National Seismic Conferences would never have gotten off the ground.

Also, I would like to express my deepest appreciation to the following individuals for all their hard work and who, during certain periods of time, worked with me almost on a daily basis to put the various pieces of the conference together. They are: Dr. Ian Buckle of University of Nevada, Reno; Dr. Frieder Seible of UCSD; Ian Friedland of ATC; Dr. Phillip Yen and Myint Lwin of FHWA; Dr. Michel Bruneau, University at Buffalo and MCEER, Mike Higgins of Soundprint Technologies, and Don Goralski, Jane Stoyle, Debbie O'Rourke, and Carolyn Baumet of MCEER.

I would like to thank all the presenters, session chairs and exhibitors for all your hard work and for helping to support this conference. Last, but not least, I thank all the participants coming from near and far to this conference. I hope all of you will have a good time in the City of Roses, while gaining valuable technical knowledge and lasting friendships through the activities of this conference.

Roland Nimis, P.E.
Chair, Steering Committee
Federal Highway Administration
Western Resource Center
San Francisco, California

Conference Steering Committee

Roland Nimis	-	FHWA, Western Resource Center (Chair)
Michel Bruneau	-	MCEER & University at Buffalo
Ian Buckle	-	University of Nevada, Reno
James Cooper	-	Federal Highway Administration
Mark Hirota	-	Oregon Department of Transportation
James Roberts	-	Caltrans (Retired) / Imbsen & Associates
Frieder Seible	-	University of California, San Diego
Jerry Weigel	-	Washington State Department of Transportation
Michael Higgins	-	Pure Technologies (Secretary)

Conference Technical Committee

Thomas Post	-	Caltrans / CH2M Hill
Donald Anderson	-	CH2M Hill
Ralph Anderson	-	Illinois Department of Transportation
Randy Cannon	-	South Carolina Department of Transportation
Gregory Fenves	-	University of California, Berkeley
Ian Friedland	-	Applied Technology Council
Neil Hawkins	-	Mid America Earthquake Center
Bruce Johnson	-	Federal Highway Administration
James Kelly	-	University of California, Berkeley
M. Myint Lwin	-	Federal Highway Administration
Geoffrey Martin	-	University of Southern California
Maurice Power	-	Geomatrix Consultants, Inc.
Mark Reno	-	California Department of Transportation
Paul Somerville	-	URS Corporation
Steve Thoman	-	David Evans & Associates
Phillip Yen	-	Federal Highway Administration

Contents

Lessons Learned from Recent Earthquakes (Since 1998)
Chair: Tom Post 1

Lessons Learned from the 1999 Kocaeli, Turkey Earthquake
Saad El-Azazy, W. Phillip Yen, Hamid Ghasemi, James D. Cooper, Roy A. Imbsen 3

Structural Movement and Damage to the Alaskan Way Viaduct Due to the Nisqually Earthquake
George Comstock and Harvey Coffman 5

Performance of Roads and Bridges in the January 26, 2001 India Earthquake
Bijan Khaleghi and Gary Norris 17

Seismic Response of Highway Bridges Subject to Near-Fault Ground Motions
Bulent Akbas and Jay Shen 31

Seismic Performance of Bridges in the Chi-Chi Earthquake,Taiwan
W. Phillip Yen, James Yeh and Liang-Hong Ho 33

Seismic Design Practices and Specifications
Chair: Michel Bruneau 39

A Proposed Bridge Seismic Design Philosophy and Criteria
Brian Maroney and Nancy McMullin Bobb 41

Seismic Retrofit of Bridges Using Shape Memory Alloy Restrainers
Reginald DesRoches and Bassem Andrawes 43

Experimental Study on Seismic Behavior of Highway Bridge Foundation during Liquefaction Process
Hiroshi Kobayashi, Keiichi Tamura, Naoki Sato and Takuo Azuma 53

Development and Implementation of a New Seismic Design Bridge Criteria for South Carolina
Roy A. Imbsen and Lucero E. Mesa 65

Seismic Retrofit of Aurora Avenue Bridge with Friction Pendulum Isolation Bearings
Hongzhi Zhang 73

Contents

Design of Major Bridges in High and Moderate Seismicity Areas
Chair: Frieder Seible 83

Seismic Design of the Ravanel Bridge, Charleston, South Carolina
Michael J. Abrahams, Jaw-Nan Wang, Peter M. Wahl and John A. Bryson 85

Seismic Investigations for the Design of the New Mississippi River Bridge at St. Louis
Thomas P. Murphy and John M. Kulicki 95

Seismic Design of the Skyway Section of the New San Francisco-Oakland Bay Bridge
Brian Maroney, Sajid Abbas, Madon Sah, Gerald Houlahan and Tim Ingham 107

Seismic Design Strategy of the New San Francisco-Oakland Bay Bridge Self-Anchored Suspension Span
Marwan Nader, Jack López-Jara and Claudia Mibelli 109

Seismic Design of the Metsovitikos Suspension Bridge, Pindos Mountains, Greece
Mike Oldham, Zygmunt Lubkowski, Xiaonian Duan and Richard Sturt 123

Effects of Near Field Earthquakes on Bridges
Chair: Jim Roberts 135

Characterizing Near Fault Ground Motion for the Design and Evaluation of Bridges
Paul Somerville 137

Designing Ordinary Bridges for Ground Fault Rupture
Stewart Gloyd, Raymond Fares, Anthony Sánchez, and Vinh Trinh 149

Design of the Lytle Creek Wash Bridge to Survive Permanent Ground Displacements due to Surface Fault Rupture
Gregory V. Brown 163

Seismic Retrofit of the Bolu Viaduct
S. W. Park, H. Ghasemi, J. D. Shen, W. Phillip Yen, and M. Yashinsky 175

PEER-Lifelines Research in Design Ground Motions
Clifford J. Roblee, Brian S.J. Chiou and Michael F. Riemer 177

Contents

International Forum

Chair: Jim Cooper 189

Revised Design Specifications for Highway Bridges in Japan and Design Earthquake Motions
Keiichi Tamura 191

The Challenge of the Rion - Antirion Bridge
Jean-Paul Teyssandier 203

Effect of Near-Fault Earthquake on Bridges: Lessons Learned from Chi-Chi Earthquake
Chin-Hsiung Loh, Wen-I Liao and Jun-Fu Chai 211

Seismic Safety Evaluation of Large Scale Interchange System in Shanghai
Lichu Fan, Jianzhong Li, Shide Hu, Guiping Bi and Liying Nie 223

Seismic Practices for Transportation Structures and Systems

Chair: Bruce Johnson 235

Seismic Vulnerability Assessment of the Seattle-Tacoma Highway Corridor Using HAZUS
Donald Ballantyne, Mark Pierepiekarz and Stephanie Chang 237

Ground Motions, Design Criteria, and Seismic Retrofit Strategies for the Bay Area Rapid Transit District Bridge and Other Structures
Tom Horton, Eric Fok, Ed Matsuda, William Hughes, Wen S. Tseng, Chip Mallare and Kang Chen 249

Pushover Analysis of Masonry Piers
Ruben Gajer, Adam Hapij and Mohammed Ettouney 261

Innovative Designs of Seismic Retrofitting the Posey and Webster Street Tubes, Oakland/Alameda, California
Thomas S. Lee, Thomas Jackson and Randy R. Anderson 271

Seismic Rehabilitation Design and Construction for the Port Mann Bridge, Vancouver, B.C.
Keith Kirkwood, Tian-Jian (Steve) Zhu, and Peter Taylor 285

Contents

Displacement Based Design
Chair: W. Phillip Yen 297

Rocking of Bridge Piers Under Earthquake Loading
Fadel Alameddine and Roy A. Imbsen 299

Legacy Parkway Seismic Design
Strategies for Developing a High Performance Structure with Typical Bridge Design Features on a Design-Build Project
Thomas R. Cooper and Joseph I. Showers 313

Plastic Hinge Length of Reinforced Concrete Bridge Columns
Robert K. Dowell and Eric M. Hines 323

Applicability of the Pushover Based Procedures for Bridges
Matej Fischinger and Tatjana Isakovic 335

Seismic Performance of Reinforced Concrete Bridge Columns
David Sanders, Patrick Laplace, Saiid Saiidi and Saad El-Azazy 345

Emerging Seismic Design and Retrofit Technologies
Chair: Mark Reno 357

Seismic Design of Concrete Towers of the New Carquinez Bridge
Ravi Mathur, Mark A. Ketchum and Greg Orsolini 359

Precast Segmental Bridge Superstructures: Seismic Performance of Segment-to-Segment Joints
Sami Megally and Frieder Seible 371

In-situ Tests of As-is and Retrofitted RC Bridges with FRP Composites
Chris Pantelides, Jeff Duffin, Jon Ward, Chris Delahanty and Lawrence Reaveley 383

Calibration of Strain Wedge Model Predicted Response for Piles/Shafts in Liquefied Sand at Treasure Island and Cooper River Bridge
Mohamed Ashour, Gary Norris and J.P. Singh 397

Seismic Performance of a Concrete Column/Steel Cap/Steel Girder Integral Bridge System
Sri Sritharan, Robert E. Abendroth, Lowell F. Greimann, Wagdy G. Wassef and Justin Vander Werff 411

Contents

Development and Testing of the New LRFD Seismic Design of Highway Bridges

Chair: Ian M. Friedland 423

Recommended LRFD Guidelines for the Seismic Design of Highway Bridges
Ronald L. Mayes, Ian M. Friedland and ATC Project Team 425

Recommended Design Approach for Liquefaction Induced Lateral Spreads
Geoffrey R. Martin, M. Lee Marsh, Donald G. Anderson, Ronald L. Mayes and Maurice S. Power 437

Application of the New LRFD Guidelines for the Seismic Design of Highway Bridges
Derrell A. Manceaux 451

Cost Impact Study for a Typical Highway Bridge Using Different Return Period Seismic Design Maps
Jeffrey Ger, David Straatmann, Suresh Patel and Shyam Gupta 463

Testing of the LRFD Bridge Seismic Design Provisions Through a Comprehensive Trial Design Process
M. Lee Marsh, Richard V. Nutt, Ronald Mayes and Ian M. Friedland 475

Poster Session

Coordinator: Myint Lwin *477*

Cyclic Testing of Truss Pier Braced Latticed Members
Michel Bruneau, Kangmin Lee, and John Mander 479

Caltrans/CSMIP Bridge Strong Motion Instrumentation Project
Pat Hipley, Tony Shakal and Moh Huang 485

Seismic Retrofitting Challenges Stimulate New Innovations for the Benicia-Martinez Bridge
Roy A. Imbsen and Moe Amini 491

West Anchorage Design of San Francisco - Oakland Bay Bridge Main Span for Seismic Loads
John Sun, Rafael Manzanarez and Marwan Nader 503

Seismic Retrofit of the US 40/I-64 Double Deck Bridge
Mark R. Capron 509

Contents

Bridge Abutment Model Sensitivity for Probabilistic Seismic Demand Evaluation
Kevin Mackie and Bozidar Stojadinovic 515

Dynamic Response of Bridge Structures Supported on Extended Reinforced Concrete Pile Shafts
T.C. Hutchinson, C.J. Curras, R.W. Boulanger, Y.H. Chai, and I.M. Idriss 521

Proportioning Substructure Columns of Short Bridges for Improved Seismic Performance
Mehmet Inel and Mark A. Aschheim 527

Near-Field Ground Motions and their Implications on Seismic Response of Long-Span Bridges
George P. Mavroeidis and Apostolos S. Papageorgiou 533

Shake Table Response of Flexure-Dominated Bridge Columns with Interlocking Spirals
Juan Correal, M. Saiid Saiidi, David Sanders and Saad El-Azazy 539

Expansion Joints for Seismic Isolated Bridges
Efthymios “Tim” Delis 545

Development of Analytical Fragility Curves for Highway Bridges Considering Strong Motion Parameters
Kazi R. Karim and Fumio Yamazaki 551

State Street Bridge: CFRP Composite Seismic Rehabilitation and Specifications
Chris Pantelides, Fadel Alameddine, Thomas Sardo, Roy A. Imbsen, Larry Cercone, and Frederick Policelli 557

Recommendations on Experimental Procedures for Bridge Column Testing
Jerry J. Shen, W. Phillip Yen, and John O'Fallon 563

Implementation of Seismic Isolators and Supplemental Dampers in Cable-Stayed Bridges
Michael J. Wesolowsky and John C. Wilson 569

Seismic Isolation of Bridges Subject to Strong Earthquake Ground Motions
Victor A. Zayas, Stanley S. Low, and Anoop S. Mokha 575

Behavior of Ductile Steel Retrofitted Deck-Truss Bridges
Majid Sarraf and Michel Bruneau 581

Contents

Appendix A

Conference Program 587
Author Index 597

Lessons Learned from Recent Earthquakes (Since 1998)

Chair: Tom Post

Lessons Learned from the 1999 Kocaeli, Turkey Earthquake

Saad El-Azazy, W. Phillip Yen, Hamid Ghasemi, James D. Cooper, Roy A. Imbsen

Structural Movement and Damage to the Alaskan Way Viaduct Due to the Nisqually Earthquake

George Comstock and Harvey Coffman

Performance of Roads and Bridges in the January 26, 2001 India Earthquake

Bijan Khaleghi and Gary Norris

Seismic Response of Highway Bridges Subject to Near-Fault Ground Motions

Bulent Akbas and Jay Shen

Seismic Performance of Bridges in the Chi-Chi Earthquake, Taiwan

W. Phillip Yen, James Yeh and Liang-Hong Ho

Lessons Learned from the 1999 Kocaeli, Turkey Earthquake

Saad El-Azazy, W. Phillip Yen, Hamid Ghasemi, James D. Cooper, Roy A. Imbsen

ABSTRACT

The North Anatolian Fault (NAF), which runs east west across northern Turkey with an approximate length of 1100 km (see Figure 1) again ruptured on August 17, 1999, resulting in a 7.4 magnitude earthquake. The epicenter of the earthquake was near the town of Gölcük, a province of Kocaeli, which is about 80 km east of Istanbul. This Kocaeli Earthquake resulted in more than 15,000 deaths and caused extensive destruction to residential and commercial buildings and industrial facilities in many cities.

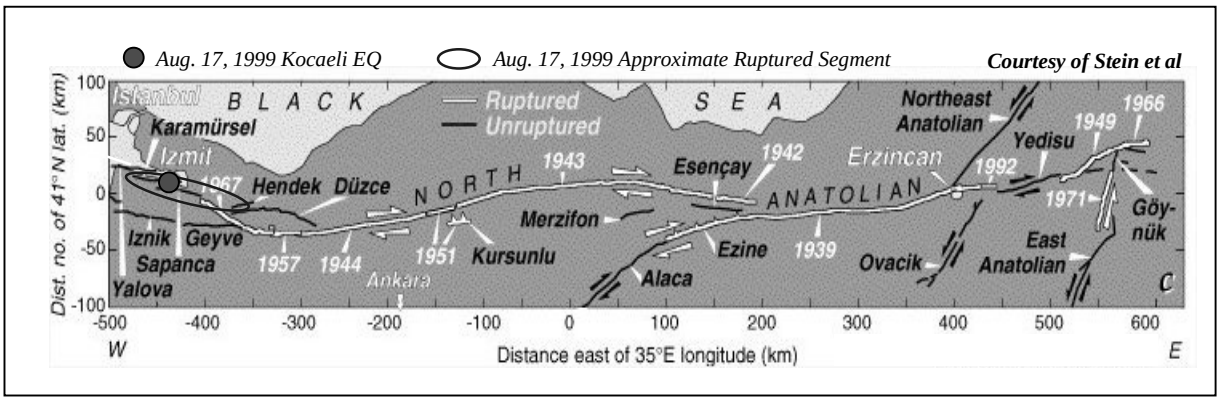

Figure 1. The North Anatolian Fault Zone

The NAF has been studied jointly by both Turkish and U.S. scientists for many years. In particular, U.S scientists have been interested in the NAF because there is a strong similarity between the creep rate and energy release of both the North Anatolian and the San Andreas fault in California. Both faults have generated large magnitude earthquakes within the last 100 years.

Since the devastating 1939 Erzincan Earthquake with its epicenter almost 1000 km east of Istanbul, earthquakes with a magnitude larger than 6.5 have occurred frequently along the NAF with their epicenters moving progressively westward towards Istanbul. This has long caused much concern in Turkey and the recent Kocaeli earthquake with its M_w of 7.4 and its close proximity to Istanbul has elevated these concerns. The scientists at the Istanbul Technical

Saad El-Azazy, PhD, PE, Senior Bridge Engineer, CALTRANS, Sacramento, CA
Phillip Yen, PhD, PE, Structural Research Engineer, FHWA, TFHRC, McLean, VA
Hamid Ghasemi, PhD, Structural Research Engineer, FHWA, TFHRC, McLean, VA
James D. Cooper, PE, Technical Director, Office of Bridge Technology, FHWA, Washington, DC
Roy. A. Imbsen, Dr. Eng., PE, President, Imbsen & Associates, Inc., Sacramento, CA

University have suggested that a large magnitude earthquake much closer to Istanbul can be expected in the near future.

Soon after the Kocaeli earthquake, an FHWA team of scientists and engineers were dispatched to Turkey at the invitation of the Turkish General Directorate (KGM) to inspect structures on the Trans European Motorway (TEM) and to evaluate their condition. In addition to scientists and engineers from the Federal Highway Administration, the team included members from the California Department of Transportation and Imbsen and Associates Inc. This team spent 3 weeks in Turkey, working very closely with their Turkish counterparts. This paper provides an overview of the Team's observations and findings on the structures along the TEM and the lessons learned.

In general the bridges on the TEM performed acceptably. There was only one bridge collapse that affected the TEM directly, and minor to moderate damage to others along the TEM.

Structural Movement and Damage to the Alaskan Way Viaduct Due to the Nisqually Earthquake

George Comstock and Harvey Coffman

This paper addresses the effects of the February 28, 2001 Nisqually Earthquake on the Alaskan Way Viaduct located on the Seattle Waterfront, approximately 35 miles from the epicenter.

Seismic ground motions at the Viaduct will be summarized from the seismic monitoring stations. Supplemental physical evidence from buildings and bridges in the vicinity provide a basis for characterizing the seismic ground motion. Preliminary findings indicate that the most significant ground movement was transverse to the bridge centerline, corresponding to seismic shear wave propagation from the epicenter, with a gravitational coefficient (g) of approximately 0.16. There is also some evidence of localized soil subsidence in the vicinity of the adjacent seawall attributable to the earthquake.

Established elastic movement and permanent deformation of the Viaduct as a consequence of the seismic ground motions is discussed. Inspection findings document information establishing conclusions presented, with information gathered from historical bridge records. These inspection findings indicate that the bridge generally moved within elastic limits transverse to the roadway centerline, with some longitudinal movement in portions of the southern end. Inspection findings subsequent to the earthquake provide the basis for discussion of structural damage, and will include structural failure of the Pier 100 East column, and structural distress to Piers 94, 97, 121, 145, and 160 including adjacent crossbeams and longitudinal beams. Other bridge conditions not directly related to the earthquake will be addressed as they affect the seismically induced damage, including settlement of selected foundations

A description of how the monitoring programs were developed and how they will be used in the future to determine structural movement is presented. Two methods for recording small structural movement have been implemented. One system is based on surveys with established control points and a second system utilizes “crack monitors” installed on the bridge over selected structurally significant cracks.

George Comstock, P.E., Regional Inspection Engineer, Bridge Preservation Office, Washington State Department of Transportation, P.O. Box 47341, Olympia, WA 98504-7341.
Harvey Coffman, S.E., Bridge Preservation Engineer, Bridge Preservation Office Washington State Department of Transportation, P.O. Box 47341, Olympia, WA 98504-7341.

This paper discusses the effects of the February 28, 2001 Nisqually Earthquake on the Alaskan Way Viaduct located in the downtown Seattle waterfront area. The structure is approximately 35 miles from the epicenter, which was centered in the South Puget Sound Nisqually Delta.

The Alaskan Way Viaduct carries north-south traffic on State Route 99 (SR 99), through Seattle from just south of Holgate Street (pier 183), north to the Battery Street Tunnel (pier 1). The Viaduct is located to the west of Interstate Route 5 (I-5), between downtown Seattle and Elliot Bay. *(See Figure I.)*

At 11,156 feet (2.1 miles) in total length, the Viaduct is a very complex structure supported on pile foundations that extend through the waterfront fill and tideflat deposits to underlying dense soil. Starting at the north end of the Viaduct the south portal of the tunnel, the first 0.4 mile (pier 1–53) of the Viaduct consists of either single or separated single-deck structures carrying the northbound and southbound lanes. Near Pike Street (pier 53), the Viaduct then transitions to a double-deck cross-section, with the southbound lanes on the lower deck and the northbound lanes on the upper deck. This configuration extends to the south for about 1.5 miles to Holgate Street (pier178). In the southerly 0.2 mile (pier 172 - 183), the viaduct

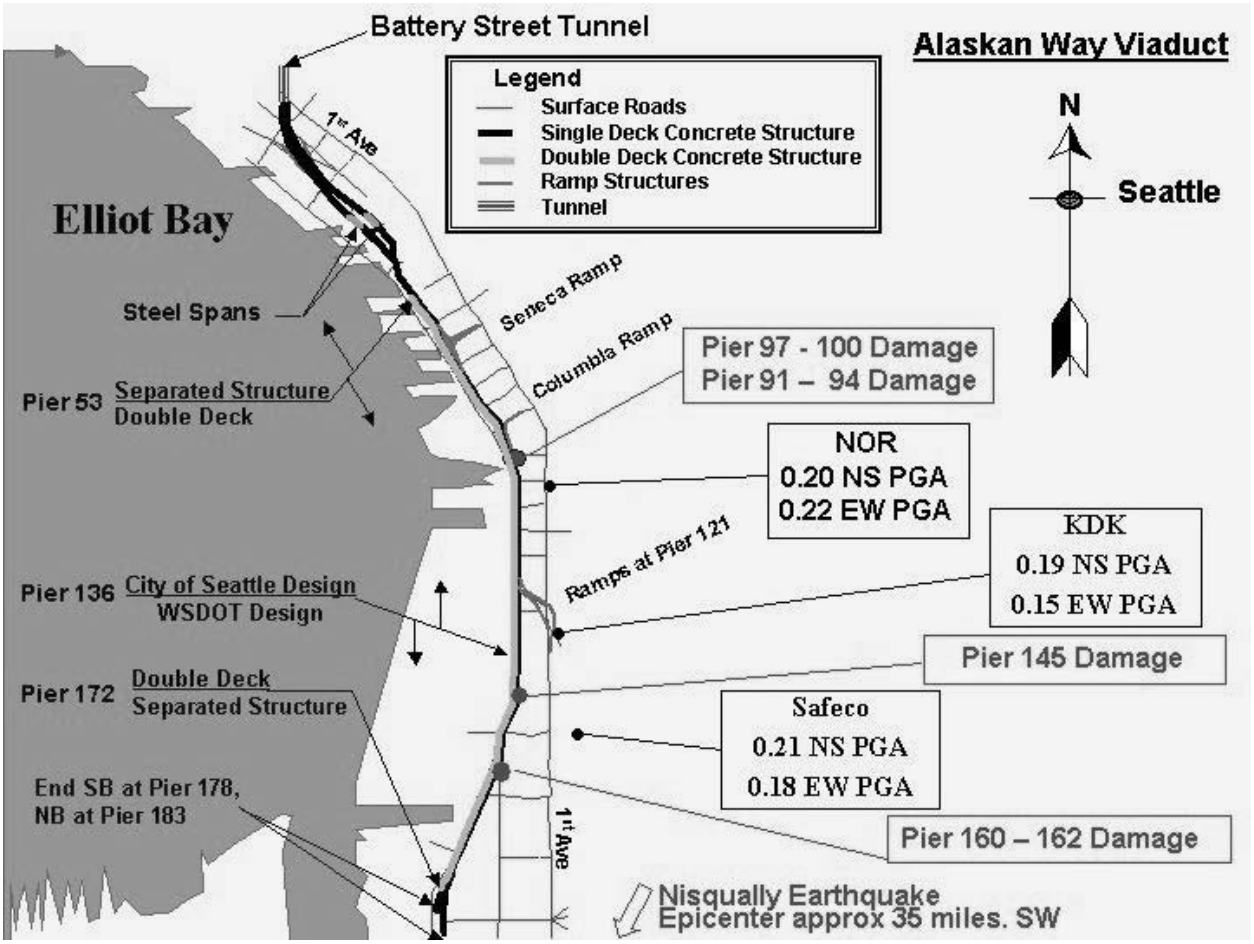

Figure I. MAP OF THE ALASKAN WAY VIADUCT AND VICINITY

reverts to a single structure carrying the northbound lanes, as the alignment of the southbound lanes moves to the west, from its location under the northbound lanes, to a new alignment. Throughout the length of the Viaduct there are five ramps providing local access.

The northerly 1650 feet (pier 1 – 40) of the viaduct is carried by a series of three-span units of continuous reinforced concrete tee-beam spans, each from 30 to 40 feet in length. Pier supports are multiple concrete columns on individual pile supported footings. At this point, the bridge (pier 40 – 44) consists of four wide-flange steel girder spans, varying in length with a maximum span of about 65 feet, carrying a reinforced concrete roadway slab and traffic over railroad tracks. Piers for these spans are transversely braced steel columns supported on individual concrete pedestals on piles-supported footings. The Viaduct continues to the south (pier 44 – 53) with another series of three-span units of continuous reinforced concrete tee-beam spans. The spans rest on multiple concrete columns on individual pile-supported footings, until the structure begins its transition into a double-deck configuration.

The one and one-half miles of double-deck structure (pier 53 – 178) has two similar, yet different configurations, related to the origin of their design, by the city (pier 1 – 136) or the state (pier 136 – 183). The basic configuration is a series of continuous three-span units, having spans in the range of 60 to 75 feet, with a unit length of from 180 to 225 feet. *(See Figure II)* Supporting piers are concrete frames, with either square or rectangular columns on each side of the roadway, and deep crossbeams at the top of the columns and below the lower roadway. The primary longitudinal supports for the spans are 7-feet deep by 1 foot 7-1/2 inch wide exterior girders rigidly connected to the pier columns. The double-deck portions of the bridge designed by the state provide four or five smaller longitudinal beams equally spaced between the exterior girders. These beams are supported on concrete crossbeams at each pier and by floorbeams located at the third points within each span. This system supports the reinforced concrete roadway slab and traffic above. The double-deck spans designed by the city are similar except that three longitudinal beams are provided between the exterior girders: a shallow beam at the center and a two deep beams, haunched at the pier cross beam at the quarter points between exterior girders. All pier frame columns are supported on individual footings founded on deep piles. Along the length of the double-deck portion, pier frames have been extended as outriggers where needed to accommodate ramps, roadway transitions or obstacles in the landscape below.

To the south of the double-deck spans the state-designed longitudinal supporting system continues for the northbound lanes (pier 178 – 183) with two four span continuous units, while the southbound lanes (pier 178 – 181) shift to the west from below the northbound lanes to a separate ground level alignment. The northbound lanes continue for an additional 454 feet as an elevated structure on a series of fifteen short, reinforced concrete, pile-supported slab spans enclosed within side walls, and end with an at-grade abutment.

CHARACTERIZING THE SEISMIC GROUND MOTIONS AND STRUCTURAL RESPONSE OF THE VIADUCT

The Alaskan Way Viaduct did not have seismic monitoring equipment in place during the Nisqually Earthquake, nor does it have any equipment now. However, there were 3 recording stations within about 1000 feet of the viaduct at the time of the earthquake. (1) These stations recorded peak ground accelerations ranging from 0.15g to 0.22g, averaging 0.19g in the East-West direction and 0.20g in the North-South direction. (*See Figure I for station locations)*

Figure II Alaskan Way Viaduct Looking North Near Pier 100

The structural response of the Alaskan Way Viaduct appears to have been predominantly East-West transverse movement of the bridge, resulting in permanent deformation of the structure at several locations. There is also evidence of North-South longitudinal structural movement, based on lower deck curb cracking and spalling at pier 121 (due to frames impacting across deck joint) and spalling of columns under lower deck edge beams at piers 130 - 140.

It is notable that other bridges in the vicinity, including the Spokane Street Viaduct and the Holgate Street Bridge also displayed seismic related damage indicating excessive movements in an East-West orientation.

There was no evidence of soil liquefaction within the Right-of-Way limits of the Alaskan Way Viaduct. However, there was one localized area of soil subsidence and suspected liquefaction adjacent to the City of Seattle Seawall near pier 60. This seawall parallels the Viaduct for much of the bridge length. There are also reports of soil liquefaction as evidenced by sand boils in several wharfs to the South of the Viaduct.

Earthquake Damage

Structural distress was found at the pier 97-100 rigid frame, including damage to the column to floorbeam, column to edge beam rigid connections *(See Figure III)*, and 3 to 4 inches of transverse lateral leaning of the frame. (2) Lateral displacement of the upper deck fog line across the joint at piers 97 and 100 confirm that the internal forces of the frame reached equilibrium in a new position as a result of the earthquake *(See Figure IV).* At pier 100 East column damage includes the fracture of steel reinforcement where the column vertical reinforcement is welded to the hooked end of the upper deck floorbeam reinforcement.
(See Figure V) The rigid frame connections were most severely distressed on the East Pier 100 column, where the concrete in the upper deck floorbeam to column connection suffered

cracking and spalling, allowing for the exposure of the reinforcement bar by hand removal of concrete rubble. Also the Pier 100 East column, the lower edge beam connection had a 6mm wide crack at the top with structural cracking of the adjacent areas of the column up to 2mm. The Pier 97 East column had very similar conditions, although the crack widths were smaller and the upper deck floorbeam to column connection had a clearly defined 2mm crack without any rubble. The interior sections of the floorbeams, girders and edge beams within this frame also displayed many old and fresh cracks ranging from hairline to 2mm in width.

Figure III North half pier 100 column damage. Three Lines of Square cross beam bars welded to square column bars. Left bar fractured.

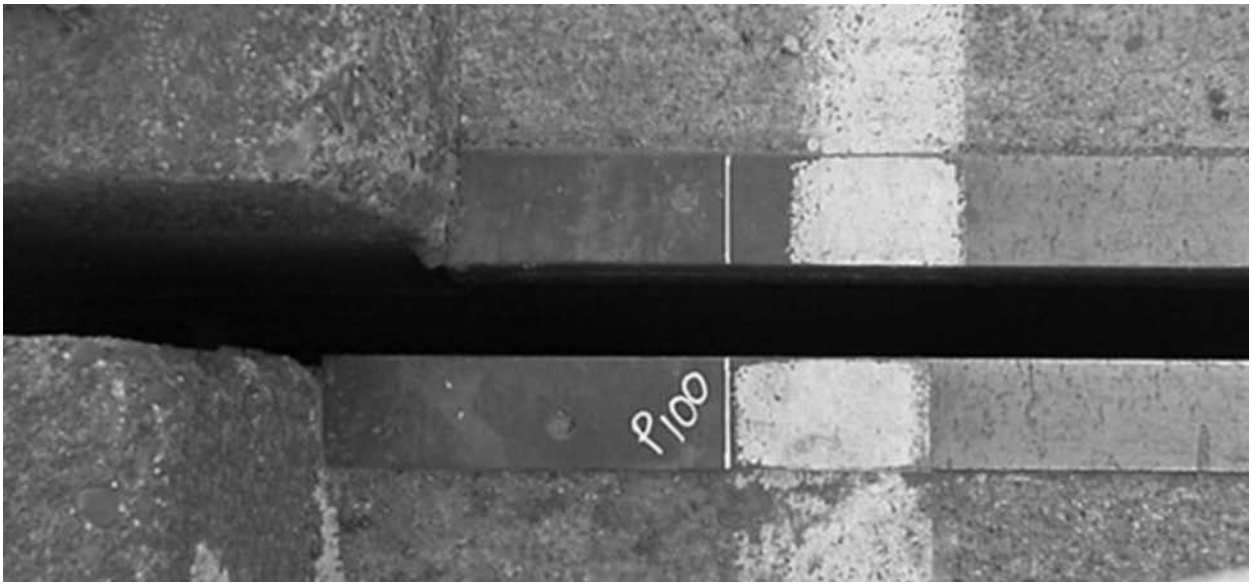

Figure IV Pier 100 - 1½ Inch Fog Line Offset And 3½ Inch Curb Offset On East Side

This damage is also associated with settlement of 5 to 6 inches at piers 98 and 99 East column footings respectively. This settlement predated the Nisqually Earthquake as evidenced by corrosion on the fractured face of the steel reinforcement at pier 100, previous inspection records documenting a 2 inch curb offset at pier 100 (3), and lack of evidence of ground subsidence around these piers immediately after the earthquake. The pier 98 and 99 East footings were exposed for inspection and no structural damage was found, suggesting that the settlement occurred in the supporting piles. A review of the soil profile indicates that there is a 25 foot dip in the underlying glacial till under piers 98 and 99. It is possible that these piles were not driven to the till during construction.

A laboratory analysis of the fractured steel reinforcement at pier 100 confirms that the failure was sudden, and indicates that a combination of extremely poor weld quality combined with brittle metal characteristics makes this detail extremely vulnerable to fracture. (4)

Taken as a whole, this damage at Frame 97-100 reduced the overall structural stability of the pier 100 frame, including substantial loss of moment continuity and shear capacity between the upper deck floorbeam and the pier 100 East column. There was also loss of strength in the connection between the pier 100 East column and the East edge beams in Span 99.

Frame 91-94 displays damage very similar to that found at Frame 97-100, though less severe. (2) This damage includes significant cracking of the columns *(See Figures VI & VII) and* 1 to 2 inches of transverse lateral leaning of the frame. Lateral displacement of the upper deck fog line across the joint at pier 91 confirms that some permanent transverse deformation of the frame occurred as a result of the earthquake.

Again mirroring the conditions found at Frame 97-100, there is settlement of approximately 3 inches at pier 93 East column footing. This settlement having predated the Nisqually Earthquake based on lack of evidence of ground subsidence around the pier immediately after the earthquake. Continuing the comparison with Frame 97-100, the soil profile indicates there is a dip in the underlying glacial till under pier 93. It is a possibility that these piles were not driven to till during construction.

Though this damage is similar to that found at Frame 97-100, no investigations have been conducted to determine if the top column reinforcement is fractured, or if the pier 93 footing is damaged.

Areas of structural distress were found between piers 160-163 with significant cracking of the longitudinal edge beams and transverse floor beams. (2) There is also 1 to 2 inches of transverse lateral leaning of the frame. Lateral displacement of the upper deck fog line across the joint at pier 160 confirms that this lean is earthquake related.

Areas of structural distress were found at the rigid frame at pier 145, including significant cracking of the transverse floor beams. (2) The pier 145 South frame shows evidence of a transverse lateral leaning of the frame between piers 145 and 148. Lateral displacement of the upper deck fog line across the joint at pier 145 confirms that this lean is earthquake related.

Cracking was found at pier 121 column at the groundline. (2) This column displayed fresh open vertical cracks on three sides of the column, all within approximately 4 feet of the groundline. This damage is considered minor and does not compromise the structural integrity of the column. The lower deck curb at the deck joint at pier 121 was also cracked and spalling, due to impact of the frames during the Nisqually Earthquake.

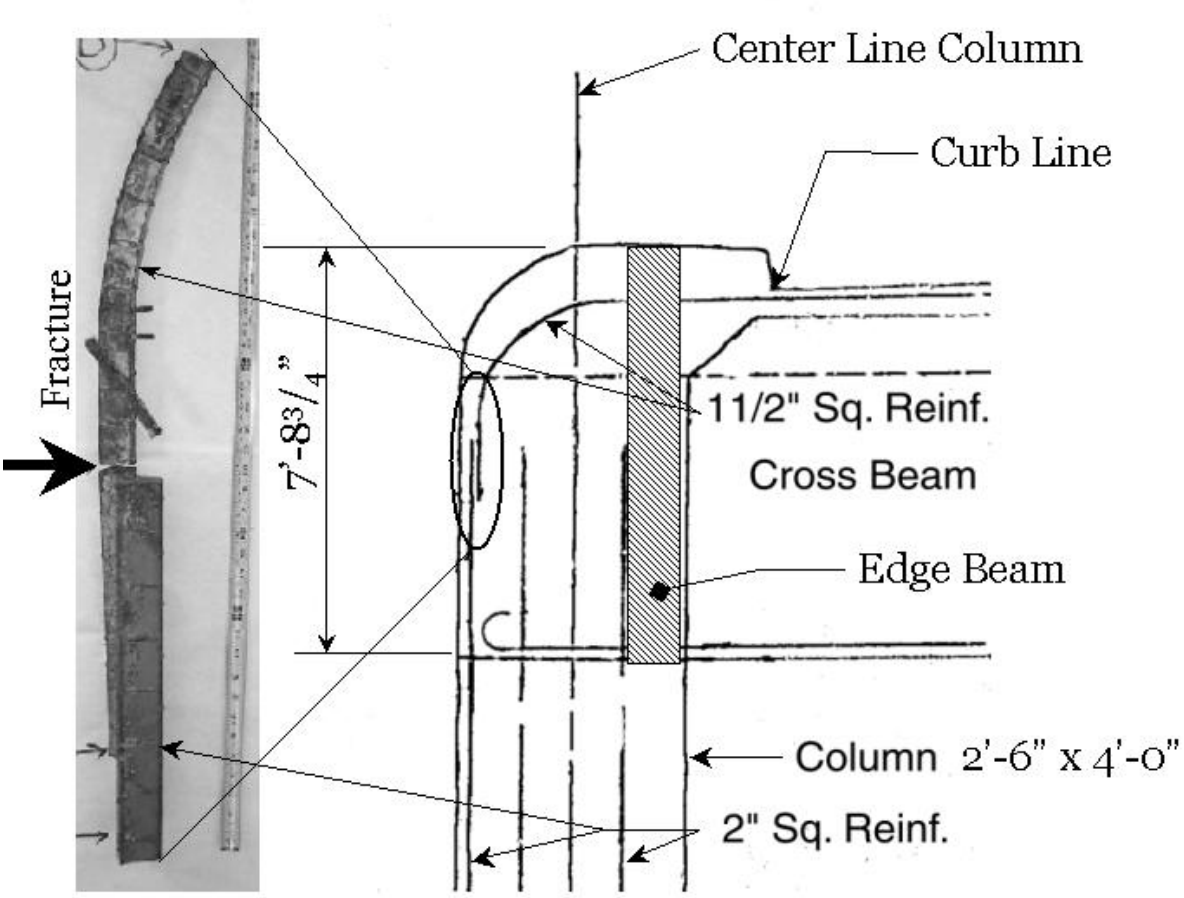

Figure V Pier 100 East Column Broken Rebar

Figure VI Pier 93 West Column Top North Face

Figure VII Pier 94 East Column West Face at Lower Deck
Note: 1mm Cracking At Curb To Column Interface

Structural Repairs

The structural repairs performed as a result of the Nisqually Earthquake are limited to Frame 97-100, and were performed in three phases:

Phase 1 Emergency Repairs consisted of strapping shoring to the pier 100 East and West columns to provide additional support to the Span 99 longitudinal edge beams and upper and lower floorbeams. This repair did not restore moment continuity to the Pier frames, but prevented any further collapse of the bridge and allowed for the use of the structure with load restrictions. This shoring was removed during Phase 2 repairs.

Phase 2 Repairs are considered permanent and consisted of grouting Pier 100 East column top; installation of new pile founded concrete pedestals at Pier 100 to support the Phase 2 shoring; installation of strongbacks and transverse post-tensioned diagonal bracing tie rods at Piers 98 and 99; placement of horizontal transverse post-tensioned tie rods and whalers between upper and lower floorbeams at Pier 97 and 100; carbon fiber wrap strengthening of girders and floorbeams; and epoxy injection of cracks in girders, floorbeams, and columns *(See Figure VIII & IX).* These repairs were intended to stabilize the frame against further transverse movement, strengthen the individual frame members to restore shear and moment capacity, and to resist a 0.10g earthquake loading. These repairs allowed for the use of the structure without any load restrictions in this frame, although it should be noted that other portions of the structure have been found structurally inadequate and require load restrictions. These repairs were modified as part of the Phase 3 repairs.

Phase 3 Repairs modified the Phase 2 repairs to remove the diagonal bracing at Piers 98 and 99, which were an obstruction to street traffic under the Viaduct. These modifications are considered permanent and are meant to last for the remainder of the structure life. The Phase 3 modifications consisted of installing post-tensioned dowels in the column top-upper deck floorbeam connection at Piers 97 and 100 to restore moment capacity; removing the diagonal transverse tie rods with a steel rigid frame under the lower deck; replacing the horizontal tie rods and whalers between upper and lower floorbeams at Piers 97 and 100; and removing the pile founded concrete pedestals for the Pier 100 shoring under the Viaduct *(See Figure X & XI).* These modifications are intended to restore the moment capacity of the column to upper floorbeam connections, allowing for the removal of those elements of the Phase 2 repairs that obstructed traffic under the viaduct.

Inspection and Monitoring Methods

The post earthquake inspection had two objectives: Determining immediate earthquake damage and establishing baseline information for use in monitoring the structure for the remainder of its service life. Several aspects of this monitoring program are on going on a semi-annual and annual inspection schedules.

The “bread and butter” post earthquake inspection consisted of a close visual inspection; systematic photographic documentation; and crack mapping of the columns, floorbeams and selected girders from pier 53 to the South abutment (pier 183) of the structure. The other portions of the bridge and ramp were inspected but not found with conditions that warranted more detailed inspection post earthquake efforts.

Figure VIII Pier 98 - 99 Phase 2 Repairs Looking North East

Figure IX Pier 98 Phase 2 Repair Looking North
Post-Tensioned Diagonal Transverse Bracing – Removed in Phase 3

Figure X Pier 97 Phase 3 Repair Looking North Note that Diagonal Bracing is Removed

In addition to this, the following inspection and monitoring methods were utilized:

A. Measurement of pier 53 to South abutment (pier 183) column transverse leaning. The results of these measurements indicate the columns are not truly vertical as shown on the plans, although conclusions are hard to reach. This is because measurement techniques and construction tolerances cloud the results, and only those areas mentioned above clearly show a transverse lean of significance.

B. Measurement of the deck joints and curb offsets. This work also included scribing lines in the steel armored deck joints to precisely establish future measurement locations. The results of these measurements correlate with findings of the leaning columns, and when compared with joint data collected in pre-earthquake inspection reports, helped to establish definitively that the Nisqually Earthquake caused permanent deformation of several frames.

C. Survey of Upper Deck Gutterlines. This survey, conducted in April 2001, provided substantiation for the settlement of the East columns at piers 93, 98 and 99, and indicates that the South end of the structure from approximately pier 150 to the South abutment has settled over time. Future gutterline surveys are planned on a regular basis.

D. Detailed 3-D Survey Data for Frame 97-100. This survey program consists of targets located on the bridge that are surveyed periodically to check for signs of movement, and is capable of detecting movement within approximately ¼ to ½ inch vertically, laterally, or

Figure XI Pier 97 East Column Phase 3 Repair
Post Tensioned Rods Installed in South Half of Split Pier Looking North

longitudinally. Repeated survey observations in 2001 did not find any uncontrolled movement of the structure, but did document movement associated with the emergency repairs in this area

E. Exposure of Footings at pier 98 and 99 East Columns. These footings were exposed to look for evidence of damage and obtain elevations for comparison with the "as-built" plans. No damage was found; measurements of the elevations at the top of the footings were inconclusive.

F. Installation and Monitoring of Crack Gauges on Structure. The Alaskan Way Viaduct currently has 28 crack gauges installed on columns girders, and floorbeams at various points on the structure, concentrated at areas of known distress. These gauges are monitored every six months for signs of structural movement across open cracks in these primary members. To date, no structural movement has been recorded.

REFERENCES:

(1) Tylin International, June 2001. Alaskan Way Viaduct Report of the Structural Sufficiency Review Committee.
(2) Washington State Department of Transportation Bridge Preservation Records, 2001.
(3) Washington State Department of Transportation 2000 Bridge Inspection Report for 99/540 NB of 12/27/00.
(4) J.M. Dwight, 2001, Alaskan Way Viaduct Re-Bar Weld Joint Analysis.

Performance of Roads and Bridges in the January 26, 2001 India Earthquake

Bijan Khaleghi, Ph.D. S.E. and Gary Norris, Ph.D.

ABSTRACT

A massive earthquake, described as the worst earthquake in India's history, struck Gujarat on Friday January 26, 2001. The earthquake was of magnitude 7.9 and relatively shallow at depth of 14.1 miles (22.7 km) below ground surface. The infrastructure was torn apart and many bridges and culvert structures suffered damage. This paper focuses on the first hand observations of damage to the bridge structures.

Bijan Khaleghi, Concrete Specialist, Washington State Department of Transportation, Bridge & Structures Office, Olympia Washington

Gary Norris, Professor of Civil Engineering, University of Nevada at Reno, Reno Nevada

INTRODUCTION

Bridges in the Kachchh region are generally stream or railroad crossings. Bridges are typically composed of short spans with span lengths of approximately 50 ft (15 m) each. Bridges are simple spans with expansion joints at each pier. L-shaped abutments are typical for all newer concrete and older masonry bridges. Both old and bridges under construction suffered extensive damage during the earthquake. Excluding the damage from the earthquake, the condition of cast-in-place concrete bridges is in general unsatisfactory and substandard.

Earthquake damage to bridge structures can be attributed to the lack of seismic design and detailing of both old bridges and bridges under construction. Bridges are typically composed of multiple simple spans supported on elastomeric bearings with no continuity of the superstructure or any fixity at the intermediate diaphragms. The substructure of most bridges is wall piers supported on shallow foundations with no consideration for ductility nor any thought for the use of deep foundations where liquefaction and lateral spreading is to be expected in a seismic event.

SEISMOLOGY OF THE REGION

The Kachchh region is located in Gujarat in western India, south of Pakistan and north of the Gulf of Kachchh. Kachchh is located in zone V, the highest zone on India's seismic zonation map (1). Gujarat has a long history of strong earthquakes, though such intraplate earthquakes are less frequent than those associated with subduction of the Indian Plate beneath the Asian Plate along the Himalayan front. The last two strong earthquakes in Gujarat took place in 1956 and 1819, with magnitudes of 7.0 and 8.0, respectively. India's seismic map is shown in figure 1.

The tectonic setting of the Kachchh region is characterized as a relatively stable continental region similar in nature to the Midwest and the Eastern United States (2). The ground acceleration records from the nearest working strong motion station in the city of Ahmedabad (in Zone 3) some 200 miles away from the epicenter are shown in figure 2. As indicated in figure 2, the thrust fault associated with the earthquake did not rupture the ground surface. East-northeast compression rides and fissures near the epicenter are largely the result of lateral spreading of the soil crust over soil beneath that liquefied.

It has been estimated (EERI, April 2001) that 10,000 square kilometers of highly susceptible deposits in low-lying salt flats, estuaries, intertidal zones and young alluvial deposits liquefied (3). Dissipation of pore water pressure from liquefaction over a wide area around Lodai, which is at sea level, caused water to pipe to the surface and erupt through boils and fissures to a reported height of 6 feet. After a couple of days, according to local sources, such flow diminished but

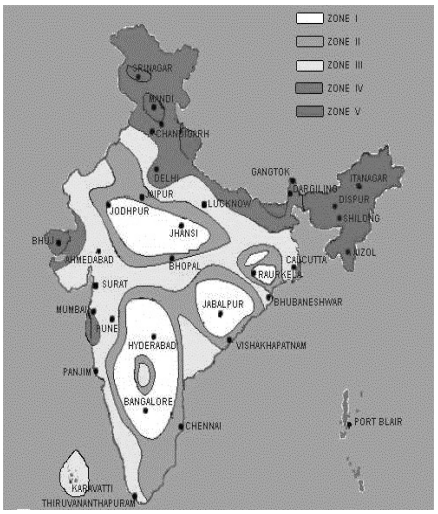

Figure 1. Seismic Zonation Maps

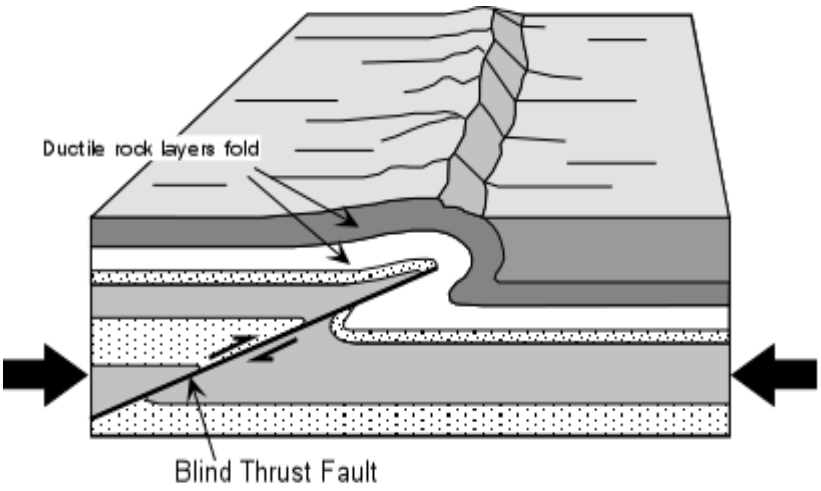

Figure 2. Fault Type Associated with the Earthquake

persisted for several weeks. As seen in figure 3, there was still standing water in places six weeks later, in spite of the warm climate.

Widespread occurrence of ground cracks and sand boils with dried ejected sediments observed at the epicenter and throughout the region ranged between 6 to 24 inches (150 to 600 mm) wide and up to 6 feet (1.8 m) deep. There was little or no vertical separation or elevation difference across these extensional features. Figure 4 is typical of the widespread occurrence of ground cracks.

Figure 3. Surface Water near the Epicenter

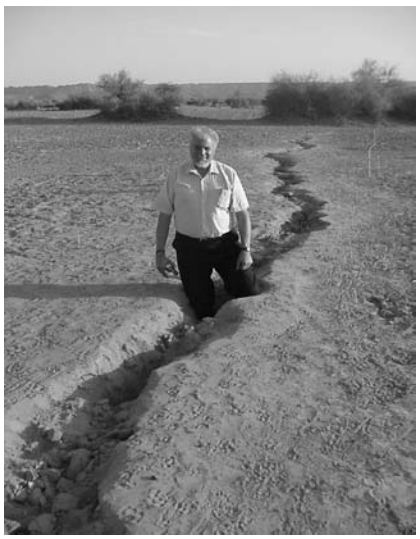

Figure 4. Ground Cracks at the Epicenter

PERFORMANCE OF ROADS

The Gujarat Roads and Buildings Department administrates design, construction, and maintenance of roadways, bridges and other structures. National Highway 8 (NH8) is the most important road in the Kachchh region. NH8A connects local ports and towns to India's highway system. The new NH8A is still under construction and is planned as a four-lane divided modern style toll road. This replacement of NH8A is being constructed at a higher elevation than the existing road to better accommodate monsoon flooding, as shown in figure 5.

Local roads in Gujarat are mostly two lanes between towns and one lane to and between villages. Such roads are in general subject to a low volume of vehicular traffic with very few heavy trucks. After the earthquake, these roads were crucial for accessibility and emergency response to remote areas.

Newly finished roadways suffered some damage. Longitudinal cracks 2 to 4 inches (50 to 100 mm) wide and approximately 12 inches (300 mm) deep developed along the shoulder and edge of the traffic lanes on the embankment. Settlement of the shoulder edge and holes about 24 inches (600 mm) in diameter and 18 inches (450 mm) deep are also visible in the photo. A longitudinal crack separated the entire guardrail system from the roadway shoulder. While rock blocks were laid and mortared in place on the face of the slope, earthquake caused settlement and down slope movement of the underlying soil as was the likely cause of such distress as shown in figure 6.

Figure 5. The new NH8A Road

Figure 6. Roadway cracking

Damage to Traffic Bearing Drainage Structures

Lack of structural adequacy resulted in the collapse of traffic bearing roadway drainage structures, as shown in figure 7. Such roadway drainage structures were, in most cases, concrete box culverts, concrete pipes and unreinforced masonry box culverts. To accommodate post-earthquake traffic, temporary detours were provided across adjacent dry season riverbeds.

Damaged drainage structures are not repairable and should be rebuilt with oversight that standards for design and construction are met.

Figure 7. Collapse of Roadway Drainage Structure

DAMAGE TO PROMINENT BRIDGES: RUDRAMATA AND SUJABARI

Due to poor construction, a harsh environment (monsoon/typhoons and saline ground water accompanied by hot dry weather) and little maintenance, bridges of the area are in substandard condition. Lack of suitable materials and the quality of construction, deterioration of concrete and rusting of reinforcing steel is common to most roadway bridges.

The Rudramata Bridge, built in 1966, is the largest precast/prestressed prestressed concrete girder bridge in the region and one of the few bridges that performed well during the earthquake. It is located on State Highway 45 in north central Kachchh about 10 miles (16 km) from the epicenter of the earthquake. The main structure of the bridge performed relatively well during the earthquake, but the north end approach suffered damage resulting in the closure of one lane of traffic. The bridge is 24 feet (7.3 m) wide and is composed of 10 simple spans of 55 feet (16.8 m) each, with expansion joint at the piers. The superstructure consists of two precast/prestressed prestressed girders with cast-in-place concrete deck and diaphragms. The substructure elements are reinforced concrete towers each supported on a large diameter caisson. Figure 8 shows the Rudramata Bridge and the collapse of the end approach and traffic barrier.

Elastomeric bearings support the prestressed girders at both ends and at intermediate piers. There were no longitudinal restrainers or transverse stops to control the superstructure movement on the piers. Due to seismic excitation, each expansion joint shifted off center on its pier. Different openings of the expansion joints on opposite sides of the deck indicate that rotation of superstructure occurred. This behavior is typical for continuous bridges made of simple spans supported on elastomeric bearings.

Lateral spreading and ground cracking at the north pier resulted in settlement of the bridge approach. As shown in figure 9, cracks in the ground at the north abutment are parallel to the stream bank. Crack were 6 to 12 inches (150 to 300 mm) wide and up to 4 ft (1.2 m) deep. There was no noticeable displacement of the end or intermediate piers due to ground movement. Gapping or separation between the pier caissons and the surrounding ground of up to 12 inches (300 mm) occurred due to movement of the surface soil.

Figure 8. Rudramata Bridge

Figure 9. Ground Cracks at Piers

The tower at Pier 2 experienced cracking as shown in figure 9. The cracks are mostly at the beam to column connection and along the exterior face of the columns. Cracks are primarily shear cracks at the connections and are due to the bending of the tower under the seismic loads. The maximum crack size is approximately ¼ to ½ inch (6 to 12 mm) in width. Some of the cracks have since been patched, though proper procedure for crack repair requires removal of spalled concrete, sandblasting and provision of adequate cover. Smaller cracks could be repaired by epoxy injection.

The Sujabari Bridge is the longest bridge in the region. Built in the fifties, it consists of 36 spans crossing the Gulf of Kachchh on NH8. The bridge is a cast-in-place box girder superstructure supported on the reinforced concrete wall piers on elastomeric bearings. The substructure is supported by well foundations composed of a stack of precast concrete rings augured into the ground to the desired tip elevation and covered by a cast-in-place reinforced concrete cap for wall pier support. Given the age of the bridge, seismic analysis and detailing were not considered in its design. There is no continuity or ductility in the structure; therefore each span acted independently and the entire structure experienced a collection of out-of-phase dynamic motions or modes.

Sand boils, lateral spreading and settlement were widespread in the gulf. The entire area under and around the bridge liquefied as a result of the earthquake. Sand boils up to 2 ft wide were widespread along the bridge alignment. The damage to the bridge indicates there was both longitudinal and transverse movement of the bridge super and substructure. The embankment at the north end of the bridge settled approximately 12 inches and moved toward the channel. This

settlement and lateral spreading of the embankment extended to the bridge abutment and resulted in settlement of the roadway.

The Sujabari Bridge suffered significant damage during the earthquake, as shown in figure 10. Due to the criticality of this transportation link, the Sujabari Bridge was kept open for one lane of select traffic a full month after the earthquake, until construction of the new bridge (parallel to it) was complete.

Figure 10. The Sujabari Bridge

Due to ground movement and liquefaction, some piers moved and associated spans shifted on bearing supports. During the earthquake the superstructure slid off its bearings at several intermediate piers and had to be jacked back to its original position. Pier 14 rocked off its foundation but was immediately repaired and limited traffic allowed. Both sub and superstructure moved, as shown in figure 11.

The in-span hinges suffered some damage with shear failure of the inclined faces of the hinge as shown in figure 12. The expansion joints were closed, rotated, and had popped out throughout the bridge. The cracks in the balusters extend into the bridge deck slab.

Figure 11. Longitudinal Movement of the Piers

Figure 12. Failure of In-span Hinge

DAMAGE TO OLDER BRIDGES

Bridges on NH8A are two lane bridges with wide unpaved shoulders. They are composed of multiple spans with an expansion joint at each pier. Spans about 50 feet (15 m) long are cast-in-place flat slabs or tee-beams. The superstructure is supported on reinforced concrete wall piers, masonry wall piers or concrete arches with masonry fascia walls on shallow foundations. Elastomeric bearings are typical for all bridges.

These bridges are all in a poor condition with spalled concrete and exposed rusted rebar. Past attempts at repair using a shotcrete layer did not protect the structure from deterioration. In spite of such poor structural condition, none of the bridges collapsed during the earthquake. This is in part due to over design, given the use of the short spans and large wall piers. Some bridges suffered more damage than the others. The bridge shown in figure 13 did not collapse during the earthquake, but suffered serious damage to end diaphragms, end pier walls, backwall, bearings and traffic barriers. The traffic barriers are in most cases post-and-beam type and their connection to the balusters and slab are completely deteriorated even prior to earthquake. Given the need to maintain traffic flow on NH8, temporary supports allow for its continued use, though the damage incurred dictates that it be replaced.

Figure 13. Failure of Super and Substructure

Figure 14. Expansion Joint Failure

Shallow foundations moved laterally with the dried crust of near surface soil in which they were embedded. Cracking of the soil surface was likely due to lateral spreading over liquefiable material at depth. Such ground separation (openings of 6 to 12 inches /150 to 300 mm) caused differential pier movements. However, due to the lack of fixity on top of the piers, no significant bending or joint failures occurred during the earthquake. There was some tilting of wall piers, which, due to the large size of the pier cap, did not cause concern.

The out-of-phase and uncontrolled movement of the bridge elements resulted in banging at the expansion joints and dislocation of the superstructure at the bearings. In some cases, the expansion joint shifted on the pier wall. Due to the poor condition of the concrete, damage of the slab at the expansion joint grew to include the cantilever slab. As shown in figure 14, the concrete at the end of the girder is sheared off and the bearing area is significantly reduced. Vertical cracks due to shear friction appear at the end of the girder. The substructure experienced diagonal cracking in the pier cap and vertical cracking in the wall pier. Cracks are ½ to 1 inch wide and require immediate repair. Epoxy injection may be considered an appropriate remedy for repair.

The masonry wall piers are supported on a continuous raft footing approximately 3 feet (900 mm) deep as shown in figure 15. The superstructure is supported on bearings, which over the years have completely deteriorated, such that their existence is hard to discern. The concrete arches are supported on the mat footing on pedestals. Due to the longitudinal movement of the bridge, the fixed connection failed and the end diaphragm cracked vertically. The end span sagged by about 2 inches resulting in cracking and spalling of the concrete at the bottom of the slab.

Figure 15. Failure of Masonry Wall Pier Bridge

The continuity of the arches and footing allowed the bridge to act as continuous structure during the earthquake. Concrete arches performed well during the earthquake, but they suffered some damage to the masonry fascia walls. Minor cracks were observed in the reinforced arches but were closed due to the compressive nature of arch action.

Damage to Bridges under Construction

The new Sujabari Bridge (adjacent to the older one) was nearly complete (two spans to finish) at the time of the earthquake. The bridge was completed within a month of the earthquake and traffic was diverted from the existing damaged bridge to this new bridge. The new bridge is a cast-in-place tee-beam girder bridge with the same number of spans and expansion joints as the older bridge.

The substructure consists of hammerhead piers supported on well foundations. There are transverse stops at pier caps but there are no longitudinal restrainers at expansion joints. Minor damage occurred at the expansion joints of both end and intermediate piers, which was repaired as the bridge was completed. The expansion joint at the end pier is supported by a short cantilever span to a L-abutment as shown in figure 16. The new Sujabari Bridge performed relatively well during the earthquake. This behavior can be attributed to attributes more suited to the seismic environment such as the use of more flexible hammerhead piers (instead of rigid wall piers) and transverse girder stops at piers to prevent the transverse movement of the superstructure.

There were a total of 10 other bridges under construction on NH8A at the time of the earthquake. Some were almost complete while others still had falsework in place for superstructure construction. They are located adjacent to older bridges so, once finished, each bridge can take two lanes of traffic in one direction. These bridges under construction were designed and detailed with the same structural concepts as the older bridges. They have short spans approximately 50 ft long with no continuity (expansion joints at each pier) or provisions for ductility. They have cast-in-place super and substructures with L- abutments at end piers. There was no indication of seismic design and detailing and in spite of the high potential for liquefaction in this seismic zone V; shallow rather than deep foundations were employed. The failure of abutments, piers, expansion joints, and settlement of approach slabs, as shown in figure 17, was typical among the bridges under construction.

Figure 16. The New (Parallel) Sujabari Bridge

Figure 17. Failure of Approach Slab

Due to the similarity of the structures, damage to these shorter bridges was nearly the same. Unfortunately, the damage to these bridges under construction was more significant than to the existing or older structures. The description of damage, though taken from several bridges, can be considered systematic to all. Due to the shorter end span of the bridge shown in figure 18, the superstructure was changed from tee-beam to shallower flat slab. To accommodate this difference in superstructure depth, an auxiliary crossbeam was provided on top of the main crossbeam. Due to the movement of the pier toward the dry stream bed the fixed connection between the two crossbeams failed and the top crossbeam slid off the lower crossbeam. The expansion joint shifted about 15 inches (375 mm) form centerline of the pier.

Due to the relative longitudinal movement of the bridge superstructure and the abutment, the superstructure banged into the abutment backwall and caused cracking and spalling of the concrete at the base of the backwall. The push from the superstructure caused the collapse of the abutment backwall, which then pushed into the approach slab. The approach backfill settled and spread out toward the wingwalls. Consequently the connection between wingwall and abutment wall failed as shown in figure 19. Settlement of the approach backfill of between 12 and 18 inches was typical. The repair of this end pier requires extensive work including rebuilding of the abutment wall, expansion joint, backwall, wingwalls, backfill and approach slab.

Figure 18. Failure of Crossbeam

Figure 19. Failure of Abutment

SEISMIC DESIGN OF BRIDGES

Bridges should be designed and detailed to minimize their susceptibility to damage from an earthquake. Bridges that are designed and detailed in accordance with the seismic requirements may suffer damage, but should have low probability of collapse due to seismically induced ground motion. Bridges may be classified for their importance by the local jurisdiction. Methods of analysis, minimum support lengths, pier design details, abutment design procedures should be specified based on the requirements of seismic zones (4).

Single-span bridges or continues bridges composed of single-spans

Connections should be designed to restrain movement between superstructure and substructure. Seat widths at expansion bearings of multi single-span bridges should accommodate the maximum possible accumulated displacement in the longitudinal direction of the bridge with consideration for the effect of span length, abutment height and skewed supports. Transverse stops and longitudinal restrainers should be provided at all expansion joints to prevent excessive movement of bridge superstructure. Restrainer may be provided between columns or piers at the expansion joints to minimize the relative movement between superstructure and substructure.

Expansion Joints

A primary focus should be the elimination of expansion joints at the end and at the intermediate piers. If expansion joints are employed the reinforcement should be epoxy coated and polymer or other type of durable concrete should be used.

Ductility

The response of structural components and connections can be characterized by ductile behavior, which is based on significant inelastic deformations before any loss of load carrying capacity occurs. It is uneconomical to design a bridge to resist seismic forces elastically. Ductility factors scale elastic forces to lower inelastic values where seismic forces exceed their design level. The ductility factors for connections are smaller than those for substructure members in order to preserve the integrity of the bridge under these extreme loads. For expansion joints within the superstructure, application of a ductility factor results in force effect magnification.

The column may yield in the transverse or longitudinal direction with plastic regions generally located at the top and bottom of columns. Shear failure of columns due to the seismic loads should be avoided by appropriate design and detailing of transverse reinforcement. The main function of transverse reinforcement is to ensure that the column ends are adequately confined after spalling and are capable to prevent buckling of the longitudinal reinforcement. The amount and the spacing of transverse reinforcement at the confinement regions are important. The concrete contribution to shear resistance within the plastic hinge zone is not assured particularly at low axial load levels, because of full-section cracking under load reversals.

Piers

The effect of active earth pressure amplification of the earth mass retained by the abutment wall and wing wall should be considered. Appropriate methods for determining the equivalent static fluid pressures of backfill soils retained by the abutment and for saturated soils susceptible to liquefaction should be used. Seismic design forces should account for wall inertia forces in addition to equivalent static forces. At abutment walls, seismic design forces should also include seismic forces transferred from the bridge superstructure through the bearing supports that do not slide freely.

Wall type piers may be analyzed as a single column in the weak direction and treated as wide a column in the strong direction provided the appropriate ductility factor for that direction is used. Wall piers with an aspect ratio greater than 2.5 have low ductility capacity and no redundancy. A small amount of inelastic deformation is expected when subjected to seismic forces. As a result, a lower ductility factor should be used in determining the reduced design forces.

CONCLUSIONS

The January 26, 2001 Gujarat earthquake was, once again, for bridge engineers, a demonstration of the need for reliable seismic design and detailing, and for greater focus on the quality of construction and the use of durable materials. Based on select information acquired from a brief visit, the authors offer the following conclusions and recommendations:

1. The main reason for damages to both bridges under construction and existing bridges was the omission of seismic design provisions and detailing. Appropriate specifications with respect to the regional seismic requirements should be considered in the design and retrofit of such bridges.
2. A seismic retrofit program should be considered for bridges currently under construction. The program should provide for longitudinal restrainers, transverse stops and column strengthening to meet the requirements for shear capacity, ductility and confinement.
3. Use of shallow foundations for bridges should be avoided where the potential for liquefaction is present. Deep foundations including driven piles and drilled shafts should be considered in the design of bridges under construction and the retrofit of bridges under construction.
4. Superstructure continuity and use of integral or semi-integral abutments should be encouraged. The seismic performance of a bridge benefits from the elimination of expansion joints. Repair and maintenance of expansion joints are costly and time consuming. If expansion joints are used, special attention should be given to restraining the adjoining segments, detailing and the quality of the materials employed in construction.
5. Due to the salt-water environment, the use of High Performance Concrete (HPC) is recommended for improved durability. Epoxy coated rebars, or other type of corrosion-protected rebar, should be used in bridge construction. Improving initial quality will result in longer service life for bridges and will reduce future maintenance and repair costs. Greater importance should be given to the curing of cast-in-place concrete by specifying continuous wet curing for an extended period of time.

ACKNOWLEDGEMENT

The National Science Foundation (NSF) and the Earthquake Engineering Research Institute (EERI) along with the NSF PEER Center sponsored this post earthquake damage assessment visit to India. The authors greatly appreciate the support.

REFERENCES

1. India earthquake Internet websites and local sources.
2. S. K. Ghosh, "Observation From the Bhuj Earthquake of January 26, 2001" PCI JOURNAL, V. 46 No. 2, March/April 2001, PP. 34-42.
3. J. P. Singh, "Preliminary Observations on the Origin an the Effects of the January 26, 2001 Bhuj (Gujarat, India) Earthquake" Earthquake Engineering Research Institute (EERI), Special Earthquake Report – April 2001
4. AASHTO-LRFD Bridge Design Specifications, 2nd Edition 1998 and interims through 2000.

Seismic Response of Highway Bridges Subject to Near-Fault Ground Motions

Bulent Akbas and Jay Shen

ABSTRACT

A multiple-span viaduct located in Izmit, Turkey was used as an example structure to investigate the effects of near-faulty ground motions on the bridges. The vibration tests were conducted to obtain as-built structural properties. The computer models simulated the structure before the dynamic analysis was carried out. The bridge was subjected to an ensemble of ground motions recorded with a range of epicentral distances. The seismic response was interpreted to discuss the characteristics of near-fault response.

Bulent Akbas and Jay Shen, Illinois Institute of Technology, 3201 S. Dearborn Street, Chicago, IL 60616, e-mail: shen@iit.edu

Seismic Performance of Bridges in the Chi-Chi Earthquake, Taiwan

By

Wen-Huei Phillip Yen[1], James Yeh[2] and Liang-Hong Ho[3]

ABSTRACT

This paper presents preliminary findings of investigating 10 bridge sites after the Chi-Chi Earthquake occurred on September 21, 1999. Damages of each bridge, and lessons learned from this particular earthquake are described.

[1] Research Structural Engineer, Office of Infrastructure, R&D FHWA, 6300 Georgetown Pike, McLean, VA 22101 Wen-Huei.Yen@fhwa.dot.gov
[2] Deputy Director-General, Taiwan Highway Bureau, Taipei, Taiwan
[3] Structural Engineer, Structures Division, National Expressway Engineering Bureau, MOTC, Taipei, Taiwan

INTRODUCTION

On September 21, 1999, at 1:47am (local time), a destructive earthquake struck the center area of Taiwan. This earthquake measured as a magnitude Mw = 7.6 had caused more than 2,400 lives loss and over 10,000 people injured according to the Taiwanese Official Report. Approximately 10,000 buildings/homes collapsed and about 7,000 were severe damaged. Highway bridges including constructed under modern seismic design codes were severe damaged as well. Based on Taiwanese Highway Bureau's preliminary report (Yeh, Nov., 1999), at least nine bridges were severely damaged including three of them were under construction. Five bridges collapsed due to the faults rupture and seven bridges were damaged in the moderate level.

With the joint efforts between Federal Highway Administration (FHWA), Ministry of Transportation and Communication (MOTC) of Taiwan, an investigation team was formed to examine and collect highway bridge performance under the Chi-Chi earthquake. The team members consisted with FHWA and Taiwanese Highway Bureau (THB) and National Expressway Engineering Bureau's (NEEB) Engineers of MOTC. During, the team visited 10 bridge sites which including 2 bridge sites of NEEB and 8 bridge sites of THB. The detail route is shown in the Figure 1. This paper presents the preliminary findings and bridge lessons learned from the team's investigation during Nov. 15-17, 1999.

Fault Rupture Type

Taiwan is located at the junction of the Manila and Ryukyu Trench in the Western Philippine Sea where the Philippine plate is being forced under the Eurasia plate. The Philippine plate is moving in a northwest direction which causes a significant strike-slip component along the northern portion of the Manila Trench and essentially creates a "transpressional" effect which has popped up the island of Taiwan microplate relative to its larger tectonic neighbors. This "thrust fault**"** or called / reverse-slip fault had elevated several locations including bridge sites lift up several feet to 30 feet high.

Bridge Design Codes

Bridge design specification used in Taiwan have been revised three times since 1960. Prior to 1960 there were several design guide specifications used for practical design. Some of them were based on Japanese design codes. In 1960, MOTC of Taiwan issued a standard specification titled "Highway Bridge Engineering Design Specifications" which was used in their design and construction of highway bridges. This design specification was based on the American Association of State Highway and Transportation Officials' (AASHTO) bridge design specifications issued in 1953. In 1987, MOTC of Taiwan revised this design code based on the 1977's AASHTO bridge design specifications. Although this code was revised again in 1995 based the 1992's AASHTO, the codes was not changed much in the seismic design area. Table 1 shows the revision changes by years. In the latest version, Chapter 2.20 of the earlier version was extracted as separated division which describes the detail of seismic design force. In the 1987's version, seismic design force used the equivalent coefficient method, and dynamic effects and soil amplification factors were included.

For bridge pier less or equal to 15 meters

$K_h = ZSIC_0$

For Bridge pier higher than 15 meters

$K_h = \beta ZIC_0$

Where

K_h : Lateral Seismic Design Force Coefficient and $K_h \geq 0.1$

C_0 : Standard Seismic Design Force Coefficient and $C_0 = 0.15$

Z : Coefficient of Seismicity (From 0.6 to 1.2)

S : Coefficient of Soil Profile (From 0.9 to 1.2)

I : Coefficient of Importance Factor (From 0.8 to 1.0)

β : Adjusting Factor.

While the latest version of design code changes the Seismic Design Force as the following

$$V = \frac{ZI}{1.2\alpha_y}\left(\frac{C}{F_u}\right)_m W$$

$(C/F_u)_m$ is the adjusted Coefficient of Acceleration Response Spectrum, and W is the design dead load. α_y is the reduction factor based on the ductility.

Seismic design forces used in the epicenter area are typical 0.15g to 0.2g. With the measured largest peak ground acceleration greater than 1.0g (986gal), the damage of bridge structures are inevitable.

Table 1. Bridge Design Codes in Taiwan

YEAR	BRIDGE SEISMIC DESIGN CODES	CODE BASIS	
Prior to 1960	Varies Bridges Design Spec.	Based on Japanese Bridge Design Codes	
1960	Standard Specification for Highway Bridges of Taiwan	Based on 1953 AASHTO Standard Specification	
1987	2nd edition Bridge Design Codes	Based on 1977 AASHTO Specification	
1995	Current Bridge Design Codes	Based on 1992 AASHTO Specifications	

BRIDGE DAMAGES

Neotsou-Si and Neotsopu Kenshi Bridges

The team first visited two bridge sites of NEEB, Neotsou-Si and Neotsopu Kenshi bridges. These two bridges are continuous spans with pre-stressed box girder superstructure; and are away from the epicenter about 60-70km. They were still under construction and suffered similar damages. In general, two bridges performed well. However, the pot bearings of both bridges were severe damaged, and superstructure offset 2-30cm. Figure 2-3 shows the pot bearing damages and

superstructure's offset in the lateral direction. Bridges under the construction by NEEB are parallel to the faults direction, and this may have less effect from this large earthquake. Nevertheless, some bridge foundations and piers were poured concrete one or two days before the earthquake, extensive NDE examinations are needed to investigate bonding issues between reinforced steel bars and concrete. Figure 4 shows the tilting of bridge pier caused by fault rupture and newly poured bridge foundation.

Eight bridge sites of THB's districts were visited including one new bridge site. Six bridges were collapsed due to fault rupture underneath or adjacent to the bridges. The average ground movement is more than 2 m.

Shi-wei bridge

It is located on the Route 3 which was constructed in September of 1994. It consists of northbound and southbound twin bridges. The total length of the bridge is 75 m, and was divided into three simply supported spans (25m each). It is a curved bridge with the bridge width of 24 m and supported by five PCI girders. Each girder is supported on elastomeric bearing pads with shear keys to provide transverse constraints. The 2nd pier of both bridges were tilting, and the first pier of northbound revealed shear cracks. The second and third spans of southbound, and the third span of the northbound collapsed due to piers tilting and large ground offsets. The fault rupture was right underneath the south abutment area. Since the bridge is skewed and curved, large ground motion might have caused bridge deck rotated and also damaged the substructures. Since bridge were design as a simple support beam and almost certain would not be able to accommodate this large ground movements.

Tong-feng bridge

This bridge is also on the Route 3 which is about 5 km away from Shi-wei bridge. Bridge has 573 m in length, and was consisted with three parts. The middle part was completed in 1966, and the bridge was widened from both sides completed in 1988. The earlier construction has 22 span with 4 PCI girders to support 9.5m wide bridge deck. Substructure is a pier wall type construction. The later construction widened the bridge deck into 30m with PCI girders support. However, the substructure used single column bridge piers. After earthquake, bridge has large vertical displacements (10-20cm) and offsets (30-50cm) in the transverse direction. PCI girders dislodged from bearings due to large transverse movements. One of girder was cracked and was temporarily supported by a steel truss. Although the bridge was severe damaged, bridge was reopen to the traffic with restricted lanes after bearings were replaced with elastomeric pads.

Bei-feng bridge

Located near by the Shi-kan Dam, this bridge is a simply supported PCI girder with multiple spans. This bridge was completed in 1991. Superstructures were collapsed due to fault rupture underneath the bridge. The fault rupture uplifted the upper steam by 5-6m, and created a new water fall. This reverse-slip fault should also shorten the bridge length and might have pushed the send pier to fail.

Wu-shi bridge

The bridge is on the Route 3 and connects Nan-tou and Tai-chung counties. The total length of this bridge is 624.5m with 25m in width, and has 18 spans. In fact this bridge has two parallel

bridges and were constructed in two different period. The superstructure of northbound bridge was constructed in 1981, but it used the original substructure (Pier-wall type) which was constructed in 1950s. The southbound was completed in 1983. They both use PCI girders in their simply supported superstructure, and have pier-wall type substructures. However, the newer bridge (Southbound) has smaller size of the older bridge (Northbound). Fault rupture occurred behind and under northern abutments of both bridges. Although two bridges suffered similar ground motions, they failed in two different ways. The first and second spans of older bridge collapsed. This failure was due to fault rupture and caused large ground movement so that the superstructures pushed back and forth and fell down from seats. Bearings are also failed due to large compression forces. The third pier of the northbound has also been uplifted. Both superstructures might also collide during the earthquake and caused some damages of substructures. Bridge piers of Northbound suffered tension crack and fractured. While southbound bridge piers have severe shear cracks and failures.

Mao-luo-shi bridge

The bridge is still on Route 3 and is between Tsou-Tun town and Nan-Tou city. It is a horizontal curved viaduct with steel superstructure. Superstructure is consisted with 4 plate girders supported on concrete, single column bents. Some of these bents are "C – bent" where the column is eccentrically connected to the cross-girder. The bridge did not collapse but has shear cracks. Most eccentric connections showed distress in the concrete columns. Some severe locations were temporarily supported by steel truss. This shear cracks could have contributed through the vertical acceleration component for this cantilever overhang superstructures.

Ji-lu bridge

The bridge is a cable-stayed bridge. It located in the Route 152, is near the Chi-Chi town. Approach spans at both ends are simply supported lead up to the two-span, single-tower structure that is approximately 240m in length. The concrete superstructure is symmetrically supported by 17 pairs of parallel cables from each side of the tower. The structure was almost completed at the tome of earthquake; only the one section under the tower and guardrail was not completed. Damages of bridge include one snapped cable, tower structure cracking and concrete spalling, pot bearings failed due to structure pounding up and down and approach spans offset in transverse direction.

These damages are typically attracted engineers' attention. For this bridge is a mid long-span bridge, and is under construction. Unbalance loading might have caused the bridge pounding vertically and laterally. Ground motion characteristics has also shown vulnerable damage to longer natural period of structures.

Tong-tou bridge

This structure located in the Route 149, and has 160m long and 9m wide. Bridge's superstructure are PCI girders supported by single column bents. The first and fourth spans collapsed. The second span tilted and rotated in transverse direction. Substructures have severe shear failure and column bents sheared out. Large movements due to the fault rupture underneath the bridge failed. The figure 10 shows the bridge's collapsed spans.

E-Jiang and Min-Tsu Bridges
These two bridges were demolished when the team visited.

BRIDGE LESSONS LEARNED

Through the extensive visits and evaluations of damaged and undamaged bridge sites, the following is a preliminary set of lessons learned from this investigation:

1. Fault rupture, directly crossing or adjacent to the bridge, is a catastrophic event and span collapse is inevitable if the dislocations are large.

2. Long-span bridge are vulnerable in the near-fault sites, especially when those still under construction

3. Ground failures may cause structural failure.

4. Shear failures must be avoided in piers.

5. Shear key and bearing design need to be consistence with pier design capacity.

6. Engineered abutment back-walls and back-fills are essential to prevent span collapses even for continuous bridges

7. Near-fault ground motion are intense and extremely punishing older structures which have not designed with modern codes.

SUMMARY

The Chi-Chi earthquake has severely damaged highway bridges due to large ground motions and fault ruptures directly underneath or adjacent to bridge sites. Even with the modern design codes, the bridge will not be able to resist such huge displacement or offset for either superstructure or substructures. The challenge tasks left for engineers is to develop a good strategy to deal with the bridge constructing across a known fault or near-by a fault.

ACKNOWLEGEMENTS

The authors like to thank Mr. James D. Cooper, Mr. John O'Fallon and Mr. Paul Teng of Office of Infrastructure, R&D of FHWA, and Mr. King Gee, Mr. Jim Hansen and Ms. Marry-Ellen Rizzo of International Program Office of FHWA for their supports. Comments of Prof. Ian Buckle of University of Nevada at Reno are very much appreciated.

REFERENCE

Ian Buckle and Jenn-Shin Hwang. " Bridge Performance in the 921 Earthquake, Chi-Chi, Taiwan," *Proceedings of the 15th US-Japan Bridge Engineering Workshop*, Tsukuba, Japan, November 1999.

Seismic Design Practices and Specifications

Chair: Michel Bruneau

A Proposed Bridge Seismic Design Philosophy and Criteria

Brian Maroney and Nancy McMullin Bobb

Seismic Retrofit of Bridges Using Shape Memory Alloy Restrainers

Reginald DesRoches and Bassem Andrawes

Experimental Study on Seismic Behavior of Highway Bridge Foundation during Liquefaction Process

Hiroshi Kobayashi, Keiichi Tamura, Naoki Sato and Takuo Azuma

Development and Implementation of a New Seismic Design Bridge Criteria for South Carolina

Roy A. Imbsen and Lucero E. Mesa

Seismic Retrofit of Aurora Avenue Bridge with Friction Pendulum Isolation Bearings

Hongzhi Zhang

A Proposed Bridge Seismic Design Philosophy and Criteria

Brian Maroney and Nancy McMullin Bobb

Since the Loma Prieta Earthquake and the report to the Governor on that earthquake, "Competing Against Time," significant attention has been focused upon bridge post-earthquake performance. Seismic design criteria continue to evolve with each new major project in California, to such a degree that consistency can be difficult to identify. This paper offers an accumulation of the California perspective of those experiences and the lessons learned. This experience is not only field experience, but actual project development experience as well, including interaction with reviewing entities external to project teams. Specific reference to experiences developing minimum seismic performance (e.g., standard bridges) and lifeline performance (e.g., San Francisco-Oakland Bay Bridge) criteria are documented.

The authors offer seismic design/retrofit philosophy and performance criteria that are essentially the product of their experiences since the Whittier Earthquake of 1987.

Brian Maroney, Principal Bridge Engineer, California Department of Transportation, Sacramento, California
Nancy McMullin Bobb, Structural Engineer, Federal Highway Administration, Sacramento, California

Seismic Retrofit of Bridges Using Shape Memory Alloy Restrainers

Reginald DesRoches and Bassem Andrawes

ABSTRACT

This paper evaluates the use of NiTi Shape Memory Alloy rods as restrainers in multi-frame bridges. Shape Memory Alloys (SMAs) are a class of alloys that display unique characteristics, based on a thermoelastic martensitic phase transformation. These properties include the shape memory effect, superelasticity, and high damping characteristics. Tests of SMA rods are performed to evaluate the superelastic properties as a function of bar size. The results show that the NiTi SMAs exhibit good superelastic properties for both SMA wire and rods. The results of the tests are used to develop analytical models of SMA restrainers. These models are used in analytical studies of the seismic response of typical multi-frame bridges subjected to moderate-to-strong ground motion. The results of the analysis show that the SMA restrainers are much more effective in limiting the relative hinge displacement compared with conventional steel cable restrainers.

Reginald DesRoches, Assistant Professor, School of Civil & Environmental Engineering, Georgia Institute of Technology, Atlanta, GA 30332-0355
Bassem Andrawes, Graduate Research Assistant, School of Civil & Environmental Engineering, Georgia Institute of Technology, Atlanta, GA 30332-0355

INTRODUCTION

During an earthquake, the relative motion between adjacent frames can result in unseating if the bridge seat width is not adequate. The 1971 San Fernando earthquake resulted in several cases of unseating at the hinge [7]. Following the earthquake, the California Department of Transportation initiated a retrofit program consisting of providing restrainer cables at hinges to reduce the likelihood of unseating. Restrainer cables typically consist of a ¾" diameter steel cable with a cross sectional area of 0.22 in^2 and a capacity of 46 kips. Recent earthquakes have shown that unseating of simple spans and frames is still a problem that has not been adequately addressed [8,3,4]. Several limitations of restrainer cables currently exist. First, restrainer cables have a small elastic strain range – typically less than 2 inches for a 10 ft cable. Therefore, restrainer cables are designed to remain elastic, which results in large forces being applied at adjacent frames. Second, recent earthquakes have shown that failure of the cable often occurs in the connection elements of the cable. To address the limitation of restrainer cables, a new technology for limiting relative hinge displacements in multi-frame bridges using shape memory alloy restrainers is studied.

SHAPE MEMORY ALLOYS

Shape memory alloys are a class of alloys that display unique characteristics, based on a thermoelastic martensitic transformation. Unlike plastically deforming metals, the nonlinear deformation is metallurgically reversible. Although several alloys exhibit the shape memory property, the most widely used shape memory alloy is Nitinol, which consist of approximately equal composition of Nickel and Titanium. In the low temperature phase, Nitinol exhibits the *shape memory effect* – strain can be recovered by heating the specimen above the transformation temperature. At a slightly higher temperature, Nitinol exhibits the superelastic effect, as shown in Figure 1. In the superelastic phase, Nitinol is initially in the Austenitic phase. However, upon loading, stress-induced martensite is formed. Upon unloading, the martensite reverts to austenite at a lower stress level, resulting in the hysteresis shown in Figure 1. The Superelastic behavior of Nitinol SMAs possesses several characteristics that make it ideal for use as restrainer cables, including (1) large elastic strain range, leading to excellent potential as a recentering device, (2) hysteretic damping, and (3) strain hardening at large strains.

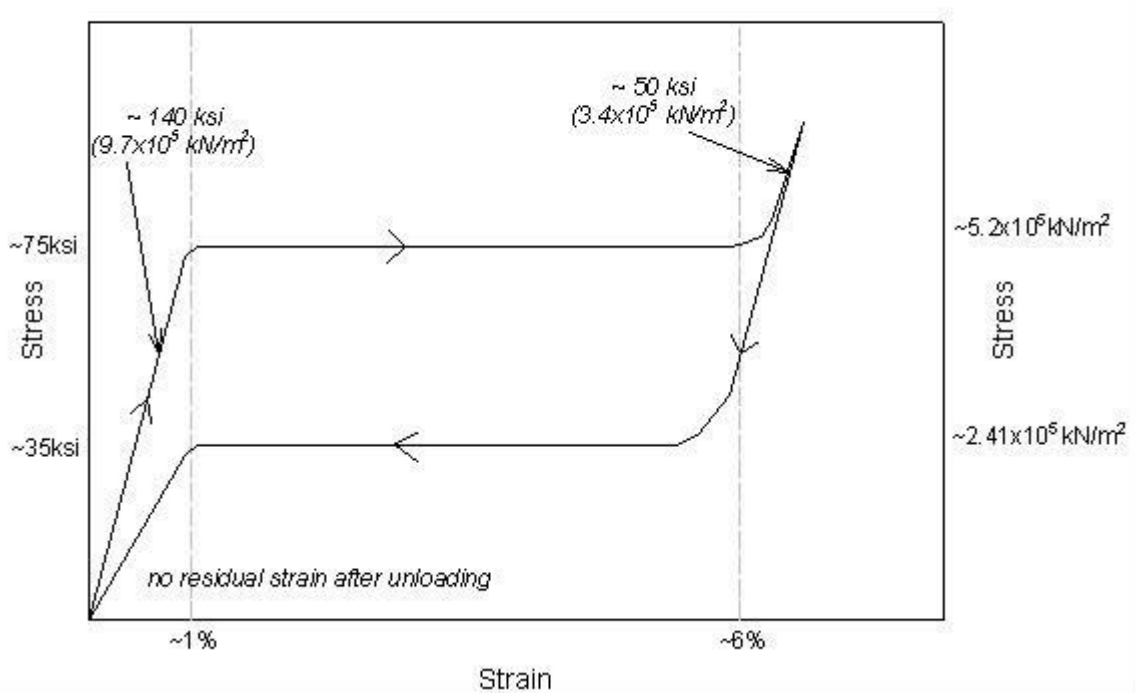

Figure 1. Idealized Stress-Strain Behavior of Nitinol Shape Memory Alloy.

EXPERIMENTAL TESTS OF NITINOL SMA WIRES AND RODS

Tests of 0.07 inch Nitinol wire and ½ inch Nitinol rods are performed to evaluate the cyclic stress-strain behavior of Nitinol wire and rods. Most of the research on Shape Memory Alloys has been in the biomedical industry where SMA sizes ranged from wire that is 0.002 to 0.04 inches in diameter [5]. It is generally thought that larger sizes do not exhibit the same superelastic properties, though few studies exists to confirm these results. The wire and rods were loaded cyclically up to a maximum strain of 6%. The loading history consists of repeated cycles at 6% since this is the strain range where the SMA restrainers will be used. The results for the wire and rod are presented below.

Nitinol SMA Wire (0.07 inch Diameter)

The results for the SMA wire, shown in Figure 2, lead to several observations. First, the loading stress ranged from approximately 80 ksi for the low strain cycles to approximately 60 ksi for the 6% strain cycles. The loading plateau shows several regions of sudden drop in stress. This was a result of minor slipping occurring at the grips in the test specimen. The unloading plateau ranges from approximately 15-20 ksi. The large difference between the loading and unloading plateau results in a wide hysteresis and an equivalent viscous damping ratio for the 6% cycle equal to 7%. The residual strain after the complete loading cycle was less than 0.50%, which indicates excellent potential for the SMA wires in re-centering applications.

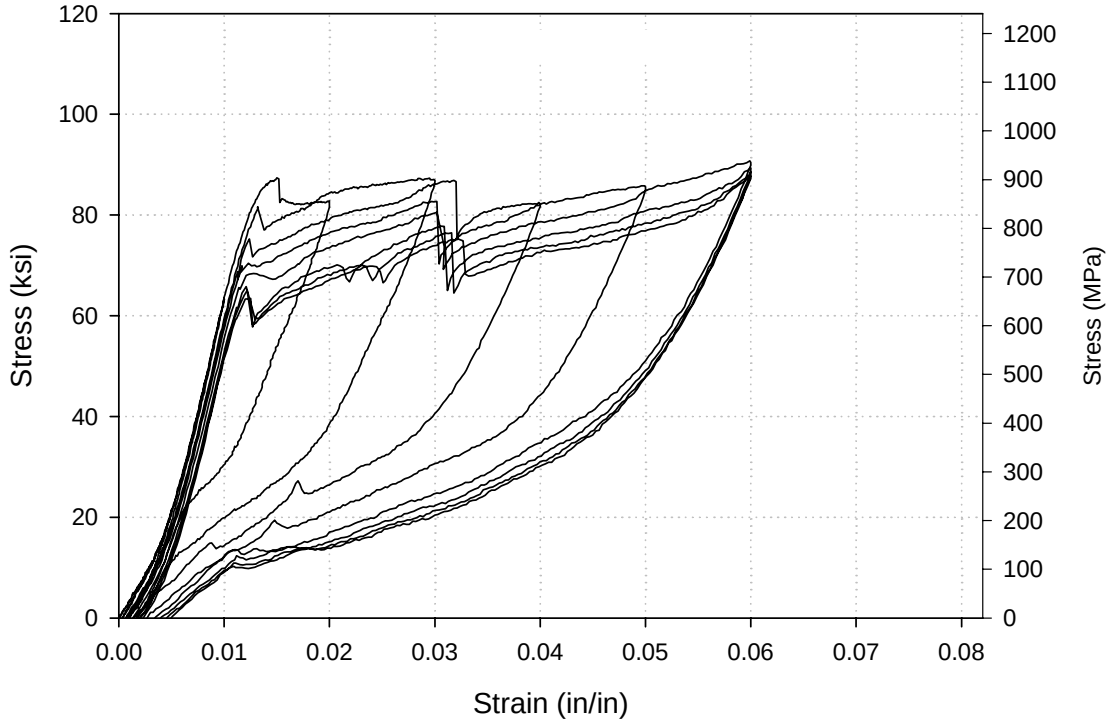

Figure 2: Stress-strain curve of 0.07 inch Nitinol SMA wire subjected to cyclical loading.

Nitinol SMA Rod (1/2" Diameter)

The results for the ½ inch SMA rod are shown in Figure 3. The rod was machined from a ¾ inch cold drawn Nitinol rod and annealed at 350 degrees C for 60 minutes. The loading history was identical to that of the 0.07 inch wire. The stress-strain curve for the rod has slightly different shape than the wire SMA. The loading plateau is not as clearly defined as it was for the wire and does not exhibit the classic "flag-shap" shown in the wire. The loading plateau occurs at approximately 40-50 ksi. At lower strains, the rod exhibits approximately 20-30 percent lower strength compared to the wire. However at higher strains, the rod exhibited much higher strength than the wire. At 6% strain, the rod had a stress of approximately 110 ksi, compared to a value of approximately 80 ksi for the wire. In terms of residual strain, the rods performed extremely well. Less than 0.30% residual strain was observed following the 6% strain loading cycles. However, the hysteresis in the rod was much smaller and the equivalent viscous damping for the 6% cycles was approximately 2.1%.

As discussed above, the wire and rod superelastic shapes are quite different. These differences are believed to be due to differences in the processing of the rod and not a general characterization of larger bars. Previous studies have shown the strong relationship between thermo-mechanical processing and strength of SMA wire and rods [6]. The differences in the stress-strain curve result in less energy dissipation potential in the rod compared to the wire. However, the recentering potential for the rod is excellent. This is the property that will be exploited in evaluating the potential of SMAs as restrainers in bridges.

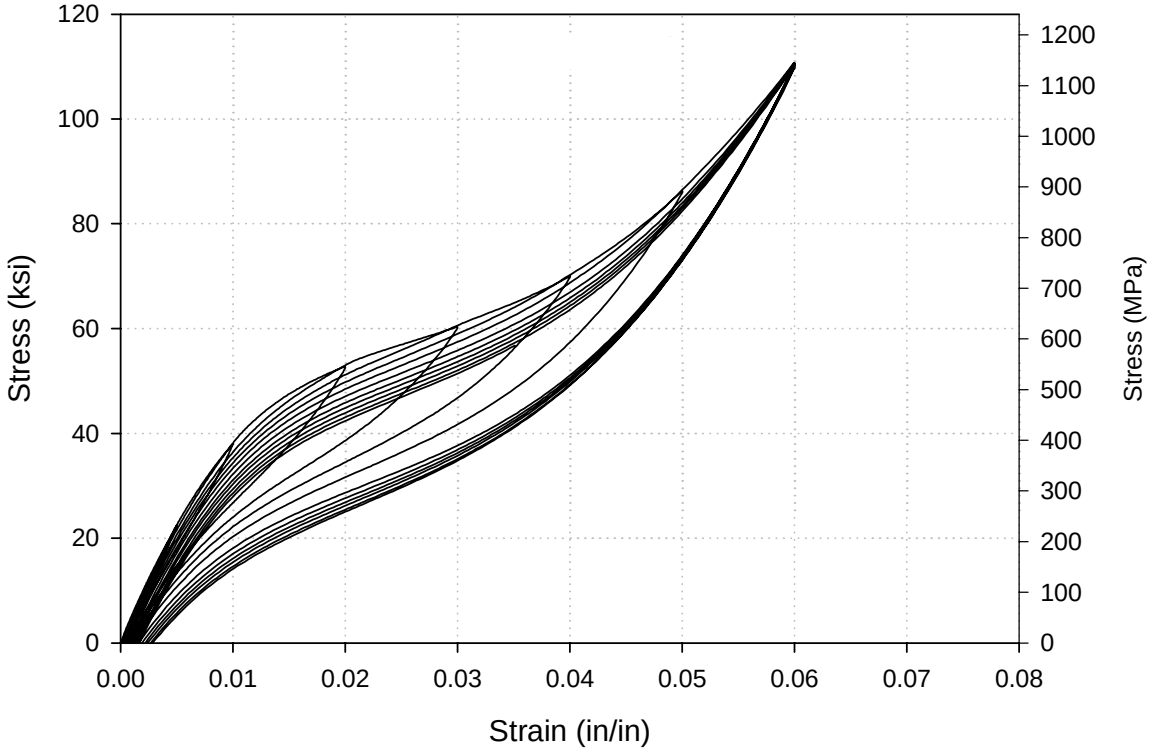

Figure 3: Stress-strain relationship of 0.50 inch diameter Nitinol SMA rod subjected to cyclical loading.

APPLICATION SMA RESTRAINERS TO MULTI-FRAME BRIDGES

The use of restrainer cables to limit the relative hinge displacement in multiple-frame bridges is a common retrofit strategy in the California and other states in moderate to high seismicity. The results of the experiment tests of the SMA rods and wires illustrated that the SMAs have excellent recentering capabilities up to strains of approximately 6%, and therefore may be a more effective alternative to conventional steel cable restrainers. In this section, the use of SMAs as hinge restrainers in a multiple-frame bridge is evaluated. The multiple-frame bridge considered in this study consist of a four-frame, 11-span reinforced concrete box-girder bridge, supported on single-column bents, as shown in Figure 4. The outer frames are each supported by two 40 ft columns, and the inner frames are supported by three 60 ft. bents. Each hinge is supported by elastomeric bearings. The gap between each frame is ½" inch.

The SMA restrainers would be connected from the end of one box girder to the beginning of the adjacent box girder, in a fashion similar to the conventional steel cable restrainers. Below, a nonlinear analytical model is used to investigate the response of the multi-frame bridge retrofitted with the SMA restrainers. In this investigation, the ½" SMA rods are used in the analytical studies.

Analytical Modeling of Multi-frame Bridge with SMA Restrainers

A 2-dimensional nonlinear numerical model of the 4-frame bridge shown in Figure 4 is developed using the DRAIN-2DX nonlinear analysis program [9]. The superstructure is modeled using linear elastic elements and the columns are modeled using the DRAIN-2DX fiber element. Each fiber has a stress-strain relationship, which can be specified to represent unconfined concrete, confined concrete, and longitudinal steel reinforcement.

The nonlinear abutment properties used in this model are based on design recommendations from Caltrans [3]. An impact element is used to model pounding between the frames in the bridge. The compression-only trilinear gap element has springs that penalize closing of the gap.

Using the results of the experimental tests of the ½ inch diameter rods, an analytical model of the SMA restrainer is developed using a combination of link and connection elements in DRAIN-2DX, as shown in Figure 5. The SMA restrainers are modeled as tension-only, multi-linear elements and represent the force-displacement relationship of the SMAs, including the yield plateau, unloading plateau, and strain hardening. The SMA restrainers are modeled with a "yield" strength of approximately 45 ksi, and unloading strength of approximately 18.5 ksi. As previously mentioned, the unloading stress and residual deformation depends on the total deformation. In the model used in this study, the residual deformation is taken as zero, and the unloading stress is kept constant, based on the average value over the strain range tested. Eighteen percent strain hardening is assumed up to 5%, and 60 percent strain hardening is assumed for strain beyond 5%, as determined from the experimental tests.

In this study, comparisons will be made between the SMA restrainer and commonly used steel cable restrainer. The restrainer cables evaluated are ¾" diameter cables that are 10 ft in length. The cables have a yield strength of 39.1 kips, at a displacement of 2.1 inches.

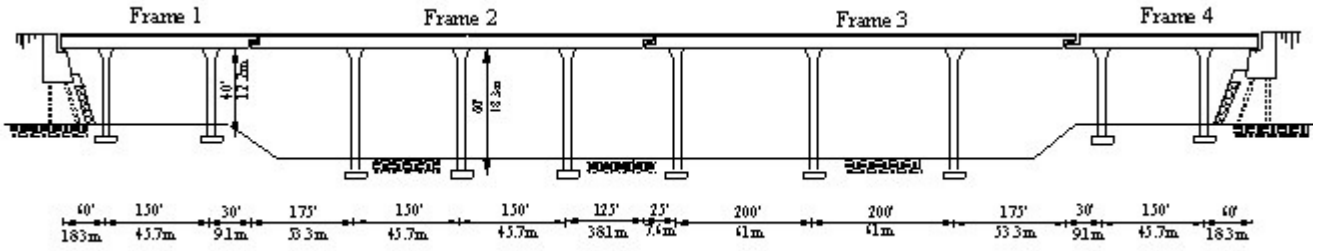

Figure 4: Typical multiple frame bridge used in analysis of SMA restrainer.

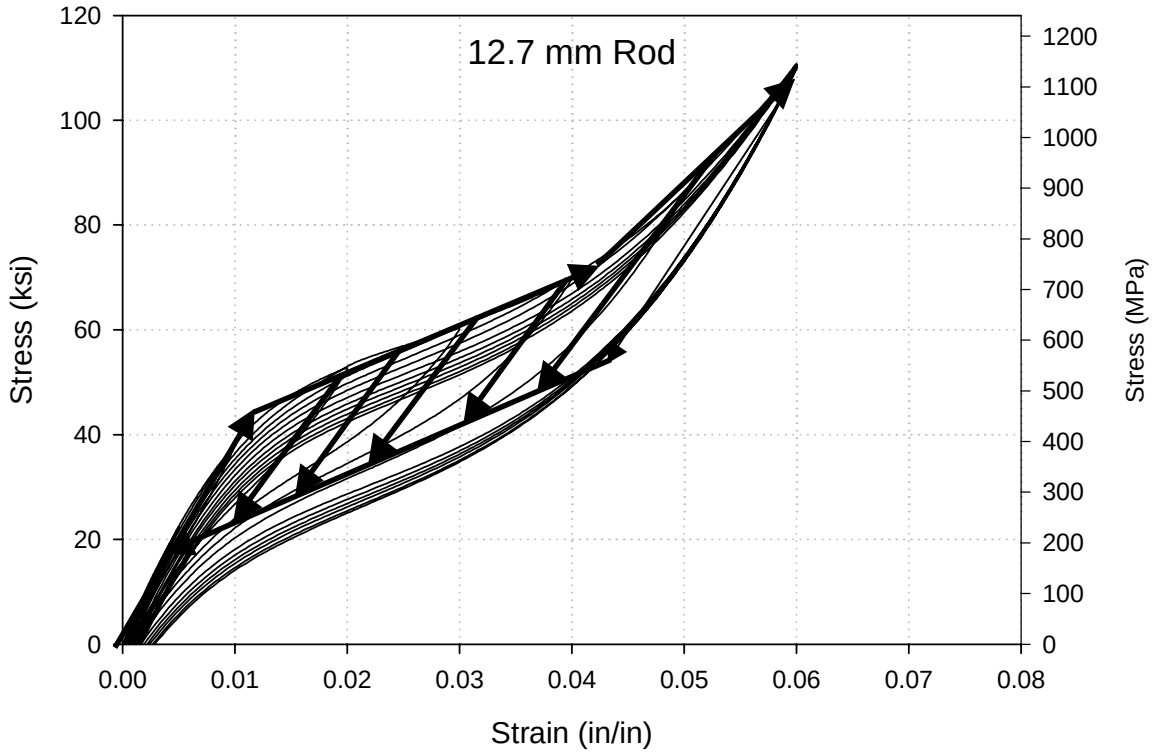

Figure 5: Analytical model of SMA restrainer (Bold) plotted with results from experimental tests.

Analytical Results

To evaluate the effectiveness of the SMA restrainers, the analytical model of the SMA restrainers is subjected to a set of ground motion, including the Oakland Outer Harbor Wharf record (1989 Loma Prieta earthquake), and the Sylmar Free Field record (1994 Northridge earthquake), and the 1940 El Centro record (Imperial Valley earthquake). All of the records are scaled to a peak ground acceleration of 0.70g. The results of the 1940 El Centro record are reported in this paper.

The conventional restrainers are designed according to the AASHTO restrainer design procedure [1], which results in 26 cable restrainers. The SMA cable restrainers are designed, such that they have the same force as the cable restrainers at their operating strain of 6%. This results in 50 36-inch long, ½" diameter SMA cable restrainers.

Figure 6 shows the response history of relative displacements between Frame 1 and Frame 2 subjected to the 1940 El Centro earthquake, scaled to 0.70g. The maximum relative hinge displacement of approximately 6.79 inches occurs in the as-built bridge. The use of conventional restrainer cables at the hinges results in a maximum relative hinge displacement of 6.05 inches – a reduction of 11% of the original displacement. The SMA restrainers, however, reduce the maximum relative displacement to 3.94 inches – a reduction of 42% of the original displacement. There are several reasons for the effectiveness of the SMA restrainers compared to the

conventional steel cables. First, since the restrainers are superelastic, they have the ability to remain elastic for repeated cycles. This results in a greater effective stiffness, as compared with the conventional restrainers. It is observed that the restrainer cables are effective in limiting the relative hinge displacement for the first couple of loading cycles. However, at approximately 3 seconds into the response, the restrainers are subjected to their maximum deformation, resulting in yielding of the cable. In subsequent loading cycles, the effectiveness of the restrainers is significantly reduced due to the large residual deformation in the cable. Note that in remainder of the response history, the hinge displacement with the restrainer cables is similar to that of the as-built bridge. This effect is also observed in the force-deformation plot of the restrainer cable shown in Figure 7. In contrast to the restrainer cable, the SMA restrainer is effective for repeated cycles. The other reason that the SMA restrainers are more effective than the conventional restrainer cables is the strain hardening that occurs in the SMAs. As shown in the experimental tests, the SMAs rods have strain hardening values of approximately 60% beyond approximately 4.5% strain. This provides significant force in resisting hinge opening during an earthquake.

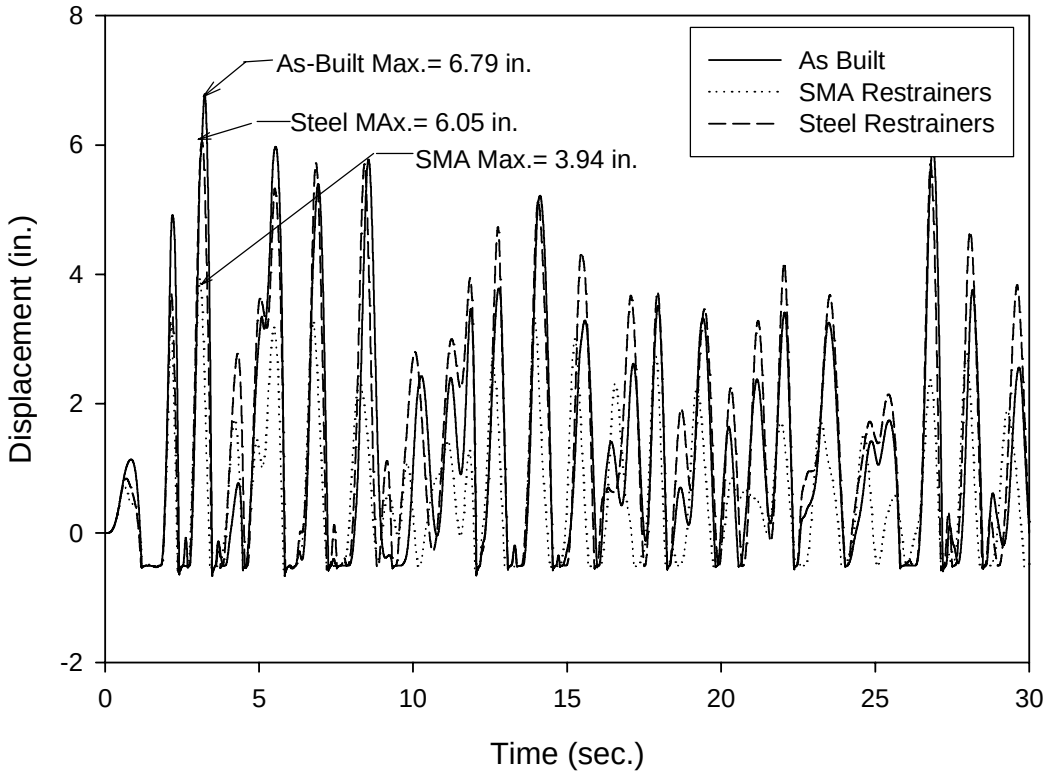

Figure 6: Response history of relative displacement between Frame 1 and Frame 2 for multiple frame bridge subjected to 1940 El Centro Ground Motion, Scaled to 0.70g.

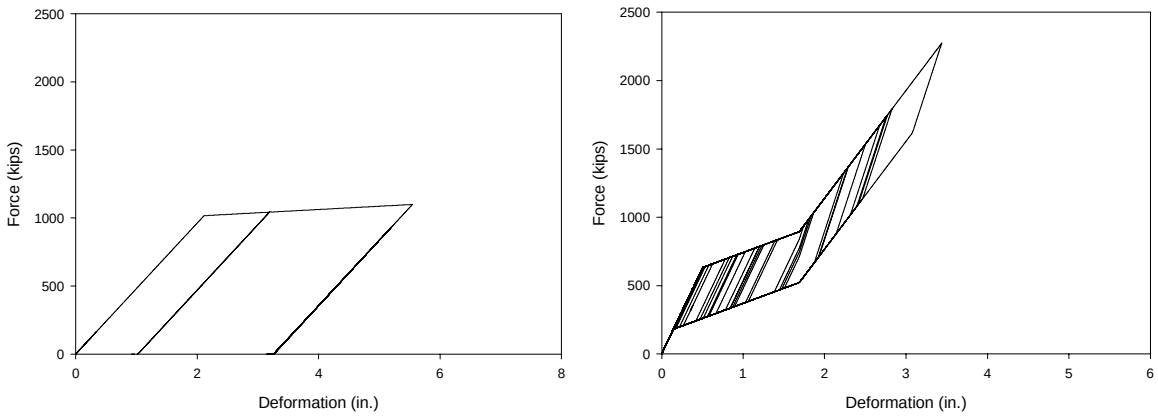

Figure 7: Force-displacement results for (left) restrainer cable, and (right) SMA restrainer rod, for 1940 El Centro ground motion.

CONCLUSIONS

This paper presents the results of a study evaluating the efficacy of using shape memory alloys as restrainers in multiple-frame bridges. Tests of SMA wire, and ½ inch diameter SMA rods subjected to uniaxial tension are conducted. The wire and rods are subjected to cyclical strains up to 6% with minimum residual deformation. The effectiveness of SMA restrainers in bridges is evaluated through an analytical study of a multi-frame bridge. The relative hinge displacement is compared with conventional restrainer retrofits using steel cable restrainers. The results show that the SMA restrainers reduce the relative hinge displacement much more effectively than conventional restrainers. The large elastic strain range of the SMA restrainers allows them to undergo large deformations while remaining elastic. In addition, the added stiffness at large strains due to strain hardening is effective in limiting the relative hinge displacement.

ACKNOWLEDGEMENTS

This work was supported primarily by the Transportation Research Board, IDEA Program, Project Number N-637. Additional funding was provided by the Earthquake Engineering Research Centers Program of the National Science Foundation under Award Number EEC-9701785 (Mid-America Earthquake Center).

REFERENCES

[1] AASHTO, 1995. American Association of State, Highway, and Transportation Officials, 1995.

[2] Bruneau, M. et al. 1996 “Performance of Steel Bridges During the 1995 Hyogo-Ken Nanbu (Kobe, Japan) Earthquake,” *Canadian Journal of Civil Engineering*, Vol 23, No. 3, June 1996, pp. 678-713.

[3] Caltrans 1990. “Bridge Design Specifications Manual,” California Department of Transportation, 1990.

[4] Chang, K. C. et al. 2000 "Seismic Performance of Highway Bridges," *Earthquake Engineering and Engineering Seismology*, Vol. 2, No. 1, Mar. 2000, pages 55-77.

[5] Duerig, T. W., Melton, K. N., Stockel, D. Wayman, C. M. 1990 “Engineering Aspects of Shape Memory Alloys”, Butterworth-Heinemann, 1990.

[6] Gall, K. and Sehitoglu, H. 1999 "The role of texture in tension-compression asymmetry in polycrystalline NiTi", International Journal of Plasticity, 15, 1999, pp. 69-92.

[7] Jennings, P. C.” Engineering Features of the San Fernando Earthquake of February 9, 1971.” *Rep No. EERL-76/18*, Earthquake Engineering Research Lab, California Institute of Technology, Pasadena, CA., 1971.

[8] Moehle, J. P. “Northridge Earthquake of January 17, 1994: Reconnaissance Report, Volume 1 – Highway Bridges and Traffic Management,” *Earthquake Spectra*, Vol. 11, No. 3, 1994, pp. 287-372.

[9] Prakash, V., Powell, G. H., and Filippou, F. C. (1992). "DRAIN-2DX: Base Program User Guide," *Report No. UCB/SEMM-92/29*, University of California at Berkeley, 1992.

Experimental Study on Seismic Behavior of Highway Bridge Foundation during Liquefaction Process

Hiroshi Kobayashi, Keiichi Tamura, Naoki Sato and Takuo Azuma

ABSTRACT

For establishing rational seismic design method of bridge foundations against soil liquefaction, it is essential to study seismic performance of bridge foundation during liquefaction process. In this study, in order to evaluate the vibration characteristics of soil and the pile foundation during liquefaction process, we conducted the shaking table test with soil and the pile foundation system, and examined the influence of vibration frequency on the pile foundation and the resonant vibration characteristics of pile foundation from the test results.

Hiroshi Kobayashi, Research engineer, Ground Vibration Research Team, Public Works Research Institute, 1-6 Minamihara, Tsukuba-shi, Ibaraki-ken, 305-8516, Japan
Keiichi Tamura, Team Leader, ditto
Naoki Sato, Chief, Eight Consultants Co., Ltd., 3-1-25 Simozawa Street, Hyogo-ku, Kobe-shi, Hyogo-ken 652-0047, Japan
Takuo Azuma, Chief, Research Administration and International Cooperation Division, National Institute for Land and Infrastructure Management, 1 Asahi, Tsukuba-shi, Ibaraki-ken, 305-0804, Japan

INTRODUCTION

According to the Specifications for Highway Bridges in Japan (1996)[1], when the soil is assumed to liquefy, the soil resistance is reduced in accordance with the degree of liquefaction. On the other hand, the design ground motion, which is applied when the soil does not liquefy, is also employed even when the liquefaction is assumed to occur. This is mostly based on the fact that the ground motion characteristics during liquefaction process is complicated and has not been clarified, and the design ground motion is so determined as to yield safe-side results. For establishing rational seismic design method of bridge foundations against soil liquefaction, it is essential to study seismic performance of bridge foundation during liquefaction process. For example, as Figure 1 indicates, the dominant frequency of soil and the pile foundation before liquefaction f_o decreases as liquefaction progresses, and becomes f_1 after liquefaction. If dominant frequency of input wave exists between f_o and f_1, the dominant frequency of input wave may coincides with that of soil-foundation structure system during liquefaction process. The resonant phenomenon arises at the same time, and it is quite likely that the large vibration amplification is arisen.

In this study, in order to evaluate the vibration characteristics of soil and the pile foundation during liquefaction process, we conducted the shaking table test with soil and the pile foundation system, and examined the influence of vibration frequency on the pile foundation and the resonant vibration characteristics of pile foundation from the test results.

OUTLINE OF THE EXPERIMENTS

In order to liquefy the saturated sand material in the container and to examine vibration characteristics of soil and the pile foundation during liquefaction process, the shaking table tests were conducted. The outline of the apparatus in this study is shown in Figure 2 and Photo 1. The physical properties of the sand and experiment model are listed in Table 1. We used the Toyoura sand as the experiment sand material and made the sand specimen of fixed relative density with boiling and preliminary shaking. We used the footing made of steel and 2*2 piles made of acrylic resin as the pile foundation model shown in Photo 2. The pile heads were rigidly connected to the footing, and their tips were also rigidly connected to the container.

As Table 2 and Table 3 show, three different input motions were employed for experiments, i.e., random wave, sinusoidal sweep wave and seismic wave. We employed earthquake motions recorded at Itajima Bridge and Kobe Maritime Observatory (JMA Kobe). Those two records were selected as representatives of ground motions caused by a plate boundary earthquake and an inland direct strike slip fault. We employed each motions with a compressed time axis to 50%, 25% and 16.7% in order to examine how the dominant frequency of input wave affects the resonant phenomenon of pile foundation. We conducted a number of experiments, in which inputted accelerations were changed.

SHAKING TABLE TESTS WITH RANDOM WAVE

We used random waves as input motions for shaking table tests, and examined transitions of the dominant frequency of the pile foundation during liquefaction process by changing the amplitude of input motion. Acceleration time histories of input wave and pile foundation head are shown in Figure 3(a), change of dominant frequency of pile foundation with time are shown in Figure 3(b) and time histories of excess pore water pressure ratio are shown in Figure 3(c). Figure 4 illustrates the calculation method of dominant frequency of pile foundation. Calculation method of the dominant frequency of pile foundation is as follows: (1) We multiply acceleration time histories of pile foundation by data window using weight function[2]. (2) The Fourier transform is conducted to the revised histories calculated by (1). (3) The dominant frequency of pile foundation is calculated with smoothing in the frequency domain. Although acceleration of pile foundation amplifies in comparison with input wave between 4sec and 10sec, it dose not amplify after 10sec. Figure 3(a) shows that the response of pile foundation shifts to the long period due to liquefaction. As Figure 3(b) indicates, dominant frequency of pile foundation, which was 30Hz at the initial condition, reduced to 15Hz due to liquefaction at the ground surface and turned out to 1Hz after liquefaction at the whole ground.

Relationships between the depth at which excess pore water pressure Lu=0.4 and dominant frequency of pile foundation in the random shaking test are indicated in Figure 5. Relationships between liquefaction degree and dominant frequency of pile foundation can be expressed by the approximate equation as shown in Figure 5 in this experiment.

SHAKING TABLE TESTS WITH SINUSOIDAL WAVE

In order to examine the resonant phenomenon during liquefaction process, shaking table tests were conducted with sinusoidal sweep wave. The test results, i. e., acceleration time histories of input wave and pile head, time histories of excess pore water pressure ratio and transition of dominant frequency in pile foundation, are shown in Figure 6. Input wave frequency f_i in Case-S1 were $f_i < f_1$, and those in Case-S2 and Case-S3 were $f_1 < f_i < f_0$. f_1 represents the natural frequency of the pile foundation model and f_0 represents that of soil and the pile foundation model. Dominant frequency of the pile foundation is calculated by the approximate equation shown in Figure 5.

In case of $f_1 < f_i < f_0$, pile head acceleration amplified in comparison with input wave acceleration during liquefaction process and a kind of resonant phenomenon were observed, however, in case of $f_i < f_1$, pile head acceleration showed the same level at input wave and the resonant phenomenon was not observed. In case of $f_1 < f_i < f_0$, pile head acceleration shows the maximum value at the time when the dominant frequency of pile foundation corresponds with that of input wave. In case of $f_i < f_1$, dominant frequency of pile foundation does not correspond with that of input wave during excitation.

Comparing two cases where the resonant phenomenon was observed, the ground condition when the resonant phenomenon arisen was different. Only ground surface liquefied in Case-S2 with higher input frequency, and nearly all ground liquefied in Case-S3 with lower input frequency. It was found from the result that the resonant phenomenon might arise on condition that dominant frequency of pile foundation corresponds with that of input wave.

SHAKING TABLE TESTS WITH SEISMIC WAVE

Figure 7 shows acceleration time histories of pile head and input wave, and transition of dominant frequency of pile foundation and input wave in cases inputted with seismic wave. Test cases shown in this Figure are Case-I2(a) where target acceleration amplitude=0.25m/sec^2 and liquefaction did not hardly occur, Case-I2(b) where target acceleration amplitude=0.4m/sec^2 and liquefaction occurred on the only ground surface, Case-I2(c) where target acceleration amplitude=0.8m/sec^2 and liquefaction occurred up to the center of the container and Case-I2(d) where target acceleration amplitude=2.5m/sec^2 and liquefaction occurred as a whole. It was identified that amplification characteristics of the pile head acceleration is different in these 4 cases. Pile head acceleration in Case-I2(a) was bigger than inputted acceleration during excitation, and the dominant frequency was not changed. Although pile head accelerations amplify with excitation in Case-I2(b) and I2(c), the acceleration shows the maximum value at 3.2 sec in Case-I2(b) and at 2 sec in Case-I2(c). Comparing these 2 cases, time that the acceleration shows the maximum value is different. The reason is that the time when dominant frequency of pile foundation corresponds with that of input wave is different. The acceleration shows the maximum value when the dominant frequency of pile foundation corresponds with that of input wave. In Case-I2(d), pile head acceleration hardly amplifies and is smaller than inputted acceleration. This is the reason why liquefaction occurred as a whole soon after excitation and dominant frequency of pile foundation does not correspond with that of input wave. Acceleration time histories of pile head shift to the long period.

Relationships between maximum acceleration of input wave and amplification ratios of maximum acceleration of pile head to that of input wave are shown in Figure 8. Diagonal sections in these Figures show the ground area where the resonant phenomenon likely arose. The dominant frequency of pile foundation in case where the ground above the diagonal section liquefies corresponds with the dominant frequency of seismic wave. In Case-I, the diagonal area are expressed by a single line because ground motion at Itajima Bridge has a specific dominate frequency. On the other hand, in Case-K, the diagonal area spread because ground motion at JMA Kobe has width dominant frequencies. We can find that the larger maximum acceleration of input wave yields the deeper liquefied ground in all cases. In cases where inputted acceleration is small and liquefaction does not occur at all, amplification ratio shows the large value. This is because the noise of shaking table might affect amplification ratio in small level excitation and ground acceleration amplify toward the surface at the non-liquefied ground. As a result, it is found that this amplification is distinct from the resonant phenomenon. In most cases where the depths at which Lu=0.4 are applicable to the diagonal area, amplification ratio become more than 1.0 and we can find that acceleration of pile foundation amplify during liquefaction process. The amplification ratio is about 1.8 in Case-I and about 1.3 in Case-K, and the amplification ratio in the case of large number of cyclic loading tends to be larger. In consequence, we can find that the larger number of cyclic loading yields the larger amplification.

CONCLUSION

Major findings of the present study are summarized as follows:

(1) In the case where shaking frequency of input wave exists between natural frequency of pile and that of soil-foundation structure system, the acceleration of foundation first increases and then decreases as liquefaction progresses.

(2) In the both cases where sinusoidal wave and seismic wave were inputted, the resonant phenomenon arises around when the dominant frequency of input wave coincides with that of soil-foundation structure system, and the acceleration of foundation is amplified.

(3) In the case where seismic wave were inputted, the resonant phenomenon was observed for the specific ground condition and the degree of acceleration amplification is smaller than the case of sinusoidal wave. The degree of acceleration amplification depends on the cyclic characteristics of input wave, and the larger number of cyclic loading yields the larger amplification.

REFERENCES

[1] Japan Road Association, 1996, *Specifications for Highway Bridges*

[2] Tatsuoka, F., Tokida, K, Yoshida, S. and Maruyama, I. 1976. "Shaking table tests on dynamic behaviors of pile foundation model in liquefying sand layers," Proc. of 5th Japan Earthquake Engineering Symposium

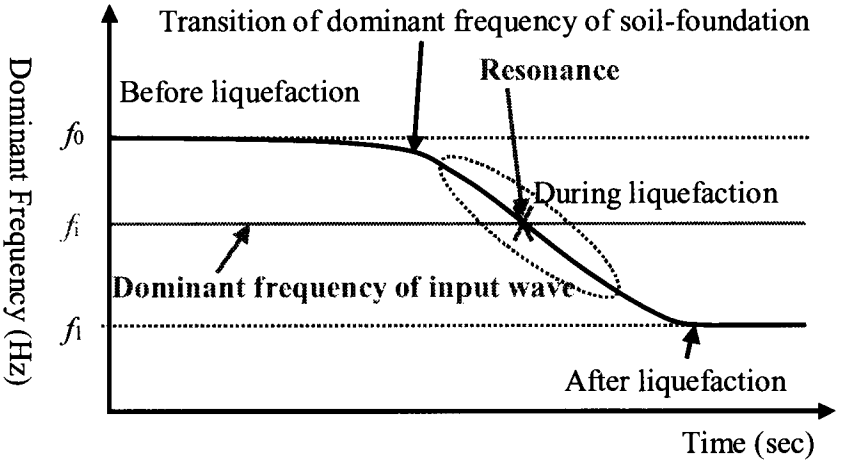

Figure 1. Transition of dominant frequency during liquefaction process

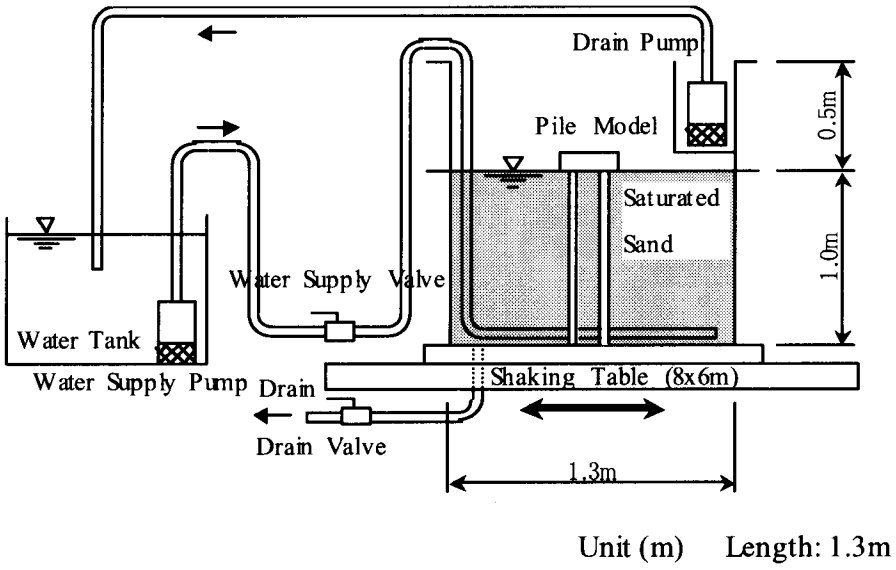

Figure 2. Outline of the apparatus

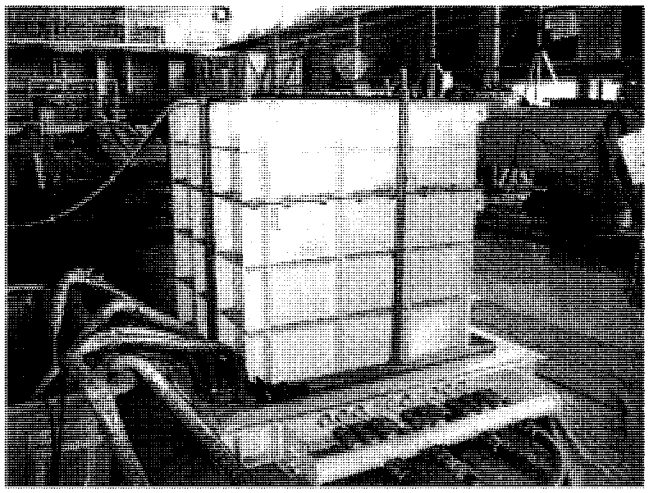

Photo 1. Overview of the container

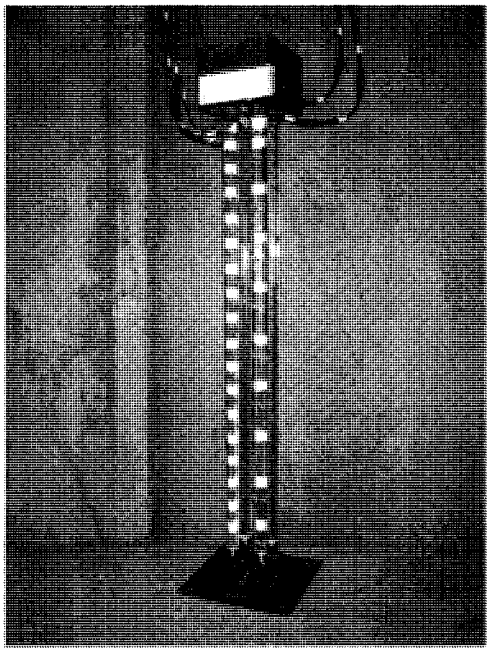

Photo 2. Pile foundation model

TABLE 1. Physical properties of the sand and experiment model

Material	Physical properties	Value
Sand Material	Specific gravity: G_s	2.635
	Maximum void ratio: e_{max}	0.925
	Minimum void ratio: e_{min}	0.604
	Relative density: D_r(%)	40
	Void ratio: e	0.797
	Saturated unit weight: γ_{sat}(kN/m^3)	18.72
	Submerged unit weight: γ ' (kN/m^3)	8.92
Pile	Diameter: D(m)	0.025
	Length: L(m)	1.0
	Young's modulus: E(N/m^2)	3.2×10^9
	Geometrical moment of inertia: I(m^4)	1.9×10^{-8}
	Space between piles	2.6 D
Footing	Size (m)	0.15*0.15
	Weight (N)	149.4
Natural Frequency	Soil and pile foundation: f_0(Hz)	30
	Pile foundation: f_1(Hz)	2.6

TABLE 2. Test cases

Cases	Input wave form	Target acceleration (m/sec^2)	Frequency (Hz)
Case-R1	Random Waves	0.0 – 4.6	0.1 – 50.0
Case-R1	Random Waves	0.0 – 4.7	0.1 – 50.0
Case-S1	Sinusoidal sweep waves	0.0– 2.0	2.0
Case-S2		0.0 – 2.0	14.0
Case-S3		0.0 – 3.0	6.0

TABLE 3. Test cases with seismic wave

Cases	Input seismic wave form	Target acceleration (m/sec^2)	Expanded time axis
Case-I1	Observed ground motion at Itajima Bridge in 1968 Hyuga-nada-oki Earthquake	0.3, 0.5, 0.8, 1.0, 1.25, 1.5, 2.0, 2.5	50%
Case-I2		0.25(a), 0.4(b), 0.5, 0.8(c), 1.0, 1.25, 1.5, 2.0, 2.5(d)	25%
Case-I3		0.4, 0.5, 0.8, 1.0, 1.25, 1.5, 2.0, 2.5	16.7%
Case-K1	Observed ground motion at JMA Kobe in 1995 Hyogo-ken Nanbu Earthquake	0.3, 0.5, 0.8, 1.0, 1.25, 1.5, 2.0, 2.5	50%
Case-K2		0.3, 0.5, 0.8, 1.0, 1.25, 1.5, 2.0, 2.5	25%
Case-K3		0.45, 0.5, 0.8, 1.0, 1.25, 1.5, 2.0, 2.5	16.7%

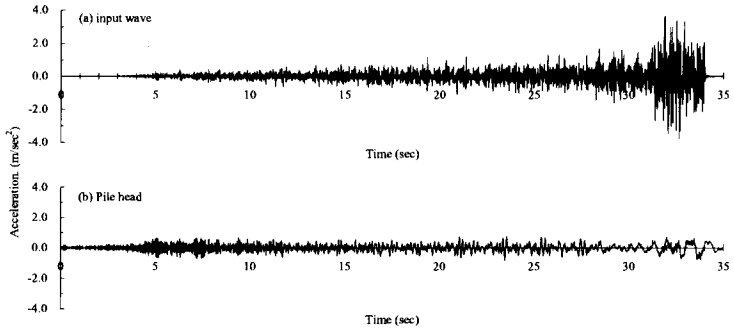

(a) Acceleration time histories (Case-R1)

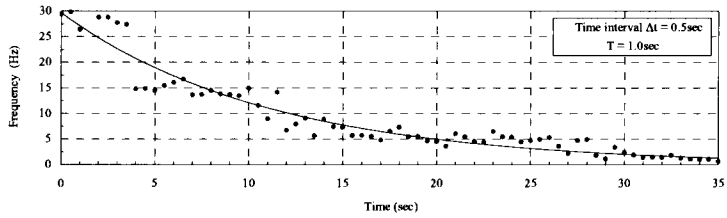

(b) Dominant frequency time histories of pile foundation(Case-R1)

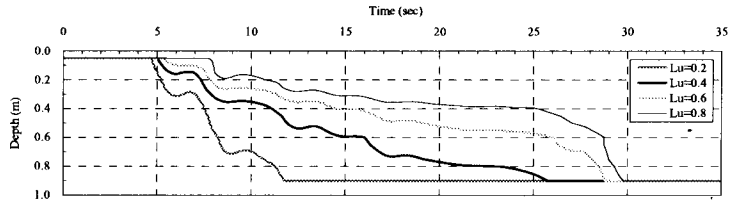

(c) Time historie of excess pore pressure ratio (Case-R1)

Figure 3. Acceleration time histories of input wave and pile head, transition of dominant frequency in pile foundation and time histories of excess pore pressure ratio Lu

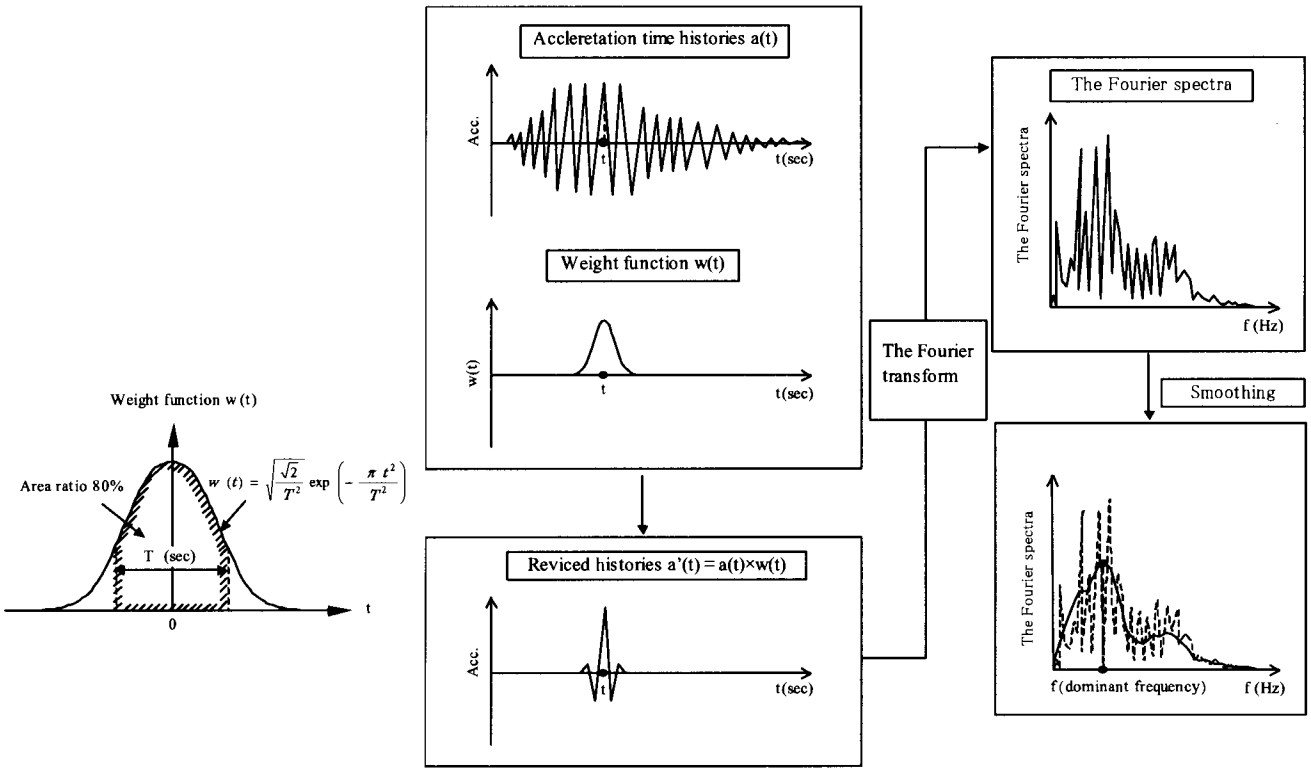

Figure 4. Calculation method of dominant frequency of pile foundation

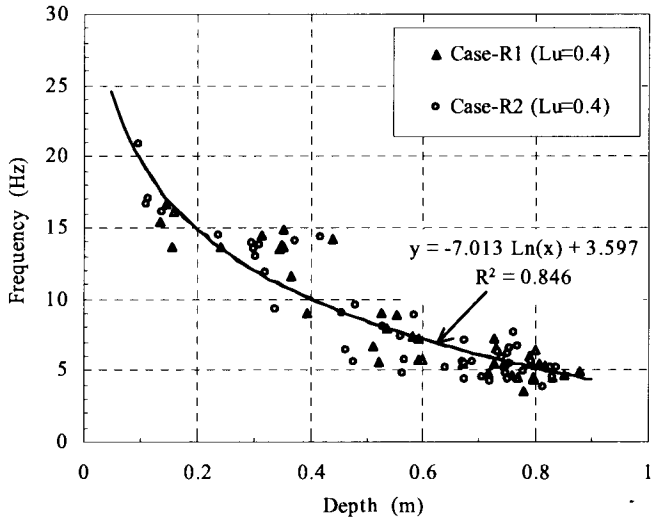

Figure 5. Relationship between the depth of Lu=0.4 and dominant frequency of pile foundation

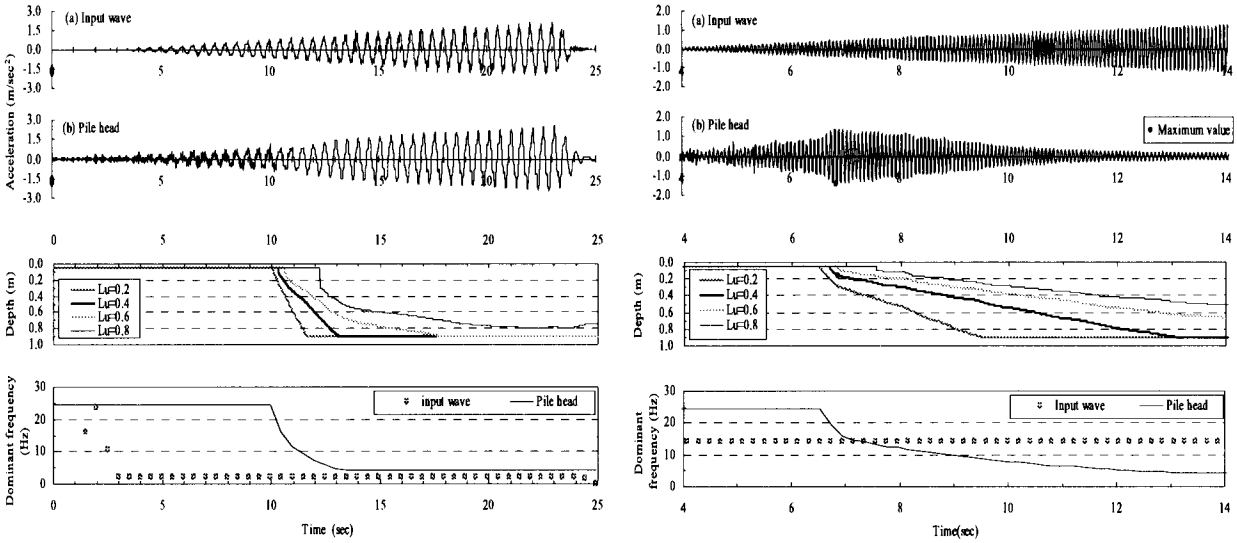

(a) Case-S1

(b) Case-S2

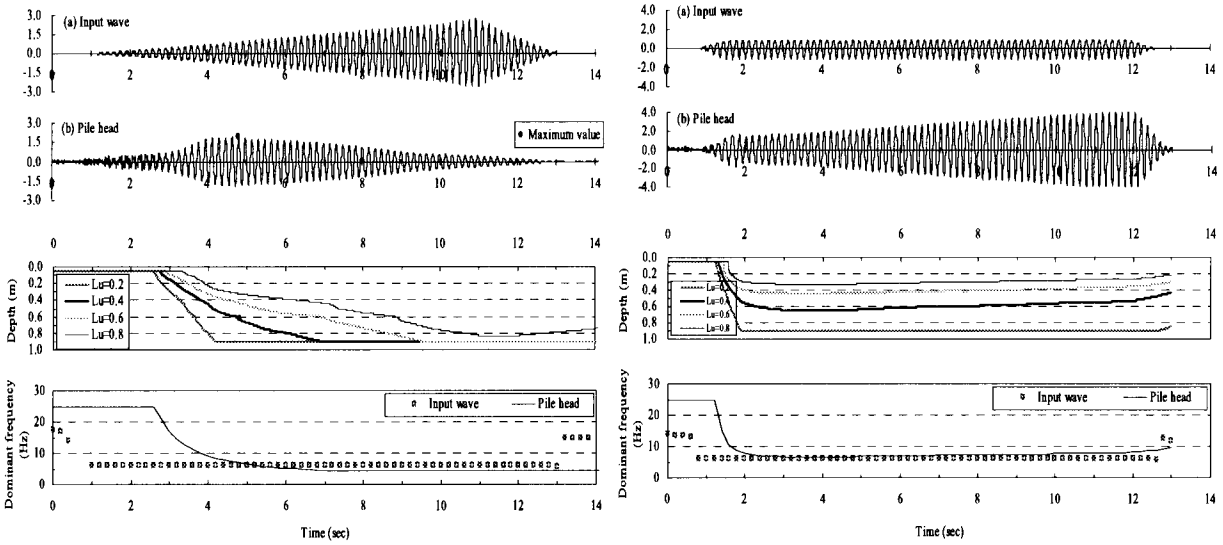

(c) Case-S3

(d) Case-S4

Figure 6. Acceleration time histories of input wave and pile head, time histories of excess pore pressure ratio Lu and transition of dominant frequency of pile foundation

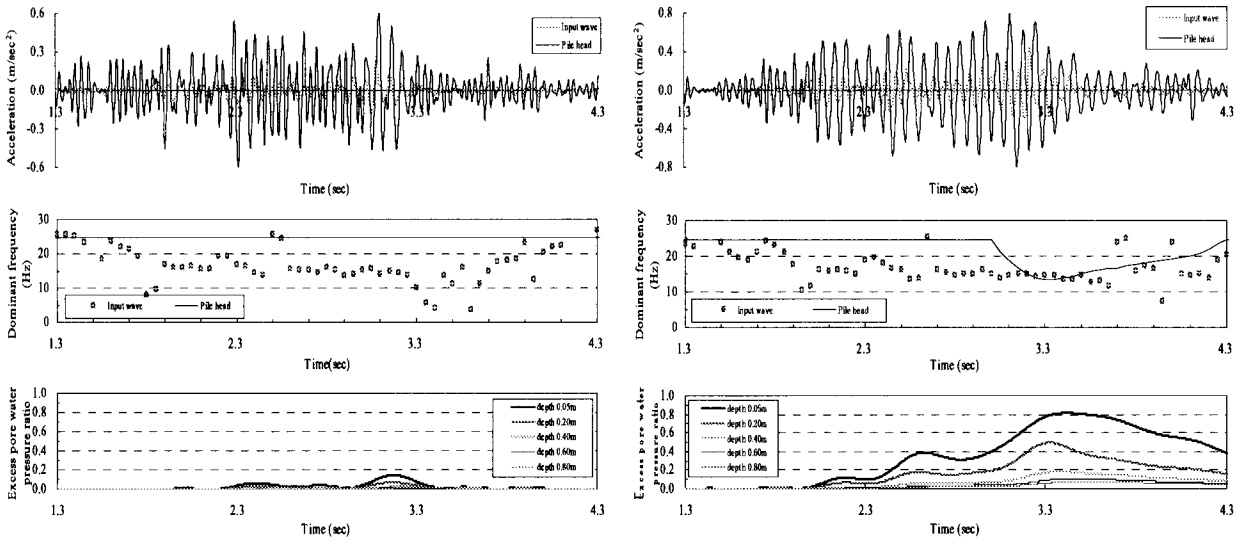

(a) Case-I2(a)

(b) Case-I2(b)

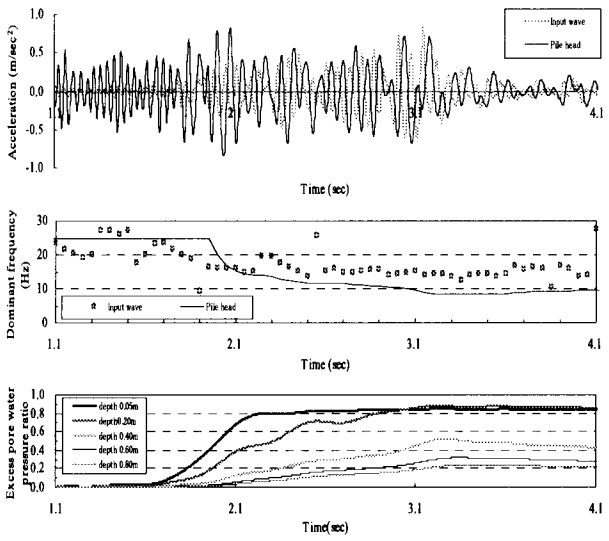

(c) Case-I2(c)

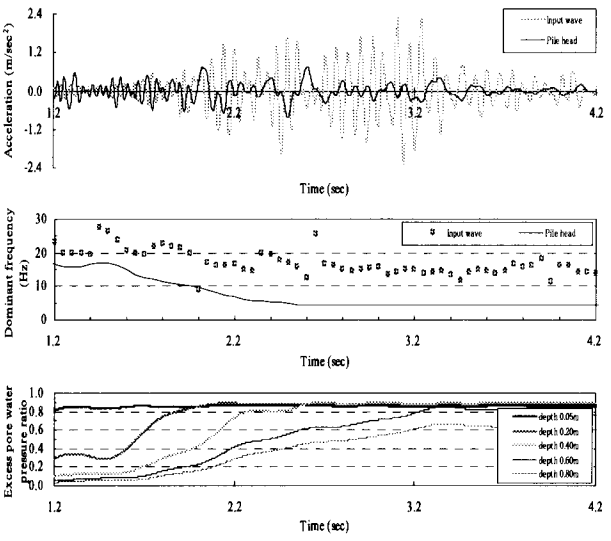

(d) Case-I2(d)

Figure 7. Acceleration time histories of input wave and pile head, and transition of dominant frequency of input wave and pile foundation

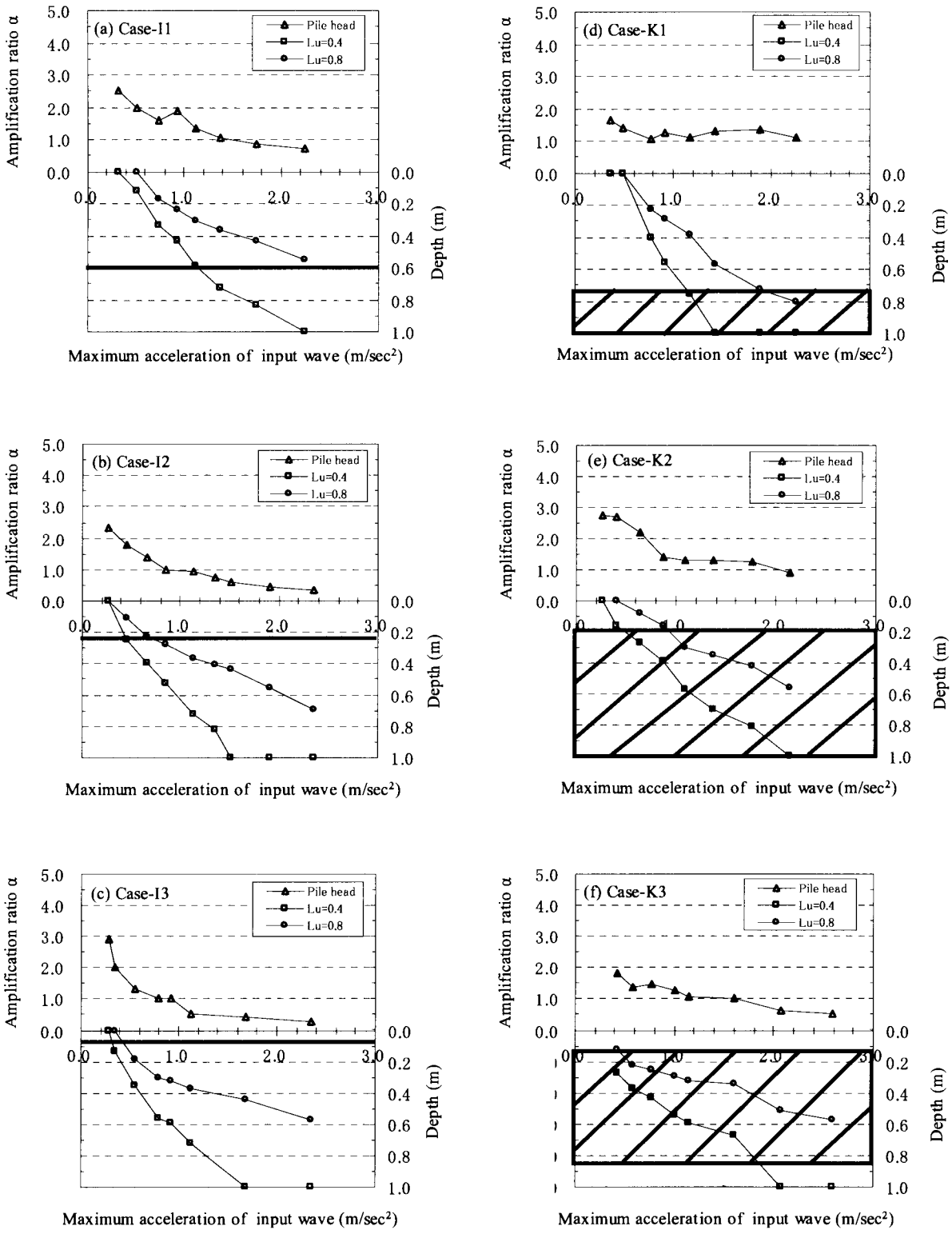

Figure 8. Relationships between maximum acceleration of input wave and amplification ratios of maximum acceleration of pile head to that of input wave

Development and Implementation of a New Seismic Design Bridge Criteria for South Carolina

Roy A. Imbsen and Lucero E. Mesa

ABSTRACT

The State of South Carolina has recently developed a new seismic design specification for highway bridges. South Carolina is in a high seismic zone similar to California and has recognized that several recent developments have occurred that are not yet implemented into AASHTO. Some of the new developments are being reviewed for implementation into future updates of the Seismic Design Specifications. The new specification has been developed and is currently being implemented into design.

The new concepts and enhancements that are incorporated into the specification include:

1. New USGS probabilistic earthquake ground motion maps
2. New design level earthquakes
3. New performance objectives
4. New soil factors
5. Displacement based design
6. Expanded design criteria for steel bridges

This paper will describe the new seismic design criteria and the implementation into practice both with the South Carolina Department of Transportation and their consultants. Additionally, the paper will describe the impact of the new criteria on the design costs.

Roy A. Imbsen, President, Imbsen & Associates, Inc., 9912 Business Park Drive, Suite 130, Sacramento, CA 95827
Lucero E. Mesa, Manager, Seismic Design, South Carolina Department of Transportation Bridge Design Section, 955 Park Street, Room 508, Columbia, SC 29202.

INTRODUCTION

The South Carolina Department of Transportation (SCDOT) has initiated the development and implementation of a bridge seismic design and retrofit program. A central feature of the new SCDOT bridge design and retrofit program is the development of new seismic bridge design criteria and standards that: 1) incorporate a new generation U.S. Geological Survey seismic ground shaking hazard maps, 2) treat certain inadequacies of existing bridge design codes to adequately address the large earthquake, and 3) associated bridge collapse and life safety issues in the central and eastern United States. This paper summarizes the upgraded bridge seismic design provisions and describes variations in national seismicity that motivated the development of the SCDOT "Seismic Design Specifications for Highway Bridges"[1]. Basically, the revised specifications specify that the design of new bridges in South Carolina directly account for the effects of the large earthquake as done by the State of California. This is to ensure conformance with the guiding principle used in the development of AASHTO provisions that the "exposure to shaking from the large earthquake should not cause collapse of all or part of the bridge." Many of the revisions were adopted from bridge design provisions of the California Department of Transportation (Caltrans), because of similar high intensity seismic hazard at the Safety Evaluation Earthquake (SEE) level and the state-of-practice progress gained due to recent earthquakes that have not yet been incorporated into AASHTO.

UPGRADED SEISMIC DESIGN REQUIREMENT

At least two developments of the U.S. Geological Survey during the past several years have been a major contribution to bridge earthquake engineering. One development was an assessment of the nature of the seismic ground shaking hazard as it varies nationally that revealed apparent inequalities in safety that result when a single level of probability common to bridge code design is used. The second development was a new generation of probabilistic ground-motion hazard maps that provide uniform hazard spectra for exposure times of 50 and 250 years and make possible the treatment of the inequality in safety of bridge code design using existing earthquake engineering design and evaluation provisions and methodology.

The new generation of probabilistic ground motion maps were produced by the USGS under the National Earthquake Hazard Reduction Program (NEHRP) with significant input from the committee on Seismic Hazard Maps of the Building Seismic Safety Council (BSSC) and the Structural Engineers Association of California (SEAOC). They allow development of uniform hazard spectra and permit direct definition of the design spectra by mapping the response spectral ordinates at different periods.

This paper presents such upgraded technical standards that have been developed incorporating the new generation ground motion maps.

TABLE 1. Seismic Performance Criteria

Ground Motion Level	Performance Level	Normal Bridges	Essential Bridges	Critical Bridges
Functional-Evaluation	Service	NR*	NR	Immediate
	Damage	NR	NR	Minimal
Safety-Evaluation	Service	Impaired	Recoverable	Maintained
	Damage	Significant	Repairable	Repairable

*Functional Evaluation Not Required.

The recommended seismic design procedures were developed to meet current bridge code objectives, including both serviceability and life safety in the event of the large earthquake. The primary function of these new provisions is to provide minimum standards for use in bridge design to maintain public safety in the extreme earthquake likely to occur within the state of South Carolina. They are intended to safeguard against major failures and loss of life, to minimize damage, maintain functions, or to provide for easy repair.

For normal or essential bridges (see Table 1), the **Single Level Design Method** is adopted by this code. This method consists of applying seismic design loading calculated based upon the value of the spectral accelerations of the 2%/50-year earthquake (i.e.,, the Safety Evaluation Earthquake).

For critical bridges and with the approval of the SCDOT, the seismic performance goals are to be achieved by a two-level design approach (i.e., a direct design for each of the two earthquakes). **(Two-Level Design Method).** In addition to the 2%/50-year earthquake (Safety Evaluation Earthquake), critical bridges shall also be designed to provide adequate functionality after the 10%/50-year earthquake (Functional Evaluation Earthquake). The minimum performance levels for the design and evaluation of bridges shall be in accordance with the level of service and damage for the two design earthquakes as shown in Table 1. Service Levels and Damage Levels are defined in Section 3 of this paper. The Bridge Category is defined in Section 4. The SCDOT may specify project-specific or structure-specific performance requirements different from those defined in the table. For example, for a Critical or Essential bridge it may be desirable to have serviceability following a 2%/50-year earthquake. The SCDOT may require a site specific design spectrum as part of the analysis.

PURPOSE AND PHILOSOPHY

This new SCDOT specification establishes design and construction provisions for bridges in South Carolina to minimize their susceptibility to damage from earthquakes. This specification is intended to be used in conjunction with AASHTO Division I [2] and as a replacement to Division I-A, Seismic Design, of the same specifications.

The principles used for the development of the new SCDOT provisions are:

Small to moderate earthquakes should be resisted within the essentially elastic range of the structural components without significant damage. The Functional Evaluation Earthquake (FEE) is adopted to represent seismic ground motion level produced by small to moderate earthquakes.

State-of-Practice seismic ground motion intensities and forces are used in the design procedures.

Exposure to shaking from large earthquakes should not cause collapse of all or part of the bridge. Where possible, damage that does occur should be readily detectible and accessible for inspection and repair unless prohibited by the structural configuration. The Safety Evaluation Earthquake (SEE) is adopted to represent seismic ground motion level produced by large earthquakes.

The seismic hazard varies form very small to high across the State of South Carolina. Therefore, for purposes of design, four Seismic Performance Categories (SPC) are defined on the basis of the spectral acceleration, $S_{D1\text{-}SEE}$, for the site and the Importance Classification (IC) as shown in Table 2. Different degrees of complexity and sophistication of seismic analysis and design are specified for each of the four Seismic Performance Categories.

TABLE 2. Seismic Performance Category (SPC)

Value of Spectral Acceleration, $S_{D1\text{-}SEE}$	Importance Classification (IC)		
	I	II	III
$S_{D1\text{-}SEE}<0.30g$	B	B	A
$0.3g\leq S_{D1\text{-}SEE}<0.45g$	C	C	B
$0.45g\leq S_{D1\text{-}SEE}<0.6g$	D	C	C
$0.6g\leq S_{D1\text{-}SEE}$	D	D	C

SERVICE LEVELS AND DAMAGE LEVELS

The performance levels, expressed in terms of service levels and damage levels, are:

(a) Service Levels

- *Immediate:* Full access to normal traffic is available almost immediately following the earthquake.
- *Impaired:* Extended closure to Public. Open to Emergency Vehicles. Possible replacement needed.
- *Recoverable:* Limited period of closure to Public. Open to Emergency Vehicles.
- *Maintained:* Short period of closure to Public. Open to Emergency Vehicles.

(b) Damage Levels

- *Minimal Damage:* No collapse, essentially elastic performance.
- *Repairable Damage:* No collapse. Concrete cracking, spalling of concrete cover, and minor yielding of structural steel will occur. However, the extent of damage should be sufficiently limited that the structure can be restored essentially to its pre-earthquake condition without replacement of reinforcement or replacement of structural members (i.e., ductility demands less than 2). Damage can be repaired with a minimum risk of losing functionality.
- *Significant Damage:* Although there is minimum risk of collapse, permanent offsets may occur in elements other than foundations. Damage consisting of concrete cracking, reinforcement yielding, major spalling of concrete, and deformations in minor bridge components may require closure to repair. Partial or complete demolition and replacement may be required in some cases.

BRIDGE CATEGORY

Bridge structures on the state highway system are classified as “normal bridges”, “essential bridges” or “critical bridges”. For a bridge to be classified as an “essential bridge” or a “critical bridge”, one or more of the following items must be present: (1) bridge is required to provide secondary life safety, (2) time for restoration of functionality after closure creates a major economic impact, and (3) the bridge is formally designated as critical by a local emergency plan.

Each bridge is classified as either Critical, Essential or Normal as follows:

(a) Critical bridges: Bridges that will be open to all traffic once inspected after the functional evaluation design earthquake and be usable by emergency vehicles and for security/defense purposes immediately after the safety evaluation design earthquake, i.e., a 2,500-year return period event.

(b) Essential bridges: Bridges that will, as a minimum, be open to emergency vehicles and for security/defense purposes after the safety evaluation design earthquake, i.e., a 2,500-year return period event and open to all traffic within days after the SEE event.

(c) Normal Bridges: Any bridge not classified as a Critical or Essential Bridge.

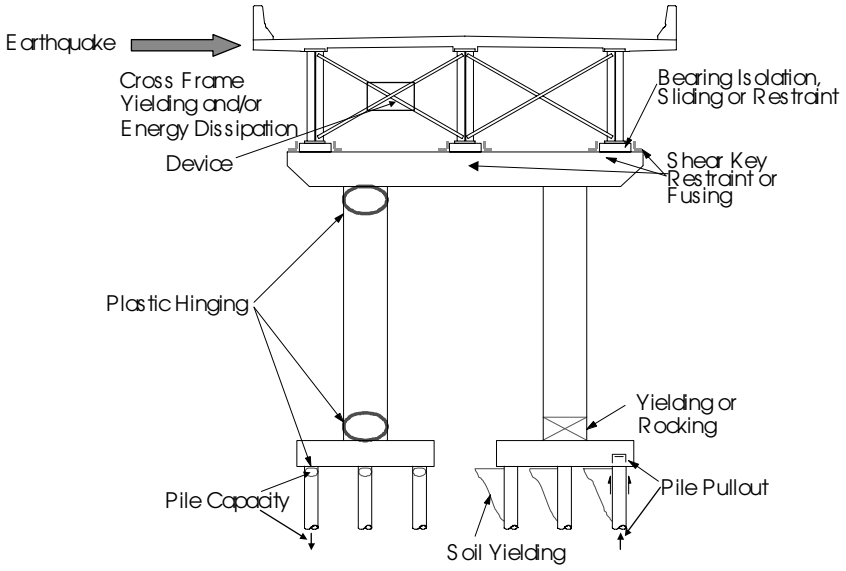

Figure 1. Seismic Load Path and Affected Components

PERFORMANCE CRITERIA

Based on the characteristics of the bridge structure, the designer has one of three choices illustrated in Figure 1:

Type 1 – Design a ductile substructure with an essentially elastic superstructure.

Type 2 – Design an essentially elastic substructure with a ductile superstructure.

Type 3 – Design an elastic superstructure and substructure with a fusing mechanism at the interface between the superstructure and the substructure.

For Type 1 choice, the displacement analysis using pushover techniques is used to achieve a ductile design of the substructure. For Type 2 choice, the design of the superstructure is accomplished using a force reduction approach. Those factors are used for the design of transverse bracing members, top laterals and bottom laterals. The reduction factors shown in Table 3 are used.

For Type 3 choice, the designer shall assess the overstrength capacity for the fusing interface including shear keys and bearings, then design for an essentially elastic superstructure and substructure. The minimum overstrength lateral design force shall be calculated using an acceleration of 0.4 g or the elastic seismic force whichever is smaller. If isolation devices are used, the superstructure shall be designed as essentially elastic.

Reference to an essentially elastic component is used where the force demand to capacity ratio of any member in the superstructure is less than 1.3.

Table 3 Reduction Factors for Steel Superstructure Bracings

	Essential or Critical Bridges	Normal Bridges
Functional Evaluation	1	2
Safety Evaluation	2	4

CONCLUSION

This criteria aims at including state-of-practice in seismic design based on displacement analysis for reinforced concrete components. Force reduction factors are used for steel superstructure due to the limited use of this approach in steel design of bridges. In addition, only limited level of ductility is so far accepted for members of a steel superstructure with a plate girder system. Implementation of the new SCDOT "Seismic Design Specifications for Highway Bridges" is now underway.

REFERENCES

[1] South Carolina Department of Transportation, "Seismic Design Specifications", October 2001

[2] AASHTO "Standard Specifications for Highway Bridges", Sixteenth Edition, 1996

Seismic Retrofit of Aurora Avenue Bridge With Friction Pendulum Isolation Bearings

Hongzhi Zhang, Ph.D., P.E
Bridge Seismic Specialist/WSDOT

The Aurora Avenue Bridge is a long-span cantilever truss structure spanning the Lake Washington ship canal at the entrance to Lake Union, in Seattle Washington (Figure 1).

The length of the bridge is 2955 feet including a five span main truss, a twelve continuous span concrete north approach and a south approach with three continuous concrete spans and three simple steel truss spans. The main truss has an 800ft main span including a 150ft drop-in span (Figure 2). The remaining truss is continuous over the piers, and the four side spans are simply supported. The vertical distances between the top of the deck to the top of the piers at Pier N1 and S1 is about 112 feet and there is another 93 feet from the top of the piers down to the top of the footing. Piers S2, N2, S3, S9 and most of the north approach piers are supported on spread footings bearing on glacially overridden soil. Piers N1, S1 and N2 are supported on timber piling that also bears on glacially overridden soil. The south approach (S4 to S8) is supported on 15-inch-square concrete piles. The bridge was designed and built between 1929 and 1931(Figure 3 and 4).

The structure has a 70ft wide of concrete deck and carries six lanes of traffic, three in each direction. Five ft sidewalks were built on both side of the bridge (Figure 5). The daily traffic on the bridge is approximately 100,000 vehicles.

A seismic vulnerability study of the bridge was completed in 1995 [1].

With a 10 % probability of being exceeded in a 50 year interval (475-year return period), the Peak Ground Acceleration (PGA) at the bridge site is about 0.3g. Liquefiable soil, at a depth up to 30 feet, is present at Pier N1, S1 and N2. Lateral spreading is expecting during earthquake.

Both spectral analyses and a 2-D Pushover analyses were performed to calculate the demand/capacity (D/C) ratio and to study the failure mechanism. Although the main piers were built with massive volumes of concrete, the analysis showed that the shear and flexure capacities are very low because of the very low reinforcement ratio. Vulnerabilities are identified at all of the piers. The D/C ratio of some truss members is also only slightly higher than 1.0.

The recommended seismic retrofit by a WSDOT consultant focused on all the vulnerable piers using a vertical post-tension strengthening method. The P/T cables would be installed at four corners of each pier and be anchored from the top of the pier to the top of the footing (Fig.6&7). Up to 40 ft of excavation at the main piers were expected during

Hongzhi Zhang, Ph.D., P.E, Bridge Seismic Specialist/WSDOT

construction. Local roads and businesses near the main piers could be severely impacted (Fig. 8). STU would be installed to distribute the seismic lateral load between piers. The post-tension strengthening method would be the solution only for the piers. The pile foundations and some of the truss members would still be vulnerable and would be more vulnerable because of the higher stiffness of the strengthened pier.

The recommended seismic retrofit of the P/T strengthening was divided into two construction stages for the main portion of the bridge: Stage I would provide the linkage of the superstructure with earthquake restrainers at the drop-in span and intermediate piers and would include installation of anchorages for P/T cables on the top of the piers. Stage II would install the post-tensioning cables for all the six main piers. In 1998, T.Y. Lin was selected to carry the final design. In 1999, the Stage I of construction was awarded to a contractor.

During construction, contaminated soils were discovered around the main piers due to ship building activities during World War II. If the post-tensioning method, to strengthen the piers, was used, the contaminated soil would need to be hauled away. Disposal of this hazard material could cost more than three million dollars. The impact on the local streets and businesses would be very high. Structurally, the strengthened piers would have higher stiffness and would, possibly, attract more seismic load into the vulnerable existing pile foundations during an earthquake.

In 1999, WSDOT/Bridge and Structures Office proposed seismic retrofit of the bridge with a totally different concept, using friction pendulum isolation bearings (Figure 9&10) to reduce the lateral seismic load and to avoid the very expensive seismic retrofits at piers and pile foundations. Friction pendulum isolation bearings have been designed and installed in buildings, as well as bridges, in recent years. Large friction pendulum isolation bearing can be more than twelve feet in diameter and have been designed and installed on Benicia-Martinez Bridge (Fig. 11&12). Many bridge seismic retrofit projects and new designs in Washington, California, Tennessee and Alaska have also selected the friction pendulum isolation concept (Fig. 13.). According to the preliminary design of the friction pendulum isolation bearings on Aurora Avenue Bridge by the manufacturer, Earthquake Protection System Inc. (EPS), four large size (81 inches in diameter) friction pendulum isolation bearings are needed on the two main piers and eight smaller bearings (43 inches in diameter) are needed on the other four piers. The period of the large bearings is 5.0 seconds (R = 244 inches) with 5% dynamic friction coefficient and the smaller bearings have a 3.0 second period (R = 88 inches) with 7% dynamic friction coefficient. The reduction of the seismic load by using friction pendulum isolation bearings would be 72% in the longitudinal direction and 87% in the transverse direction, respectively, per the preliminary study. With this concept for retrofit, WSDOT will avoid the expensive excavation and retrofit of the main piers and the pile foundations.

In 2000, the WSDOT decided to proceed with friction pendulum isolation bearings instead of the P/T strengthening for the seismic retrofit of the Aurora Avenue Bridge. The decision included cancellation of all retrofit activities around the main piers planned for Stage I construction and a stop to the final design of Stage II, to accomplish P/T

strengthening of all the main piers. The WSDOT regional office was happy to initiate this changing seismic retrofit concept resolve the constructability problems.

Two independent feasibility studies to investigate friction pendulum isolation bearings by Imbsen & Associates, Inc. (IAI) and T. Y. Lin International (TYLI) were initiated in June of 2000 and completed in February of 2001. These two parallel studies used nonlinear time-history analyses to analyze the reduction of lateral loads using friction pendulum isolation bearings. Geotechnical engineers were brought into the study to provide seismic input and foundation stiffness [2]. Three earthquake records, representing crustal, intra-plate and subduction earthquakes, were used in the nonlinear time-history analysis.

After spending more than six months to compare and debate the results from the two nonlinear time-history analysis in the parallel studies, both IAI and TYLI concluded that it was feasible to install friction pendulum isolation bearings on four of the six main piers, leaving two piers to carry same high tensile forces which are caused by dead loads and tension forces which are caused by the frame actions in an earthquake. But the tension forces of the frame action will be less than before isolation. Seismic damage of the Aurora Avenue Bridge, including all the piers and the pile foundations, would be greatly reduced by using friction pendulum isolation bearings [3] & [4].

In July of 2001, TYLI started the final design of the seismic retrofit with friction pendulum isolation bearings and completed the design by February of 2002. The sizes of the friction pendulum isolation bearings are smaller and the heights are shallower than the existing bearings, therefore the jacking requirement for the installations of the isolation bearings are minimal. Except for strengthening the pier cap with post-tensioned cables, the jacking and installation will have very little impact on the existing structure and the surrounding area.

Conclusion: The seismic retrofit, with friction pendulum isolation bearings, on the Aurora Avenue Bridge provides a more efficient way to increase the survivability of the structure during an earthquake and will also save millions of dollars in construction over alternative P/T strengthening methods.

References

1. “SR99/560 Aurora Avenue Bridge Seismic Vulnerability Assessment and Retrofit Concept Study”; December of 1995; Parsons Brincherhoff Quade & Douglas, Inc.

2. “Geotechnical Report of Aurora Avenue Bridge Seismic Renovation”; December of 2000; PanGeo Inc.

3. “Aurora Avenue Bridge Seismic Retrofit – Seismic Isolation Feasibility Study”; February of 2001;

4. Imbsen & Associates, Inc. “SR99-Aurora Avenue Bridge – Friction Pendulum Base Isolation Feasibility Study”; January of 2001; T. Y. Lin International

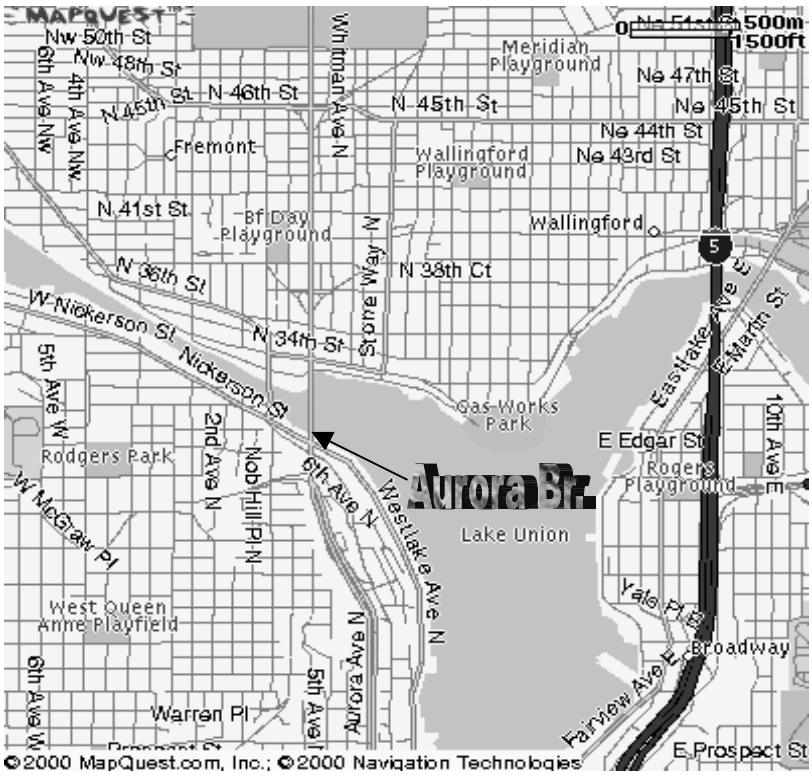

Figure 1. Aurora Avenue Bridge and Vicinity Map

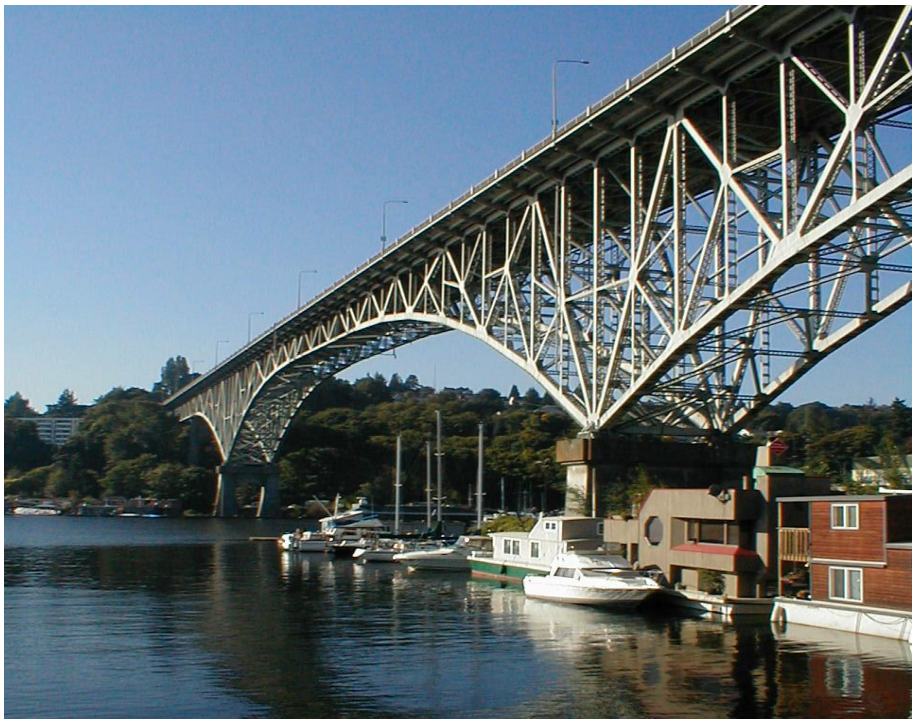

Fig. 2. Main Span of Aurora Avenue Bridge

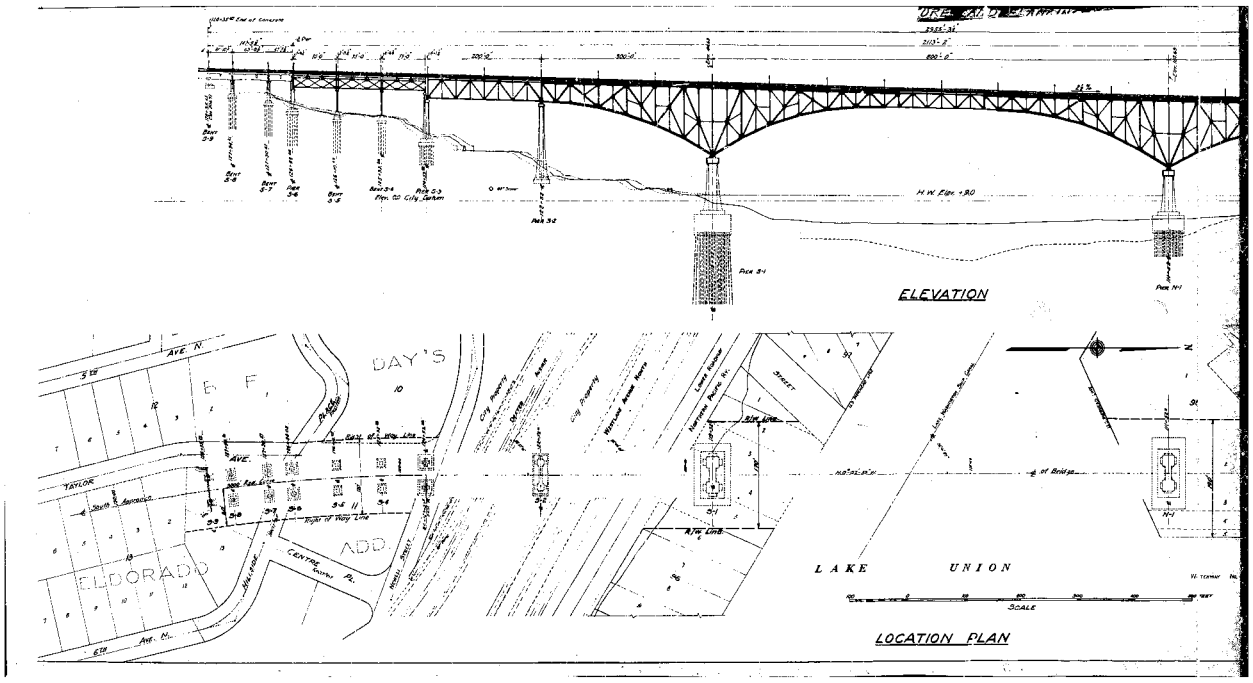

Fig. 3. Aurora Avenue Bridge Layout (South Portion)

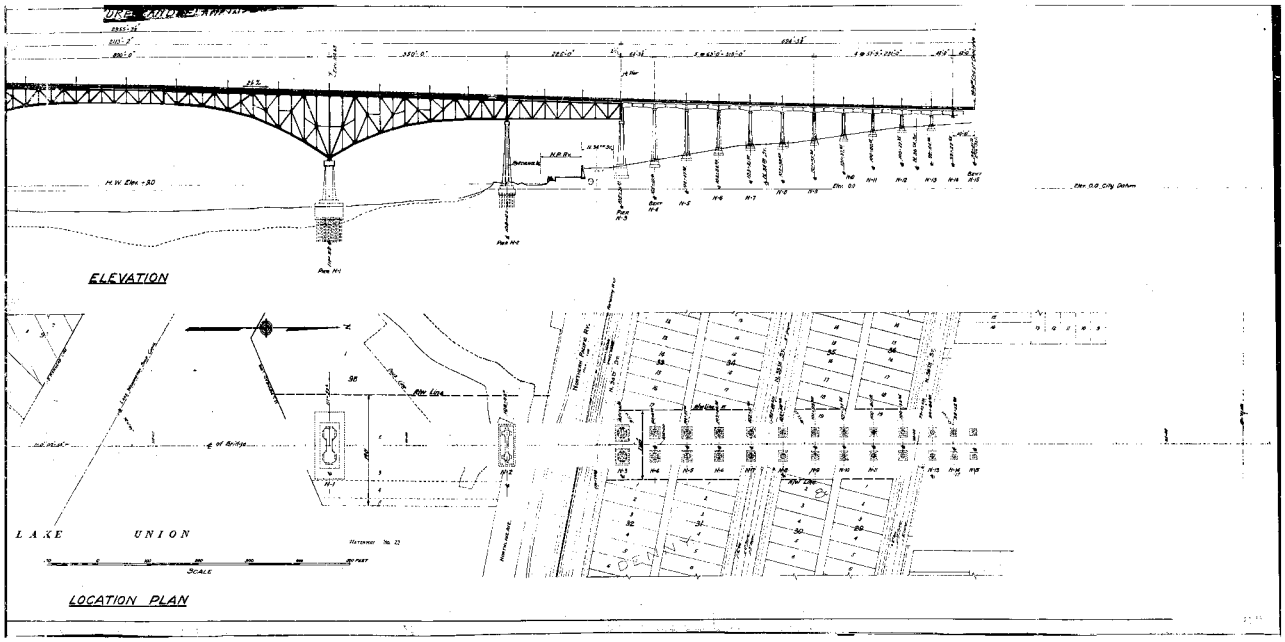

Fig. 4. Aurora Avenue Bridge Layout (North Portion)

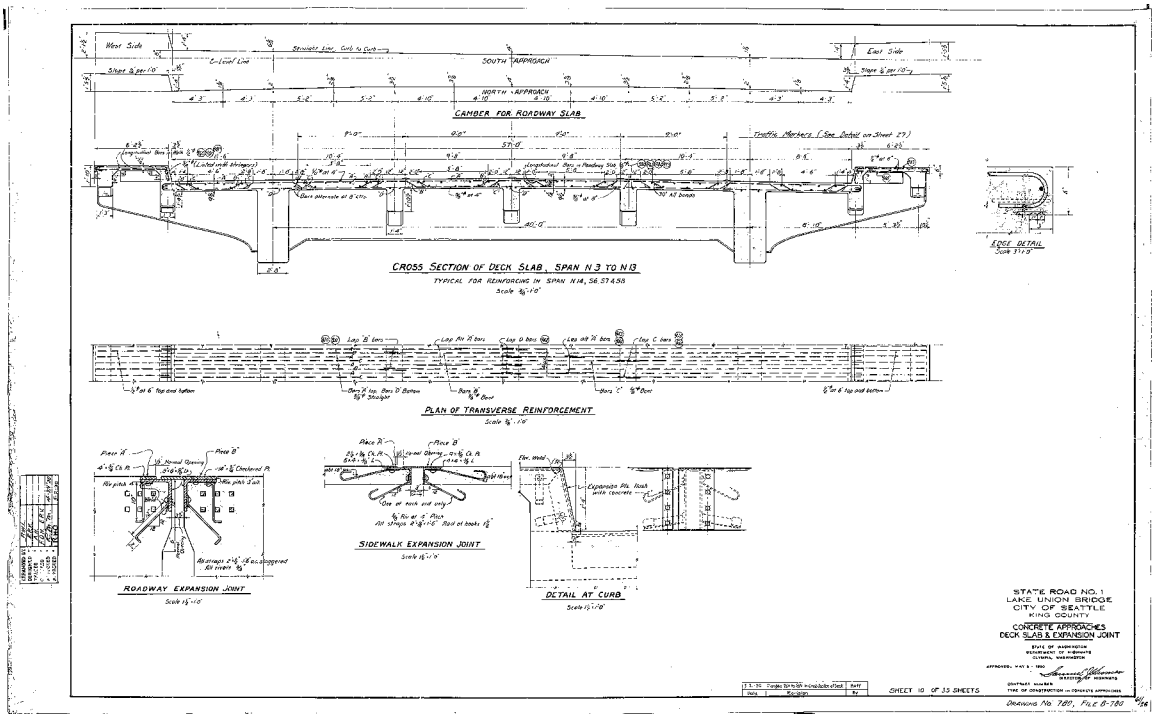

Fig. 5. The Cross Section of Aurora Avenue Bridge

Figure 6. Pier N1 of Aurora Avenue Bridge

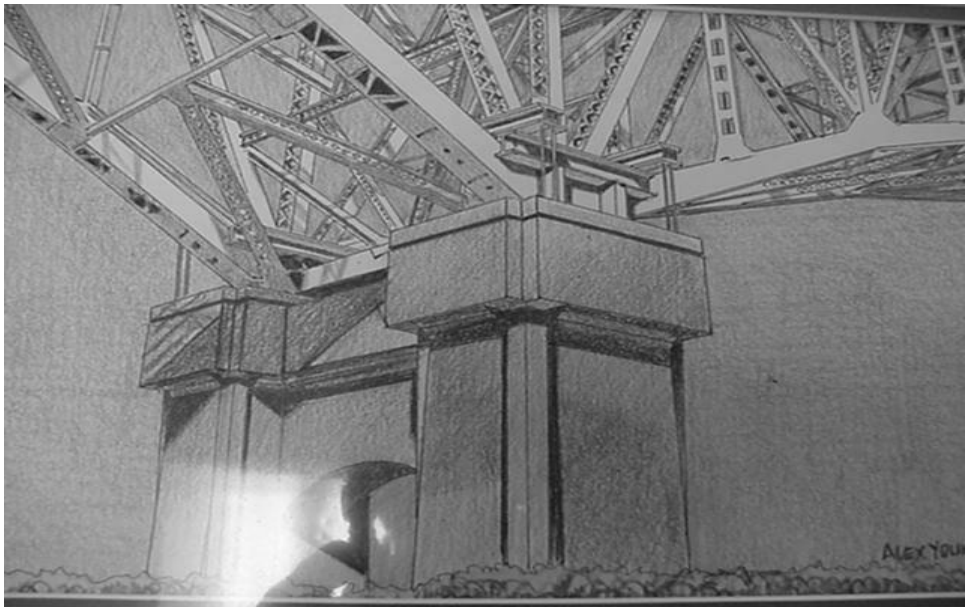

Fig. 7. Proposed Strengthening with Post-tensioned Cables at Main Piers

Figure 8. Parking Area and Local Roads at Pier N1, N2 and Ne3

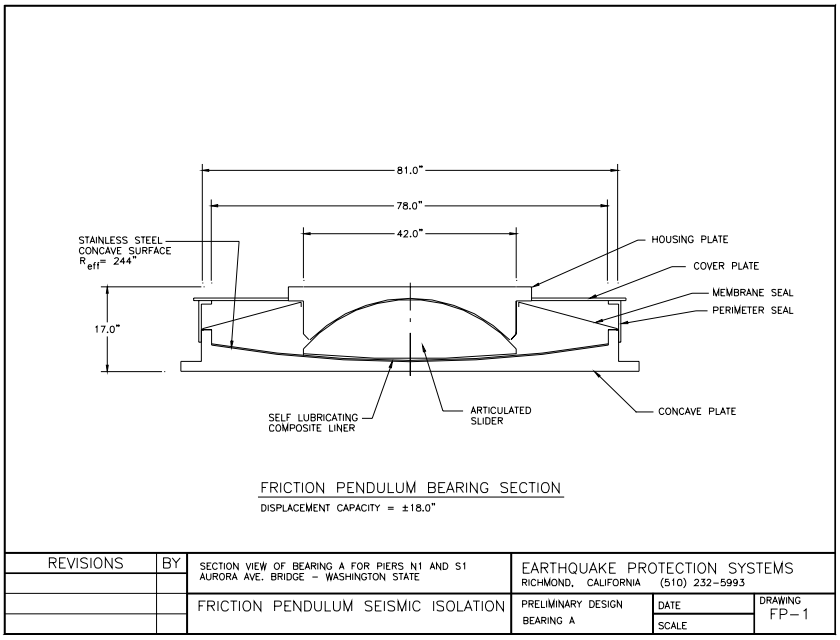

a) Cross Section

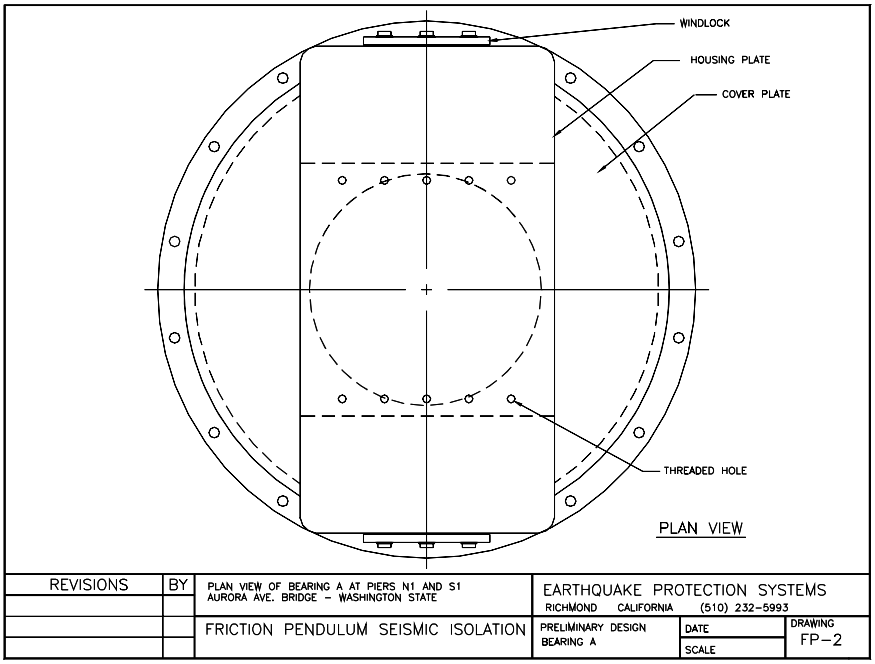

b) Plane View

Figure 9. Friction Pendulum Isolation Bearing

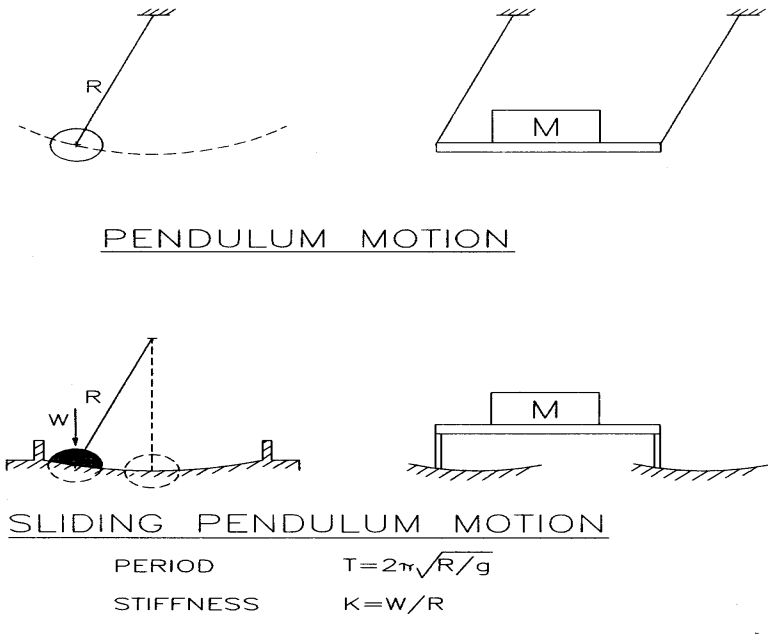

Figure 10. Basic Principles of Friction Pendulum Isolation Bearing

Figure 11. A Large Friction Pendulum Isolation Bearing

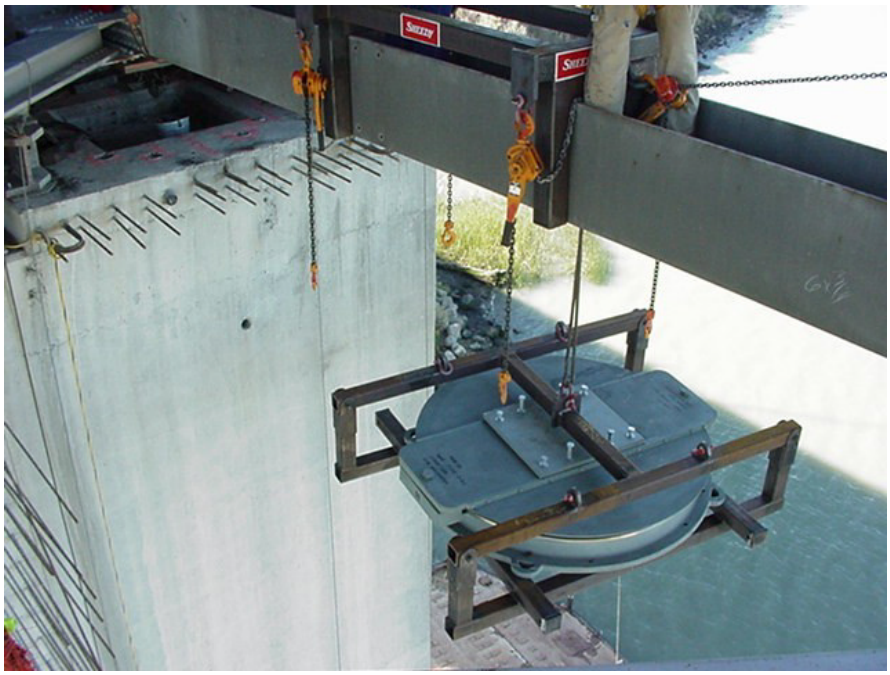

Fig. 12. Installing Friction Pendulum Isolation Bearing

Figure 13. The Installed Friction Pendulum Isolation Bearing

Design of Major Bridges in High and Moderate Seismicity Areas

Chair: Frieder Seible

Seismic Design of the Ravanel Bridge, Charleston, South Carolina

Michael J. Abrahams, Jaw-Nan Wang, Peter M. Wahl and John A. Bryson

Seismic Investigations for the Design of the New Mississippi River Bridge at St. Louis

Thomas P. Murphy and John M. Kulicki

Seismic Design of the Skyway Section of the New San Francisco-Oakland Bay Bridge

Brian Maroney, Sajid Abbas, Madon Sah, Gerald Houlahan and Tim Ingham

Seismic Design Strategy of the New San Francisco-Oakland Bay Bridge Self-Anchored Suspension Span

Marwan Nader, Jack López-Jara and Claudia Mibelli

Seismic Design of the Metsovitikos Suspension Bridge, Pindos Mountains, Greece

Mike Oldham, Zygmunt Lubkowski, Xiaonian Duan and Richard Sturt

Seismic Design of the Ravanel Bridge, Charleston, South Carolina

Michael J. Abrahams, Jaw-Nan Wang, Peter M. Wahl and John A. Bryson

ABSTRACT

Charleston South Carolina is well known for the 1886 magnitude 7.3 (moment magnitude, Mw) earthquake that was reported to have caused church bells to ring from Cuba to Boston. Recent site specific seismic studies suggest that during the past 2000 to 5000 years up to 6 large earthquakes of magnitudes similar to the 1886 event have occurred and they appear to have resulted from the same earthquake source.

This paper will discuss the Ravanel Bridge, a cable-stayed bridge being designed to span the Cooper River, as a replacement for two older truss type bridges. The design was selected by the SCDOT, based on a design-build competition. Upon its scheduled completion in 2004, the new bridge will be the longest cable stayed bridge in North America, with a main span of 1546 feet and a cable supported span length of 3296 feet. It will carry 8 lanes of traffic and a 12 foot walkway/bikeway. Including the high level approaches, ramps and interchanges, approximately 11,300 feet of new bridge structure is being constructed under this project.

The superstructure for the cable-stayed span consists of two 6'-6" deep steel edge girders and steel floorbeams composite with precast concrete deck panels. The high level approach spans will utilize continuous composite steel girders, while the lower level interchanges will utilize composite precast prestressed concrete bulb tee girders and composite steel girders on the lower level curved ramps. Drilled shaft foundations will be used throughout.

Due to the history of large earthquakes and presence of deep underlying soil deposits, there are important seismic design issues to be addressed for the Ravanel Bridge. The new design utilizes 10 foot diameter drilled shafts over 200 feet deep at the main span towers, with an ultimate capacity of approximately 27,000 kips per shaft. Similar sized drilled shafts are used throughout the high level approach spans.

Michael J. Abrahams, Technical Director, Major Bridges, Parsons Brinckerhoff Quade & Douglas, Inc., One Penn Plaza, 250 West 34th Street, New York, New York 10119
Jaw-Nan Wang, Senior Professional Associate, Parsons Brinckerhoff Quade & Douglas, Inc., One Penn Plaza, 250 West 34th Street, New York, New York 10119
Peter M. Wahl, Supervising Structural Engineer, Parsons Brinckerhoff Quade & Douglas, Inc., One Penn Plaza, 250 West 34th Street, New York, New York 10119
John A Bryson, Supervising Structural Engineer, Parsons Brinckerhoff Quade & Douglas, Inc., One Penn Plaza, 250 West 34th Street, New York, New York 10119

A detailed finite element model of the main bridge and adjacent high level approaches was developed for use in analysis of seismic and non-seismic loads. Foundation elements (pile caps, piles and soil stiffnesses) are explicitly defined in the global analytical model. In addition to linear multi-mode response spectrum analysis, inelastic nonlinear time history analysis is being utilized for seismic design of the main and high level approach spans. The time history analyses includes spatial variation time histories (multiple support excitation) to capture wave travel, local site and spatial incoherence effects of ground motions and nonlinear soil springs, determined based on extensive site-specific geotechnical evaluations.

The paper discusses the overall project with particular emphasis on the seismic design and detailing and how key issues are being addressed under a tight schedule in a design-build environment.

INTRODUCTION

The Ravanel Bridge is currently under construction and when completed will provide a 3,296 foot long cable stayed main span over the Cooper River between the City of Charleston and the Town of Mount Pleasant in South Carolina, see Figure 1. This will be the longest cable stayed bridge in North America.

The bridge evolved from studies begun in 1988 in order to address the need to replace the deficient existing Silas T. Pearman and Grace Memorial Bridges between Charleston and Mount Pleasant and to a more recent need to improved shipping clearances in the upper reaches to the Charleston Harbor, a significant port of commerce for over 300 years. In order to address traffic and shipping demands as well as community requests, the new bridge will provide a 1000 foot horizontal and 186 foot vertical clearance over the main channel and a 250 foot horizontal and 65 foot vertical clearance over a secondary channel, Town Creek.

The roadway will provide for 8 traffic lanes and a 12 foot wide walkway/bikeway. The main span, is 1546 feet long with back spans 650 and 225 feet on each side, for an overall length of 3296 feet. It will utilize a composite concrete deck with steel edge girders. As shown in Figure 2, the sidewalk/bikeway will be cantilevered outside of the south edge girder.

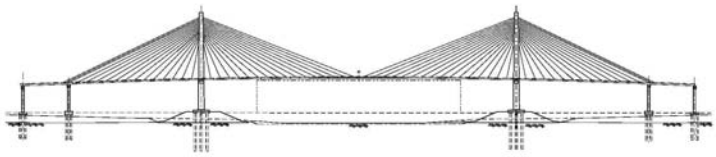

Figure 1: Elevation

Figure 2: Typical Section

The high level approaches will also utilize composite steel construction with steel girders spaced 12 feet on centers. The high approaches are jointless and 4350 feet long on the Charleston side and 2090 feet long on the Mount Pleasant side. Beyond the high level approach spans there are low level approach spans and interchanges structures. These utilize composite precast concrete girders for the straight portions and composite steel girders for the curved ramps.

The entire site is characterized by a layer of stiff clay known as Cooper Marl at a depth of 50 to 60 feet. Above the marl, the river has soft alluvial deposits, while the land portions of the projects have relatively soft surficial soils, so the bearing stratum throughout the site is the Cooper Marl.

DISCUSSION

The preliminary design was developed in response to a request for proposals issued by the South Carolina Department of Transportation and was developed in a two phase review process, with Phase 1 generally focusing on an overall concept and Phase 2 requiring a more advance development of the design in response to a revised design criteria. The design criteria,[(1)] which was part of the Request For Proposal (RFP), was generally based on the AASHTO Standard Specifications for Highway Bridges,[(2)] but included a number of project specific requirements. There was also a project specific Seismic Design Criteria.[(3)] And while some other project specific data were furnished, such as an extensive geotechnical investigation and testing program (including full scale dynamic tests of 8 foot diameter drilled shafts), ship collision design loads based on a Method 1 analysis and preliminary wind loads based on a preliminary study, it was up to the design-build team to develop much of the criteria as well as additional survey and geotechnical testing, a corrosion control plan, an independent wind tunnel testing program and a ship collision analysis. So while much of the criteria has been established at the time of the proposal, other items have been defined as the design has evolved.

At the time of the preparation of this paper the final design is still underway but most major design issues have been resolved. This paper will focus on a number of the seismic design related issues that were part of the preliminary design package that formed the proposal package or design issues that have been developed and resolved as the design has progressed.

Charleston is well known for the 1886 Magnitude 7.3 (moment magnitude, Mw) earthquake that was reported to have caused church bells to ring from Cuba to Boston, Massachusetts. Recent studies that have led to the development of a project specific seismic hazard analysis[(4)] suggest that during the past 2000 to 5000 years up to 6 large earthquakes of similar magnitude have occurred and they appear to have resulted from the same source. The methodology used in this determination was based on the identification and carbon dating of sand boils associated with these events. By correlating the extent of the sand boils and the date of their occurrence a record of past events was established. Based on these records, a probabilistic seismic hazard analysis was conducted to develop a site specific criteria for this project. The criteria specified that for a 2500 year event, the main span and designated portions of the approach structure could not suffer significant damage and would need to be able to be reparable and returned to service shortly after such an event. The remaining portions of the structure could suffer considerable damage but could not collapse.

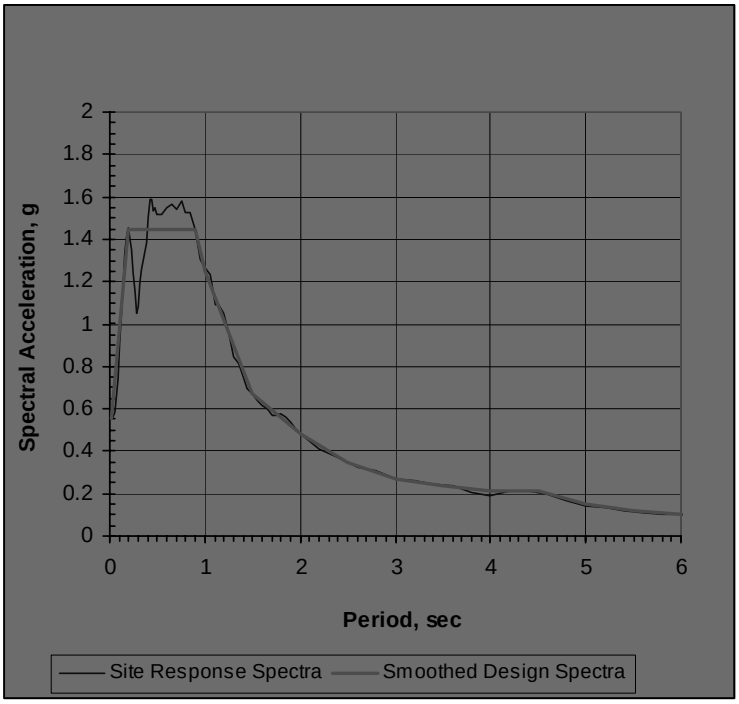

Figure 3: 2500 yr. spectra

For a 500 year event the structure was to remain in the elastic range.

The solution to these demanding criteria in a very competitive design-build environment, with a client who had only a limited budget proved to be the major design challenge.

In general the solution adopted, particularly for the main span and high level approach spans, was to minimize the structure weight to provide enough flexibility in the structure so that seismic demands were minimized. The use of 10 foot diameter drilled shafts in the foundations minimized the number of shafts. For the main span piers only 11 of the high capacity drilled shafts are required while on the high level approaches typically only two drilled shafts are required per pier, see Figures 4 and 5.

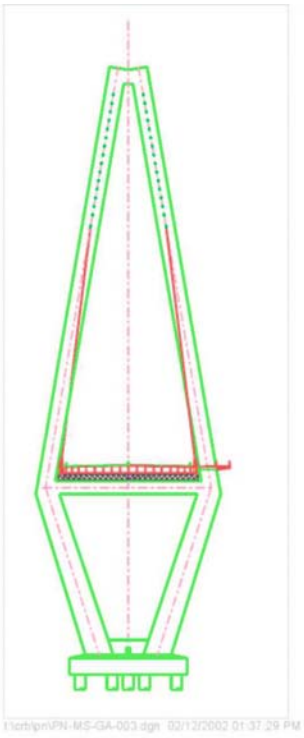

Figure 4: Main span foundation

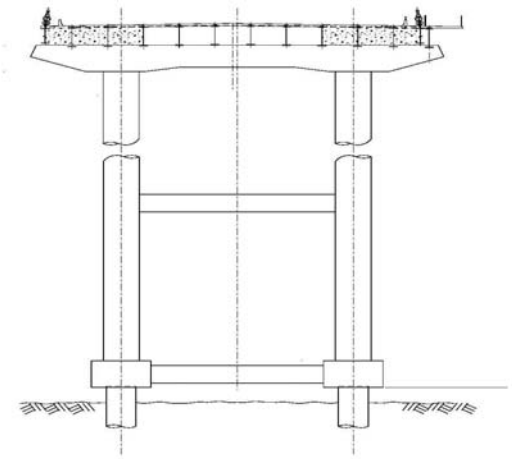

Figure 5: Approach span foundation

The height of the high level approach span piers proved to be too flexible along the axis of the bridge so the solution adopted was to make the approach spans continuous over a significant length, 4350 feet on the west approach and 2090 feet on the east approach, so that the shorter piers of the lower portions of the approaches act to brace the taller piers. This has an advantage

of minimizing expansion joints but has required considerable analysis to properly establish the relative stiffnesses of the piers to address the desired behavior.

Seismic Analysis

The project Seismic Design Criteria requires a time history analysis using records from three different events as part of the final design of these portions of the bridge. This was accomplished using ADINA, with a specific subroutine prepared by SC Solutions to track the moment curvature behavior of those sections of the structure that undergo inelastic behavior during a seismic event. While the AASHTO Standard Specifications provided specific detail criteria for most of the structure, the behavior of the hollow cross sections of the main span piers was not well covered by existing criteria. As a result, an investigation into available recently published reports on the non linear behavior of hollow reinforced piers was required.

Time History Analysis

The project Seismic Design Criteria included a site specific design spectrum as well as three scaled earthquakes, the Tabas, Imperial Valley and Joshua Tree to be utilized in the analysis. The intent was that the designer would utilize an spectrum analysis for the preliminary design of the cable stayed main span and high level approaches together with a time history analysis of those same elements as a part of the final design. However the experience in this project, which is on a very compressed design schedule and for which the foundations design must be completed first, is that the time history has proven to be very cumbersome tool that does not lend itself to design modifications as the work evolves. The spectrum analysis has proven to be a much more useful tool in arriving at a design solution.

Vertical Motions

The seismic analysis uses horizontal motions in two horizontal directions and combined with vertical motions using either the SRSS method or the 40% rule (e.g. 1.0L +0.4T+ 0.4V). A site response analysis with SHAKE (a computer program) is used to establish ground motions. While SHAKE has produced reasonable results for the horizontal ground motions, it has not been useful in determining vertical motions. It has therefore been agreed that vertical motions will be based on a percentage of the base horizontal motions reduced by a factor. The factor is currently under consideration and is anticipated to be between 2/3 and 0.8.

Hollow Rectangular Piers

The criteria found in the Seismic Design Criteria was based on the recommendations of Breen,[5] but these investigations were limited to evaluating hollow columns up to a strain limit of 0.003 and did not address the issue of cyclic loading. However an evaluation of available references found that if adequately detailed, hollow piers would perform well. Pinto et al[6] and[8] Pinto reported that "The piers exhibited a ductile behavior with quite stable hysteretic loops. Equivalent displacement ductilities of about 6 were observed.[7]" Similarly Mo (8) has reported a ductility factor of 5.0 to 8.4. It was also found that where without proper confining steel, failure occurred due to rupture of the longitudinal reinforcement, Pinto et al (9) and (10).

Drilled Shaft Design

The Seismic Design Criteria indicates hinging should be prevented below grade in the foundations elements. As the project is founded on large diameter drilled shafts, the shafts vary from 10 foot diameter on the main span to 6 to 8 foot diameter on the low level spans, the design of the drilled shafts has in general been controlled by the plastic hinge capacity of the columns above the drilled shafts. Since most of the shafts are in approximately 50 feet of soft soil, the shafts have had their maximum moment at the level of the stiff marl just below the soft upper soil layer. This has resulted in having more reinforcing steel at the mid portion of the drilled shaft than at the top, a somewhat unusual arrangement but one dictated by the site conditions.

Reinforcing Details

The Seismic Design Criteria generally referred to AASHTO Division 1A, Seismic Performance Category, for detailing requirements. These requirements have proven to be inappropriate in detailing the reinforcing for the main span and approach spans for a number of reasons. For example splices in columns are to be restricted to the middle half of column height for normal overpass bridges with modest column heights these may be appropriate but for spans whose columns sometimes exceed 100 feet in height such restrictions are not practical. As a result it has been proposed to utilize the provision of ATC-32 (12) to design the hinge area in columns and to allow lap splices anywhere outside of the hinge zone. And while it is desirable to eliminate splices within a hinge zone, this is not always realistic when designing large columns. Therefore, for this project it has been proposed that if splices are required within a hinge zone, only mechanical splices will be used and that the splices will conform to the requirements of the International Conference Of Building Officials, (13), which specify a cyclic testing protocol for mechanical spices. A somewhat similar, but less restrictive requirement for mechanical slices in hinge zones can be found in ACI (14).

Another issue relates to the tie requirements in the hollow pier columns. The current requirements in AASHTO when applied to the columns has resulted in very dense reinforcing, which while good for ductile behavior, make for very difficult placement and the possibility of voids in the concrete. Less restrictive requirements can be found in both ATC 32 and ACI, and these requirements are also under discussion to see if a more appropriate spacing can be established.

CONCLUSIONS

The use of the design build method is relatively new in the United States, and the Ravanel Bridge is believed to be one of the first major bridge projects in which it has been used. There have been many challenging requirements for the project, including the need to accommodate an area of high seismicity and hurricane force winds. This process appears to have resulted in a design approach that has met the challenge**.**

ACKNOWLEDGMENTS

Design-build is an evolving process and is most successful when everyone works as a team. When a proposal is prepared not every issue can be known and defined, nor can every aspect of the design be worked out. Thus as the design and construction proceed everyone - the owner and his review team, the contractor, and the designer - need to work together. This has proved to be the case on the Ravanel Bridge. The contractor, Palmetto Bridge Contractors, (PBC) is a joint venture of Tidewater Construction Company, Virginia, and Flatiron Contractors, Colorado. Their project manager is Wade Watson. To assist in the design review process the owner, the South Carolina Department of Transportation, assisted by the Federal Highway Association, has retained a team of consulting engineers, led by T.Y. Lin, San Francisco California, and HDR, Engineering, Inc. Pittsburgh, Pennsylvania, together with Wilbur Smith Associates, Columbia, South Carolina. The Department has also retained a Seismic Review Panel to provide oversight and guidance as to the seismic design issues of the project. The Panel is chaired by Dr. Frieder Seible, University of California, San Diego, and the Panel members are Gerry Fox, consultant, Dr. Po Lam, Dr. Roy Imbsen, Imbsen and Associates, and Tim Ingram, T.Y. Lin. The panel has met with the design team several times and they have proved to be a very valuable source of guidance on a number of design issues.

There are a large number of individuals involved in the project, including Bobby Clair, Program Manager, SCDOT, Charleston, South Carolina; Charles Dwyer, SCDOT, Charleston South Carolina; Ken Johnson, FHWA, Columbia, South Carolina; and John Pohle, Design Manager, PBC, Charleston, South Carolina. The design team includes Dr. Peter Taylor and Roger Welch, Buckland & Taylor, Vancouver, British Columbia; Bob Bittner, Henrich Gluver and Liang Shen, Ben C. Gerwick Inc., Oakland, California; Judy Thomason and Jeff Mulligan, LPA Associates, Columbia, South Carolina; Dr. Peter Irwin, Dr. Stoyan Stoyanoff and Deborah Near, RWDI, Guelph, Ontario; Alex Krimotat and Hassan Sedarat, SC Solutions, San Francisco, California; Dan Carrier, Project Manger, Parsons Brinckerhoff (PBQD), Charleston, South Carolina; and Dan Dock, Deputy Project Manger, PBQD, Raleigh, North Carolina. Other key staff at PBQD include Raymond Castelli, Ke Fan, Joe Tse, and Ian Fraser.

REFERENCES

(1) SCDOT, February 2001, Bridge Design Criteria, Cooper River Bridge Replacement, Charleston, South Carolina.

(2) American Association of State Highway and Transportation Officials, 1996, Standard Specifications for Highway Bridges.

(3) SCDOT, August 2000, Supplemental Criteria for Seismic Design U.S. 17 Cooper River Bridges, Charleston, South Carolina.

(4) Geomatrix Consultants, 2000, Final Report: Cooper River Bridges Replacement Project – Ground Motions Hazard Analysis,.

(5) Taylor, Powell and Breen, ACI Structural Journal, May-June, 1995, Behavior of Thin-Walled Concrete Box Piers.

(6) Pinto, A.V., Verzelli, G., Negro, P., Guedes, J., 1995. "Cyclic Testing of a Squat Bridge Pier," European Laboratory for Structural Assessment, Ispra, Italy, Report EUR 16247 EN.

(7) Pinto, A.V., Verzeletti, G., Pegnon, P., Magonette, G., Negro, P. Guedes, J., 1996. "Psuedo-Dynamic Testing of Large-Scale R/C Bridges," European Laboratory for Structural Assessment, Ispra, Italy, Report EUR 16378 EN.

(8) Y.K. Yeh and Y.L. Mo, International Workshop on Mitigation of Seismic Effects on Transportation Structures, Taipei, Taiwan, July 1999, Seismic Performance of Rectangular Hollow Bridge Columns.

(9) Pinto, A., Molinia, J., Tsionis, G., 2001. "Cyclic Test on a Large-Scale Model of an Existing Short Bridge Pier (Warth Bridge - Pier A40)," European Laboratory for Structural Assessment, Ispra, Italy, Report EUR 19901 EN

(10) Pinto, A., Molinia, J., Tsionis, G., 2001. "Cyclic Test on a Large-scale Model of an Existing Tall Bridge Pier (Warth Bridge - Pier A40)," European Laboratory for Structural Assessment, Ispra, Italy, Report EUR 19907 EN

(11) American Concrete Institute, 1999, ACI 318, Building Code Requirements for Structural Concrete, Chapter 21, Special Provisions for Seismic Design, 21.2.6.1 Mechanical Splices, (b) Type (2).

(12) Applied Technology Council, 1996, ATC-32, Improved Seismic Design Criteria for California Bridges: Provisional Recommendations.

(13) International Conference of Building Officials, 2001, AC133, Acceptance Criteria for Mechanical Connectors for Steel Bar Reinforcement.

Seismic Investigations for the Design of the New Mississippi River Bridge at St. Louis

Thomas P. Murphy and John M. Kulicki

ABSTRACT

This paper describes the proposed New Mississippi River Bridge at St. Louis and the preliminary seismic analyses. A high seismic performance level is set for the bridge, and a site specific design spectrum is developed. The bridge will be a cable stayed structure with a main span of 2000' carrying 8 lanes of traffic and 4 full shoulders resulting in 12 design lanes. The sidespans will be cast-in-place post-tensioned concrete cellular structures, connected integrally with the towers, and will extend approximately 70' into the main span. The remainder of the main span will consist of steel edge box girders supporting steel floor beams and a concrete deck. The important mode shapes and periods in the three principle directions of the bridge were investigated. The results of a preliminary multi-modal response spectrum analysis are presented, and the response of the bridge is evaluated.

Thomas P. Murphy, Structural Engineer, Modjeski and Masters, Inc., 4909 Louise Drive, Mechanicsburg, PA 17055
John M. Kulicki, President and Chief Engineer, Modjeski and Masters, Inc., 4909 Louise Drive, Mechanicsburg, PA 17055

Figure 1. The New Mississippi River Bridge

INTRODUCTION

This paper describes the preliminary seismic design of the proposed New Mississippi River Bridge (NMRB) at St. Louis. Situated north of the Eads and south of the Martin Luther King Jr. bridges, this bridge will carry eight lanes of interstate I-70 and I-64 across the Mississippi river just north of downtown St. Louis.

General Description

The design is for a cable-stayed bridge with two main single pylon towers located at the edges of the river, as shown in Figure 2. The main span is 2000', which will make it the longest bridge of its type in the western hemisphere when completed. The bridge type and major appearance features resulted from extensive public involvement, the participation of the owners, and an integrated engineering-architecture design team. The side spans are pier supported, and consist of four spans in Missouri (147.5'-140'-140'-147.5') and three spans in Illinois (191.7'-191.7'-191.7'). The towers are single pylons with centroids inclined 7 degrees from the vertical away from the river. They are situated between the two travel directions, in a 40-foot slot down the middle of the bridge. The Missouri tower is supported by a spread footing on rock; the depth to rock at this location is only approximately 25'. The Illinois tower will be supported by a dredge well caisson sunk nearly 100' to rock. The superstructure is

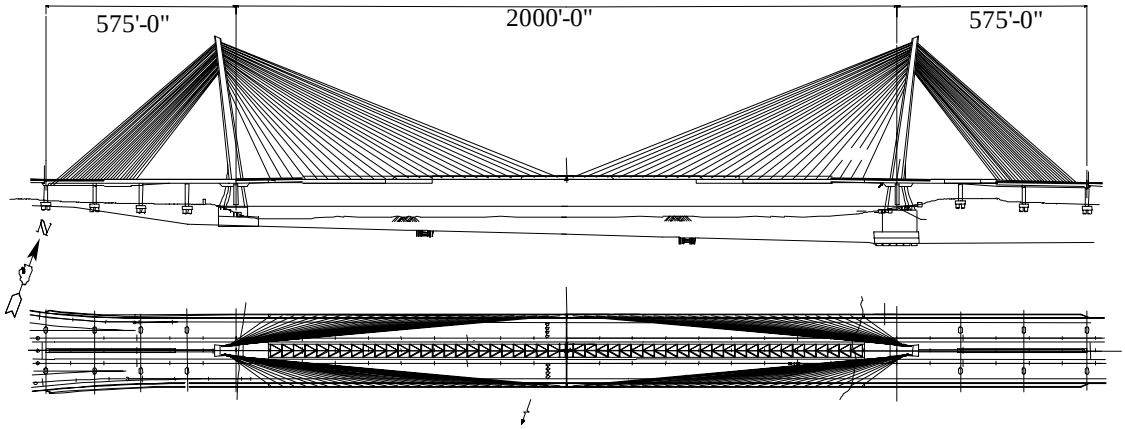

Figure 2. General plan and elevation

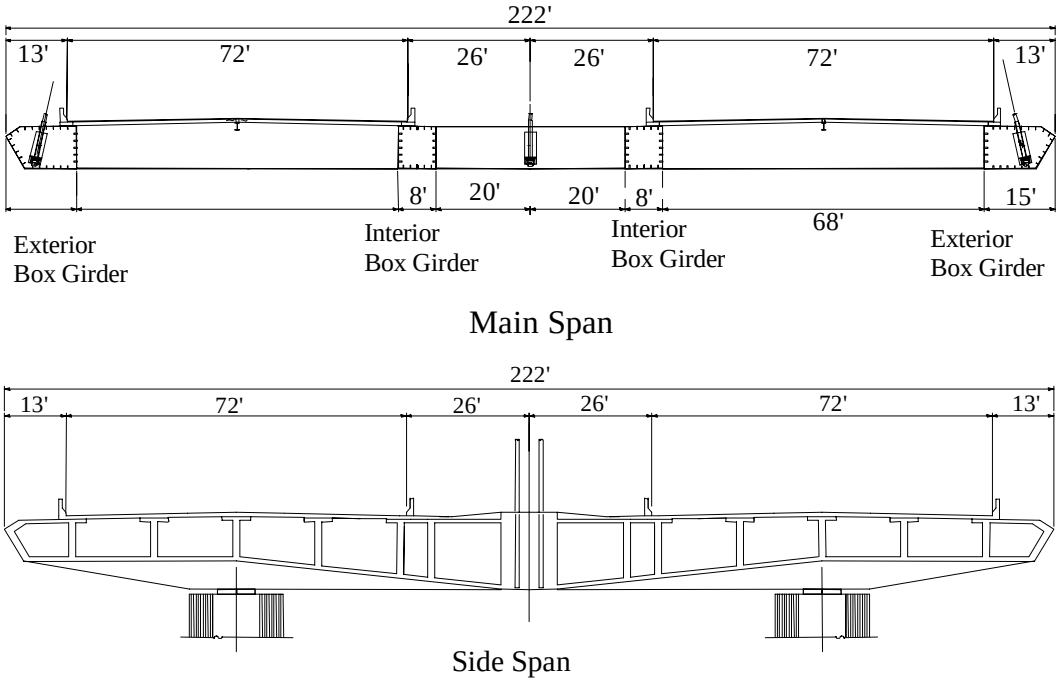

Figure 3. Main and side span cross sections

constructed integrally with the tower, and also supported by curved struts at the tower center line. There are three cable planes in the main span arranged in the semi-fan pattern, anchoring at the center and both edges of the deck. The majority of the main span is a composite steel-concrete superstructure, while the side spans are cast-in-place cellular concrete box girders. The anchor cables are arranged in two parallel planes along the center of the concrete box girder, and are splayed longitudinally along the ends of the side spans.

Cross Section

The out-to-out width of the main span is an extraordinary 222', the extra width occurring due to the passage of the tower up through the center of the cross-section as well as the provision for full width shoulders along both sides of each roadway. With full width shoulders, the bridge can be expanded to carry a total of 12 lanes in the future, if need be. The main span cross-section, shown in Figure 3, may be thought of as consisting of two individual cross-sections, one for each direction of traffic, straddling the towers and joined along the center gap. Each cross-section consists of an interior and an exterior steel box girder arranged along the edges, the interior box is on the side of the center gap. Steel floorbeams span between box girders and support the post-tensioned concrete deck.

The exterior box girders are 9 feet deep, 15 feet wide and are shaped to improve the aerodynamic performance of the bridge. The shape has not been finalized at this writing, aerodynamic studies are ongoing. The inner box girders along the sides of the slot are 9 feet deep x 8 feet wide rectangles. The box girders are constructed of stiffened steel plates, utilizing HPS grade 70 steel where required. The side planes of cables are anchored within the exterior box girders.

The typical floor beams are approximately 5 ft. deep, and span 68' between the faces of the box girders. They are spaced at 11'-8" and have widened top flanges to accommodate the erection of precast deck panels. A small longitudinal beam, spanning between floor beams, also serves as an edge support for precast panels. At each cable anchorage location, a main floor beam spans between the box girders and across the center gap. These are full depth steel beams, moment connected to the box girders. In addition to supporting the concrete deck, they carry the transverse bending moments and anchor the central plane of cables. In order to reduce the maximum size of stay cable required and to increase the torsional stiffening effect of the outer planes of cables, the vertical loads were distributed uniformly to each plane of stays, so that each plane carries the same vertical force. The main floorbeams, therefore, carry the transverse moments resulting from this distribution.

The concrete deck consists of precast panels, two per half bridge, which will be post-tensioned together after erection. Due to the long main span of the NMRB, the efficiency of the deck will have a large impact on the magnitude of the forces in the cables and tower.

In addition to the main floor beams, the center gap contains two planes of bracing, one in the top plane of the boxes, one in the bottom plane. These tubular struts resolve the longitudinal components of the cables anchored in the main floor beams. In addition, they carry shear forces due to transverse bending in the main span.

Towers

The single pylon inclined towers, approximately 520' tall from high water elevation, are perhaps the most distinctive feature of the bridge. Figure 4 shows the towers in elevation and cross-section. They are constructed of concrete and maintain an approximately rectangular cross-section through most of their height. The front face is inclined at a constant 9 degrees from the vertical, while the back and side faces vary over the height to allow for changes in the cross-section dimensions. The cross section of the tower is a concrete box with interior cross walls and exterior spurs that start and end along the height. In the cable nest area, the cross section transitions to a solid H-shape. The cables, three planes from the main span and two planes from the side spans, pass through the web of the H and anchor across from each other. Facia panels are used to cover the anchorage areas in this region.

The concrete superstructure is made integral with the tower where the two intersect. The depth of the superstructure is locally increased around the tower to reduce the post-tensioning required to resist live and dead load moments. This region resembles a column capital from building construction.

Side Spans

The superstructure cross-section for the side spans consists of two multi-cell box girders joined in the center by cable anchorage members, as shown in Figure 3. The box girders are 6,500 psi cast-in-place concrete and longitudinally post-tensioned to resist local dead and live loads. The box girders match the approximately 9-foot depth and shape of the steel main span and are continuous over their full-length from the end of the 575-foot side span to the interface with the steel main span approximately 70 feet into the main span.

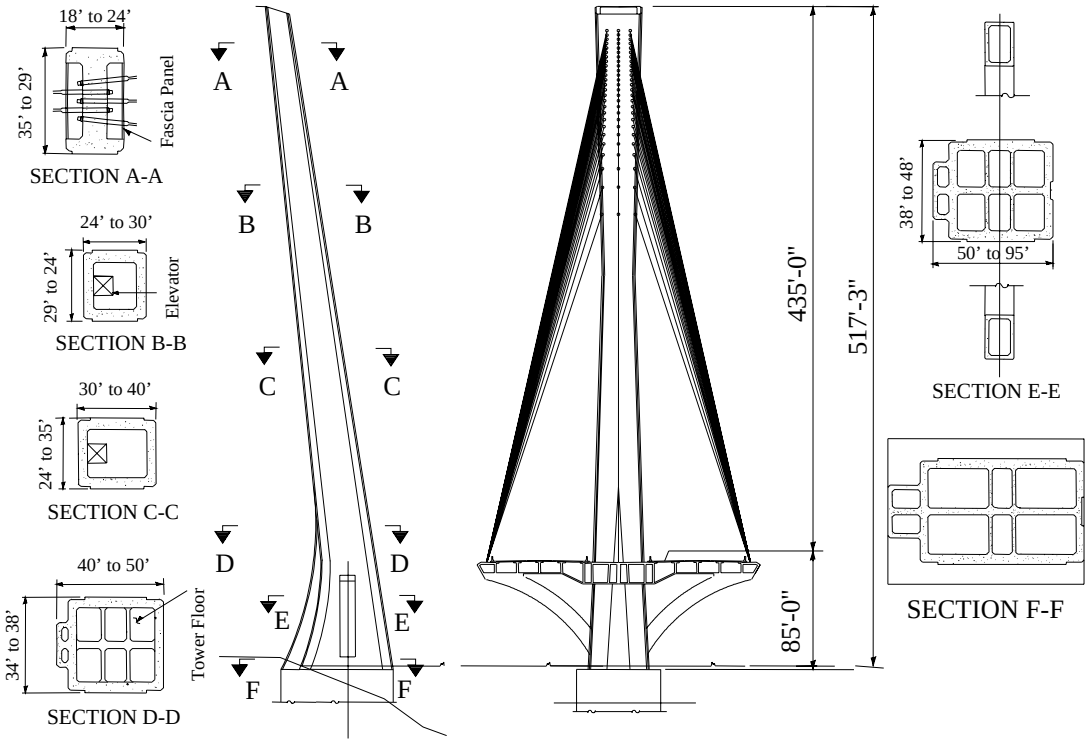

Figure 4. Tower elevations and cross sections

The 26 cable-stay pairs anchor into a centrally located, massive, solid concrete cable girder. This longitudinally post-tensioned cable girder is 14 feet wide and varies in depth from 10 to 16 feet. The cable girder is in turn supported by transverse floorbeams, which are located at each stay location and at the pier lines. The post-tensioned transverse floorbeams, which run from out-to-out of the bridge, form a grid system with the webs of the box girders and serve to mobilize the weight of the side spans in resisting the vertical component of the cable forces. The floorbeam located at the end of the side span is notched to create a bridge seat for the approach spans. This will allow a portion of the approach span weight to be used in resisting the uplift forces from the stays.

Diagonal thrust girders are provided to create a direct load path for the conveyance of longitudinal thrust (resulting from the horizontal component of the inclined stays) from the cable girder to the outside cells of the concrete box girder. These cells align with the four steel box girders of the main span. This will help balance the thrust distribution in the side spans to match that of the main span. The outside cells of the box girders are closed sections. To facilitate deck replacement, the webs of the box girders are topped with "sub-flanges", which will effectively replace the top flange (deck slab) of the box section when the deck slab is removed. This will allow the side span superstructure to support its dead load and remain stable in the absence of the deck slab. Therefore, shoring of the superstructure will not be required for deck replacement operations.

Nontraditional reinforcing steels, including stainless steels, are being considered in certain locations to eliminate corrosion potential of critical members. These locations include: all reinforcing in the cable girder, stirrups projecting from box girder sub-flanges into the deck slab, and surfaces of the end floorbeams exposed to potential leakage from deck joints.

SEISMIC HAZARD

The most important seismic zone in the central United States is the New Madrid Seismic Zone (NMSZ). The New Madrid zone is located about 140 miles south of St. Louis. The fault system extends 150 miles southward from Charleston, Missouri, and Cairo, Illinois, through New Madrid and Caruthersville, Missouri, following I-55 to Blytheville and Marked Tree, Arkansas. It crosses five state lines, the Mississippi River three times and the Ohio River twice.

The largest earthquake recorded on this system of faults was the series of quakes and aftershocks that occurred during the winter of 1811-1812. Of the hundreds of earthquakes that occurred at this time, three were of very large magnitude, the largest estimated at greater than 7.5. These events all but destroyed the small town of New Madrid (population 400) and caused widespread destruction.

Only recently has the full potential of the NMSZ to produce damaging earthquakes been realized. In the 1970's, widespread monitoring of the region was instituted. Since that time, thousands of earthquakes have been recorded, although most are too small to be felt. A magnitude 4.0 or greater event occurs almost annually, magnitude 5.0 or greater events occur nearly every decade, and magnitude 6.0 or greater about once every century. The return period for events of the magnitude of the 1811-1812 quakes is estimated at somewhere between 300 to 1,200 years. Obviously, the small amount of data available about larger events results in high uncertainties in their predictions.

Aside from the NMSZ, earthquakes can occur virtually anywhere in the St. Louis region. The probability of such an event is relatively low, but must be considered when identifying the seismic hazard. The possible existence of as yet unknown faults which can produce earthquakes is termed "background hazard." The size of such hypothetical quakes is expected to be relatively small to moderate. However, even a small quake can cause damage if the epicenter is close to the structure.

Site Hazard

Current AASHTO seismic design procedures use a hazard level of 10% in 50 years (i.e. a return period of 475 years, commonly stated as 500 years), meaning the design earthquake has a 10% probability of being exceeded in a time window of 50 years. Only one hazard level is considered.

Recent draft seismic provisions, i.e., ATC-32 and NCHRP 12-49, recommend a two level design process, where a lower hazard level is used to represent a frequently occurring event during which the structure is expected to sustain very low damage levels, and a higher hazard level representing a rare, strong earthquake. The exceedence probabilities for these two levels are 40% in 50 years (return period of 100 years) for the frequent event and 2% in 50 years (2,500 year return period) for the rare earthquake. Performance levels are selected to be appropriate for each of the two design events.

Early in the project, a desire to design the bridge to a high level of seismic safety was expressed. The bridge will be an important lifeline for the St. Louis area, and it is essential that it remains functioning after a major disaster, such as an earthquake, in order to accommodate emergency response efforts. In addition, the anticipated 150-year life span of the bridge is two to three times longer than normally expected from a bridge. It would be very undesirable to design the bridge to a currently acceptable standard only to have more stringent requirements come into effect in the near future which would require retrofitting of the bridge. Because of the above, the design hazard level for the bridge has been chosen as 2% in 50 years (i.e., an earthquake with a return period of 2,500 years), the service level has been identified as "immediate", and the damage level has been chosen as "minimal to none." An "immediate" service level is defined as allowing full access to normal traffic after a seismic event, with perhaps a short period of closure while the bridge is visually inspected. The "minimal to none" damage level means that there should be no apparent deformations, although narrow cracking of the concrete may occur. In order to achieve these goals, the R factor for the main bridge has been set at 1.5 for the 2500 year event.

Rock Spectra

The NCHRP 12-49 Draft LRFD Design Specifications utilize uniform hazard maps developed by the USGS. A spectrum is developed using the two point method, where two values of the spectrum are obtained from the maps at periods of 0.2 and 1.0 seconds and the remainder of the spectrum is obtained by fitting standard curves to the two points. Previous methods used only the peak ground acceleration and a spectrum shape that was the same for all locations in the country.

In order to more accurately identify the hazard level at the site, synthetic ground motions representative of those expected at St. Louis were used to develop a site-specific design spectrum. Researchers at the Mid-America Earthquake Center have developed a suite of ten time histories representative of the motions expected in St. Louis due to large earthquakes from the NMSZ and due to smaller earthquakes generated by the background hazard. These motions, along with the spectra from NCHRP 12-49 were used to develop a site-specific spectrum for this project.

Figure 5 shows the maximum, minimum, and median rock response spectra from the suite of synthetic motions along with the NCHRP 12-49 Soil Class B spectrum. At longer periods, the maximum of the suite of motions exceeds the design spectrum. Therefore, a modification to the design spectrum is shown which has

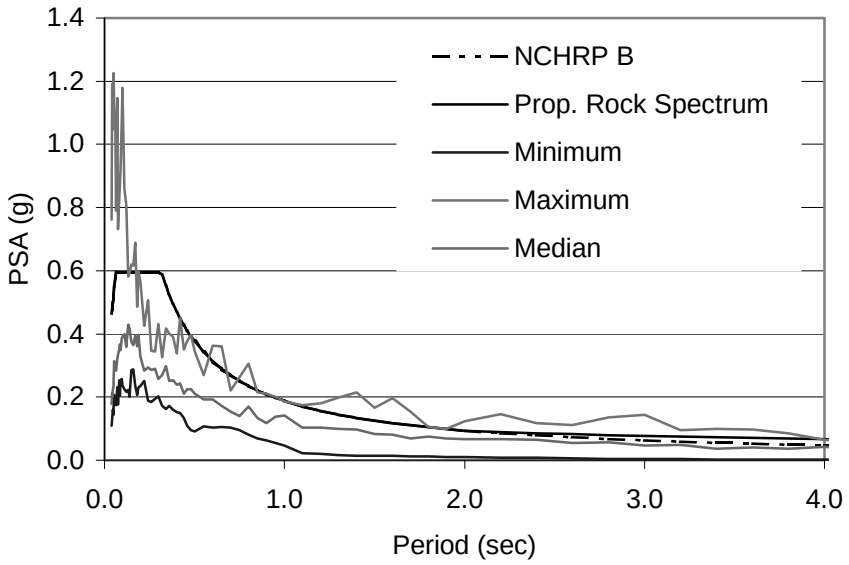

Figure 5. Design spectra

project design guidelines for structures with foundations providing direct lateral connection with the bedrock, such as dredge well caissons.

Liquifaction Induced Lateral Spread

In addition to the inertial forces due to the earthquake accelerations defined by the above spectra, the foundations of the main span will be subjected to significant lateral spread forces arising from the susceptibility of the local soils to liquifaction. Preliminary investigations identified potential liquifaction zones as deep as 50 ft below grade on the Illinois side of the river and extending hundreds of feet eastward into Illinois.

These liquifaction zones along with the cut formed by the Mississippi river presents a potential for gross soil movements toward the river. As the foundations to the bridge will present obstructions to the flow of soil, large riverward horizontal forces will be induced. Investigations have been begun into potential soil improvement techniques to reduce the extent of the liquifaction zones, but for the present the foundations will be sized to accommodate the full lateral spread forces.

STRUCTURAL BEHAVIOR

The behavior of the bridge in the longitudinal direction under seismic loads is in large part determined by the articulation option chosen. For the NMRB, the use of inclined towers introduces additional constraints which affect the articulation of the main span, and thus the seismic behavior.

Articulation

In most self-anchored cable-stayed bridges, the permanent force horizontal components of the main span cables and the anchor cables exactly balance. The towers supply only vertical support. An inclined tower has the potential to create enormous moments due to the centroid of the tower at the base having a large eccentricity from the vertical cable forces unless structural actions are taken.

One way to reduce this bending moment is to turn the resultant of the cable forces to the inclination of the tower. This is achieved by releasing some load from the side span cables through the selection of cable camber and creating an imbalance in the horizontal component of the cable force. However, the imbalance in cable forces is reflected in an imbalance in the deck forces in the main span and side spans.

There are two different approaches for dealing with the unbalanced forces in the deck. One option is to use the deck as a tension tie, allowing the two towers to pull against each other. The other approach is to fix the deck to both towers, using the unbalanced force in the deck to equilibrate the horizontal component of the inclined tower force. In this case, an expansion joint will need to be introduced at midspan to allow for thermal movements of the superstructure.

It was found that the second option, utilizing and expansion joint at midspan and integrally connecting the superstructure to the tower, possessed significant advantages. They are:

- Vertical loads to the foundations. The resultant of the inclined force in the tower and the unbalanced horizontal thrust in the deck is vertical below the deck level, resulting in no dead load shear on the foundations, unlike the other approach.
- Minimal thermal tower moments. By essentially de-coupling the towers by the introduction of the midspan expansion joint, the thermal moments induced in the towers drop to a negligible level.
- Elimination of bearings. The removal of the requirement of the superstructure to slide at one or both towers, as would be required in the other approach, allows an integral connection between the superstructure and the tower, eliminating the need for sliding bearings at the tower.
- Simplified construction. Because the state of the bridge during construction and in service are the same, no redistribution of forces is required during construction, eliminating a potentially difficult erection step.

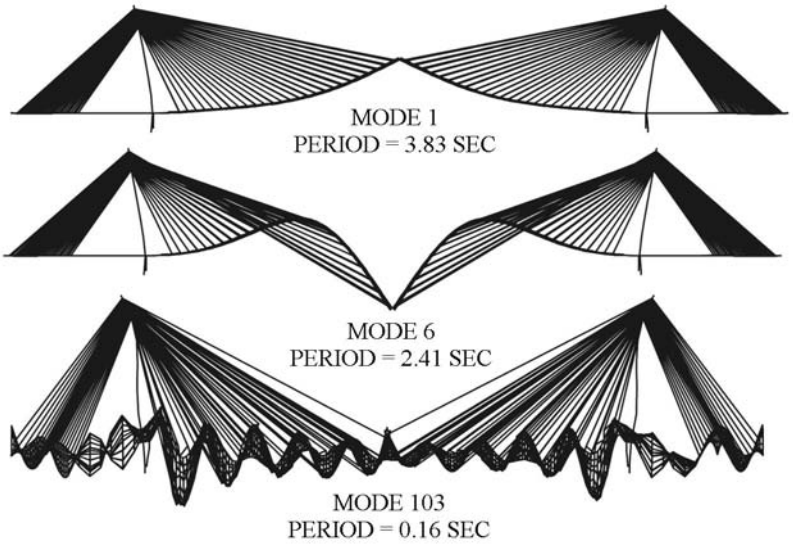

Figure 6. Vertical mode shapes

The expansion joint at midspan will be able to transmit both vertical and transverse shears between the two halves of the bridge, and also torsional moments. The bending moments in the remaining two directions, along with axial thrusts, will not be transmitted. This type of joint has been used in previous cable stayed bridges, most notably the Dame Point bridge in Florida and the Barrios de Luna bridge in Spain. Additionally, prestressed segmental concrete bridges often use similar hinges at the midspan or quarterspan.

Mode Shapes

The dynamic properties of the bridge are best evaluated by examining the modal shapes and periods. Cable stayed bridges are characterized by having a relatively large number of closely spaced modes which contribute to the dynamic properties. It is instructive to categorize as much as possible the modes as vertical, longitudinal, or transverse in nature.

Vertical modes

Because of the long span length of the bridge, the first modal periods are relatively long. Figure 6 shows three important vertical modes of the bridge. Mode 1 is a symmetrical bending mode with a period of 3.83 sec. This is the longest period of the bridge. The action of the center expansion joint is clearly visible. Mode 6 is the next symmetrical bending mode with a period of 2.41 sec. Both of these modes primarily involve movement in only the main span. The towers do not become active until mode 103, a vertical vibration mode of primarily the towers, with a period of only 0.16 sec.

Transverse modes

Due top the large structural width of the bridge, and the three dimensional arrangement of the cable stays, the transverse modal periods are relatively short for a bridge of this span. The first transverse mode, mode 2, shown in Figure 7, has a period of 3.07 sec., much less than the first vertical mode. It is a symmetric, simple transverse bending mode. The next important transverse mode is mode 17 with a period of 1.01 sec. In this mode, the side spans have become activated due to the transverse flexibility of their supporting piers. This is an unsymmetrical mode shape, due in part to the differing side span arrangements. Mode 26, another symmetric lateral mode, has a period of only 0.69 sec.

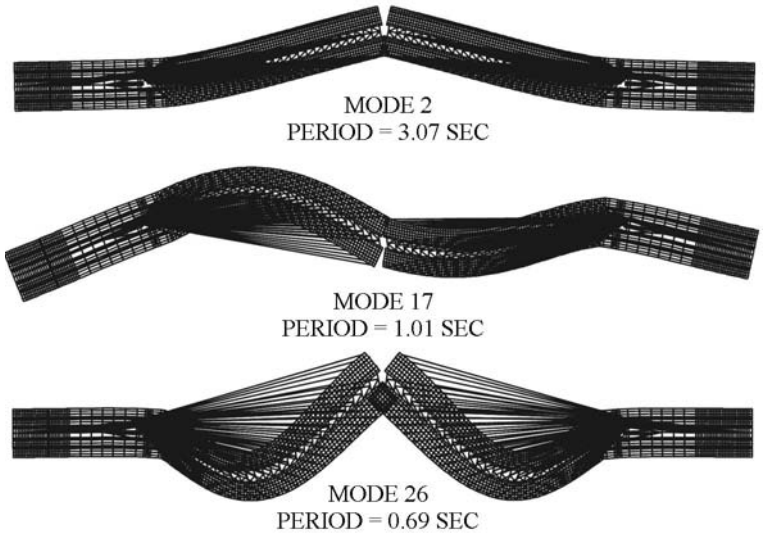

Figure 7. Lateral mode shapes

Longitudinal modes

Because the superstructure is integrally connected to both towers, and because the tower sections below deck level are very stiff, the longitudinal periods of the bridge are much shorter than in the previous directions. The first longitudinal mode has a period of only 0.74 sec. Figure 8 shows three important longitudinal modes. Because of the different tower foundation stiffnesses, and the different side span arrangements, all of the longitudinal modes are unsymmetrical.

Other modes

Because of the unique features of this bridge, there is a large amount of coupling between mode shapes, such that many modes have significant components in one or more of the bridge axes. In addition, there exist also a number of torsional modes. However, these do not have much impact on the seismic response of the bridge.

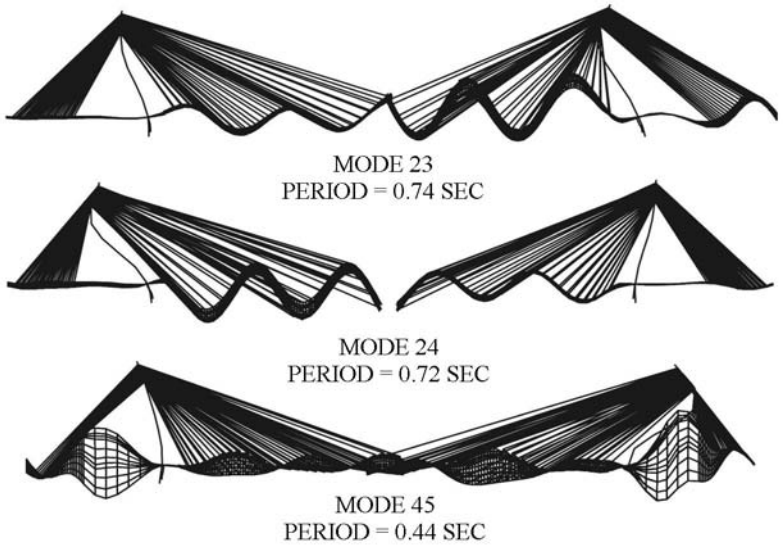

Figure 8. Longitudinal mode shapes

SEISMIC LOADS

For this preliminary analysis, the multi-modal response spectrum analysis was used. The design spectra was applied in both horizontal directions, along with 2/3 of the spectrum in the vertical direction. Of interest at present is the determination of the global response of the structure, and not the demands on the individual components of the structure. The global response will be characterized by examining the base reactions, the global displacements, and the tower moment diagram.

Reactions

Table 1 lists the reactions at the bases of the Missouri and Illinois towers due to the seismic loads. Forces are given in kips and moments in kip-ft. The longitudinal direction is parallel to the direction of traffic, while the transverse is perpendicular. For the moments, the longitudinal moment acts about the longitudinal axis, as does the transverse moment about the transverse axis, while the torsional moment acts about the vertical axis.

Examining the reaction forces, the longitudinal forces are nearly twice those from the other two directions. This occurs due to the much stiffer, and hence shorter period, behavior of the bridge in this direction. In general, as the period decreases, the seismic demands increase, as is shown in the design spectrum. This large longitudinal force then induces the large moment about the transverse axis.

The torsional moments come from two sources; inertia of the tower, and transverse bending of the superstructure. Because the tower is inclined, transverse forces will induce a torsional moment about a vertical axis. This is equally valid for transverse inertia forces such as those induced by seismic ground accelerations. The second source of torsion comes from the fixed nature of the integral connection between the superstructure and the tower. The rotational restraint provided by the tower to the deck against rotation about a vertical axis creates the torsional moment.

Displacements

Despite the large magnitudes of the seismic base reactions, the displacements remain relatively small. Table 2 shows the seismic displacements at midspan and at the tower top. The maximum displacements of the deck occur at midspan. The order of the displacement values follows that displayed in the modal periods. The longitudinal direction is stiffest, and has the smallest displacements, followed by the transverse and the vertical directions. The vertical displacements, although the largest, is still very small when compared to the length of the main span. Expressed as fraction of the span length, the displacement is roughly equal to L/2000.

The tower top displacements show a similar trend, only in this case the vertical displacement is the smallest. Again, this agrees with the modal results, as the first vertical mode the includes vertical tower motions has a very short period. In evaluating the magnitudes of the tower displacements, it is useful to note that the maximum displacement is roughly only 0.1% of the tower height.

TABLE I. SEISMIC REACTIONS AT TOWER BASE

Tower	Longitudinal Force	Transverse Force	Vertical Force	Longitudinal Moment	Transverse Moment	Torsion
Missouri	40,000	15,000	22,000	1,100,000	3,100,000	410,000
Illinois	38,000	16,000	21,000	1,100,000	2,800,000	340,000

TABLE II. SEISMIC DISPLACEMENTS

Location	Longitudinal	Transverse	Vertical
Mid-span	0.119	0.779	1.14
Tower top	0.213	0.446	0.027

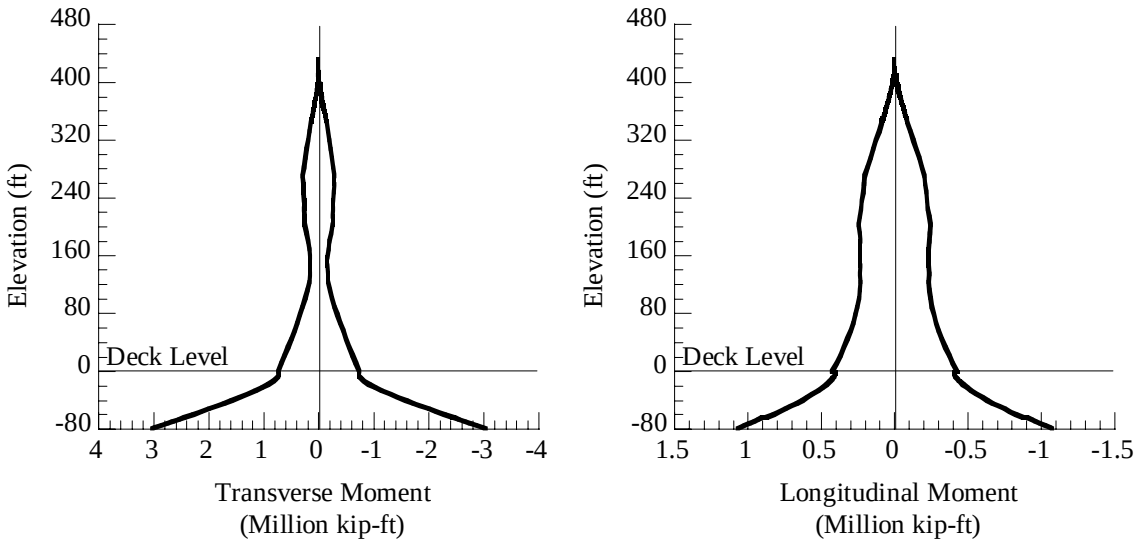

Figure 9. Tower seismic moments

Tower Moments

The moments in one tower due to seismic loads are shown in Figure 9. The moments are plotted versus elevation, where zero corresponds to deck level. Nomenclature is the same as for base reactions. From the graph it is clear that the majority of the transverse moment at the base is due to the inertia forces from the deck. For the longitudinal moments, this is still true although the contribution of the tower above deck level is somewhat higher. The flat slop of the moment diagram below deck elevation indicates a very high shear force. The forces from the tower above the deck, either due to the vibration of the tower itself or to load entering the tower through the cables, are small in comparison to the large shears at deck level.

SUMMARY

The NMRB is an inclined tower cable stayed bridge with a main span of 2000', which will make it the longest bridge of its type in the Western Hemisphere. It crosses the Mississippi river just north of downtown St. Louis. The seismic design is based on a 2500 year return period event, with the performance objectives of minimal damage and immediate serviceability.

The bridge articulation consists of integrally connecting the superstructure to the towers and providing expansion joints at midspan and at the connections to the approaches. This creates relatively short period modes of vibration in the longitudinal direction of the bridge. The transverse modes are also shorter due to the width of the superstructure. The seismic base reactions in the longitudinal direction are roughly twice those in the transverse direction. Most of the seismic moments in the lower portion of the towers comes from the superstructure and not from the tower itself or through the cables.

ACKNOWLEDGEMENTS

The NMRB project is a collaboration between the Missouri and Illinois Departments of Transportation, with Illinois as the lead owner. HNTB, Inc. is the Project Management Consultant. The preliminary engineering phase of the design of the NMRB was conducted by a team of consultants. The major team members were:

Modjeski and Masters, Inc.	Prime Consultant - Design of main bridge
Alfred Benesch & Co., Inc.	Design of approach spans and main bridge foundations
Hanson Professional Services, Inc.	Geotechnical consultant
TRC –	Side span consultant
H2L2, Inc. –	Lead Architects, preliminary plans
Rosales Gottemoeller & Associates, Inc.	Architectural consultant
KAI, Inc.	Architectural consultant
Jacobs Facilities	Architectural consultant

REFERENCES

[1] ATC/MCEER 2000. "NCHRP 12-49: Comprehensive Specifications for the Seismic Design of Highway Bridges - Draft," National Cooperative Highway Research Program, Washington, D.C.

[2] Hanson Engineers 2001. "Preliminary Geotechnical Report I-70 Mississippi River Bridge St. Louis County, Missouri, St. Clair County, Illinois," Hanson Engineers Inc., Springfield, Illinois.

[3] Wen, Y.D. and Wu, C.L. 2002. "Uniform Hazard Ground Motions for Mid-America Cities," *Earthquake Spectra* 17(2):359-384.

Seismic Design of the Skyway Section of the New San Francisco-Oakland Bay Bridge

Brian Maroney, Sajid Abbas, Madon Sah, Gerald Houlahan and Tim Ingham

ABSTRACT

The seismically vulnerable eastern span of the San Francisco-Oakland Bay Bridge will be replaced with a dual, 3.5-kilometer long parallel structure. The bridge will be situated between the Hayward and the San Andreas faults, which can generate large earthquakes. Performance criteria require that the bridge be operational following a 1500-year return period earthquake from either of these two faults.

The middle 2.0 kilometers of the new bridge consist of a segmental concrete "skyway" with spans varying from 96 to 160 meters in length. This will be constructed using the balanced cantilever method of segmental construction. The superstructure is a box girder 9 m deep at the pier and 5.5 m deep at midspan. The box is 25 meters wide and designed to carry either 5 lanes of highway traffic with standard shoulders or 4 lanes of traffic with a light rail system. Mid-span hinges between longitudinal frames allow longitudinal expansion and contraction due to creep, shrinkage and temperature changes. An internal steel beam assembly at the hinge provides shear transfer and moment resistance in addition to controlling deflections at the cantilever end of each frame.

A typical footing is supported by six 2.5 meter diameter battered piles. The average length of these piles is about 100 meters. They consist of driven steels shell with a composite reinforced concrete fill in the upper section. The design of the pile caps is based on capacity design principles. In order to transfer the over-strength moments from both the pier and the piles, they are to be constructed from (concrete encased) structural steel.

The piers are box shaped and sculpted to architecturally match the main pylon of the signature suspension bridge. The typical dimensions are 6.5 m x 8.5m. The main reinforcement is placed in the four corners of the box; heavy confinement is provided with closely spaced hoops to ensure ductile behavior. The pier is the most critical element in the bridge from a seismic design standpoint; it is the only element designed to yield and form plastic hinges during a safety evaluation earthquake.

The design approach was to adopt a stiff foundation system thereby controlling pile cap elastic displacements to acceptable levels and minimizing the potential for permanent pile cap offsets. A relatively stiff foundation system was achieved through the use of large diameter battered piles.

Brian Maroney, Ph.D., P.E., Brian_Maroney@dot.ca.gov, 510-286-5885
Sajid Abbas, Ph.D., P.E.;sabbas@tylin.com, 415-291-3741
Madon Sah, P.E.; msah@tylin.com, 415-291-3770
Gerard Houlahan, P.E.; ghoulahan@moffattnichol.com, 415-227-4080
Tim J. Ingham, Ph.D., S.E.; tingham@tylin.com, 415-291-3781, T.Y. Lin International, 825 Battery Street, San Francisco CA 94111

Seismic Design Strategy of the New San Francisco-Oakland Bay Bridge Self-Anchored Suspension Span

Marwan Nader, Jack López-Jara and Claudia Mibelli

ABSTRACT

The East Spans of the San Francisco Oakland Bay Bridge were closed in 1989 when a 50-ft portion collapsed due to the 7.1 M Loma Prieta Earthquake. Seismic evaluation of the bridge performed by the California Department of Transportation concluded that replacing the East Bay Bridge was more cost effective than a seismic upgrade of the 50 year old bridge. T.Y.Lin International and Moffatt & Nichol, a joint venture, were hired in 1998 to design the new bridge which consisted of a skyway portion and a signature span. This paper focuses on the seismic design strategy that was employed in the selection process of the signature span type and the design phase.

A total of six design options for the signature span were proposed and developed including cable-stayed bridges and self-anchored suspension bridges. The three alternatives of each bridge type consisted of a single tower, dual portal towers and three-legged tower. Each of these design alternatives was evaluated based on its seismic response, construction cost and aesthetics. Because this is a seismic safety replacement project, the seismic behavior and design of each option were the most important factors in the selection process.

The Bay Bridge is located between the Hayward fault and the San Andreas fault which are capable of producing a magnitude 7.5 and 8 earthquakes, respectively. Design criteria for the Bay Bridge require it to be operational within 24 hours after a major earthquake. The seismic behavior of each solution was evaluated based on dynamic analysis, push-over analysis and various parametric studies to evaluate the structural lateral system. The selected design was a single tower asymmetric self-anchored suspension bridge.

To provide a seismically reliable design, the selected alternative included: (1) Shear Links between the tower shafts which would yield in the event of a major earthquake, these links may be replaced afterwards if necessary (2) a floating deck isolated from the tower; and (3) a tie-down/counter weight at the West pier (W2) to insure stability after the pier yields.

Marwan Nader, T.Y.Lin International, 825 Battery St. San Francisco, CA 94111
Jack López-Jara, T.Y.Lin International, 825 Battery St., San Francisco, CA 94111
Claudia Mibelli, T.Y.Lin International, 825 Battery St., San Francisco, CA 94111

INTRODUCTION

The San Francisco-Oakland Bay Bridge was constructed in 1936. At that time, it was one of the longest high-level bridges in the world. Today, it carries 280,000 vehicles a day and is the busiest bridge in the world. Figure 1 shows the bridge's geographical location. The 1989 Loma Prieta Earthquake seriously damaged the East Span of the bridge when a 15-m portion above Pier E-9 collapsed onto the lower deck; the bridge was closed for repairs for a period of four weeks. Post-earthquake inspections revealed that another portion above Pier E-23 nearly experienced a similar collapse. Seismic evaluation of the bridge performed by the California Department of Transportation concluded that replacing the East Span of the Bay Bridge was more cost effective than a seismic upgrade of the 50-year old bridge.

T.Y.Lin International and Moffatt & Nichol, a joint venture, were hired in 1998 to design a new bridge consisting of a skyway portion and a signature span. A Self-Anchored Suspension bridge (SAS) and twin 2.4-km concrete viaducts will replace the existing and seismically unsafe eastern crossing. This design was selected by the Metropolitan Transportation Commission out of four other competing designs (Figure 2). The span lengths planned for this bridge make it the longest self-anchored suspension bridge in the world. The new bridge will carry 5 lanes of highway traffic, however, it is designed to carry 4 lanes of highway and one lane of light rail transit as a future alternative to improve the transit in the Bay Area.

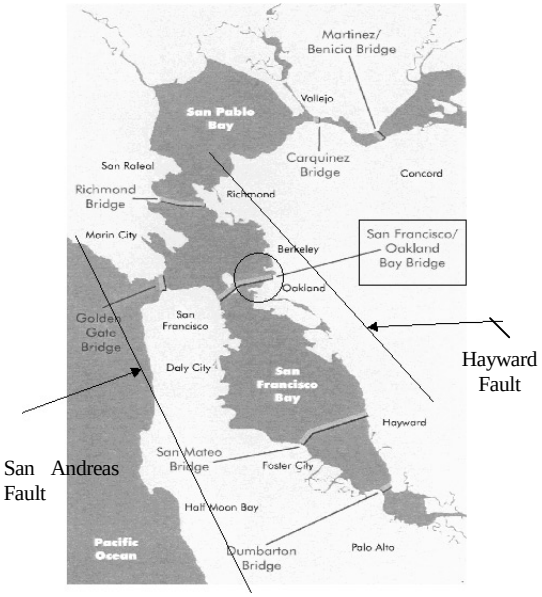

Figure 1. Geographical Location of Bridge

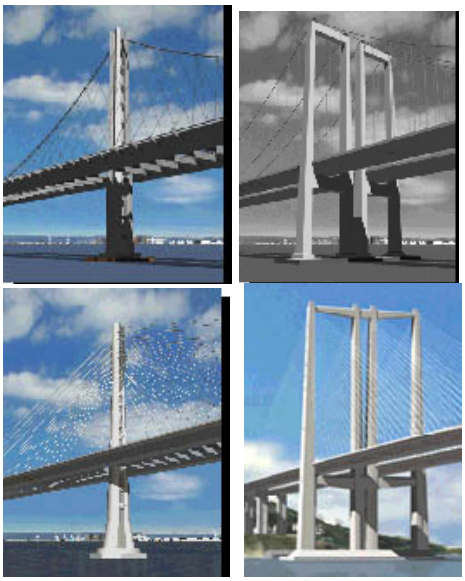

Figure 2. Design Alternatives for the Signature Span

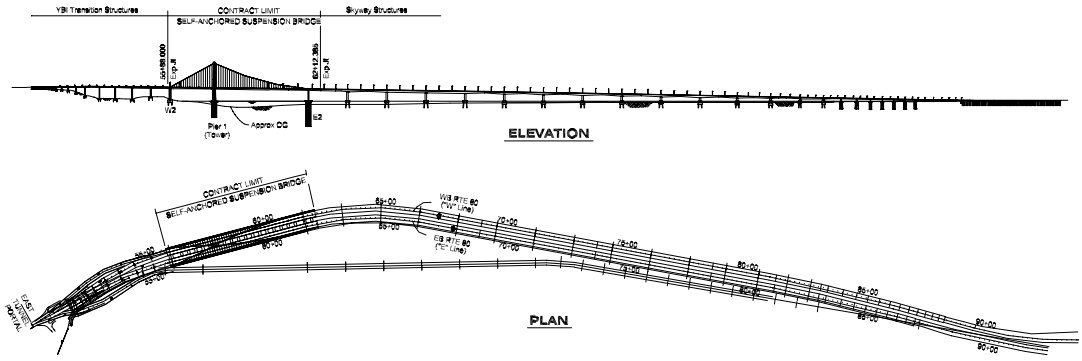

Figure 3. General View of the New East Bay Bridge

DESCRIPTION OF THE BRIDGE

The Self-Anchored Suspension Bridge consists of a 385m main span and a 180m back span supported by a cable system connected to a single tower (Figures 4 and 5). The lateral resisting system of the bridge consists primarily of the West Piers (W2) and East Piers (E2). The 0.78m diameter cable is anchored to the deck at the East bent (E2) and is looped around the West bent (W2) through deviation saddles. Unlike traditional suspension bridges, these deviation saddles are fixed to the West bent and the cable force on either side is balanced during construction using a jacking saddle (Figure 6). These saddles are supported by a pre-stressed cap beam, which is designed to carry differential stresses during service and seismic loads. The weight of this cap beam is designed to balance the dead load uplift at the West bent arising from the asymmetry of the bridge. The cables at the tower do not cross and are secured in a single saddle. The saddle at the East pier is supported by the box girders and is designed to move in order to balance the cable forces on either side. The suspenders, spaced at 10m, are splayed to the exterior sides of the box girders. The superstructure consists of dual hollow, ASTM Grade 50, orthotropic steel boxes (Figure 7). These boxes are in compression (supporting the cable tension forces) and are a part of the gravity load system. Diaphragms spaced at 5m support the orthotropic deck and distribute the suspender loads to the box. The box girders are connected together by 10m-wide, 5.5m-deep crossbeams spaced at 30m. These crossbeams carry the transverse loads between the suspenders (span of 72m) and ensure the composite action of both boxes during wind and seismic loads.

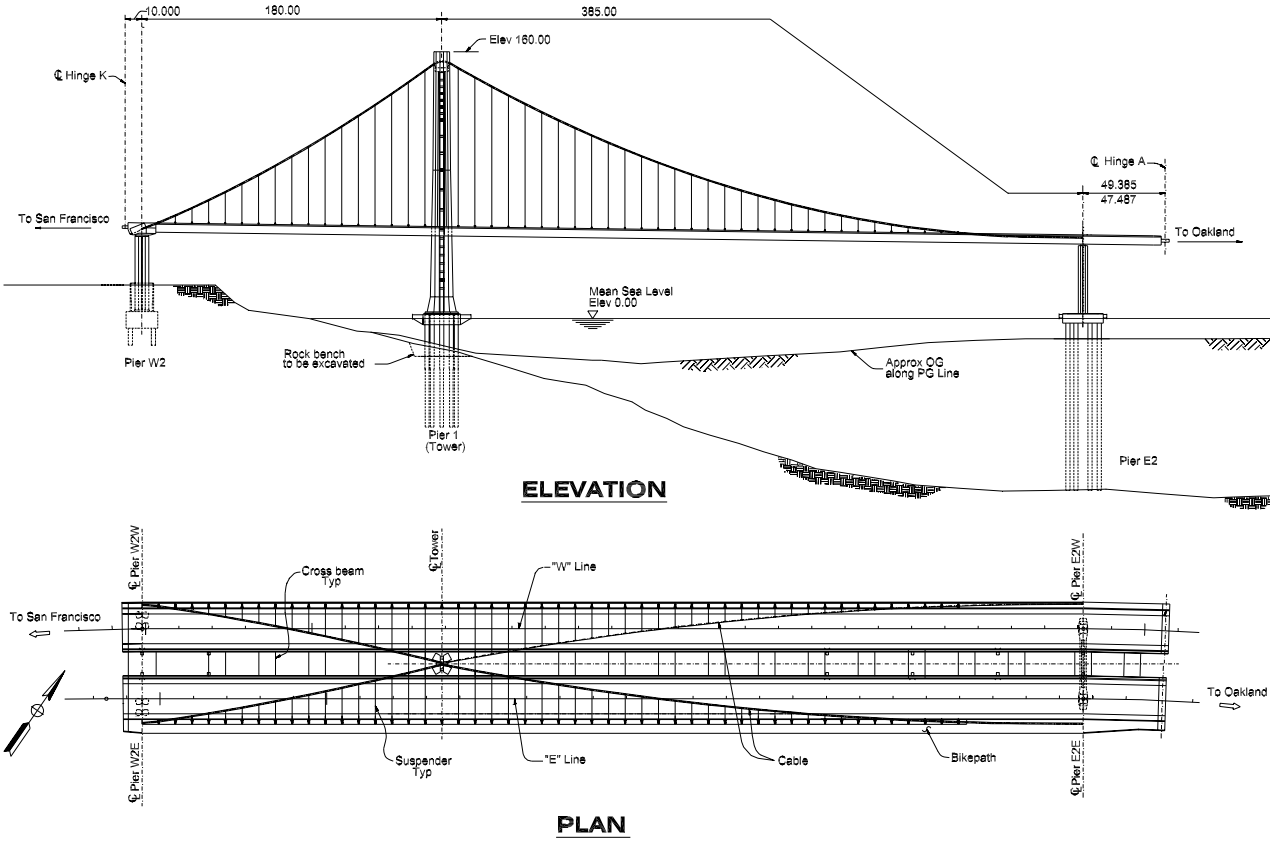

Figure 4. Elevation and Plan of the Self Anchored Suspension Bridge

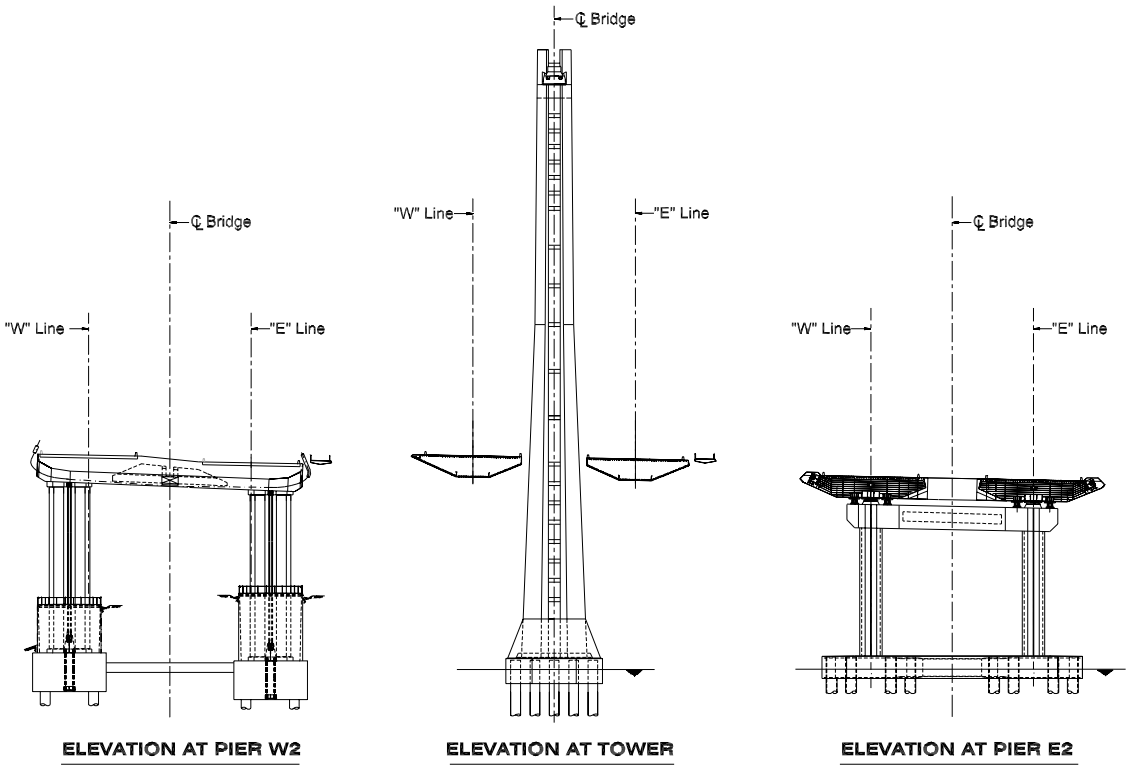

Figure 5: Elevation of Bridge at Piers and Main Tower

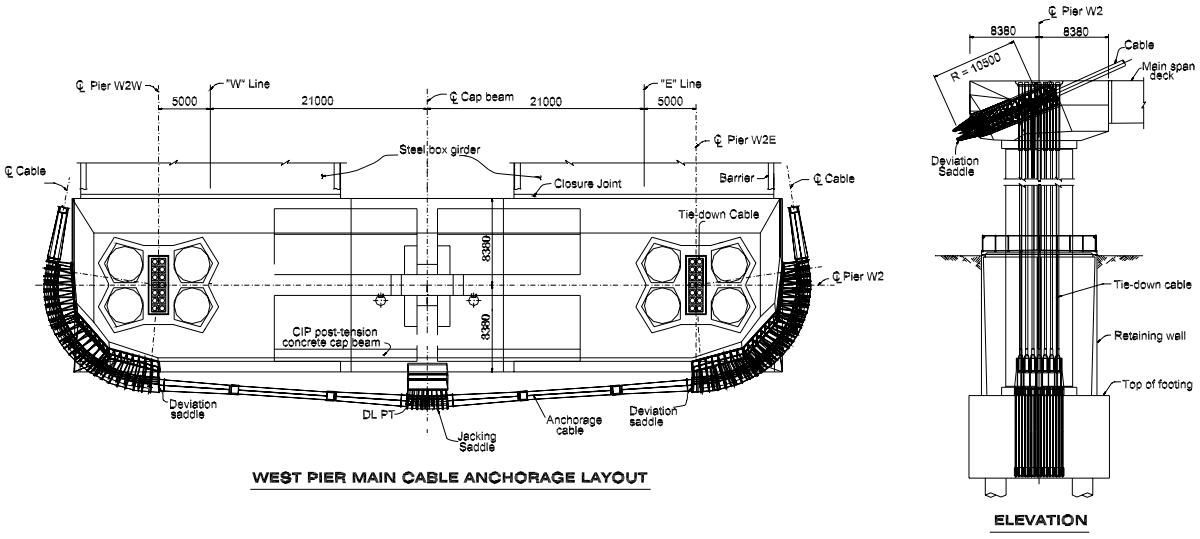

Figure 6. West Anchorage – Looped Cable throughout two Deviation Saddles.

As shown in Figure 6, the bridge carries a pedestrian path on the south side. This eccentric load is balanced by a counter-weight on the north side. At the West bent, the box girders frame into the cap. The connection between the orthotropic steel box girders and concrete cap beam is subjected to the compressive forces of the cables. Additional pre-stress is added through longitudinal post-tension strands at each rib .

The single tower is 160m tall and is composed of four shafts connected with shear links along its height (Figure 5). The tower shafts are tapered, stiffened, steel box members, with diaphragms spaced at 3m. The tower is fixed to the 6.5m deep pile cap (consisting of steel moment frame encased with concrete) and is supported on 13 - 2.5m steel shell pipe piles (filled with concrete) which in turn are embedded and fixed into rock. The rock slope is benched to give the piles equal lateral stiffness and avoid torsional response (pile clear length is about 20m). The East piers are made of reinforced concrete supported on 16 – 2.5m steel pipe piles. These piles are 100 m long and are filled with concrete for the top 55m. The West piers are reinforced concrete columns that are monolithic with the pre-stressed cap beam (forming the West bent). The tie down system at the West pier, designed to resist the seismic uplift, consists of 28 cables (61-15mm diameter strands each) which are anchored into a gravity foundation with 4-2.5 CIDH piles that serve as shear keys. At the East piers the box girders are supported on bearings. Shear keys and tie rods are provided to carry lateral loads and uplifts, respectively. The box girders are supported at the East and West pier and are "floating" at the tower. The transition spans between the Skyway, Suspension Bridge and Yerba Buena Island Structure are connected through hinges. These hinges are designed to allow the structures to move relative to each other in the longitudinal direction only (Figure 8).

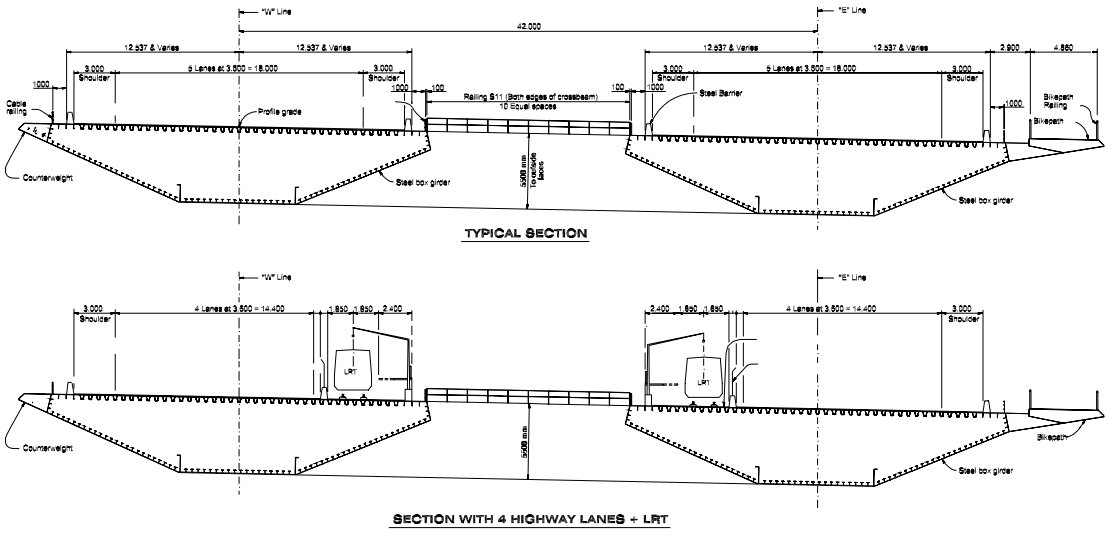

Figure 7. Bridge Typical Cross Section Alternatives.

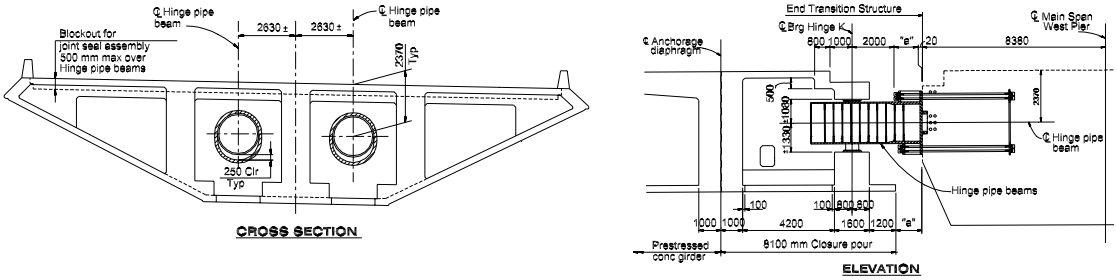

HINGE BETWEEN SELF ANCHORED SUSPENSION BRIDGE AND YBI STRUCTURE

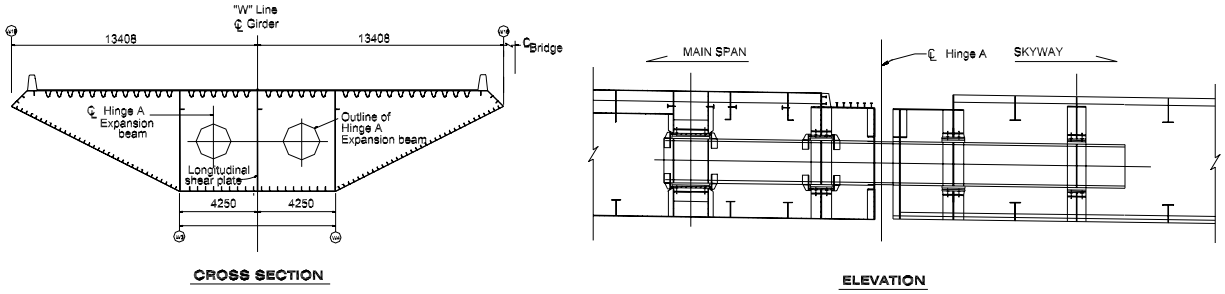

HINGE BETWEEN SELF ANCHORED SUSPENSION BRIDGE AND SKYWAY STRUCTURE

Figure 8: Hinges between Transition Structures and Self-Anchored Suspension Bridge.

SITE CONDITIONS AND SEISMICITY

The Bay Bridge is located between the Hayward and the San Andreas faults which are capable of producing magnitude 7.5M and 8M earthquakes, respectively. The proposed bridge alignment is underlain by variable subsurface conditions. While the West pier sits on Yerba Buena Island and the tower is located on relatively shallow sloping bedrock, the East piers and the remainder of the skyway will be founded in deep soils. Spectrum compatible ground motions were generated for this site (three for Hayward and three for San Andreas). Figure 9 illustrates the fault normal spectral accelerations for San Andreas Ground Motion No. 3. As noted, the characteristics of these motions are very distinct.

SEISMIC PERFORMANCE CRITERIA

The bridge is designed to provide a high level seismic performance. It is designed to resist two levels of earthquake, a functional evaluation earthquake (FEE) and a safety evaluation earthquake (SEE). After a functional evaluation earthquake, the bridge will provide full service almost immediately and there will be minimal damage to the structure. Minimal damage implies essentially elastic performance and is characterized by minor inelastic response, narrow cracking in concrete, no apparent permanent deformations, and damage to expansion joints. After a safety evaluation earthquake, the bridge will provide full service almost immediately and will sustain repairable damage to the structure. Repairable damage is damage that can be repaired with minimum risk of losing functionality; it is characterized by yielding of reinforcement, spalling of concrete cover and limited yielding of structural steel.

In addition, the bridge has been designed to satisfy the following criteria: (1) provide a clearly defined plastic mechanism for response to lateral loads with all components (except the E2 and W2 Piers, the Main Tower shear links, and the hinge pipe beams) designed to remain essentially elastic under all known seismic demands; (2) provide fully ductile load paths for all critical components, thus, they have been detailed to be ductile under hypothetical overload conditions at any location; and (3) the detailing and proportioning requirements for full-ductility structures.

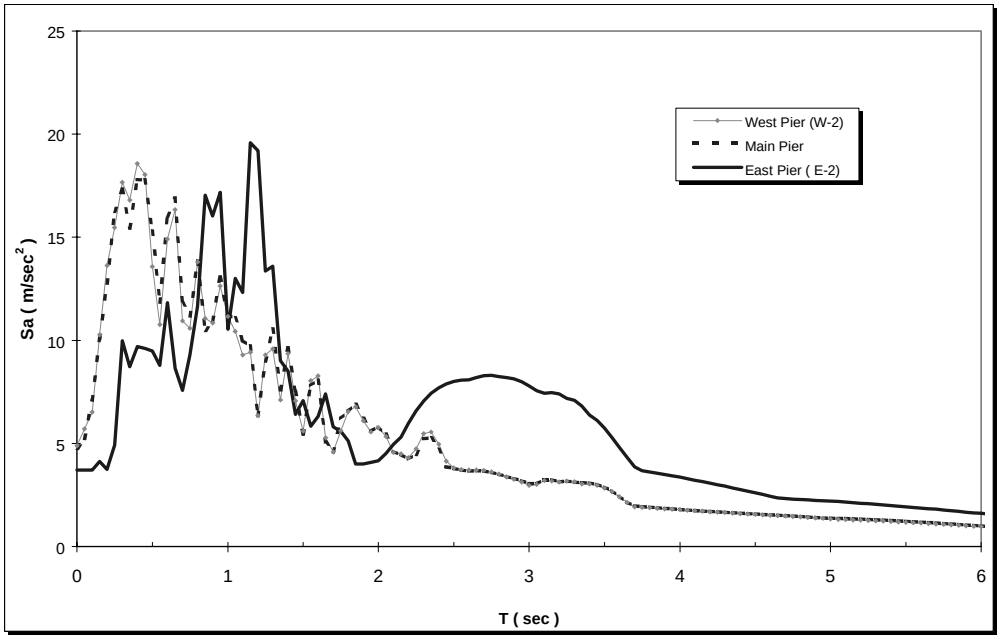

Figure 9. Fault Normal Response Spectrum of the San Andreas Ground Motion No. 3

ANALYSIS METHODOLOGY

Seismic analysis was performed using the ADINA general-purpose finite element program. Three forms of analysis were employed: time history analysis (global model), push-over analysis and local detailed analysis. Time history was used as the primary means of analysis for several reasons. Foremost among these is that the bridge foundations are subjected to different excitations. The tower and West pier of the bridge are founded on rock while the East pier is supported in deep soil. The ground motions at these supports are completely different in character and intensity. This was reflected in the analysis by applying different time histories of ground displacement at the supports. Large displacement analysis and the use of nonlinear material properties where necessary, allow the designers to capture the true behavior of the bridge (geometric stiffness of bridge, P-delta effects, slacking of suspenders, plastic hinging of piers, tower shear links, etc.). The model was ”built” in a single step, in the dead load state. Initial strains in the deck, cables and suspenders were applied in this single step rather than simulating the construction sequence of the bridge. Time history analyses were done as restart analyses from the dead load state. Push-Over analyses were primarily used to evaluate ductility of critical elements and to establish failure mode sequence. Local detailed analyses were used to establish local strain/stress demands and to evaluate the modeling used for the global model.

DESCRIPTION OF ANALYTICAL MODEL

In addition to the Self-Anchored Suspension Span structure (SAS), the ADINA global model includes boundary frames representing the transition structure on Yerba Buena Island (YBI) and the first frame of the Skyway to ensure accurate boundary conditions (Figure 10). The model consists of linear and nonlinear beams and truss elements.

The bridge deck is modeled with two parallel spines comprised of elastic beam elements representing the axial, bending, and torsional properties of the box girders. Their axes coincide with the box girder cross sections centers of gravity, and follows the prescribed bridge alignment and profile. Beam elements extending from the spine to the edge of the bridge deck provide connection points for the suspenders at their working point locations. These elements capture the deck stiffness for vertical deformations and are rigid for transverse deformations.

Beam elements are cantilevered out from the East Bound spine to the bike path's center of mass location, where the masses of the bike path are lumped. Similar beam elements also extend towards the counterweight center of mass at the West bound. The crossbeams were also modeled with elastic beams. A local detailed model of the dual box girders and cross beams was used to evaluate and calibrate the stiffness of the crossbeams. Due to warping and shear flexibility, the actual stiffnesses are significantly less than those that could have been calculated based on simplified beam theory. Based on the detailed model, an equivalent shear area was used for the crossbeam.

The suspenders were modeled with non-linear tension-only truss elements. This was done to allow the suspenders to go slack, if necessary, under dynamic loading. The cable is modeled with elastic truss elements and passes through the cable PIs (intersection points of the tangents to the cable profile where cable changes direction through the saddles) at Pier W2, the Main Tower, and Pier E2. The cable terminates at the working point of the East anchorage. The cable model does not loop around W2. Instead, it is modeled by forces at each of the two PIs equivalent to the cable forces directed towards each other as dictated by equilibrium conditions. Since the W2 deviation saddles are fixed, each PI is connected to the saddle working point through rigid beam elements. This technique is a reasonable representation since the friction between the cable and deviation saddle is sufficient to secure the cable against sliding.

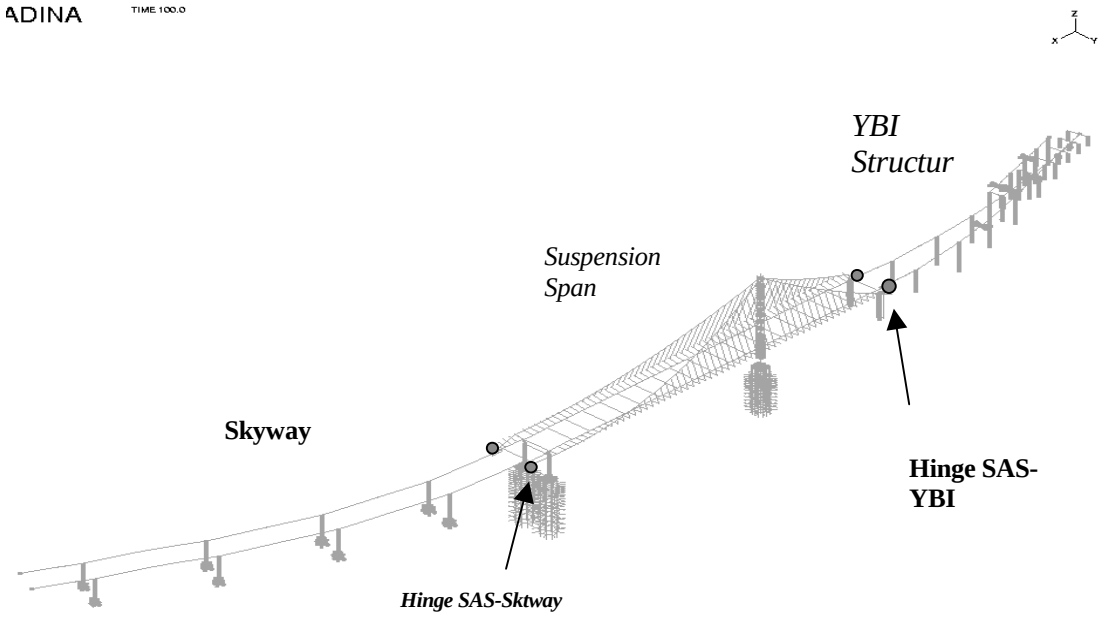

Figure 10:SAS Global ADINA Model

The main tower saddle PIs are connected to the tower through "rigid links" The tower saddle is bolted to the tower grillage. Friction between the cable and saddle troughs secures the cables against sliding. The East Saddle PIs are connected directly to the East saddle crossbeam through a flexible member, since the saddles at this location can have relative movements with respect to the deck. This flexible member has local coordinates such that it allows for relative movement between the cable and the deck in the plane of sliding of the East saddle.

The four tower shafts were modeled with elastic beam-column elements. The tower base was modeled as a single leg with elastic beam-column elements and properties that account for all shear walls and stiffeners. At the top of the tower, the grillage rigidly connects the 4 tower shafts (Figure 11).

The shear links between the main tower shafts were modeled with inelastic moment-curvature beam elements. These inelastic beam elements were calibrated based on the shear-displacement relationship obtained from a detailed

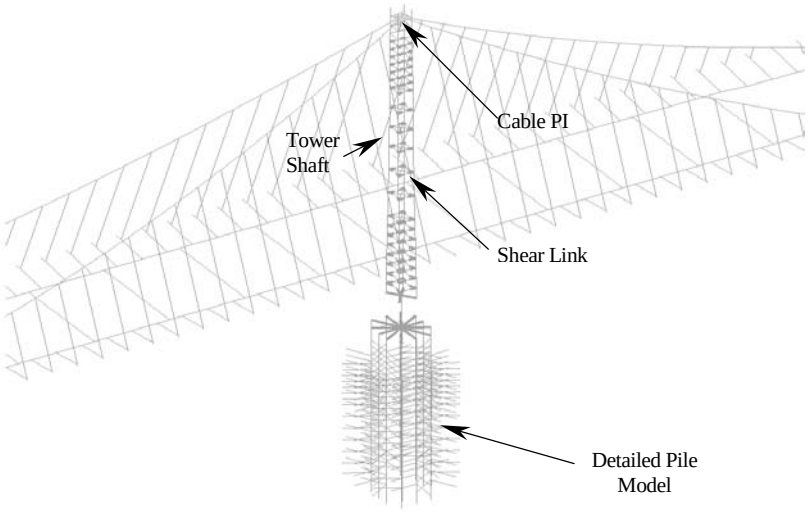

Figure 11: Main Tower Model.

local model. The yield moment of the inelastic beam elements are set to obtain the corresponding shear capacity of the shear link for the same yield vertical displacement. The rotation of the beam plastic hinges serves as a measure of the shear deformations of the links.

The East and West piers were modeled with nonlinear beam-column elements. The moment-curvature relationships were calculated for a wide range of axial forces to capture the variations that occur during an earthquake. The pier elements are connected to the deck elements according to realistic constraints. Pier W2 is monolithically connected to the cap beam while Pier E2 and the deck are connected through bearings and shear keys (Figure 12). The nodes representing the bearing and shear key location are connected to the top of the pier through two rigid beam elements. Additional nodes at the same location are rigidly connected to the geometric center of the spine at the pier location. The coincident bearing nodes (a pair of nodes for each bearing, two bearings separated by 8.5m for each pier) are constrained to move together in the vertical direction. An additional pair of coincident nodes for the shear key is constrained to move together in the longitudinal and transverse directions. Relative rotations are permitted.

Each pile in the Main Tower and E2 Pier foundation was modeled explicitly with several nonlinear beam elements, extending from the bottom of the pile cap to the pile tip. The soil and rock stiffness was modeled with p-y and t-z non-linear springs varying along the height with properties corresponding to each pile location. The mass of the foundation (including rotational mass inertia as well as hydrodynamic mass) was lumped at the center of gravity of the pile cap.

Since the West pier is founded on rock it was assumed fixed, and the ground motions were applied directly to the bottom of the pier.

The effective damping at the pile cap level at the E2 pier and Main Tower was tuned to achieve 5% and 2% damping respectively, by adding a viscous damper at the pile cap elevation. The effective damping in the model was confirmed by plucking the pile caps and measuring the log decrements of the displacements. Displacements in the order of SEE demands at the pile cap were used.

The skyway foundation model consists of beam elements representing each pile from the bottom of the pile cap to the mud-line. Below the mud-line, each pile was modeled with a 12 degree of freedom stiffness and damping matrices (spanning between two six degree of freedom nodes). The coefficients of the impedance matrices were varied with design iterations, according to the mud-line displacement of the piles. The ground motion was applied at the "bottom" nodes of the pile springs.

The hinges between the SAS and the Skyway (Hinge A) as well as the SAS and the YBI structure (Hinge K) were modeled explicitly. The hinge pipe beams were modeled using non-linear beams along with the proper constraints at the bearing locations.

Hinge K beams were fixed to W2 cap beam and constrained to the YBI structure at the bearing location in the transverse direction only. Gap elements were introduced in the vertical direction to torsionally decouple the SAS and

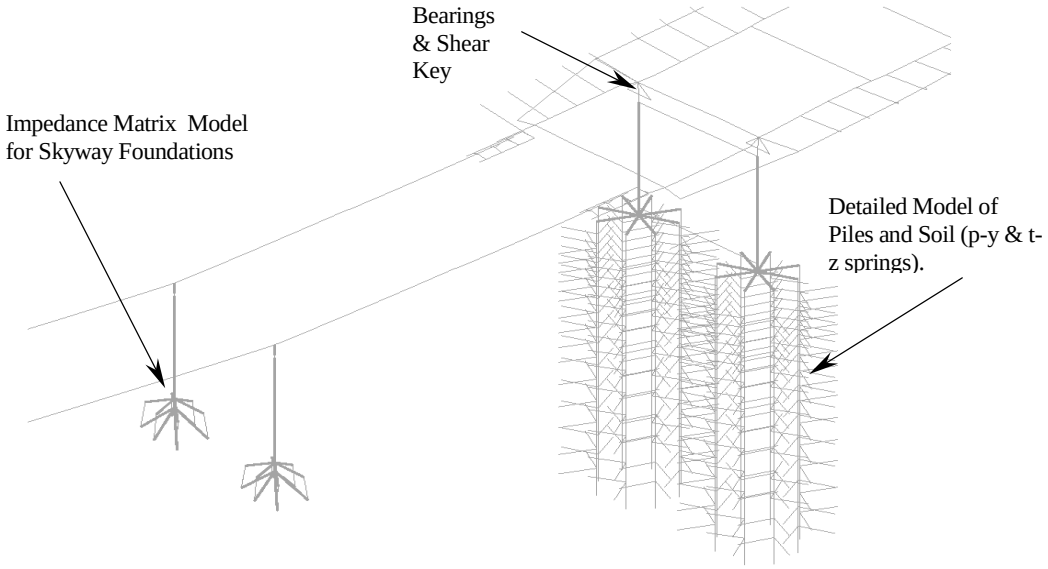

Figure 12: Foundation and bearing models

YBI Structures; the element allows uplift at the bearing during a SEE event, (see Figure 8). The gap element is comprised of a vertical spring with large stiffness under compression and very small stiffness under tension.

SEISMIC RESPONSE

The SAS design is primarily governed by Safety Evaluation Earthquake (SEE) demands. Distortion is limited to imperceptible levels and no immediate repair is required. The bridge, in accordance to the lifeline criteria adopted for this project is serviceable immediately following the SEE scenario.

The bridge is a long period structure and is mainly in the region of constant displacement demand, which improves the reliability of the structural response. The bridge vertical, longitudinal and transverse fundamental periods of vibration are 4.50 sec, 3.80 sec, and 3.64 sec respectively. Figure 13 summarizes the displacement demands on the bridge.

As discussed earlier, the bridge is designed to have a clearly defined plastic mechanism. Therefore, it remains largely elastic with the exception of the East Piers, the West Piers and the Tower Shear Links, which are designed to undergo inelastic deformations (Figure 14).

The maximum rotation demand on the Shear Links is 0.05 radians compared with an ultimate rotation capacity of 0.08 radians calculated per AISC- LRFD. A testing program was sponsored by Caltrans to verify the maximum capacity and ductility of the Shear Links. An ultimate rotation capacity of 0.07 radians was reported as a result of the full-scale testing of the shear link at the University of California at San Diego (UCSD), and 0.13 radians as a result of the half-scale testing performed at the laboratory of the University of Nevada, Reno (UNR). To avoid the premature stress concentrations that were observed at the juncture of the flange/ web/stiffener at the UCSD test, a cope size at the shear link stiffeners was increased thus, further improving the behavior as shown with the UNR test.

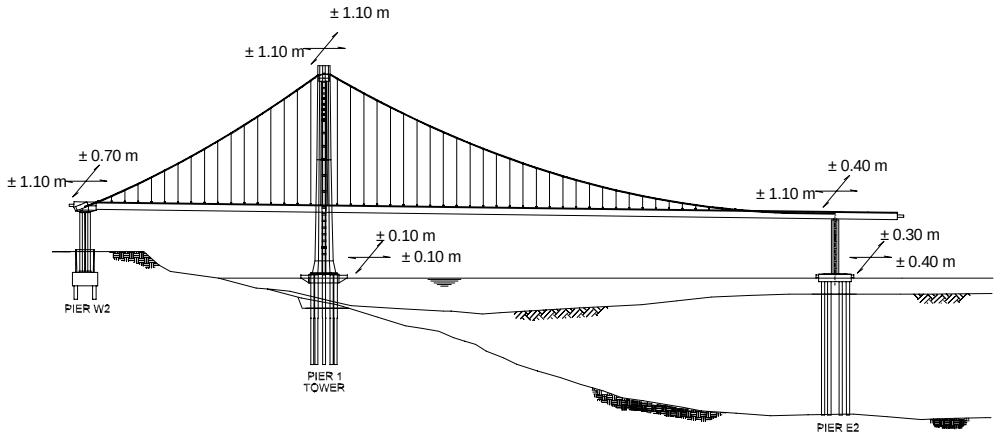

Figure 13. Seismic Displacement Demands

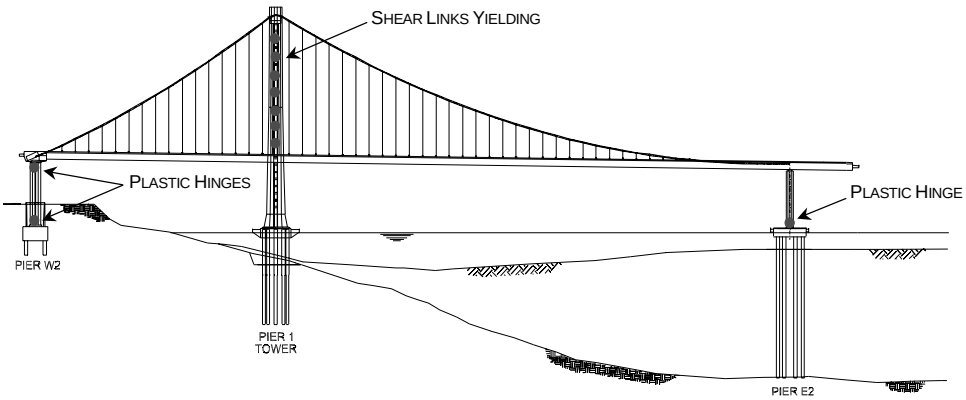

Figure 14. Seismic Displacement Demands

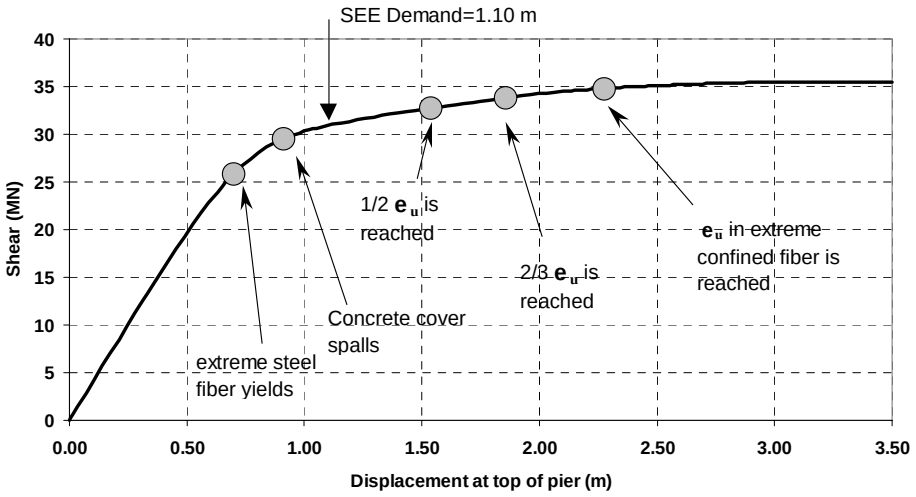

Figure 15: Longitudinal Pushover Analysis of West Pier.

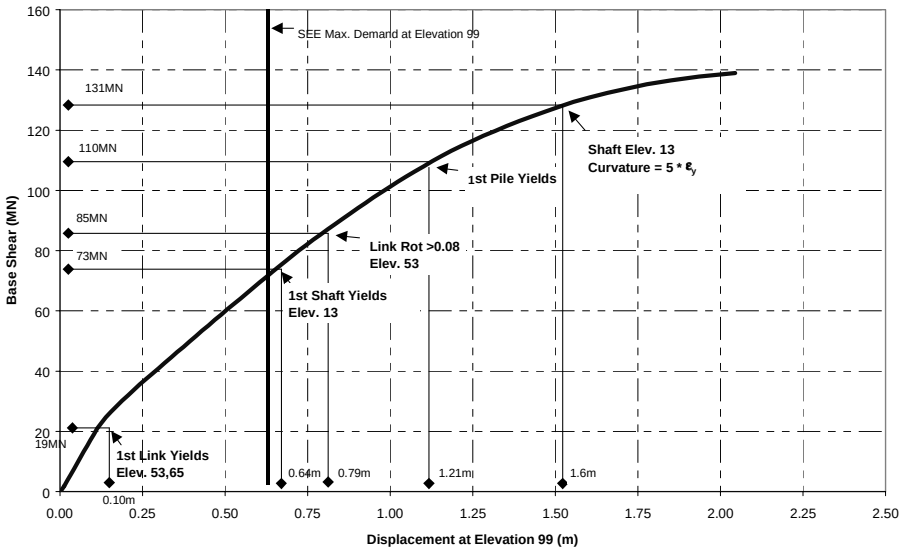

Figure 16. Pushover Analysis of the Single Tower (Displacement applied at elevation 99m)

The plastic strain in the piers is limited to 2/3 of the ultimate strains based on Mander's equation for confined concrete columns. The results of the longitudinal pushover of the West Pier (Figure 15) identifying yield events for various levels of displacement demand, show that at the SEE demand of 1.10 m, ½ ε_u has not been reached. A Test of the West Pier is also in progress to verify its ductility. The piles were designed to sustain minimal damage (strains less than 0.01 for concrete and 0.02 for steel) when subjected to the SEE displacement demands.

Pushover analyses of the Main Tower were also performed with the following main objectives: to evaluate the base shear versus displacement relationship; to evaluate lateral ductility and to identify yield events for various levels of displacement demand. During an earthquake the inertial load vector on a structure varies continuously, while in a pushover the load vector remains constant. Hence, it is necessary to consider more than one load pattern in order to bound the expected lateral behavior. Up to three load patterns were used. These are: (i) shape of participating modes, (ii) deformed shape of the tower at a time step corresponding to maximum drift in the global time history analysis and (iii) a uniform load vector. Figures 16 shows results of a longitudinal push-over analysis of the Tower. As noted, the Tower has a stable behavior for displacements much larger than SEE displacement demands.

ACKNOWLEDGEMENTS

The authors would like to acknowledge the invaluable contribution of the California Department of Transportation personnel, namely:Brian Maroney, Ade Akinsanya, Vong Toan and Reza Valijadeh. The authors would also like to acknowledge the contribution of Weidlinger Associates, Inc. for their collaboration in the design of the bridge.

REFERENCES

[1] First Annual Progress Report San Francisco Oakland Bay Bridge, July 1934.
[2] Vulnerability Reports on the Seismic Performance of the Existing East Span of the San Francisco Oakland Bay Bridge, California Department of Transportation.
[3]The San Francisco-Oakland Bay Bridge East Span Seismic Safety Project, 30% Design Report, May 11, 1998 – Prepared by T.Y. Lin International – Moffatt & Nichol, Joint Venture - Prepared for the State of California Business, transportation and Housing Agency.
[4] The San Francisco-Oakland Bay Bridge East Span Seismic Safety Project, Supplement to Final 30% Design Report, June 22, 1998 – Prepared by T.Y. Lin International – Moffatt & Nichol, Joint Venture - Prepared for the State of California Business, Transportation and Housing Agency.
[5] The San Francisco-Oakland Bay Bridge East Span Seismic Safety Project, 85% Design Report, May 11, 1998 – Prepared by T.Y. Lin International – Moffatt & Nichol, Joint Venture - Prepared for the State of California Business, Transportation and Housing Agency
[6] ADINA R & D, Inc, 71 Elton Avenue, Watertown, MA 02172 USA
[7] Design Criteria of the San Francisco- Oakland Bay Bridge East Span Seismic Safety Project (2001), T.Y. Lin International – Moffatt & Nichol, Joint Venture
[8] Design of the New San Francisco-Oakland Bay Bridge, Rafael Manzanarez et. al, 16th International Bridge Conference, Pittsburgh, Pennsylvania, 1999.
[9] Seismic Analysis of Bridges with Pile Foundations, Tim Ingham et al., 12th Adina Conference, June 1999
[10] Cyclic Testing of Suspension Tower Shear Links of the San Francisco – Oakland Bay Bridge, Cole McDaniel et al, September 2001
[11] Shear Link Testing at University of Nevada, Reno, Peter Dusicka, November 2001. Report in Progress.

Seismic Design of the Metsovitikos Suspension Bridge, Pindos Mountains, Greece

Mike Oldham, Zygmunt Lubkowski,
Xiaonian Duan & Richard Sturt

ABSTRACT

This spectacular landmark suspension bridge has been designed to span the Metsovitikos River in the Pindos Mountains of Western Greece, an area of significant seismic activity. The rock anchored suspension bridge spans 550m (1800ft) across a steep sided valley between tunnel portals at each end of the bridge. The steel deck is supported on suspension cables spanning 800m (2640ft) to rock anchorages in the mountainside above the abutments.

This unique structure has presented a number of seismic engineering challenges whose solutions have required state-of-the-art computational techniques. The Performance Based seismic design basis has adopted the principles of ATC-32.

A number of innovative ground assessment methodologies have been developed during the design. The stability of the anchorages on the mountainside has been demonstrated using a combination of two-dimensional and three-dimensional explicit non-linear, finite element analyses. The rock matrix has been modeled using a ubiquitous joint failure model.

The cable form adopted provides an excellent concept for seismic resistant design. The long period structure is naturally isolated during the design earthquakes and the P-delta effects present are stabilizing because the anchorages are located well above the bridge center of mass. Even in this region of significant seismic activity, the earthquake loads do not govern the design of the primary structural elements.

Xiaonian Duan, Arup Advanced Technology Group, 13 Fitzroy Street, London W1T 4BQ, UK
Zygmunt Lubkowski, Arup Geotechnics, 13 Fitzroy Street, London W1T 4BQ, UK
Mike Oldham, Arup Advanced Technology Group, 13 Fitzroy Street, London W1T 4BQ, UK
Richard Sturt, Arup Advanced Technology Group, The Arup Campus, Blythe Gate, Blythe Valley Park, Solihull, West Midlands B90 8AE, UK

METSOVITKOS SUSPENSION BRIDGE

In 1998 Egnatia Odos AE held an international design competition for a landmark structure as part of a new motorway across Greece. Arup Consulting Engineers and Wilkinson Eyre Architects won the competition with the dramatic design shown below and have since carried out the detailed design of the structure. The bridge site is in the Pindos Mountains of Western Greece, a region of significant seismic and wind hazard.

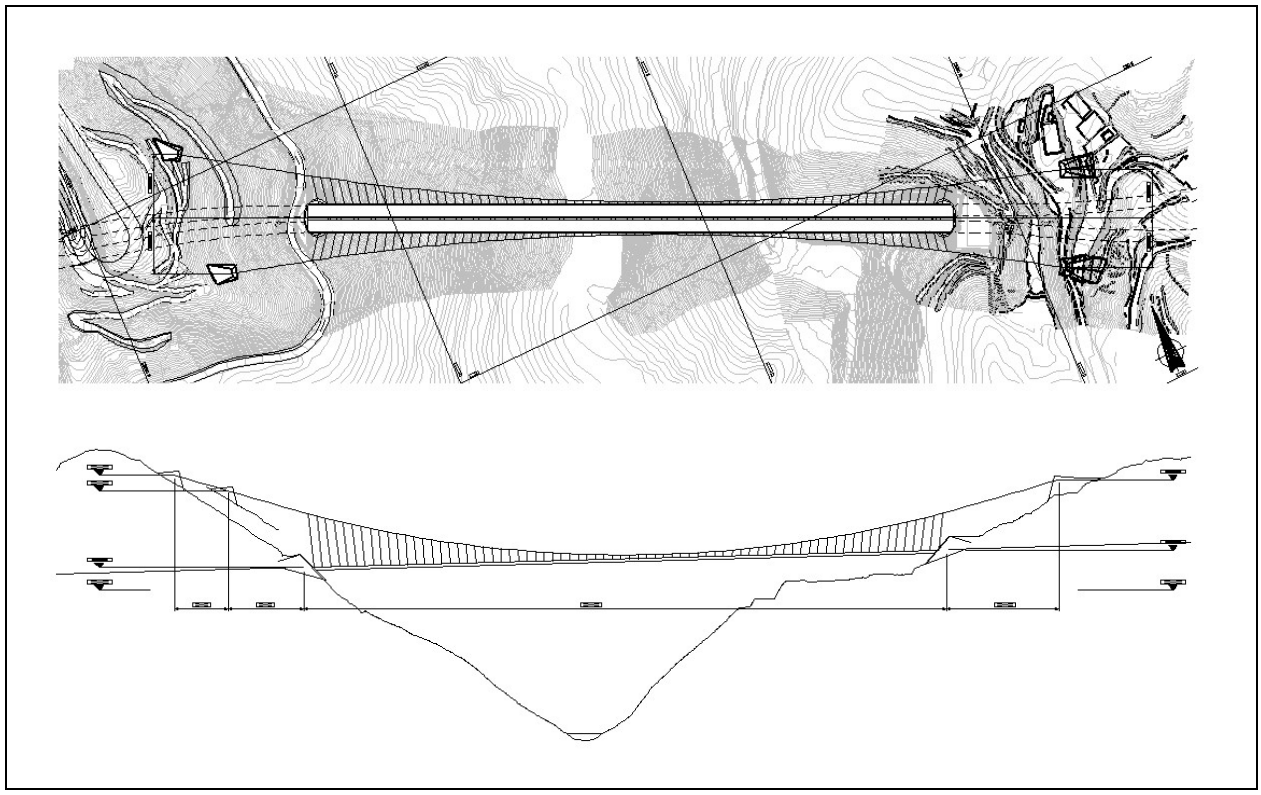

Figure 1. Plan View and Elevation of the Metsovitikos Suspension Bridge.

The rock anchored suspension bridge spans 550m (1800ft) across a steep sided valley, some 150m above the Metsovitikos River. The main cables are anchored directly to the rock of mountainside and span 800m (2640ft) between anchorages. The main suspension cables are 561mm (22in) diameter galvanized high strength steel wire; the unfactored cable load under permanent loads is some 88MN (20 000kips). The main cables are fixed directly back to the mountainside with two gravity anchorages and two tunneled socket rock anchorages. Inclined hangers at 7.5m (26.5ft) centers support a twin hull, orthotropic steel deck.

The hangers at the ends of each deck hull are pre-tensioned to give a 3MN (340kips) tie-down force, which is taken into the abutments through an articulated pendal arrangement. These end hangers provide virtual-towers that control the deflection of the suspension cables and the deck rotations at the abutments.

SEISMIC CONDITIONS AT BRIDGE SITE

The bridge site is a region of significant seismic activity. The earthquake catalogue developed by Papazachos and Papazachou (1997) [1] records seven earthquakes greater than 6.0M_w within 50km of the site since 550BC. The closest earthquake to the site was a 6.4M_w event, which occurred in Arta in 1967. Modified Mercalli intensities of VII+ were observed in the nearby village of Metsovo. Figure 2 shows the complete earthquake catalogues for events greater than 6.5 M_w and 4.5 M_w.

A detailed probabilistic seismic hazard assessment using a logic tree approach was carried out as part of the project to derive the uniform hazard acceleration and displacement response spectra for the seismic design basis. The analyses took account of the topography and subsequently time histories were generated at each anchorage location.

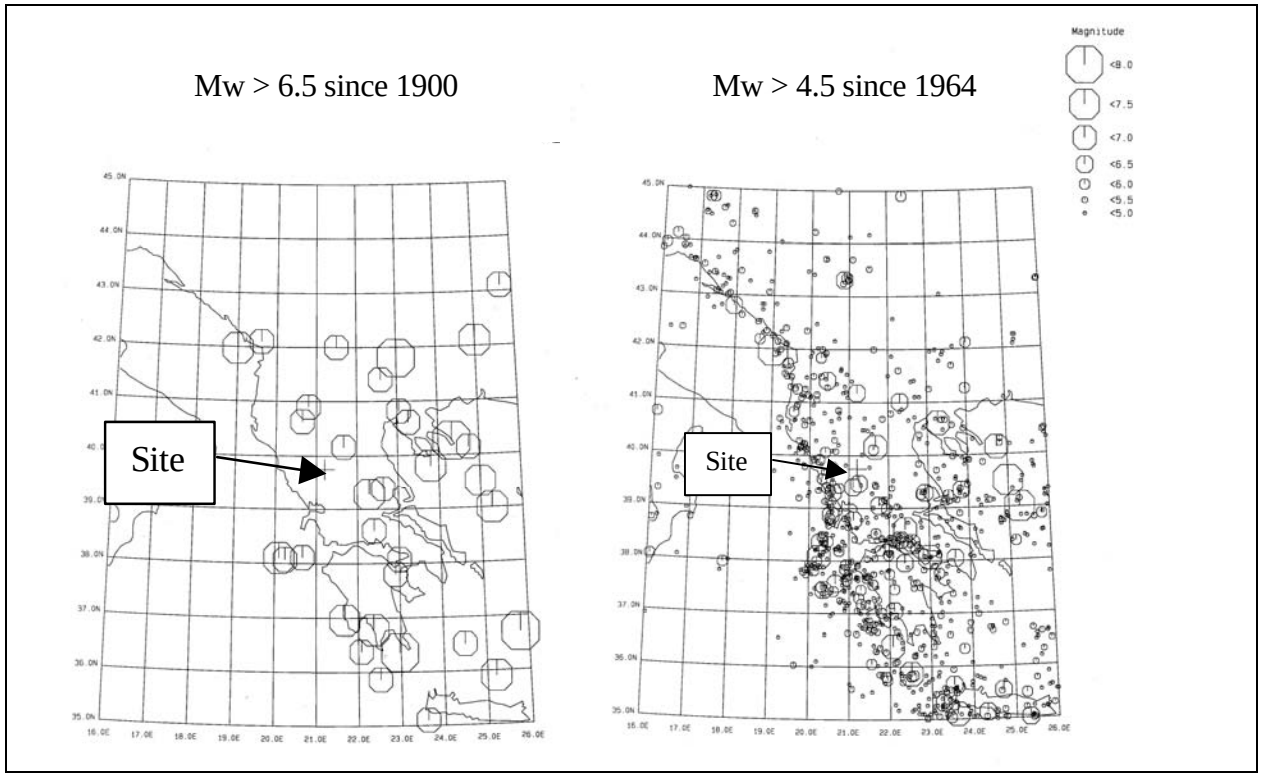

Figure 2. Complete Earthquake Catalogues.

PERFORMANCE BASED SEISMIC DESIGN BASIS

Due to the structural form and relative importance of the bridge, the seismic design falls outside normal seismic design codes. In fact suspension bridges are specifically excluded from many codes of practice. A structure specific design basis was developed following the principles of ATC-32 [2].

Two levels of seismic performance were specified: a frequent Functional Evaluation Earthquake and a rare Safety Evaluation Earthquake were defined. In addition, collapse prevention under the Maximum Credible Earthquake was considered. The seismic design basis is summarized below.

Design Ground Motions		**Seismic Performance Criteria**			**Load Combinations**
Evaluation Level	**Probability of Exceedance in 120 year useful life**	**Service Level**	**Damage Level**	**Limit on Ductility Demand**	
Functional	40% 235 year return period	Immediate	Minimal damage Elastic design	1.0	Dead + Superimposed Dead + 40% Live Traffic Load
Safety	10% 1139 year return period	Immediate, with reduced traffic	Repairable damage Elastic design	1.0	Dead + Superimposed Dead

Table 1. Seismic Performance Objectives of the Metsovitikos Bridge

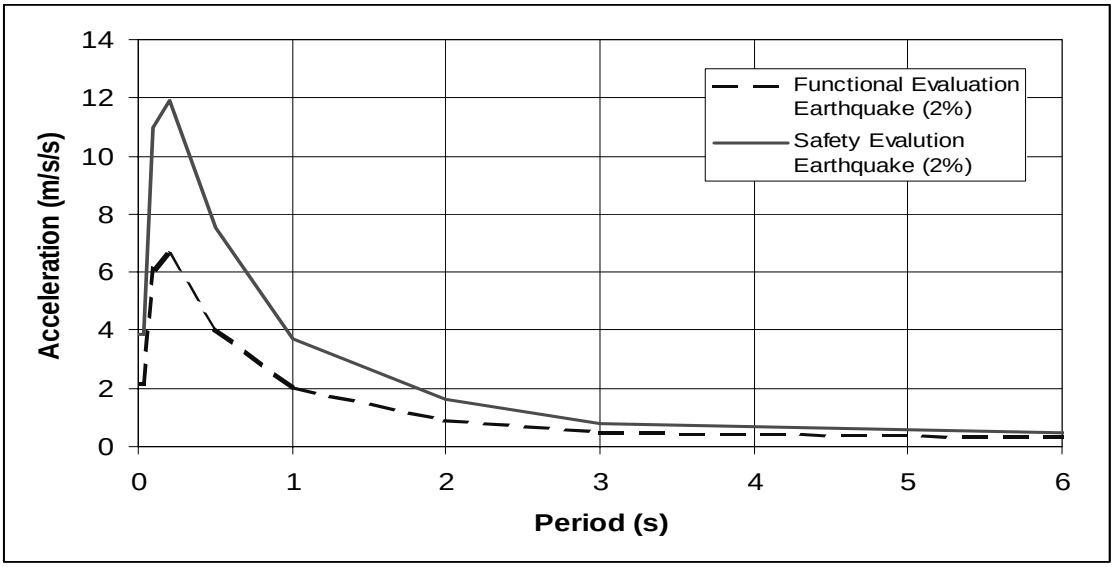

Figure 3. Design Response Spectra (2% Damping)

ANCHORAGE SEISMIC DESIGN

Some of the greatest challenges have been faced in the ground engineering of anchorages, which are fixed directly to the rock slopes above the bridge abutments.

The valley slopes comprise a combination of thick-bedded sandstones that dip steeply into the valley and thinly bedded siltstones with a strong tectonic fabric. The presences of an historic landslide required the relocation of the South West anchorage resulting in a slight asymmetry of the bridge. Below the Eastern anchorages a thrust fault separates the sandstones below from the siltstones above, and this fault dips away from the bridge at approximately 50°.

Differences in the topography and rock types at each anchorage location resulted in the choice of gravity solutions for the South West and North East anchorages and tunneled socket rock achors at the North West and South East supports.

3D & 2D Slope Stability Analysis with Ubiquitous Joint Model

A combination of 2D and 3D explicit, non-linear finite element analyses were used to demonstrate the stability of the slopes under the seismic loads. Analyses using a ubiquitous joint model for the rock (Pande et al 1990 [3]) were carried out using the commercially available software *Oasys* SAFE, *Vips* VISAGE and *Oasys* LS-DYNA.

The rock is modeled as a continuum with a specified strength and stiffness. A reduced strength is specified along the planes orientated in the direction of the discontinuities and no tension is permitted normal to these planes. The 3D finite element model is shown below.

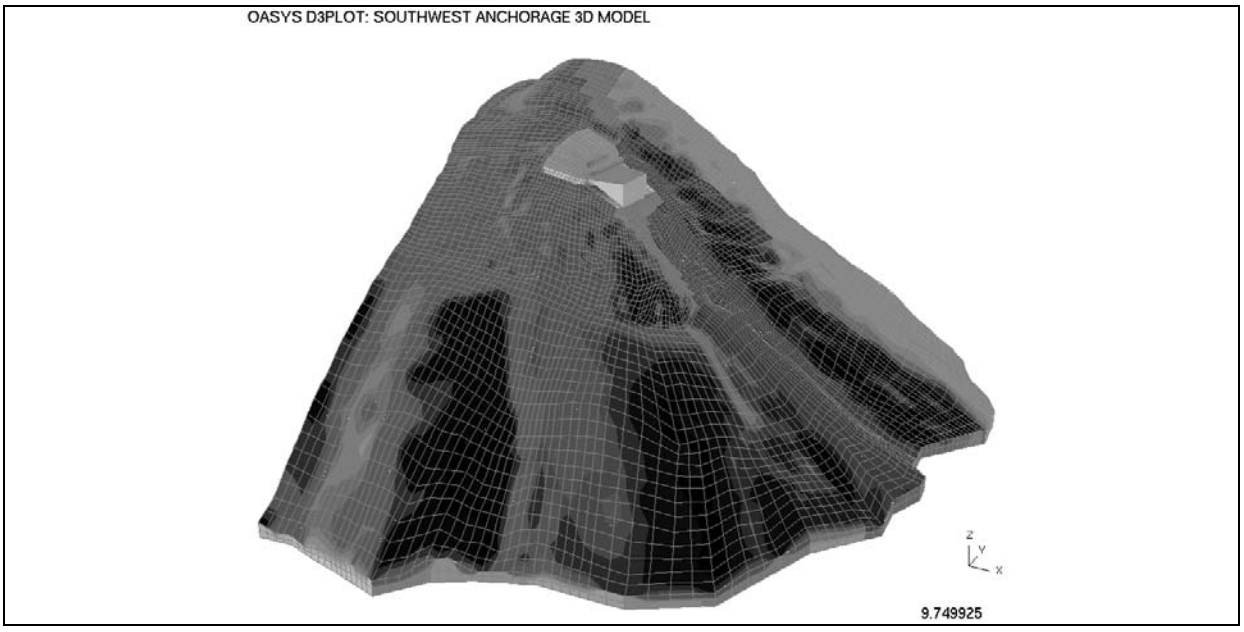

Figure 4. 3D FE Model of SW Anchorage and Slopes

For the seismic load case, quasi-static analysis was carried out. Increasing vertical and horizontal seismic accelerations were imposed until the limit of slope stability was found. Figure 8, below, shows the displacement of the slope against the applied acceleration. The results shown are for seismic acceleration applied along the length of the bridge.

From this graph, it can be seen that the rock slope begins to slide at an applied acceleration of 0.28g. Having determined the critical acceleration for slope stability, the displacements under the design earthquakes can be calculated, as described below.

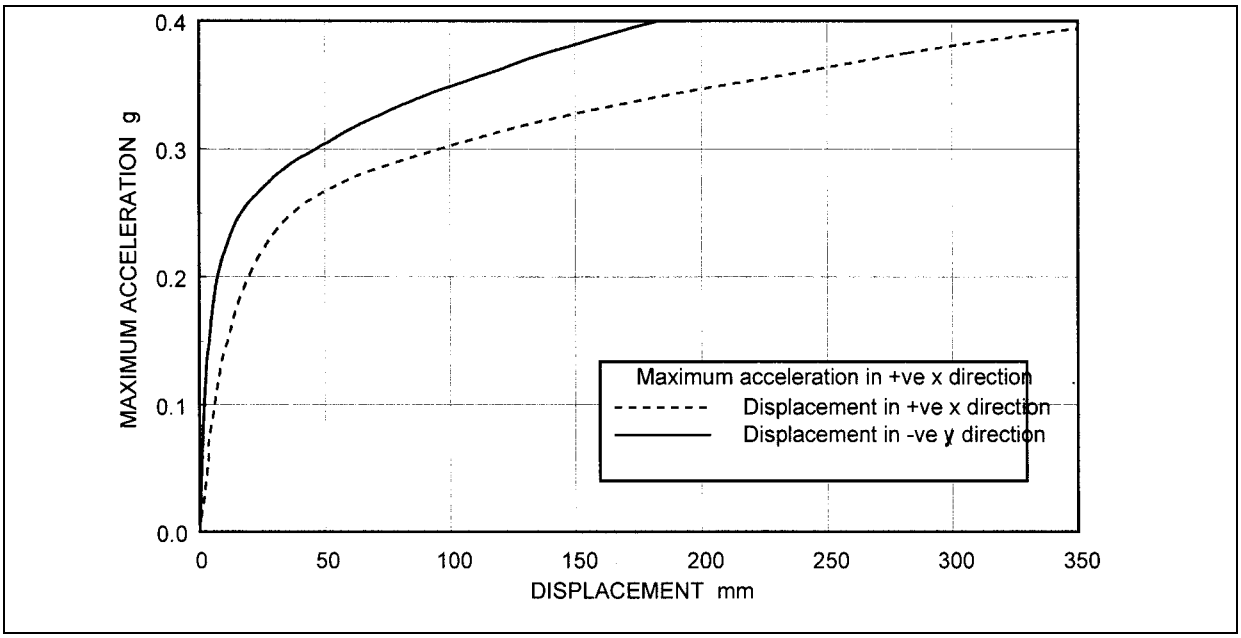

Figure 5. Slope Stability Predictions from 3D Finite Element Modeling

2D Limit Equilibrium Analyses

The results of the 3D stability analyses have been fed into 2D dynamic equilibrium analyses carried out using a Newmark type [4] sliding block methodology. The earthquake time history is applied to the 2D representation of the ground and sliding is assumed to occur when the applied acceleration is greater than the critical acceleration of 0.28g. The total extent of sliding duringa a given seismic record can therefore be predicted.

Using this method, a permanent displacement of 5mm (0.20in) was predicted after the Safety Evaluation Earthquake and the stability of the slope is satisfactory.

SUPERSTRUCTURE SEISMIC DESIGN

Whilst ATC-32 permits repairable, moderate structural damage more stringent criteria have been adopted for this bridge. The primary structural elements are required to remain elastic during both design earthquakes because the high strength steel cables and hangers have little ductile capacity and there is obviously no redundancy in the support system. In addition, damage to the main structural elements would not be repairable without effectively replacing the bridge. Damage to secondary elements, such as the expansion joints and flexing panel is tolerable under the safety evaluation event.

Due to the form and importance of the bridge it is crucial that the analyses were able to represent:

- Simultaneous application of the ground motion in all three directions, because the natural modes of the bridge are coupled.
- Spatial variability of the ground motion. The phase shift and loss of coherence between the anchorages is significant.
- Non-linear structural behavior, both in terms of geometry and material properties.

The seismic design of the superstructure was carried out with the aid of two methods of finite element analysis. Linear elastic response spectrum analyses were carried out during the design iterations. Final verification of the bridge was carried out using non-linear, dynamic time-history analyses using the explicit non-linear finite element software *Oasys* LS-DYNA.

As the rock material is very stiff compared with the bridge fundamental frequency, it was possible to decouple the superstructure and ground response analyses.

Dynamic Characteristics of the Bridge

The Metsovitikos Suspension Bridge is a relatively long period structure and the fundamental modes of the structure are between 4 and 6.5 seconds. The first three modes of the bridge are shown in Figure 6, below.

An interesting feature of the dynamic response is the way in which the cable form couples the modes of vibration in all three directions. The main cables couple the vertical and longitudinal modes. In addition, the inclined hangers couple the transverse mode to the vertical response of the deck. As a result of this coupling, it is important that the seismic loads in the three orthogonal directions are considered simultaneously.

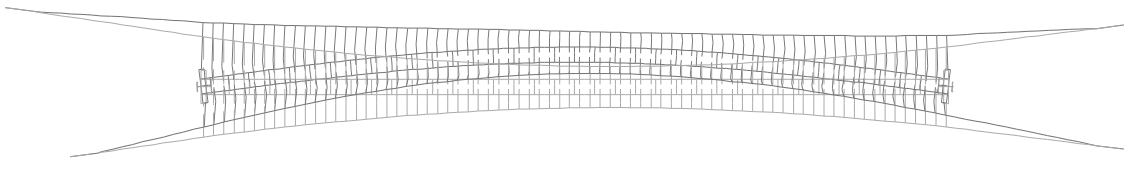

Transverse Mode: 6.5 second period

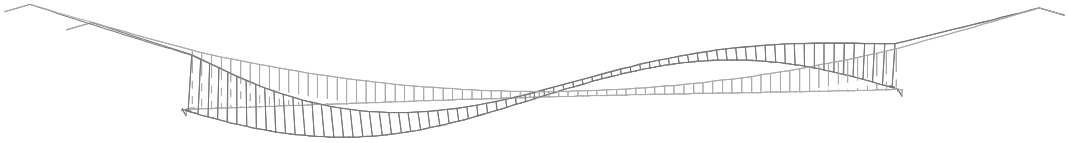

Longitudinal Mode: 5.3 second period

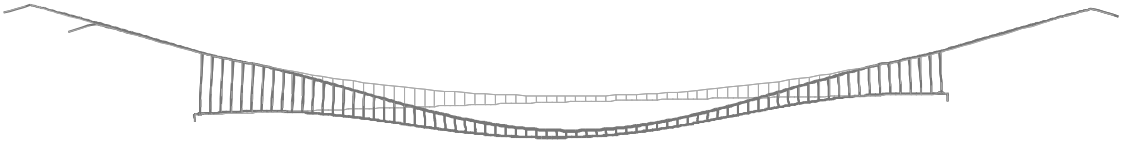

Vertical Mode: 4.3 second period

Figure 6. Natural Modes of the Bridge

Seismic Loads in Bridge Superstructure

The cable system we chose for the suspension bridge produces a structure that has an inherent seismic isolation. Even this area of significant seismic activity, the earthquake loads are not governing the design of the superstructure. In addition, the P-delta effects that are present in the structure are all stabilizing because the points of support are well above the center of mass of the bridge.

The cable force during the Safety Evaluation Earthquake is shown in Figure 11, below. The unfactored cable force under the action of permanent loads can be seen to 88MN (20 000kips). The seismic event produces approximately ±8MN (±900kips) about the mean cable force. For comparison the cable force under the maximum traffic live load of 125MN (14 000kips) is also plotted.

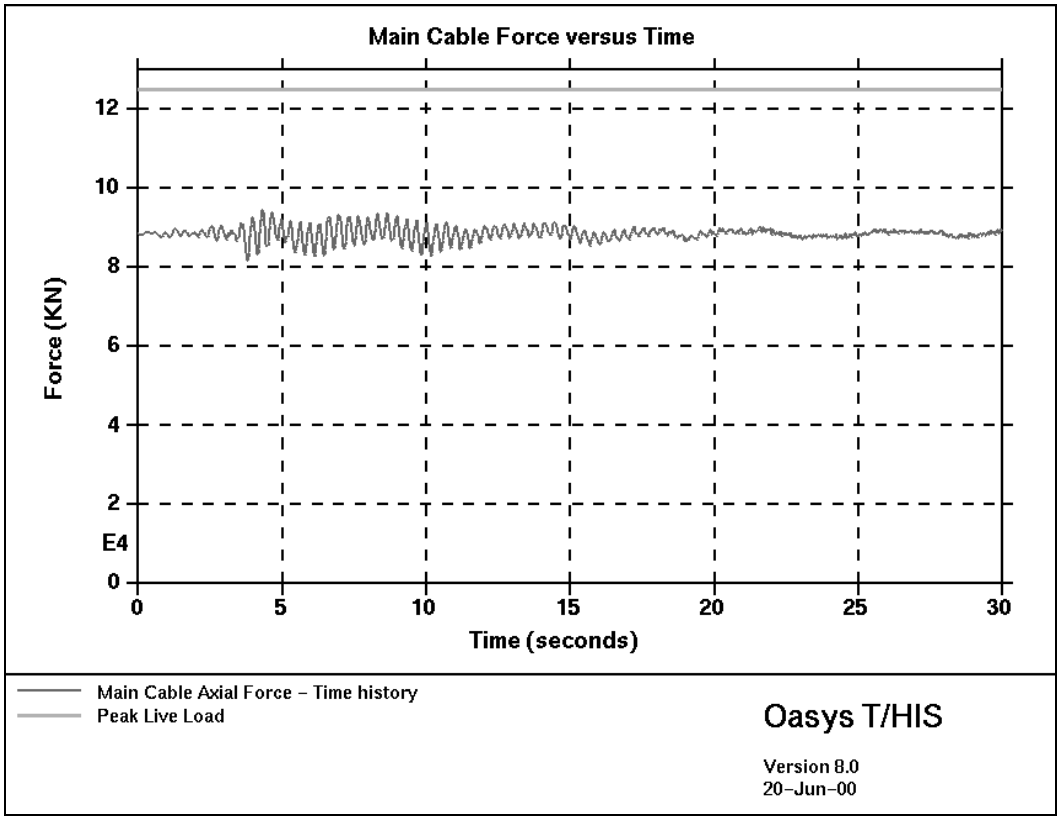

Figure 7. Main Cable Force During Seismic Event

Figure 8, below, shows the displacement at the abutment expansion joints during the Safety Evaluation Earthquake. With an isolated structure, the trade-off for reduced force is an increased displacement. As a result of the cable system and the relatively low spectral displacements associated with the rock site, the seismic displacements are bounded by the displacements under the maximum traffic load combinations.

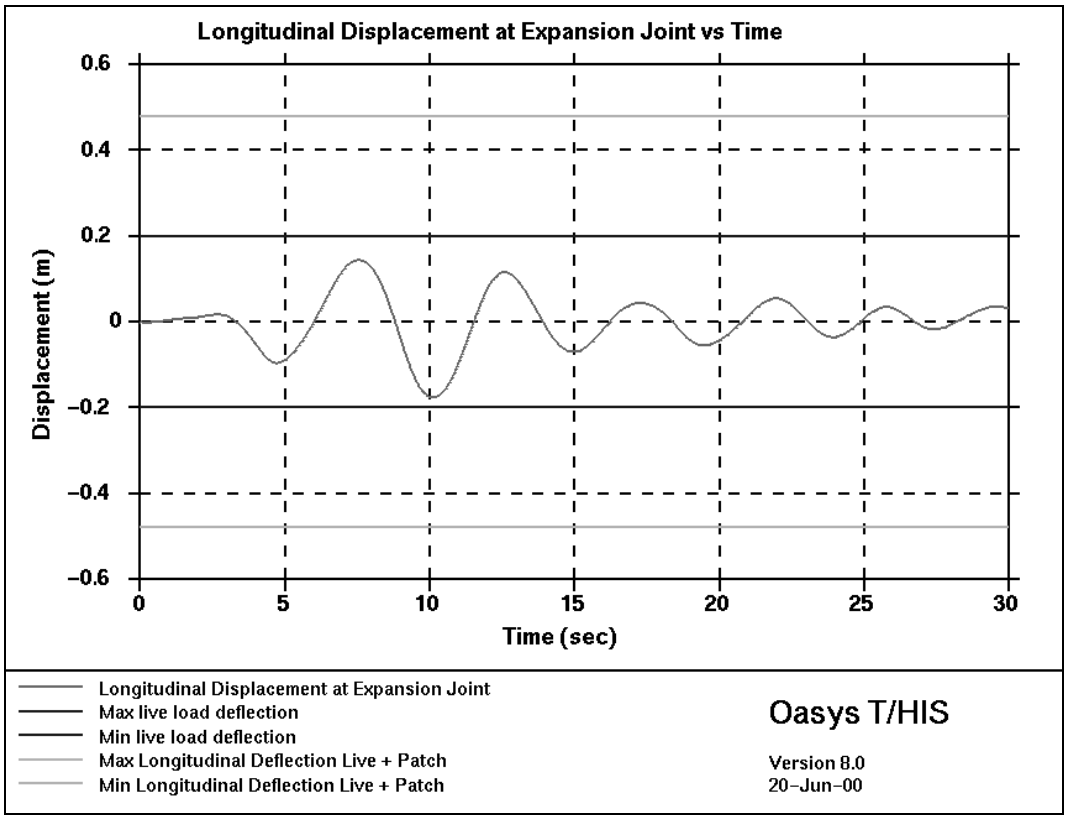

Figure 8. Longitudinal Displacement at Expansion Joint

CONCLUSION

The innovative design of the Metsovitikos suspension bridge has presented a series of seismic engineering challenges throughout the design period. A structure specific, performance based seismic design basis has been developed following the principles of ATC-32. This incorporates a site-specific probabilistic seismic hazard assessment.

A number of innovative ground assessment methodologies have been developed during the design. The stability of the anchorages on the mountainside has been demonstrated using a combination of two-dimensional and three-dimensional non-linear finite element analyses, which have modeled the rock matrix using a ubiquitous joint model.

The cable form adopted provides an excellent concept for seismic resistant design. The long period structure is naturally isolated during the design earthquakes and the P-delta effects present are stabilizing because the anchorages are above the bridge mass. Even in this region of significant seismic activity, the seismic loads do not govern the design of the primary structural elements.

REFERENCES

1. Papazachos BC & Papazachou CB (1997)
   "The Earthquakes of Greece"
   P Ziti & Co, Thessaloniki

2. ATC-32
   "Improved Seismic Design Criteria for California Bridges: Provisional Recommendations"
   Applied Technology Council

3. Pande GN, Beer G & Williams JR (1990)
   "Numerical Methods in Rock Mechanics"
   John Wiley

4. Newmark (1995)
   "Effects of Earthquakes on Dams and Embankments"
   Geotechnique. Vol 15. No 2 pp 139-160

Effects of Near Field Earthquakes on Bridges

Chair: Jim Roberts

Characterizing Near Fault Ground Motion for the Design and Evaluation of Bridges

Paul Somerville

Designing Ordinary Bridges for Ground Fault Rupture

Stewart Gloyd, Raymond Fares, Anthony Sánchez, and Vinh Trinh

Design of the Lytle Creek Wash Bridge to Survive Permanent Ground Displacements due to Surface Fault Rupture

Gregory V. Brown

Seismic Retrofit of the Bolu Viaduct

S. W. Park, H. Ghasemi, J. D. Shen, W. Phillip Yen, and M. Yashinsky

PEER-Lifelines Research in Design Ground Motions

Clifford J. Roblee, Brian S.J. Chiou and Michael F. Riemer

Characterizing Near Fault Ground Motion For The Design And Evaluation Of Bridges

Paul Somerville

ABSTRACT

Near-fault ground motions are different from ordinary ground motions in that they often contain strong coherent dynamic long period pulses and permanent ground displacements. The dynamic motions are dominated by a large long period pulse of motion that occurs on the horizontal component perpendicular to the strike of the fault, caused by rupture directivity effects. Near fault recordings from recent earthquakes indicate that this pulse is a narrow band pulse whose period increases with magnitude, as expected from theory. This magnitude dependence of the pulse period causes the response spectrum to have a peak whose period increases with magnitude, such that the near-fault ground motions from moderate magnitude earthquakes may exceed those of larger earthquakes at intermediate periods (around 1 second). The static ground displacements in near-fault ground motions are caused by the relative movement of the two sides of the fault on which the earthquake occurs. These displacements are discontinuous across a fault having surface rupture, and can subject a bridge crossing a fault to significant differential displacements. The static ground displacements occur at about the same time as the large dynamic motions, indicating that the static and dynamic displacements need to be treated as coincident loads.

At the FHWA/NCEER Workshop on the National Representation of Seismic Ground Motion for New and Existing Highway Facilities held in San Francisco on May 29-30, 1997, a consensus was reached that the response spectrum alone is not an adequate representation of near-fault ground motion characteristics, because it does not adequately represent the demand for a high rate of energy absorption presented by near-fault pulses. This is especially true for high ground motion levels that drive structures into the non-linear range, invalidating the linear elastic assumption on which the elastic response spectrum is based. To fully portray the response of structures to near-fault ground motions, nonlinear time history analysis may be required. Fortunately, near fault ground motions containing forward rupture directivity may be simple enough to be represented by simple time domain pulses, thus simplifying the specification of ground motion time histories for use in structural response analyses. Preliminary equations relating the period of the pulse to the earthquake magnitude, and the effective velocity of the pulse to the earthquake magnitude and distance, have been developed. The directivity pulse can be combined with the static fault displacement to provide a complete description on near-fault ground motions. The effect of the simultaneous dynamic and static ground motions on the response of a bridge should be analyzed using time histories that include both types of motion.

The probabilistic approach to seismic hazard analysis has an important advantage over the deterministic approach in that it takes into account the degree of activity of the faults that contribute to the hazard, providing explicit estimates of the likelihood of occurrence (or return period) of the hazard level that is specified in the design ground motions.

Paul Somerville, Principal Seismologist, URS Corp., 566 El Dorado St., Pasadena, CA 91101

INTRODUCTION

An earthquake occurs when elastic strain that has gradually accumulated across a fault is suddenly released in the process of elastic rebound. The elastic energy stored on either side of the fault drives the motion on the fault. The elastic rebound generates dynamic strong ground motions that last for a few seconds to a few minutes, constituting a primary seismic hazard. The elastic rebound also generates static deformation of the ground. The static deformation of the ground consists of a discontinuity in displacement on the fault itself, and a gradual decrease in this displacement away from the fault on either side of the fault. If there is surface faulting, the static displacements are discontinuous across the fault at the ground surface, constituting a primary seismic hazard. Even if the fault does not break the surface, there is static deformation of the ground surface due to subsurface faulting.

Strong ground motions recorded on digital accelerographs in recent earthquakes, including the 1985 Michoacan, Mexico, 1999 Chi-chi, Taiwan and 1999 Kocaeli, Turkey earthquakes, contain both dynamic ground motions and static ground displacements. Figure 1 shows the strong motion recording of the strike-slip Kocaeli earthquake at Yarimca. The static displacement of the ground is about 2 meters in the east-west direction, parallel to the strike of the fault, consistent with geological and GPS data. The large dynamic ground velocity pulse is oriented north-south, in the fault normal direction. The static ground displacement is coincident in time with the largest dynamic ground velocities, as shown in Figure 1, and occurs over a time interval of several seconds. It is therefore necessary to treat the dynamic and static components of the seismic load as coincident loads.

In some earthquakes, faulting of the ground surface occurs on a distributed system of sub-parallel faults instead of occurring on a single fault trace. This distributed fault system may have a width of several tens to hundreds of meters. This does not have a significant impact on the estimation of dynamic ground motions, but can complicate the estimation of the static ground displacement field, including surface faulting. Ground shaking can cause secondary ground deformation by inducing soil liquefaction with concomitant lateral spreading, and landslides. Excluding these complications and secondary effects, the near fault ground motion hazards that influence an individual bridge support include:

- Dynamic displacements at a bridge support due to seismic waves
- Permanent displacements at a bridge support due to the static displacement field

These dynamic and static ground displacements need to be quantified in separate hazard analyses, because they are not strongly correlated, as shown below. Once they have been separately quantified, the two components of the hazard can then be combined into a single ground motion time history, like those shown in Figure 1, that contains both dynamic and static ground displacements at a bridge support.

Bridges have multiple supports and are thus also affected by differential displacements of the ground. These differential displacements may be caused by both dynamic and static ground displacements. The kinds of seismic hazards that cause differential ground displacements of bridge piers in the near fault environment include:

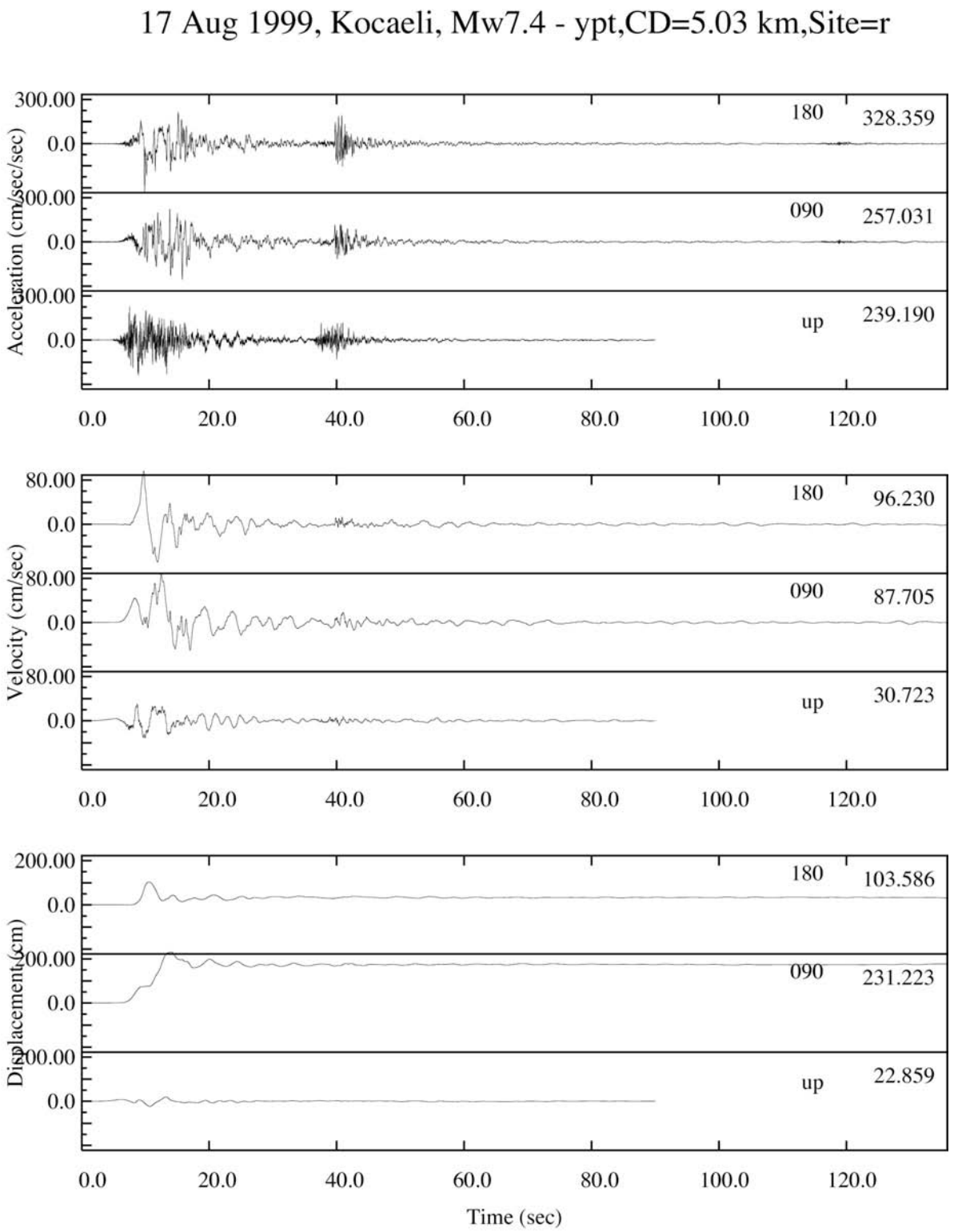

Figure 1. Strong motion recording of the south (180), east (090), and vertical (up) components of the 1999 Kocaeli, Turkey earthquake at Yarimca.

- Dynamic differential displacements between supports due to seismic waves. These include the effects of wave passage, and differences in the amplitude and phase of ground motions at multiple supports due to wave incoherence effects [1].

- Permanent differential displacements between supports due to the static displacement field. These are potentially large when surface faulting occurs between supports. Even without surface displacements between supports, differential displacements may occur due to spatial variations in the static displacement field, which may be significant near the fault.

These dynamic and static differential displacement hazards need to be quantified in separate hazard analyses. However, both components of the hazard can be specified together by suites of ground motion time histories at multiple supports that contain both dynamic and static ground displacements whose differential values between supports are consistent with the estimated differential displacement hazards.

NEAR FAULT RUPTURE DIRECTIVITY PULSE

An earthquake is a shear dislocation that begins at a point on a fault and spreads at a velocity that is almost as large as the shear wave velocity. The propagation of fault rupture toward a site at a velocity close to the shear wave velocity causes most of the seismic energy from the rupture to arrive in a single large pulse of motion that occurs at the beginning of the record [2], [3]. This pulse of motion represents the cumulative effect of almost all of the seismic radiation from the fault. The radiation pattern of the shear dislocation on the fault causes this large pulse of motion to be oriented in the direction perpendicular to the fault plane, causing the strike-normal component of ground motion to be larger than the strike-parallel component at periods longer than about 0.5 seconds. To accurately characterize near fault ground motions, it is therefore necessary to specify separate response spectra and time histories for the strike-normal and strike-parallel components of ground motion.

Forward rupture directivity effects occur when two conditions are met: the rupture front propagates toward the site, and the direction of slip on the fault is aligned with the site. The conditions for generating forward rupture directivity effects are readily met in strike-slip faulting, where the rupture propagates horizontally along strike either unilaterally or bilaterally, and the fault slip direction is oriented horizontally in the direction along the strike of the fault. However, not all near-fault locations experience forward rupture directivity effects in a given event. Backward directivity effects, which occur when the rupture propagates away from the site, give rise to the opposite effect: long duration motions having low amplitudes at long periods.

The conditions required for forward directivity are also met in dip slip faulting. The alignment of both the rupture direction and the slip direction updip on the fault plane produces rupture directivity effects at sites located around the surface exposure of the fault (or its updip projection if it does not break the surface). Unlike the case for strike- slip faulting, where forward rupture directivity effects occur at all locations along the fault away from the hypocenter, dip slip faulting produces directivity effects on the ground surface that are most concentrated in a limited region updip from the hypocenter.

ORIENTATION OF DYNAMIC AND STATIC NEAR FAULT GROUND MOTIONS

The top part of Figure 2 schematically illustrates the orientations of dynamic and static near fault ground motions. The strike-slip case is shown in map view, where the fault defines the strike direction. The rupture directivity pulse is oriented in the strike-normal direction and the static ground displacement ("fling step") is oriented parallel to the fault strike. The dip-slip case is shown in vertical cross section, where the fault defines the dip direction; the strike direction is orthogonal to the page. The rupture directivity pulse is oriented in the direction normal to the fault dip, and has components in both the vertical direction and the horizontal strike normal directions. The static ground displacement is oriented in the direction parallel to the fault dip, and has components in both the vertical direction and the horizontal strike normal direction.

The bottom part of Figure 2 schematically illustrates the partition of near fault ground motions into the dynamic ground motion, which is dominated by the rupture directivity pulse, and the static ground displacement. For a strike-slip earthquake, the rupture directivity pulse is partitioned mainly on the strike-normal component, and the static ground displacement is partitioned on the strike-parallel component. If the static ground displacement is removed from the strike-parallel component, very little dynamic motion remains. For a dip-slip earthquake, the dynamic and static displacements occur together on the strike-normal component, and there is little of either motion on the strike-parallel component. If the static ground displacement is removed from the strike-normal component, a large directivity pulse remains.

PRESERVING ORIENTATION IN THE ARCHIVING, ANALYSIS AND APPLICATION OF NEAR FAULT GROUND MOTIONS

Figures 1 and 2 demonstrate that near-fault ground velocities and displacements have orientations that are controlled by the geometry of the fault, specifically by the strike, dip, and rake angle (direction of slip) on the fault. Consequently, it is necessary to treat them as vector, rather than scalar, quantities. The simplest method or treating them as vector quantities is to partition them into strike-normal and strike-parallel components. The dynamic and static motions are distinctly different on these two components at all near-fault locations.

Accordingly, near-fault ground motion recordings should be archived in the strike-normal and strike-parallel components, as shown on the left side of Figure 3. The rotation of the two recorded components North (N) and East (E) into strike-parallel and strike-normal components SP and SN is accomplished using the following transformations:

$$SP = N \cos \phi + E \sin \phi; \quad SN = -N \sin \phi + E \cos \phi$$

where ϕ is the strike of the fault measured clockwise from North. If the recording orientation is not North and East but rotated clockwise by the angle ψ, then ϕ would be reduced by ψ.

Distinct models for the strike-normal and strike-parallel components of near-fault ground motions, derived from appropriately archived recordings and from simulations based on seismological models, are needed for seismic hazard analysis. In order to represent near-fault effects, ground motion simulations need to be based on the summation of complete Green's functions that contain near-, intermediate-, and far-field terms. This is done using the

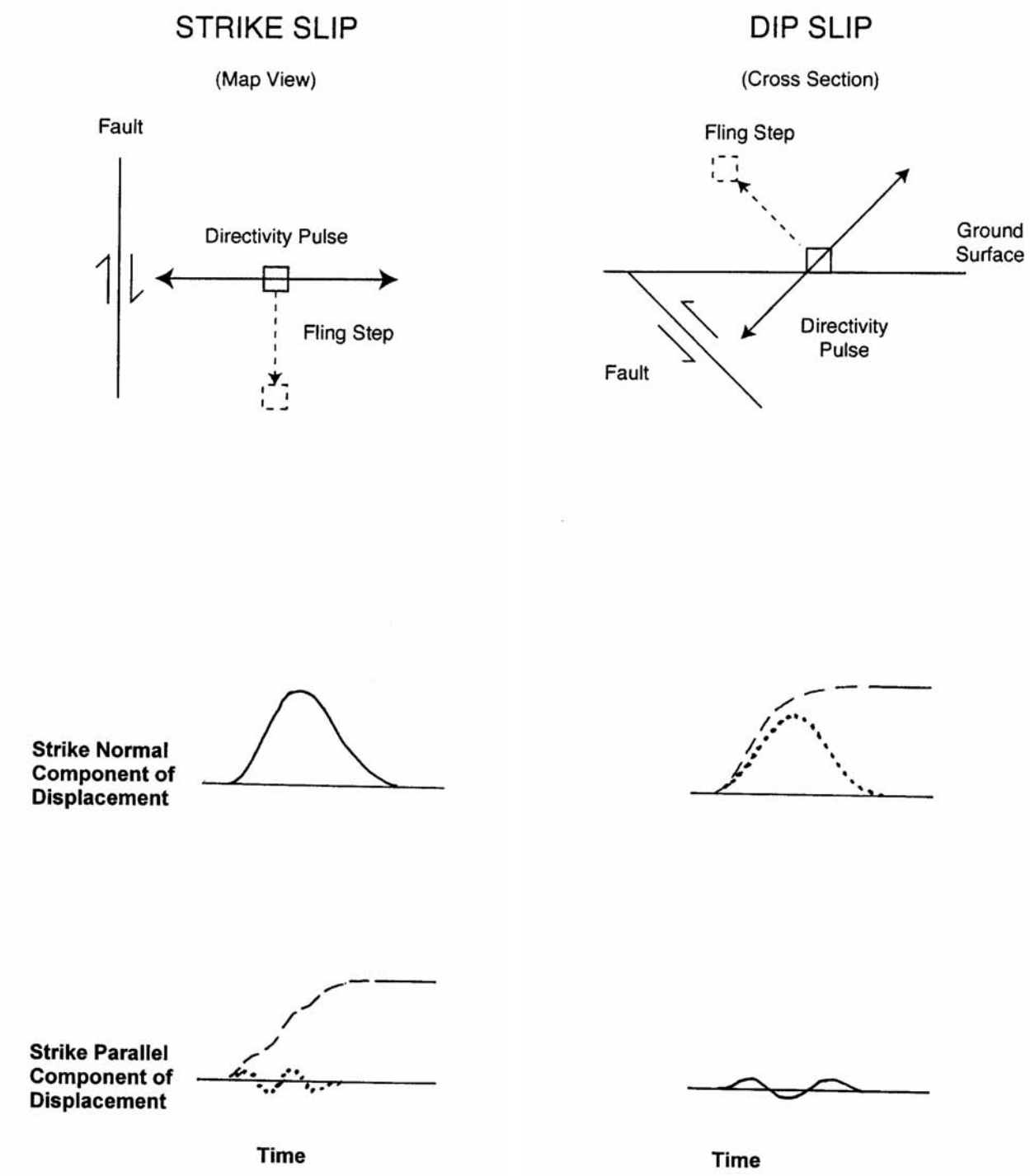

Figure 2. Top: Schematic orientation of the rupture directivity pulse and fault displacement ("fling step") for strike-slip (left) and dip-slip (right) faulting. Bottom: Schematic partition of the rupture directivity pulse and fault displacement between the strike normal and strike parallel components of ground displacement. Waveforms containing static ground displacement are shown as dashed lines; versions of these waveforms with the static displacement removed are shown as dotted lines.

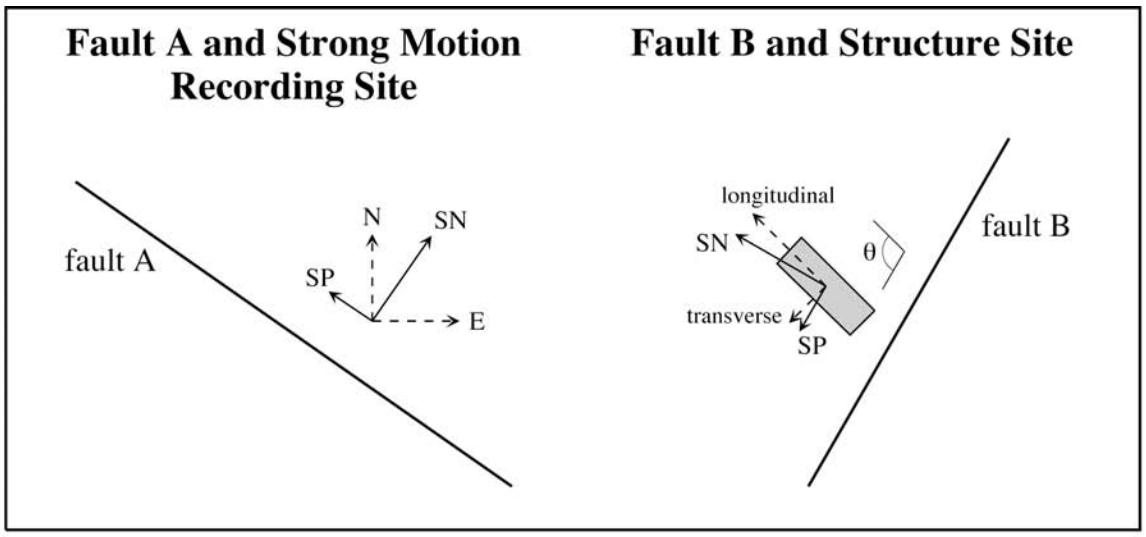

Figure 3. Archiving (left) and application (right) of strike-normal and strike-parallel components of ground motion.

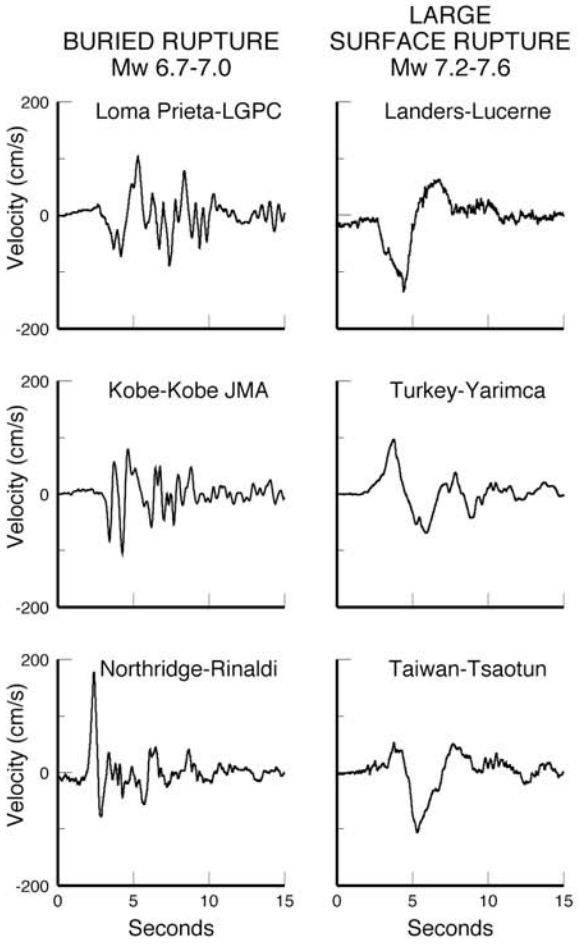

Figure 4. Fault-normal velocity pulses recorded near three moderate magnitude earthquakes (left column) and three large magnitude earthquakes (right column), shown on the same scales.

elastodynamic representation theorem, which states that the ground motion U(t) can be calculated from the convolution of the slip time function D(t) on the fault with the Green's function G(t) for the appropriate distance and depth, integrated over the fault rupture surface [4]:

$$U(t) = \sum D(t) * G(t)$$

When a near-fault ground motion time history is used for the analysis of a structure at a site, the strike-normal and strike-parallel components need to be oriented with respect to the strike of the fault that dominates the seismic hazard at the site. The strike-normal and strike-parallel components may be transformed into longitudinal and transverse components, preserving the orientation of the motions with respect to the fault strike, as illustrated on the right side of Figure 3. If the axis of the structure is aligned at some angle θ to the strike of the fault, then the longitudinal and transverse time histories can be derived from the strike-normal (SN) and strike-parallel (SP) time histories using the following transformation:

$$long = SP \cos\theta + SN \sin\theta; \quad trans = SP \sin\theta - SN \cos\theta$$

NEAR FAULT GROUND MOTION MODELS

The relationships between the dynamic and static components of near-fault ground displacements are quite complex, as illustrated in Figure 2. For example, the rupture directivity pulse and the static ground displacement occur on orthogonal components in strike-slip faulting, but on the same component in dip-slip faulting. The rupture directivity pulse can be very strong off the end of a strike-slip fault, where there is little or no static displacement. The 1989 Loma Prieta and 1994 Northridge earthquakes produced strong rupture directivity pulses even though they did not rupture the ground surface. This indicates that separate models are needed for predicting the dynamic and static components of near-fault ground displacements at a site. The separately estimated dynamic and static components of the ground motion can be combined to produce ground motion time histories representing both effects. In the following, we present models for predicting dynamic near fault ground motions. The static displacement field of earthquakes can be calculated using theoretical methods [4], and surface fault displacements can be estimated using empirical models [5].

Broadband Directivity Model

Somerville et al. [3] developed a model for near-fault ground motions that assumes monotonically increasing spectral amplitude at all periods with increasing magnitude. This model can be used to modify conventional ground motion attenuation relations to account for the amplitude and duration effects of rupture directivity. Abrahamson [6] demonstrated that incorporation of a modified version of this model in a probabilistic seismic hazard calculation results in an increase of about 30% in the spectral acceleration at a period of 3 seconds for an annual probability of 1/1,500 at a site near a large active fault.

Narrow Band Directivity Model

Strong motion recordings of the recent large earthquakes in Turkey and Taiwan indicate that the near fault pulse is a narrow band pulse whose period increases with magnitude. In Figure 4, forward rupture directivity pulses of earthquakes in the magnitude range of 6.7 to 7 are compared with pulses from earthquakes in the magnitude range of 7.2 to 7.6. The narrow band nature of

these pulses causes their elastic response spectra to have peaks, as shown in Figure 5. The fault normal components (which contain the directivity pulse) are shown as solid lines, and the fault parallel components, which are much smaller at long periods as expected, are shown by long dashed lines. The 1994 UBC spectrum for soil site conditions is used as a reference model for comparison. The spectra for the large earthquakes (right column) are compatible with the UBC code spectrum in the intermediate period range, between 0.5 and 2.5 seconds, but have a peak at a period of about 4 seconds where they significantly exceed the UBC code spectrum. The spectra of the smaller earthquakes (left column) are very different from those of the larger earthquakes. Their spectra are much larger than the UBC code spectrum in the intermediate period range of 0.5 - 2.5 sec, but are similar to the UBC spectrum at longer periods.

The recent large earthquakes in Turkey and Taiwan, which caused large surface ruptures, have surprisingly weak ground motions at short and intermediate periods. These new observations are consistent with our finding from previous earthquakes that the strong ground motions of earthquakes that produce surface faulting are weaker than the ground motions of events whose rupture is confined to the subsurface. All of the earthquakes in the magnitude range of 6.7 – 7.0 shown in Figures 4 and 5 are characterized by subsurface faulting, while all of the earthquakes in the magnitude range of 7.2 to 7.6 are characterized by large surface displacements. Consequently, some of the differences seen in these figures may be attributable not only to magnitude effects, but to the effects of buried faulting [7].

The magnitude scaling exhibited in the data in Figures 4 and 5 is contrary to all current models of earthquake source spectral scaling and ground motion spectral scaling with magnitude, which assume that spectral amplitudes increase monotonically at all periods. However, these magnitude scaling features are the natural consequence of the narrow band character of the forward rupture directivity pulse. The period of the near fault pulse is related to source parameters such as the rise time (duration of slip at a point on the fault) and the fault dimensions, which generally increase with magnitude.

Preliminary response spectral models that include the magnitude dependence of the period of the rupture directivity pulse are shown in Figure 6. These models are derived from empirical relations between pulse period and magnitude [7]. Figure 6 compares the response spectra for rock and soil predicted by this model with the standard model of Abrahamson and Silva [8], which does not explicitly include directivity effects, and the broadband model of Somerville et al. [3], whose directivity effects are based on the monotonic increase of ground motion amplitudes with magnitude at all response spectral periods. The narrowband model produces larger response spectra in the period range of about 0.5 to 2 seconds for earthquakes smaller than M_w 7.5, and smaller response spectra at all periods for earthquakes larger than M_w 7.5, compared with the broadband model.

TIME DOMAIN MODELS OF NEAR FAULT GROUND MOTIONS

The response spectrum models shown in Figure 6 do not adequately represent the demand for a high rate of energy absorption presented by near-fault pulses. Near fault ground motions containing forward rupture directivity may be simple enough to be represented by simple time

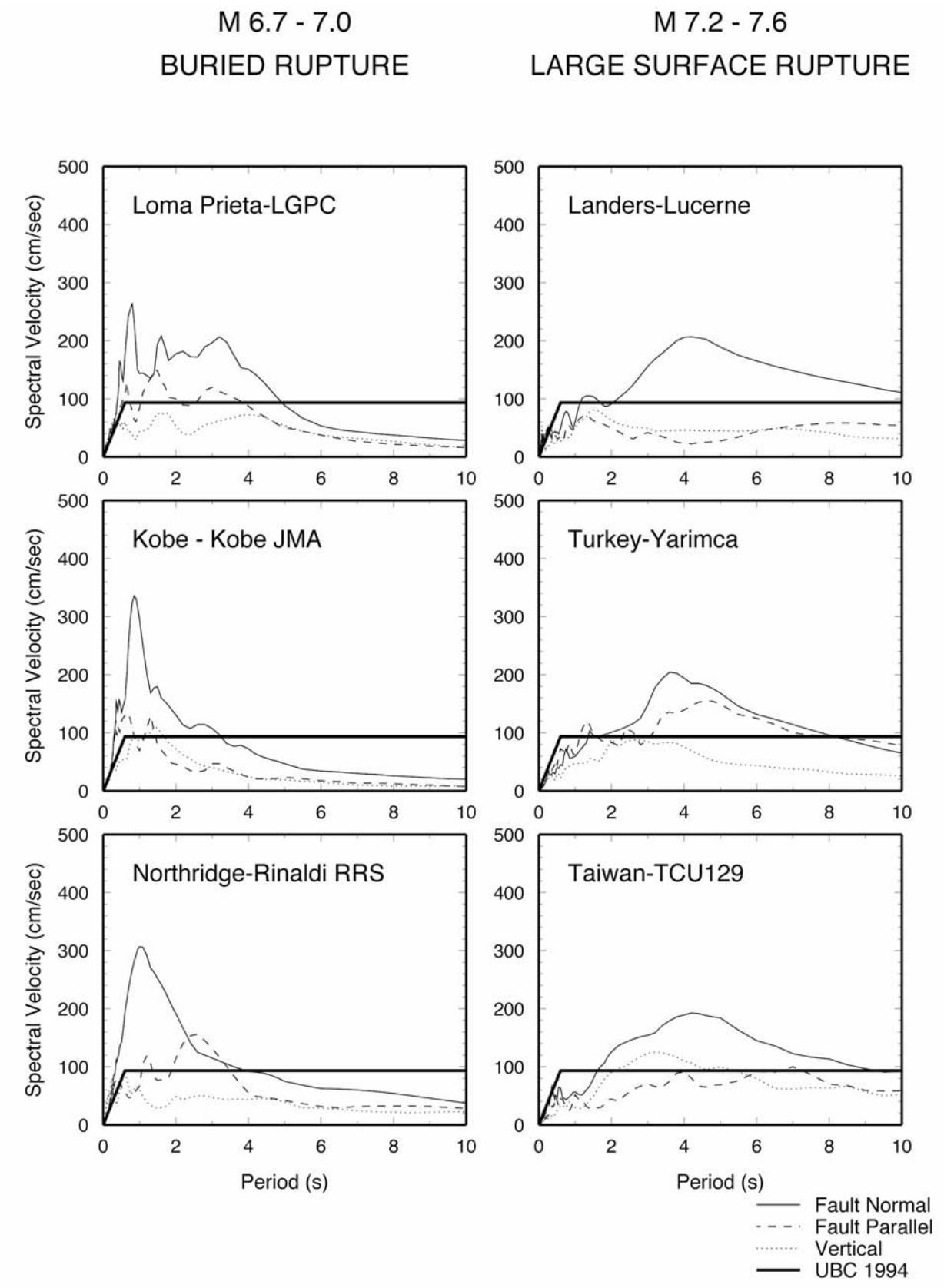

Figure 5. Spectral velocity of fault-normal pulses of moderate (left) and large (right) earthquakes.

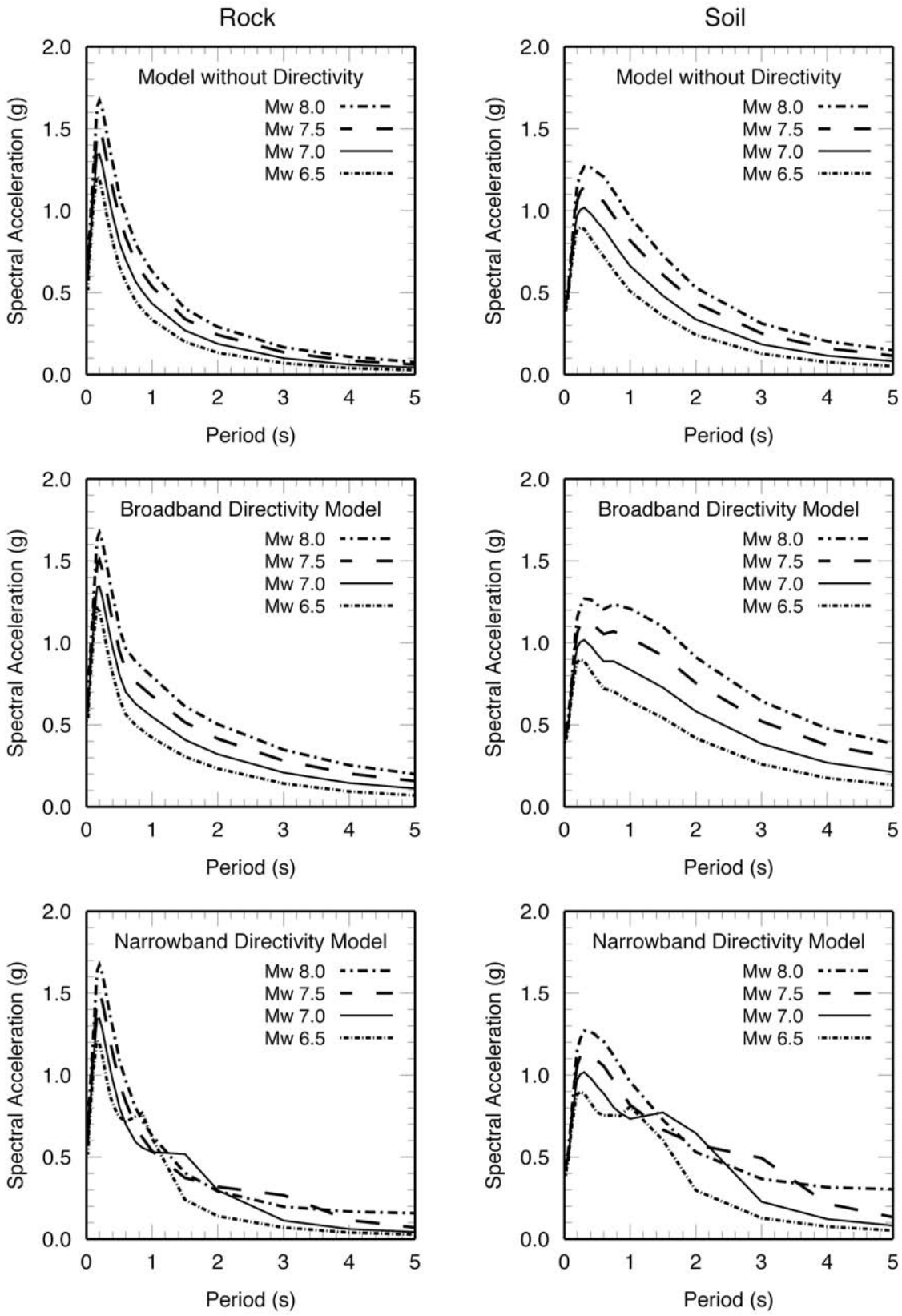

Figure 6. Near fault response spectral model, strike-slip, 5km for rock sites (left) and soil sites (right). Top: model without directivity (Abrahamson and Silva, 1997). Middle: Broadband directivity model (Somerville et al., 1997). Bottom: Narrow band directivity model (Somerville, 2001).

domain pulses, thus simplifying the specification of ground motion time histories for use in structural response analyses. Preliminary equations relating the period of the pulse to the earthquake magnitude, and the effective velocity of the pulse to the earthquake magnitude and distance, have been developed by Somerville [7], Somerville et al. [9], Alavi and Krawinkler [10], and Rodriguez-Marek [11]. The effect of the simultaneous dynamic and static ground motions on the response of a structure can be analyzed using time histories that include both the dynamic rupture directivity pulse and the static ground displacement.

CONCLUSIONS

Near-fault ground motions differ from ordinary ground motions in that they often contain strong coherent dynamic long period pulses and permanent ground displacements. The dynamic motions are dominated by a large long period pulse of motion that occurs on the horizontal component perpendicular to the strike of the fault, caused by rupture directivity effects. Near fault recordings from recent earthquakes indicate that this pulse is a narrow band pulse whose period increases with magnitude, as expected from theory. This magnitude dependence of the pulse period causes the response spectrum to have a peak whose period increases with magnitude, such that the near-fault ground motions from moderate magnitude earthquakes may exceed those of larger earthquakes at intermediate periods (around 1 second). The static ground displacements in near-fault ground motions, caused by the relative movement of the two sides of the fault on which the earthquake occurs, are discontinuous across a fault having surface rupture, and can subject a bridge crossing a fault to significant differential displacements. The static ground displacements occur at about the same time as the large dynamic motions, indicating that the static and dynamic displacements need to be treated as coincident loads.

REFERENCES

[1] Abrahamson, 1993. Spatial variation of multiple support inputs. *Proceedings of the first U.S. symposium on the seismic evaluation and retrofit of steel bridges*, U.C. Berkeley, October 18.

[2] Archuleta, R. J. and S. H. Hartzell, 1981. Effects of fault finiteness on near-source ground motion. *Bull. Seismol. Soc. Am*., 71: 939-957.

[3] Somerville, P.G., N.F. Smith, R.W. Graves, and N.A. Abrahamson (1997). Modification of empirical strong ground motion attenuation relations to include the amplitude and duration effects of rupture directivity, *Seismological Research Letters* 68, 199-222.

[4] Aki, K. and P.G. Richards (1980). *Quantitative Seismology: Theory and Methods*. W.H. Freeman & Co.

[5] Wells, D.L. and K.J. Coppersmith (1994). Analysis of empirical relationships among magnitude, rupture length, rupture area, and surface displacement, *Bull. Seismol. Soc. Am. 84*, 974-1002.

[6] Abrahamson, N.A., 2000. Effects of rupture directivity on probabilistic seismic hazard analysis. Proceedings of the 6th International Conference on Seismic Zonation, Palm Springs, Earthquake Engineering Research Institute.

[7] Somerville, P.G. (2001). Magnitude scaling of the near fault rupture directivity pulse. *Proceedings of the International Workshop on the Quantitative Prediction of Strong-Motion and the Physics of Earthquake Sources*, October 23-25, 2000, Tsukuba, Japan

[8] Abrahamson. N.A. and W.J. Silva, 1997. Empirical response spectral attenuation relations for shallow crustal earthquakes. *Seismological Research Letters*, 68: 94-127.

[9] Somerville, P.G., H. Krawinkler and B. Alavi, 2000. Development of improved ground motion representation and design procedures for near-fault ground motions. *Final Report to CSMIP Data Utilization Program*, Contract No. 1097-601.

[10] Alavi, B. and H. Krawinkler, 2000. Design considerations for near-fault ground motions. *Proceedings of the U.S. – Japan Workshop on the Effects of Near-Fault Earthquake Shaking*, San Francisco, March 20-21.

[11] Rodriguez-Marek, A., 2000. Near fault seismic site response. Ph.D. Thesis, Civil Engineering, University of California, Berkeley, 451 pp.

Designing Ordinary Bridges for Ground Fault Rupture

Stewart Gloyd, Raymond Fares, Anthony Sánchez, and Vinh Trinh

ABSTRACT

Ground fault rupture from past seismic events, both vertical and horizontal, was discovered by site trenching during the final design phase of an otherwise ordinary freeway completion project in San Bernardino, California. Several existing and proposed new bridges of various span lengths and column height configurations are in the area of the fault rupture and it was not feasible to avoid the entire fault zone by revising the roadway alignments. With no established criteria or precedent for considering ground fault rupture at ordinary bridges, special design approaches were necessary. A determination of fault rupture magnitude for design or evaluation of structures was made using both deterministic and probabilistic methods. Concept studies were performed to determine whether or not it was feasible to use the Caltrans normally preferred continuous span monolithic frame structure configuration for the new bridges. There was also the question of whether to design for fault rupture as a separate loading condition or in combination with the severe near fault ground shaking applicable at this site, and if so how to do this. A special technical advisory panel was used by the California Department of Transportation (Caltrans) to provide additional guidance on both the seismic and structural issues. The resulting design method provides a reasonable measure of confidence regarding collapse prevention from possible future seismic ground rupture permanent displacement, and accomplisheshis without a highly complex bridge design procedure.

Stewart Gloyd, P.E., Senior Engineering Manager, Parsons Brinckerhoff, 685 E. Carnegie Drive, Suite 210, San Bernardino, CA 92408
Raymond Fares, P.E., Structural Engineering Manager, Parsons Brinckerhoff, 685 E. Carnegie Drive, Suite 210, San Bernardino, CA 92408
Anthony V. Sánchez, Ph.D., P.E., Associate Bridge Engineer, T.Y. Lin International, 5030 Camino de la Siesta, Suite 204, San Diego, CA 92108
Vinh Trinh, S.E., Project Manager, W. Koo and Associates, Inc., 600 The City Parkway West, Suite 310, Orange, CA 92868

INTRODUCTION AND PROJECT DESCRIPTION

Segment 11 is a freeway-to-freeway interchange project in San Bernardino, California. Parsons Brinckerhoff (PB) is preparing the final design and PS&E for the project. PB is assisted by subconsultants T.Y. Lin International and W. Koo & Associates, Inc., for structural design.

This long planned new east-west freeway will be designated as SR-210, replacing the existing SR-30 (See Figure 1). All of the structures for the project are considered to be of an ordinary nature, that is, there are no unusually long spans or complex geometric shapes involved. These highways are important to the transportation of the immediate region but are not designated as critical state or defense routes.

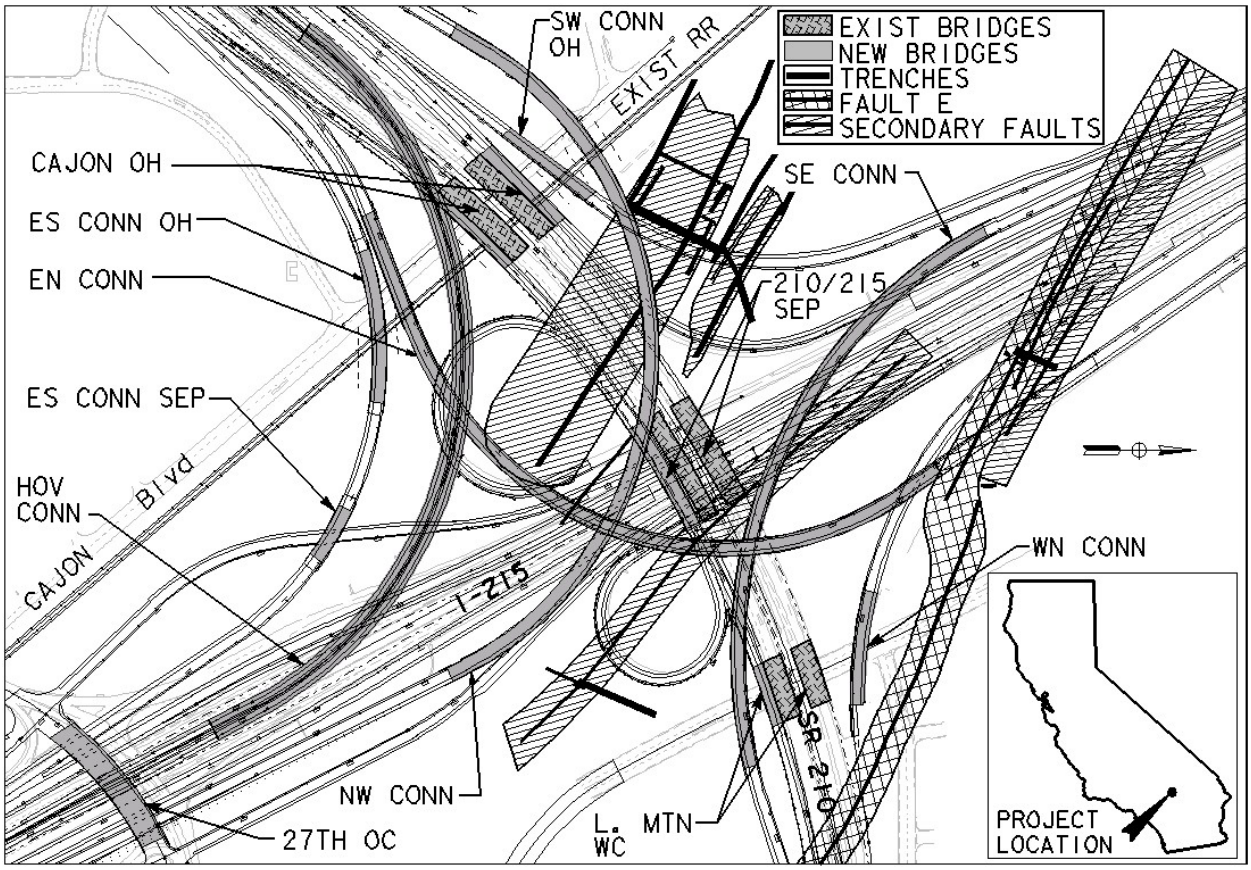

Figure 1. Project Location with Fault Rupture Zones

Geographically this project lies between two major known seismic faults: the San Jacinto fault is about 3 km to the west; the San Andreas fault is about 6.5 km to the east. Preliminary geotechnical studies indicated that possible evidence of past ground fault rupture existed in this area, and recommended that the design program include a more thorough investigation.

An investigation of past fault rupture was made by Earth Mechanics, Inc. (EMI), a geotechnical subconsultant to the PB team. Surface fault rupture evidence was found, and the results were interpreted as requiring design consideration for fault rupture within the freeway to freeway interchange area [1]. See Figure 1 for project location and interchange configuration.

Altogether, the structures in this fault risk area include four existing bridges to be widened, four new long multi-span high level connector structures, four other connector structures, and a new four span freeway overcrossing structure.

DISCOVERY OF GROUND FAULT RUPTURE

The PB team geologist first reviewed early aerial photographs and other references to identify potential fault rupture traces. A trenching program was then conducted to determine whether actual fault rupture had historically occurred in the vicinity of the planned structures. Figure 1 shows fault traces and trench locations. Trenches were excavated transversely across the potential traces to intercept the suspected fault lines.

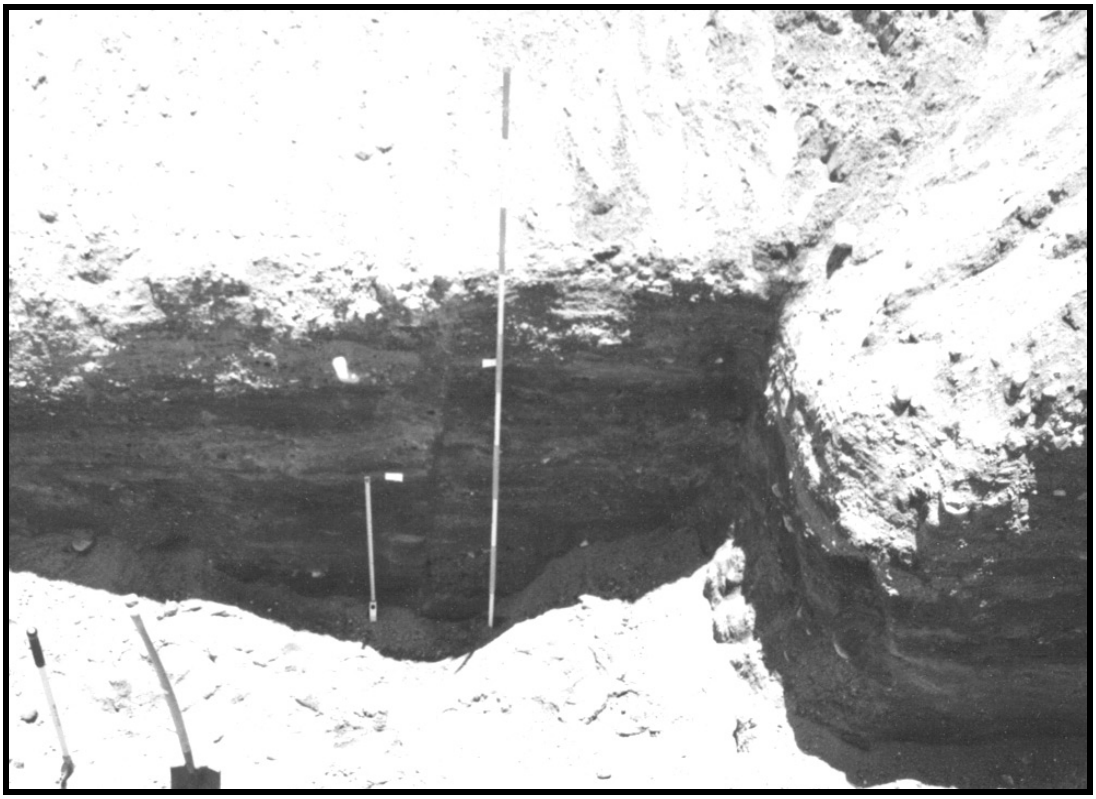

Figure 2. Trench Showing Vertical Fault Rupture of about 0.6 m.

Fault rupture was noted at many locations within the interchange area of the project. Figure 2 shows a vertical fault rupture at a typical trench face.

The findings were that most of these fault ruptures were of a secondary nature caused by ground distortion associated with the nearby major faults. However, one of the fault traces where rupture was found was interpreted to be a primary fault (Fault E).

Future fault rupture is more likely to occur in the same places as past fault rupture. The state of the art for other major infrastructure such as schools and hospitals is a deterministic approach that assumes that another rupture of similar magnitude as was observed in the trenching program could occur during the life of the structures being designed. To account for uncertainty in the location, a setback zone of 15 to 20 meters is used. The PB team geologist made design recommendations based on this approach. The recommendations included fault rupture magnitudes, both horizontal and vertical, and specific locations and zones where foundation placement is to be avoided. The zones are shown on Figure 1.

Caltrans practice when fault rupture is encountered is to avoid building bridges across the faults, but there were no feasible alternatives that would accomplish this objective. Due to the unprecedented nature of this situation, Caltrans called for a Technical Advisory Panel (TAP) to review the information and provide expert recommendations. The PB design team provided information and assistance to the TAP. The TAP concurred with the EMI findings regarding the nature of the observed faulting in this area, but concluded that future rupture could occur anywhere within the interchange area, and therefore recommended a "floating fault" concept for design purposes. Using a probabilistic approach the TAP determined the range of magnitudes that could occur associated with various return periods [2].

Caltrans strongly recommended that no structures be built across Fault E [3]. Design concepts for avoiding a structure over that location are being identified so that at least one feasible solution is available for future implementation.

There was not a consensus on the issue of whether it is necessary, for the purposes of structure design, to combine the effects of ground shaking with surface fault rupture. EMI did not recommend combining the effects because they believe the peak values do not occur simultaneously. The TAP believed that although the design level ground shaking can occur without surface fault rupture, surface fault rupture will definitely be accompanied by strong ground shaking. The TAP felt that a time history analysis was necessary to properly determine the combined effect.

DESIGN ISSUES AND CRITERIA

Structures Affected by the Fault Rupture

The deterministic faults identified by EMI are at specific locations, and effect only the structures within the setback zones. However, the floating faults introduced by the TAP for consideration of possible fault surface displacements from secondary faults would affect all the structures within close proximity of the SR-210/ I-215 Interchange. Floating faults can occur anywhere: between bents, between columns in a multi-column bent, within a foundation, or within an abutment.

Table I lists the structures affected by either the deterministic or floating fault displacements.

TABLE I- SUMMARY OF BRIDGE STRUCTURES POTENTIALLY AFFECTED BY FAULT RUPTURE

Bridge Name[2]	Length/ Width (m)	Spans	Bent Type[1]	Probabilistic Fault Type	Intersects Deterministic Fault
Cajon Blvd OH Widen	84/27	2	M	Floating	None
210/215 Separation Widen	97/30	3	M	Floating	None
Little Mtn Dr UC Widen	50/26	1	-	Floating	None
WN Connector Widen	59/13	1	-	Floating	None
27th Street OC (Replace)	116/21	4	M	Floating	None
NW Connector	648/13	13	S	Floating	G & H
SW Connector OH	88/13	2	S	Floating	None
HOV Connector (ES/NW)	933/18	20	S	Floating	None
EN Connector	1042/13	26	S	Floating &	A, E, & G
ES Connector OH	128/13	2	S	Floating	None
ES Connector SEP	43/13	1	-	Floating	None
SE Connector	492/13	9	S	Floating	None

[1]Bent Type: S = Single Column Bent, M = Multi-Column Bent

[2] All Structures are CIP/PS Box Girders

Surface Displacement Demands

The surface displacement demands have been developed from the geotechnical investigation conducted specifically for the purpose of establishing the fault rupture design criteria for this project. Two sets of displacements were considered: probabilistic and deterministic. The probabilistic surface displacement demands are as recommended by the TAP and defined in the Probabilistic Fault Displacement Hazard Analysis (PFDHA) Study [2]. The deterministic displacements were developed by EMI and represented the expected maximum surface displacement values at the various faults [1]. The project design criteria is to consider the upper limit of the probabilistic displacement values described in Table II, preferably with the displacement capacity based on normal material properties [4]. In addition, the design is to consider the deterministic displacement values, but the realistic ultimate (experimentally based) values for displacement capacity can be used for this design condition.

TABLE II-SURFACE DISPLACEMENT VALUES

	Fault	Return Period (years)	Horizontal Displacement Component	Vertical Displacement Component	Affected Structures
PROBA-BILISTIC	E	1500-5000	0 - 0.6 m (2 ft)	0 - 0.2 m (8 in.)	All
	Floating	1500-5000	0 - 0.2 m (8 in.)	0 - 0.2 m (8 in.)	All
DETERMI-NISTIC	A		1.000 m (3.3 ft)	1.000 m (3.3 ft)	EN & SE Connectors
	E		1.500 m (5.0 ft)	0.500 m (1.6 ft)	EN Connector
	E [1]		0.050 m (2.0 in.)	0.500 m (1.6 ft)	EN Connector
	G		0.125 m (0.4 ft)	1.250 m (4.1 ft)	EN & NW Connector
	H		0.060 m (2.4 in.)	0.600 m (2.0 ft)	NW Connector

[1] Subsidiary faults associated with Fault E.

Fault Rupture Load Cases

The surface displacement demands applied to the structures constituted an additional seismic load case, Group VII_{FR}. Group VII_{FR} loading was considered in addition to the standard Group I – VII loading as defined in the code [5].

Group VII_{FR} loading is as follows, where FR is the static loading resulting from applying the design fault rupture displacements to the structure, and D, E, B, SF, PS, EQ and β_E are as defined in the code. Note that ground shaking (EQ) is included in Group VII_{FR-1} only.

$$\text{Group } VII_{FR-1} = 1.0\,[1.0\,D + \beta_E\,E + 1.0\,B + 1.0\,SF + 1.0\,PS + 1.0\,EQ + 1.0\,FR] \quad (1)$$

$$\text{Group } VII_{FR-2} = 1.0\,[1.0\,D + \beta_E\,E + 1.0\,B + 1.0\,SF + 1.0\,PS + 1.0\,FR] \quad (2)$$

For Group VII_{FR-1}, probabilistic surface displacement (FR) demands are to be combined with the demands resulting from the associated ground shaking (EQ). The directions of ground shaking and the direction of the surface displacement within the specified range are to be selected to maximize the effects under consideration. For Group VII_{FR-2}, deterministic surface displacements (FR) are to be used without ground shaking.

The strength reduction factor, $\Phi = 1.0$ is used unless otherwise specified.

Performance Objectives

The performance objectives for the fault rupture load case is as outlined below.

- Performance Level – No Collapse
- Damage Level - Significant Damage
- Service Level – Minimally serviceable to unserviceable after event

The standard definition of the "No Collapse" criteria has been that the ductile components (columns) may reach their ultimate limits and undergo significant inelastic action and sustain major damage. The capacity design philosophy, as applied by Caltrans, dictates that even under this level of damage to the ductile components, the capacity protected components (superstructure, bent caps and foundations) are to remain essentially elastic and undamaged [6]. For the fault rupture load case, the "No Collapse" performance level is amended to allow limited inelastic action in the capacity protected components. However, a ductility analysis must be performed to verify the deformation capacity of any component that is allowed to deform beyond the essentially elastic level.

Structure Vulnerability

Table III summarizes the potential vulnerabilities of the bridge structures subjected to the fault rupture surface displacements.

TABLE III-POTENTIAL STRUCTURAL VULNERABILITIES FROM FAULT RUPTURE

	Displacement	Vulnerabilities	Comments
Superstructure	Horizontal	None expected	Displacements accommodated primarily by flexural hinging of the columns. Torsional demands on box girders not expected to be significant. Unseating of hinges should be considered.
	Vertical	High flexural and shear demands	For short span or existing structures, may not be practical to design superstructures to remain elastic as per SDC. Therefore, design for adequate ductility. Bearing uplift at hinges should be considered.
Bent Cap	Horizontal (Transverse)	Flexural demands	Bent cap capacity protected by plastic hinging in columns. Group VII demands expected to control.
	Horizontal (Longitudinal)	Torsional demands	Longitudinal hinging in columns causes torsional demands on cap, similar to Group VII. No special analysis should be required for monolithic box girder structure.
	Vertical	Flexural and Shear demands	Hinging expected in columns for two-column bents. Flexural hinges may develop in bent caps with three or more columns.
Column	Horizontal	Flexural hinging	Not expected to control design. P-delta effects in the transverse direction should be considered.
	Horizontal (Footing Rotation)	High torsional demands	Compatibility torsion is dependent on column stiffness (cracked). May control the transverse reinforcement design.
	Vertical	None expected	Displacements accommodated by superstructure.
Footing	Horizontal	None expected	Preferred pile head connection is a pin-type to limit moment transfer into the pile cap. Displacements accommodated by flexure of the piles.
	Vertical	Flexural and Shear demands	Resulting force couple limited by column plastic hinging and effects of global axial loads. Not expected to control design.
Pile	Horizontal	Flexural demands	Piles shall be designed to have sufficient flexural strength and ductility to accommodate the displacements.
	Vertical	Additional axial forces	Resulting force couple limited by column plastic hinging. Not expected to control design.

Horizontal Mechanism

Figure 3 describes the generally expected deformation of multi-span structures subjected to horizontal fault rupture. Columns form plastic hinges and thereby accommodate the displacement demand without significant effect on the superstructure.

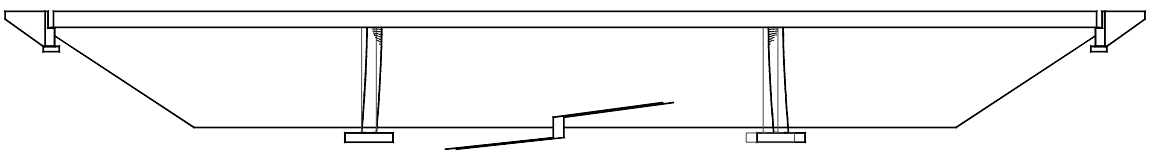

Figure 3. Longitudinal Displacement in Main Span Causes Hinging in Columns

Vertical Mechanism

Figure 4 describes the expected deformation of continuous structures subjected to vertical fault rupture. Plastic hinges will form in the superstructure when the elastic capacity is

exceeded. Collapse prevention is accomplished by ensuring adequate displacement and shear capacity.

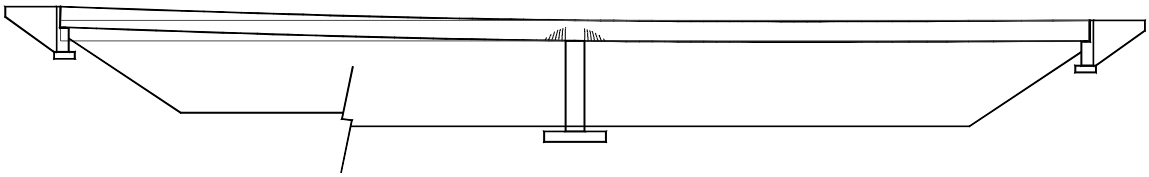

Figure 4. Vertical Displacement Between Abutment And Bent Causes Hinging In Superstructure

Combining Fault Rupture with Ground Shaking Displacements

To account for the coincidence of ground shaking and fault rupture displacements, the probabilistic based design displacements are combined with the displacements generated from ground shaking. A vector combination of the maximum fault rupture displacement (in the controlling fault direction) with the displacements generated from the elastic dynamic analysis (under earthquake shaking in a direction normal to the fault) was adopted for design purposes. See Figure 5. This simple method is used in lieu of a time history analysis recommended by the TAP.

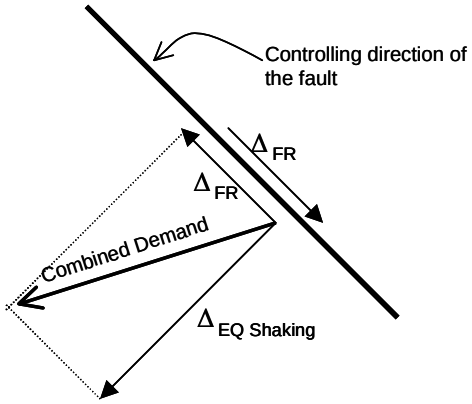

Figure 5. Combined FR and EQ Shaking Displacements

Combinations such as the 30% rule usually used for uncertainty of dynamic shaking direction were not used when combining the effects of fault rupture displacements in a known direction.

When using the deterministic surface displacements values, a static check for the surface displacements alone is sufficient; i.e. combining the deterministic surface displacements with the effects of ground shaking is not required. This is based on the team geologist's belief that the peak effects do not occur simultaneously.

STRUCTURE DESIGN IMPLEMENTATION

Design Concepts

A design concept study was performed to evaluate several potentially viable structure types that could be well suited to the special conditions of the project site, namely the ability to

accommodate large permanent horizontal and vertical ground displacements from a surface fault rupture event [4]. The preliminary design concepts included the following:

1. Standard CIP/PS concrete box girder superstructure with monolithic bents
2. Decoupled CIP/PS box girder superstructure on bearings
3. Modified box girder with secondary systems
4. Monolithic superstructure with very long spans - 250 to 350 ft
5. Steel girder superstructure on bearings
6. Multiple simple-span superstructure
7. Back to back cantilever spans - hinge in alternate spans at L/2
8. Bridge structure on continuous, rigid grade beam

Additional criteria used to evaluate the viability of the various concepts were: constructibility, serviceability and maintenance characteristics, impacts to geometrics of interchange, performance under standard seismic loading (ground shaking), and construction and life cycle costs. After evaluating and ranking the concepts according to their ability to accommodate the ground displacements as well as the additional criteria, concepts 1, 2 and 3 were chosen for detailed consideration for the new bridges on the project.

Adopted Structure Configuration

The standard CIP/PS concrete box girder with monolithic bents, incorporating modified details and secondary systems was chosen as the most viable design concept. The reasons for this type selection were as follows: relative ease of construction by established methods, excellent serviceability and low maintenance characteristics, well suited to curved alignment of interchange ramps, proven performance under standard seismic loading (ground shaking), low construction and life cycle costs. In addition, the use of long spans and special detailing allows this structure type to accommodate the large permanent horizontal and vertical ground displacement demands.

Superstructure Design

According to established bridge seismic design philosophy, the columns are designed to hinge under imposed horizontal displacement demands [6]. Hence, the critical demands on the superstructure are a result of relative vertical displacement demands between adjacent supports, as can be seen in Figure 4. As such, the following approach was used for the design of the superstructures:

- Take advantage of inherent displacement and flexural capacity of well-detailed, ductile concrete members
- Strengthen and/or detail critical superstructure regions for additional demands caused by vertical displacements
- Strengthening measures can include additional mild steel reinforcement, increased prestress force, thickened slabs and girders and increased concrete strength

- If it is not practicable to provide sufficient strength to resist the flexural demands elastically, then adequate ductility must be ensured by proper detailing and verified with a ductility analysis
- Measures to increase ductility can include thickened slabs with seismic ties to enhance confinement and including mild steel reinforcement in top and bottom slabs
- Consider using secondary systems to support dead load of superstructure

Substructure Design

The design of the substructure follows much of the current seismic design concepts, where the columns are sized and detailed to be the ductile elements, and are able to accommodate large horizontal displacement demands.

Bent Cap Design

As per standard seismic design criteria [6], under horizontal displacement demands, the columns are designed to form plastic hinges. The bent caps are designed with sufficient moment capacity and shear strength to resist the moment input and joint shear forces from the columns. However, relative vertical displacements between columns in a bent with three or more columns can result in large displacement demands and plastic hinging within the bent caps. Thus, when practicable, bent caps are designed with either one or two columns to avoid the potential for increased flexural demands.

Column Design

The columns are designed with enhanced ductility to respond to the increased demands from horizontal fault rupture displacements as can be seen in Figure 3. Some special considerations for the design of the substructure for fault rupture ground displacements included:

- Consider the horizontal displacement demands from ground shaking in combination with the demands from the surface displacements from fault rupture.
- Consider the effects of the vertical displacements on the columns in the form of increased axial loads and moment demands from the superstructure.
- Consider the effects of tension demands on the columns from uplift of the superstructure at adjacent support, or downward vertical displacement of the ground beneath the column. These effects include reduced shear and moment capacity.
- Consider rotational demands on the columns from horizontal displacements at the footing or within the pile group.
- Consider demands on bent caps from vertical column displacements

Foundation Design

Areas of concern for foundations include the nature of load application, footing rotation, flexural and shear capacity of the foundation components, and pile response.

Desirable attributes of the preferred foundation system include compactness and ductility. A compact foundation will minimize the possibility of the fault rupture occurring within the foundation system, while ductility in the chosen system will ensure dependable strength and displacement capacity in the event that a fault rupture occurs within the foundation. CIDH pile shafts are the most compact foundation type, and have demonstrated high levels of ductility in laboratory tests. As such, they were given serious consideration for use on the project.

The structural elements of the foundation system were designed with sufficient strength and/or ductility to resist the maximum loads and displacement demands caused by a fault rupture through the foundation system. Realistic upper bounds for the ultimate foundation capacities including soil bearing pressure, soil-pile cap coefficient of friction, pile skin-friction and compression and tension capacities for the piles, are used for the fault rupture load case to ensure that failure does not occur in the structural components of the foundation system.

Abutment Design

The current standard for seismic design of abutments allows for large displacements by including large seat widths and sacrificial components such as the back-wall and shear keys. Special considerations for the design of the abutments include:

- Providing additional seat width to accommodate the increased displacement demands from the fault rupture event
- Designing the abutment for increased vertical forces from uplift of the abutment or downward displacement at the adjacent support

DESIGN RESULTS

Superstructure

The superstructures have been designed elastically to resist the moment demand generated the fault rupture load cases by adding mild steel over the bent as shown on Table IV for designs now completed or in progress.

TABLE IV – ADDITIONAL SUPERSTRUCTURE REINFORCEMENT

Structure	Additional Mild Steel
Cajon Blvd OH (Widen)	15-#36 Top, 10-#36 Bottom
Route 210/215 Separation (Widen)	32-#36 Top, 64-#36 Bottom
27th Street OC (Replace)	35-#36 Top, 48-#32 Bottom
NW Connector	72-#43 TOP, 80-# 43 Bottom

The structures listed above are subject to the probabilistic fault rupture load case of 0.2 m vertical displacement and ground shaking (column Mp), except for the NW Connector, which is subject to additional deterministic fault rupture load case of 0.6 m vertical displacement. The added mild steel is relatively extensive but can be accommodated within the superstructure deck and soffit slabs.

Substructure & Foundations

The columns are designed with adequate ductility capacity to resist the displacement generated by combining fault rupture displacement and ground shaking as shown in Table V for designs now completed or in progress.

TABLE V – SUBSTRUCTURE DUCTILITY AND DISPLACEMENT DEMANDS

Structure	Ductility Demand		Displacement D/C	
Fault rupture in the longitudinal direction	Ground Shaking	Combined	Ground Shaking	Combined
Cajon Blvd OH (Widen)	4.20	5.00	0.75	0.83
Route 210/215 Separation (Widen)	2.61	3.08	0.75	0.95
27th Street OC (Replace)	4.05	4.75	0.86	0.95
NW Connector[1]	2.80	3.40	0.80	0.98
Fault rupture in the transverse direction	Ground Shaking	Combined	Ground Shaking	Combined
Cajon Blvd OH (Widen)	1.92	2.50	0.45	0.54
Route 210/215 Separation (Widen)	2.01	2.29	0.90	0.94
27th Street OC (Replace)	4.39	5.61	0.92	1.00

[1]The NW Connector is on a curve and there is no apparent longitudinal or transverse direction.

For multi-column bents, where the columns are pinned at the bottom, the structure is modeled with one footing losing half of the piles and it is found that the increase in the structure displacement is minimal because there are other footings to share the load.

For tall single column bents, the large diameter cast-in-drilled-hole (CIDH) concrete shaft foundations are designed for the combined displacement demand without difficulty.

CONCLUSIONS

Prior to this project there was no precedent in California for the design of ordinary bridges for the effects of ground fault rupture. The discovery of ruptures in unavoidable locations at the site of this project presented challenges to the design team, the program management agency, and owner.

One approach would be to rationalize that fault rupture is very unlikely during the life of the project therefore the risk can be disregarded. This was rejected because the risk was comparable to extreme ground shaking and the state of the art is to design for at least no-collapse behavior for that occurrence.

A very conservative approach would be take the time to carefully research and test candidate structural systems to assure that behavior under fault rupture as well as ground shaking was satisfactory, and to develop design procedures for such systems. This was rejected because of cost and delay to the overall transportation project.

The approach used on this project was pragmatic. Determination of design displacements used both state of the art deterministic and probabilistic approaches, giving assurance that the design was reasonable. Bridge performance objectives were selected comparable to those accepted for extreme ground shaking, i.e. no collapse. The bridge configuration used is the now well tested and understood ductile frame system that is reliable for ground shaking effects. The additional demands for vertical fault rupture are accommodated by allowing plastic hinging of the superstructure if necessary. Demands for horizontal fault rupture were added to the displacement demands in the column. In some cases, displacement capacity was extended beyond normal design, but remained within levels that have been verified by large-scale testing.

The bridges were designed for the special project criteria without undue difficulty or significant extra cost to the construction or maintenance requirements. Although this project shows that ordinary bridges can accommodate some fault rupture, avoiding structures at fault rupture is still a prudent solution.

ACKNOWLEDGEMENTS

The San Bernardino Associated Governments (SANBAG) is the overall program manager for the Route 210 design and construction. The California Department of Transportation (Caltrans) owns and operates Route 210 as well as Interstate 215, and provided design oversight and special seismic design resources.

REFERENCES

[1] Earth Mechanics, Inc., “Fault Investigation, Segment 11 of State Route 30, East of Interchange 215, San Bernardino County, California.”, July 2000.
[2] Technical Advisory Panel, “Design Guidance for Fault Rupture Displacements at the SR 210/I-215 Interchange in San Bernardino.”, January 2001.
[3] Zelinski, Ray, “Route 210 Fault Rupture.” Caltrans Memorandum, March 2001.
[4] Parsons Brinckerhoff, et al. “Project Specific Seismic Design Criteria, SR 210/I-215 Segment 11.”, December 2001.
[5] California Department of Transportation, Bridge Design Specifications, LFD Version, April 2000.
[6] California Department of Transportation, Seismic Design Criteria (SDC), Version 1.2, December 2001.

Design of the Lytle Creek Wash Bridge to Survive Permanent Ground Displacements due to Surface Fault Rupture

Gregory V. Brown, PE

ABSTRACT

As part of the State Route 210 project in San Bernardino County, California, a new highway bridge will be constructed to span the Lytle Creek Wash. The bridge site is within one kilometer of the San Jacinto fault, which is capable of generating an earthquake with a magnitude of 7.5. Based on recorded earth movement in the project area, it is suspected that a splay of this fault lies beneath the wash and that permanent ground displacements on the order of 3.0 meters horizontally and 0.3 meter vertically could occur within the limits of the new bridge.

In addition, hydraulic studies indicate that long-term degradation of the stream bed will be significant and that additional headcutting and local scour at supports will be large, resulting in foundation conditions that will vary significantly over the anticipated life of the structure.

Due to the complexity of these issues and the lack of historic precedence in the design and construction of bridge structures under these conditions, the development of the design criteria to be used for this project was a difficult endeavor. This paper will describe the process by which the project-specific design criteria were established and highlight some of the design features of the final solution, which is currently being designed.

Gregory V. Brown, PE, Vice President, DMJM+HARRIS, 999 Town & Country Road, Orange, California 92868.

INTRODUCTION

The overall State Route 210 (SR-210) Improvements Project extends from the San Bernardino/Los Angeles county line to Interstate Highway 215 (Barstow Freeway.) The project is divided into 11 segments and includes the freeway system and interchanges, highway/street/road improvements, drainage facilities and other appurtenant features. DMJM+HARRIS is under subcontract with the San Bernardino Associated Governments (SANBAG), in cooperation with the California State Department of Transportation (Caltrans), for design work in Segment 10. DMJM+HARRIS is responsible for the design of a new bridge to carry SR-210 over Lytle Creek Wash, where a suspected earthquake fault lies.

The Lytle Creek Wash Bridge is proposed to be 170 meters long and carry a total of 8 lanes of traffic. The width of the bridge will vary from approximately 48 meters to 55 meters to accommodate the geometry of on-ramps and off-ramps from an adjacent interchange. Concrete slope protection will be added to the sides of the wash but the bottom will remain unimproved. For the majority of the year, the wash is dry; during the rainy season, very high-velocity flows can occur. The bridge soffit elevation must be established to convey the 100-year flood volume. An aerial photo of the bridge site is shown in Figure 1.

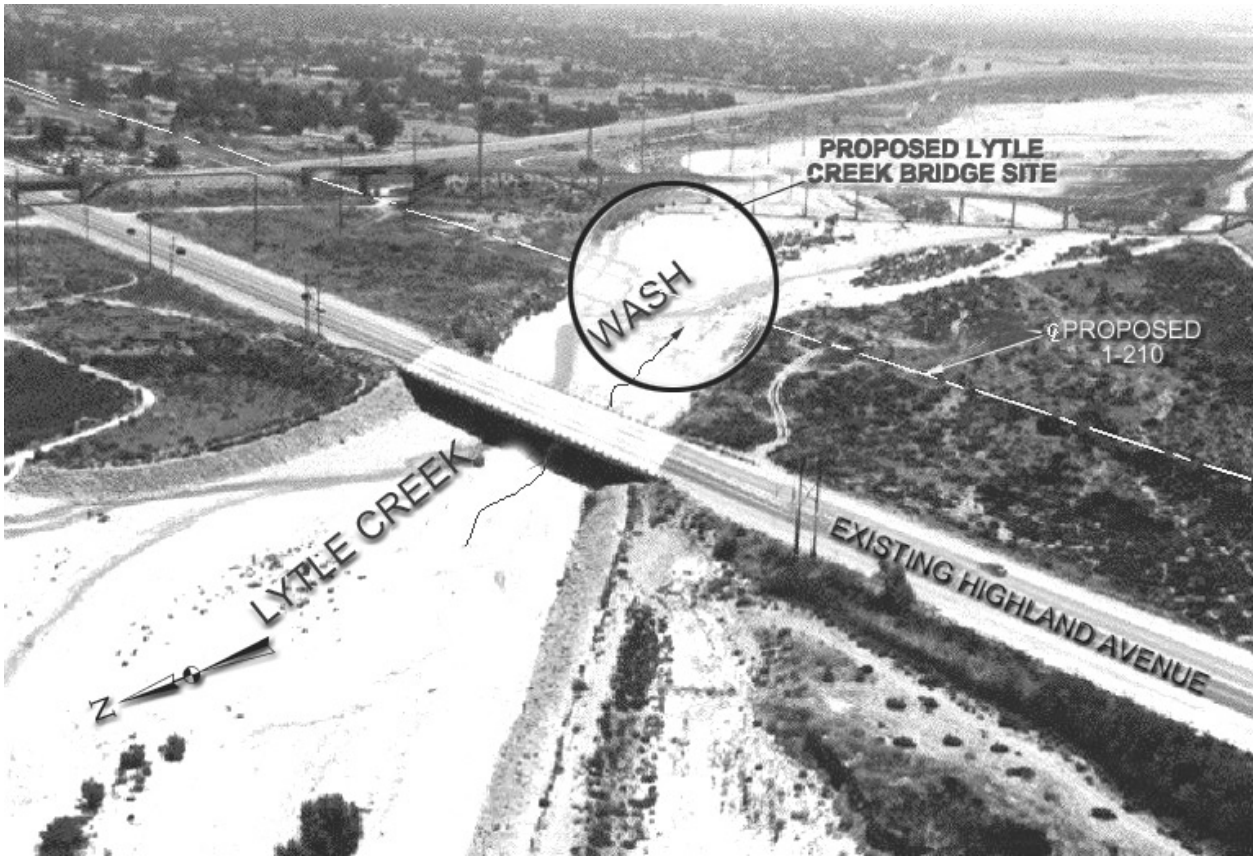

Figure 1. Aerial photo of the bridge site.

Immediately upstream of the site is the existing Highland Avenue crossing of the Lytle Creek Wash. Highland Avenue currently is State Route 30, which will be replaced by SR-210; the existing roadway and bridge will remain in service as a local route. Immediately downstream is an existing Union Pacific Railroad bridge.

SITE GEOLOGY AND SEISMICITY

Earth Mechanics, Inc. (EMI), the project geotechnical consultant, performed a geotechnical investigation of the bridge site. EMI also initiated a study to identify the potential for permanent ground surface fault rupture. It was suspected that a splay of the nearby San Jacinto fault lay within the wash.

In an adjacent project to the east of this site, a trenching study was performed to locate similar fault splays that would impact the design of interchange bridges. In fact, several fault splays were located within that interchange site. It was agreed that, unfortunately, the young alluvial sediments left by seasonal flooding within the Lytle Creek Wash would mask any traces of fault splays and that a trenching study would not be conclusive at this site.

A deterministic fault displacement hazard analysis was performed for the Lytle Creek Wash Bridge site, and the results indicated that permanent displacements could be as great as 3.0 meters horizontally and 0.3 meter vertically.

This project may represent the first time in California that geological fault surface displacements were evaluated as a separate seismic hazard in the form of a Fault Rupture (FR) design event for new bridges. In order to assist Caltrans and SANBAG with the hazard assessment for this FR design event, a Technical Advisory Panel (TAP) consisting of Dr. Scott Ashford (University of California at San Diego), Dr. Bruce Clark (Leighton & Associates), Dr. Paul Somerville (URS Corporation), and Dr. Frieder Seible (University of California at San Diego), Chair, was formed to provide technical review and input to the demand and capacity assessment for bridge structures in this special seismic event.

A summary report evaluating the demand assessment for this FR design load case was prepared by the TAP. The intent of this report is to provide Caltrans, SANBAG, and the design consultants with guidance on how to select and quantify possible fault surface rupture displacements as a design basis for specific bridge structures in this area. The report is based on a probabilistic approach to the assessment of the displacement hazard and recommends lower values for the fault rupture displacements than those based on the deterministic approach. However, Caltrans, who will be the owner of the structure, has recommended to design for the full amount based on the deterministic analysis for the proposed Lytle Creek Wash Bridge. Table I summarizes the proposed criteria for seismic and foundation design.

TABLE I. PROPOSED SEISMIC/FOUNDATION DESIGN CRITERIA

Type of foundation recommended	Cast-in-drilled hole concrete piles
Pile diameter	2.1 meters at bents, 1.8 meters at abutment
Maximum credible earthquake (MCE)	7.5
Maximum horizontal bedrock acceleration	0.7g
Causative fault	San Jacinto fault (< 1 km)
ARS curve recommendation	Modified Caltrans SDC, Figure B.5 @0.7g
Soil profile	Type C (per Caltrans SDC)
Fault displacement	3.0 meters horizontal and 0.3 meter vertical

Due to the proximity of the structure to the San Jacinto fault (less than one kilometer), the modification to the Caltrans Seismic Design Criteria (SDC) curve will include a 20 percent increase of spectral accelerations for periods greater than 1.0 second, no increase for periods less than 0.50 second and a linear interpolation to be used for periods between 0.50 and 1.0 second.

CREEK BED DEGRADATION AND SCOUR

This paper focuses primarily on the seismic issues related to fault rupture; however, creek bed scour has complicated the seismic design significantly since the foundation support conditions are anticipated to change dramatically over the life of the structure.

A number of factors influence changes in the elevation of the creek bed. First, several construction companies are actively removing material from the wash to produce aggregate upstream and downstream of the bridge site. These companies have permits to continue to mine the material, which will influence the rate at which the wash degrades.

Second, the foundations of the two existing bridges upstream and downstream of this site are already scour critical or near scour critical. The footings of the railroad bridge downstream are exposed and the Union Pacific Railroad has periodically been adding large rip-rap in the form of a check dam just downstream of the bents in order to maintain the grade at the foundations. If this check dam were to fail or if it were removed in the future due to a replacement of the railroad bridge, headcutting scour would rapidly make its way upstream to the Lytle Creek Wash Bridge.

Third, the creek can experience very high flow velocities; therefore, the local scour in the sand and gravel creek bed at the proposed piers can be significant.

The various amounts of anticipated scour over the 75-year design life of the bridge are summarized in Table II.

TABLE II. ANTICIPATED SCOUR OVER 75-YEAR DESIGN LIFE

Long-term degradation	4.5 meters
Headcutting scour	2.4 meters
Local scour	4.0 meters
Total scour	10.9 meters

It is recognized that these scour amounts would not necessarily occur at the same rate over the width of the creek so that the effective length of the columns/pile at different bents could be different at any given time.

Originally, the column/pile length assumed for evaluation of the fault rupture scenario was proposed to be based on the 75-year stream bed degradation plus one-half of the local scour plus headcutting that could result from the failure of the check dam downstream of the bridge. It was agreed that it was unlikely that the fault rupture would occur during a maximum flood stage and that it was unlikely that, if the dam failed, it would be left unrepaired. For these reasons, the effective column length was revised to include only the 75-year stream bed degradation. Of course, the total scour value was used to establish the tip elevation of the large cast-in-drilled hole (CIDH) piles for service loads.

DESIGN STRATEGY

The most significant design factors are potential fault rupture and a significant amount of anticipated hydraulic scour.

The design must accommodate fault rupture resulting in permanent ground displacements of 3.0 meters horizontally and 0.3 meter vertically. Since the fault is suspected to run somewhat parallel to the wash and since the bents would also be parallel to the wash, it is anticipated that the fault would occur either between the bents or possibly at a bent. If it occurs between bents, the result would be that one group of bents would move in relation to the rest. If the rupture occurs within a bent, however, it would likely result in some damage to that bent, reducing its capacity to support the structure. This issue was discussed with the TAP, and it was agreed that, due to the type of proposed foundation, this would not likely result in collapse.

The hydraulic study indicates that the anticipated long-term degradation of the stream bed will be significant and that additional headcutting and local scour at supports will also be large. These conditions may result in column effective lengths that not only change over time, but vary greatly from bent to bent. If this occurs, the period of vibration of the overall system will change and the loads will migrate to the supports, which are currently the stiffest.

A General Plan of the proposed bridge is shown as Figure 2 on the following page. The following items summarize the design recommendations proposed for the Lytle Creek Wash Bridge project.

- Use a continuous superstructure with no hinges.
- Provide seat-type abutments with seat width in both the longitudinal and transverse direction to accommodate the anticipated fault rupture displacements in any direction without collapse of the superstructure.
- Provide a deep diaphragm on the seat abutment to mobilize a large quantity of soil in the longitudinal direction.
- Support the abutment on large-diameter CIDH piles to provide a forgiving redundant support system for the fault rupture scenario.
- Design the transverse abutment keys to fail prior to failure of the large abutment piles or the superstructure girders. This provides a significant amount of restraint so that the bridge will not displace significantly during minor earthquakes. The abutment is allowed to travel along the transversely extended abutment seat after the keys have failed.
- Configure the bents with multicolumn, large-diameter pile shaft extensions that are founded deeper than the total long-term degradation and local scour.
- Provide drop bent caps that connect the columns at the top but without any shear or moment connection to the superstructure. Add post tensioning to the bent cap to increase ductility, in the event that ground rupture occurs within a bent. Extend the bent caps beyond the edge of the soffit to provide support if the superstructure translates in relation to the bent in a transverse direction.

The philosophy of this alternative is to allow the superstructure to move independently from the substructure during the MCE or fault rupture event, thus avoiding the introduction of large lateral loads to the bents (which will have continuously changing stiffnesses over the life of the bridge). The transverse abutment keys will maintain the alignment of the structure during lesser events and fail during the MCE or fault rupture event, protecting the abutment piles and superstructure girders. Wide seats and continuous drop bent caps will provide adequate support to accommodate large movements. Further elaboration on the individual structure components follows.

SUPERSTRUCTURE

A cast-in-place prestressed continuous concrete box girder superstructure is proposed due to economic and aesthetic considerations, as well as the need for continuity of the deck structure to accommodate fault rupture displacement. The bridge total length is 170 meters. The span lengths vary from 36.5 meters to 48.5 meters. The proposed superstructure depth is 2 meters, resulting in a minimum depth-to-span ratio of 0.04. A 3-meter-deep drop-end diaphragm is proposed to engage more soil passive resistance against the backwall of the abutment under seismic events.

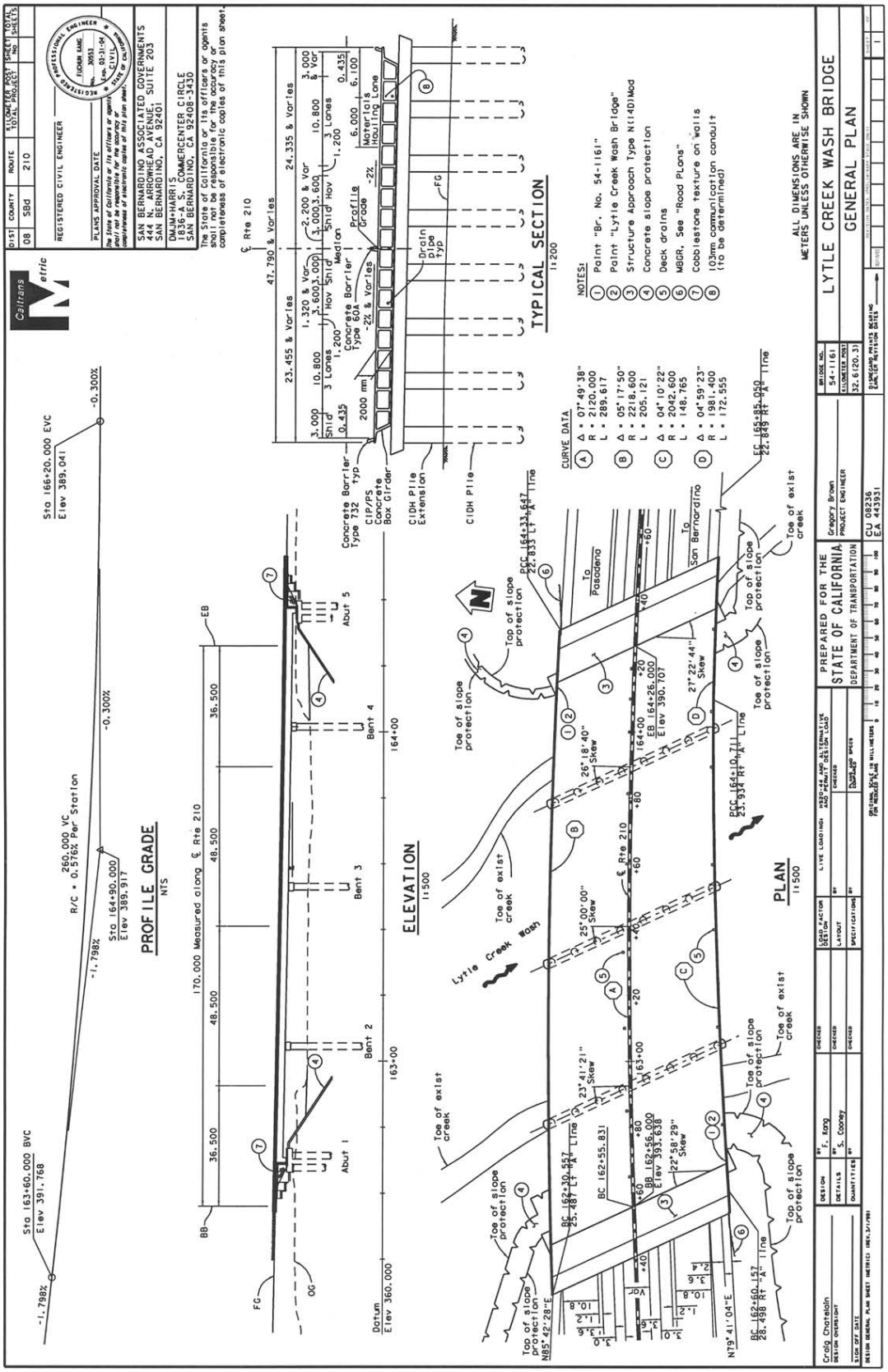

Figure 2. Lytle Creek Wash Bridge General Plan.

BENTS

Eight 2.1-meter-diameter CIDH pile extensions (columns) with no flares are proposed at each bent. The skew angles of the bents vary from 23 degrees to 26 degrees to match the alignment of the creek. The drop cap will extend 3 meters beyond the superstructure soffit at each end of the cap to ensure adequate support for a 3-meter horizontal fault displacement. The superstructure is supported on elastomeric bearing pads on top of drop cap with no moment or shear connection between the superstructure and bent cap. The columns have a fixed connection to the cap and are continuous with the CIDH piles. The intent of this detail is to allow large relative horizontal movement of the superstructure without inducing large loads into the columns. Figure 3 shows the details for the bent section.

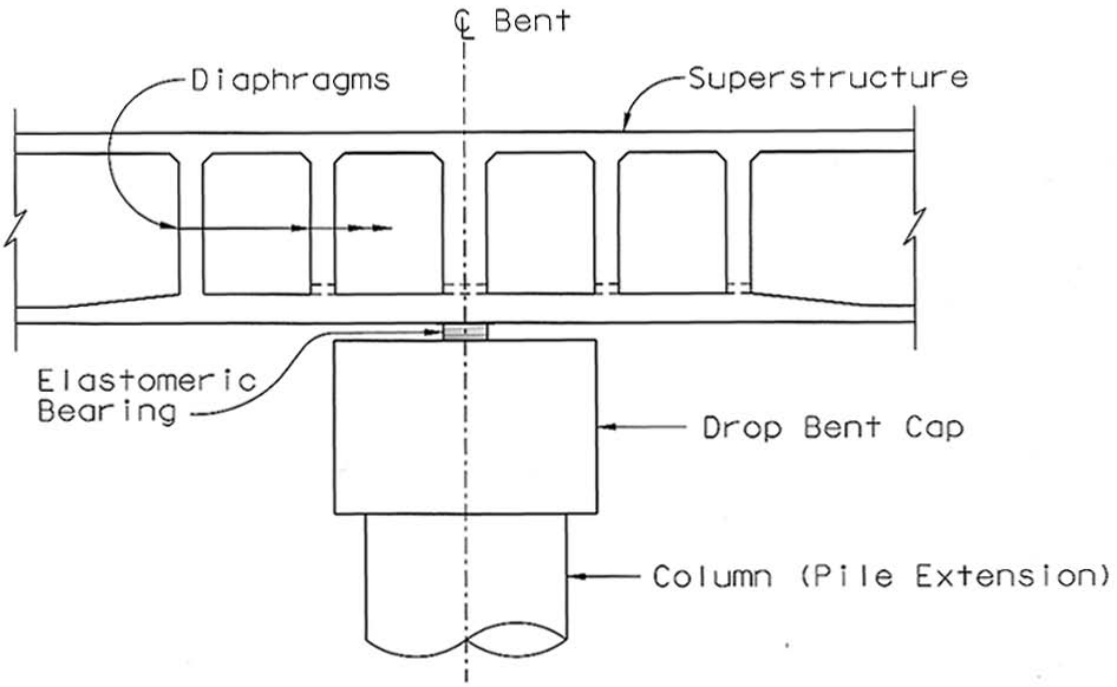

Figure 3. Bent section details.

In the fault rupture scenario, the elastomeric bearings will likely shear, and the soffit will bear directly on the drop cap. The reaction of the cap would then be fairly evenly distributed to all of the girders. In order to ensure even better load distribution and preclude girder buckling in this event, we proposed to provide several internal transverse diaphragms spread over a 6-meter length of the superstructure at each bent rather than one single internal bent cap.

ABUTMENTS

Seat type abutments are proposed to support the drop-end diaphragm of the superstructure. The abutments are founded on 1.8-meter-diameter CIDH piles. For longitudinal seismic loads on the abutment, the backwall is designed to fail and the end diaphragm will be designed to mobilize the resistance of the soil mass. The transverse abutment shear keys will be designed to fail prior to the piles or the superstructure. The abutment seat will be extended both longitudinally and transversely to accommodate the large horizontal fault rupture displacements without unseating the superstructure. Figure 4 shows the details for the abutment section.

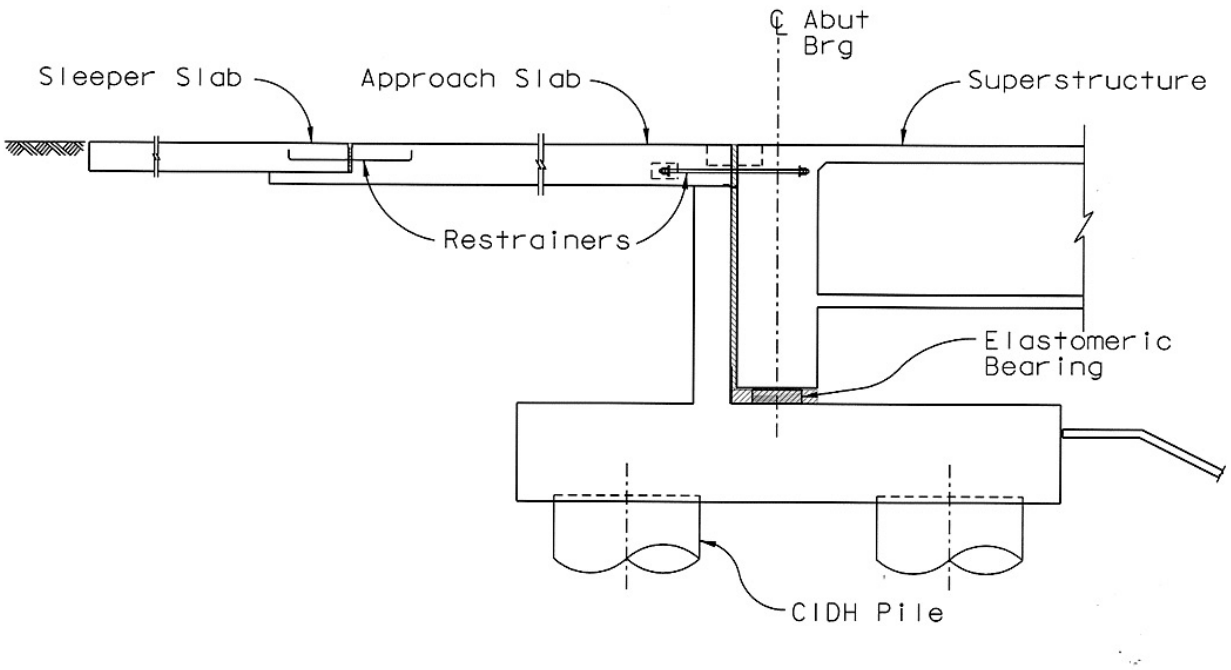

Figure 4. Abutment section details.

Approach slabs, 13.5 meters long, are recommended for the approaches by Caltrans' "Memos to Designers." Due to the large potential ground displacements, the superstructure could permanently move longitudinally away from the abutment backwall, resulting in a large opening in the roadway into which a vehicle could drop. It is proposed to modify the standard approach slab so that it could be dragged by the superstructure, effectively spanning this opening. There is also the potential for significant settlement of the approach fill directly behind the abutment. If the structure approach consists of a single slab, it will not be able to conform to the ground settlement as it is pulled across the top of the abutment backwall. For this reason, we proposed to add a sleeper slab, which would articulate with the main slab.

ANALYSIS

Since there are no shear keys at the bents, the superstructure can impose lateral loads only up to the limit of the frictional force on the bent cap. In the original analysis, a friction coefficient of 0.4 was used based on test information concerning the contact between elastomeric bearing pads and concrete. If horizontal fault rupture occurs, and the displacements are large, it is assumed that the bearings will fail but that the friction force between the concrete soffit and the top of the concrete drop cap will still be approximately 0.4W. This is based on information obtained from tests conducted on the coefficient of friction between two smooth concrete surfaces. This friction value was later increased to 0.5 to ensure a conservative design. The bent total deflection demands will be the summation of friction displacements due to 50 percent of superstructure dead load reaction and the cap/column/pile dynamic response displacements at each bent. Additional analyses were performed with the inclusion of an increased axial load on the bent due to vertical fault rupture.

In order to capture the effects of the changing creek invert elevation in the displacement analysis, a variety of different CIDH pile embedment scenarios were investigated. They ranged from the condition where no degradation or scour has occurred to the condition where total degradation has occurred. The point of fixity of the CIDH piles was assumed to be at approximately three times the pile diameter below the ground surface for column/pile lateral displacement demand calculations.

A steel reinforcement ratio of 1.75 percent was used in the 2.1-meter-diameter column/CIDH pile with transverse confinement reinforcement per Caltrans SDC to provide a ductile supporting system.

Computer program SAP2000 was used to identify the lateral displacement demand of the bent. LPile, WFrame, and XSECTION programs were used for lateral displacement capacity analysis.

The controlling condition in the design was based on the assumption that the vertical fault rupture could occur simultaneously with the horizontal fault rupture and maximum ground shaking. The original analysis assumed a worst-case scenario for vertical fault rupture, wherein a single bent could be displaced upward with the others remaining at their as-built elevations. This resulted in a dramatic increase in vertical load at the subject bent, which then resulted in higher lateral loads when the friction coefficient was applied. It was agreed that this also was unlikely; a more realistic and still very conservative approach was adopted that assumed an adjacent bent would likely displace upward, thereby sharing some of the additional vertical load. In the revised analysis, it was assumed that an adjacent bent would also displace upward by a

prorated percentage of the maximum vertical fault rupture value, based on the adjacent span length.

The results of this analysis indicate that, for the worst-case scenario, the maximum displacement demand/capacity (D/C) ratio would be 1.07 with a P-delta value equal to 26 percent of the column plastic moment capacity (Mp). These values slightly exceed the limits of 1.00 and 20 percent, respectively, established by the Caltrans Seismic Design Criteria (SDC) for ordinary structures. However, it was agreed that these were acceptable values for a loading combination that has such a low probability of occurrence. It was then agreed that the final project-specific design criteria would set upper limits of D/C = 1.10 and P-delta = 30 percent of Mp to allow for minor changes during final design and independent check.

It was also agreed that the elastomeric bearings would have to survive minor seismic events without damage. To accommodate this criterion, it was proposed to size the thickness of the pads so that the superstructure could move longitudinally a distance sufficient to completely close the backwall gap at the abutments without bearing damage.

Finally, a displacement capacity analysis was performed on the superstructure itself to evaluate the impact of the vertical fault rupture on the prestressed concrete box girder. A vertical differential displacement of 0.3 meter between bents was assumed as described above. The analysis was performed using the XSECTION program, modified to account for the prestressing steel model. The results indicated that the displacement demands were all well within the ultimate displacement capacity for these spans and that the superstructure would be capable of accommodating the 0.3-meter vertical displacement.

CONCLUSIONS

Permanent ground displacements of several meters would destroy most conventional bridges due to the enormous loads imposed on critical structural members by the differential movement of the foundations with respect to each other. Combine this situation with a rapidly degrading creek bed with constantly changing foundation conditions, and the problem becomes complex.

For the design of a new structure to meet the unique requirements of these conditions, the solution may be simple−and fairly inexpensive. In the case of the new Lytle Creek Wash Bridge, it was proposed to simply release all the joints that would typically cause distress to the structure if they were to displace differentially. The supports would be wide enough to accommodate the unpredictable movement of the superstructure without unseating, and the foundation system would be very ductile and redundant.

If not for the scour problem, which requires very deep foundations to accommodate the future degradation, the cost of this proposed structure would be little more than that of a conventional post-tensioned concrete box girder. At the time of the writing of this paper, the bridge design was nearing completion and a marginal construction cost estimate had not yet been prepared. The preliminary estimate, however, totaled $11.6 million, which equals $1,331 per square meter or $124 per square foot of deck area.

Seismic Retrofit of the Bolu Viaduct

S. W. Park , H. Ghasemi, J. D. Shen, W. P. Yen, and M. Yashinsky

ABSTRACT

An evaluation of the seismic isolation design of Bolu Viaduct 1 in Turkey and an assessment of its performance in the 1999 Duzce Earthquake were conducted through nonlinear finite element simulation of near-fault earthquake ground motions. The analysis indicated that the near-fault effects of ground motion at the site induced responses that exceeded the design displacements and capacities of the seismic isolation systems. This resulted in significant damage to the bearings and energy dissipation systems as observed on site. Analysis highlights the distinction between the responses of the viaduct to near-fault and far-field ground motions.

INTRODUCTION

Developments in seismic isolation and energy dissipation devices have permitted considerable advances in seismic protection of highway bridges. However, existing seismic protection strategies are largely based on design ground motions that do not consider near-fault features. A number of recent earthquakes, such as Northridge, Kobe, Duzce and Chi-Chi earthquakes, have pointed to the need to account for the effects of near-fault ground motions in the seismic design of bridges.

A near-fault ground motion is commonly characterized by a long-period, pulse-like component in its velocity profile, and the characteristics of the ground motion depend on the specific nature of the fault rupture involved and the directivity of the rupture propagation. While seismically isolated bridges, due to their lengthened fundamental period, can be effectively protected from far-field ground motions with sharp, high-frequency accelerations, they might be vulnerable to near-fault ground motions containing rapid, long-period components. In general, for the same peak ground acceleration and duration of shaking, a near-fault ground motion induces far greater displacement and force demands than a far-field motion.

In this paper, the effects of near-fault earthquake ground motions on the seismic isolation of highway bridges are studied through a numerical analysis of Bolu Viaduct #1 subjected to the 1999 Duzce Earthquake. Viaduct #1 is in north central Turkey and is part of the Trans-European Motorway (TEM) which runs from Ankara to Europe. The 2.3-km viaduct, with its 59 dual spans, was approximately 95% complete at the time of the earthquake. The superstructure consists of seven lines of simply-supported, prestressed-concrete box girders seated on sliding bearings with stainless steel/PTFE slider interfaces. The deck slab is monolithic over 10-span segments and each segment is 392 m long which is supported by 11 piers. An energy dissipation

S. W. Park and J. D. Shen, LENDIS Corporation @ Federal Highway Administration, Office of Infrastructure R&D, 6300 Georgetown Pike, McLean, VA 22101, USA
H. Ghasemi and W. P. Yen, Federal Highway Administration, Office of Infrastructure R&D, 6300 Georgetown Pike, McLean, VA 22101, USA
M. Yashinsky, California Department of Transportation, Division of Engineering Services, Earthquake Engineering, Sacramento, CA 95816, USA

system of yielding-steel type is also installed on each pier cap to form, together with the sliding bearings, a seismic isolation system for the viaduct.

NUMERICAL SIMULATION

Numerical simulation is conducted via a nonlinear time-history analysis of a typical ten span segment of the viaduct subjected to a number of recorded and simulated earthquake ground motions including those recorded at the Bolu and Duzce stations. The viaduct's superstructure and piers are modeled using 3-D beam elements. Special nonlinear link elements are used to model sliding bearings, EDUs, and shear keys. The foundation conditions at each pier base are modeled by elastic translational and rotational springs. All three (longitudinal, transverse, and vertical) components of a ground motion are used as the input, and non-synchronous ground motions at different pier bases are also taken into account in the analysis. In particular, the surface fault rupture crossing the 10-span segment is modeled by applying a different ground motion to each side of the segment divided by the rupture crossing.

SUMMARY OF FINDINGS

The analysis indicates that the calculated displacement paths of the sliding bearings are consistent with the scoring marks observed on the stainless steel plates. Analysis of the seismically-isolated viaduct with ground motions recorded at the Bolu station resulted in displacements exceeding the capacity of the isolation bearings but not large enough to engage shear keys. However, analysis with simulated near-fault ground motions resulted in displacements far exceeding the capacities of the isolation bearings and EDUs and resulted in engagement of the shear keys. The close proximity of the fault rupture to the viaduct caused significant superstructure movement relative to the substructure resulting in severe damage to bearings and EDUs. The simulation, however, shows that the shear keys played a critical role in keeping the girders from dropping off the pier caps thus preventing a collapse of the viaduct.

PEER-Lifelines Research in Design Ground Motions

Clifford J. Roblee, Brian S.J. Chiou and Michael F. Riemer

ABSTRACT

The Lifelines Program of the Pacific Earthquake Engineering Research (PEER) Center is a government-industry-academia partnership that conducts a coordinated program of applied seismic research to provide scientific and engineering underpinning needed to improve the design and operation of lifelines infrastructure. This article provides an overview of PEER-Lifelines Program research activity in the area of design ground motions with emphasis on applications to California highway and bridge design.

Design earthquake ground motions in California are typically governed by large magnitude events (e.g. Mw > 6.5) at close distances (eg. <20 km). Recorded motions from previous earthquakes show variability of load demand approaching a factor of 10 for sites at the same distance and magnitude. This variability arises from differences in a variety of source, path and site effects. A primary theme of the PEER-Lifelines Program is the execution of a coordinated suite of research projects aimed at systematically developing a better understanding and accounting for variability in recorded ground motions. Broadly, these projects acquire new field and laboratory data, calibrate numerical procedures of ground-motion simulation and develop new design tools. Together, these projects are expected to yield improved design capabilities to estimate loads, along with uncertainties, that are imposed on built facilities.

This article introduces several projects from the PEER-Lifelines Program that contribute to improved ground-motion models, and presents some of the early findings. First, activities involving improvements to empirical procedures are presented that include uniform processing of new recordings from recent international earthquakes, characterization of local conditions at these recording sites, and the impacts on attenuation relations. Next, projects involving improved numerical simulation of "near field" motions are described that focus on joint calibration of three 1-D techniques relative to both recent empirical data and to newly-generated physical model data. Also, initial findings from a joint calibration of multiple 3-D "basin modeling" techniques are presented. Finally, research directions and implementation strategies are discussed with an emphasis on the implications for highway and bridge design.

Clifford Roblee, Chief of Geotechnical/Geological Research, California Department of Transportation, Office of Research, 5900 Folsom Blvd., Sacramento, CA 95819.
Brian S.J. Chiou, Chief of Seismological Research, California Department of Transportation, Office of Research, 5900 Folsom Blvd., Sacramento, CA 95819.
Michael F. Riemer, PEER Lifelines Program Manager, Pacific Earthquake Engineering Research Center, 1301 S. 46th Street, Building 451, University of California at Berkeley, Richmond, CA 94804.

THE PEER-LIFELINES PROGRAM

The Lifelines Program of the PEER Center is a government-industry-academia partnership that was created to perform applied design-oriented seismic research to complement the more fundamental long-range research mission of the PEER "Core" program. Charter partners in the entire Lifelines Program include the California Department of Transportation (Caltrans), the Pacific Gas and Electric Company (PG&E), the California Energy Commission (CEC), the United States Geological Survey (USGS), and the PEER Center. Additionally, project-specific partners currently include the National Science Foundation (NSF), the Federal Emergency Management Agency (FEMA), the California Division of Mines and Geology (CDMG), the Taiwan National Center for Research in Earthquake Engineering (NCREE), the Kajima Corporation of Japan, and the Japan Ports and Airport Research Institute (PARI).

The PEER-Lifelines Program conducts applied seismic research to provide scientific and engineering underpinning needed to improve the design and operation of lifelines infrastructure. A primary theme of the program is the execution of a coordinated suite of research projects aimed at systematically developing a better understanding and accounting for variability in recorded ground motions. Broadly, these projects acquire new field and laboratory data, calibrate numerical procedures of ground-motion simulation and develop new design tools. Together, these projects are expected to yield improved design capabilities to estimate loads, along with uncertainties, that are imposed on built facilities. These improved capabilities are providing the scientific underpinning for the demand-side of performance-based engineering design that is at the core of PEER's mission.

Major common-interest research initiatives within the PEER-Lifelines program fall under four general categories: 1) engineering seismology, 2) geotechnical site effects, 3) ground deformation, and 4) network risk and reliability. Tables 1a through 1d provide brief descriptions of current major initiatives for each of the four general categories. Projects addressing each initiative listed in Table 1 are either now underway or were recently completed. This paper will introduce only a selection of recent findings that contribute toward improved ground-motion models. For additional information on the overall PEER Lifelines Program or specific project updates, refer to the PEER web site (http://peer.berkeley.edu/).

Table 1a) Engineering Seismology Research Goals

Ground Motion Database	Develop current web-accessible database of uniformly processed earthquake ground motions for attenuation studies and selection of seed time histories.
Attenuation Relations	Improve existing and develop "next generation" design ground-motion attenuation relationships for response spectra and key non-spectral parameters.
Directivity Models	Improve design models for characterization of "near-fault" ground motion effects (fling step, directivity pulse) using empirical and experimental data.
Calibration of 1-D Simulation Techniques	Joint calibration of 3 different 1-D source-path-site ground-motion modeling techniques against major earthquakes and laboratory directivity data.
Calibration of 3-D "Basin" Simulation Techniques	Joint calibration of 4 different 3-D "basin modeling" techniques against theoretical cases and major earthquakes.
Consensus Design Ground-Motion Library	Develop library of consensus-based "seed" time histories appropriate for time-domain analysis for various combinations of fault mechanism, magnitude, distance, azimuth and site condition.

Treasure Island Testbed	Estimate rock outcropping motion from future large earthquake scenarios using calibrated simulation techniques with emphasis on comprehensive characterization of parametric and modeling uncertainty.

Table 1b) Geotechnical Site Effects Research Goals

ROSRINE Database of Site Information	Develop subsurface geophysical, geotechnical and geologic information for key recording sites. Validate alternative geophysical techniques, and develop generalized geotechnical models.
Archive & Dissemination Standards for Geo-Data	Develop national consensus standards for the electronic archive and web-based dissemination of geological, geotechnical, and geophysical data.
Regional-Scale Site Amplification Methods	Evaluate and improve alternative "generic" methods for estimating site response using surface-geology and/or other regionally mapped quantities.
Benefit of Site-Specific Analyses	Quantify the marginal benefit of using site-specific site-amplification methods over generic or regional-scale methods
G&D Material Model	Improve design material models used in site-response analyses to better account for high confining pressure, large strain, and soil disturbance effects.
Vertical Site Response	Develop guidelines for site-specific analysis of vertical ground motions.
Calibration of Non-Linear SRA codes	Joint calibration of $\geq$3 independent non-linear site response modeling techniques against a standard data set. Of recordings and design cases.

Table 1c) Ground Deformation Research Goals

Design Surface Fault-Rupture Model	Develop a comprehensive hazard model for fault surface rupture as a function of earthquake magnitude, distance from mapped fault, and facility footprint.
Liquefaction Deformation Case History Database	Develop database of high-quality case histories of liquefaction-related deformation for use in improving lateral spread and settlement models.
Probabilistic Liquefaction Triggering	Develop improved probabilistic-based models for liquefaction triggering using SPT, CPT and velocity data.
Lateral Spread Model	Develop improved models for liquefaction deformation with an emphasis on displacements of less than 2 meters.
Regional Liquefaction Deformation Hazard	Examine the feasibility of developing regional liquefaction *deformation* hazard maps for a case study in the Santa Clara Valley.
Calibrate SSI Methods for Lateral Spread	Perform large-scale field tests and analyze data for calibration of lateral spread loads and group effects on pile foundation systems.

Table 1d) Network Risk and Reliability Research Goals

Unified Network Risk/Reliability Platform	Create and implement initial phases a long-term plan to develop a unified *network* risk/reliability platform for use in examining impacts on goods flow of various earthquake scenarios, mitigation measures, and lifeline interactions.
Verification of Probabilistic Seismic Hazard Analysis Codes	Joint verification of commonly used public-domain and proprietary software for probabilistic seismic hazard analysis.
Rational Cost Functions	Develop rational cost functions, for various standard bridge types, as a function of ground motion amplitude for improved quantitative assessment of the cost impacts of designing for alternative hazard levels.
Earthquake Risk Decision Making Processes	Examine the decision processes and information flow used by various lifeline organizations and their control agencies to initiate major earthquake mitigation programs.

GROUND MOTION VARIABILITY

Design earthquake ground motions in California are typically governed by large magnitude events at close distances (say <20 km). Recorded motions from previous California earthquakes show variability approaching a factor of 10 for sites at the same distance and magnitude. This variability arises from the differences in source, path and site effects.

Figure 1 provides an example illustrating the variability of near-field ground motions. Velocity time histories in the direction normal to fault strike are presented for two sites that are both within 3 km of the fault trace during the 1979 Imperial Valley earthquake. Clearly, the El Centro #6 (E06) recording shows a large velocity pulse that is not evident in the Bonds Corner (BCR) record. The map shows the location of the two stations relative to the trace, and the star denotes the point where fault rupture initiated. The color vector plot in Fig. 1 depicts the distribution of co-seismic slip along the fault plane and shows a large asperity about midway along strike. The difference in amplitude between the recordings at the two stations is primarily attributed to rupture directivity. The E06 station is in the forward directivity direction (i.e. the fault rupture propagates toward E06), while the BCR station is in the back azimuth. However, the E06 station is also located much closer to the large asperity where energy release is greatest, thus obscuring conclusions regarding the exact contribution of directivity to the observed velocity pulse. Regardless of the cause, the difference in motions between these sites can have serious ramifications for the response of built facilities, and point to the need for improved ground-motion models.

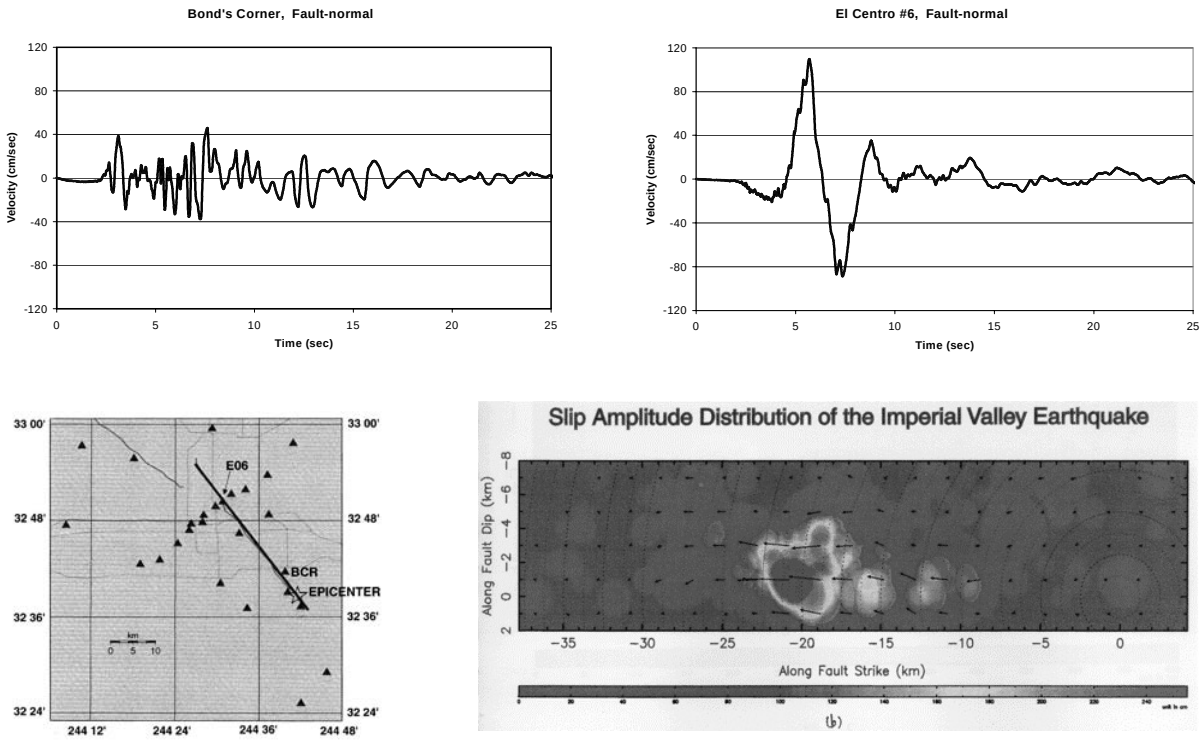

Figure 1) Fault-normal velocity time histories for two near field sites, map of fault trace, and fault slip distribution from the 1979 Imperial Valley earthquake. Both sites are within 3 km of fault trace, but the El Centro array is further along in the direction of the rupture.

GROUND TRUTH: RECORDED DATA

Direct observations from of near-field (<20 km) ground motions from large magnitude (M >7) earthquakes provide the standard against which any predictive methods should be compared. Unfortunately, until recently there have been little data available, since large events are rare and strong motion instruments were sparsely distributed in the past. During 1999, however, the Kocaeli and Duzce earthquakes in Turkey, and the Chi-Chi earthquake in Taiwan provided a wealth of new information. The addition of recordings from these events expanded the database of near-field ground motions approximately tenfold.

The "raw" data recorded by accelerometers often requires substantial evaluation and processing to produce a reasonable estimation of actual ground motions. With many different recordings from multiple earthquakes around the world involved, this processing must be especially consistent and be able to extract the full useable bandwidth to be of greatest engineering value. The PEER Strong Motion Database (http://peer.berkeley.edu/smcat/) has been developed with these goals in mind. The database provides a user-friendly web-based search engine to access recordings that have been uniformly processed by Dr. Walt Silva (Pacific Engineering and Analysis). The PEER-Lifelines program has enhanced the database by supporting Dr. Silva's work to incorporate main shock data from the Turkey and Taiwan earthquakes. Additionally, the PEER-Lifelines Program supported efforts by Dr. Willie Lee (USGS emeritus) to screen and process the large body of data gathered from the Taiwan aftershock sequence recorded by the Taiwan Central Weather Bureau's extensive instrumentation network. Dr. Douglas Dreger (UC-Berkeley Seismological Station) is now establishing source characteristics for approximately 30 aftershocks, including slip distributions for the larger events. This will allow the data to be used in attenuation relationships and for the study of site effects where multiple recordings were obtained at individual sites.

To optimize the value of the recent recordings, the PEER-Lifelines Program is supporting the development of a new generation of attenuation relations. As a preliminary step, Dr. Brian Chiou (Caltrans, formerly with Geomatrix) recently completed an update of the Sadigh relationship to incorporate recent data from Turkey and Taiwan. Preliminary findings show a decrease in median near-field motions, but a concurrent increase in the total uncertainty. The next phase of this work will be the reformulation of attenuation relationships to better account for near-field phenomena. It is now envisioned that this "next generation" formulation will be coordinated through a national working group.

SITE CHARACTERIZATION

To maximize the value of recorded data to improve ground-motion models, the subsurface conditions beneath the recording site needs to be characterized. This allows the recordings to be appropriately grouped for the development of attenuation relationships, and provides critical inputs to better account for site-to-site variations when ground-motion numerical modeling is employed.

The PEER-Lifelines Program is contributing to continuing efforts to characterize key recording sites both in the U.S. and abroad. In the U.S., support is being provided to the on-

going ROSRINE effort to systematically collect and disseminate geologic, geotechnical, and geophysical data from instrument sites. Dr. Bob Nigbor (University of Southern California) is leading the field site investigations, and is working closely with Dr. J.P. Bardet and Dr. Jennifer Swift (also at USC) in web posting the logs using a GIS-based search engine (Fig. 2).

Dr. Ken Stokoe and Dr. Ellen Rathje (University of Texas at Austin) and Dr. Jim Bay (Utah State University) have used the Spectral-Analysis-of-Surface-Waves (SASW) technique to measure the shear wave velocity profiles at selected strong motion sites in the US, Turkey and (soon in) Taiwan. This quick, portable, and noninvasive method has proven to be a valuable and cost-effective approach for characterizing site conditions.

Dynamic geotechnical material properties for samples collected at instrument sites are being developed by a team coordinated by Dr. Don Anderson (CH2MHill) with state-of-the-art laboratory testing provided by Dr. Ken Stokoe (UT) and Dr. Mladen Vucetic (University of California at Los Angeles. These new fundamental data are providing the basis to extend current design engineering models used for site-response analysis to significantly greater confining pressures and strain levels.

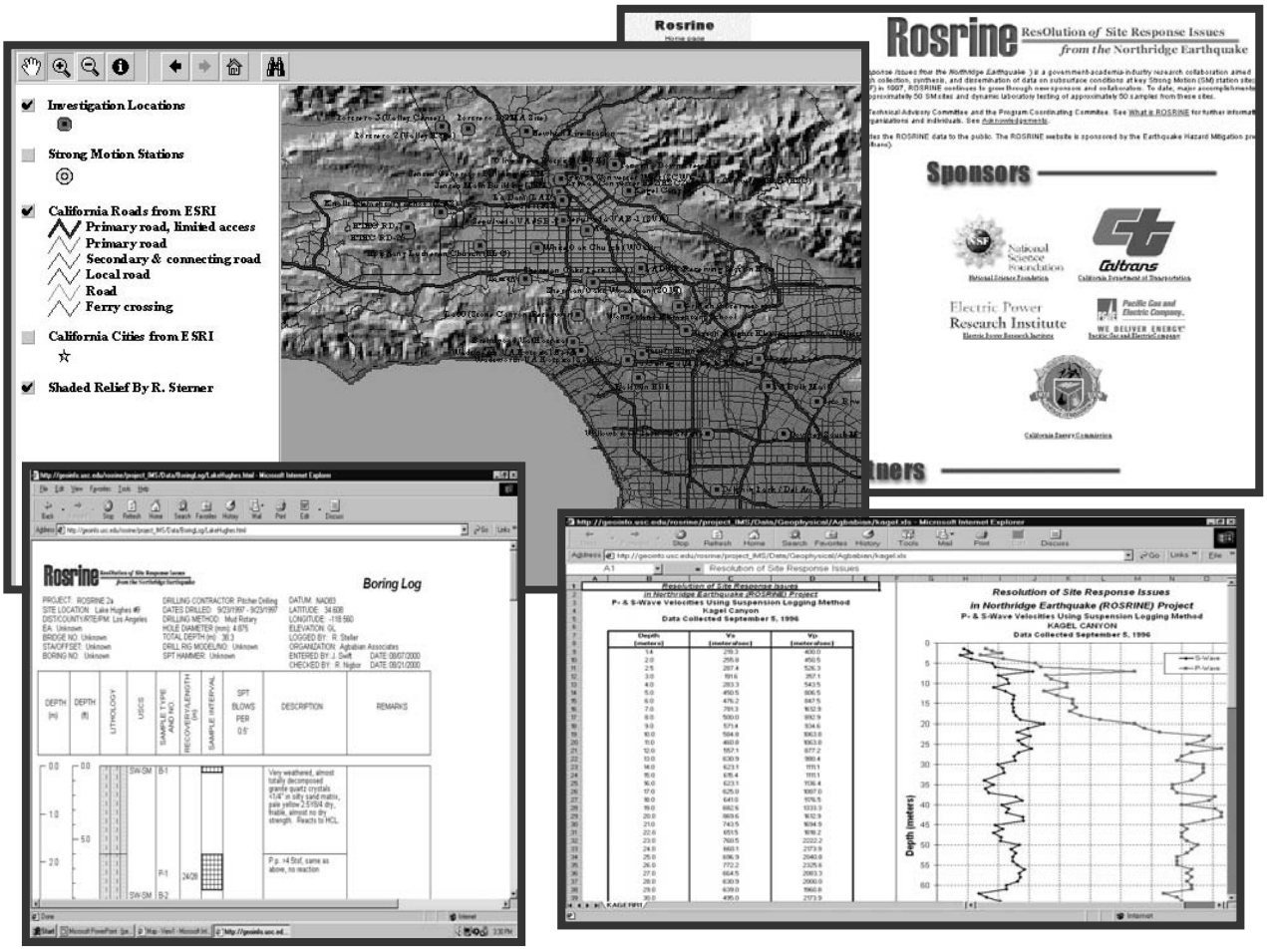

Figure 2) The ROSRINE web site (http://geoinfo.usc.edu/rosrine/) disseminates geological, geophysical and geotechnical data on subsurface conditions beneath EQ recording sites.

MODELING OF NEAR-FIELD GROUND MOTIONS

Procedures to numerically simulate ground motions from a finite fault rupture have been developed over many years, with sophisticated procedures now capable of incorporating near-field effects. These effects include "directivity pulse" (wave field buildup in the direction of rupture propagation), "fling step" (motions very near the fault trace associated with permanent offset of the ground surface), and the polarization (radiation pattern) of energy release that causes different motions to occur in the fault-parallel and fault-normal directions. The simulation procedures are currently used in practice to guide the development of attenuation relationships and to generate synthetic motions for conditions where little or no recorded data is currently available. In the future, there will likely be an increased reliance on simulation approaches to account for the various physical processes that contribute to ground motion variability. Acceptance of results from numerical simulation procedures requires careful calibration and validation against available earthquake data and new experimental data sets (see next section).

Toward this end, the PEER-Lifelines Program is supporting a comprehensive validation exercise involving three teams of researchers: Dr. Paul Somerville, Dr. Robert Graves and Dr. Arben Pitarka of URS Corporation; Dr. Walter Silva of Pacific Engineering and Analysis; and Dr. Yuehua Zeng and Dr. John Anderson of the University of Nevada, Reno. In the first phase of the work, now complete, each team applied its own procedures to simulate five large earthquakes from which some near-field data were recorded (1979 Imperial Valley, 1989 Loma Prieta, 1992 Landers, 1994 Northridge, and 1995 Kobe). These calibrations focused on directivity issues, and results showed that each of the procedures were comparable in terms of the degree of fit to recorded data, though significant differences between the simulations and the observed motions were still observed at specific locations. The initial study also highlighted the need to treat site effects in a consistent manner during the development of the fault slip model and subsequent simulation of recorded motions. As pointed out earlier, the Turkey and Taiwan earthquakes of 1999 are providing a wealth of additional near-field data, and are therefore being used in the current phase of the modeling validation exercise.

These models will also be validated against data collected in a series of experiments designed to physically produce directivity effects of the rupture processes, as described below. Once the validation studies are completed, it is anticipated that the strengths and limitations of each numerical procedure can be assessed with confidence, and that directivity effects on near-field ground motions can be simulated using these models and the results incorporated into the next generation attenuation relationships.

EXPERIMENTAL DATA FOR DIRECTIVITY

The validation of numerical simulation techniques for directivity effects using field data is hampered by the lack of near-field recordings and differences in subsurface properties for the available data. Therefore, the PEER-Lifelines Program is sponsoring an investigation by Dr. James Brune and Dr. Rasool Anooshehpoor at the University of Nevada, Reno designed to produce directivity effects in the laboratory under carefully controlled conditions. Fault rupture is being physically simulated by slippage between two large blocks of foam rubber, while precise

measurements of the acceleration and displacement time histories are made at critical locations both along the "ground surface" and on the fault plane (Fig. 3). The low density and stiffness of the material allows high-resolution measurement of wave propagation over laboratory scales, while the uniform properties minimize complexities in the response caused by inhomogeneities. Multiple tests performed under nominally identical conditions will also provide valuable information on the variability in the buildup of directivity. In addition to developing data for uniform slip, fault-plane roughness will be altered locally in a variety of patterns to examine the impact of asperities on the buildup and saturation of rupture directivity effects. In effect, these experiments allow for direct control of two separate physical phenomena that are difficult to separate in current field recordings. The numerical procedures described in the previous section will be jointly calibrated against these new laboratory data.

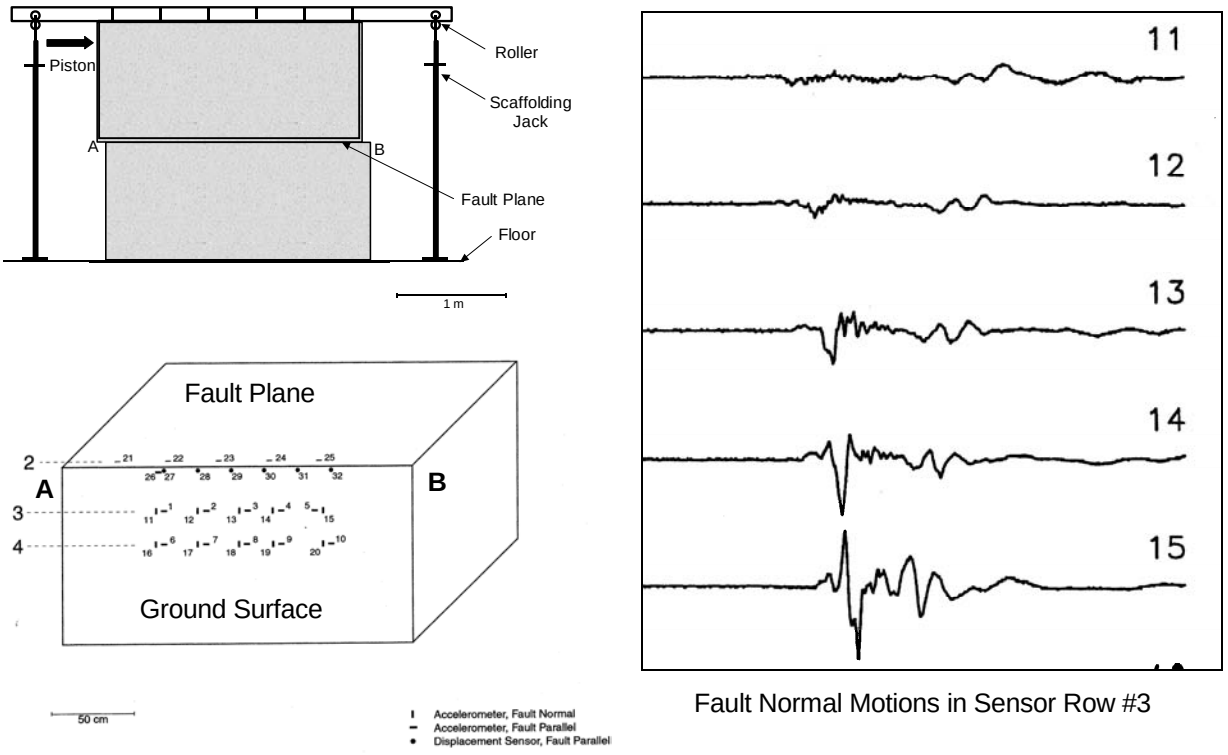

Figure 3) Equipment, instrumentation schematics and typical data for physical modeling experiments of near-field ground motions using foam rubber blocks. Sensors for all data traces on right are equidistant from fault plane. Traces 11 and 15 are in the back and forward directivity directions relative to rupture propagation direction from A to B.

BASIN STUDIES

Ground motion characteristics, such as the spectral acceleration and the duration of strong shaking, can be significantly affected by seismic energy being trapped in sedimentary basins. In recent years, a variety of numerical "basin modeling" procedures have been developed to model long-period (>1 sec) wave propagation in a 3-D medium. The PEER-Lifelines Program

is sponsoring a national team of investigators in partnership with the Southern California Earthquake Center (SCEC) in a joint calibration exercise headed by Dr. Steve Day at San Diego State University. Modeling is being performed by Dr. Jacobo Bielak of Carnegie Mellon University, Dr. Shawn Larsen and Dr. Doug Dreger at Lawrence Livermore National Laboratory and UC Berkeley, respectively, Dr. Kim Olsen at UC Santa Barbara, and Dr. Robert Graves and Dr. Arben Pitarka of URS Corporation. Each team is applying its own numerical codes to analyze a series of increasingly complex "standard" problems. An initial study, now complete, involved only a series of simple problems for which exact solutions were available. A surprising finding from this early work was the large discrepancies between results for the simplest problem comprised of a point source in an elastic half space. The cooperative framework for the calibration exercise enabled the teams to isolate and rectify errors in their models, and consistent results are now being obtained. The full set of problems has been made available via web to a wide community of international researchers and is therefore providing a valuable standard beyond the direct limits of the funded research.

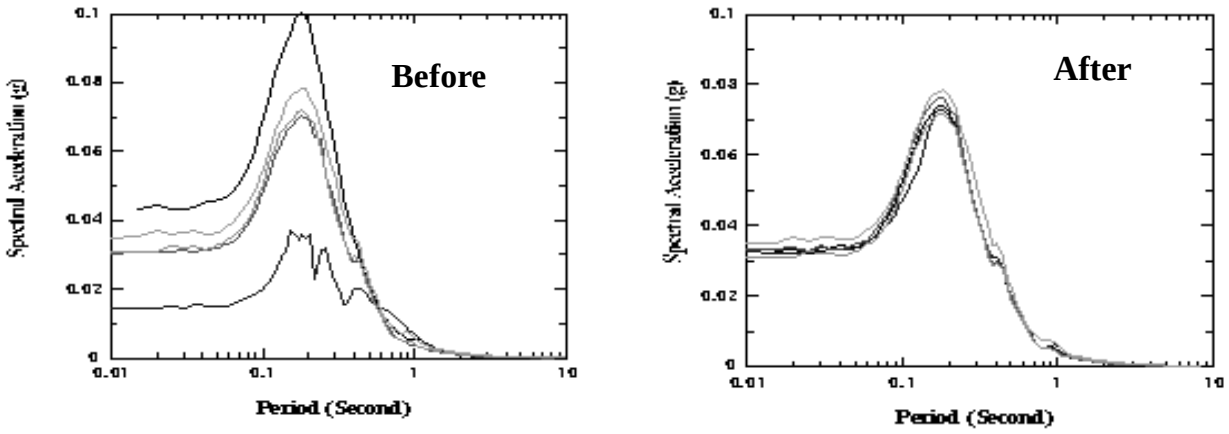

Figure 4) Results before and after joint calibration of four independent 3-D numerical "basin" modeling techniques for the problem of a point dislocation in an elastic half space.

With basic validation complete, the models are now being applied to more realistic problems including simulation of the 1994 Northridge earthquake using the 3-D velocity model developed for SCEC by Dr. Harold Magistrale (San Diego State University) and others (Fig. 5). In this phase of calibration, the teams will evaluate the quality of simulation results by direct comparison to each other and to recorded data. In addition, the results will be contrasted to those simulated from site-specific 1-D velocity models to identify the benefit of using increasingly sophisticated models.

This stepwise approach to calibration is considered essential to acceptance of results in practice. Once the individual models are fully calibrated, the codes will become useful tools both for predicting responses in a particular basin due to specific events and for evaluating the parametric effects of basins on the amplitude and duration of motion. Ultimately the PEER-Lifelines Program, in conjunction with SCEC, plans to apply these codes to selected scenarios for both the Los Angeles Basin and the greater San Francisco Bay Area.

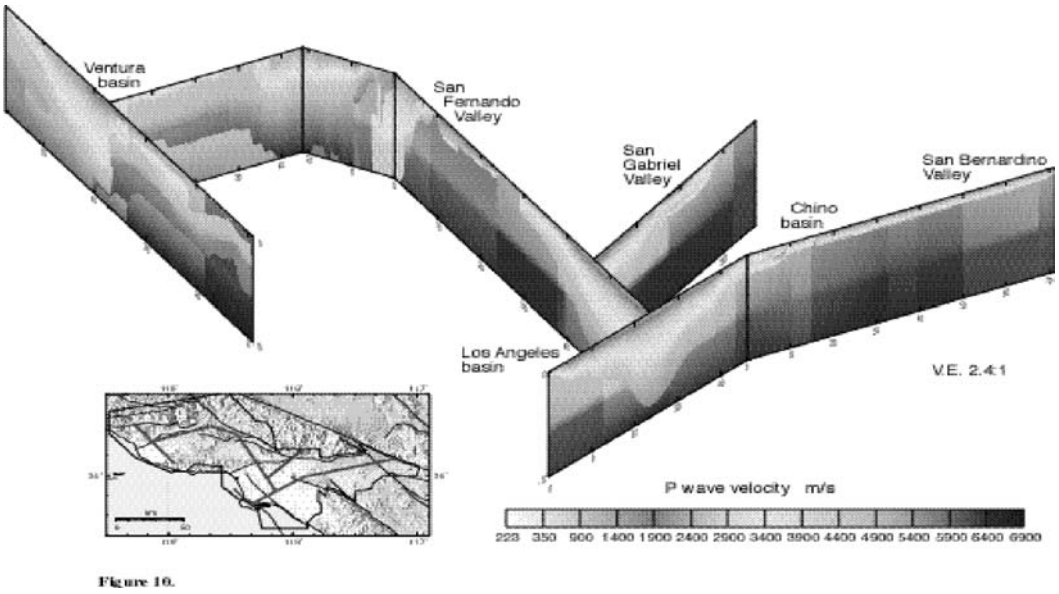

Figure 10.

Figure 5) Cross sections through the SCEC 3-D subsurface velocity model of the Los Angeles basin that is being used in current joint calibration exercises of "basin" modeling numerical simulation procedures.

IMPROVED EMERGENCY RESPONSE

Developments in ground-motion modeling capability are also providing benefits to the emergency response community. The PEER-Lifelines Program is supporting research headed by Dr. Doug Dreger to integrate fundamental features of finite-fault and near-field effects modeling into the *ShakeMap* software developed by the U.S. Geological Survey. The improved system will provide better estimates of near-field ground shaking immediately after an earthquake in areas that are currently only sparsely instrumented (Fig. 6).

IMPLEMENTATION

For this or any other research program to make a positive impact on the reliability of lifeline systems in future earthquakes, the improvements must be implemented into practice. This focus on implementation is a major feature of the PEER-Lifelines Program and drives the motivation to keep the various related tasks coordinated within an overall framework. Individual projects are already beginning to have impact on practice. However, the most significant payoffs are expected in the coming years when the calibrations and validations in light of the new high quality data are completed. Then, it is anticipated that sufficient confidence and experience will have been gained to apply the improved models widely in practice both directly and in the formulation of simpler design guidelines.

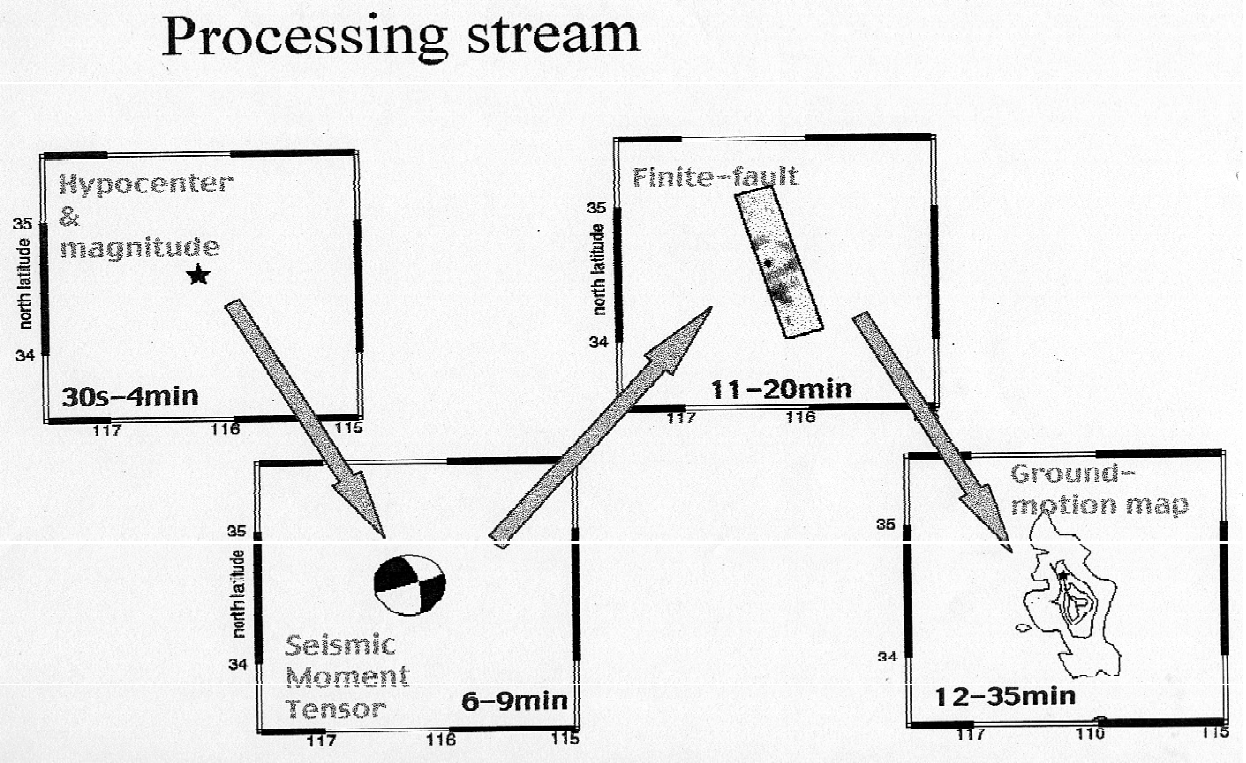

Figure 6) Data processing stream for near-real-time maps of ground shaking intensity in areas of poor instrument density. Data from regional broad band instruments are used to estimate hypocenter, magnitude and seismic moment tensor. Newly developed capabilities infer the dimensions and slip distribution of a finite fault, then use simulation procedures to estimate shaking intensity where strong-motion data is not available.

ACKNOWLEGEMENTS

The authors extend their sincere appreciation to past and current participants in the Joint Management Executive Committee of the PEER Lifelines Program including Bob Anderson of the California Seismic Safety Commission, David Chambers of the CEC, Tom Shantz of Caltrans, Lloyd Cluff, Norm Abrahamson and Stuart Nishenko of PG&E, Jack Moehle and Greg Fenves of UC-Berkeley and Woody Savage of the USGS. The authors also applaud the over 30 principal investigators nationwide that are supported by the program who have both produced outstanding research and have diligently coordinated with their colleagues. The personal dedication of these individuals speaks highly of the earthquake profession and of future opportunities to advance seismic safety practices.

International Forum

Chair: Jim Cooper

Revised Design Specifications for Highway Bridges in Japan and Design Earthquake Motions

Keiichi Tamura

The Challenge of the Rion - Antirion Bridge

Jean-Paul Teyssandier

Effect of Near-Fault Earthquake on Bridges: Lessons Learned from Chi-Chi Earthquake

Chin-Hsiung Loh, Wen-I Liao and Jun-Fu Chai

Seismic Safety Evaluation of Large Scale Interchange System in Shanghai

Lichu Fan, Jianzhong Li, Shide Hu, Guiping Bi and Liying Nie

Revised Design Specifications for Highway Bridges in Japan and Design Earthquake Motions

Keiichi Tamura

ABSTRACT

The Design Specifications for Highway Bridges in Japan were revised in March 2002. The most important change regarding seismic design in this revision is the adoption of performance-based design criteria. Although we had similar design concepts in the previous specifications, they are systematically arranged in the newly revised specifications. Two levels of design ground motions, which are further classified into three kinds of ground motions, three levels of seismic performance criteria and corresponding limit states are prescribed. A new concept has also been introduced to the provision of design earthquake motion, and a site-specific ground motion can be conditionally employed for design practice.

INTRODUCTION

The first requirements for seismic design of highway bridges in Japan were included in the Details of Road Structures (draft), which were issued in 1926, following the 1923 Kanto earthquake. Since then, the seismic design regulations for highway bridges have been repeatedly revised, based on earthquake disaster experience and progress of research. Among them, the most comprehensive revision was made after the 1995 Hyogo-ken Nanbu (Kobe) Earthquake, which caused the worst damage to various structures including highway bridges since the 1923 Kanto earthquake [1, 2]. After this earthquake, the Design Specifications for Highway Bridges were revised in 1996, in which a number of new design techniques were incorporated [3, 4]. They include:

1) Seismic design force that represents destructive near-field ground motion caused by an inland earthquake,
2) Ductility design method that is applicable to bridge pier, foundation, bearing support and unseating prevention system,
3) Seismic isolation design,
4) Seismic design of unseating prevention system.

The Design Specifications for Highway Bridges in Japan were revised in March 2002 [5]. This revision is not large in scale, comparing to the previous one in 1996, however, several important additions and modifications are included. Among them, the most important change regarding seismic design is the adoption of performance-based design criteria. This revision also allows the designer to develop a site-specific design ground motion, in addition to using the standard design ground motion or design spectrum.

Keiichi Tamura, Team Leader, Ground Vibration Research Team, Public Works Research Institute
1-6 Minamihara, Tsukuba-shi, Ibaraki-ken 305-8516 Japan

This paper first summarizes the basic concepts and principles of current seismic design of highway bridges, where an emphasis is put on the new design philosophies introduced to the specifications. Also presented in this paper are the prediction of site-specific earthquake ground motion and a numerical example.

BASES AND PRINCIPLES OF SEISMIC DESIGN

Basic Concepts of Seismic Design

A Bridge shall be designed to achieve the required seismic performance in accordance with the level of design ground motion and the importance of the bridge. In designing a bridge, the earthquake-resistant structural type shall be selected based on topographical, geological and site conditions, and both individual members and the bridge as a whole system shall be ensured to be earthquake-resistant.

Highway bridges play key rolls for evacuation, rescuer, first aid, fire fighting and transporting relief supplies after an earthquake. Hence, it is most essential to secure the safety of bridge against an earthquake and minimize the influence of its functional deterioration on social activities. Reflecting such important rolls of bridge, a bridge shall be designed to achieve the required seismic performance according to the level of design ground motion and the importance classification.

Principles of Seismic Design

Design Ground Motion

In designing bridges, two levels of design ground motions, i.e., ground motion likely to occur during the service period of bridge and destructive ground motion less likely to occur during the service period shall be considered. These design ground motions are termed Level 1 ground motion, and Level 2 ground motion, respectively. Level 2 ground motion contains the ground motion resulting from a large plate-boundary earthquake and that from an inland earthquake which occurs at short distance from a construction site. The former and latter ground motions are designated as Type I and Type II ground motions, respectively. These design ground motions are the same as adopted in the previous specifications that were issued in 1996. Type I ground motion is characterized by large amplitude and large number of cycles, while Type II ground motion has short duration and destructive strength.

Importance of Bridge

In the specifications, each bridge is classified either ordinary bridge or important bridge, according to the road classes, function and structure of the bridge. Table 1 indicates this classification.

Seismic Performance

The seismic performance of bridge is categorized into the following three levels based on the seismic behavior of a whole bridge system:

- Seismic performance 1; to secure integrity.
- Seismic performance 2; to limit damage and secure rapid restoration of function.
- Seismic performance 3; to prevent fatal damage.

Table 2 shows the seismic performance objectives, which is prescribed by the combination of design ground motion and importance of bridge.

The seismic performance is established from the three different standpoints, i.e., safety, serviceability and reparability, which are further classified into three levels, respectively, as summarized in Table 3. Safety is the seismic performance to prevent loss of human lives due to unseating of superstructure. Serviceability represents the performance to maintain the original traffic function after an earthquake and serve as a route for evacuation, rescuer, first aid, fire fighting and transporting relief supplies. Reparability represents the performance to be able to repair the damage caused by an earthquake.

Requirement for Preventing Unseating of Superstructure

An additional requirement is to prevent the unseating of superstructure due to unexpected seismic behavior of the bridge and ground failure. As Type II ground motion, those recorded in the 1995 Kobe earthquake that influenced the most destructive effects on structures were incorporated into the specifications, whereas even greater ground motions could occur. There still remain large uncertainties to predict such ground motion characteristics and reflect them to the seismic design of bridges. Furthermore, ground failure and unexpected response of structural members may cause unpredictable effects to the bridge structure. Even under such circumstances, it is intended to secure safety against the unseating of superstructure.

DESIGN GROUND MOTION

General

The standard design response spectrum, which is presented later in this paper, may by used as design ground motion, whereas a site-specific design ground motion shall be developed when the ground motion at a construction site can be appropriately predicted, based on the information of past earthquakes, active faults, plate-boundary earthquakes, geological structure, local site condition, recorded ground motions, and so forth. Reflecting the recent research and development in the area of ground motion prediction, the site-specific design ground motion shall be established, if enough information is available to appropriately predict ground motion at the site. Otherwise, the standard design response spectra may be used as design ground motions.

Standard Design Response Spectra

Level 1 Ground Motion

Level 1 ground motion in terms of acceleration response spectrum S may be determined from the following equations:

$$S=c_Z \cdot c_D \cdot S_0 \quad (1)$$

$$c_D=1.5/(40h+1)+0.5 \quad (2)$$

where c_Z is the zone factor (=1.0, 0.85, 0.7), c_D is the modification factor by damping ratio h, and S_0 is the standard acceleration response spectrum. This standard response spectrum was established from attenuation relations of spectral acceleration, characteristics of past earthquake damage and ground vibration, and so on. Since ground motion characteristics and resultant structural damage is closely related the soil condition, the standard acceleration response spectra are defined for the three different soil classes that are given in Table 4. Table 5 and Figure 1 show the standard acceleration response spectra of Level 1 ground motion.

Level 2 Ground Motion

Similar to the case of Level 1 ground motion, Level 2 motion is also prescribed by acceleration response spectrum, and Type I and Type II ground motions, which are denoted by S_I and S_{II}, are expressed as

$$S_I=c_Z \cdot c_D \cdot S_{I0} \quad (3)$$

$$S_{II}=c_Z \cdot c_D \cdot S_{II0} \quad (4)$$

where S_{I0} and S_{II0} indicate the standard acceleration response spectra of Type I and Type II ground motions, respectively. Table 6 and Figure 2 give these standard response spectra. Type I ground motion stands for ground motions in Tokyo by the 1923 Kanto earthquake, for instance. The acceleration response spectrum of this ground motion is estimated from attenuation relations and past experiences. The acceleration response spectrum of Type II ground motion, which represents ground motion generated by an inland earthquake at short distance, was developed by smoothing the response spectra that are computed from the ground motions records obtained in the 1995 Kobe earthquake.

VERIFICATION OF SEISMIC PERFORMANCE

General

In order to verify the seismic performance of bridge, the limit states of individual structural members shall be first established, based on the limit state of bridge as a whole, which is described in the following section. Then, the seismic response of individual members shall be verified not to exceed the corresponding limit state, in which an appropriate method depending on design ground motion, structural type and limit state should be selected. In the specifications, standard static and dynamic verification methods are prepared for the bridges whose seismic behavior is uncomplicated and complicated, respectively. In addition to this, it is necessary to verify to prevent unseating of superstructure due to unexpected structural response and ground failure, for which the standard method is also provided in the specifications.

Limit State of Bridge against Seismic Performance 1

The limit state of bridge against seismic performance 1 shall be appropriately determined so that the seismic response of whole bridge system remains within the elastic range. This limit state is determined to maintain function of bridge after an earthquake and limit structural damage to be minor. Corresponding to this limit state of the bridge as a whole, the limit states of individual structural members may generally be established so that seismic response of individual members remains within the elastic range.

Limit State of Bridge against Seismic Performance 2

The limit state of bridge against seismic performance 2 shall be appropriately determined so that the plastic deformation is limited to the structural members that are allowed to be plastic and secure reparability. This limit state is determined to ensure rapid restoration of bridge function after an earthquake. As the structural members that are allowed to be plastic, members that can reliably absorb energy and be presently repaired shall be selected. The designer shall appropriately combine members that are allowed to be plastic and properly establish the limit states of individual members. For general bridges, bridge piers may be regarded as the structural members that can absorb energy and be easily repaired. In case of the bridges equipped with isolation bearings, the limit states of individual members shall be established so that energy can reliably be absorbed at the bearings.

Limit State of Bridge against Seismic Performance 3

The limit state of bridge against seismic performance 3 shall be appropriately determined so that the plastic deformation is limited to the structural members that are allowed to be plastic and plastic deformation does not exceed the plastic deformation capacity. This limit state is determined to prevent fatal damage or collapse of bridge. As the structural members that are allowed to be plastic, members that can reliably absorb energy shall be selected. The designer shall appropriately combine members that are allowed to be plastic and properly establish the limit states of individual members.

Verification Method of Seismic Performance

The seismic performance of bridge shall be verified by an appropriate method, based on design ground motion, structural type and limit state. For the bridges whose seismic behavior is uncomplicated, the static verification method prescribed in the specifications may be employed as a verification method of seismic performance. The conventional seismic coefficient method and ductility design method are applicable as static verification methods. In case of the bridges that have complicated seismic behavior, the dynamic verification method in the specifications may be applicable to verify the seismic performance. The bridges that have complicated seismic behavior generally correspond to the following cases:

1) The principal vibration mode is definitely different from that assumed in the static verification method of seismic performance.
2) Two or more vibration modes which dominate the seismic response of bridge exist.

3) Plural plastic hinges are assumed to be formed in the verification of seismic performance against Level 2 ground motion or location of plastic hinges cannot be identified.
4) The applicability of energy-constant rule based on the nonlinear characteristics of structural member or whole bridge system is not sufficiently confirmed.

Figure 3 illustrates the standard procedure of seismic design.

DEVELOPMENT OF SITE-SPECIFIC DESIGN GROUND MOTION

Ground Motion Prediction Method

As previously mentioned, in the newly revised design specifications for highway bridges, a site-specific design ground motion shall be developed when the ground motion at a construction site can be appropriately predicted, based on the information of past earthquakes, active faults, plate-boundary earthquakes, geological structure, local site condition, recorded ground motions, and so forth. This provision does not restrict methods of ground motion prediction, and the recorded ground motion data and various techniques, such as attenuation relations, semi-empirical and theoretical ground motion simulation methods may be used for this purpose.

The semi-empirical ground motion synthesizing technique, in which ground motion record from a small event is used as a Green's function, has been applied to ground motion prediction [6, 7]. This technique has an advantage of automatically incorporating the complicated earthquake source mechanism and seismic wave path effects into calculation. On the other hand, this method requires an actual small event record, and it is obvious that an appropriate record is not always available at a construction site of new structure. To compensate this disadvantage, a stochastic Green's function technique has been proposed, in which the stochastically simulated small event motion is used as a Green's function [8, 9]. As an example of site-specific ground motion prediction, ground motion predicted by a stochastic Green's function technique is presented in the following section.

Ground Motion Prediction for the Kanto Earthquake

We herein simulate ground motion at Kannonzaki, which is located at the mouth of Tokyo Bay, from a Kanto earthquake [10, 11]. Kanto earthquake recurrently occurs off the coast of Tokyo, and the latest one occurred in 1923 caused destructive damage to Tokyo metropolitan area. We assume the fault plane model proposed for the 1923 Kanto earthquake, and systematically change the location of hypocenter and asperities to examine the effects of uncertainties of source parameters on the calculation results. This is because it is hardly possible to predict the location of these quantities for a future earthquake, which is essentially important for seismic design of structures. Figures 4 and 5 indicate the fault plane model and the changed locations of hypocenter and asperities. The length and width of the fault plane are assumed to be 130km and 70km, respectively. The following numerical results correspond to those estimated on the outcropping layer with shear wave velocity v_S=700m/s.

Figure 6 shows the synthesized acceleration time history that has the largest peak acceleration among the computed results and the corresponding velocity time history. The 5 % damped acceleration response spectra obtained from all the numerical simulations are plotted in Figure 7. We see from this figure that the spectral amplitude varies about four times for an

arbitrary natural period due to uncertainty of hypocenter and asperity locations. The thick line in this figure indicates the spectral level that has a 90 % probability of not being exceeded for each natural period. This spectral line exceeds 1G over the wide natural period range $0.1<T<2$ (s), and reaches 2G for $0.1<T<0.6$ (s). Although further detailed study is necessary, the presented result seems to be consistent with ground motion characteristics from a large earthquake.

CONCLUDING REMARKS

The Design Specifications for Highway Bridges were revised in March 2002. The major modification in this revision is the introduction of performance-based design criteria. This paper presented the basic concepts and principles of seismic design of highway bridges including design ground motion, seismic performance and limit states. In the revised specifications, a site-specific ground motion can be conditionally employed as design ground motion. To predict a site-specific ground motion, we adopted a stochastic Green's function technique. The ground motion at the mouth of Tokyo Bay was simulated, in which a Kanto earthquake was assumed. Based on numerical results, effects of source parameter uncertainties on the simulated ground motions were examined.

ACKNOWLEDGEMENT

The draft of Design Specifications for Highway Bridges, Part V Seismic Design was developed by the Working Sub-Committee on Seismic Design (Chair: Dr. Shigeki Unjoh) and approved by the Committee on Bridges (Chair: Dr. Shoichi Saeki) under the auspices of the Japan Road Association.

REFERENCES

[1] Japan Society of Civil Engineers (1996). *The 1995 Hyogoken-Nanbu Earthquake – Investigation into Damage to Civil Engineering Structures –*.
[2] Public Works Research Institute (1997). "Report on the Disaster Caused by the 1995 Hyogoken Nanbu Earthquake", *Journal of Research*, Public Works Research Institute, Vol.33.
[3] Yokoyama, K. and Unjoh, S. (1997). "Seismic Design and Retrofit of Highway Bridges in Japan", Second National Seismic Conference on Bridges and Highways, Sacramento, CA, U.S.A.
[4] Japan Road Association (2000), *Design Specifications for Highway Bridges, Part V Seismic Design* (English edition).
[5] Japan Road Association (2002), *Design Specifications for Highway Bridges, Part V Seismic Design* (in Japanese).
[6] Hartzell, S. (1978). "Earthquake Aftershocks as Green's Functions", *Geophysical Research Letters*, Vol.5, No.1.
[7] Irikura, K. (1983). "Semi-Empirical Estimation of Strong Ground Motions during Large Earthquakes", *Bulletin of Disaster Prevention Research Institute*, Kyoto University, Vol.33, No.298.
[8] Boore, D. M. (1983). "Stochastic Simulation of High-frequency Ground Motions based on Seismological Models of the Radiated Spectra", *Bulletin of Seismological Society of America*, Vol.73, No.6.
[9] Kamae, K., Irikura, K. and Fukuchi, Y. (1991). "Prediction of Strong Ground Motion based on Scaling Law of Earthquake", *Journal of Structural and Construction Engineering*, Architectural Institute of Japan, No.430 (in Japanese).
[10] Yasuda, M. *et al*. (2000). "Seismic Design Ground Motions for Strait-crossing Projects in Japan", Thirty-second Joint Meeting, U.S.-Japan Panel on Wind and Seismic Effects, UJNR, Tsukuba, Japan.
[11] Tamura, K. and Kataoka, S. (2000). "A Procedure for Setting up Level-2 Earthquake Motions for Seismic Design of Bridges", Sixteenth U.S.-Japan Bridge Engineering Workshop, U.S.-Japan Panel on Wind and Seismic Effects, UJNR, Lake Tahoe, NV, U.S.A.

TABLE 1. IMPORTANCE CLASSIFICATION

Bridge class	Bridges included
Class-A bridges	- Bridges other than Class-B bridges
Class-B bridges	- Bridges on national expressways, urban expressways, designated city expressways, Honshu-Shikoku bridge highway and general national highways - Double-section and overpass bridges on prefectural highways and municipal roads, and other bridges and viaducts that are important in view of regional disaster prevention plans, traffic flow volume, etc.

TABLE 2. DESIGN GROUND MOTION AND SEISMIC PERFORMANCE

		Class-A bridges (Ordinary bridges)	Class-B bridges (Important bridges)
Level 1 ground motion		Secure integrity	
Level 2 ground motion	Type I ground motion	Prevent fatal damage	Limit damage and secure rapid restoration of function
	Type II ground motion		

TABLE 3. SEISMIC PERFORMANCE CRITERIA

Seismic performance criteria	Safety	Serviceability	Reparability	
			Short-term	Long-term
Seismic performance 1	Secure safety against collapse	Secure pre-earthquake function	Need no repair for restoration of function	Need minor repair
Seismic performance 2	Secure safety against collapse	Secure rapid restoration of function	Emergency repair enables restoration of function	Possible to perform permanent repair easily
Seismic performance 3	Secure safety against collapse	–	–	–

TABLE 4. SOIL CONDITION CLASSIFICATION

Soil classification	Natural period (s)	Geological description
Group-1	T_G<0.2	Rock or shallow soil deposits
Group-2	0.2≤T_G<0.6	Diluvium or alluvium
Group-3	0.6≤T_G	Soft alluvium

TABLE 5. LEVEL 1 STANDARD DESIGN RESPONSE SPECTRA

Soil classification	Spectral acceleration S_0 (cm/s^2) at natural period T (s)		
Group-1	S_0=431$T^{1/3}$ for T<0.1 (S_0≥160)	S_0=200 for 0.1≤ T ≤1.1	S_0=220/T for 1.1< T
Group-2	S_0=427$T^{1/3}$ for T<0.2 (S_0≥200)	S_0=250 for 0.2≤ T ≤1.3	S_0=325/T for 1.3< T
Group-3	S_0=430$T^{1/3}$ for T<0.34 (S_0≥240)	S_0=300 for 0.34≤ T ≤1.5	S_0=450/T for 1.5< T

TABLE 6(1). LEVEL 2 STANDARD DESIGN RESPONSE SPECTRA
(a) Type I ground motion

Soil classification	Spectral acceleration S_{I0} (cm/s^2) at natural period T (s)		
Group-1	S_{I0}=700 for T ≤1.4		S_{I0}=980/T for 1.4< T
Group-2	S_{I0}=1505$T^{1/3}$ for T<0.18 (S_{I0}≥700)	S_{I0}=850 for 0.18≤ T ≤1.6	S_{I0}=1360/T for 1.6< T
Group-3	S_{I0}=1511$T^{1/3}$ for T<0.29 (S_{I0}≥700)	S_{I0}=1000 for 0.29≤ T ≤2.0	S_{I0}=2000/T for 2.0< T

TABLE 6(2). LEVEL 2 STANDARD DESIGN RESPONSE SPECTRA
(b) Type II ground motion

Soil classification	Spectral acceleration S_{II0} (cm/s^2) at natural period T (s)		
Group-1	$S_{II0}=4463T^{2/3}$ for $T<0.3$	$S_{II0}=2000$ for $0.3\leq T\leq 0.7$	$S_{II0}=1104T^{-5/3}$ for $0.7< T$
Group-2	$S_{II0}=3224T^{2/3}$ for $T<0.4$	$S_{II0}=1750$ for $0.4\leq T\leq 1.2$	$S_{II0}=2371T^{-5/3}$ for $1.2< T$
Group-3	$S_{II0}=2381T^{2/3}$ for $T<0.5$	$S_{II0}=1500$ for $0.5\leq T\leq 1.5$	$S_{II0}=2948T^{-5/3}$ for $1.5< T$

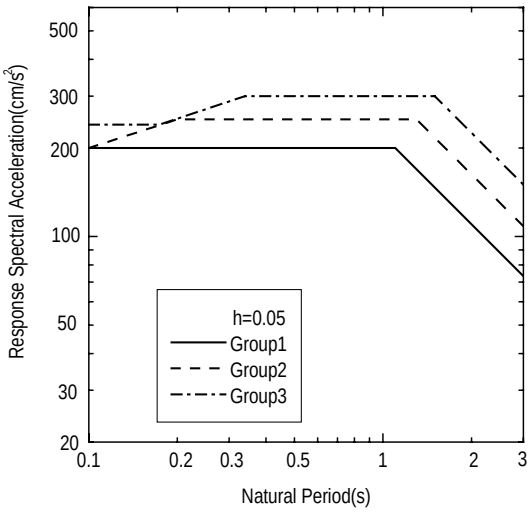

Figure 1. Standard acceleration response spectra of Level 1 ground motion

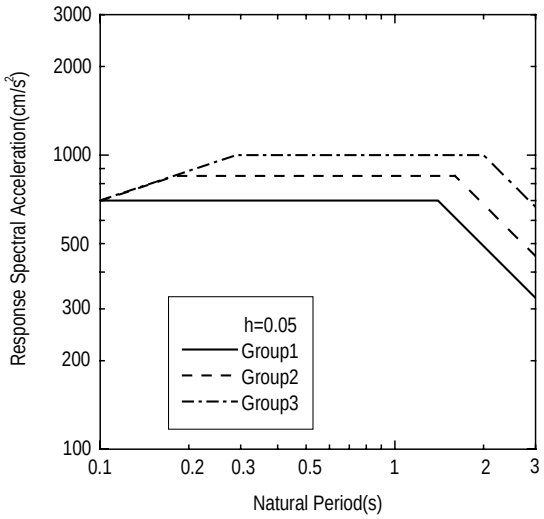

(a) Type I ground motion

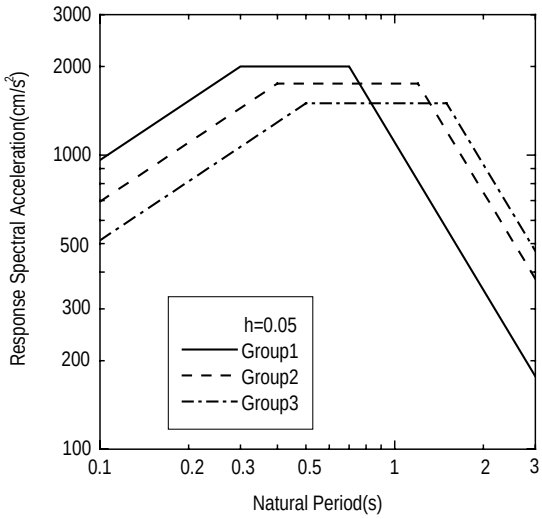

(b) Type II ground motion

Figure 2. Standard acceleration response spectra of Level 2 ground motion

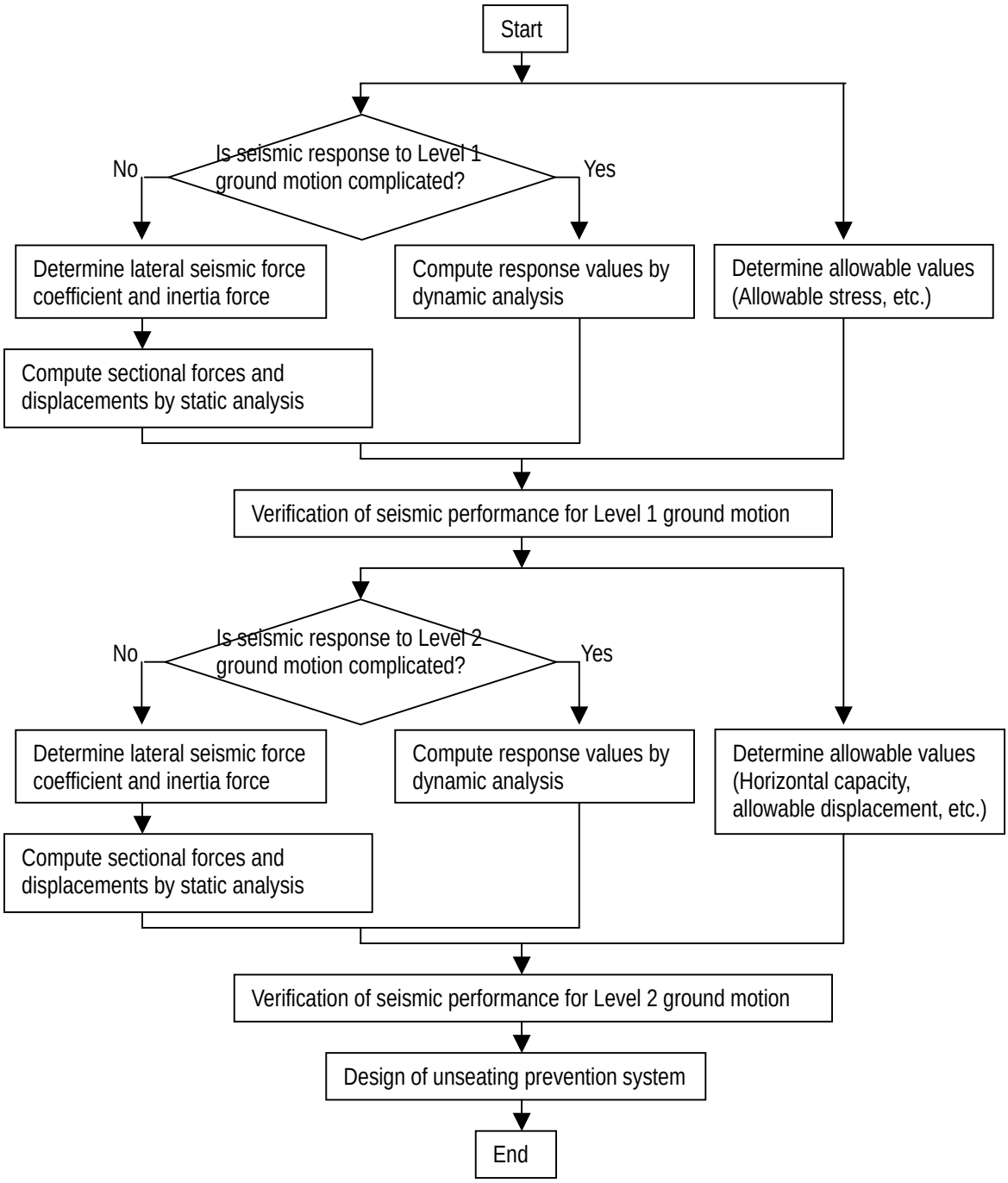

Figure 3. Standard procedure of seismic design

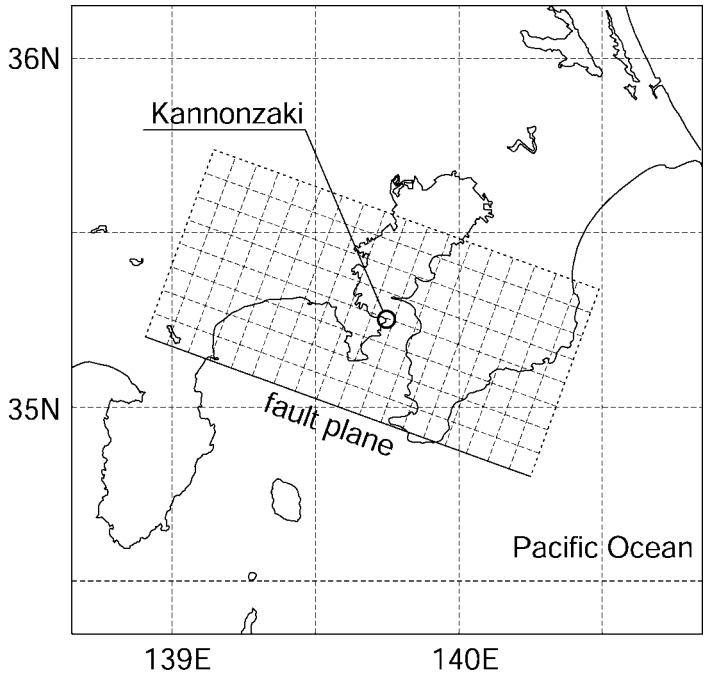

Figures 4. Fault plane model of Kanto earthquake

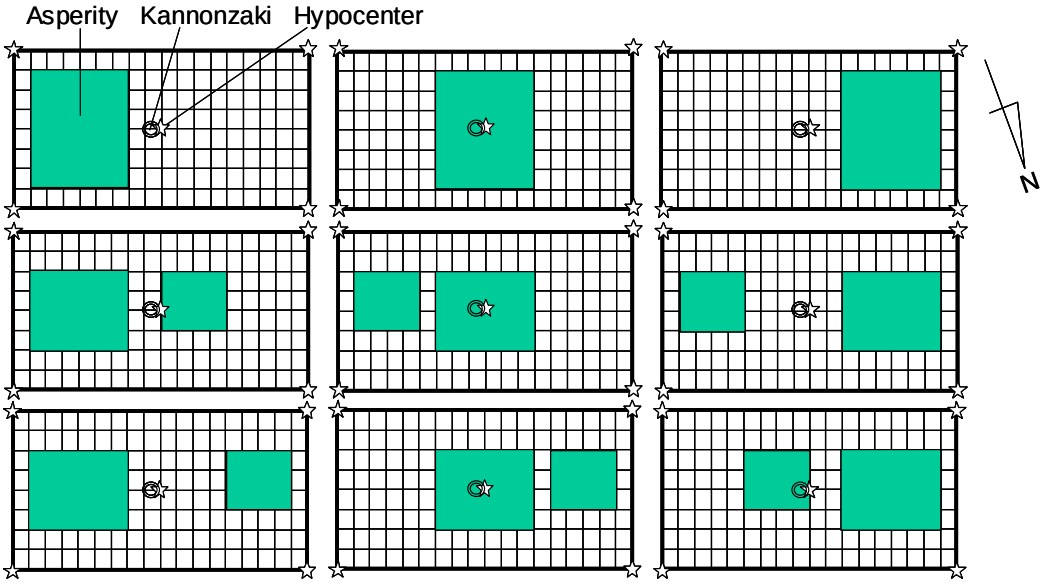

Figure 5. Locations of hypocenter and asperities

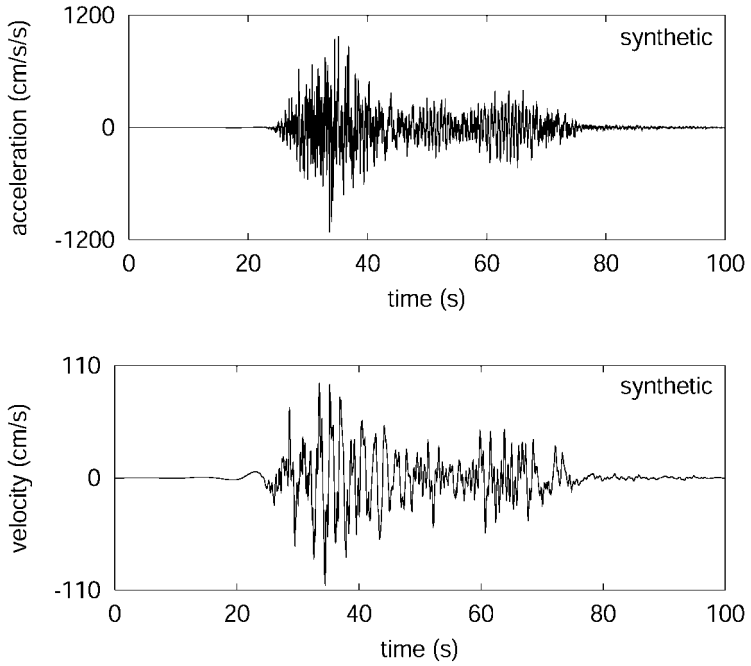

Figure 6. Simulated ground motion

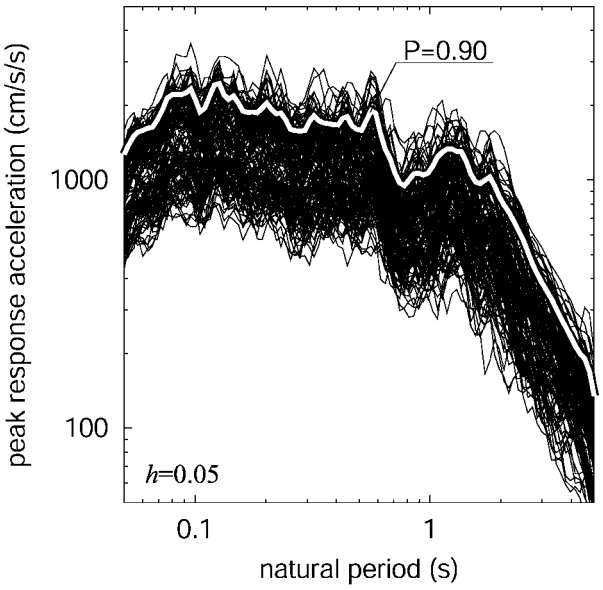

Figure 7. Acceleration response spectra

The Challenge of the Rion - Antirion Bridge

Jean-Paul Teyssandier

ABSTRACT

The Rion-Antirion Bridge in Greece is located in a zone of difficult environmental conditions characterized by deep soil strata of weak alluviums, large water depth, strong seismic design motion and possible tectonic movements. All these constraints have called for an original design.

The main bridge presents series of cable-stayed spans, 560 m long each, for a total length of 2,252 m. Foundations consist in large diameter (90 m) caissons resting on the seabed. The top 20 m of soils need to be strengthened. This is achieved by means of metallic inclusions, based on an innovative concept.

Another unique feature of this project lies in its 2.2km long continuous cable-stayed deck which, in addition to being the longest in the world, is totally suspended, achieving an effective isolation system. However, this disposition necessitates damping system of unusual characteristics.

Construction methods for foundations are those commonly used for offshore concrete platforms. However, dredging the seabed and driving 500 inclusions in a depth of water reaching 65 m is an unusual marine operation demanding special equipment and procedures.

In conclusion, the Rion-Antirion Bridge is a major structure, presenting exceptional features in term of design and construction methods, adopted mainly to achieve its seismic resistance.

Jean-Paul Teyssandier, Managing Director, Concession Company GEFYRA S.A., (VINCI Group),
2, Rizariou str., 15233 Halandri (Greece).

MAIN DATA

The RION-ANTIRION Bridge is located over the Gulf of Corinth, Western Greece, and is intended to replace an existing ferry system.

Its environment presents an exceptional combination of physical conditions which makes this project quite complex:

- large water depth (up to 65 m)
- deep soil strata of weak alluviums
- a strong seismic activity
- possible tectonic movements

The structure will span a stretch of water of some 2,500 m. The seabed presents fairly steep slopes on each side and a long horizontal plateau at a depth of 60 to 70 m.

No bedrock has been encountered during soil investigations down to a depth of 100 m. Based on a geological study, it is believed that the thickness of sediments is greater than 500 m.

General trends identified through soils surveys are the following:

- a cohesionless layer is present at mudline level consisting of sand and gravel to a thickness of 4 to 7 m, except under pier M4, where its thickness reaches 25 m.
- underneath this layer, the soil profile, rather erratic and heterogeneous, presents strata of sand, silty sand and silty clay.
- below 30 m, the soils are more homogeneous and mainly consist in silty clays or clays.

In view of the nature of the soils, liquefaction does not appear to be a problem except on the north shore, where the first 20 m are susceptible of liquefaction.

The seismic conditions to be taken into account are presented in the form of a response spectrum at seabed level given in figure 1. The peak ground acceleration is equal to 0.48 g and the maximum spectral acceleration is equal to 1.2 between 0.2 and 1.0 s. This spectrum is supposed to correspond to a 2000 year return period.

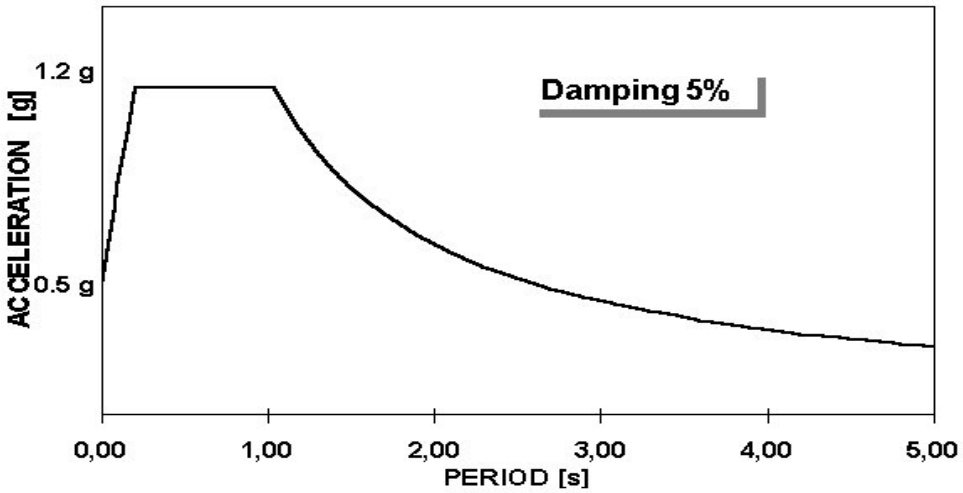

Figure 1: Design horizontal spectrum

In addition, the bridge has to accommodate possible fault movements up to 2 m in any direction, horizontally and/or vertically.

DESCRIPTION OF THE BRIDGE

These difficult environmental conditions called for an original design based on large foundations able to sustain seismic forces and large spans in order to limit the number of these foundations.

The bridge consists of (see figure 2):

- the cable-stayed main bridge, 2,252 m long, built on 4 large foundations with a span distribution equal to 286 m – 560 m – 560 m – 560 m – 286 m
- the approach viaducts, 392 m on Rion side and 239 m on Antirion side, made of prefabricated prestressed beams.

Foundations consist of large diameter (90 m) caissons, resting on the seabed (see figure 3). The top 20 m of soils are rather heterogeneous and of low mechanical characteristics. To provide sufficient shear strength to these soil strata, which have to carry large seismic forces coming from structural inertia forces and hydrodynamic water pressures, the upper soil layer is reinforced by inclusions. These inclusions are hollow steel pipes, 25 to 30 m long, 2 m in diameter, driven into the upper layer at a regular spacing of 7 to 8 m (depending on the pier); about 150 to 200 pipes are driven in at each pier location. They are topped by a 3 m thick, properly levelled gravel layer, on which the foundations rest. These inclusions are not required under pier M4 owing to the presence of a thick gravel layer.

The cable-stayed deck is a composite steel structure made of two longitudinal plate girders 2.2 m high on each side of the deck with transverse plate girders spaced at 4 m and a concrete slab, the total width being 27 m (see figure 4).

Each pylon is composed of four legs 4 x 4 m, made of self-compacting high strength concrete, joined at the top to give the rigidity necessary to support unsymmetrical service loads and seismic forces (see figure 5). The pylons are rigidly embedded in pier head to form a monolithic structure, up to 230 m high, from sea bottom to pylon top.

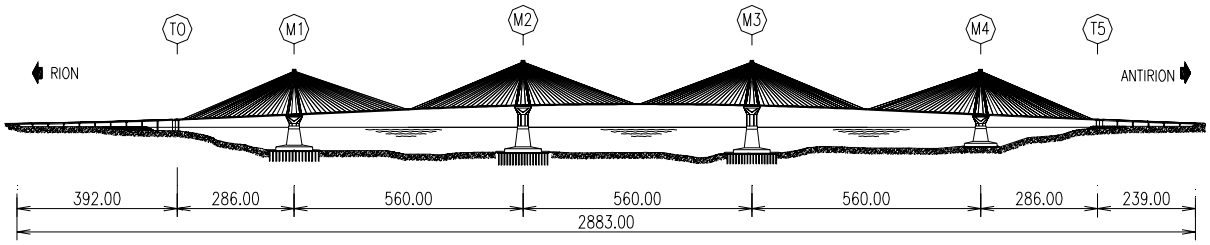

Figure 2: Bridge elevation

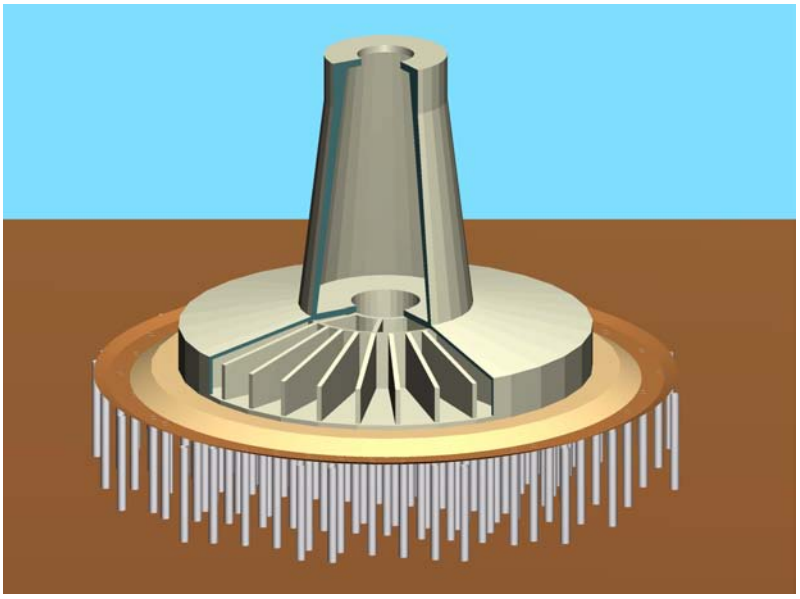

Figure 3: Foundation and inclusions

The stay cables, forming a semi-fan shape, are in two inclined arrangements, with their lower anchorages on deck sides and their upper anchorages at the pylon top. They are made of parallel galvanised strands individually protected.

The deck of the main bridge is continuous and fully suspended by means of stay cables for its total length of 2,252 meters. In the longitudinal direction, the deck is free to accommodate all thermal and tectonic movements. At its extremities, expansion joints are required to accommodate movements of 2 m.

In the transverse direction, the deck is connected to each pylon with 4 hydraulic dampers. The capacity of each damper is in the range of 3,500 kN, operating in both tension and compression. The dynamic relative movement between the deck and the pylon, during an extreme seismic event will be in the order of 3.50 m, with velocities up to 1.6 m/sec.

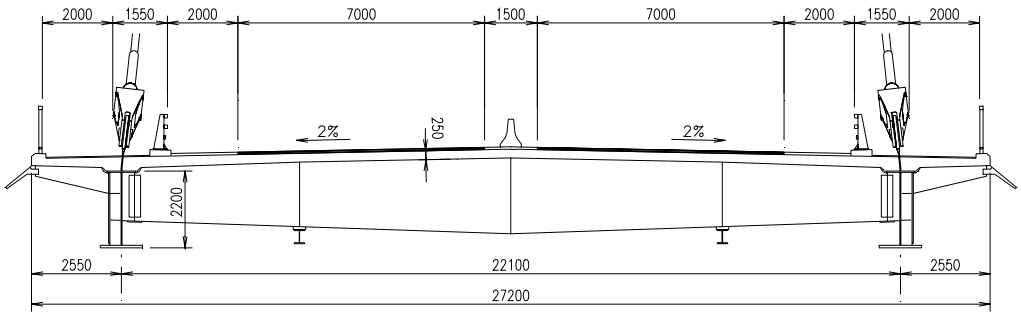

Figure 4: Typical deck cross section

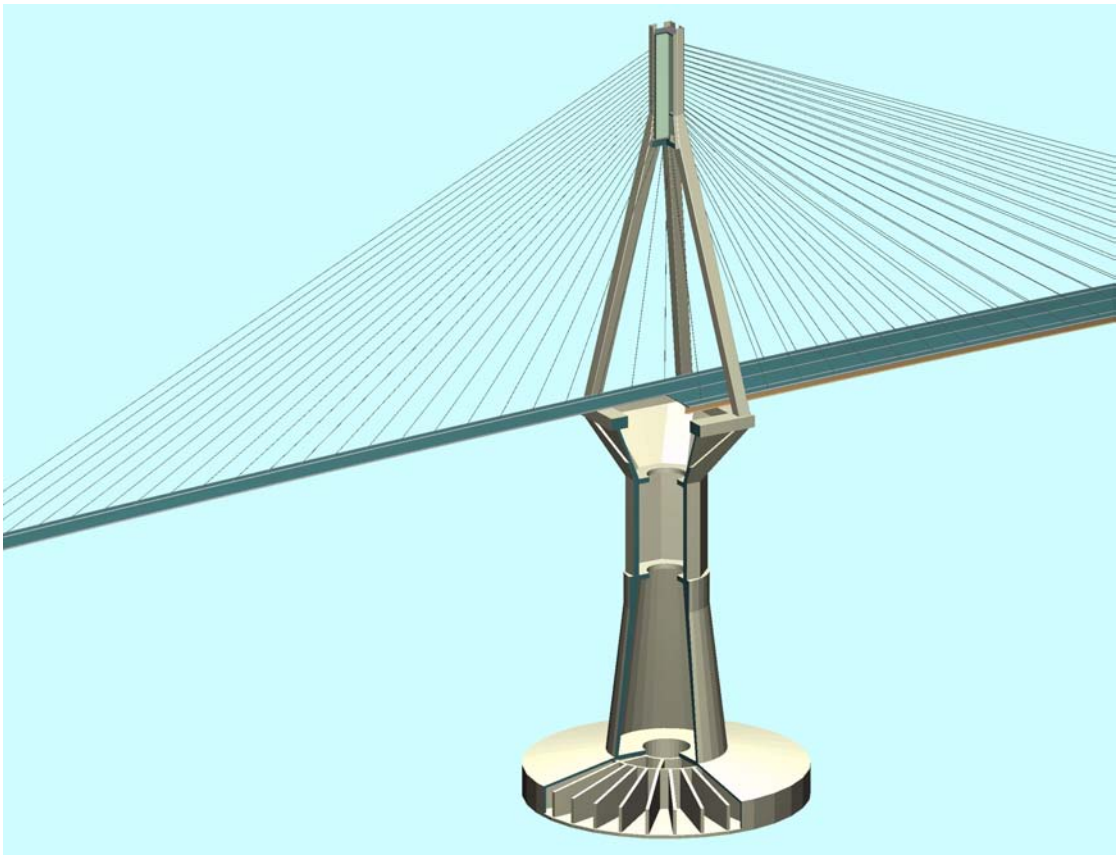

Figure 5: Pier and pylon

DESIGN CONCEPT

From the beginning it has been clear that the critical load for most of the structure is the design seismic loading, despite the fact that the bridge also has to sustain the impact of a 180,000 dwt tanker sailing at 18 knots.

The choice of the present design was made after examination of a wide range of possible solutions in term of span type (suspension spans vs. cable-stayed spans) and foundation concepts.

Particularly with regard to the foundations, the bearing capacity was a major concern in these difficult environmental conditions characterized by poor soil conditions, significant seismic accelerations and large depth of water. Alternative foundation concepts (such as pile foundations, deep embedded caissons and soil substitution) have been investigated with their relative merits in terms of economy, feasibility and technical soundness.

This analysis showed that a shallow foundation was the most satisfactory solution as long as it was feasible to significantly improve the top 20 m of soils. This has been achieved by means of metallic inclusions, as described here above. Although these foundations resemble piled foundations, they do not at all behave as such: no connection exists between the inclusions and the caisson raft, which will allow for the foundation to uplift or to slide with respect to the soil; the density of inclusions is far more important and the length smaller than would have been the

case in piled foundations. This type of soil reinforcement through metallic inclusions is quite innovative and necessitated extensive numerical studies and centrifuge model tests for its validation in the Laboratoire Central des Ponts et Chaussées (France).

Another unique feature of this project lies in its continuous cable-stayed deck, which, in addition to being the longest in the world, is totally suspended. This creates an effective isolation system significantly reducing seismic forces in the deck and allowing the bridge to accommodate fault movements between adjacent piers. However, this disposition necessitates installing at each pylon transversal damping devices able to limit lateral displacements of the deck and dissipate large amount of energy during a seismic event. This isolation system must also allow slow tectonic movement and restrain the deck for wind action. For that reason, the deck is connected to each pylon by an horizontal strut of 10,000kN capacity which will break during a seismic event of low occurrence (over 350 year return period), then allowing dampers to go into action. A prototype test for these dampers was recently performed in the CALTRANS testing facility at the University of California San Diego.

CONSTRUCTION METHODS

Construction methods for the foundations are those commonly used for the construction of offshore concrete platforms:

- construction of the foundation footings in a dry dock up to a height of 15 m in order to provide sufficient buoyancy;
- towing and mooring of these footings at a wet dock site;
- construction of the conical part of the foundations at the wet dock site;
- towing and immersion of the foundations at final position.

However some features of this project make the construction process of its foundations quite exceptional.

The dry dock has been established near the site. It is 200 m long, 100 m wide, 14m deep, and can accommodate the simultaneous construction of two foundations. It has an unusual closure system: the first foundation is built behind the protection of a dyke, but once towed out, the second foundation, the construction of which has already started, is floated to the front place and used as a dock gate.

Dredging the seabed, driving 500 inclusions, placing and levelling the gravel layer on the top, with a depth of water reaching 65 m is major marine operation which necessitates special equipment and procedures. In fact, a tension-leg barge has been custom-made, based on the well known concept of tension-leg platforms but used for the first time for movable equipment. This concept is based on active vertical anchorage to dead weights lying on the seabed (see figure 6). The tension in these vertical anchor lines is adjusted in order to give the required stability to the barge with respect to sea movements and loads handled by the crane disposed on its deck. By increasing the tension in the anchor lines, the buoyancy of the barge allows the anchor weights to be lifted from the seabed, then the barge, including its weights, can be floated away to a new position.

As already stated, once completed the foundations will be towed then sunk at their final position. Compartments created in the footings by the radial beams will be used to control trim by differential ballasting. Then the foundations will be filled with water to accelerate settlements,

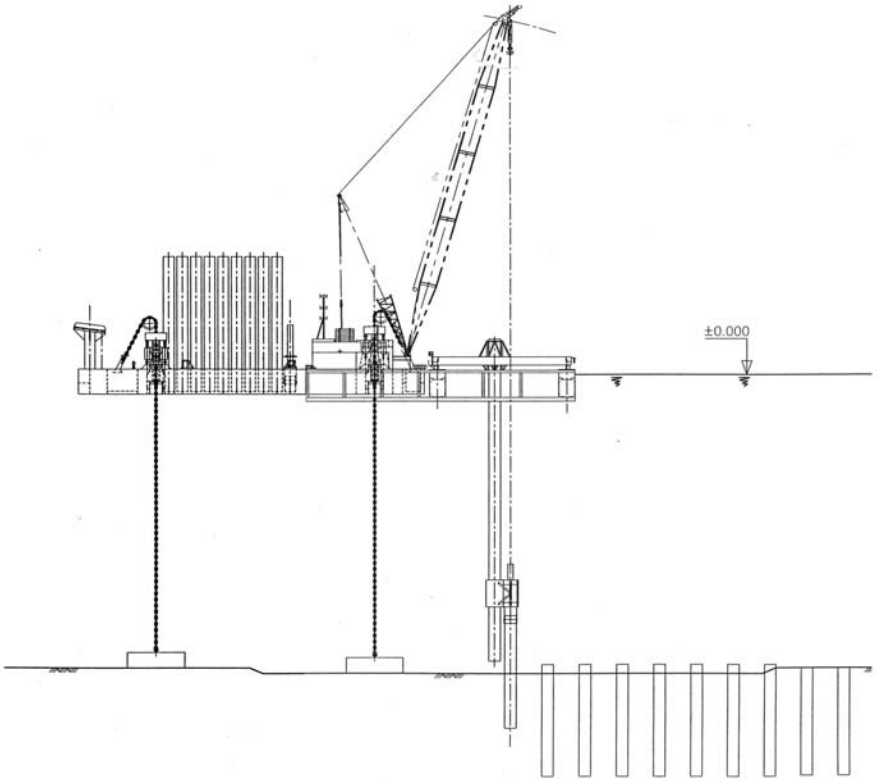

Figure 6: Tension-leg barge

which are expected to be significant (between 0.2 and 0.3 m). This pre-loading will be maintained during pier shaft and pier head construction, thus allowing a correction for differential settlements before erecting pylons.

The deck of the main bridge will be erected using the balance cantilever technique, a usual construction method for cable-stayed bridges, with deck elements 12 m long.

CONCLUSION

The Rion-Antirion bridge is a major structure, presenting exceptional features in term of design and construction methods, mainly commanded by its seismic resistance.

The design and construction of this highly innovative project have been undertaken under a private concession scheme, led by the French company VINCI. The detailed design is completed, the four foundations are in place and the four piers under construction for a completion of the whole project due in 2004.

REFERENCES

Teyssandier, J.P., Combault, J. and Morand, P. (2000), "The Rion-Antirion Bridge design and construction", *Proceedings 12th WCEE- Auckland*.
Combault, J., Morand, P. and Pecker, A. (2000), "Structural response of the Rion-Antirion Bridge", *Proceedings 12th WCEE- Auckland.*
Combault, J. and Morand, P. (1998), "The exceptional structure of the Rion Bridge in Greece", *Proceedings IABSE Symposium – Kobe*.
Pecker, A., Teyssandier, J.P., Guyot, T. and Combault, J. (1996), "Seismic design for the foundations of the Rion-Antirion Bridge", *Proceedings IABSE Congress – Copenhagen*.
Pecker, A. (1998), "Capacity design principles for shallow foundations in seismic areas", *Proceedings Xith European Conference on Earthquake Engineering – Paris*.
Pecker, A. and Teyssandier, J.P. (1998), "Seismic design for the foundation of the Rion-Antirion Bridge", *Proceedings Institution of Civil Engineers, Geotechnical Engineering*.
Teyssandier, J.P. (1997), "The Rion-Antirion Bridge", *Proceedings International Conference, New technologies in Structural Engineering – Lisbon*.
Website: www.gefyra.gr

Effect of Near-Fault Earthquake on Bridges: Lessons Learned from Chi-Chi Earthquake

Chin-Hsiung Loh[1] , Wen-I Liao[2] and Jun-Fu Chai[2]

ABSTRACT

The objective of this paper is to describe the responses from academic and engineering communities of Taiwan in relating to the revision on seismic design guidelines of bridge structure after the Chi-Chi earthquake. Because a lot of variable near-fault ground motion data was collected from the rupture of Chelungpu fault, seismic response of bridge structure subjected to these near-fault ground motions were examined carefully. To reflect the near-fault ground motion effect on bridge seismic design guideline with the consideration of near-fault ground motion effect was developed and implemented and two-level seismic design of bridge structure was studied and proposed. Finally, a risk assessment methodology, based on vulnerability, is also developed to assist in decisions for reducing seismic risk due to failure of bridges.

INTRODUCTION

Taiwan is located at the active arc-continent collision region between the Luzon arc of the Philippine Se plate and the Eurasian plate. The Philippine Sea plate is colliding onto the Eurasian continent at a rate of 7-8 cm/yr, resulting high seismicity in this region. Most earthquake in the western seismic zone are shallowly seated. On September 21, 1999, at 1:47am local time (17:47pm Sept. 20, UT), an earthquake of magnitude $M_L = 7.3$ and $M_W = 7.7$ took place in the central part of Taiwan. The epicenter of the earthquake located at 120.82°E and 23.85°N near the town of Chi-Chi, Nautou county. The focal depth was 8.0km. A surface rupture along Chelungpu fault with length of about 105km was observed with the largest measured vertical offset reaching more than 9 meters. Ground and geophysical surveys also showed that the shock resulted from reactivation of the Chelungpu fault. The rupture was generated by the combination of reverse, strike-slip and normal movements, particularly in the northern part of the fault, thus far more complicated than that of a simple fault. As a direct result of this earthquake, 2469 lives were lost and more than 700 peoples were severely injured, and many civil infrastructures were damaged, including roads and bridges, communication systems, water supply systems, gas supply systems and electric power systems. On the basis of the number of deaths, this was Taiwan's worst disaster since the Shin-Chu Taichung earthquake of magnitude 7.1 (1935-4-2 earthquake).

Immediately after the earthquake, the NCREE mobilized more than 1,200 scientists and engineers to conduct field surveys systematically and to collect scientific data in order to learn as

[1]Professor, Department of Civil Engineering, National Taiwan University, Taiwan; Director of NCREE.
[2]Associate Research Fellow, National Center for Research on Earthquake engineering (NCREE), Taiwan.

much as possible from this disastrous event [1]. These reports are to describe the lessons learned from the damage investigation of structures. From the damage investigation of civil infrastructure the responses been taken after the Chi-Chi earthquake are: (i) development of seismic design code for bridge to include near-fault ground motion effect, (ii) development of risk assessment methodology of bridges. This paper will describe the actions been taken in relating to the development of guidelines for seismic design of bridge.

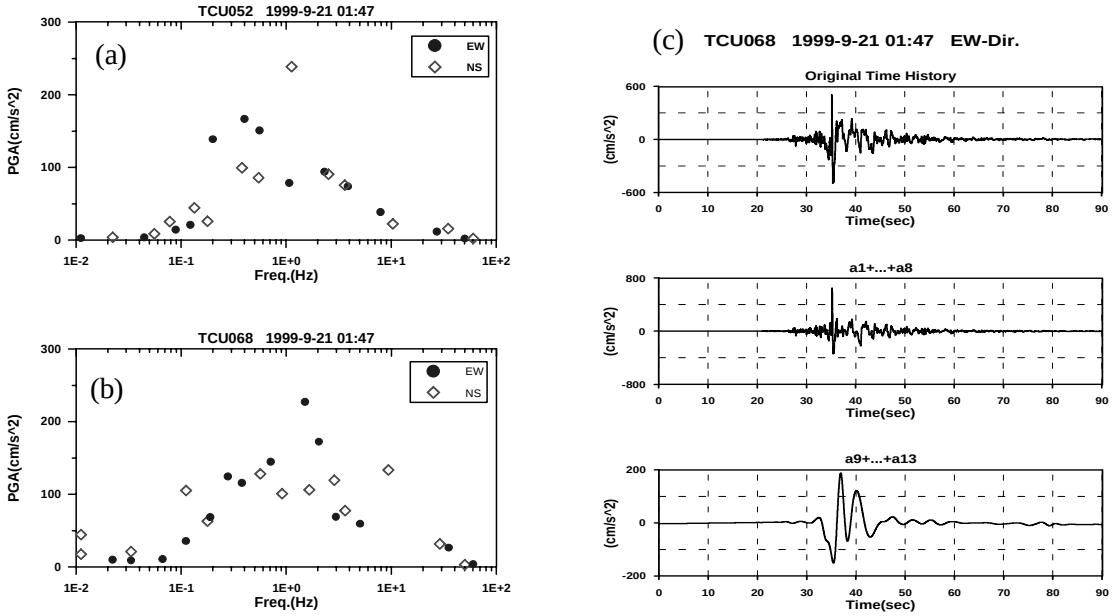

Figure 1: (a) & (b) Distribution of PGA value with respect to its dominant frequency for each IMF from data collected at station TCU052 and TCU068, (c) Separation of recorded ground acceleration into two signals; below 1.0 Hz and higher than 1.0 Hz.

NEAR-FAULT GROUND MOTION CHARACTERISTICS

To investigate the near-fault ground motion characteristics the empirical mode decomposition method was used to decompose the recorded ground acceleration into several intrinsic mode functions (IMF) [2]. The peak acceleration of each IMF was identified. Because each IMF is un-correlated to each other then dominant frequency of each IMF can also be estimated. Figs.1a and 1a show the peak ground acceleration (PGA) of each IMF with respect to the identified dominant frequency of each IMF for data recorded at station TCU052 and TCU068. From these figures the distribution of peak ground acceleration of each IMF with respect to its corresponding dominant frequency can be observed. It is found that near-fault data from stations TCU068 and TCU052 (Chi-Chi earthquake) large PGA value was observed in low frequency band (0.1Hz and 0.2Hz). Based on each IMF $a_i(t)$, two groups of IMF can be separated. As shown in Fig.1c, for example, data from TCU068, one group of high frequency signals is defined as dynamic wave, $a_1(t)+\ldots+a_8(t)$ and the other group of low frequency signals is defined as pulse-like wave, $a_9(t)+\ldots+a_{14}(t)$. The contribution of pulse-like wave in the recorded ground acceleration can be observed. The PGA value is significant even in the pulse-like wave with frequency content lower than 1.0 Hz.

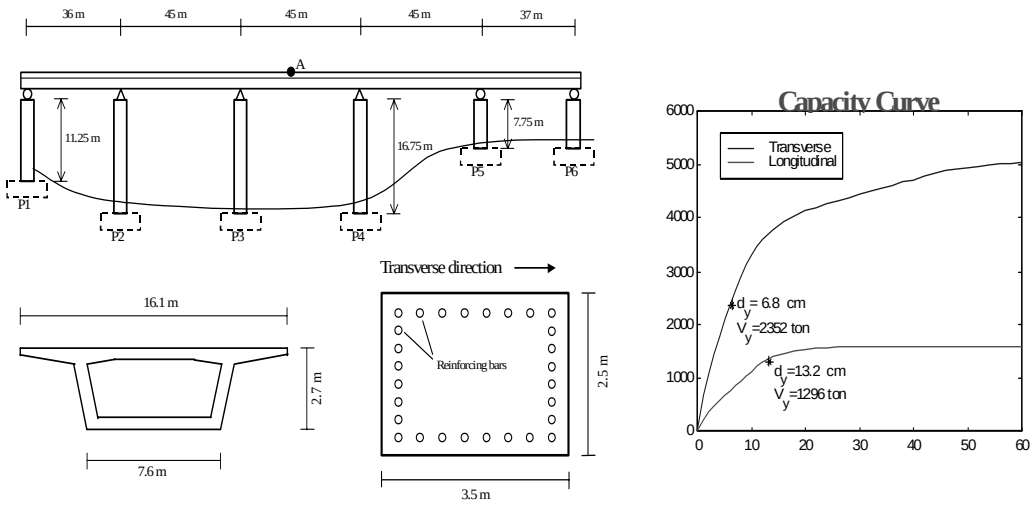

Figure 2: A five span continuous bridge for dynamic analysis subjected to near-fault ground excitation. The capacity curves of the bridge were also shown.

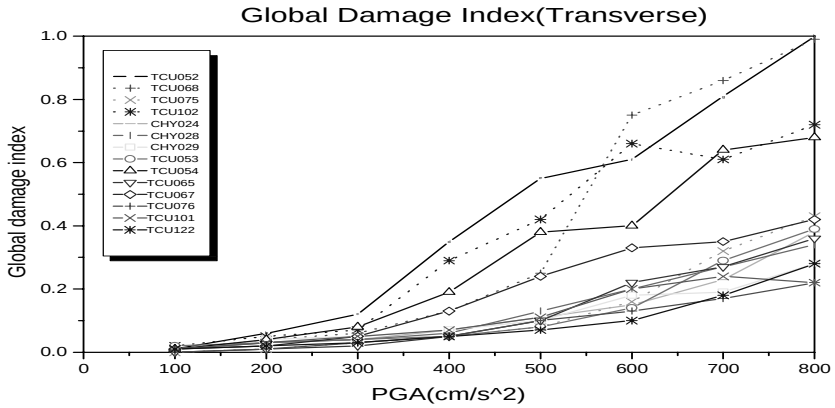

Figure 3: Plot of global damage index of the 5-span continuous bridge versus various PGA level of excitation for different set of ground motion collected from Chi-Chi earthquake.

SEISMIC RESPONSE OF BRIDGE TO NEAR-FAULT GROUND EXCITATION

In order to understand the effect of near-fault ground motion on the bridge structure two examples are selected for the analysis of seismic response of bridge to near-fault ground motion excitation. In the first example a 5-span continuous girder bridge with both hinge and roller supported by the concrete pier in the longitudinal direction and fixed connection in the transverse direction was considered first. This bridge was designed according to the Taiwan seismic design code of bridge, as shown in Fig.2. The design concrete nominal strength and yield strength of reinforcement are 280 kg/cm^2 and 4200 kg/cm^2. The natural period of this bridge in longitudinal direction and transverse direction is 1.06 sec and 0.59 sec, respectively. The capacity curves of this bridge can be obtained from pushover analysis. The yield base shear (V_y) and corresponding displacement (d_y) in the longitudinal direction are V_y=1296 ton and d_y=13.2 cm, and in the transverse direction are V_y=2352 ton and d_y=6.8 cm, respectively. The IDARC computer program

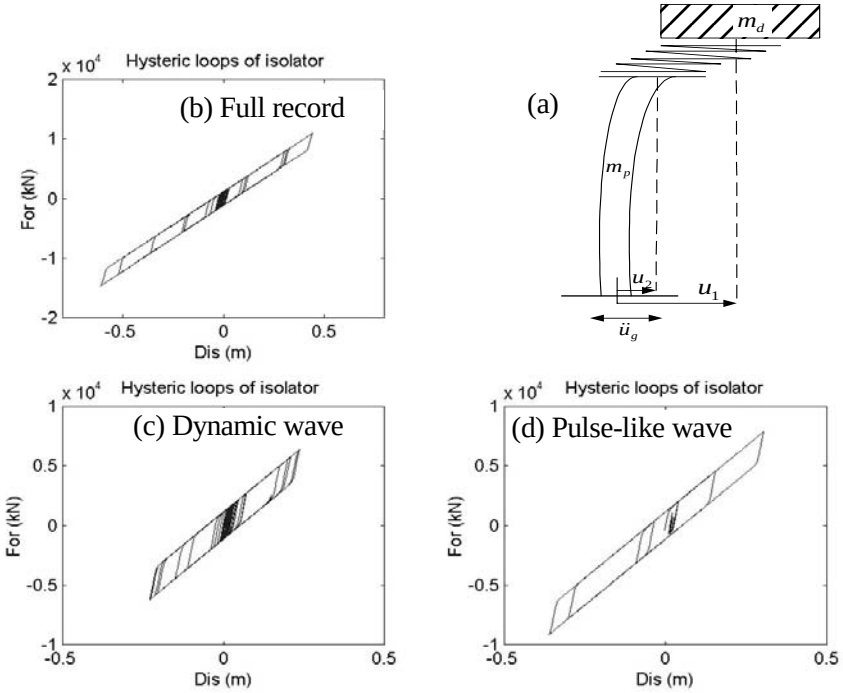

Figure 4: (a) Simplified isolated bridge structure, (b) hysteretic loop of the isolator using record from TCU068, (c) and (d) the hysteretic loop of the isolator using dynamic wave and pulse-like wave of data from TCU068, respectively

was used for the dynamic analysis of the bridge. The model parameters of bridge column were determined from the pseudo-dynamic testing of a 1/2-scale model of bridge column. The near-field ground motion data collected from the Chi-Chi (Taiwan) earthquake was used as input ground motion to study the dynamic response of the bridge structure.

To examine the effect of bridge response to earthquake load a damage model for expressing the potential damage of reinforced concrete component is used as damage index, *D*, and expressed as [3]

$$D = \frac{\delta_m}{\delta_u} + \frac{\beta}{Q_y \delta_u} \int dE \tag{1}$$

where δ_m is the maximum displacement obtained during cyclic loading, δ_u is the ultimate displacement to failure under monotonic loading, Q_y is the shear force at the yield moment, dE is the incremental hysteretic energy dissipated, and β is a non-negative parameter. In these parameters, δ_m and $\int dE$ are determined from the response of the structure while δ_u, Q_y, β are independent of the loading history and depend only on the properties of the reinforced concrete member. When damage index $D > 1$, it represents a complete collapse or total damage of the structure and the over all damage index $D < 0.4$ represents repairable damage, and $D > 0.4$ represents damage beyond repair. The overall damage index is computed using weighting factors based on dissipated energy at element level. It is now defined the global damage index as follows:

$$\mathrm{DI}_{global} = (\lambda_i)_{element} (\mathrm{DI}_i)_{element} \tag{2a}$$

$$(\lambda_i)_{element} = [\, \mathrm{E}_i / \Sigma \mathrm{E}_i \,] \tag{2b}$$

$(\lambda_i)_{element}$ is the energy weighting factors, and E_i is the absorbed energy by the element "*i*". Eq.(2) will be used to measure the response of the bridge structure subjected to different degree of damage. Fig. 3 indicated the damage index of this particular bridge subjected to different kind of input ground motion. From this study it is found that the excitation which contains the pulse-like wave in the velocity wave forms (such as ground motion at station of TCU052, TCU102, TCO068 and TCU075) will cause a significant damage as compare to other input motions.

In the second example, a three-span (34m-52m-34m) continuous bridge with post-tensioned box girders is considered in this study. A simplified pier-bearing-deck model was considered for dynamic analysis, as shown in Fig.4a. The pier is assumed to have ideal smooth bilinear hysteretic behavior with initial stiffness K_p, yield strength F_{yp} and yield displacement d_y. The bearing (isolation system) is modeled by Bouc-Wen hysteretic model [4]. The accuracy of the simplified model for earthquake excitation was verified by comparing the seismic response of the bridge using IDARC-BRIDGE computer program. The Near-fault ground motions collected from Chi-Chi earthquake was used as input ground motion for examining the relative displacement of isolator using this simplified model. Fig.4b-4d shows the hysteretic loops of isolator subjected to three different excitations: (a) full record of station TCU068, (b) dynamic wave of TCU068, and (c) pulse-like wave of TCU068. It is found that the maximum displacement of the isolator for this near-fault ground excitation was about 50 cm and the restoring force due to pulse-like wave and the dynamic wave were in a similar order of magnitude, about 25~35 cm. It is found that the displacement of isolator is very significant when subjected to the excitation of near-fault pulse-like wave.

SEISMIC DEMAND FOR NEAR-FAULT SITES

After the Chi-Chi earthquake seismic design force in Taiwan was revised [5]. Instead of using seismic zone factor Z and normalized design spectrum C [6], the site adjusted spectral acceleration at a period of T=0.3 sec (S_{DS}) and T=1.0 sec (S_{D1}) with a uniform seismic hazard level of 5% probability of exceedance within 50 years (return period of 475 years) were used, and the seismic design force was expressed as

$$V = \frac{ZICW}{1.2\alpha_y F_u} \quad \Rightarrow \quad V = \frac{S_{aD} IW}{1.2\alpha_y F_u} \tag{3}$$

where α_y is the first yield seismic force amplification factor that is dependent on the design method and the related load combination method. F_u is the structural system seismic reduction factor dependent on structure ductility capacity, *I* is the important factor, and *W* is the seismically effective weight of the bridge. The site adjusted S_{DS} and S_{D1} was provided in each township and county from which the design spectrum can be constructed, as shown in Fig.5.

To consider the effect of near-fault ground motion in seismic design, both the probabilistic analysis based on the seismic hazard analysis at a return period of 2500 years and the deterministic analysis based on the attenuation law corresponding to the maximum potential magnitude of the fault are implemented. Based on the maximum potential magnitude of an active fault, the attenuation relations $S_{S,Att}(r)$ and $S_{1,Att}(r)$ for the median 5% damped spectral acceleration demands at short periods (e.g. 0.3 second period) and at 1 second are determined firstly. For example, the Chi-Chi earthquake can be considered as the maximum potential earthquake for Chelungpu fault.

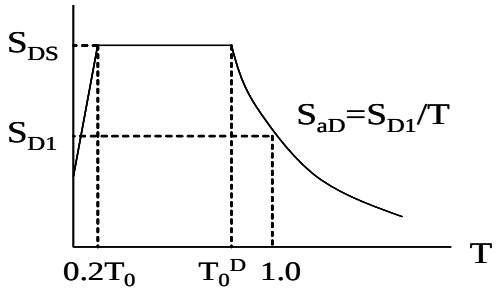

$S_{DS} = F_a S_S^D$; $S_{D1} = F_v S_1^D$

S_S^D	0.5	0.6	0.7	0.8
S_1^D	0.30	0.35	0.40	0.45
EPA	0.20	0.24	0.28	0.32

Figure 5: Seismic design spectrum used in Taiwan. Four different level of S_S^D , S_1^D and related EPA is also shown in the table.

Table 1: Near-fault factor N_a and N_v

	$r \le 2\,km$	$r = 5\,km$	$r = 8\,km$	$r > 11\,km$
N_A	1.74	1.46	1.19	1.00
N_V	1.77	1.49	1.23	1.00

Compared the result with the spectral response acceleration at short periods (S_S^M) and at 1 second (S_1^M) that are determined from uniform hazard analysis at a return period of 2500 years, the near-fault factors $N_A(r)$ and $N_V(r)$ can be defined:

$$N_A(r) = 1.5 S_{S,Att}(r) / S_S^M \quad ; \quad N_V(r) = 1.5 S_{1,Att}(r) / S_1^M \tag{4}$$

The factor of 1.5 implies the consideration of 1σ deviation of uncertainty of fault movement and the component effect (fault-normal). For site with the consideration of $N_A(r)$ and $N_V(r)$ larger than 1.0 will be considered as the effect of near-fault ground motion, and hence the two-level design should be implemented for bridge structure within this site. With the consideration of site amplification the site-adjusted spectral response acceleration parameters S_{MS} and S_{M1} are determined by

$$S_{MS} = F_a N_A S_S^M \quad ; \quad S_{M1} = F_v N_V S_1^M \tag{5}$$

It is noted that the site coefficients F_a and F_v should be evaluated based on the ground shaking level of $N_A S_S^M$ and $N_V S_1^M$, respectively. The spectral acceleration S_{MS} and S_{M1} are used for the ultimate checking level. Table 1 shows the near-fault factor for Chelungpu fault. The required spectral response acceleration S_{aM} at the checking level can be defined by

$$S_{aM} = \begin{cases} S_{MS}\left[0.4 + (1-0.4)T / \left(0.2T_0^M\right)\right] & ; \quad T \le 0.2T_0^M \\ S_{MS} & ; \quad 0.2T_0^M < T \le T_0^M \\ S_{M1} / (T) & ; \quad T > T_0^M \end{cases} \quad \text{with} \quad T_0^M = \left(\frac{S_{M1}}{S_{MS}}\right)$$

CAPACITY CHECK FOR BRIDGES AT NEAR-FAULT SITES

The seismic design code of bridge structure is followed by the conventional force based design method (seismic coefficient method). The designed seismic force is considered for an earthquake

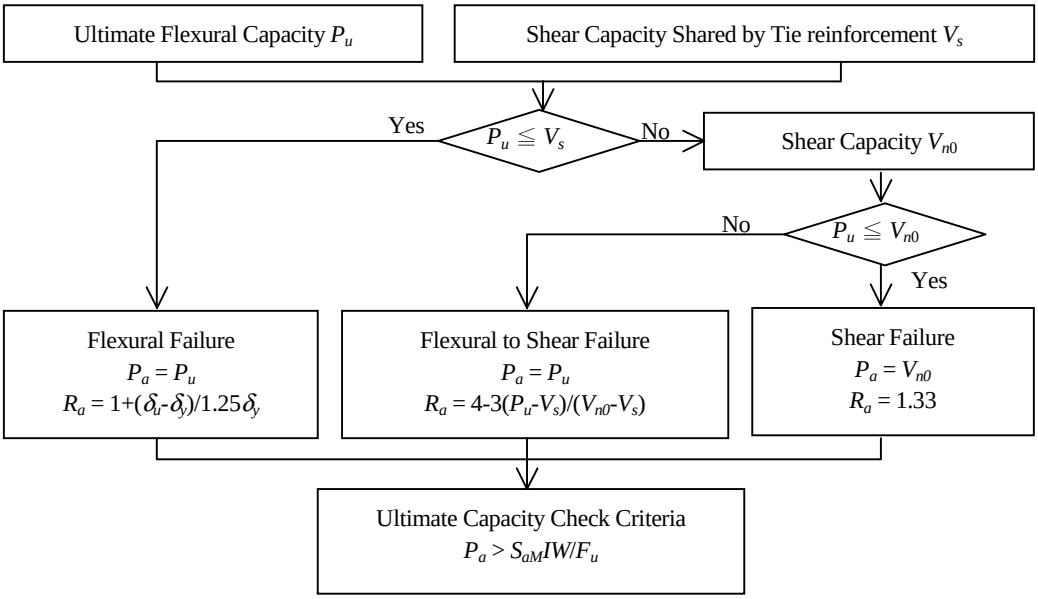

Figure 6: Procedures for the ultimate capacity check of bridges located in the near-fault area.

with return period of 475 year as shown in Eq. (3). For the protection of collapse of the bridge, the seismic capacity check is required for the bridge located in the near-fault area. The earthquake level for capacity check adopted is the earthquake motion with return periods of 2500 year. To check the seismic capacity of the RC bridge pier, in the beginning, the moment-curvature method [7, 8] was adopted to calculate the moment capacity and curvature of the pier in accordance with the reinforcement details and stress-strain curves of both concrete and reinforcement. It then calculates the ultimate allowable lateral capacity and allowable ductility capacity. Based on the ductility capacity, it calculates the reduced seismic force demand using equal energy principle for the near-fault area and compares with the allowable lateral capacity to determine the bridge pier is seismically adequate or not. The whole procedures for the capacity check of the bridge pier are resumed in Fig. 6. The shear capacity V_n of the RC pier are evaluated by $V_n=V_s+V_c$, where V_s and V_c represent the shear capacity shared by the reinforcement and concrete, respectively, and they are defined by

$$V_s = A_v f_{yh} d / s \quad ; \quad V_c = 0.53(k+F)\sqrt{f_c'} A_e \tag{6}$$

where

$$F = N/(140 A_g) \tag{7a}$$

$$k = \begin{cases} 1.0 & \text{(outside the plastic hinge zone)} \\ (R_a - 1.0)/3.0 & \text{(inside the plastic hinge zone)} \end{cases} \tag{7b}$$

where A_v and d are the sectional area and height of the tie reinforcement, s is the spacing of the tie reinforcement, A_e (=0.8A_g) and A_g are the effective shear area and total cross section area, f_{yh} and f_c' are the design strength of reinforcement and concrete, and k and F are the adjustment factors related to the allowable ductility ratio R_a and axial force N, respectively.

After calculating the ultimate bending capacity and the shear capacity of the RC pier

column, failure mode inside the plastic hinge zone can be determined. Failure modes are categorized to flexural failure, flexural to shear failure and shear failure based on the ultimate capacity and shear capacity of the pier as

$$\begin{aligned} &P_u \le V_s && : \text{flexural failure} \\ &V_s < P_u \le V_{n0} && : \text{flexural to shear failure} \\ &V_{n0} < P_u && : \text{shear failure} \end{aligned} \tag{8}$$

where V_{n0} : the shear capacity with factor k =1.0.

Based on the failure mode, the lateral capacity P_a and the allowable ductility capacity R_a of a pier are evaluated as

$$P_a = \begin{cases} P_u & : \text{for flexural failure and flexural to shear failure} \\ V_{n0} & : \text{for shear failure} \end{cases} \tag{9}$$

$$R_a = \begin{cases} 1.0 + (\delta_u - \delta_y)/1.25\delta_y & : \text{for flexural failure } (R_a \le 4.0) \\ 4.0 - 3(P_u - V_s)/(V_{n0} - V) & : \text{for flexural to shear failure} \\ 1.33 & : \text{for shear failure} \end{cases} \tag{10}$$

In the above equation if the flexural failure was identified the allowable ductility capacity only use 80% of the ductility capacity and limits the maximum R_a value up to 4.0. The main considerations are (1) moment curvature method does not consider the degrading of the bending strength and stiffness under the cyclic loading; (2) prevent the structure from collapse because use of all the ductility capacity; and (3) P-Δ effect increases because increase in lateral displacement. Once the allowable ductility capacity is obtained, the earthquake force reduction factor F_u can be calculated. If a RC pier column has adequate seismic capacity, its allowable lateral capacity must be larger than the horizontal earthquake force demand, i.e.

$$P_a > \frac{S_{aM} IW}{F_u} \tag{11}$$

SEISMIC DESIGN BASED ON DUCTILITY AND CUMULATIVE DAMAGE DEMANDS

Under earthquake loading different hysteretic model may have different percentage of contribution to the displacement damage index and to the hysteretic damage index of the Park & Ang's damage index model. It can be clearly found out that for case of model with either lap splice failure or shear failure the contribution of hysteretic damage to the overall damage index is much smaller than the contribution from model with flexure failure. Several structural members were damaged during the Chi-Chi earthquake due to these kinds of failure mode. To develop inelastic response spectra with specified damage level, several nonlinear single degree of freedom systems must be established to consider different hysteretic model with stiffness and strength degradation. A series of experiment was conducted in National Center for Research on Earthquake Engineering (NCREE) to study the capacity of reinforced concrete column. Cyclic loading test had been carried out on the reinforced-concrete column to observe the capacity of column from different design philosophy. Eight different types of column were designed and tested. The cross section of the rectangular column is 75 cm by 60 cm. Specimen BMR1 is a rectangular column and is designed

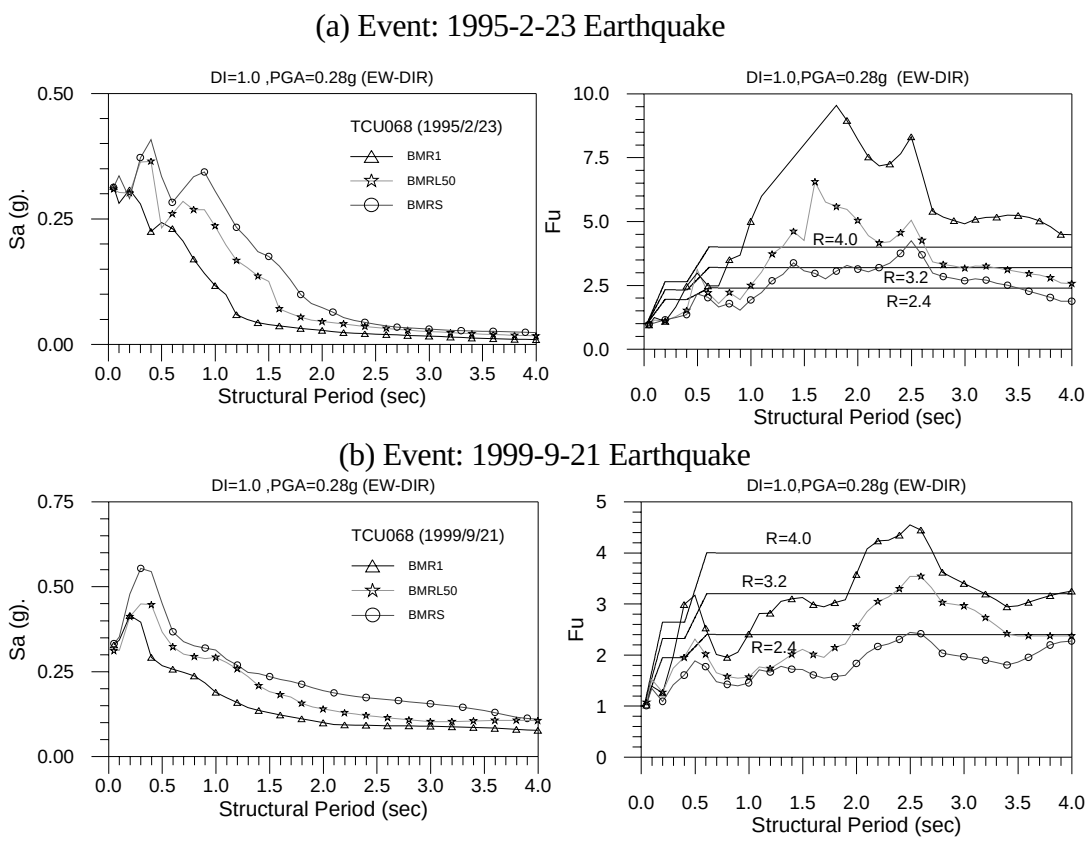

Figure 7: Plot of inelastic acceleration response spectrum and its corresponding reduction factor by using different hysteretic model with damage index equals to one (BMR1, BMRL50, and BMRS).

according to the 1995 version of Taiwan design code. The longitudinal reinforcement consists of 32 No.6 bars throughout all the height of the column. The shear reinforcement consists of No. 3 stirrups spacing at 10 cm with 135 degrees and 90 degrees hook at the two ends respectively. The specimen BMRL50 (failure in lap splice 50%), and BMRS (shear failure) are designed according to the 1982 version of Taiwan design code. The longitudinal reinforcement consists of 32 No.5 bars throughout all the height of the column. The shear reinforcement consists of No. 3 stirrups spacing at 24 cm with double U Welded. Based on the proposed modified Bouc-Wen model the model parameters were identified.

Ground motion data of two events recorded at station TCU068 (a station in Taiwan CWB strong motion instrumentation) were used as input ground motion (i.e. data from 1995-2-23 earthquake and 1999-9-21 earthquake). Three different inelastic models were selected to study the seismic demand for different hysteretic rules. The inelastic acceleration response spectrum, with the control of damage index equals to one (DI=1), was generated, as shown in Fig.7. To examine the effect of hysteretic model and ground motion characteristics on seismic demand of SDOF system, the code-specified strength reduction factor for different ductility ratio was also calculated (strength reduction factor is defined as the ratio between elastic acceleration response spectrum to inelastic acceleration response for a specified ductility ratio). Comparison between the estimated reduction factor (DI=1) to the code-specified reduction factor was also shown in Fig.7. It is clear that for the case of near-fault ground motion the code-specified reduction factor can not provide enough design base shear force for structure despite the hysteretic model. Since the structure was

designed based on the code provided reduction factor, but different hysteretic model as well as near-fault ground motion excitation may reduce different results for reduction factor, the modification factor for reduction factor must be used to evaluate the capacity of the bridge structure when subjected to near-fault ground motion.

VULNERABILITY ASSESSMENT OF BRIDGES

The Chi-Chi earthquake causes significant losses in civil infrastructures. The need to mitigate seismic risk to highway bridges has become evident after the earthquake. Besides the collection of data on bridge damage from earthquake, assessment of damage to highway systems from earthquake and estimation of consequent loss provide more valuable information for post-earthquake planning and risk mitigation. The methodology can serve as a tool in the decision process for emergency response operation and retrofitting of critical structure in the system as a mean of pre-disaster mitigation. The vulnerability assessment of bridges includes hazard analysis, classification of the critical component of bridge structure and fragility analysis. In order to evaluate the seismic response of a large number of bridges, bridges first can be categorized into different classes according to their structural characteristics. Procedures for developing fragility curves of a typical bridge type are listed as follows:

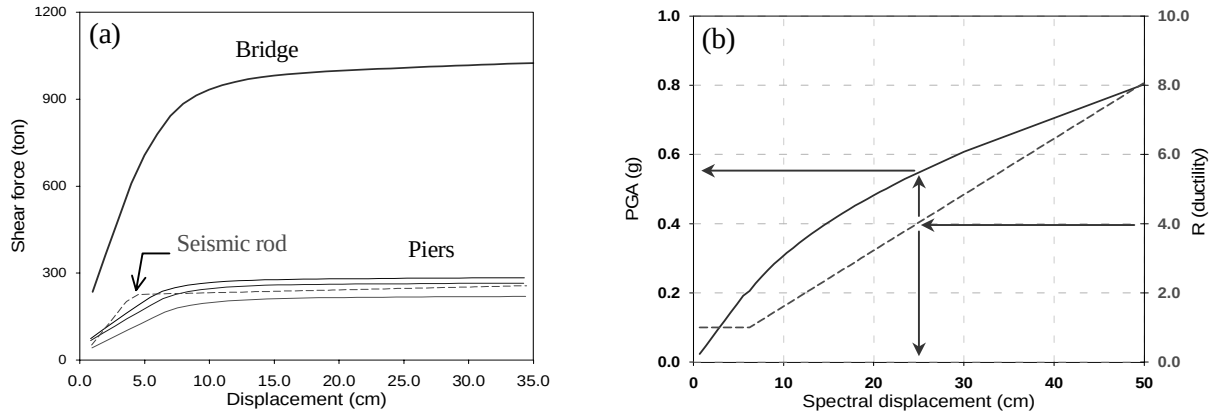

Figure 8: (a) Capacity curves of a bridge structure, (b) Plot of the ductility ratio (dash line) and PGA (solid line) with respect to spectral displacement.

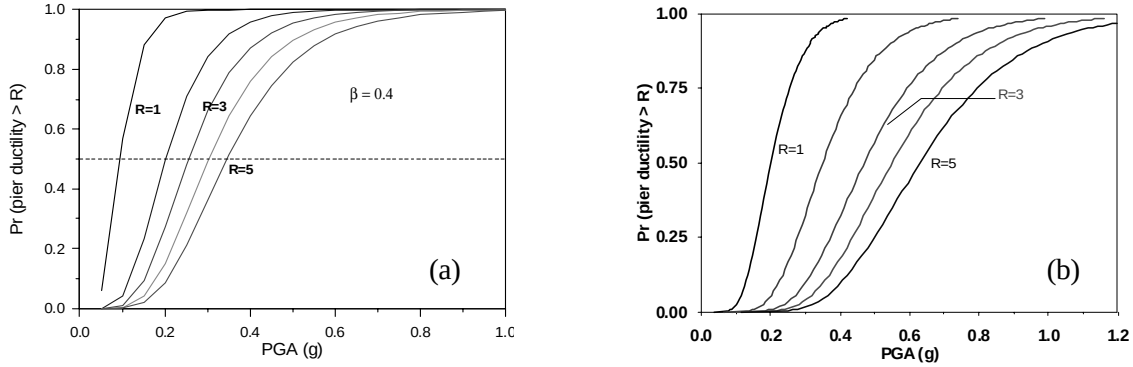

Figure 9: Fragility curves of continuous bridge (a) for semi-ductile designed bridge and (b) for ductile designed bridge.

(1) Conduct the static pushover analysis of bridge structure to develop the capacity curve. The capacity curve was expressed in terms of the shear force with respect to displacement for each structural components and the whole bridge. Fig.8a shows the typical capacity curves of the structural components and the whole bridge of a continuous bridge.

(2) Establish the relationship between ductility ratio and spectral displacement S_d from the capacity obtained from step (1): The elastic-perfect plastic force-displacement relationship was assumed to represent the capacity curve of each structural components and structural system. Transform the system capacity curve into the capacity spectrum followed ADRS format [9].

(3) Construct the inelastic demand diagram: Establish the relationship between peak ground acceleration (PGA) and spectral displacement S_d of the bridge structure by using the following equation

$$PGA = \frac{S_{ay} F_u}{C} \tag{12}$$

where S_{ay} is the yield spectrum acceleration of the elastic-perfect plastic capacity spectrum. Fig. 8b shows the relationship of the spectral displacement (S_d), ductility ratio and the peak ground acceleration (PGA) value using code specified reduction factor F_u and normalized design spectrum C for a typical bridge structure.

(4) As shown in Fig. 8b, with a specified ductility ratio from capacity curve the spectral displacement can be determined. Then with the estimated S_d value the PGA can be identified from demand diagram. The arrows shows in Fig.8b represent the rule to find the relationship between the spectral displacement, the ductility ratio and the PGA value.

(5) Generate fragility curves for a specified ductility ratio R: The identified PGA value from step (4) and the corresponding ductility ratio will be defined as the median value of the bridge fragility curve. Fig. 9 shows the fragility curves of typical continuous bridge structure with two different designed methodologies. The identified fragility curves can provide useful information to perform the seismic assessment of transportation system.

CONCLUSIONS

The purpose of this paper is to describe the lessons learned and actions been taken after the damage investigation of civil infrastructures during the Chi-Chi earthquake. From this earthquake the effect of near-fault ground motion has a significant impact on the response of structures. The seismic design standard in Taiwan, particularly on the design of bridges, was revised to take into consideration on the near-fault ground motion characteristics. The following conclusions are drawn:

1. Through numerical analysis and filed damage investigation of bridges, the effect of near-fault ground motion is significant on the response of structures. Based on the ground motion data of Chi-Chi earthquake the N_a and N_v factors were generated and implemented into the code-specified seismic design forces.

2. A two-level design concept for bridge was proposed. The designed seismic force is considered for an earthquake with return period of 475 year. For the protection of collapse of the

bridge, the seismic capacity check is required for the bridge which located in the near-fault area. The earthquake level for capacity check adopted is the earthquake motion with return periods of 2500 year.

3. The extensive vulnerability of the existing bridge inventory, as revealed by this earthquake, must be addressed before other equally destructive earthquake strike again in Taiwan. The seismic risk assessment methodology of bridge structure was developed. In this method the fragility curves of different type of bridge were developed from this study. The result can be applied for seismic loss estimation of transportation system.

ACKNOWLEDGEMENTS

This research was supported by National Science Council (Taiwan) under the grant No. NSC90-2211-E-002-028. Attribute data of bridges provided by T. Y. Lin (Taiwan) International Ltd. was appreciated.

REFERANCES

[1] National Center for Research on Earthquake Engineering, 2000. Reconnaissance Report of Chi-chi Earthquake, Vol.1-Vol.11, (in Chinese).

[2] Loh, C.H., T.C. Wu and N.E. Huang, 2001. "Application of EMD+HHT Method to Identify Near-Fault Ground Motion Characteristics and Structural Responses," ***BSSA***, Special Issue of Chi-Chi Earthquake (Editor: T. Teng), Vol.91, No.5, 1339-1357.

[3] Loh, C.H., S. Wan and Y.W. Chang, 2001. "Evaluation of Seismic Damage in a Continuous Bridge," Int. J. of Structural Stability and Dynamics, Vol.1, No.2, 235-246.

[4] Wen, Y. K., 1976. "Method of Random Vibration of Hysteretic Systems," *Journal of Eng. Mech. Div.* ASCE Vol. 102(EM2) 249-263.

[5] MOTC, 2001. The Modification of Seismic Design Provision and Commentary for Highway Bridges (Drafts), Ministry of Transportation and Communication, Taiwan (in Chinese).

[6] MOTC, 1995. Highway Bridge Seismic Design Criteria, Ministry of Transportation and Communication, Taiwan (in Chinese).

[7] CALTRANS, 1999. CALTRANS Seismic Design Criteria, Version 1.1

[8] Japan Road Association, 1995. Design Specification of Highway Bridges Part V. Seismic Design, translated and edited by S. Unjoh and T. Terayma.

[9] Mahaney J. A., Freeman, S. A., Paret, T. F., and Kehoe, B. E., 1993. "The Capacity Spectrum Method of Evaluating Structural Response During the Loma Prieta Earthquake", Proc. 1993 National Earthquake Conference, pp. 501-510, Memphis.

[10] ATC-32, 1996, Improved Seismic Design Criteria for California Bridges: Provisional Recommendations, Applied Technology Council.

[11] Park, Y.J., Ang, A.H.S., and Wen, Y.K., 1984. "Seismic damage analysis and damage limiting design of RC buildings," *Civil Engineering studies, Structural Research series* No. 516, University of Illinois at Urbana Champaign.

Seismic Safety Evaluation of Large Scale Interchange System in Shanghai

Lichu FAN, Jianzhong LI, Shide HU, Guiping BI and Liying NIE

ABSTRACT

The report for the seismic evaluation and retrofit of a large scale interchange system in Shanghai Xin-zhuang has been completed by Stare Key Laboratory for Disaster Reduction of Civil Engineering (SLDRCE) in Tongji University. In this paper, the important problems of the seismic evaluation procedure and the analysis model were investigated. The suggestions for local models of plate girder bridges and continuous girder bridges in a large scale interchange system were given. Additional studies were conducted to determine pounding effects at the structure interfaces in bridges.

INTRODUCTION

Xin-zhuang interchange system is the largest transportation engineering in Shanghai, and it is also the largest interchange system in Asia at present as shown in Figure 1. The interchange site is between the outer ring road's station at the No.1 Subway and the Xin-zhuang's station. The site locates approximately at 1km south west of the Xin-zhuang Town, and is the start-point of the Hu, Hang, Yong's freeway. Xin-zhuang interchange system includes four trunk highways with six entrances and exits. The four layers interchange system with 20 directional bifurcated girders to make a complex cloverleaf interchange. The whole system has 11.1km-long bridges with total plan area of more than 84 thousand square meters. The highest construction at the interchange system is 21 meter. In the original seismic design, according to the China Code for Seismic Design of Highway Engineering (JTJ 041-89)[1], the seismic intensity 7 is considered for the interchange system.

Lichu FAN, Professor, SLDRCE, Tongji University, Shanghai 200092, P.R.C.
Jianzhong LI, SLDRCE, Tongji University, Shanghai 200092, P.R.C.
Shide HU, SLDRCE, Tongji University, Shanghai 200092, P.R.C.
Guiping BI, PhD Candidate, SLDRCE, Tongji University, Shanghai 200092, P.R.C.
Liying NIE, PhD Candidate, SLDRCE, Tongji University, Shanghai 200092, P.R.C.

STRUCTURE CHARACTERISTICS

The superstructure of bridges in Xin-zhuang interchange system includes four kinds of girders:

(1) The concrete hollow plate girders with the depth ranging from 0.95m to 1.05m;
(2) The posttensioned box girders with uniform depth ranging form 1.1m to 1.6m;
(3) The irregular box girders with varied width;
(4) The steel and concrete composite girders.

The heights of columns of the piers range from 2m to 20m. The girders are directly supported on the teflon bearings and the elastomeric bearings without connection between the bearings and girders or cap beams. The teflon bearings are located at expansion joints. For simple girder bridges, the inverse T type cap beams are used as shown in Figure 2. Most piers have a specified concrete compressive strength of 30 Mpa with l**ongitudinal steel reinforcement ratio ranging from 1.4% to 2.5%**. The volumetric ratio of lateral steel reinforcement provided inside the plastic is about 0.3%.

In the bridges in the interchange system, the shear keys and seismic concrete block structures (shown in Figure 3) were widely used to prevent a girder fall.

SEISMIC SAFETY EVALUATION PROCEDURE

According to the characteristics of Xin-zhuang interchange system, seismic evaluation procedures for the overall bridge have evolved as outlined below:

(1) Earthquake safety assessment at site. This includes site-specific information on the expected ground motion that consist of a basic responses spectrum shape, or shapes, with peak ground acceleration related to annual probability, and artificial generated accelerograms that closely match the responded spectrum.

(2) Testing of material behavior and investigating of structural component at site. In order to determine the difference between the design and actual bridges, the concrete and reinforcement strength of actual bridges in Xin-zhuang interchange system were tested and were compared with the design values.

(3) Two level dynamic analysis. Linear Level-1 with global model of entire interchange system and linear local models was first performed using three-dimensional elements. The global model focuses on the overall behavior and includes all structural components. The global model analysis is an important first step in the initial assessment of the seismic vulnerabilities of a structure. Such analysis can provide initial indication of "hot spots" to plan an evaluation strategy, categorize members by their demand/capacity ratio, and envelope peak response quantities to a design spectrum. The linear local analysis models were applied to investigate the difference between linear dynamic analysis of global and local models to get simplified model methods. Nonlinear level-2 analysis is defined as nonlinear dynamic time history analysis with considerations of geometrical nonlinearity, nonlinear boundary conditions, other inelastic

Fig. 1 Xin-zhuang interchange system

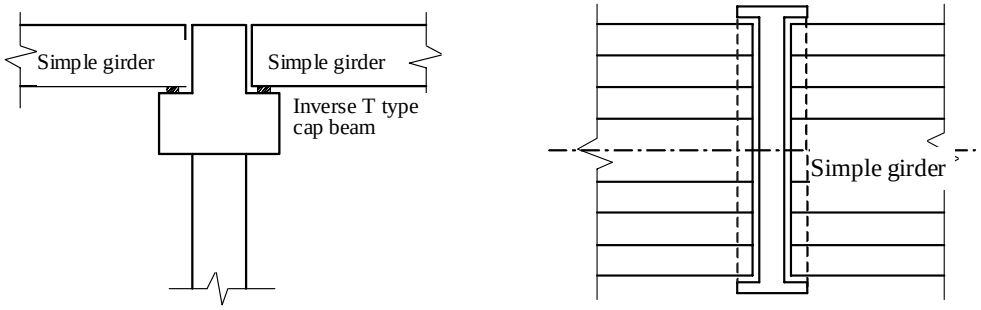

Fig. 2 Inverse T type cap beam

Fig.3 Seismic concrete block structure

element (for example, bearings) and inelastic members. Level-2 analysis is mainly applied to local models. The local models emphasize the localized behavior, especially complex inelastic and nonlinear behavior.

(4) Determination of capacity for piers, bearings and connection elements. Based on material properties for concrete and reinforcement, nominal flexural strength, shear strength of structural components have been determined in accordance with specified code formula.

(5) Capacity/demand ratio analyses. Based on the results of nonlinear dynamic time history analysis, capacity/demand ratio analyses were carried out. Based on the results of capacity/demand ratio analyses, the suggestion plan for retrofit is given.

The flow chart outlining the step in the seismic evaluation procedures for a large scale interchange system is given in Figure 4.

.

ANALYSIS MODELS

Global Model

The global model focuses on the overall behavior and includes all structural components in interchange system as shown in Figure 5. The superstructure is modeled by three-dimensional linear elastic beam-column elements placed at the geometric centroid of the cross section. At end of each continuous beam or simple beam, the three-node frame ends are connected by rigid elements that extend transversely from the centerline of the superstructure (detail A in Figure 5). For models of the straight bridge, the rigid elements extend perpendicular to the centerline. For skewed models, the rigid elements extend at skew angle. Three-dimensional linear elastic beam-column elements are also used to model the column and cap beam for each of the piers in the bridges in the global model. Each elastomeric bearing in bridges is modeled by a linear spring element as shown in detail A in Figure 5. Total of 6310 three-dimensional linear elastic beam-elements and 2104 linear spring elements were used in the global model.

Nonlinear Local Model

Based on the analysis results of global model and characteristics of the Xin-zhuang interchange system, the linear and nonlinear analysis local models were established. The detail description of linear local analysis models was presented in the report of the seismic evaluation of Xin-zhuang interchange system [2]. Here, the typical nonlinear elements and nonlinear local models are discussed as following:

Pier Columns

The inelastic three-dimensional beam-column element with a fiber model of the cross section [3] was used to model each column of the piers in the bridges. Figure 6 shows the fibers

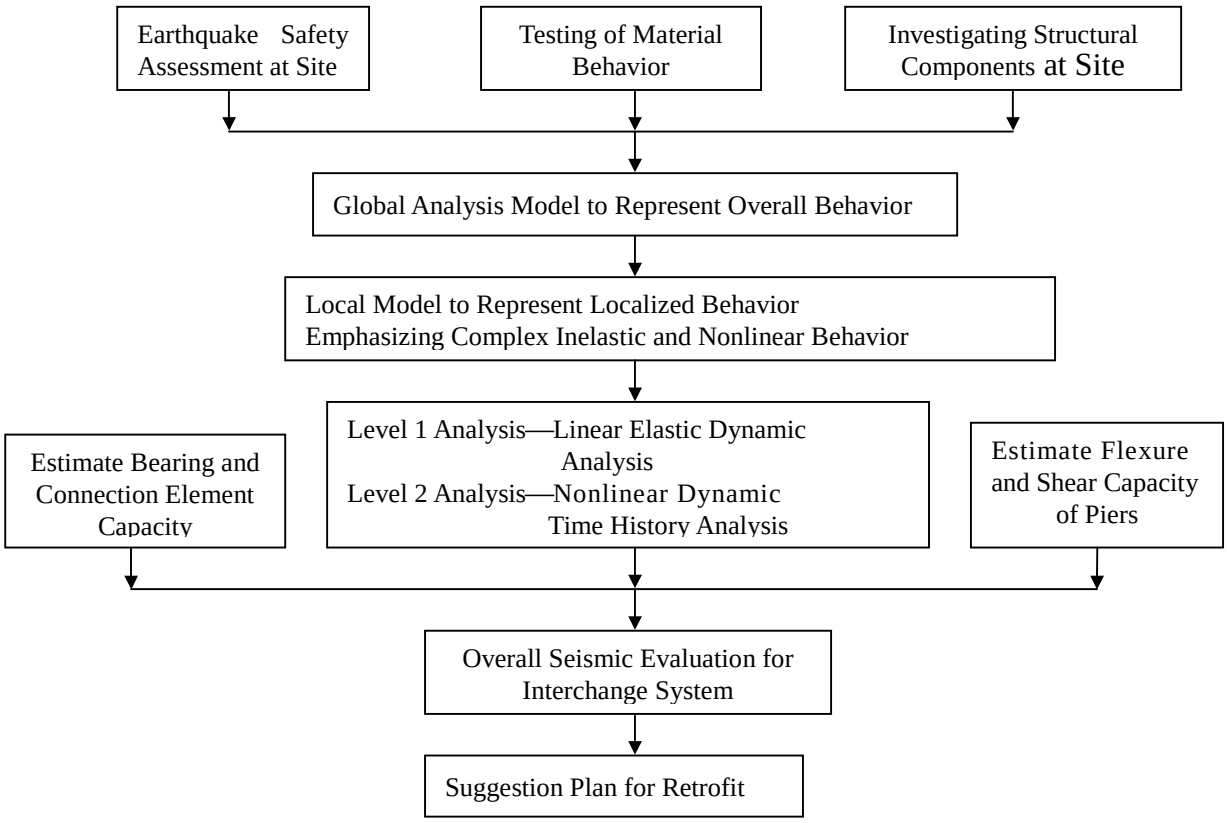

Fig.4 Seismic evaluation procedures

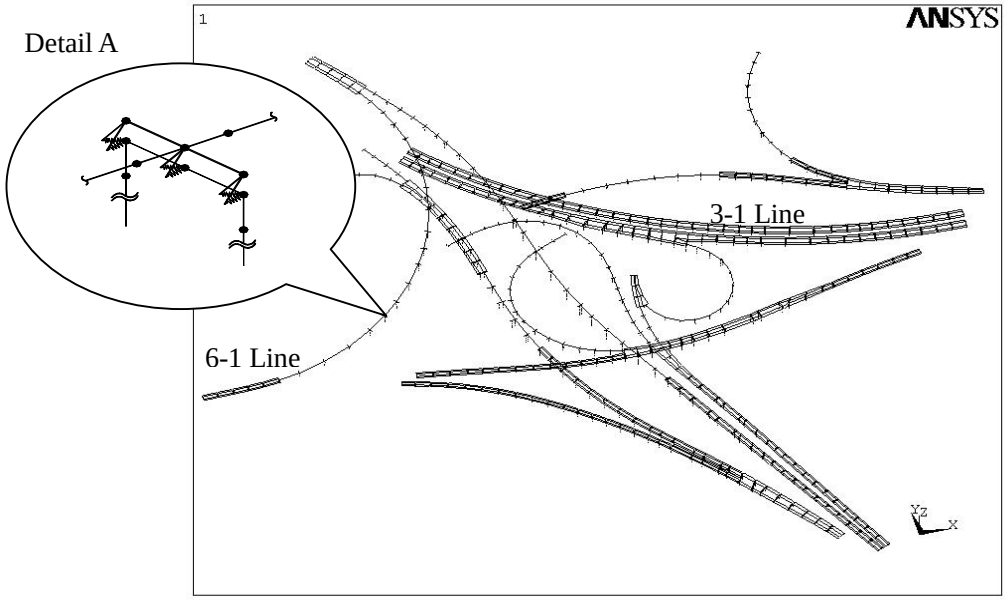

Fig. 5 Global computer model

of the section. Each fiber has a specified stress-strain relationship, which can be specified to represent unconfined concrete, confined concrete, and longitudinal steel reinforcement. The distribution of inelastic deformation and forces is simply by specifying cross section slices along the length of the element. The fiber model approach provides versatile modeling of bi–axial moment-axial force interaction with distributed inelastic hinges and can represent the loss of stiffness caused by concrete cracking, yielding of reinforcing steel, and stain hardening. In this study, Mander's model for confined concrete and unconfined concrete [4] were used to represent the stress-strain behavior of concrete as is shown in Figure7

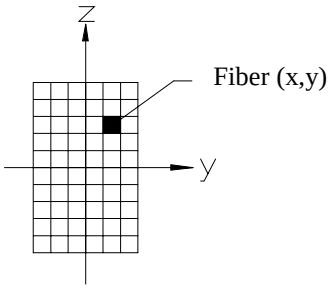

Fig. 6 Column elements with fibers

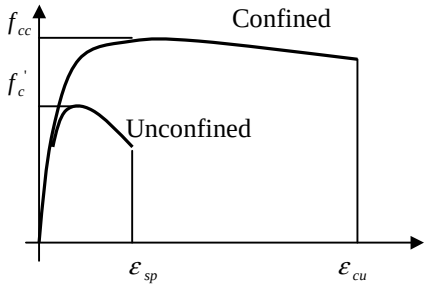

Fig.7 Stress-strain behavior of concrete

Bearings

As mentioned above, the girders in the bridges in the Xin-zhuang interchange system are directly supported on the teflon bearings and the elastomeric bearings without connection between the bearings and girders or cap beams. The horizontal sliding behavior of interface between the bearings and girders or cap beams is presented by nonlinear spring elements with bilinear model shown in Figure 8. The value of initial stiffness k_0 for the bilinear model is determined by shear stiffness of a bearing. The frictional force, F_f, at a sliding interface, may be described by following equation.

$$F_y = \mu_d R \tag{1}$$

in which R= the vertical reaction force of a bearing; u_d =sliding fraction coefficient of interface.

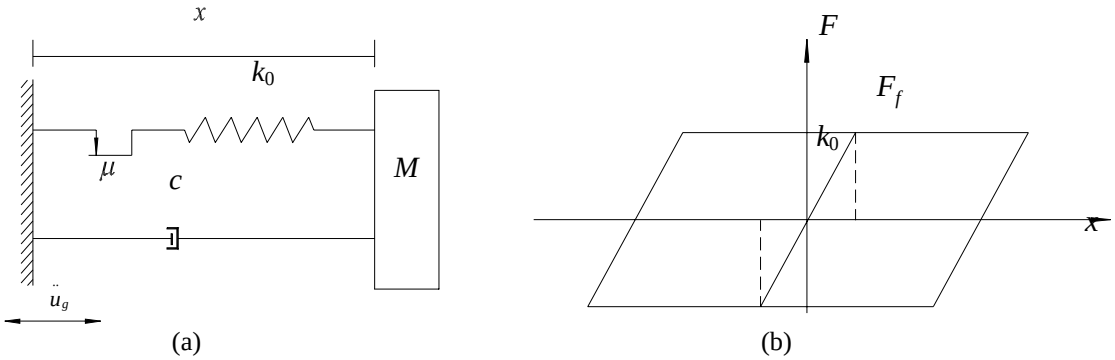

(a) (b)

Fig. 8 (a) Nonlinear spring element; (b) Bilinear mode

Pounding Effects

Based on the characteristics of Xin-zhuang interchange system, following three kinds of collisions may occur during earthquakes;

(1) Collisions between the simple girders and inverse T type cap beams;
(2) Pounding of adjacent girder segments at expansion joints for the continuous girder;
(3) Collisions between the girders and the seismic concrete block structures;

The collision is modeled by a nonlinear spring element with gas as shown in Figure 9. The nonlinear spring element with gas becomes active when the relative displacement between ad adjacent structures is smaller than the initial gap D_0. The initial stiffness k_0 and post-yield stiffness k_1 of the spring are used to represent the elastic and plastic behavior of pounding structures.

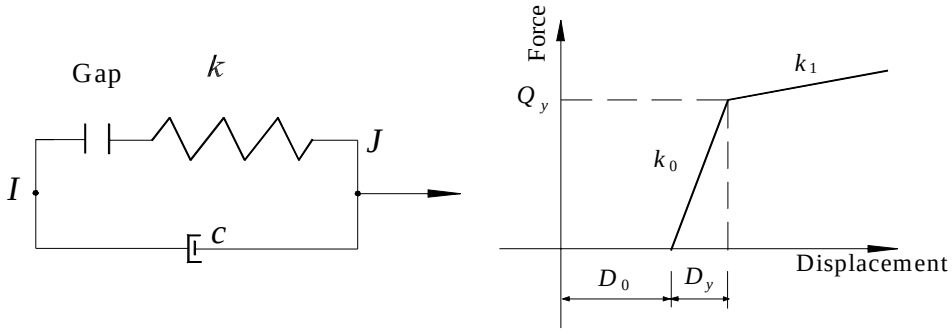

Fig. 9 Nonlinear spring element with gas

Nonlinear Local Models

As mentioned above, in the bridges in the Xin-zhuage interchange system, there are three kinds of bridge, simple girder bridges, curve continuous girder bridges and bifurcated girder bridges. Here the typical nonlinear local models for a simple girder bridge and a curve continuous girder bridge are given as following.

The 3-1 Line in Xin-zhuang interchange is a 36 span bridge with simply supported concrete hollow plate superstructure. Pier10 to pier 12 are two column bents, and other piers are single column bents. The column heights vary considerably over the bridge from 1m to 15m. The 6-1 Line includes simply supported girder and continuously supported girder bridges. The part of continuous bridge is a 13 span bridge with box girder superstructure and single column pier. The expansion joints located at top of pier 5, pier 10, pier 14 and pier 18.

The nonlinear local analysis models for simple the girder bridge in 3-1 Line and the continuous girder bridge in the 6-1 Line are presented in Figure 10 and Figure 11 respectively. The superstructure and the cap beam are modeled by three-dimensional linear elastic beam-column elements. A nonlinear spring element with gap is used to model impact (Detail A in Fig.10 and Fig.11). To be able to capture impact caused by in-plane rotation of the superstructure,

three nonlinear springs are used at each end of rigid element. The nonlinear spring element with bilinear was used to model horizontal sliding behavior of interface between the bearings and girders or cap beams. For the interface between the teflon bearing and girder (cap beam), sliding fraction coefficient 0.02 is suggested; for the interface between the elastomeric bearing and girder (cap beam), 0.15 is suggested. Each column of the piers in the bridge is modeled by inelastic three-dimensional beam-column element with a fiber model.

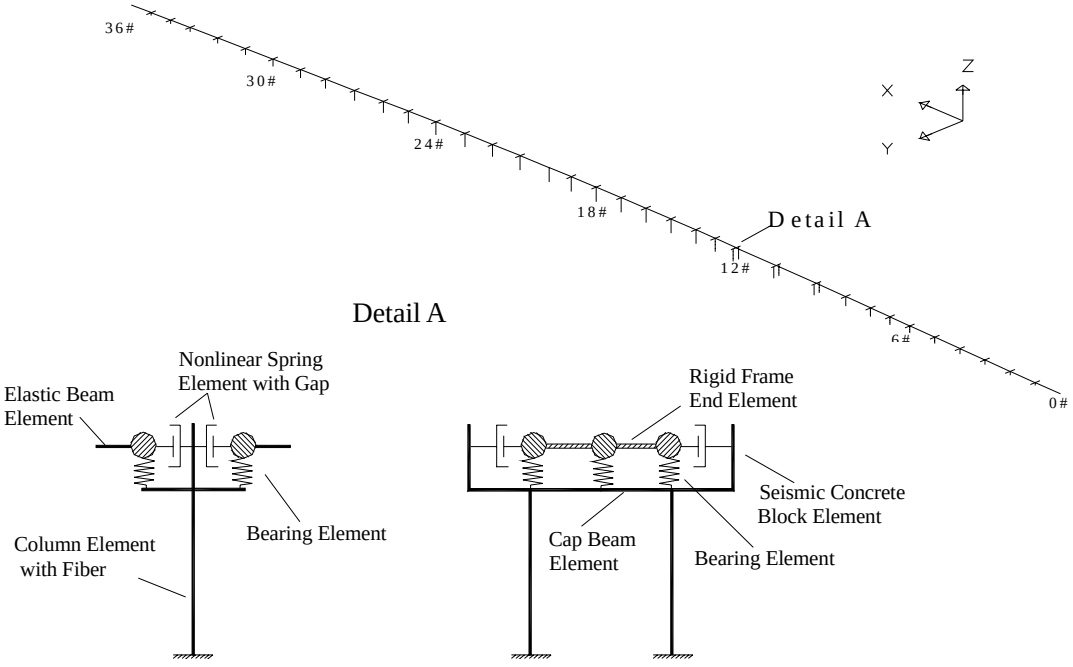

Fig.10 Nonlinear local model of simple girder bridge in 3-1line

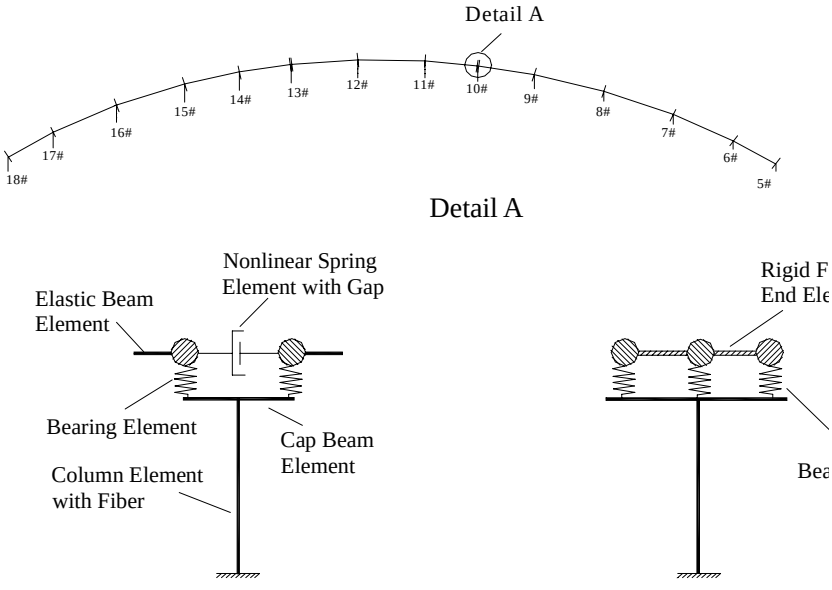

Fig.11 Nonlinear local model of continuous girder bridge in 6-1 line

EARTHQUAKE LOADING

According to earthquake safety assessment at site, site-specific acceleration coefficient (shown in Figure 12) and typical site-specific time histories of input acceleration for a 10% and 2% probability of exceedance in 50 years are provided. The input acceleration for a 10% probability of exceedance in 50 years was used to represent design earthquake and the input acceleration for a 2% probability was used to represent severe earthquake in the seismic safety evaluation of the Xin-zhuang interchange system.

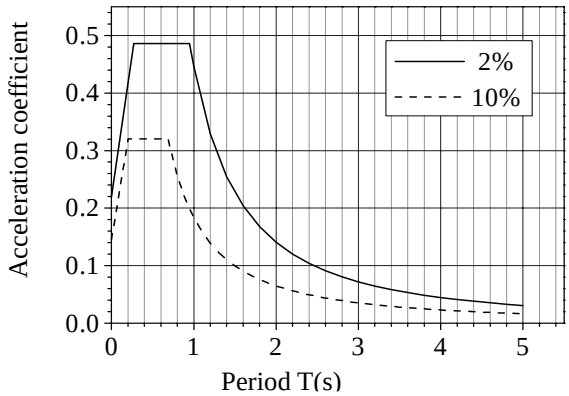

Fig.12 Site- specific acceleration coefficient

ANALYSIS RESULTSS

The computer program ANSYS [5] was used to perform linear spectral analysis for the global and linear local model. For the nonlinear dynamic time history analysis, the specific computer program developed by Stare Key Laboratory for Disaster Reduction of Civil Engineering in Tongji University was adopted.

To assess the response, the maximum relative displacements between the girder and the pier, column displacement, column curvature ductilities, column bent moments, column shear forces and the impact forces for seismic concrete block were calculated with the site-specific input acceleration of a 10% and 2% probability, respectively. The detail analysis results are presented in the report of the seismic evaluation of Xin-zhuang interchange system. Parts of import results are discussed as following.

Under Design Earthquake

The pier columns in the interchange system work generally in the elastic range and the shear capacity of the columns is adequate to resist the design earthquake. Because the girders in the bridges are directly supported on the elastomeric bearings without connection between the

bearings and girders or cap beams, the horizontal sliding between the elastomeric bearings and girders or cap beams in simple girder bridges occur. The collisions between the girders and the seismic concrete block structures induce a large impact force in simple girder bridges. The maximum values of impact force between the girders and the seismic concrete block structures in the 3-1 Line are about 9320kN.

Under Severe Earthquake

Parts of pier columns enter to plastic work range and maximum demand/capacity ratio of curvature ductility is about 5.293. The shear capacity of the columns is adequate to resist the severe earthquake according to China Seismic Code for Urban Bridges [6]. The horizontal sliding between the elastomeric bearings and girders or cap beams in simple girder bridges and parts of continuous occur. The typical sliding displacement history between the elastomeric bearing and girder at pier 35 in 3-1 Line is shown in Figure 13.

The collisions at concrete block structures, expansion joints and inverse T cap beams induce a large impact force, and may cause considerable damage or even lead to collapse of colliding structures under severe earthquake. The typical pounding time history between the girder and the seismic concrete block at pier 2 and moment time history at column bottom of pier2 in 3-1 line are presented in Figure 14 and Figure 15. Figure 16 and Figure 17 show the typical pounding time histories between the girder end and inverse T cap beam at pier 35 and moment time history at column bottom of pier35 in 3-1 Line.

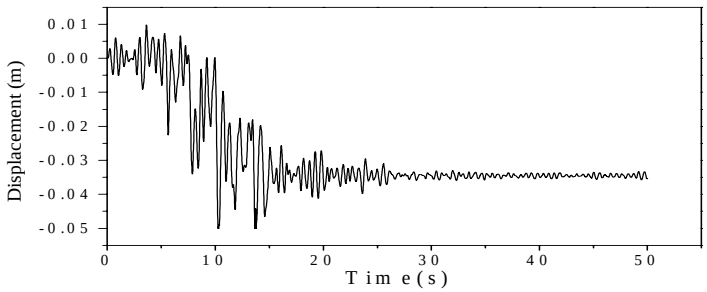

Fig.13 The typical sliding displacement history between the elastomeric bearing and girder

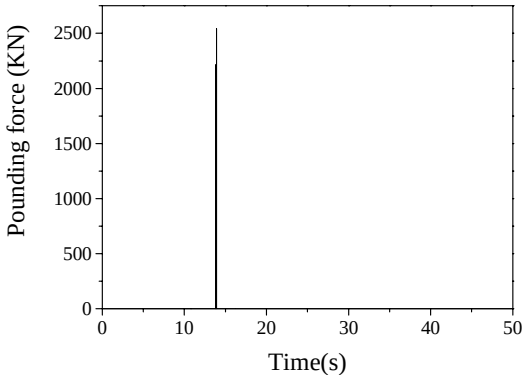

Fig. 14 Pounding time histories at the concrete block

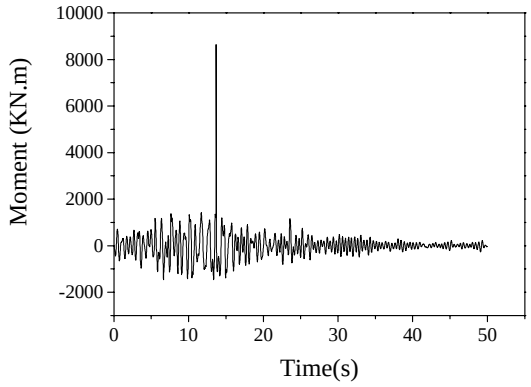

Fig.15 Moment time histories at column bottom

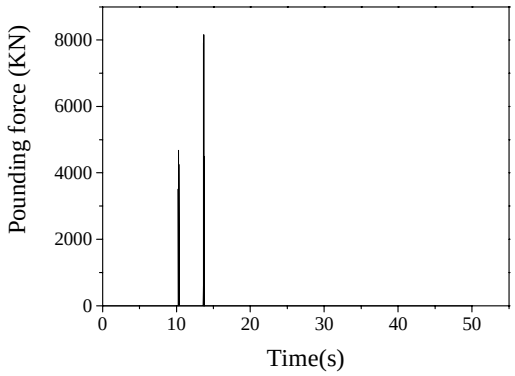

Fig.16 Pounding time histories at inverse T cap beam

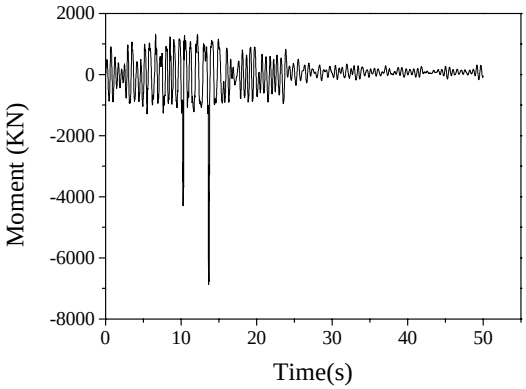

Fig.17 Moment time histories at column bottom

Retrofit Suggestions

Based on the analysis results of the Xin-zhuang interchange system, following suggestions are given for retrofit.

(1) To insure that sliding between the elastomeric bearings and girders or cap beams does not occur under design and severe earthquakes, the bolts should be applied to connect elastomeric bearings with girder or cap beam. The links shall be adequate to resist the design and severe earthquakes.

(2) To reduction of pounding effects in the interchange system, the rubber layer should be attach on the inner side of seismic concrete block. A rubber layer on the interface of pounding can reduce the pounding time, than reduce pounding forces.

CONCLUSIONS

Based on the characteristics of the large scale interchange system, the seismic evaluation procedures have been investigated. Three kinds of analysis models, global model, linear local

and nonlinear local models are established, and two level dynamic analysis, linear spectral analysis and nonlinear dynamic time history analysis were carried out for Xin-zhuang interchange system.

The analysis results were investigated. The results show that the horizontal sliding between the elastomeric bearings and girders or cap beams occur under design earthquake and severe earthquakes. The collisions at concrete block structures, expansion joints and inverse T cap beams induce a large impact force, and may cause considerable damage or even lead to collapse of colliding structures under severe earthquake. Based on the analysis results, suggestions are given for retrofit.

REFERENCES

[1] Transportation Ministry of P.R.C. 1989. “Code for Seismic Design of Highway Engineering (JTJ 041-89)”

[2] Lichu Fan, Jianzhong Li, Shide Hu, Guiping Bi and Liying Nie. 2001. “Seismic Safety Evaluation of xin-Zhuang interchange system,” Stare Key Laboratory for Disaster Reduction of Civil Engineering in Tongji University.

[3] Enrico Spacone, Filip. C. Filippou and Fabio F. Taucer. 1996. “Fiber Beam-Column Model for Nonlinear Analysis of R/C Frames: Part 1. Formulation,” Earthquake Engineering and Structure Dynamics.25 (4):711-725.

[4] J. B. Mander, M. J. N. Priestley and R. Park. 1988. “Theoretical Stress-Stain Model for Confined Concrete,”ASCE Journal of Structure Engineering. 114 (8):1804-1826.

[5] ANANS, Inc.1997. “ ANASYS Workbook Release 5.4,” Third Edition. SAS, IP Inc.

[6] Stare Key Laboratory for Disaster Reduction of Civil Engineering. “China Seismic Code for Urban Bridges (Draft 20001),’’ Shanghai, P.R.C.

Seismic Practices for Transportation Structures and Systems

Chair: Bruce Johnson

Seismic Vulnerability Assessment of the Seattle-Tacoma Highway Corridor Using HAZUS

Donald Ballantyne, Mark Pierepiekarz and Stephanie Chang

Ground Motions, Design Criteria, and Seismic Retrofit Strategies for the Bay Area Rapid Transit District Bridge and Other Structures

Tom Horton, Eric Fok, Ed Matsuda, William Hughes, Wen S. Tseng, Chip Mallare and Kang Chen

Pushover Analysis of Masonry Piers

Ruben Gajer, Adam Hapij and Mohammed Ettouney

Innovative Designs of Seismic Retrofitting the Posey and Webster Street Tubes, Oakland/Alameda, California

Thomas S. Lee, Thomas Jackson and Randy R. Anderson

Seismic Rehabilitation Design and Construction for the Port Mann Bridge, Vancouver, B.C.

Keith Kirkwood, Tian-Jian (Steve) Zhu, and Peter Taylor

Seismic Vulnerability Assessment of the Seattle-Tacoma Highway Corridor Using HAZUS

Donald Ballantyne[1], Mark Pierepiekarz[2], and Stephanie Chang[3]

ABSTRACT

The seismic vulnerability of 214 bridges along three highways, I-5, SR-167, and SR-99 between Seattle and Tacoma, Washington, was modeled using HAZUS.

The USGS developed six ground motion scenarios for representative earthquakes from the Cascadia Subduction Zone, the Deep Benioff Zone, and crustal earthquakes. The ground motions were amplified for site response using modified NEHRP amplification factors based on soil classifications developed by the Washington State Department of Natural Resources (DNR). The resulting ground motion maps were input into HAZUS 99. DNR also developed liquefaction mapping for the study area that was input into HAZUS.

Bridge data was provided by the Washington State Department of Transportation (WSDOT), and modified to properly represent bridges had been upgraded. Bridges in the WSDOT database were classified in accordance with the HAZUS bridge types. Some bridge classifications were modified to better represent the year various design standards were implemented in Washington. Pushover analyses were conducted on several representative bridges to check the validity of the fragility curves in HAZUS 99. There was good concurrence.

HAZUS 99 was run, and expected bridge damage states for the six scenarios output and mapped. For the 3 intermediate scenarios, an average of 26 out of 214 bridges were estimated to suffer extensive damage or collapse. In the most severe scenario, 40 bridges were rendered unusable. Based on individual bridge damage states, the probability of each highway segment along the corridor was estimated. Recovery times were estimated by HAZUS 99 and mapped by highway segment indicating the probability of being open immediately following, 3 months, 6 months, and one year following the event. Three scenarios had highway segments that had closures exceeding 6 months, and the most severe scenario, closures exceeding a year.

The regional economic impact due to one of the smaller events was estimated. Over twenty businesses were interviewed to identify the likely effect on their operations, costs, and revenues. Highway outage and recovery times were provided to each business. Based on these results and a regional economic model, impacts were estimated at $3 billion in reduced business income, and a loss of 39,000 jobs in the year following the event.

[1] Donald Ballantyne, P.E., VP Lifeline Services, ABS Consulting (formerly EQE International), 1915 63rd St. NE, Tacoma, WA 98422, dballantyne@absconsulting.com

[2] Mark Pierepiekarz, P.E., S.E., Group Manager, ABS Consulting, (formerly EQE International) 1411 4th Ave. Bldg., #500, Seattle, WA 98101, mpierepiekarz@absconsulting.com

[3]Stephanie Chang, Research Assistant Professor, University of Washington, Dept. of Geography Box 353550, Seattle, WA 98195-3550 sec@u.washington.edu

INTRODUCTION

Washington is the most trade-dependent state in the country, where one in four jobs rely on international trade. The airplane, software, financial, forest product, and biomedical industries are all key to the region's economic success. Two and a half million people (40% of the State population) reside along the north-south corridor supporting these industries. One hundred billion dollars in goods moves through the ports of Seattle and Tacoma annually. Much of the cargo, 60 percent, moves through the region to inland domestic markets. The Puget Sound region accounts for seven percent of the nation's international trade, but is home to only one percent of the population. In the highly competitive import-export shipping business, disruption of service from a disaster could deal a terrible blow to the Puget Sound economy, shifting business to foreign and domestic West Coast ports.

In this region, the I-5 corridor is funneled by the Cascade Mountains to the east, and the Puget Sound to the west, so there is minimal transportation "redundancy" in the event one of the major routes is damaged in an earthquake. The I-5 corridor moves about 200,000 vehicles per day north south between Tacoma and Seattle, where most of region's businesses are located. Parallel routes, including SR-167 and SR-99, have a total capacity about half that of I-5, and are already jammed. Boeing (the nation's largest exporter) is dependent on moving airplane components along the corridor, as part of their manufacturing process. All employers depend on the corridor to get people to work to ship and receive goods, and for access of customers.

In 1998, Washington's King and Pierce counties combined their Project Impact funding to address regional issues. When they convened a group of public and private sector citizens and asked them to identify their greatest concern following a disaster, the overriding consensus was transportation. Not only is transportation critical to provide emergency response but it provides the lifeblood to maintain the long-term economic vitality of the region. And transportation systems in the Pacific Northwest are already at maximum capacity.

With that direction the counties developed a project to evaluate the post-earthquake reliability of a key section of the regional transportation system, and if it were not operational, to estimate the regional economic impact. Consulting with their partners, the Counties defined the study area as the "Port to Port" Corridor connecting the nation's fifth and sixth busiest container ports: Seattle and Tacoma. Ultimately, the counties are planning to use the project results to help spur development and implementation of effective mitigation strategies.

Based on the background presented above, the project team established the following five project objectives that were used to formulate the project approach, and as guidance throughout the project.

1. Engage business and government participation.
2. Evaluate post-earthquake transportation system survivability.
3. Develop an emergency response and recovery plan.
4. Estimate the economic impact of transportation system outage.
5. Promote mitigation of high-risk bridges on critical lifeline corridors.

The project carried out a four-step evaluation process to estimate the earthquake risk associated with the transportation corridor.

1. Hazard assessment - quantifying hazards, including ground motions and liquefaction.

2. Loss estimation - evaluating individual bridge vulnerability/reliability, route reliability, and recovery time.
3. Economic analysis - estimating the regional economic impact if the corridor is disrupted.
4. Contingency planning – developing plans to detour around key collapsed bridges.

HAZUS was used as the platform to integrate the hazards and individual reliabilities. HAZUS 99 is an earthquake loss estimation software developed and funded by FEMA to help communities to prepare, plan, and build stronger and safer communities. Among many HAZUS 99 uses are analysis of disaster-related damages; identification of vulnerable areas; assessment of vulnerability of housing, essential facilities and lifelines; estimation of potential losses; and aid in development of response and recovery plans.

Highway transportation systems generally consist of roadways, bridges, and tunnels. Road damage occurs due to surface fault ruptures or extreme soil failure. Bridge damage can occur due to extreme ground shaking and or site soil failure. Loss of bridge function usually results in significant disruption to the transportation network, and thus is a key component to reliability of these lifelines. The project focused on the loss estimation methodology used in HAZUS 99 for bridges.

The reliability of individual bridge structures was estimated based on the local earthquake hazards, the bridge structural design characteristics, and performance of similar structures in previous earthquakes. Most of the bridges along the I-5 corridor were constructed before the mid-1970s, when more rigorous seismic design codes were initiated.

The reliability of the transportation corridor "system" was estimated by combining the reliabilities of the individual bridge structures. The reliability of each bridge in a linear system such as I-5 has a dramatic impact on the overall route reliability. In the Puget Sound region, there are limited redundant routes compared to the grid, or network of highways that were available in Los Angeles following the Northridge Earthquake.

The potential regional economic impact was estimated considering the likely bridge/highway segment outage time, associated increased travel times, and the resulting impact on a cross section of the region's employers.

Contingency planning was developed by stakeholders with interests in each county including the counties (public works and sheriffs), cities, the WSDOT, and the State Police.

HAZARDS ASSESSMENT

A hazard assessment was performed for six earthquake scenarios. Ground motion assumptions were developed, site amplification estimates applied, and liquefaction susceptibility mapping prepared.

Ground motions were developed independently due to the limitations of HAZUS generated scenarios. HAZUS does not allow site amplification of user supplied ground motions within the program, so “amplified” ground motions were input into HAZUS.

The scenario ground motion approach was selected rather than using probabilistic ground motions. The premise of probabilistic ground motions is that they will not be exceeded over the associated return period. This may result in overestimating the impact as several different

earthquakes may contribute to those ground motions. Ground motions for the scenarios were used to better approximate what may occur for a single event. The scenarios modeled included:

- Seattle Fault M6.5 (shallow crustal)
- Seattle Fault M7.0 (shallow crustal)
- Tacoma Fault, M6.7 (shallow crustal)
- Cascadia Subduction M9.0
- Deep Benioff zone M6.5
- Deep Benioff zone M7.1

The expected return period for the scenarios is: Deep Benioff – 50 to 100 years; Cascadia Subduction, Tacoma or Seattle M6.5 – 300 to 1,000 years; and Seattle M7.0, over 1,500 years.

Site amplification for peak ground acceleration and 1-second spectral acceleration were taken as developed in NEHRP, and applied in HAZUS. The amplification values were renormalized to better represent the their original basis.

DNR provided liquefaction mapping. Liquefaction and lateral spread can have a dramatic impact on bridge foundations and highways segments. The Puget Sound region has a higher potential for liquefaction than many other areas, because of high water tables in river valleys with young geologic deposits, such as in the Green and Duwamish river valleys. Liquefaction can result in loss of bearing, and lateral movement (spread) can occur, measured in meters.

HAZUS uses liquefaction susceptibility map data in determining a conditional liquefaction probability used in subsequent damage-state calculations. The program translates a relative liquefaction susceptibility (ranging from very high to none) into a conditional liquefaction probability. The conditional probabilities are adjusted for earthquake magnitude (duration) effects and variation in the depth to groundwater. These probabilities are then used to calculate the expected permanent ground displacement both from lateral spreading and settlement. The permanent ground displacements then modify direct damage estimates.

BRIDGE VULNERABILITY EVALUATION

General Model and Preliminary Screening

Earthquake damage can be estimated for various transportation components based on anticipated ground accelerations and ground deformation. The required data to estimate bridge damage includes:

- Geographical location/longitude and latitude
- Bridge classification (structure type)
- Site spectral accelerations at 0.3 seconds and 1.0 seconds
- Permanent-ground deformation (PGD)
- Peak-ground acceleration (for PGD-related calculations)

HAZUS 99 classifies bridges into 28 categories based on the following structural characteristics:

- Seismic design
- Number of spans
- Structure type and material
- Pier type
- Abutment type
- Span continuity

General bridges with good seismic design features can accommodate relatively higher seismic input and allowable drift limits. The general fragility curves for each of the 28 bridge classes can be further refined in HAZUS 99 using bridge specific data such as: bridge length/span length/number of spans, bridge width, and skew. The effects of these parameters for several bridge types were investigated using sensitivity spreadsheet analyses. The bridge inventory was divided into the 28 categories as shown in Table I. More detailed analysis focused on the bridge categories with the least lateral capacity, HWB 12 and HWB 17.

TABLE I. SUMMARY OF BRIDGE CLASSES AND ASSOCIATED CAPACITIES

Bridge Class	Number/ Percent of Total		Lateral Capacity (g)	PGD Capacity (in)	Bridge Type
HWB10	76	36%	1.05	3.9	Continuous Concrete
HWB17	68	32%	0.44	3.9	Multi-Col. Bent, Simple Support-P/T Concrete
HWB23	23	11%	1.05	3.9	Continuous - Prestressed Concrete
HWB22	12	6%	1.05	3.9	Continuous - Prestressed Concrete
HWB11	11	5%	1.05	23.6	Continuous Concrete
HWB3	9	4%	1.1	3.9	Single Span
HWB4	4	2%	1.1	3.9	Single Span
HWB12	4	2%	0.44	3.9	Multi-Col. Bent, Simple Support- Steel
HWB15	3	1%	0.76	3.9	Continuous Steel
Other	4	2%	varies		
Total	214				

Definition of Damage States

HAZUS 99 defines four bridge damage states (as modified by WSDOT) plus no damage, that are related to the damage ratio (i.e. the repair-to-replacement cost) for evaluation of direct economic loss:

- Slight damage - minor cracking or spalling to concrete bridge elements. Bridge remains structurally sound.
- Moderate damage – Any column experiencing moderate cracks but remaining structurally sound, moderate superstructure displacement (< 2 inches), any damaged connections, bearing failure or moderate (< 6 inches) settlement of approach. Requires temporary repair and/or capacity or functionality reduction.
- Extensive damage – Any columns degrading without collapse – shear failure (column structurally unsafe), significant permanent displacement at connectors or major settlement (6 inches or greater) of an approach, or differential structural alignment.
- Complete damage – Any column collapsing or span losing all bearing support that may lead to imminent span collapse, tilting of structure due to foundation failure.

Damage Algorithms for Bridges

The HAZUS 28 primary bridge classes are defined for the above damage states as a function of ground motion and ground displacement. The assumptions in the development of these damage algorithms were reviewed and verified for applicability in this project. The verification focused on the most vulnerable bridge types that generally consist of simple-span bridge structures lacking modern seismic design features. A typical plot of a family of highway bridge fragility curves as the function of spectral acceleration is presented in Figure 1. For ground deformation, HAZUS considers incipient unseating and collapse as the possible types of damage due to ground failure. Initial damage to bearings, which correspond to slight damage from ground failure, is not considered.

Restrainers do not have a significant effect on the shape of the fragility curve for ground motion but will modify the expected performance of bridges when subjected to liquefaction/lateral spread.

The "extensive" and "complete" damage states were of primary interest since they result in loss of functionality. Figure 1 shows probabilities that a given bridge structure will not be extensively damaged.

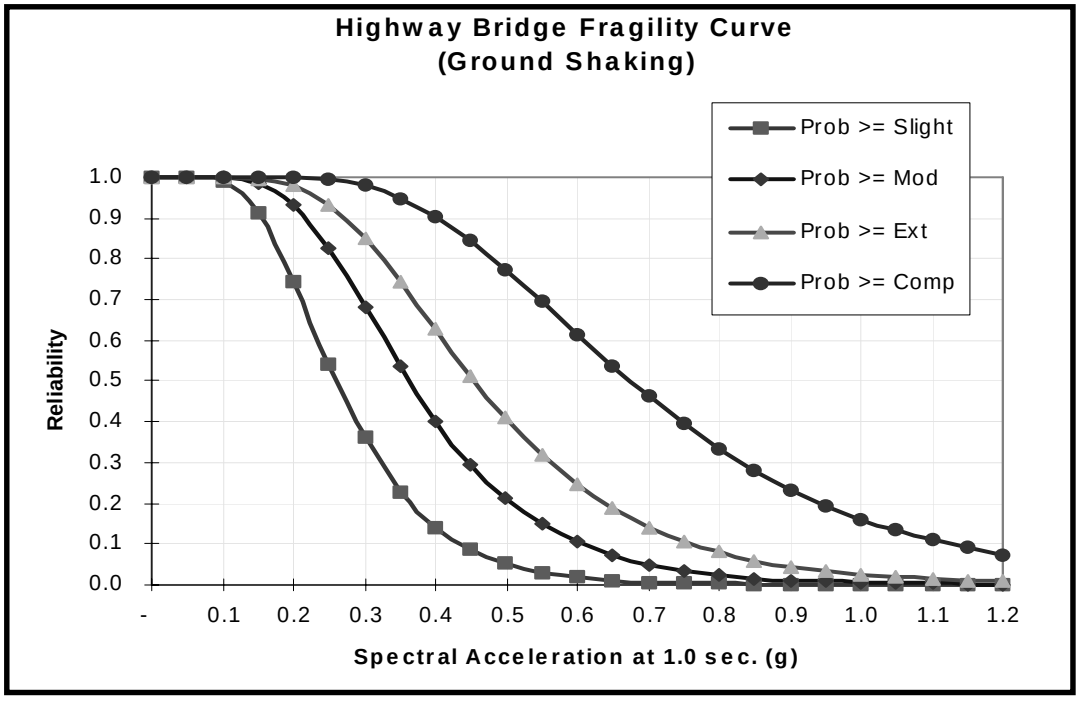

Figure 1. Highway Bridge Fragility - Prestressed Concrete Bridge Multi-Column Bent, Simple Support

Evaluation Inventory Considerations and Verification

The important questions to ask when applying HAZUS-based bridge vulnerability functions to Project Impact port-to-port corridor study are the following:

1. Is the bridge data currently in HAZUS database accurate relative to bridge location, physical characteristics, and key descriptors important for seismic performance?
2. Do damage functions, particularly for the most vulnerable bridges, accurately reflect Washington State bridge stock and design practice?
3. What modifications need to be made to appropriately model corridor bridges and assess the vulnerability of the lifeline network?

First, the existing HAZUS geographic database for the port-to-port corridor was examined to see whether bridges are accurately located. Second, the HAZUS database and WSDOT bridge database fields were mapped against each other to verify consistency of the key descriptors such as bridge type, bridge length, span length, number of spans, construction date, etc. Bridges with data discrepancies were discussed with WSDOT staff to establish an accurate input data for those structures. Furthermore, new structures, retrofitted bridges, and bridges with unique seismic features were also discussed to appropriately classify these within the available 28 HAZUS bridge classes.

Based on our discussions with WSDOT Bridge and Structures engineers, it is apparent that WSDOT has closely followed California DOT (Caltrans) seismic design practice. Consequently, for this the bridge categories were modified to use of these three curves as follows:

1. "Seismic design" category will be applied to all Washington State bridges built during or after 1982. WSDOT adopted ATC-6 provisions at that time.
2. The second category, originally intended to correspond to pre-1975 construction in California, will be applied to WSDOT bridges built between 1973 and 1982 according to AASHTO 1973 provisions.
3. The third category, intended for those bridges that lacked key seismic features or were designed to very low seismic forces, will be applied to WSDOT bridges built in Washington State prior to 1973.

The date of construction of the WSDOT bridge inventory is compared with the dates when the applicable design codes were in place. The plot, shown in Figure 2, shows that a significant number of the state bridges were built prior to the advent if adequate seismic codes.

Pushover Analysis

A nonlinear static pushover analysis for typical transverse bridge bents for selected bridges along State Route 167 was performed. This was of interest since column behavior governs WSDOT bridge response for simple span bridges. A pushover analysis is used to determine the load-deformation behavior of a structure prior to failure. Failure is defined as that point at which the structure becomes unstable resulting in collapse. The analysis was performed using a two-dimensional finite element model of a transverse bridge bent. The lateral force can

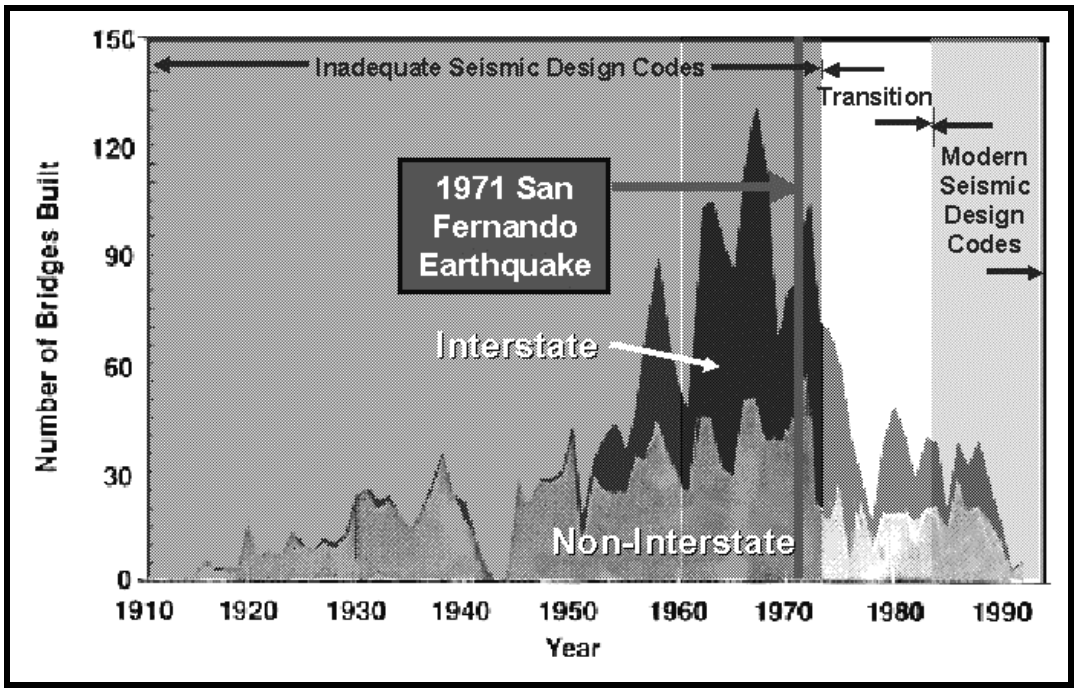

Figure 2. Construction of Washington State Bridges and the Relevant Seismic Codes.

be related to the spectral acceleration, and further normalized to spectral acceleration at one-second period to compare with existing HAZUS bridge fragility models.

Pushover analysis included the following assumptions:

- Model transverse bridge bent.
- Use cracked concrete section properties.
- Include "widened" section properties.
- Include gravity "deck" loads.
- Model soil stiffness (linear springs).
- Failure of bridge bent controlled by column plastic moment capacity (Mp) – verified.

Pushover analysis procedure includes:

- Increase lateral load until Mp is developed at column.
- Determine bent stiffness based on load and deflection prior to failure.
- Calculate spectral acceleration (Sa) at failure given bent stiffness and the weight of the structure.
- Compare to HAZUS bridge fragility curves for non-ductile detailing (pre-1973 WSDOT bridges).

The maximum calculated displacements for sample bridges range from 2.2" to 3.7" (this is just prior to the last hinge forming. At this displacement level, a bridge is extensively

damaged, but has not yet failed. The corresponding HAZUS value is 3.9", which is in reasonable agreement. The "failure" displacement of HAZUS is 13.9" – i.e., the bridge can probably accommodate additional displacement after the full hinge mechanism is formed. This corresponds to some reduced moment capacity (i.e. non-zero moment strength) in the columns, after the hinges have formed.

Vulnerability To Long-Duration Earthquakes

It is important to consider long-duration earthquakes, such as those originating on the Cascadia Subduction zone, and their effects on bridge performance. Long-duration effects apply at 0.23 g lateral force representing the median value for onset of cracking in bridge columns. Bridge vulnerabilities are based on: 90% probability of failure is at 0.40 g and 90% probability of cracking is at 0.28 g. Thus, if a bridge responds in the "plastic" range (above 0.28 g), in a long duration event, then it could degrade and fail. Therefore, the vulnerability of bridges under these conditions is reduced by a factor of 1.4 (0.4 g/0.28 g).

RESULTING BRIDGE DAMAGE AND HIGHWAY SEGMENT RELIABILITIES

The estimated number of bridges damaged (extensive or complete) for each of the six scenarios is shown in Table II.

TABLE II. REGIONAL BRIDGE DAMAGE ESTIMATES (EXTENSIVE/ COMPLETE DAMAGE)

Earthquake Scenario	Project Area Bridges Damaged	Regional Impact Multiplier	Regional Bridges Damaged	Damage Category	Additional Soft Soil/ Lique-faction	Additional area affected by shaking
Benioff M6.5	6	1	6	Low	No	Limited
Benioff M7.1	13	1.25	16	Low	No	Limited
Tacoma M6.7	23	1.5	35	Moderate	Nisqually	I-5 south to Olympia, SR-16 (competent soils), I-705, SR-509, SR-410, SR-18.
Seattle M6.5	28	1.5	42	Moderate	Limited	I-5, I-405 and SR-99 north to Snohomish County Line (-). I-90, SR-520, SR-522.
Seattle M7.0	40	2	80	High	Limited	I-5, I-405 and SR-99 north to Snohomish County Line (+). I-90, SR-520, SR-522
Cascadia Subduction M9.0	29	3	87	High	Significant	Entire state west of the Cascades. All alluvial valleys along I-5 corridor. All state routes west of I-5.

Highway segment reliabilities immediately following the earthquake were calculated by multiplying together the reliabilities of individual bridges in the segment. The results on shown on the project web site. Bridge reliabilities are combined using this approach immediately after

the earthquake because the probabilities of failure of each bridge are not influenced by restoration management decisions. The reliability of highway segments after restoration is based on the restoration of the individual bridge that HAZUS estimates has the longest restoration time.

Restoration time will be influenced by the availability of resources. The general approach assumes that for "low" damage category earthquakes, there will be adequate resources to pursue restoration of all bridges immediately following the earthquake. For "moderate" and "large" damage category earthquakes (refer to Table II), it is assumed that bridge restoration will be delayed for lower priority bridges.

The HAZUS restoration curve shows that on the "average" bridge will be about 67 percent restored within 3 months. It is assumed that many of the resources that would be used in the initial stages of bridge restoration would be freed up after 3 months, and could be applied to other bridges. For high damage category earthquakes, bridges are divided into 3 priorities for restoration, with delays for starting restoration of 3 and 6 months respectively for 2nd and 3rd priority highway segment bridges.

In order to establish the bridge damage categories in Table II, bridge damage results are used to estimate the total number of bridges across the state that will have at least extensive damage. This done by multiplying the average probability of being in the damage state times the total number of bridges. This approach is applied to main line bridges, as those are the bridges required to resume near full traffic volumes. The estimated number of bridges with at least extensive damage is shown in Table II for each earthquake scenario.

The study area only encompasses a portion of the interstate bridge system that would likely be impacted by an earthquake. The WSDOT would be responsible for restoration of all state owned bridges. Therefore an order of magnitude estimate is provided of the total number of interstate bridges that would be damaged as shown in Table II. This estimate takes into account the location, type, and expected distribution of ground motions of each earthquake, and the location of bridges in areas with significant site amplification and liquefaction susceptibility. In general, the study area encompasses the largest liquefiable areas in the region. To the north, the next large liquefiable area is the Snohomish River valley/delta just north of Everett. To the south, the next significant liquefiable are is the Nisqually River valley/delta. Each earthquake scenario affects bridges differently. Those affects are described in Table II. The result is the total number of bridges with at least extensive damage for the entire region, as shown in Table II.

The six earthquake scenarios are subdivided into 3 groups for low, moderate, and high levels of earthquake bridge damage, based on the total number of bridges with at least extensive damage. High levels of damage are expected for the Cascadia Subduction M9.0 earthquake and the Seattle M7.0 earthquake. Moderate levels of damage are expected for the Seattle M6.5 and the Tacoma M6.7 events. Low levels of damage are expected for the Benioff earthquakes. For the high level of damage category, it is assumed that bridges will be restored in 3 priorities: 1) I-5, 2) SR-167 north of SR-18 to I-405, and SR-518, and 3) all other highways. For moderate levels of damage, 2 priorities are identified: 1) I-5, and 2) all others. For low levels of damage, it is assumed that restoration will start on all bridges at the same time.

ECONOMIC IMPACT

The economic impact analysis evaluated only one earthquake scenario, the M7.1 deep Benioff earthquake centered under the City of SeaTac. This therefore should not be considered a worst-case scenario. However, the projected economic impact is severe. The earthquake's transportation related effects could mean:

- Reduced business revenues of $3 billion.
- Loss of 39,000 jobs costing over $1 billion in income.
- Tax losses to local government of $72 million.

Trucking firms, port related businesses, "just-in-time" manufacturers and retailers depending on customer access to stores could be hard hit. Small businesses without financial reserves could face bankruptcy. Furthermore, these estimates of economic loss are based only on the study area, and not the entire region.

CONTINGENCY PLANNING

The contingency planning efforts by both counties revealed significant challenges in redirecting up to 200,000 cars per day (I-5) onto surface streets. Simultaneous route outages could bring traffic to a standstill, with few arterial substitutes to carry daily traffic. Earthquake damage to multiple bridges would disable entire routes for up to three to six months. One of the major benefits of this multi-jurisdictional contingency planning was that it brought together transportation planners for the first time to address these types of issues.

FINDINGS AND CONCLUSIONS

For earthquakes with ground motions that are expected to be exceeded in the order of every 50 to 100 years, the maximum probability of failure of any single bridge is less than 35 percent, and overall may result in loss of use of about 3 to 6 percent (6 to 13 bridges) of the 214 bridges in the study area. However, for earthquakes that produce ground motions that are expected every 300 to 1,000 years, 10 to 15 percent of the bridges (23 – 29 bridges) are fail functionally, with nearly 20 percent (40 bridges) failing in an M7.0 earthquake on the Seattle fault.

Restoration of these bridges following the 300 – 1,000 year event will exceed six months, and be over a year for the larger event.

With failure of only six bridges in the deep Benioff M6.5 event (the smallest modeled event), the region is expected to lose $3 billion in business revenues, and lose 39,000 jobs due to the impact on the regional transportation system, including effects on Boeing, and the ports of Seattle and Tacoma.

REFERENCES

King and Pierce County Project Impact, Port-to-Port Transportation Corridor Earthquake Vulnerability Project Report, performed by ABS Consulting (formerly EQE International), 2000. The report is available in printed format (text only) and online with text and hazard, bridge damage state, and highway segment recovery status maps at: www.eqe.com/impact.

HAZUS Loss Estimation Software and Technical Manuals developed by the National Institute of Building Sciences with funding from the Federal Emergency Management Agency, available at http://www.fema.gov/hazus.

Ground Motions, Design Criteria, and Seismic Retrofit Strategies for the Bay Area Rapid Transit District Bridge and Other Structures

Tom Horton, Eric Fok, Ed Matsuda, William Hughes, Wen S. Tseng, Chip Mallare, and Kang Chen

ABSTRACT

In 1989, the Loma Prieta earthquake caused significant damage to the transportation infrastructure in the San Francisco Bay Area. However, the Bay Area Rapid Transit (BART) system sustained very minor damage and was able to resume service within a few hours. The BART system was critical to meeting transportation needs following the Loma Prieta earthquake, especially between the East Bay and San Francisco. It is acknowledged that ground motions impacting BART during future earthquakes could greatly exceed those experienced during the Loma Prieta earthquake. Consequently, the system is being evaluated for retrofit, incorporating the latest ground motion and design technology lessons learned. The California Department of Transportation (Caltrans) is providing funding assistance and oversight for BART structures that cross over public streets and highways.

The work on the retrofit project began in September 2000 and is expected to continue in phases over the next 5–9 years with a total construction cost currently estimated at $1.3 billion. Over the next year, BART and the General Engineering Consultant (Bechtel/HNTB) will be performing the following tasks:

- Development of design ground motions and seismic retrofit design criteria. Emphasis is placed on using latest technology to maintain serviceability after a major earthquake.
- Identifying seismic vulnerabilities and developing retrofit measures for bridges and other structure elements.

The following sections provide an overview of the BART system and its history, and then discuss the special challenges faced by the retrofit program team. The authors describe how risk management methodologies are being applied to the development of retrofit alternatives, and provide some history of BART seismic design criteria and their development. The critical understanding of ground motions acting on the BART system is discussed extensively, as are a variety of possible retrofit alternatives.

Tom Horton, PE, BART Program Manager, Bay Area Rapid Transit District Seismic Retrofit Capital Program, 1330 Broadway, Suite 1200, Oakland CA 94612
Eric Fok, SE, BART Principal Engineer, Bay Area Rapid Transit District Seismic Retrofit Capital Program, 1330 Broadway, Suite 1200, Oakland CA 94612
Ed Matsuda, SE, BART Engineering Manager, Bay Area Rapid Transit District Seismic Retrofit Capital Program, 1330 Broadway, Suite 1200, Oakland CA 94612
William Hughes, PE, Consultant Deputy Project Manager, Bay Area Rapid Transit District Seismic Retrofit Capital Program, 1330 Broadway, Suite 1200, Oakland CA 94612
Wen S. Tseng, PhD, PE, Consultant Ground Motion/Criteria Manager, Bay Area Rapid Transit District Seismic Retrofit Capital Program, 1330 Broadway, Suite 1200, Oakland CA 94612
Chip Mallare, PE, Consultant Bridge Retrofit Manager, Bay Area Rapid Transit District Seismic Retrofit Capital Program, 1330 Broadway, Suite 1200, Oakland CA 94612
Kang Chen, PE, Consultant Design Criteria Manager, Bay Area Rapid Transit District Seismic Retrofit Capital Program, 1330 Broadway, Suite 1200, Oakland CA 94612

INTRODUCTION – OVERALL BART SYSTEM

The San Francisco Bay Area Rapid Transit (BART) District was created by the California Legislature in 1957 to provide rapid transit facilities to the Bay Area. Construction began in 1964 and was completed in 1976. The original 75-mile long system includes 25 miles of aerial guideway structures, 34 stations, 22 miles of subway and twin-bore tunnels, and 27 miles of track supported at grade and on embankments. The original system also includes the 3.6-mile long Transbay Tube connecting the East Bay to San Francisco and the Berkeley Hills Tunnel (3.2 miles) which connects Oakland to Contra Costa County. (See Figure 1)

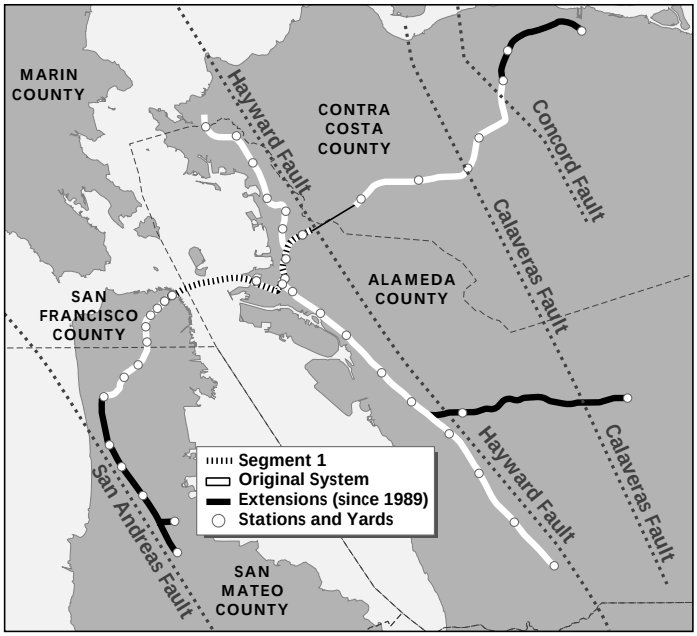

Figure 1 BART System and Major Bay Area Faults

In the 1990s, BART began a massive program to add more than 30 miles of extensions and nine stations to the original system. Five stations and 24 miles of track in the East Bay and Colma have been completed and opened for service. Nearly 9 miles of track and four stations extending BART to San Francisco International Airport are currently under construction.

Recently, BART began a 5½-mile extension south from Fremont to Warm Springs, and in November 2001, the BART Board of Directors approved design and construction of a BART extension from Warm Springs to Santa Clara County. In addition to track and stations, the system consists of train control and communication facilities, traction power facilities, ventilation structures, the Central Operations Center, administrative buildings, parking structures, and miscellaneous structures. There are also five maintenance shop/yard facilities servicing the system.

BART's critical contribution to Bay Area transportation was highlighted following the 1989 Loma Prieta earthquake, which destroyed major roadways around the region and left numerous others unusable. However, BART was able to resume limited passenger service in the East Bay within 12 hours after the quake and full service within 2 days. In fact, BART carried an additional 100,000 passengers each day during this period, increasing patron loads by 40 percent over pre-earthquake service. Today, the system carries over 310,000 passengers during the weekdays, about 45 percent of the commuters crossing the bay, and operates more than 50 trains during peak hours.

In light of its criticality to Bay Area transportation, BART has initiated a seismic retrofit program to enhance the seismic performance of the system in the event of a future major earthquake, employing a team led by Bechtel Infrastructure Corporation and HNTB Corporation as the General Engineering Consultant.

The team is performing a system-wide seismic vulnerability study to 1) determine the susceptibility of all facilities, structures, and equipment in the BART system to earthquakes, and 2) to develop an overall retrofit strategy and scope (through a risk management plan) to improve the seismic performance of the system. The Vulnerability Study is to be completed in the summer of 2002 and the program will then proceed to preliminary and final design. For retrofit of aerial guideways that cross local roadways, the California Department of Transportation (Caltrans) will provide Federal Highway Administration (FHWA) funding through the Local Seismic Safety Retrofit Program.

This paper focuses on ground motions, design criteria, and seismic retrofit strategies for aerial guideways because a large portion of total program expenditures will go toward retrofitting these struc-

tures. Typical BART aerial guideway structures consist of simply supported precast prestressed concrete box girders with spans between 80–100 feet. (In a few locations composite steel girders, steel through girders, or cast-in-place prestressed concrete box girders are used.) The prestressed girders are typically single-cell trapezoidal boxes with girder ends dapped, or notched, to allow pier caps to be partly contained in girder depths.

Superstructure spans are typically seated on elastomeric bearing pads. A closure pour is provided on top of pier caps between the ends of superstructure girders. One end of a superstructure girder is pinned with horizontal dowels into the closure pour, which in turn is restrained laterally by vertical concrete-filled steel pipe shear keys. The other end of the girder is free to slide longitudinally and restrained laterally by one horizontal concrete-filled steel pipe shear key connecting the girder end to the closure pour.

Substructures for aerial guideways consist of concrete columns, piers, and abutments. The majority of bents are single concrete T-bents, or hammerhead bents, that support two parallel track girders. Columns are supported on either spread footings or pile foundations. Other bent types include single rectangular concrete columns supporting a single-track girder with no bent cap, single or multiple columns with in-fill walls that support multiple track girders, and multicolumn bents with bent caps.

CHALLENGES AND UNIQUENESS OF THE PROGRAM

Upon embarking on its seismic retrofit program, BART managers recognized that program challenges stem primarily from two sources – BART's rigorous performance requirements, and the uniqueness of the BART system itself.

Performance Criteria

BART has established Seismic Performance Categories or (SPCs) to guide seismic evaluation of the BART system. **SPC-1** requires that primary revenue structures be capable of returning to revenue service within 72 hours after a "Maximum Credible Earthquake" (MCE). The 72-hour standard was designed to allow time to inspect the system and declare it safe for operation before resuming service. This criterion essentially means that SPC-1 structures should be operational immediately after a major earthquake. Structures falling into this category include aerial guideways, stations, trackways, subways, and the Transbay Tube.

SPC-2 dictates secondary facilities, including train control and power systems, mechanical and electrical systems, track, and the Central Operations Center, return to service within 60 days after an MCE. Restricted levels of service based on temporary repairs were allowed as part of this criterion. It is envisioned that the SPC-2 system components will be brought back on line gradually as mechanical, electrical, and track systems are restored, with the entire system back in operation by the 60-day mark.

SPC-3 applies to noncritical facilities such as shop buildings, training facilities, office structures, and parking structures. These facilities are required to meet life safety or noncollapse guidelines.

Unique Features of the BART System

A primary unique feature of the BART system is its extensive reliance on mechanical and electrical systems for operations. While highways are usable with minimal electrical and mechanical support, BART simply cannot operate without such systems. Thus, the retrofit of these systems is a vital component of the overall retrofit plan.

Also unlike most highway systems, BART has little redundancy. If a particular section of track, tunnel or station goes out of service, there are no alternate routes around it, and areas on opposite sides of the nonoperational section will be isolated from each other. Since BART does not have a loop system, failure at a critical location can split the system in half, greatly reducing its effectiveness. This characteristic was the prime factor in BART's organizing the retrofit program in phases. The first phase

istic was the prime factor in BART's organizing the retrofit program in phases. The first phase of work includes the "core" system, which is located at the center of the BART alignment. Subsequent phases start at the core and work their way out to the ends of the system.

Additionally, BART structures contain unique characteristics that limit the team's ability to model them on earlier retrofit experience. Notable among these is the large amount of reinforcing steel in aerial structure columns (as much as 6 percent). This makes columns quite strong, but also quite stiff, and thus their behavior can be significantly different than more lightly reinforced columns.

The team also has had to deal with the recently recognized *near-field effect*. This consists of a short-lived "spike" or "fling" in ground motion, fault rupture directivity, and other effects. These effects are most pronounced within 10 kilometers of an earthquake fault, and their precise effect on structures is not completely understood. Since practically the entire BART system is within one near-field effect zone or another, the team has had to account for these large motions and create design criteria for detailed design that include requirements for the near-field effect.

The particulars of rail system vulnerability also drive criteria development. Unlike highway systems, railroads cannot tolerate large relative displacements. Temporary displacements during an earthquake can cause train derailments or even cause trains to fall off aerial structures. Moreover, excessive permanent displacements cause difficulties in realigning tracks and may interfere with resumption of train service. The team is establishing the acceptable amount of temporary and permanent rail displacement, taking into account not only the structural considerations but characteristics of the rail cars, maintenance practices, and the specific characteristics of BART track.

RISK MANAGEMENT PLAN COST/BENEFIT ANALYSIS

A risk management plan is being implemented as part of the overall BART Seismic Retrofit Program. The plan demands attention to the affordability and cost-effectiveness of any proposed solutions. This is not only the "right thing to do," but is required by BART's current or potential funding partners. This concern has driven a substantial risk analysis effort. The plan has three main objectives. The first objective is to demonstrate the need for the BART system to be seismically retrofitted. The second is to assist BART in establishing acceptable seismic performance goals for the BART system. The final objective is to determine the level of funding needed to carry out such a program and to facilitate funding procurement. Development of risk management-directed retrofit alternatives starts with assessing the impact of high-likelihood, high-magnitude deterministic earthquake scenarios on the system in its present condition (to establish the *Status Quo* alternative), then establishing the retrofits required to mitigate life safety risks. Next, assessing earthquake scenarios' impact on operability (assuming life safety mitigation retrofits are in place) establishes the *Life Safety* alternative. Assessing whether and where retrofit beyond life safety should be considered to improve operability, and developing retrofit schemes to achieve various levels of enhanced operability establishes *Operability* alternatives. Cost /benefit analysis of retrofit alternatives evaluates them based on acceptable operability/system recovery and cost benefit justification. These alternatives are then evaluated by Peer Review Panels to yield recommendations that can be communicated to decision-makers and other interested parties for their action. This process is illustrated in Figure 2.

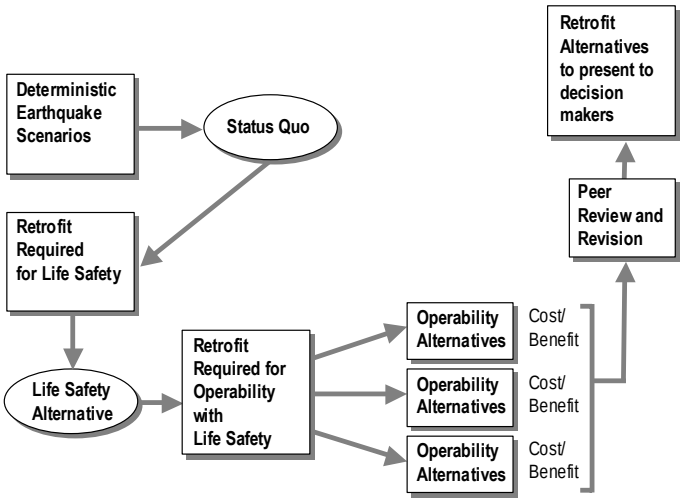

Figure 2 Development of Risk Management Alternatives Through Application of Deterministic Earthquake Scenarios

The *Status Quo* assessment should demonstrate the program's need quite convincingly: it will reveal problems with the existing system, the extent of the problems, and consequences if the retrofit program is not adopted. One of these consequences might include impacts to life safety. Moreover, because BART is a vital part of the Bay Area transportation system, there will be significant economic impacts should the BART system stop operating. The risk management plan will document and quantify these consequences.

The plan will also assist BART in finalizing the performance goals and requirements for the system. BART's "upper bound" requirement meets the SPC-1 criteria, meaning that aerial guideway structures need to be fully functional following an MCE. The "lower bound" requirement is retrofitting to a *Life Safety* level. The risk management plan addresses the cost/benefit of these two bounding alternatives; it also establishes retrofits for different levels of operability and calls for cost/benefit analyses of each. One alternative may be to retrofit all aerial structures to allow limited damage, including damage to foundations, such that trains can safely run on the structures immediately after a scenario earthquake without any shoring or repair. Another alternative is to upgrade the core of the system to a high level of performance, but allow more damage and downtime to less critical stations and segments. In this case, aerial structures on less critical segments might need to be shored to allow trains to run over them in the short term, and extensively repaired or replaced to restore to normal use. The prudence of allowing additional damage would depend on many factors including the consequences of additional downtime, probability of a damaging earthquake occurring, relative pre-earthquake and post-earthquake construction costs, and annualized cost/benefit ratios. Through these studies, the Risk Management Plan will provide BART with the information needed to define the seismic performance goals for their system.

The risk management plan will establish the level of funding needed by determining cost-effective performance goals and set the levels and costs of retrofit required. Demonstrating the cost-effectiveness of the retrofit program is essential because of its anticipated scope and cost, as well as significant competition for funding in the region. The performance-based system and cost/benefit analysis in the risk management plan is more complicated and time-consuming than traditional methods of assessing and retrofitting individual structures and components to a given ground motion and structural criteria. However, the process reduces conservatism, facilitates prioritization, and will provide strong justification for requested funding.

The risk management plan was developed to demonstrate that the retrofit program is needed, prudent, and cost-effective, and should have a high priority for funding. BART has arranged for outside peer review under the direction of the Pacific Earthquake Engineering Research (PEER) Center to help ensure that the process and recommendations are technically sound, economically feasible, and responsive to system operational goals. Technical soundness was a primary consideration of design criteria development, discussed below.

BART SEIMIC RETROFIT PROGRAM DESIGN CRITERIA

BART first developed design criteria in 1963 for construction of the original system. Since then, the criteria have been updated twice: for construction of the East Bay Extensions in 1990 and the SFO Extension in 1995. The design criteria currently under development for the seismic retrofit program are based on previous updated BART design criteria; Caltrans seismic design and bridge structure evaluation and retrofit design guidelines; and Federal Emergency Management Agency (FEMA) design guidelines. The design methodology has changed since 1963 from allowable stress design to displacement and allowable material strain based performance (deformation control) design.

BART's original aerial structures seismic design was based upon both elastic and plastic theories. Structures were designed elastically, with up to 0.1g load applied as an equivalent static lateral seismic load using the allowable stress design method. In addition, structures were checked for inelastic horizontal displacement capacity under higher ground motion, with 0.33g or 0.5g loads for foundations on firm and soft ground, respectively. The ultimate displacement capacity of structures was defined as the column

longitudinal steel reaching a maximum strain of twice the yield point strain. Detail designs were in accordance with then-current American Concrete Institute (ACI) and American Association of State Highway and Transportation Officials (AASHTO) requirements.

The retrofit criteria currently under development cover structural seismic evaluation, design methodology and analytical procedures, and retrofit design requirements for various BART facilities. These include aerial structures and bridges; passenger stations; cut-and-cover and bored tunnels; the Transbay Tube and ventilation structures; buildings; equipment; and equipment supports. The criteria are based on 1995 BART criteria modified to suit retrofit specifics, current Caltrans practice and design methodology in seismic retrofit design, and FEMA design guidelines in seismic evaluation and retrofit design.

Principal Features of Aerial Guideway Retrofit Design Criteria

Aerial guideways are classified as SCP-1 structures, which requires them to be capable of returning to revenue service within 72 hours of an MCE. Due to the difficulty of repairing foundation damage, the current criteria for aerial structures mandates that foundations remain essentially elastic under the design earthquake. Therefore, inelastic behavior is limited to elements above the foundation, such as the column and possibly bent caps. To force yielding to occur at the desired location or locations, all other members and connections in the seismic load path of the structural system must remain elastic, and must be designed to meet the strength requirements under the seismic group load combination.

BART has adopted deformation control design methodology based on allowable material strain using inelastic analytical procedures for facilities' seismic design. These procedures involve advanced analytical technologies including nonlinear analysis, soil-structure interaction, and computer-aided evaluation.

Considerations were also given to the structural contribution of the continuously welded direct fixation rails. The rails are fastened to the structural deck and participate during seismic events as part of the overall structural system. Considerations also must be made for the allowance of structure residual movement related to the train operation. These are features unique to BART structures with respect to typical highway structures.

Physical Testing Program

A laboratory testing program is under way to verify several assumptions made during development of the design criteria and vulnerability study. Two half-scale column-pile cap units are to be built and tested at the University of California, San Diego under quasi-static reversed cyclic loading conditions resembling earthquake loading expected in an MCE. The test results will address the following issues:

- Transfer of very large shear forces across the column-pile cap joint region. Plastic column hinging forces could result in shear stresses of the order of 17 sqrt (f'c) in some existing joints.
- Pile cap shear strength enhancement through the use of S-shaped vertical dowels or the use of double T-headed bars.
- Effects of column longitudinal bar curtailment.

The final test report will also provide strain/damage relationships assumed in the design, such as size of cracks, extent of spalling corresponding to concrete strain, and recommendations for allowable concrete and steel strain limits.

GROUND MOTIONS

The BART system is located in the heart of the San Francisco Bay Area, one of the most seismically active regions in the world. There are numerous faults in the region and BART lines are close to these faults, as indicated in Figure 1. Because so many major faults are present, and the BART system's proximity, the probability of a large-magnitude earthquake having a major effect on the system is very high. Consequently, a major task of the retrofit program is the development of a suitable set of seismic input criteria.

The BART system is composed of long segments of at-grade, above-, and underground engineered facilities of many different kinds. Since different structure types have different seismic response characteristics, the development of seismic input criteria must recognize specific seismic ground motion parameters that are critical to each type of structure. Furthermore, considering the long alignment of the system, criteria must take into account the spatial variation of ground motions. Additionally, because of close proximity to major faults, the criteria must also incorporate near-field effects, such as fault-rupture directivity, ground motion polarization directivity, and large velocity pulse or "fling" in near-field ground motions.

Seismic Hazard Analyses

Seismic ground motion criteria development consists of specifying appropriate ground motion parameters that characterize ground-shaking hazards including near-field effects, spatial variation of ground motions in the project region, and fault-rupture offset displacement where BART lines cross major faults. In developing these criteria, both deterministic and probabilistic seismic hazard analysis approaches have been employed.

In the deterministic approach, development of the criteria was based on MCE conditions as represented by the maximum earthquake magnitude judged to be likely at each major fault. Derivation of ground motions at BART facility locations under MCE conditions was based on an average of up to five published ground motion attenuation relationships. The ground motion parameters consist of three-component peak-ground acceleration (PGA), velocity (PGV), and displacement (PGD) values, and their 5%-damped acceleration response spectra (ARS).

Six site conditions have been considered, designated as Site Classes B, B/C, C, D, E, and F, defined in accordance with NEHRP (1997)[1] site classification definitions. Site condition B/C represents rock-site conditions in the project area. Recognizing scattering in empirical ground motion data, three intensity levels have been selected to represent design-level ground-shaking intensities: median, median $+0.5\sigma$, and median $+1.0\sigma$ levels, where σ represents the standard deviation of empirical ground motion data. Median $+0.5\sigma$ was selected because it results in ground motion intensity corresponding closely to the level used in BART's most recent extension – San Francisco Airport (SFO) – which is currently under construction.

In the probabilistic approach, all earthquake magnitudes that could occur at each major fault, and areal sources located among the major fault zones, are considered in the hazard analysis. Based on the same attenuation relationships used in the deterministic approach, probabilistic estimates of uniform-hazard ARS and other ground motion parameter values (corresponding to those generated using the deterministic approach) were generated for several return-periods: 500, 1,000, and 1,500 years. The 500-year probabilistic values generated for the SFO extension sites compare very well with the deterministic median $+0.5\sigma$ values at corresponding sites. Since 500-year probabilistic values have been used as the basis for many current design codes, the final design intensity level representing BART system-wide ground shaking hazards is the greater of deterministic median $+0.5\sigma$ and probabilistic 500-year values. Likewise, the greater of deterministic median $+1.0\sigma$ and probabilistic 1,000-year values was selected to represent the higher level of design ground motion.

Presently the deterministic median level ground motion intensity has been selected as the basis for assessing system-wide BART facilities to meet operation performance goals. The greater of deterministic median +0.5σ and probabilistic 500-year intensity level was selected for assessment to meet life-safety performance goals. However, for the critical Transbay Tube and its associated ventilation structures, the corresponding levels are the greater of deterministic median +0.5σ and probabilistic 500-year level for operations, and the greater of deterministic median +1.0σ and probabilistic 1,000-year level for life safety.

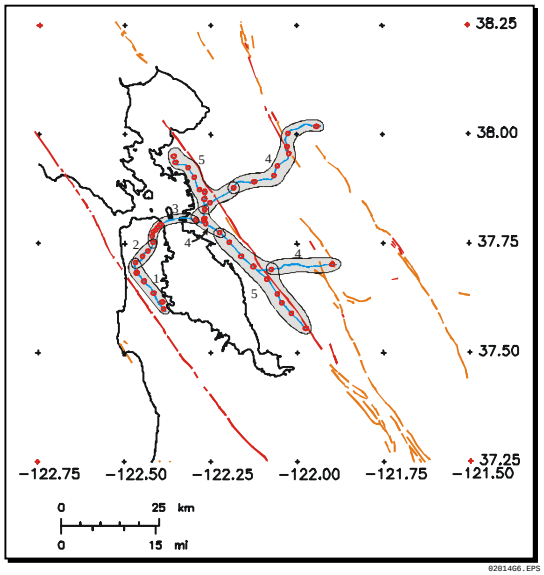

Figure 3 Five Bay Area Seismic Zones

Acceleration Response Spectra

Using the methodology described above and incorporating near-field effects, three-component values (horizontal fault-normal (FN), fault-parallel (FP), and vertical of PGA, PGV, and PGD), and horizontal and vertical ARS were generated for 17 selected facility locations in the BART system. These parameters were generated first for the rock-site condition (B/C) and then modified for other soil-site conditions (B, C, D, and E). (Site-specific site response analyses are required for the special F soil site condition.) To simplify criteria for application, ground motion parameters generated at 17 selected locations were grouped, based on their geographic locations and relative distances from the hazard-controlling faults, into five distinct Seismic Zones along the entire BART alignment. These five zones are shown in Figure 3. Figure 4 shows an example of the ARS curves representing the greater of deterministic median +0.5σ and probabilistic 500-year intensity for Seismic Zone 1, for all five site-classes. As can be seen from the figure, the ARS curves developed for seismic assessment of BART facilities represent a rather high level of ground shaking.

Time Histories

Due to high ground-shaking intensities, seismic assessment of BART facilities necessarily involves post-elastic nonlinear seismic response behaviors, for which nonlinear time-history response analyses are required. Three-component sets of time histories representing design-level ground-shaking conditions were generated by modifying near-field actual-earthquake accelerograms using the method developed by Lilhanand and Tseng (1988)[2]. The time histories match PGA, PGV, PGD, and ARS values and satisfy strong-motion duration guideline values specified in the ground motion criteria; the

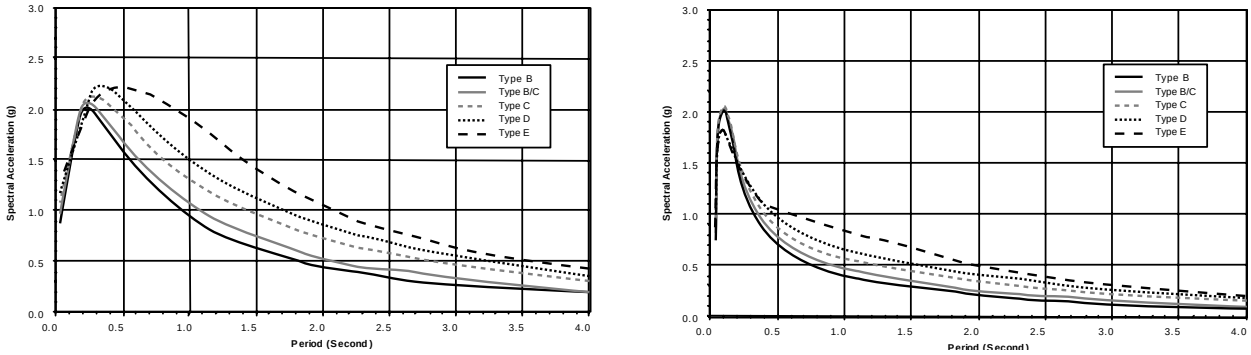

Figure 4 ARS Curves for Seismic Zone 1

generated motions are response spectrum-compatible time histories. Recorded motions for time-history modification considered such geologic and seismologic factors as earthquake magnitude, faulting mechanism, source-to-site distance, and site conditions appropriate for each Seismic Zone and site-soil class. Distinct horizontal FN and FP and vertical components of ground motion time histories have been developed for each seismic zone and each site class.

Spatial Variations

For seismic evaluation of BART's long, continuous, elevated viaduct and underground structures such as the Transbay Tube and bored tunnels, spatial variation of ground motions resulting from seismic wave passage and spatial coherency effects has also been considered. Based on results of analyses of strong-motion instrument-array data, an apparent horizontal wave-propagation speed equal to 2.5 km/sec was selected to characterize the wave passage effect. To represent the seismic wave spatial coherency effect, spatial coherency functions derived by Abrahamson, et al (1991)[3], which characterize spatial coherency of seismic waves as function of wave frequency and separation distance, have been used. For seismic assessment, response spectrum- and coherency-compatible time histories were developed for multiple ground stations along specific segments of the BART alignment using a method developed originally by Hao, Oliveira, and Penzien (1989)[4] and extended later by Tseng, Lilhanand, and Yang (1993)[5]. It is worth mentioning that, for long underground structures sensitive to ground deformation gradients, and due to the presence of long-period near-field velocity pulses that usually control seismic response, the wave passage effect is usually much more important than the spatial coherency effect.

Fault Crossing Displacements

BART lines cross five major faults: Hayward, Calaveras, Concord, Franklin, and Pleasanton. To assess the consequences of fault-rupture displacements on BART structures at fault-crossing locations, expected fault offset displacement values consistent with the selected MCE conditions need be estimated. The assessment of fault-offset hazards was made using both deterministic and probabilistic methods. The deterministic assessment used Wells and Coppersmith (1994)[6] empirical relations between maximum fault displacement and earthquake magnitude to estimate the median value and standard deviation; the probabilistic assessment used the same hazard analysis procedure used to assess ground-shaking hazards. Fault-offset displacements for 500-, 1,000-, and 1,500-year return-periods were estimated. Based on the results of these analyses, fault-offset displacements equal to 3.3, 1.4, 0.5, and 0.3 meters were selected for seismic evaluations where BART lines cross the Hayward, Calaveras, Concord, and Pleasanton strike-slip faults, respectively. These displacements are to be treated as resultants of horizontal and vertical offset components having a horizontal-to-vertical ratio of 8 to 1. For the BART line crossing the Franklin reverse fault, the offset displacement estimated is 0.3 meters with a horizontal-to-vertical ratio of 1 to 1. The above fault-offset displacements are based on probabilistic 1,000-year return period values with a lower bound limit set at 0.3 meters. Ground motions developed through the above process were applied during the development of possible retrofit concepts, described below.

AERIAL GUIDEWAY RETROFIT CONCEPTS

Although the original BART system was designed and constructed in the 1960s, BART had the foresight to include seismic demands in their original design criteria. As a result, many of the as-built aerial guideway structures include details that allow them to withstand seismic forces much better than other bridges designed and built during the same period. These features include well-anchored column reinforcement, closely spaced column horizontal reinforcement, generous bearings seats with restrainers, and an absence of column lap splicing.

However, the magnitude of seismic forces used in the original design criteria was well below that used today, and recent seismic analysis of BART elevated structures reveals a number of seismic vulnerabilities. Many of the seismic deficiencies found in BART aerial guideway structures are similar to those found in California highway bridges and therefore some the retrofit approaches planned for the elevated structures are similar to those taken for Caltrans highway bridges.

The retrofit alternatives and details developed to date reflect the SPC-1 performance criteria initially set by BART. They represent, more or less, upper bound solutions which are meant to allow train operations to resume within 72 hours of a major seismic event. As stated previously, BART may revise the acceptable performance level based on results from the Risk Management Plan. This in turn would change the retrofit approach taken by the design engineers.

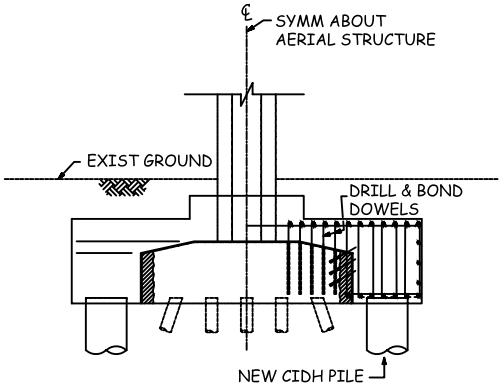

Figure 5 Foundation Retrofit Alternative

Foundations

Aerial guideway as-built pile foundations were found to have a number of seismic deficiencies that include inadequate pile capacities, inadequate pile-to-pile cap connections, inadequate pile cap flexural reinforcement, inadequate footing shear strength, and excessive joint shear stress. Retrofit details proposed for pile foundations include increasing the footing size to provide for additional piles and adding a footing overlay that incorporates a top mat of reinforcing. (See Figure 5)

Because of low overhead and limited access, two pile alternatives are currently being investigated: large cast-in-drilled-hole (CIDH) piles and micro- or pin-piles. Micropiles may be battered, as are many of the as-built piles, to increase their lateral resistance and to limit lateral displacement. Footing pedestals are also being considered to increase footings' joint shear performance. Pedestals will reduce the joint shear stresses in footings without increasing the depth of the entire footing.

Another unique detail being considered is extending vertical drill and bond dowels to the bottom of footings.Extending dowels to the bottom of footings, in conjunction with using button headed reinforcing, will increase footings' shear capacity and provide better joint shear performance.

Columns

As-built columns have generally good seismic performance, with the columns having sufficient strength, stiffness, and ductility to resist expected seismic demands. However, many columns are either deficient in shear capacity or close to their shear capacity as compared to their plastic shear. Therefore, column casings are proposed where needed to increase the overall shear capacity of columns. Common steel casing retrofit procedures would involve elliptical steel shells at rectangular columns and circular casings at hexagonal columns. However, since shear strength enhancement is the primary goal, fabricating casings to closely match the shape of the columns is a possible option. This would offer aesthetic advantages as well as potential savings in material costs. Furthermore, shaped casings would minimize column flexural strength increases that could require further costly strengthening at the footings. Where additional column ductility is needed, circular or elliptical steel casings, (or perhaps composite material jacketing) can be used. The composite material jacketing offers some advantages over steel jackets. For example, column flexural strength enhancement is negligible using composite jackets, provided unidirectional composites are used. Also, composite casing can readily conform to the rectangular or hexagonal shapes of BART columns while still providing greater ductility enhancement over the shaped steel jackets, and installation may be simpler in highly congested areas.

Bent Caps

Study reveals that as-built shear keys typically have insufficient strength to resist the plastic shear force of the columns. To resist transverse seismic forces, external shear keys are proposed to be attached to the bent caps at the exterior surfaces of the girders. Longitudinal forces will be resisted by placing bearing material, or "bumpers" such as steel plates or elastomeric pads, between the ends of the girders and the face of the bent caps. The existing shear keys also impart large torsional moments to the bent caps since the longitudinal seismic force is currently transferred through the shear keys at the top of the bent cap. The bumpers would decrease these torsional demands on the bent caps and thereby eliminate the need to retrofit the bent cap for torsional forces.

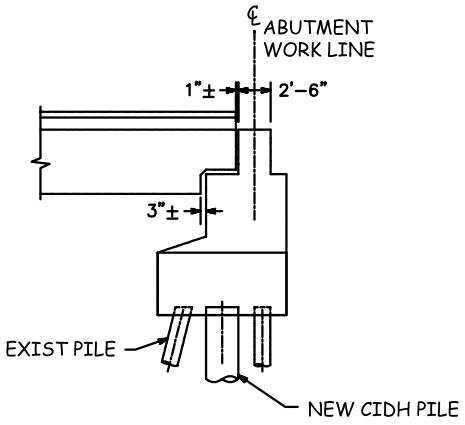

Figure 6 Abutment Retrofit Alternative

Abutments

The typical BART aerial guideway structure has short seat type abutments on piles, with the superstructure supported on low-profile elastomeric bearing pads. As-built abutments typically have a 1-inch expansion joint between the ends of the girders and the abutment backwall. The gap between the dapped face of the girder and the front face of the abutment is typically 3 –4 inches. Concrete shear keys at both sides of the girders secure them from transverse movement. (See Figure 6)

Longitudinal Response

In a typical Caltrans bridge retrofit, the abutment backwall is allowed to fail. The longitudinal restraining force is then supplied by the soil behind the backwall. However, the typical BART aerial guideway structure has a mildly reinforced, 2-½ foot-thick backwall. Because of this large backwall, piles are expected to fail prior to failure of the backwall.

To satisfy BART's original requirement of preventing foundation damage, three possible retrofit schemes are being investigated for abutments. The first is to open abutment gaps to provide sufficient distance to either eliminate abutment engagement or reduce displacement and force demands on the abutments to an acceptable level. However, this approach is difficult to implement without affecting BART operations. The second approach is to weaken the abutment backwall so that it will fail prior to damaging the piles. This could be done by coring a hole transversely near the front face of the backwall, thereby removing the front face of reinforcing. If this approach is chosen, BART would have to accept some damage to the abutments after a major (or even moderate) seismic event. Although this backwall damage would eventually need to be repaired, it is not likely to affect train operations. The third approach would be to strengthen the abutment foundation sufficiently to prevent failure by providing additional piles. This is the most costly alternative, but it would limit the amount of damage to the existing abutment and abutment foundation.

Transverse Response

In normal Caltrans bridge design, transverse abutment shear keys are sized so that they fail prior to damaging pile foundations. However, shear keys on the BART aerial guideway structures are generally much stronger than the pile foundations. Two retrofit alternatives are currently being investigated for transverse response. The first is to replace existing shear keys with weaker keys or other sacrificial elements that will fail before damaging the piles. However, analyses have shown that the transverse

movement of the girders using this type of system would be quite large, on the order of 1½–2½ feet. This amount of movement would severely damage the rails and existing elastomeric bearing pads and would likely prevent train operation. Replacement of the rails could be done quickly, but replacement of the bearing pads would require jacking superstructure girders and could take longer than the 60-day guideline. The second alternative would be to increase the foundation's capacity by using either large diameter CIDH or battered micropiles. These piles could be used for both the transverse and longitudinal seismic forces.

CONCLUSION

BART has always maintained twin goals of protecting the community's investment in the system while planning for the future. Given the public's need for additional transportation capacity, the system has regularly expanded, with new extensions and capacity enhancements in various stages of conceptual planning, final design, and construction. However, portions of the current system are aging and in need of maintenance and upgrading. BART will use the information developed as a part of the seismic retrofit program, and in particular the seismic risk management plan, to guide decision-making relative to seismic retrofit options.

Seismic upgrading of transit systems is a complex issue. Major factors that influence results include identifying appropriate ground motions, reasonably evaluating the integrity and performance of the structures, and developing the appropriate, affordable upgrades to protect and benefit the public who use and depend on the system. The initial seismic data developed suggest that some measures of seismic upgrading will be prudent. This important fact allows BART to begin implementation planning for the retrofit program internally, and with the public and interested external agencies. In particular, Caltrans and FHWA have become important partners assisting BART in defining and implementing the retrofit program.

The remaining challenges for the program will be to specifically define the level of retrofit, procure the balance of funding necessary, comply with environmental guidelines, and properly design and construct the improvements in an efficient manner with the least disruption to BART's patrons and neighbors. BART is committed to operating a safe and reliable system, and the seismic retrofit program is an expression of that commitment.

References

[1] National Earthquake Hazard Reduction Program NEHRP (1997), "Recommended Provisions for the Development of Seismic Regulations for New Buildings and Other Structures," Vol. 1 (Provisions), Vol. 2 (Commentary).

[2] Tseng, W. S., Lilhanand, K., and Yang, M. S. (1993), "Generation of Multiple-Station Response-Spectrum-and-Coherency-Compatible Earthquake Ground Motions for Engineering Applications," Proceedings, 12th International Conference on Structural Mechanics in Reactor Technology," Paper No. K01/3, Stuttgart, Germany, August 15-22.

[3] Abrahamson, N. A., Schneider, J. F., and Stepp, J. C. (1991), "Empirical Spatial Coherency Functions for Application to Soil-Structure Interaction Analyses", Earthquake Spectra, Vol. 7, No. 1.

[4] Hao, H., Oliviera, C. S., and Penzien, J. (1989), "Multiple-Station Ground Motion Processing and Simulation Based on SMART-1 Array Data", Nuclear Engineering and Design, III (6), 2229-2244.

[5] Lilhanand, K. and Tseng, W. S. (1988), "Development and Application of Realistic Earthquake Time Histories Compatible with Multiple-Damping Design Response Spectra", Processings, 9th World Conference on Earthquake Engineering, Vol. II, Tokyo-Kyoto, Japan.

[6] Wells, D. L., and Coppersmith, K. J. (1994), "Empirical Relationships among Magnitude, Rupture Length, Rupture Width, Rupture Area, and Surface Displacement," Bulletin of the Seismological Society of America, Vol. 84, No. 4, 974-1002.

Pushover Analysis of Masonry Piers

Ruben Gajer, Adam Hapij, and Mohammed Ettouney

ABSTRACT

Masonry towers/piers have been used in bridge construction for hundreds of years. They are present in the construction of all types of bridge systems. The behavior of these masonry towers during seismic events is of concern to bridge owners, as well as bridge engineers. A distinctive characteristic of masonry structures is their composition of two distinct materials: the masonry blocks and the mortar. Masonry blocks can be natural stones, such as granite or limestone, oven-backed clay, or concrete blocks. Reinforcement has been used in the past to add strength., however its detailing may not be sufficient to add ductility. Any of these materials can exhibit very different engineering properties. The composition and properties of mortar also vary considerably. When dealing with older masonry towers, the effects of aging can also make the properties of blocks and mortar even more varied. The tensile strength of the mortar is much weaker that the compressive strength of both the mortar and the masonry blocks. This inherent nonlinearity of the masonry towers/piers makes it particularly difficult to approximate the seismic behavior of the masonry system using an equivalent linear (elastic) approach. For a realistic seismic analysis and safe, yet cost effective, retrofit measures, an analysis method that recognizes the basic material properties of both mortar and masonry blocks is needed.

Pushover analyses have been utilized in the recent past to address the structural nonlinearities during seismic events, in a simple manner. This paper investigates the use of pushover analysis method for the seismic analysis of masonry towers/piers. First, a baseline, high-resolution analysis method is utilized to investigate the effects of different factors on the pushover behavior of masonry piers. Second, two simplified analytical methods are introduced and their results are compared with the baseline method. It is shown that even though the computational effort of the simplified methods is much less than the high-resolution method, the simplified methods produce realistic and accurate results.

Ruben Gajer, Senior Associate, Weidlinger Associates, Inc. 375 Hudson Street Fl #12, New York, NY 10014-3656
Adam Hapij, Senior Research Engineer, Weidlinger Associates, Inc. 375 Hudson Street Fl #12, New York, NY 10014-3656
Mohammed Ettouney, Principal, Weidlinger Associates, Inc. 375 Hudson Street Fl #12, New York, NY 10014-3656

INTRODUCTION

Masonry piers have been used in many of existing bridges of all sizes. Satisfactory seismic evaluation of these piers requires accurate evaluation of the inherent nonlinear behavior of the components of the pier, i.e., masonry blocks and mortar. Many authors have studied the seismic behavior of masonry walls, Madan and Reinhorn. [1] and Taghdi, *et al.* [2]. The seismic behavior of masonry piers was studied by Azevedo, *et al*.[3], while the different computational strategies for masonry structures were summarized by Lourenco [4].

This study will apply the pushover method [5] to masonry piers. A high-resolution analysis method will be utilized to establish a base line behavior, as well as to investigate different sensitivities to specific parameters. Two simplified methods of analysis will then be introduced and compared to the baseline method. It will be shown that simplified methods of analysis can produce accurate pushover results.

PUSHOVER METHOD

Pushover method is a static nonlinear method that is intended for evaluating the lateral seismic behavior of structures. The method has the advantage of relative simplicity, while accounting for nonlinearities of the structure. Its basic approach entails applying a monotonically increasing lateral load on the structure of concern. The vertical distribution of the load remains constant; only a scalar factor that controls the magnitude of the load is increased monotonically. In addition, a vertical gravity load is also applied to the structure before the start of the lateral loading process application. As the lateral load increases, the structure behaves in an increasingly nonlinear fashion. The lateral ”pushing” continues until a control point in the structure reaches a target lateral displacement level. In addition to reaching the global target, this method allows the engineer to establish the internal state of stress and deformations of the structure

Some of the disadvantages of the pushover method are a) it accounts only for monotonically increasing static loads, and b) its results might be sensitive to the assumed lateral load distribution.

Once the capacity of the structure is established, it is compared to the seismic demand, which depends on the applied seismic load. This study will only investigate various analytical approaches to simulate the behavior of a masonry system in order to determine the structural capacity of masonry piers.

ANALYTICAL METHODS

General Description of the Masonry Pier

A typical masonry pier will have a rectangular elevation view. The height and width of the pier are H and B, respectively. The thickness of the stone pier in this study is assumed to be one block. The pier contains two components, masonry units and mortar. The masonry units are assumed to be rectangular, with dimensions h and b, respectively. The thickness of the mortar, t, is assumed to

be constant throughout the pier. The compressive strength of the stone masonry and cementitious mortar are 15 *ksi* and 2 *ksi*, respectively. The shear strength of the masonry and mortar are 1.5 *ksi* and 1.4 *ksi*, respectively. The tensile strength of the masonry and mortar are 0.6 *ksi* and 0.04 *ksi*, respectively. Finally, the modulus of elasticity of the masonry and mortar are 4,500 *ksi* and 3,000 *ksi*, respectively. The average unit weight of the pier is assumed to be 150 *pcf*. The assumed vertical distributions of the lateral pushover loading are shown in figure 1. They are a) uniform loading, b) linearly varying loading and c) concentrated loading at the top of the pier, corresponding to commonly used static load approximations of the dynamic excitation imposed by an earthquake.

High Resolution Modeling

Within this study, the high resolution modeling of masonry piers accounts for all components of the pier individually. Each masonry unit is modeled using a set of continuum, 3-D finite elements. The mortar that connects each of the masonry units is also modeled using a set of continuum, 3-D finite elements. Nonlinear material models were used for both masonry and mortar elements, with explicit crushing and cracking capabilities. Utilizing a special feature of the ANSYS computer code, [6], enabled the accurate modeling of the tensile strength of both the masonry and the mortar materials; this feature permits the elimination of any element in the model when the normal principal stresses reach the tensile strength limit. In all the case studies of this work, the tensile strength of mortar, being much lower than the tensile strength of the masonry blocks, governed the behavior of the piers.

There are two important limitations to this approach. First, it is computationally taxing as it requires the modeling of all components of the masonry structure. Second, it is not suitable for any situation where the developed cracks might close, due to load reversal. However, the pushover approach does not include any such reversal, so this limitation does not reduce the accuracy of results. Therefore, given that the computed results of the high-resolution model are accurate, it can be used as baseline for assessing simpler analytical methods.

Approximate Models: Frame Analogy

Modeling 2-D, or 3-D systems by utilizing 1-D components are known as frame analogy method. For example, Szilard [7], presented the use of beam elements to model a plate behavior. Ettouney [8], utilized one dimensional bar elements to model nonlinear reinforced concrete beams. In modeling seismic behavior of in-fill masonry walls, Madan and Reinhorn. [1] suggested a simple strut model which was validated by experimental data. In this study, the frame analogy will be utilized to simulate the pushover behavior of masonry piers.

The application of the frame analogy to masonry piers is simple; utilize a rectangular grid, figure 2, where all of the framing members are struts (resisting only axial forces). The stiffness of the struts in the model is based on an equivalent strut area of $A_{strut} = \alpha\, L\, t$, where L is the length of the strut, t is the thickness of the masonry component and $\alpha = 0.75$; the value recommended by Szilard [7]. Each strut is assumed to have an elastic-perfectly plastic force-deformation relationship. The strength of each strut is assumed to be $F_{\pm y} = \beta\, A\, \sigma_{\pm y}$. The tensile and compressive strengths of the strut are represented by $F_{\pm y}$. Also $\sigma_{\pm y}$ are the tensile and compressive yield stresses, respectively. The contributory area of each strut is A. Values

of $\beta = 0.25$ (for tension) and $\beta = 1.0$ (for compression) produced the best results for this class of problems.

Approximate Models: Beam Analogy

Upon observing the behavior of numerous high-resolution models of masonry piers undergoing a pushover loading, the following trends are observed. For taller masonry piers, with height-to-width ratios larger than 2, which are subjected to a lateral seismic load, the structure will behave as a nonlinear beam. As soon as tensile cracking develops in a particular area, that area will quickly form a plastic hinge. This plastic hinge will dominate the subsequent behavior of the pier. This raises the possibility of a simple method of modeling masonry piers as vertical beams with a specialized moment-rotation behavior of the cross section.

The limit states of the stress-strain of a masonry cross section are shown in figure 3. At rest, the stress distribution of the cross section is uniform, since only the vertical axial compressive gravity forces are in effect. As the pushover lateral forces gradually increase, the stress distribution along the cross section varies linearly along the cross section. The first limit state is when the stress at the tension-side of the pier reaches zero value. Any lateral load increase after that, the mortar will be assumed to crack under any tensile stresses; only compressive normal stresses will exist within the cross section. The next limit state is when the maximum compressive stress at the compression side of the pier reaches crushing stress level. The final limit state is reached when the resultant force affecting the cross section reaches the edge of the cross section. Beyond that, the cross section is assumed to unstable.

The stress-strain relationship of the cross-section can be summarized as $\sigma = E\ \varepsilon(e\ ,\ N)$, where σ and ε are the normal stresses and strains. The axial gravity load is N and the distance between the point of application of N and the centerline of the cross section is e. The modulus of elasticity is E. By integrating the stress-strain equation, the moment-curvature of the cross section, $M = K_{\varphi}\ \varphi(e\ ,\ N)$, can be obtained. Where M, K_{φ} and $\varphi(e\ ,\ N)$ are the cross sectional moment, the tangent bending rigidity, and the curvature of the cross section. The relationship of the moment-rotation of the cross section is $M = K_{\theta}\ \theta = \ell\ K_{\varphi}\ \varphi(e\ ,\ N)$. Where θ is the rotation of the cross section and ℓ is an assumed length of the plastic hinge. Analyses were performed with nonlinear rotational springs simulating the formation of the plastic hinges, using the moment-curvature relationships defined earlier.

RESULTS

Behavior of Masonry Piers

The sensitivity of masonry pier to different geometric and loading parameters are investigated in this section. Only the high-resolution analytical method is used for this purpose. This will help in understanding some behavioral aspects of masonry bridges. In addition, this will form a baseline of data that the results of the approximate methods can be compared to.

Effects of Dimensions of Masonry Units and Mortar

The effects of the relative sizes of the masonry units and the pier itself are studied in this section. A masonry pier with height of 56 ft. and width of 12 ft. is studied. Several masonry unit sizes were considered. The height and width of those different units are a) 2 ft. and 4 ft., b) 1 ft. and 2 ft. and c) 0.5 ft. and 1 ft. The thickness of the mortar is kept constant at ¼ in. Figure 4 shows the pushover capacity of those different configurations. It seems that the pushover capacity of the masonry pier is insensitive to the size of masonry blocks.

The effects of the mortar size are investigated in figure 5. The same 56 ft. by 12 ft. pier is considered, with masonry block sizes of 2 ft. by 1 ft. Three sizes of mortar were investigated. They are ¼ in., ½ in. and ¾ in. From figure 5 it is evident that the pushover capacity of the pier is insensitive of the mortar thickness.

Effects of Dimensions of Piers

The sensitivities of the pushover capacities to the dimensions of the masonry pier are shown in figure 6. All the masonry piers in the figure have a width of 12 ft. The heights of the piers are 56 ft., 34 ft. and 12 ft. The pushover capacity of the different piers varies considerably, as shown in figure 6. As expected, higher piers are more vulnerable to lateral loads than shorter piers.

Effects of Load Distribution

The three pushover lateral load distributions of figure 7 are applied to a masonry pier with height and width of 56 ft. and 12 ft., respectively. The masonry pier is sensitive to the vertical distribution of the lateral load, as shown in figure 7. Extreme care is needed when selecting a pushover distribution of the lateral load along the height of the pier. In some cases, more than one loading profile should be considered. Also, if there is any concentrated mass that is attached to the pier, such as a tributary portion of a bridge deck, the relative magnitude of the pushover force that results from this mass should be carefully accounted for in the analysis.

Comparison of Methods

In comparing the different analytical methods, only 56 ft. by 12 ft. pier is considered, with masonry block sizes of 1 ft. by 2 ft. A mortar thickness of ¼ in. connected those masonry blocks. A uniform vertical lateral load distribution was utilized in the pushover comparisons.

Figure 8 shows a comparison of the pushover capacity of the high-resolution method and the frame analogy method. There is a good agreement between the two methods. Figure 9 shows a comparison of the pushover capacity of the high-resolution method and the beam analogy method. A good agreement is also observed. The assumed length of plastic hinge that produced this good agreement is $\ell = 0.01\,B$. Note that Paulay and Priestley [9] indicated that the extent of plastic hinges in reinforced concrete beams are on the order of $\ell = 0.5\,B$. The difference between the masonry piers and the reinforced concrete beams is that the masonry pier that was considered in this study is brittle, with no reinforcement, thus limiting the length of the hinging,

i.e, all the rotation demand is concentrated in a localized region. For reinforced masonry piers, typically the length of the plastic hinge will be longer.

CONCLUSIONS AND RECOMMENDATIONS

The pushover behavior of masonry piers was studied. It was found that the pushover capacity of masonry piers is insensitive to relative sizes of masonry blocks as well as mortar thickness. The height to width ratio of the pier and the vertical distribution of the pushover lateral load were found to have considerable effects on the pushover capacity of the piers.

Two simplified methods of analysis were compared with a high-resolution finite element method. The frame analogy and the beam analogy methods were found to produce good agreement with the high-resolution method. It should be noticed that care is needed when assigning factors that control the results of both simple methods.

For future research work, the behavior of 3-D masonry piers using any / all of these methods needs to be studied. For simplified methods, the magnitude of the controlling factors such as, α and β needs to be further investigated. Finally the additional studies are required to investigate the effects of simulating reinforcements in masonry, for example steel rebars or carbon fibers.

REFERENCES

[1] Madan, A. and Reinhorn, A. M. 1998. "Modeling of Masonry Infill Panels for Structural Analysis," *J. of Structural Engineering, ASCE,* 123(10):1295-1302.

[2] Taghdi, M, Bruneau, M., and Murat S. 2000. "Analysis and Design of Low-Rise Masonry and Concrete Walls Retrofitted Using Steel Strips," J. of Structural Engineering, ASCE, 126(9)

[3] J. Azevedo, G. Sincraian, J. Lemos. 2000. "Seismic Behavior of Block Masonry Structures," Earthquake Spectra, 16(2): 337-365.

[4] Lourenco , P.J.B.B. 1996. "Computational Strategies for Masonry Structures," Proefschrift, Department of Civil Engineering, Delft University, Netherlands.

[5] Applied Technology Council 1996. "ATC-40 : Seismic Evaluation and Retrofit of Concrete Buildings," Report, SSC 96-01, California Seismic Safety Commission: Proposition 122 Seismic Retrofit Practices Improvement Program.

[6] SAS IP, 2001. ANSYS ® Release 6.0 UP20010919.

[7] Szilard, R. 1974. *Theory and Analysis of Plates: Classical and Numerical Methods.* Englewood Cliffs, NJ, Prentice-Hall, Inc. pp. 253-269.

[8] Ettouney, M. M. 1979. "Inelastic Analysis of Plane Stress Problems," Proceedings of Fifth International Conference on Structural Mechanics in Reactor Technology, Berlin, West Germany.

[9] Paulay, T. and Priestley, M.J.N. 1992. *Seismic Design of Reinforced Concrete and Masonry Buildings*.New York, NY: John Wiley & Sons, Inc., pp.135-146.

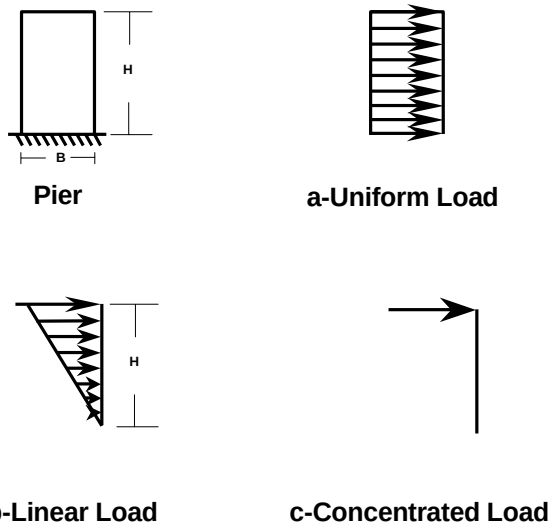

Figure 1. Vertical Distributions of Pushover Loads

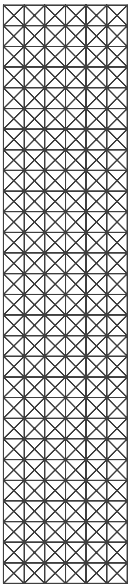

Figure 2. Frame Analogy

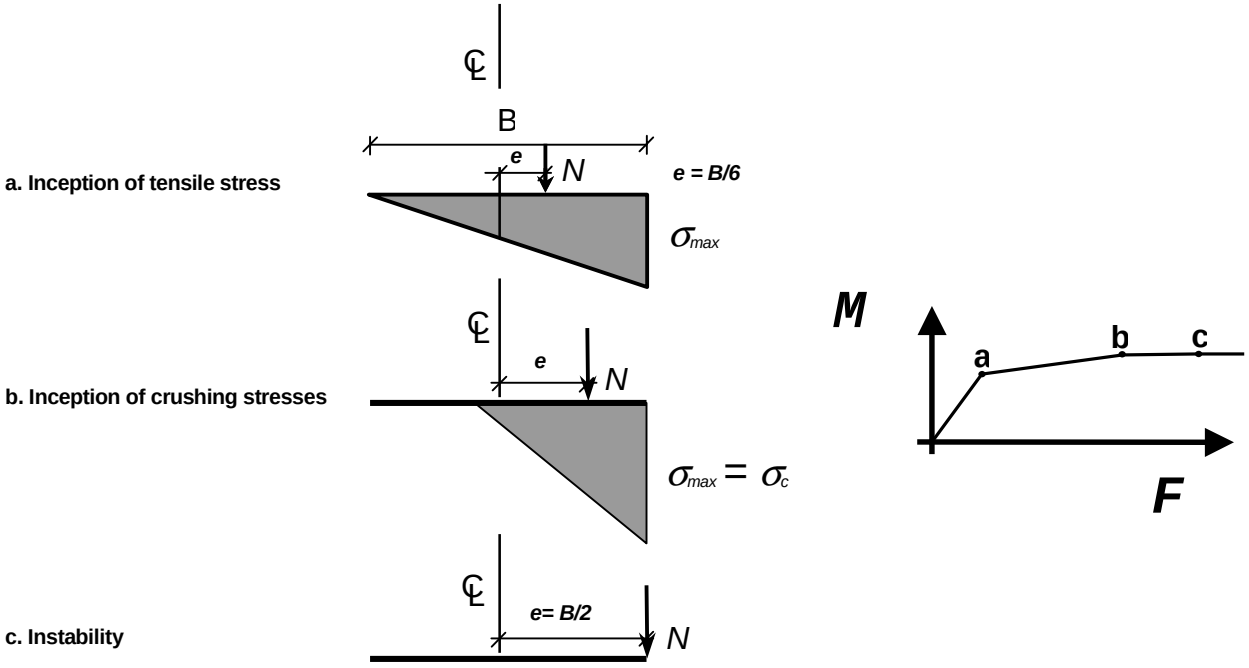

Figure 3. Limit States of the Stress-Strain of a Masonry Cross Section

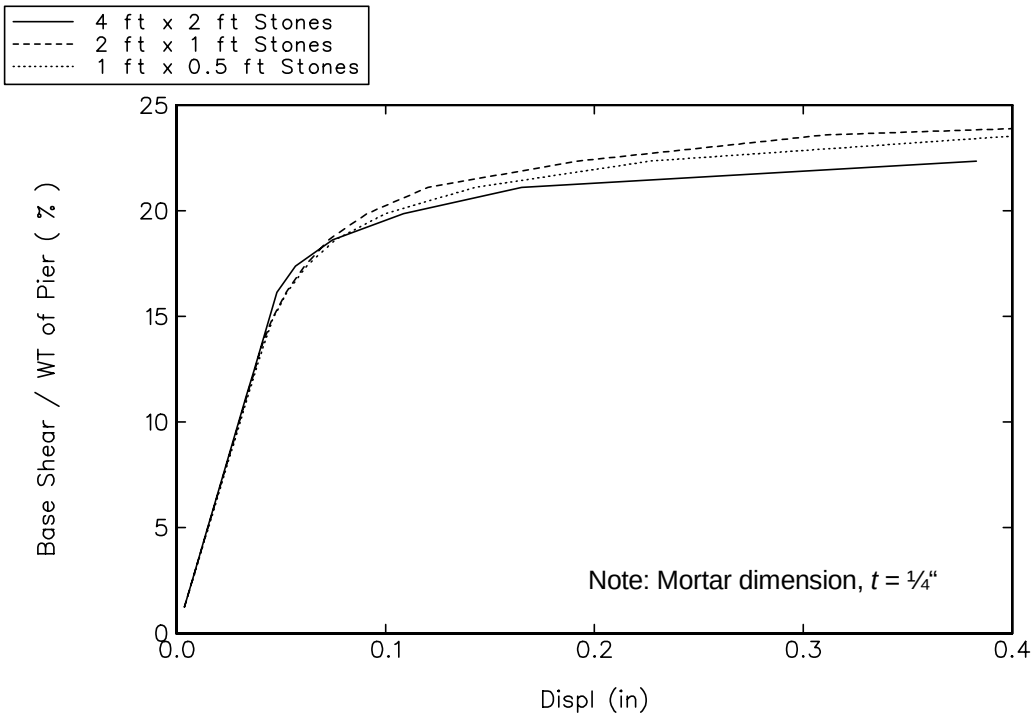

Figure 4. Effect of Dimensions of Masonry Units

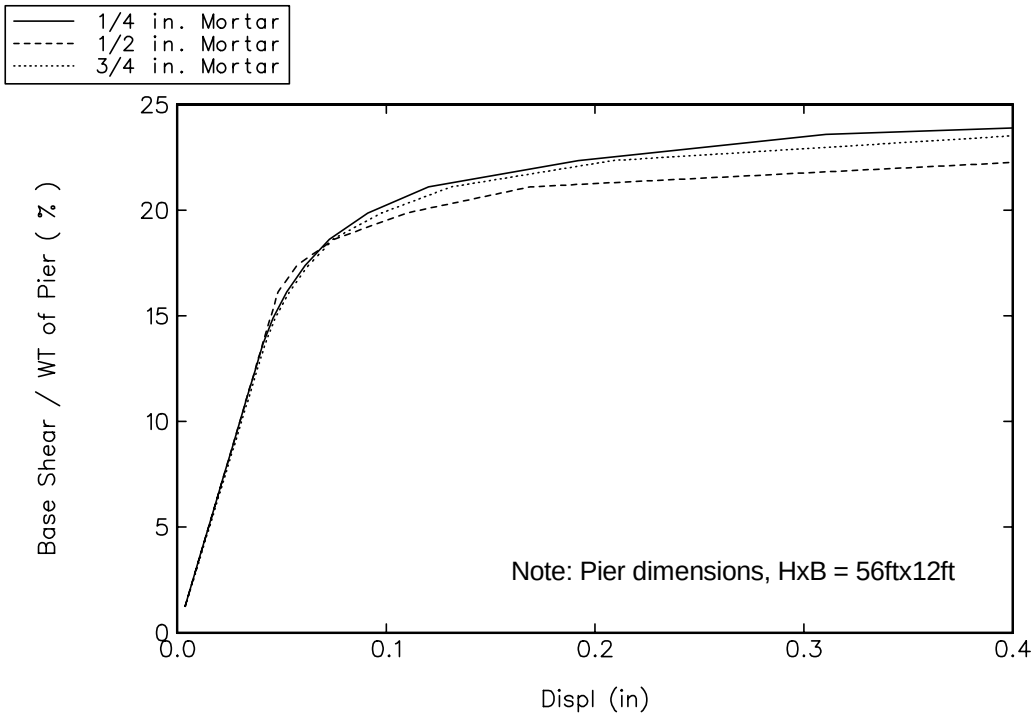

Figure 5. Effect of Dimensions of Mortar Size

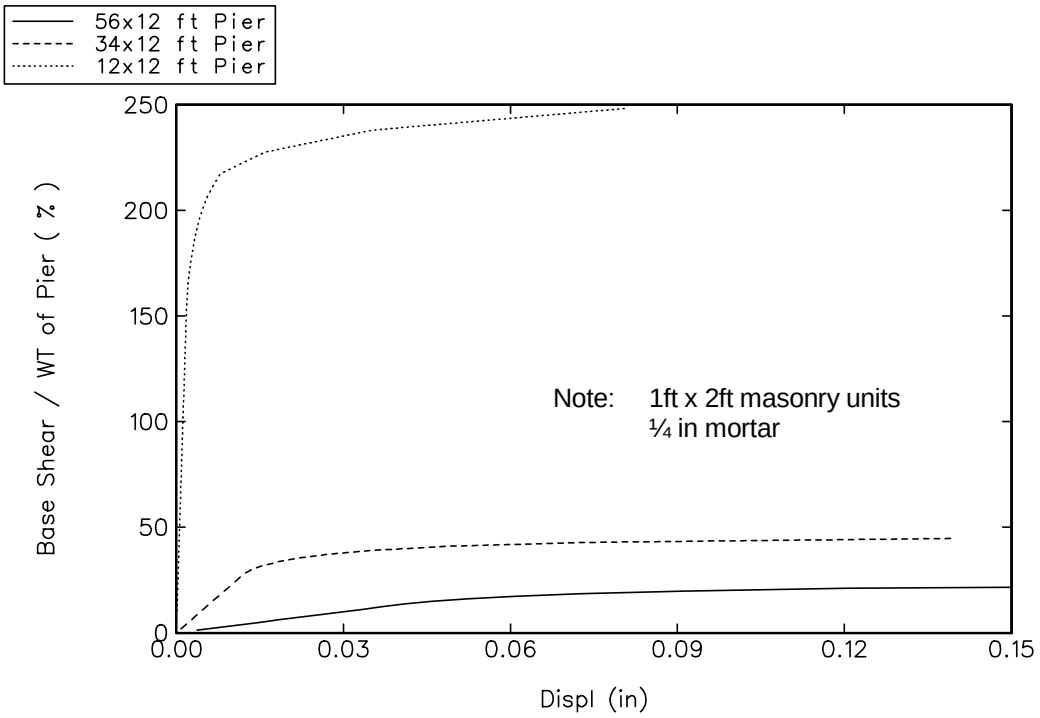

Figure 6. Effect of Dimensions of Pier

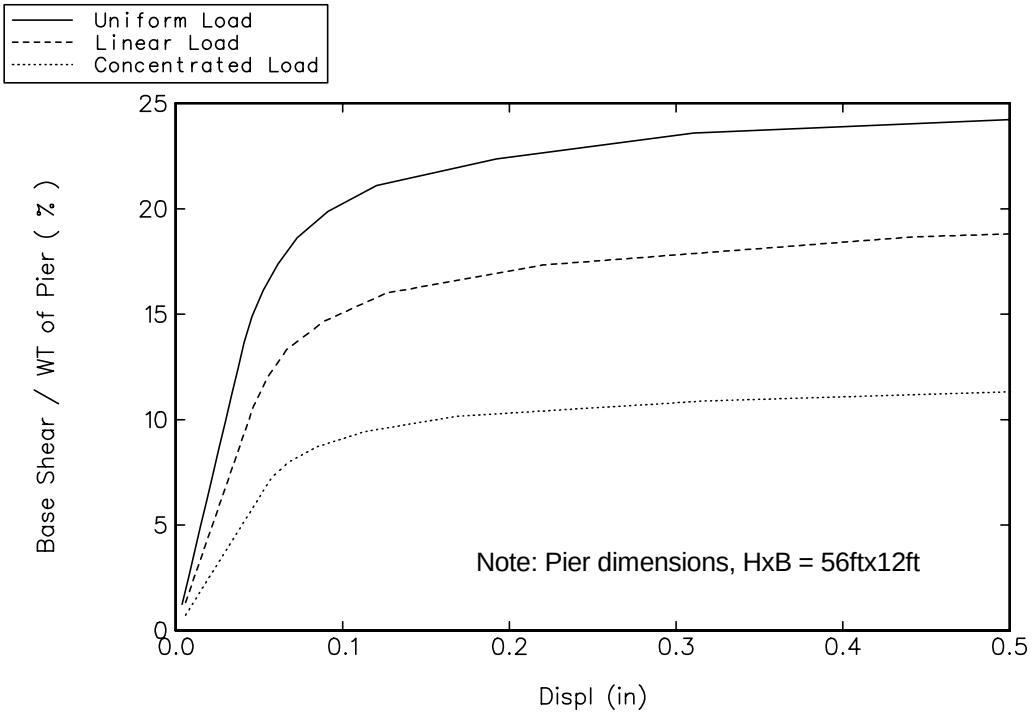

Figure 7. Effect of Vertical Distribution of Pushover Loads

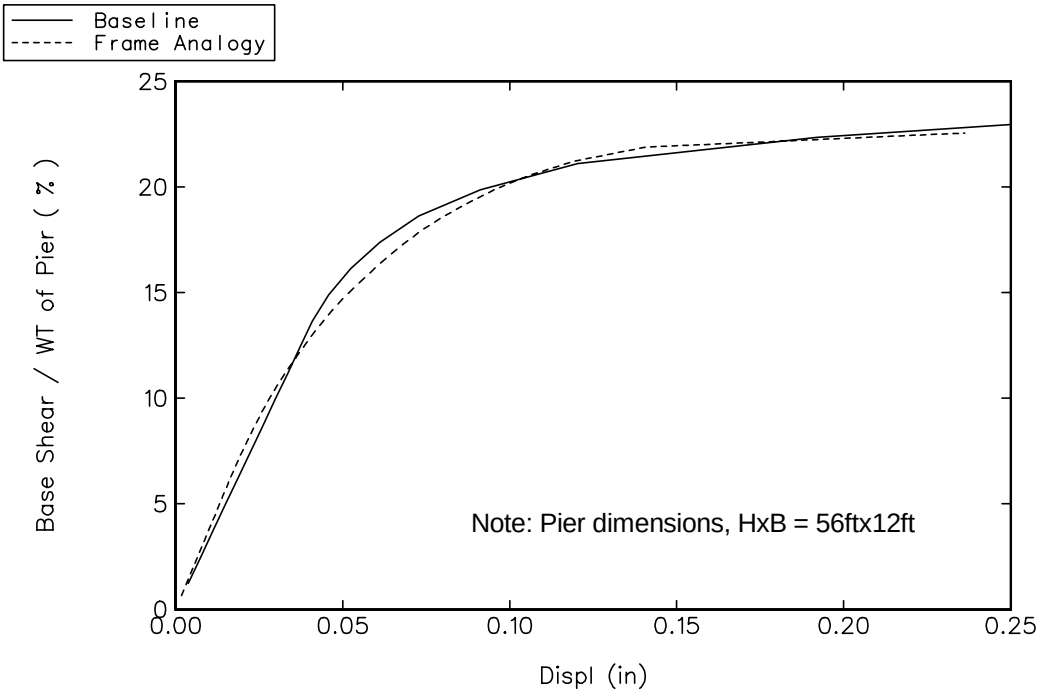

Figure 8. Comparison of Frame Analogy with Baseline

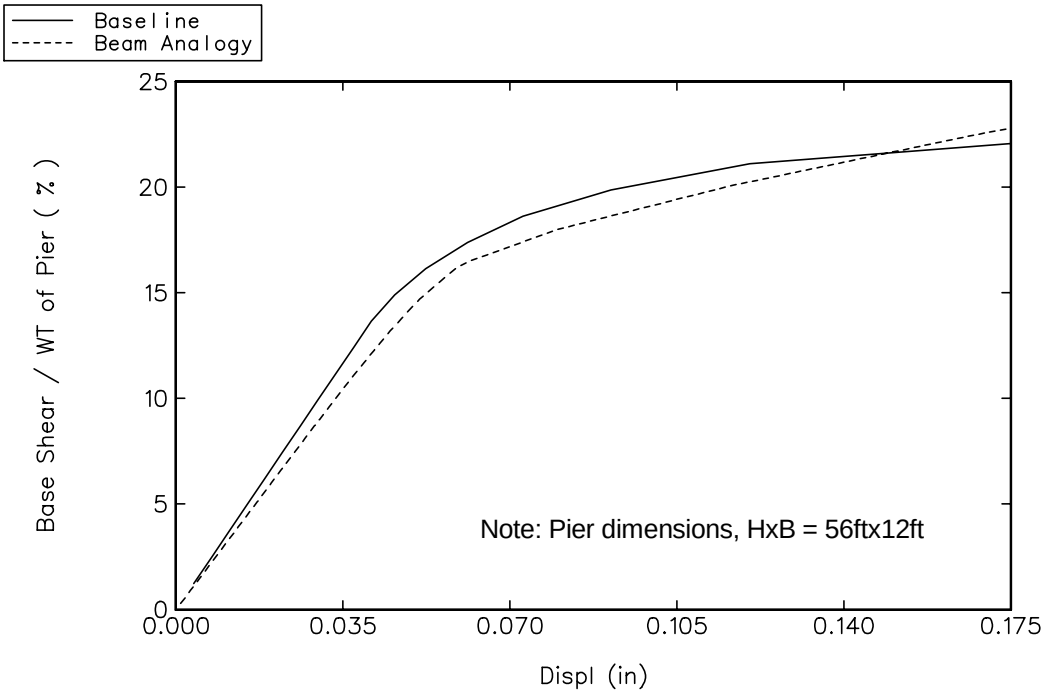

Figure 9. Comparison of Beam Analogy with Baseline

Innovative Designs of Seismic Retrofitting The Posey & Webster Street Tubes, Oakland/Alameda, California

Thomas S. Lee[1], Thomas Jackson[1], and Randy R. Anderson[2]

ABSTRACT

This paper presents state-of-the art and practice for an innovative seismic retrofit of the Posey and Webster Street Tubes in the San Francisco Bay area. The tubes are immersed tunnels, connecting Oakland with the Island of Alameda, California. The tubes are located between two major faults, Hayward Fault and San Andreas Fault in the State of California, both capable of generating horizontal ground acceleration of about 0.5g at the site. The Loma Prieta earthquake in 1989 with an estimated horizontal ground acceleration of about 0.2g at the site was the most recent major seismic event that occurred near Posy-Webster Street Tunnels. Caltrans officially recognized these two tubes as candidates for retrofit in the comprehensive seismic retrofit program for highway structures throughout California.

This paper will discuss the innovative design of seismically retrofitting the two tubes. Liquefaction of the hydraulically placed backfills could cause buoyancy of the tubes with the resulting displacements causing catastrophic failure of the tubes' precast joints. Two different design approaches are used to mitigate liquefaction potentials. For the Posey Tube, the design involves installing jet grout columns to create cut-off walls adjacent to the tube to prevent potential buoyancy of the Tube during and after a M-7.25 earthquake. This design is innovative as it isolates the liquefied soil from flotation by the jet grout walls, and is considered to be first of its kind to be employed in an immersed tunnel. For the Webster Street Tube, two methods of installing stone columns are used to densify sandy soils surrounding the Tube; one is the called the Pipe-pile method and the other the bottom feed vibroflotation method. The Pipe-pile method is believed to be the first of its kind to be applied to densify soils adjacent to an immersed tube in the world. The bottom feed vibroflotation method, though used to stabilize loose soils, has never been employed to densify soils surrounding an immersed tube in the U.S.

To verify the design concept and the constructibility of the three methods, a demonstration program was instituted and implemented by the State of California Department of Transportation in the summer of 2000. Results of the demonstration program have been incorporated into the Phase I construction where the joints between precast segments and the joints between the tubes and portal buildings are being released to allow displacements and limit the forces. This paper will also present some of the findings and recommendations of the demonstration program as well as the joint repair work performed at the site.

[1] Thomas S. Lee and Thomas Jackson, both Senior Professional Associates of Parsons Brinckerhoff Quade & Douglas, Inc., San Francisco, CA.

[2] Randy R. Anderson, Design Contract Manager, California Department of Transportation, Sacramento, CA.

PROJECT DESCRIPTION

The Posey and Webster Street Tubes are two immersed tunnels carrying vehicular traffic between Oakland and Alameda in the San Francisco Bay Area, California as shown in Figure 1. Caltrans, the California Department of Transportation, under the seismic retrofit program, determined that the structures would be subject to liquefaction damage during a 7.25M level event along the Hayward Fault. Subsequently, a consortium led by Parsons Brinckerhoff of San Francisco, California was retained by Caltrans to carry out an extensive seismic study on the two immersed structures and to provide recommendations for the seismic retrofit of the two tubes. Tasks included performing a detailed seismic evaluation of the sites, developing and presenting alternative retrofit strategies.

PROJECT BACKGROUND

The project consists of two immersed tube tunnels, each carrying two-lane vehicular traffic between Oakland and Alameda, California. The tunnels were constructed in different time periods about 30 years apart, but are nonetheless, remarkably similar.

The Posey Tube was constructed in 1928 – the first highway immersed tube tunnel in the world at that time. George A. Posey, the chief engineer for the former California Highways, designed the tube. The construction was started by dredging a trench across the Oakland Estuary. Pre-fabricated, 37-ft diameter cylindrical concrete tubes were placed and connected to each other. Each segment of the tube is 200 feet in length and consists of a reinforced concrete ring of 2.5 feet thick. In addition, a collar and a bracket were provided at each end of the segment. The trench was then backfilled with dredged material from the bay. The backfill, consisting of soft clay and loose sand, was dumped from barges over the Oakland estuary. The backfill serves as a protection to the tube from possible damage by shipping crossing over the tube and to furnish sufficient weight to provide a reasonable of safety to resist hydrostatic uplift. Loose sand bedding fill was placed below the tube to facilitate construction of the tube.

In the 1950s, the Port of Oakland required that the estuary be deepened. As the Posey tube relied upon the backfill overburden pressure to prevent flotation, it was necessary to remove backfill and replace with a thinner 4-ft thick layer of heavy iron ore (magnetite) constructed in stages. The iron ore aggregate, with a maximum size of 1.25 inch, was mixed with sand to obtain a maximum density. The side slopes of the iron ore were reported to be at 45 degrees.

The Webster Street tube, which is parallel to the Posey tube, was completed in 1963. The design was almost identical to that for the Posey tube, even including the iron ore backfill to counteract the flotation at the estuary. The trench backfill for the Webster Street tube was composed of barge-dumped clean sand fill with silt; no attempt was made to densify the fill and the iron ore aggregate. Loose sand bedding fill was also dumped to facilitate laying of the tube segments.

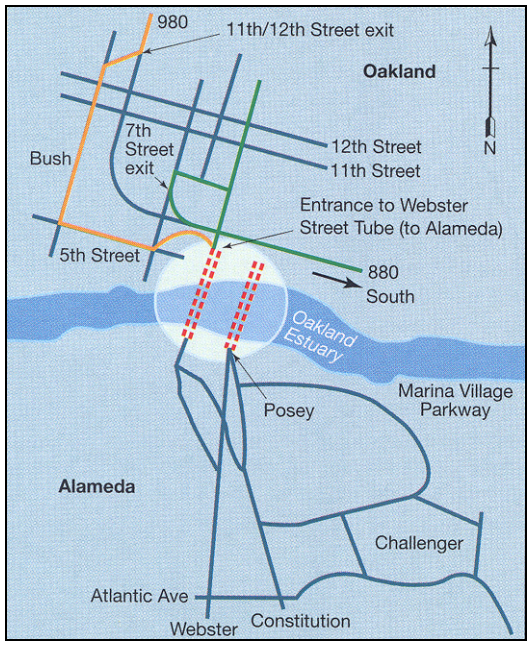

Figure 1 Site Location Plan [1]

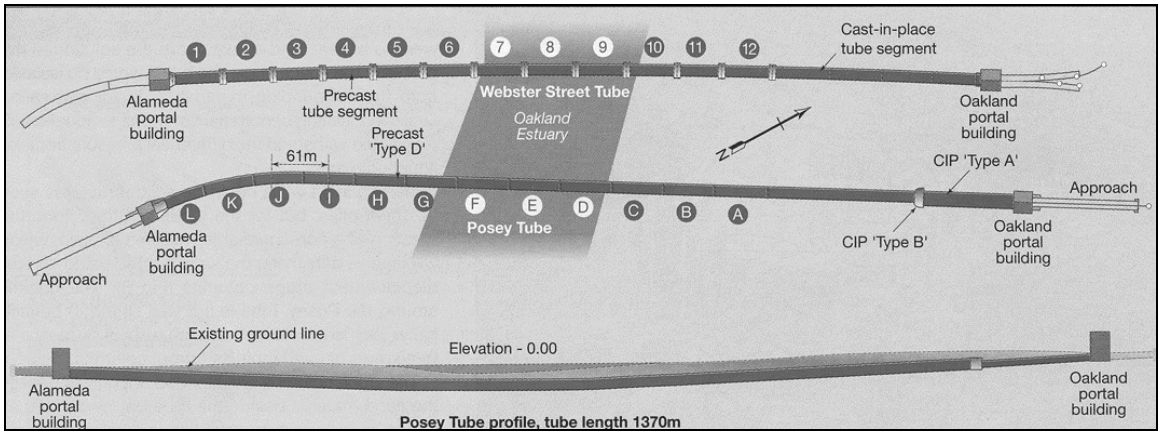

Figure 2 Site Plan and Profile [1]

The Webster Street tube backfill along with the sand bedding fill around the bottom of the tube, consisting of loose sand with an average of SPT blowcounts of less than 10 would most likely liquefy in major earthquakes, posing severe danger that the tube would float. In 1989, the Loma Prieta earthquake caused modest liquefaction damage to a bulkhead above the Alameda Landing of the Webster Street tube. Liquefaction spouts and back displacements were also seen above the adjacent Posey tube. It was estimated that the horizontal ground acceleration of about 0.2g was felt at the site and minimal damage to the tubes was noted.

Although the two tubes are not the only lifelines to Alameda from Oakland, California, they are heavily used; and the transportation between Oakland and Alameda would be severely impacted by a disruption in service of the tubes. Consequently, the

two tubes were officially recognized by Caltrans in 1995 as candidates for seismic retrofit under a comprehensive seismic retrofit program for highway structures throughout California.

RETROFIT DESIGN

A number of options were considered to stabilize the loose to soft backfill surrounding the two tubes, thereby mitigating potential liquefaction and arresting flotation of the tubes. Two basic approaches can be adopted; one is to improve conditions of the ground such that it would not liquefy, and the other is to permit liquefaction, but to prevent flotation of the tubes by confining the liquefied material within impermeable or highly densified zones. This approach is hereby called the isolation principle.

Improving Soil Conditions of the Tubes

1. Densifying the sand backfill material by vibroflotation and other means may seem to be a method, but it cannot reach the loose sand bedding fill immediately below the tubes. In addition, densifying the material under the tubes would cause settlements.
2. Grouting the backfill material from the ground or the estuary could be a solution. However, great difficulty was foreseen in reaching the materials below the tubes with directional drilling.
3. Grouting from inside the tube bottom would be a difficult task in view of the tight space in the lower plenum and the possibility of drilling numerous grout holes in the tubes under 75 ft water pressure, the operation of which could exacerbate the structural integrity of the tubes, but also a single failure of the process could flood the tunnel.

Isolation Principle[1]

For an immersed tube tunnel to move upward in a liquefied soil mass, the liquid must be able to flow under the tube as it moves up (Figure 3). If this mechanism is prevented, the tube would not float, even if the soil under the tube were to liquefy. Thus was born the isolation principle [1]. The space under the tubes can be isolated from the surrounding material by building “isolation” walls, consisting of material that would not liquefy and that would withstand differential pressure from the liquefied mass. The isolation walls can be sheet piles, but for the Webster Street Tube which is surrounded by sandy backfill, a non-liquefiable wall consisting of vertical displacement stone columns is adopted. According to Mitchell (1994) [2], soils most suitable for densification by vibroflotation method should:

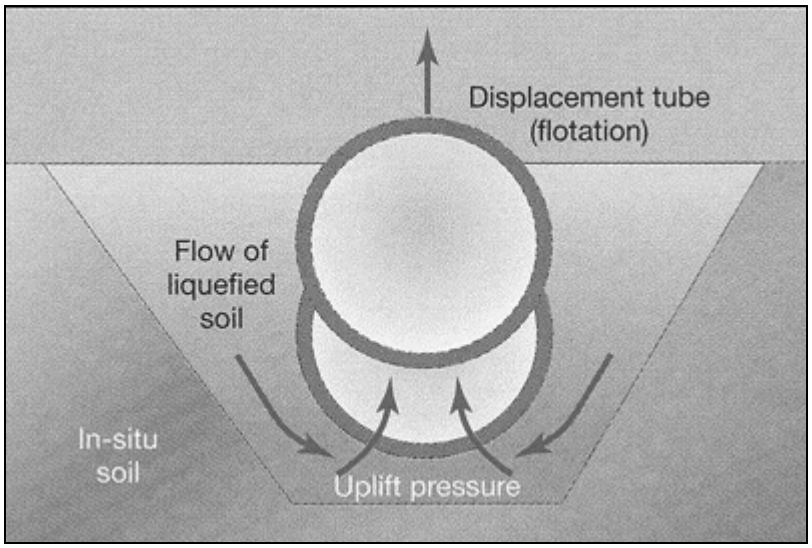

Figure 3 Potential Flotation Mechanism of the Tube [1]

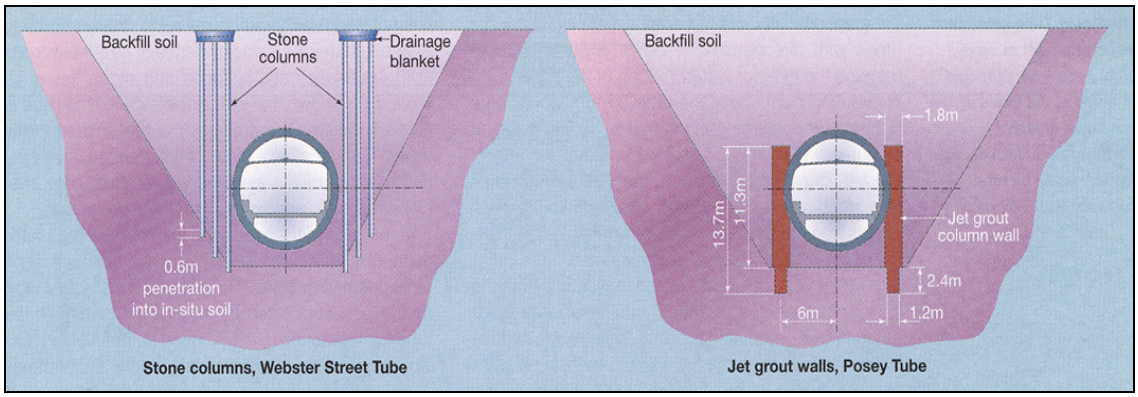

Figure 4 Isolation Walls for the Two Tubes [1]

1. Be granular and free draining with $d_{10} > 0.03$ mm;
2. By the Cone Penetration Test (CPT) have: Friction ratio <1% and Cone tip resistance greater than 50 tsf (if <50 tsf, likely to indicate silt, clay, and organic material).
3. Have coefficient of permeability $k>1 \times 10^{-4}$ cm per second.

Besides the vibroflotation method, there are other methods available to densify the sandy soils. One of them considered for design is called the Pipe Pile Stone Column Method which can densify the sandy soils via displacement and vibration actions of the pipe pile.

The stone columns are also intended to act as vertical drains, quickly relieving the high water pressures generated during major earthquakes. The backfill surrounding the Posey Tube is composed of clays and lenses of sand and is considered not to be suitable

for densification using stone columns. Here, the isolation walls consist of a row of continuous jet grout columns at each side of the tube.

The isolation principle to be used here to prevent flotation is unique in the sense that it has never been used to seismically retrofit immersed tubes in the U.S. But there is some evidence of its effectiveness based upon Japanese case histories and model tests. One drawback is that, although the tube will not float as a result of liquefaction, the liquefied sand below the tube will reconsolidate after major earthquakes and some settlements will occur.

The liquefiable materials below the tubes are about 5 to 7 feet thick and the reconsolidation pressure is very small. The tubes are relatively quite rigid and in part supported by clusters of piles at the tube joints, which were employed for positioning during construction. In addition, large volumes of tremie concrete were used to make the tube joints. As a result, it is expected small settlements will occur which would not damage the structural integrity of the tubes.

Seismic Vulnerabilities of the Tubes

The overall seismic retrofit of the Posey and Webster St. Tubes identified a number of seismic vulnerabilities of the tubes and adjacent structures. Design criteria provided a performance standard that tubes must remain open for 30 minutes following a maximum credible event on the nearby Hayward Fault. The primary vulnerability is the uplift of the tube that could be caused by liquefaction of the hydraulically placed backfill material. Secondary vulnerabilities were also identified based on results of the time history analyses performed on the tubes. The primary vulnerability can be dealt with by stabilizing the soils surrounding the tubes using the isolation principles above. The secondary structural vulnerabilities will be briefly described as follows.

Due to ground motions propagating across the estuary, the tubes may be forced into a wide range of deformations. The most serious deformations cause significant axial, shear and flexural stresses in the concrete tube structures. The tubes are composed of twelve precast concrete large diameter pipe segments. Each of the 32 ft. diameter segments is 200 feet long. The joints between segments were formed by placing tremie concrete collars around the outside of the sealed joints as well as casting a reinforced concrete inner sleeve through the joint zone. The joints provide a slight irregularity in stiffness so stresses accumulate at the joints. The analysis results indicate that the most serious internal stresses are the tension stresses in certain reaches in the tubes. These tension stresses could cause uncontrolled cracking in the segments and particularly at the segment joints. The same longitudinal ground movements force a very substantial reaction at the portal buildings. The analyses results indicate that the reaction at the portal buildings can exceed 100,000 tons. This force is not just a brief spike, but a full contact pulse lasting for 1.5 to 2 seconds. Such a force would shatter the portal buildings. Shear stresses in the tubes were found to be within the structure capacity. Flexure stresses were high and barely within capacity of the un-retrofitted structure.

Our solution to the high stress buildup was to introduce releases into the structural system. The releases will limit the stresses and concentrate the deformations by allowing the structure to move with the ground in shorter segments. This approach also significantly reduces flexural stresses. In order to create the releases, a new secondary

flexible water seal system was required. Further the shear capacity through the released tube joints had to be maintained to limit relative transverse displacements. Details were developed for installing new water seals at selected segment joints and including those seals within a heavily reinforced concrete and steel shear ring.

In order to release the potential reaction at the portal buildings, the tube had to be physically separated from the buildings at each end. At the same time, traffic, ventilation, lighting, drainage and other services have to be maintained. To provide the separation details were developed to cut a slot through the tubes including the roadway and plenum concrete slabs. Larger versions of the joint seals were required to accommodate up to 6 inches of compression movement as well as some exterior waterproofing. Further, special ground improvement in the form of jet grouting has been incorporated to help provide vertical support to the ends of the tubes. Additionally permeation and compaction grouting have also been used to reduce potential water flow against the new joint seals.

DEMONSTRATION PROGRAM

To verify the effectiveness and overall constructibility of the isolation wall principle discussed above, a demonstration (demo) program was instituted in August 2000. The program consisted of two sites. The jet grout columns were conducted at the Jack London Square over the Posey Tube. The stone columns, which used vibroflotation and pipe pile methods, were installed over the Webster Street Tube at the Marina Square in Alameda. The two sites were chosen in areas where effects on local traffic could be kept to a minimum by the construction works. Both sites were located on a parking lot.

Another goal of the Demonstration Program was to verify the parameters used for design of the jet grout columns and the stone columns using the vibroflotation and pipe pile method. Design requirements stated in the contract are as follows:

Tube	**Soil Type/Method**	**Property/Test**	**Design Value**
Posey	Clay/Jet Grouting	Compressive Strength/ Unconfined Compressive Strength Test	600 psi
		Permeability/Packer Test	<1 Lugeon
Webster	Sand/Pipe Pile Stone Column	Standard Penetration Test	$(N_1)_{60}$ ≥25bl/ft
		Cone Penetration Test (CPT)	Q_{nc} ≥ 125 tsf
	Sand/Vibroflotation Stone Column	Standard Penetration Test	$(N_1)_{60}$ ≥30bl/ft
		Cone Penetration Test (CPT)	Q_{nc} ≥ 150 tsf

[1] $(N_1)_{60}$ stands for SPT blow count corrected for overburden effects to 1 tsf and for energy effects to an energy ratio (ER) of 60%.
[2] Q_{nc} represents cone tip bearing resistance in tsf.

Posey Tube

For the Posey Tube, which is surrounded mainly by soft silty clays with lenses of sand, a row of twelve 6-ft diameter jet grout columns were installed at a selected area on

the Jack London Square Parking lot. The jet grout columns were spaced at 4.5 feet center to center, resulting in an overlap of 1.5 feet between two columns. For anchorage purposes, the jet grout columns were drilled to at least 8 feet into firm native soils prior to the start of jet grouting.

The jet grout columns were installed in August 2000. The jet grouting technique employed by the Contractor to construct the jet grout columns is called the "double fluid" jet grouting which utilized ultra-high pressures (typically 5,800 to 8,700 psi) to impart energy to an air/grout fluid stream that was injected into the soil at a velocity of about 800 to 1,000 feet per second. The high speed fluid cut and mixed the in situ soils with a cementitious grout mixture. During the grout injection process, columns were formed when the drill rods were continuously rotated while simultaneously lifting the drill string. The most distinctive feature of the double fluid jet grouting system is the simultaneous injection of high velocity grout within a cone of compressed air. The introduction of compressed air around the cutting jet was capable of creating columns of up to 6 feet in diameter.

The design depth to the bottom of each jet grout column varied from 86 feet to 89 feet including 8 feet into the firm native ground. Prior to construction of the 12 production jet grout columns, four test jet grout columns were installed using different sets of installation parameters and were subsequently exposed for visual inspection. Construction of the production jet grout columns was carried out using the same installation parameters as determined from the test columns. Drilling of the columns to the required depths was very easy, indicating the soft to very soft nature of the clayey backfill adjacent to Posey tube. Drilling of each column typically took approximately 10 minutes. Grout jetting of the columns took about 100-120 minutes per column. Estimated grout take of each of the 12 production columns ranged from 29 to 33 cy.

Substantial ground heave up to 2.5 feet was observed during construction of the 12 production columns. This was because the top of the jet grout columns was only two to three feet below ground surface and the ground was "lifted" by the shroud of air/grout under high pressure. However, much less ground heave (less than 0.5 inch) was noted at the drilling rig west side of the production columns as the weight of the rig counteracted the "uplift". In conjunction to the ground heave, cracks and bubbling water were noted on the asphalt pavement of the parking lot area during construction. Cracks as far as about 30 feet from the production columns were observed.

To determine the overall structural integrity of the jet grout columns, coring of selected jet grout columns was made following completion of the columns. The percent recovery of the cores was typically greater than 90 percent, except for the core performed in the center of one column which had very poor recovery. Cores often broke at sandy to gravelly seams. In general, the percent RQD in core runs was much lower than the percent recovery. Rock Quality Designation (RQD) is a measure of rock quality and is calculated for each core run (typically 5 feet). RQD typically ranged between 20 to 50 percent.

All the soilcrete cores taken from the production columns achieved a minimum compressive strength of 600 psi as in accordance with the Contract design requirement. The maximum compressive strength measured is about 1,970 psi which is comparable to lean concrete. Bulk density varied from 96 to 105 pcf, indicating that the soilcrete is not as heavy as typical grout cubes. This is because soilcrete formed in situ is a hybrid of

clayey to sandy soils and cement grout coupled with voids full of air, and hence renders an overall lighter material. In addition, the soilcrete formed by the double fluid system has a higher air content and hence has the lowest compressive strength among other jet grout systems.

In conjunction to coring, packer tests were performed to determine the overall tightness of the jet grout columns. A total of four tests were done in selected cored holes. For assessing the tightness of the jet grout column, 1 Lugeon (LU) is used as an impermeabilization criterion for the cut-off wall. The test results, in general, indicated that the soilcrete mass is essentially tight to very tight with less than 1 LU and is therefore considered to be highly impermeable.

Webster Street Tube

The existing soils surrounding the Webster Street tube are composed of loose to very loose sandy backfill placed during construction of the tube. The trench backfill was believed to have been dumped in place by barges without any compaction. Pre-construction borings and cone penetrometer tests indicated that the sandy backfill is loose to very loose with average blow counts of 4 blows per foot and that silt contents increased at depths of 40 to 60 feet. Below the trench backfill is the firm to compact native fat clays to silty clay with consistency being medium stiff to stiff. Tip resistance decreased gradually with depth from more than 150 tsf in the top 5 feet to less than 10 tsf at a depth of 60 feet.

Stone Columns

Stone columns consisting of subsurface columns of graded aggregates were constructed at the Webster Street tube using “pipe pile” method and vibroflotation method to densify existing soils and provided drainage of pore water in the soil mass.

Pipe Pile Method

Pipe pile method used in the Demonstration project, involved driving a 18-inch diameter closed end steel pipe with a give-away end plate (sometimes called as boot plate) to a predetermined depth of about 70 feet, filling the pipe with stone aggregate from the top via a hopper and then withdrawing the pipe with a vibratory hammer. This procedure is continued until the column is filled with stone to the ground surface. The Pipe Pile method densifies the loose sandy trench fill by displacement (via a impact hammer Delmag-D46) and dynamic vibratory action (via vibrating hammer 200-C) and results in the stone columns in place that are clean and uncontaminated. The pipe pile equipment utilized a fixed lead system to guide the driving of the pipe pile to ensure an overall verticality of the stone columns which were only 1.5 feet away from the edge of the Webster Street tube.

Pipe pile method to install stone columns has been employed previously in relatively small sites which are prone to liquefaction potentials. It is believed that the use of this method to stabilize sandy soils adjacent to an immersed tube such as the Webster Street tube is first of its kind in the U.S., and may also be one of its kind in the world.

Nineteen stone columns, each 1.5 ft in diameter, were installed on the west side of the Webster Street Tube at the Mariner Square site in Alameda. Two phases of installation were conducted; the first phase consisted of constructing ten stone columns at a predetermined triangular grid pattern of 4.5 feet and at a pipe withdrawal rate of 3 to 7 feet per minute. The second phase involved in nine stone columns installed in a much lower rate of withdrawal of the vibrating pipe, i.e., the pipe was withdrawn at a rate of 2.5 feet per minute and maintained with vibration without extracting at each 5-ft interval for one minute.

Comparisons between pre- and post-construction $(N_1)_{60}$ (Figure 5) indicate that the existing fine sands to silty fine sands have been significantly densified by the pipe pile stone columns using a much slower rate of pipe withdrawal. The data further reinforce the notion that sandy soils can be substantially densified by the vibration effects of the pipe pile installation. In other words, the more vibration imparted to the sandy soils, the higher is the densification.

No apparent increase in overall densification in the native silty clays below the depth of 60 to 62 feet. The lack of densification in the native silty clays is expected as the displacement and vibration of the steel pipe pile could not increase the consistency of the silty clays.

Vibroflotation Method

Vibroflotation method is another approved method used to install the stone columns adjacent to the Webster Street Tube at the Mariner Square site in Alameda. The vibro-displacement method is used to construct the stone columns. This method is a dry, top feed or bottom feed method that involves using a vibrating probe (sometimes called vibro-flot or vibro-probe) without the use of jetting water to advance a hole. For short columns, the stone can be fed into the annulus created by the vibrating probe from the ground surface – which is called the top feed method. For deeper stone columns, just like the ones proposed for the Demonstration project, the stone is fed into the bottom of the vibrating probe through an auxiliary tube – which is therefore called as the bottom feed method. The stone delivery is assisted by compressed air. The vibrating probe densifies and compacts the surrounding soils from the lateral force that is developed by rotating eccentric weights.

Seventeen stone columns, each of 2 feet in diameter, were constructed by means of the dry, bottom feed vibroflotation method. They were located on the west side of the Webster Street Tube at the Mariner Square site in Alameda (Figure 1). These stone columns were performed in two phases; nine in Phase 1 and eight in Phase 2. The sequence of the installation was to construct the first row adjacent to the tube first, then the second and third rows away from the tube. Pre- and post-construction borings and CPTs were made prior to and upon completion of each of the two phases of vibro stone columns to evaluate the effect of the construction.

Phase 1 vibro stone columns were spaced at 6 ft and 8 ft on centers while Phase 2 vibro stone columns at 10 ft and 12 feet. The purpose of these two phases was to determine the optimal spacing of the vibro stone columns.

Comparisons between post-construction $(N_1)_{60}$ and pre-construction $(N_1)_{60}$ (Figure 6) indicate that the existing fine sands to silty fine sands have been significantly

densified by the vibro stone columns. $(N_1)_{60}$ at post-construction borings ranged from 23 to 52 blows per foot which is much higher than the design values..

On the average, higher blows were obtained from the boring which is located at the center of a 6-ft triangular grid than those from that located at the center of an 8-ft triangular grid (Figure 6). Much more densification was obtained at the top 40 feet where the existing soils are basically sandy materials than that between depths of 40 and 60 feet where the existing soils are more silty in nature. No apparent increase in overall densification in the native silty clays below the depth of 60 to 62 feet. The lack of densification in the native silty clays is expected as the displacement and vibration of the vibroflot would not be able to increase the consistency of the silty clays.

Just like the Pipe Pile stone column installation, native soils composed of fat to lean clays show little increase in both cone and soil penetration resistances as reflected Figure 6.

The above findings confirm the generally accepted notion that excessive fines are the single most inhibiting factor to deep densification by dynamic and vibratory methods [2], [3]. The inhibiting influence of a given content of clay fines is as great as 5 to 10 times as much silt fines content [2]. This is not surprising given that liquefaction resistance also increases with increasing fines contents.

CONCLUSIONS

A jet grout wall of width at least 6 feet could be constructed by a double-fluid system to a depth of 75 feet. The demonstration wall had compressive strength in excess of 600 psi and permeability less than 1 Lugeon.

Both Pipe Pile and Vibroflotation methods achieved the required density of the sandy soils. Overall increase in density of the sandy soils was found to be 300% to 800% for the Pipe Pile stone columns and 400 to 1,000% for the Vibro stone columns. The time to construct a Pipe Pile stone column of depth of 70 feet was 75 to 95 minutes, which is approximately 2.5 times longer than that of a vibro stone column (i.e., 30 to 45 minutes) for the same depth.

Substantial ground heave of up to 2.5 feet was observed during construction of the jet grout columns due to the shallow depth to the top of the jet grout columns. On the other hand, ground settlements up to 2 feet were induced by both Pipe Pile and Vibroflotation stone column installations, which is equivalent to approximately 1.5% to 2% of the ground volume within which the stone columns were constructed.

CLOSURE

The isolation walls proposed for the seismic retrofit of the Posey and Webster Street Tubes at Oakland-Alameda, California can be constructed adjacent to the immersed tunnels to confine the liquefied soils in place and to prevent flotation of the tubes. The Stage II ground stabilization package is scheduled to start in the spring of 2002. Construction of the isolation walls will take approximately 2 to 2.5 years. To prove the reliability of the isolation walls and the overall effectiveness of the ground stabilization works, we have to await a major earthquake (7.25M in magnitude) which, the authors hope, will never come.

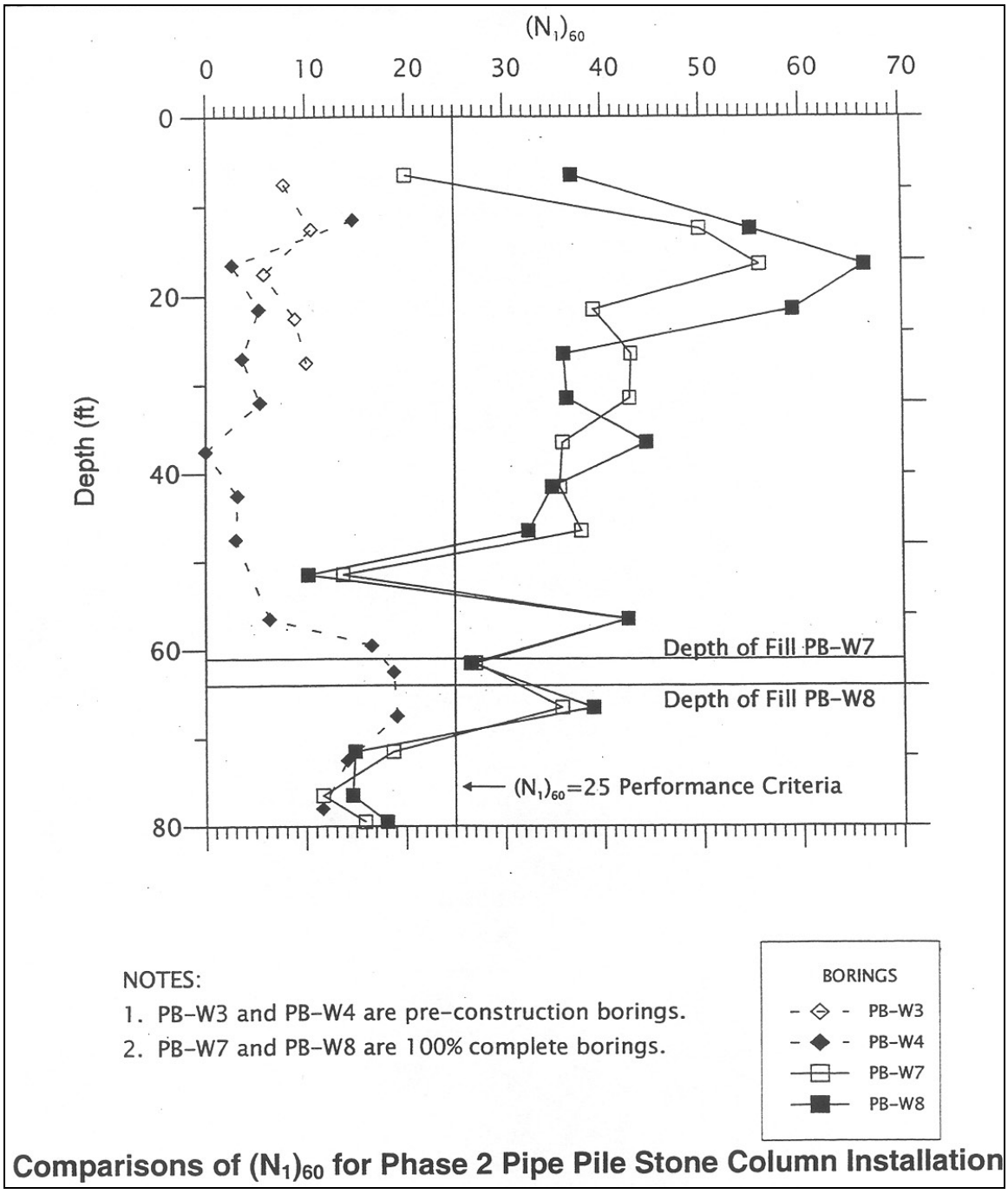

Figure 5 Results of Pre- and Post-Construction $(N_1)_{60}$ for Pipe Pile Stone Column Installation [4]

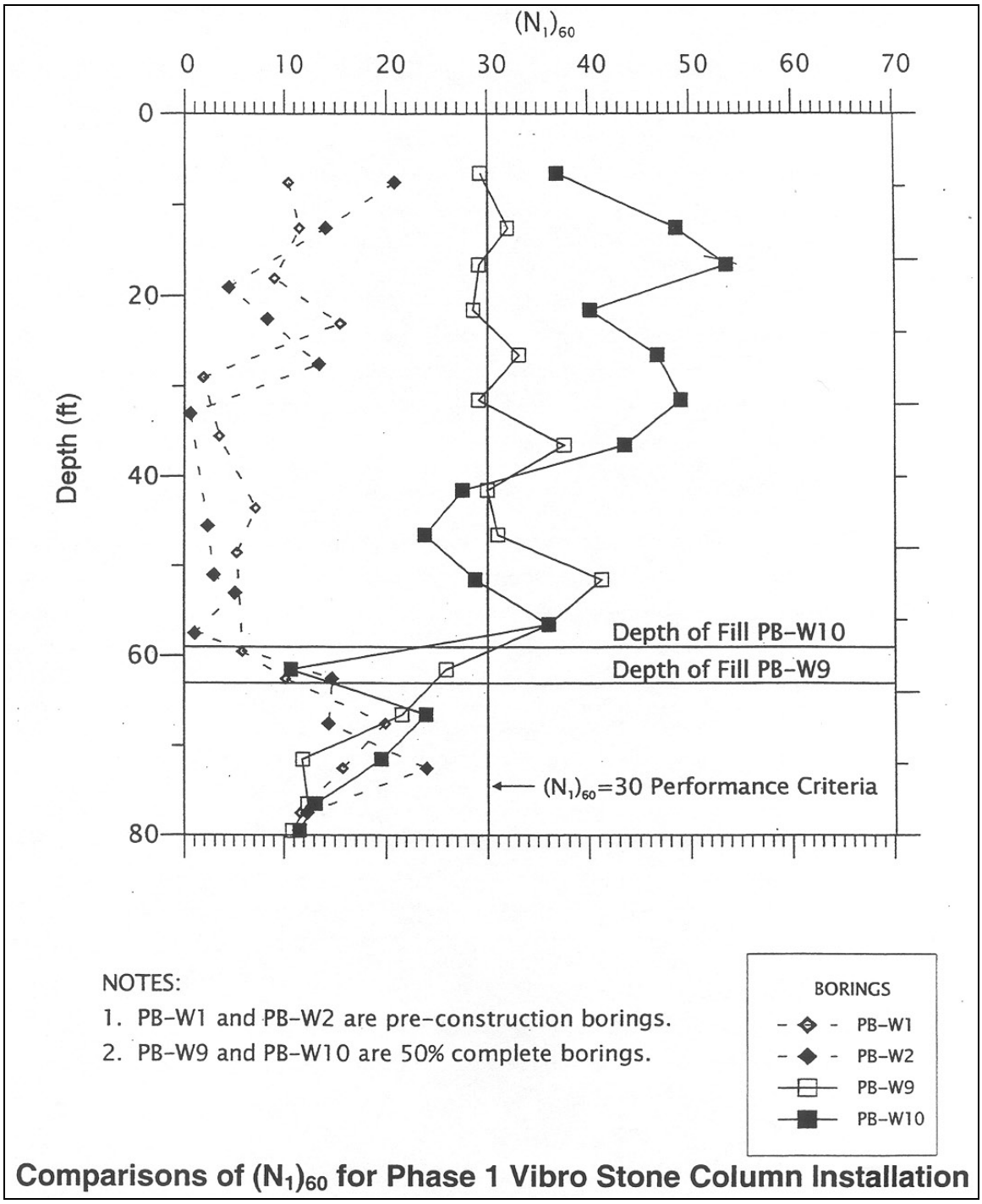

Figure 6 Results of Pre- and Post-Construction $(N_1)_{60}$ for Vibro Stone Column Installation [4]

ACKNOWLEGEMENTS

The first two authors would like to thank the California Department of Transportation for the execution of the demonstration program, without which the design concepts for the isolation wall principle cannot be put into practice. The contents of this paper reflect the views of the authors, but do not necessarily reflect official views of the State of California. This paper does not constitute a standard, specification, or regulation.

REFERENCES

[1] Schmidt, B., Hashash, Y., and Stimac, T., November 1998. "US Immersed Tube Retrofit" *Tunnel and Tunnelling International Magazine*; 22-24

[2] Mitchell, J. K., 1994; Mitigation of Liquefaction Hazard and "Other" Issues, presented for the short course in Geotechnical Engineering, University of California, Berkeley, June.

[3] Harder, L. F., Jr. (1992); Evaluation of Becker Soundings Performed at Mormon Island Auxiliary Dam in Conjunction with Upstream Remediation, Report to the Sacramento District, Corps of Engineers.

[4] Subsurface Consultants, Inc., 2000; Test Boring/CPT Report for Webster Tunnel Ground Improvement Demonstration Project, Vibroflotation Installation of Stone Columns, Alameda, California; October 25.

Seismic Rehabilitation Design and Construction for the Port Mann Bridge, Vancouver, B.C.

Keith Kirkwood, P.Eng., Tian-Jian (Steve) Zhu, P.E., Peter Taylor, P.E.

ABSTRACT

The Port Mann Bridge spans the Fraser River and is a vital link in the transportation infrastructure of Vancouver, British Columbia carrying approximately 110,000 vehicles per day. Constructed between 1960 – 64 the bridge totals 6866 ft (2092m) in length and is currently being seismically rehabilitated to safety level standards.

The elegant 1920 ft (585 m) long main span is the second longest continuous tied-arch in the world and was the first orthotropic steel deck bridge constructed in North America. The deck is supported by closely spaced transverse floorbeams that span between main tie girders that are, in turn, supported by arch ribs. The tie girders and arch ribs are large steel box cross-sections.

The north and south approaches are curved in plan and are, respectively, 3223 ft (982 m) and 1723 ft (525 m) long and consist of three-span-continuous steel girders supporting a composite concrete deck. Three different span lengths (and associated girder depths) are found: 125 ft (38.1 m), 175 ft (53.3 m) and 225 ft (68.6 m).

This paper examines both design and construction challenges of the seismic upgrade which consists of rehabilitating elements of the main span, approach spans and north approach soils densification (including soils under the river itself).

Major analysis and design efforts were undertaken to optimize the interaction of the superstructure, substructure and soils to arrive at a cost-effective rehabilitation solution. Both subduction and non-subduction earthquakes were considered. Time-history analyses with multi-support excitation were performed with concrete pier stiffnesses based on push-over analysis results. An iterative process was used to adjust pier stiffnesses to arrive at matching displacement demands between push-over and time-history analyses.

Geotechnical challenges were posed by the greatly varying soil profiles along the bridge alignment. For analysis purposes, six zones were designated, each with its own dynamic characteristics for propogating firm rock accelerations to ground level. Furthermore, foundation types and conditions vary, requiring close collaboration among the geotechnical and structural design team members to ensure superstructure-substructure-soil interaction compatability. This paper examines the rationale behind the various types of retrofits and the interdependence of superstructure, substructure and soil behaviour.

Keith Kirkwood, P.Eng., Senior Design Engineer, Buckland & Taylor Ltd. Bridge Engineering, North Vancouver, B.C.

Tian-Jian (Steve) Zhu, P.Eng., P.E., Senior Design Engineer, Buckland & Taylor Ltd. Bridge Engineering, North Vancouver, B.C.

Peter Taylor, P.Eng., P.E., Principal, Buckland & Taylor Ltd. Bridge Engineering, North Vancouver, B.C.

INTRODUCTION

The Port Mann Bridge, shown in Figure 1, is comprised of two different general structural forms, one for the approach spans and one for the main span crossing the navigation channel of the river. A general arrangement of the bridge is shown in Figure 2.

This paper examines both design and construction challenges of the seismic upgrade which consists of rehabilitating elements of the main span, approach spans and north approach soils densification (including soils under the river itself).

Figure 1. General Overview of Port Mann Bridge

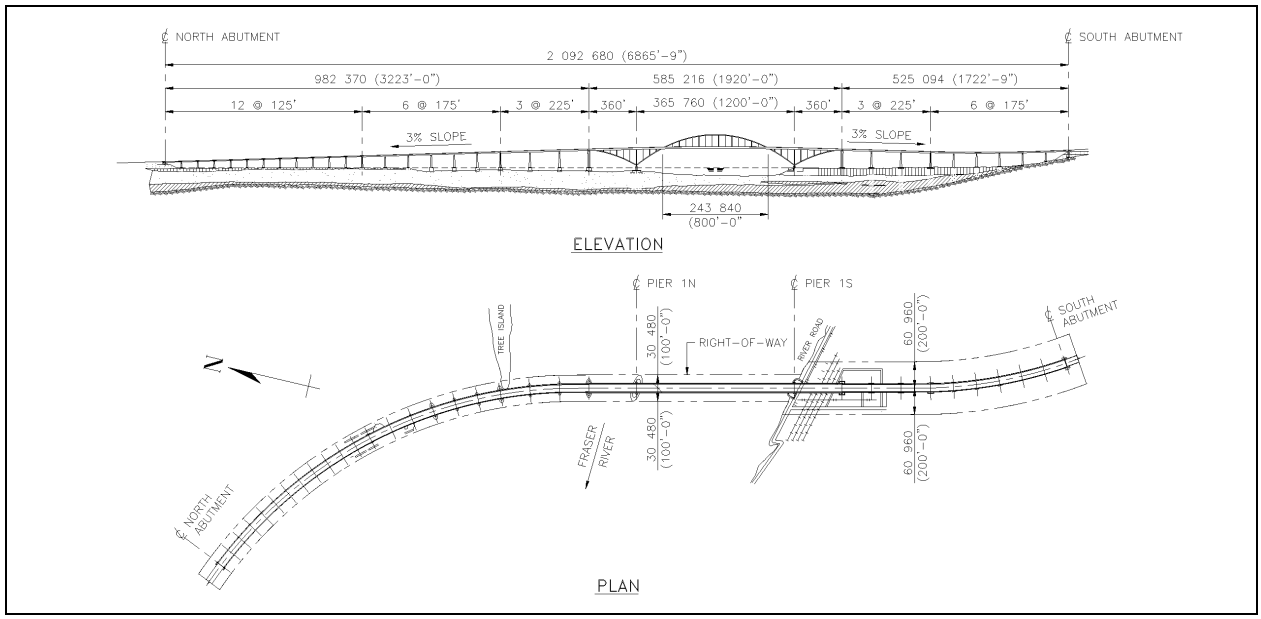

Figure 2. Bridge General Arrangement

DESIGN EARTHQUAKE AND SITE RESPONSE ANALYSIS

Two potential sources of earthquake were considered: non-subduction earthquake and subduction earthquake. The non-subduction earthquake corresponds to a M7.0 event occurring at a distance of about 84 km from the bridge site, and the subduction event is a M8.25 earthquake occurring at a distance of about 120 km from the site. For each earthquake source, a firm ground design response spectrum was developed, and two sets of firm ground input time histories were developed to be compatible with the firm ground design spectrum.

The soil profiles vary greatly along the bridge alignment. For site response analysis purposes, six soil zones were identified along the bridge length. For each soil zone, ground response analyses were carried out to derive four sets of ground surface horizontal time histories, based on a representative soil column and using the four sets of firm ground horizontal time histories (two sets for each earthquake source) as inputs. Ground surface vertical time histories were taken as 67% of the firm ground horizontal time histories. The ground surface time histories were time lagged at each support to model seismic wave travel. Typical design response spectra at ground surface are shown in Figure 3.

COMPUTER MODELLING AND DYNAMIC ANALYSIS

A computer model was initially developed for the two approach structures and the main span using Buckland & Taylor Ltd.'s in-house program CAMIL. The CAMIL model was calibrated with ambient vibration survey data. In addition, SAP models were developed for the two approach structures because of the ability in SAP2000 to use non-linear damper elements and to model gaps. The SAP model was calibrated with the CAMIL model.

Time-history analyses were carried out using the CAMIL and SAP models. Multi-support excitations were considered with different inputs in six soil zones. Static push-over analyses were performed for the approach concrete piers and their foundations. The push-over analyses were used to identify brittle failure modes and to generate nonlinear lateral force-deformation curve for the concrete piers. Iterations were performed on the secant stiffness of the concrete piers in the time-history analyses to match the static push-over curves of the piers and their foundations.

Many iterations were carried out using the time-history analyses to arrive at an optimized solution minimizing capital cost while achieving the specified performance level of "safety retrofit". Such iterations included different seismic isolation schemes, and different bearing fixity schemes in both the transverse and longitudinal directions.

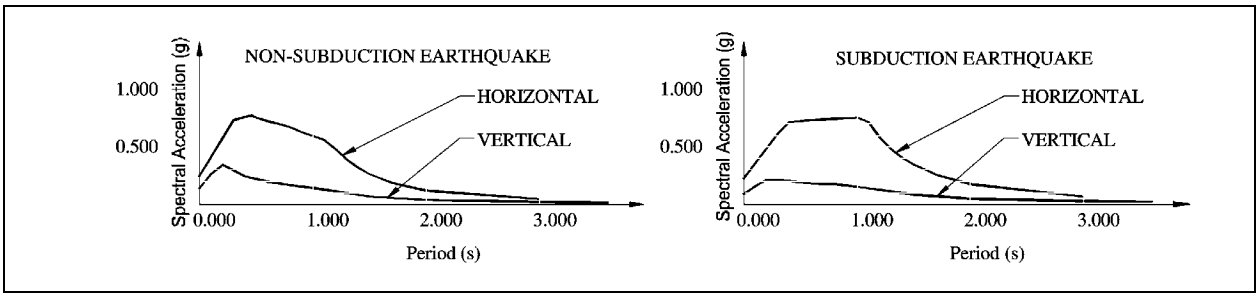

Figure 3. Design Earthquake Spectra at Ground Surface

PROJECT DESIGN PHILOSOPHY

Major analysis and design efforts were undertaken to optimize the interaction of the superstructure, substructure and soils to arrive at a cost-effective rehabilitation solution. Time-history analyses with multi-support excitation were performed with concrete pier stiffnesses based on push-over analysis results. An iterative process was used to adjust pier stiffnesses to arrive at matching displacement demands between push-over and time-history analyses.

APPROACH SPANS

Lateral Connectivity Between Superstructure and Substructure

Two options were explored regarding superstructure-substructure connectivity in the lateral direction. The first - fixing the superstructure to all piers - resulted in all piers needing retrofit, to varying levels. The second - fixing the superstructure only to "end" piers of successive three-span continuous units and letting the superstructure "float" over the two interior piers on new elastomeric bearings - resulted in many interior piers not requiring retrofit at all. This second method was adopted for the project because of its overall lower cost. This is because, while end piers required more retrofit, the savings in providing costly construction access at the interior piers not retrofitted were substantial.

Superstructure Modifications

The superstructure of the bridge has recently been widened to increase the number of lanes from four to five. The widened cross-section of the approaches is shown in Figure 4.

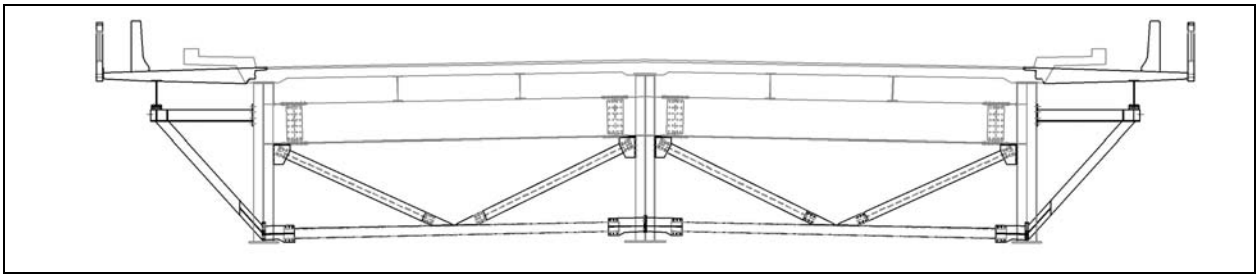

Figure 4. Widened Approach Span Cross-Section

During the widening contract recently completed, all superstructure modifications above bearing level to improve seismic performance were incorporated. These improvements include the addition of new intermediate diaphragm bracing and new pier diaphragms.

Other superstructure improvements will be carried out in later phases of the project. These include bearing replacements or modifications and the installation of longitudinal and/or transverse shear keys to alter superstructure-substructure articulation.

New Intermediate Diaphragm Bracing and Pier Diaphragms

As indicated in Figure 4, new intermediate diaphragm bracing has been added between the interior and exterior girders to increase overall torsional stiffness of the deck and better

distribute increased live load due to the widened bridge deck. This new bracing, combined with new bottom plan bracing shown in Figure 5, also helps to deliver seismic loads from deck level to bearing level.

Figure 5. New Superstructure Plan Bracing.

The original deck cross-section was relatively "open" at the piers resulting in a laterally soft and unstable load resisting system. As shown in Figure 6, transverse "infills" have been installed above the existing pier floorbeam (between longitudinal deck supporting stringers) and solid plate pier diaphragms have been provided between the underside of the floorbeams and the bottom flanges of the main girders. This establishes a direct load path to transfer large horizontal deck shears to the bearings.

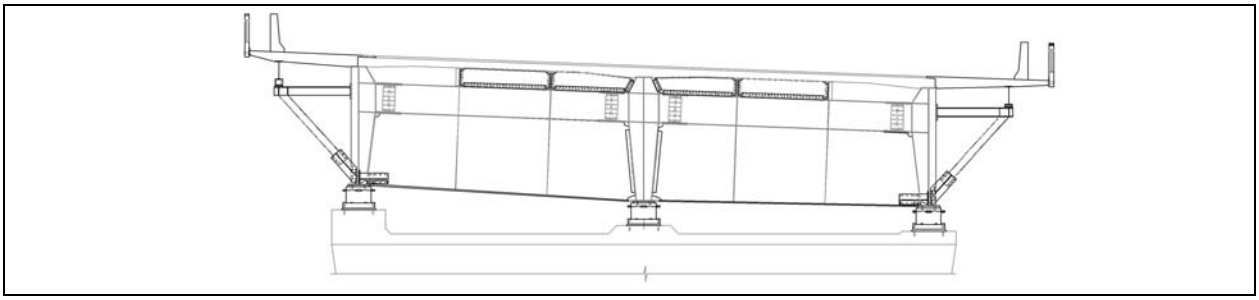

Figure 6. New Pier Diaphragms.

Transverse and Longitudinal Shear Keys

Analysis showed that horizontal seismic demands were too large to be taken in fixed bearings. Existing bearing pedestal reinforcing was also deficient to resist such large loads. Schemes for externally strengthening the pedestals were examined but it was concluded that provision of independent transverse and longitudinal shear keys was economically more advantageous. Transverse shear keys are provided at the underside of pier diaphragms and are cast into cap beam encasement retrofits, as shown in Figure 9.

One longitudinal shear key is provided for each three span girder unit. An example is shown in Figure 7. Each shear key is attached to the underside of the center deck girder and to

the pier cap beam via longitudinal Dywidag rods in holes cored through the pier cap beam. Laminated elastomeric bearings are situated between the shear key steel and the concrete face of the cap beam to allow thermal movement and girder rotations due to live load.

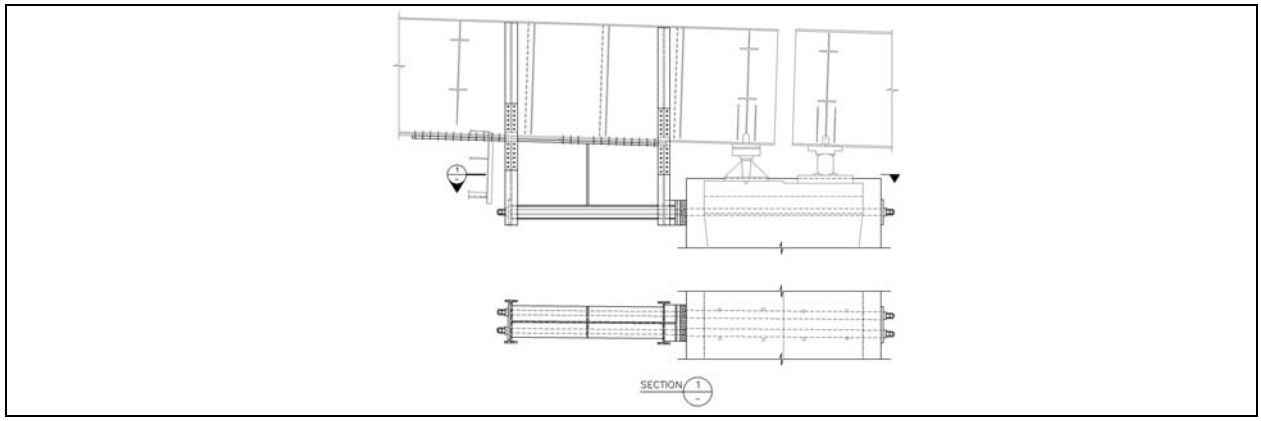

Figure 7. New Longitudinal Shear Key.

Bearing Replacement and Modifications

All existing bearings on the bridge are seismically deficient and are being either replaced or retrofitted. Existing roller bearings at end piers consist of truncated cylinders with limited movement capabilities. As shown at the top of Figure 8, infills are being attached to these bearings to create full cylinders to increase capacity. Interior pier bearings consist of two cylinders and are being replaced with laminated elastomeric bearings as shown in the middle of Figure 8. Fixed (pintle) bearings are being bolstered by longitudinal shear keys discussed above. To allow relative rotation of girders to pier cap beams under this new arrangement, teflon-stainless steel plates are being inserted between the bearing cap plate and the girder bottom flange, as shown at the bottom of Figure 9.

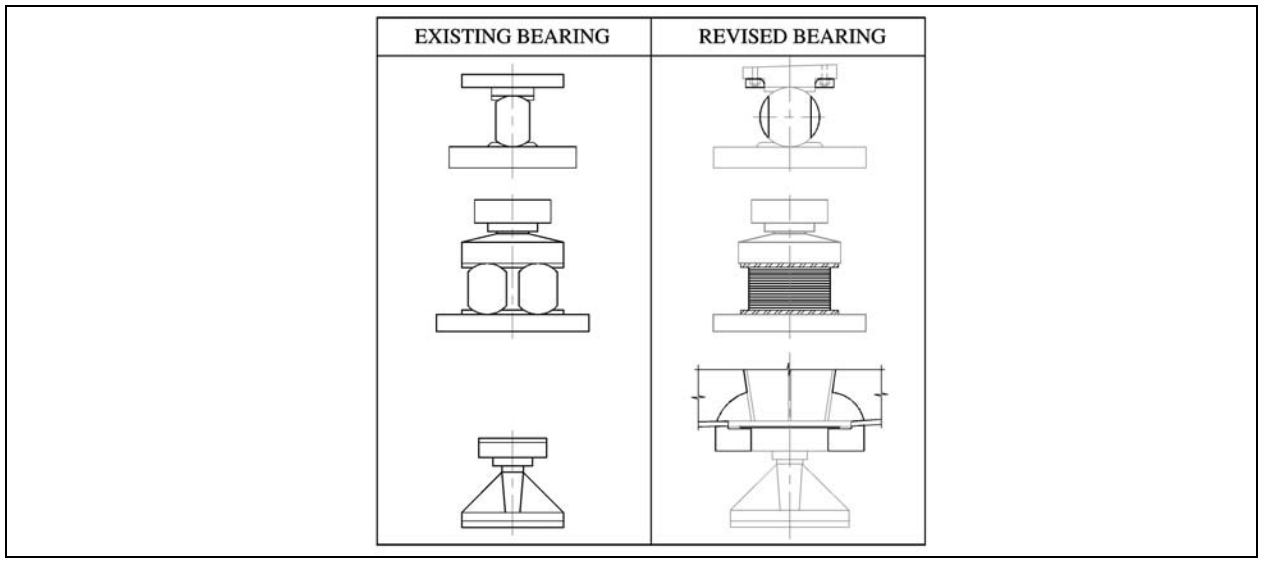

Figure 8. Bearing Replacement and Modifications.

Substructure Retrofit

Cap Beam Encasement or Post Tensioning

For the bents where plastic hinges will form in the columns, the demands on the cap beam were evaluated based on the formation of a hinge mechanism (two top and two bottom column hinges) and an overstrength factor of 1.3 to 1.5 for column flexural capacity. The cap beam was found to be inadequate in both flexural and shear capacity. Concrete encasement of the cap beam is adopted to increase its flexural and shear capacity, as shown in Figure 9. New top and bottom horizontal bars are used to increase flexural capacity, and closed stirrups with couplers are used to increase shear capacity. Bonding between existing and new concrete is enhanced by rebar dowels. The encased cap beam will remain elastic after formation of plastic hinges in the columns.

For several bents where the seismic demands on the cap beams are moderate, post-tensioning of the cap beams is adopted to save construction cost, as shown in Figure 9. Two holes with diameter ranging from 120 to 150 mm are cored drilled in existing concrete through the full length of each cap beam. Multi-strand tendons are installed, post-tensioned, and grouted in the cored holes. The tendon anchors are cast in the new concrete end blocks at the two ends of the existing cap beam. The post-tensioning tendons increase both the flexural and shear capacities of the cap beam.

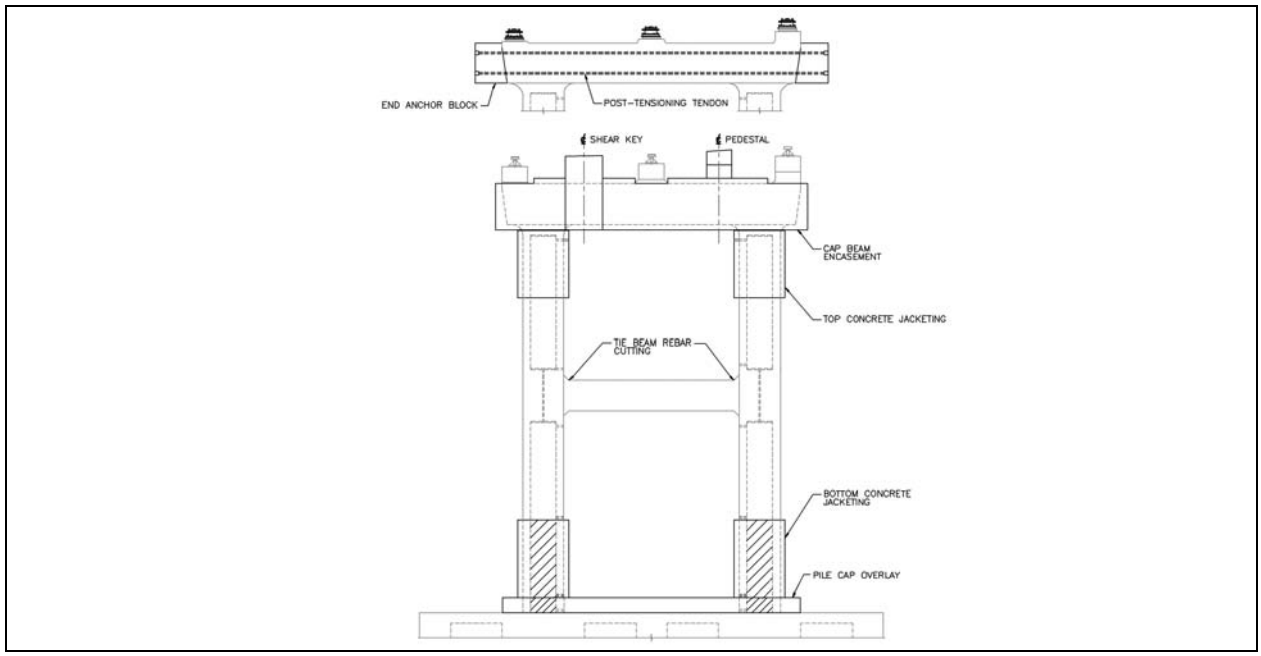

Figure 9. Pier Retrofit

Column Top and Bottom Encasement

There are lap splices in the exterior stirrups of the bent columns. Plastic hinges will form at the top and bottom of the columns for some of the bents, based on the seismic analysis results. For these bents, the stirrups become ineffective after spalling of concrete cover in the column

plastic hinges. Shear failure and buckling of main longitudinal rebars would occur prior to development of the required curvature ductility demand in the plastic hinges. To provide confinement and increase shear capacity, concrete jacketing is used in the top and bottom column plastic hinge regions, as shown in Figure 9. In the top and bottom encasement regions, new closely spaced stirrups are installed, and cross ties in both directions are used to engage the stirrups. These ties go through holes cored through column walls. The base of the columns is subjected to the most severe axial compression. Therefore, the center hollow cell in the bottom column plastic hinges is filled with new concrete to prevent buckling of main longitudinal rebars inward during cyclic response. The adopted column retrofit enables the development of the required flexural ductility demand in the plastic hinge regions without premature brittle failure modes.

Intermediate Tie Beam Deconstruction

For the taller bents, there is an intermediate tie beam at about mid column height, as shown in Figure 9. The assessment indicates that plastic hinges will form at the two ends of the tie beam in the early stage of seismic response. The joints between the tie beam and the columns would not have sufficient capacity to resist the plastic moments developed at the ends of the tie beam. The principal tensile stress in the joint corresponding to the development of negative plastic moment at the tie beam end would be higher than the allowable stress for diagonal cracking. Instead of strengthening the joint, deconstruction is adopted as a more cost-effective retrofit. Several existing top layer #11 bars in the tie beam are cut near the joint to reduce the negative moment capacity and hence the input into the joint. With this deconstruction retrofit, principal tensile stress in the joint is reduced to a level lower than the allowable stress.

Pile Cap Overlays

For the bents where plastic hinges will form in the columns, the demands on the pile caps were evaluated based on the formation of a column hinging mechanism and an overstrength factor of 1.3 to 1.5 for column flexural capacity. For the other bents, elastic seismic demands were used for the pile caps. Some of the pile caps were found to be inadequate in negative moment capacity. The two columns of each concrete bent have a common pile cap. Failure of the pile cap could result in independent vertical settlement, horizontal movement, and tilting of the two columns. This could significantly increase the structural demands on the concrete bents and lead to failure of the bents. Therefore, concrete overlay is used to increase the negative moment capacity of the pile caps, as shown in Figure 9. With this retrofit, integrity of the pile caps would be maintained during seismic response.

Special Foundation Strengthening at Piers 7S and 8S

Special foundation strengthening is required at south approach piers 7S and 8S because the soil layer between the footing and the firm till below is very soft and compressible peat. Octagonal concrete piles supporting the footings of these piers are expected to break in brittle fashion. To avoid catastrophic settlement of the piers, 16 vertical pipe piles are to be driven to firm till around the exteriors of each existing footing and then filled with concrete. These piles are then made integral with the existing footing through post-tensioning and strengthening of the footing, as shown in Figure 10.

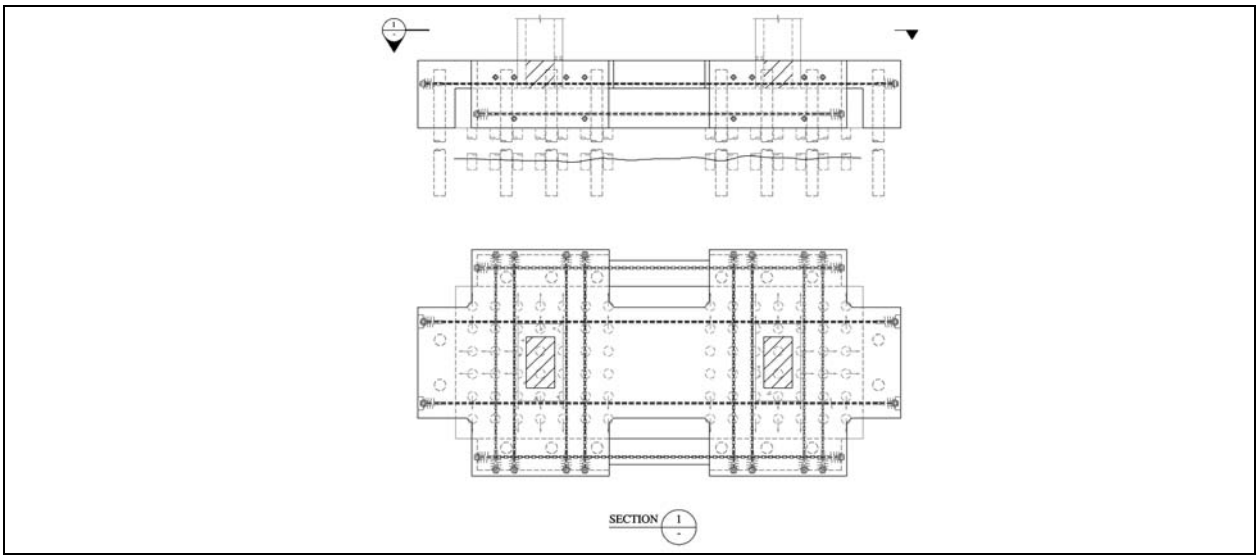

Figure 10. Special Foundation Strengthening at Piers 7S and 8S.

North Approach Soils Densification

The approach on the north side of the Fraser River is founded on loose, liquefiable sands. These sands exist for both piers in the river and those on the riverbank. Close cooperation between the geotechnical and structural engineering teams occurred to develop a densification scheme that provided consistent substructure-soil interaction that would ensure overall structural safety. Analysis predicts that concrete piles supporting the land based piers will break in brittle fashion just below pilecap level. Once densification is complete, the broken piles are expected to act as soil reinforcing elements to limit vertical deflection of the piers. This failure mechanism is significantly more cost effective than adding capacity to each footing through the addition of external piling and pilecap strengthening.

Timber Piles and Seismic Drains for Land Piers

The most economical densification method for the land piers was determined to be the driving of timber piles in concentric rings around each footing. At regular intervals, seismic drains consisting of gravel columns will also be installed to alleviate deleterious pore pressure build-up.

Performance-Based Criteria for Water Piers

Three different possible densification methods are considered feasible for the water based piers: vibro-replacement with stone columns, installation of gravel compaction piles or driving timber compaction piles, or combinations of these methods. It was concluded that the most cost effective solution to choosing which option to use would best be left to contractors via a performance based design criteria. Thus, required densification values have been specified in the contract documents, as well as testing criteria to ensure that the values are reached by the contractor's chosen method.

MAIN SPAN

Superstructure Analysis and Design

The main span superstructure is a relatively light continuous tied arch with orthotropic steel deck. The main arches and tie girders are box members. The superstructure was analyzed using Buckland & Taylor Ltd.'s in-house computer program CAMIL. Time history ground motions were input at each main pier and tie-down piers. Demands were determined and compared to capacities and deficiencies were found to be relatively localized in the above deck portal beam, the diaphragms at the tie-down piers, the main sway bracing and the main bearings. Neither the arches nor the main tie girders were found to be deficient. Complicating analysis of the tie girders is the fact that they are constructed of two grades of steel (for efficiency of original design).

Portal Beam Retrofit

The joint of the portal beam to the main arch was determined to be deficient during earthquake rocking motions due to fastener pull-out. Therefore, a strengthening of this joint, shown in Figure 11, was undertaken during the widening contract recently completed because it could be constructed behind the temporary construction barrier used during widening work.

Diaphragms and Shear Keys at Tie-Down Piers

Tie downs at the ends of the main span connect to the pier below and must be kept intact during a seismic event for overall structure stability. Therefore, no significant relative deflection between the pier and the superstructure can be tolerated. To eliminate relative deflections, a large diaphragm with shear key below is being added between the main span box girders.

Main Pier Sway Bracing and Tie Downs

The main pier sway bracing, shown in Figure 11, was determined to be deficient in local buckling of the webs of the box member. An innovative technique was developed to stiffen the webs through the addition of simple flat bar stiffeners and change the failure mode from local plate buckling to overall buckling instability of the box member. Sufficient capacity increase results from this procedure that no other member strengthening is required.

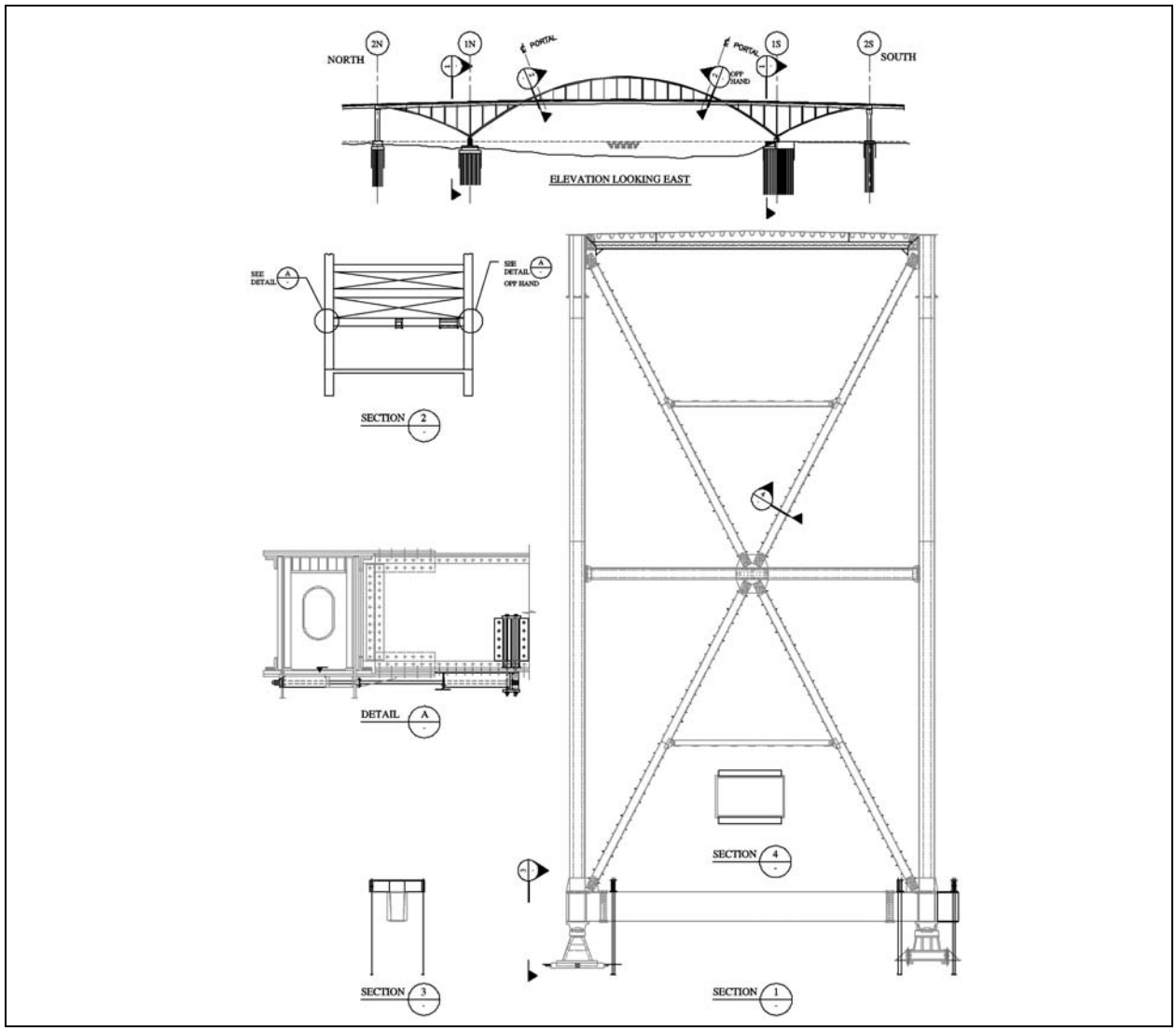

Figure 11. Main Span Retrofits

Main Pier Bearing Encapsulation

The southern main arch bearings are currently cogged rolling bearings that are skewed in their running tracks and are, therefore, frozen. It is believed that their sudden release in a seismic event would result in a damaging release of energy. Therefore, they are to be encapsulated in concrete to fully fix them to the pier.

The northern main arch bearings are fixed but are unable to withstand the large horizontal shears resulting from the design earthquakes. As such, they are also being encapsulated in concrete. Both north and south pier retrofits are shown in Figure 12. Temperature and live load movements at bearing level will be accommodated by flexing of supporting piles. This behaviour was verified during ambient vibration measurements undertaken during preparation of the Seismic Strategy Report (1995).

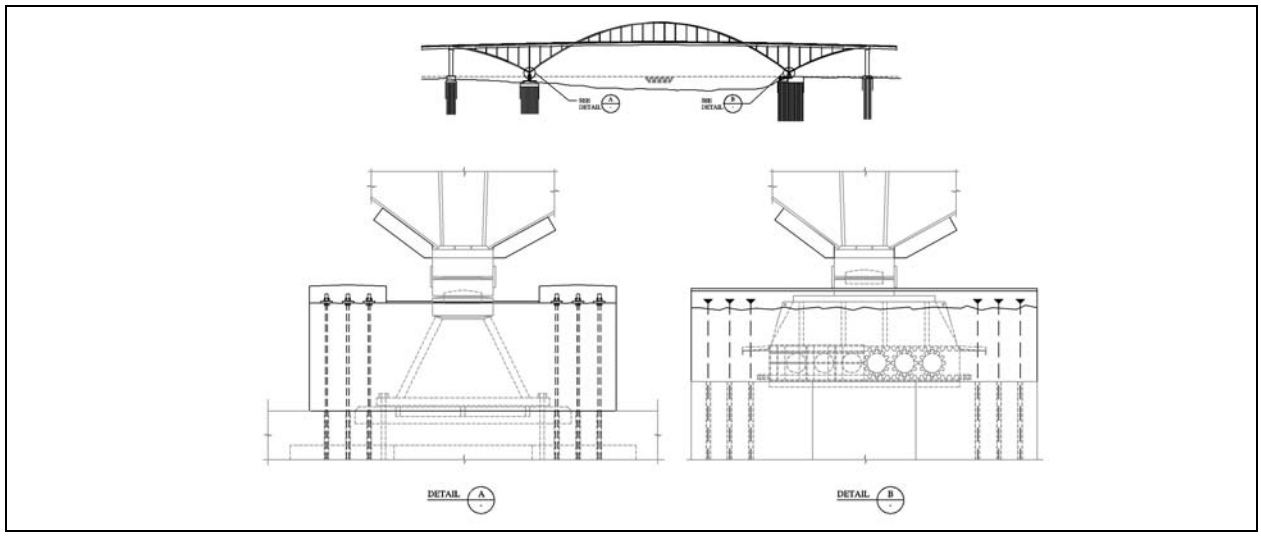

Figure 12. Main Span Bearing Encapsulation.

CONCLUSIONS

Significant design and analysis efforts were expended to arrive at a cost-effective seismic retrofit solutions for this bridge. Close collaboration between the geotechnical and structural engineering teams resulted in an efficient design at low capital cost. The strategic decision to concentrate retrofits at end piers of three span units while decoupling the superstructure and substructure at interior piers eliminated considerable retrofits at interior piers. Bearing retrofits were kept to a minimum due to the significant construction costs associated with girder jacking for bearing replacement.

ACKNOWLEDGEMENTS

The authors would like to acknowledge Mr. Dan Gould, P.Eng., and Mr. Bill Szto, P.Eng., of the British Columbia Ministry of Transportation for their cooperation in authorizing the publishing of this paper.

Gratitude is extended to the seismic retrofit peer review team members Dr. Don Anderson, P.Eng., and Dr. Peter Byrne, P.Eng., both formerly of the University of British Columbia and Mr. Don Gillespie, P.Eng. of the B.C. Ministry of Transportation.

Gratitude is also expressed to geotechnical team members Mr. Ernie Naesgaard, P.Eng. and Mr. Uthaya Uthayakumar, P.Eng. of Terra Macleod Enginnering. Finally, the analysis and design of many of the retrofits for this bridge were undertaken by Mr. David Calder, P.Eng. The authors would like to express their deep gratitude for his valuable contributions to the overall success of the project.

REFERENCES

[1] "Port Mann Bridge #1614, Seismic Assessment and Preparation of a Seismic Safety Retrofit Strategy – Final Report," Buckland & Taylor Ltd. for British Columbia Ministry of Transportation, 1995 March 31.

Displacement Based Design

Chair: W. Phillip Yen

Rocking of Bridge Piers Under Earthquake Loading

Fadel Alameddine and Roy A. Imbsen

Legacy Parkway Seismic Design

Strategies for Developing a High Performance Structure with Typical Bridge Design Features on a Design-Build Project

Thomas R. Cooper and Joseph I. Showers

Plastic Hinge Length of Reinforced Concrete Bridge Columns

Robert K. Dowell and Eric M. Hines

Applicability of the Pushover Based Procedures for Bridges

Matej Fischinger and Tatjana Isakovic

Seismic Performance of Reinforced Concrete Bridge Columns

David Sanders, Patrick Laplace, Saiid Saiidi and Saad El-Azazy

Rocking of Bridge Piers Under Earthquake Loading

Fadel Alameddine and Roy A. Imbsen

ABSTRACT

Current design of a seismically resistant bridge column with a fixed connection to the footing requires the plastic hinge to form in the column away from the footing. This mechanism is used in new design but is rather expensive to achieve in older structures to be retrofitted for enhanced seismic performance. In some situations, rocking still needs to be evaluated for new structures where spread foundations are used. In California, older columns are supported on footings that can be lumped into two categories:

a) Spread footings resting on relatively dense material or footings resting on piles with weak tension connections to the footing cap. This latter group is treated similarly to spread footings since a strategy can be considered to ignore the supporting piles in tension provided the existing footing has enough structural capacity to overcome the limited demand from the piles going in tension.

b) Footings with adequate capacity to resist the piles tension and compression forces.

This study focuses on the first category where rocking behavior of the bent is used since it offers an alternative to the use of tie-downs for the footing or adding more piles to create a fixed condition. Favorable rocking behavior was reported back in 1963 by Housner [1] comparing the post earthquake survivability of slender structures despite the appearance of instability against the damage of much more stable appearing structures. The effect of duration on overturning is also discussed in that paper. Housner mentioned also that the concept of representing the effect of an earthquake by a certain static lateral force may be quite misleading.

Fadel Alameddine, Senior Bridge Engineer, Caltrans Office of Earthquake Engineering, 1801 30th Street MS 9 2-51, Sacramento, CA 95816.
Roy A. Imbsen, President, Imbsen & Associates, Inc., 9912 Business Park Drive, Suite 130, Sacramento, CA 95827.

INTRODUCTION

During the seismic retrofit program of bridges in California, rocking analysis was used based on procedures that were reported by Preistley & Seible [2]. The program "WinRock" was developed based on these procedures and used by Caltrans engineers and consultants. The general procedure includes the following steps:

1. Develop a relationship between the top of the column displacement and rocking period.
2. Develop a displacement response spectrum from the design acceleration response spectrum.
3. Use a trial and error approach where the displacement is initially guessed, the period is then calculated followed by calculation of the displacement until convergence is reached between the initially guessed displacement and the calculated displacement. Stability is unattainable where convergence is not reached.

For the case of a single column bent (see Figure 1) where no tensile capacity is associated with the footing, the footing is considered to be supported on a rigid perfectly plastic soil with uniform compressive capacity "p_c ". The overturning and rocking on the foundation can be simplified using a linear force/deflection relationship as outlined in the following:

- Guess the displacement "Δ". (1)
- Calculate the applied force at the superstructure level "F".

$$F = W_t*(L-a)/2H - W_s*\Delta/H \quad \text{where } a= W_t/(B*p_c) \tag{2}$$

- Calculate the equivalent system stiffness $K=F/\Delta$.
- Calculate the period "T" of the bent system based on "K" and W_s.
- Recalculate "Δ" considering 10% damping; this would typically reduce the spectral acceleration ordinates S_a of a 5% damped spectrum by approximately 30%.

$$\Delta=(T^2/4\pi^2)*(0.7\ S_a) \tag{3}$$

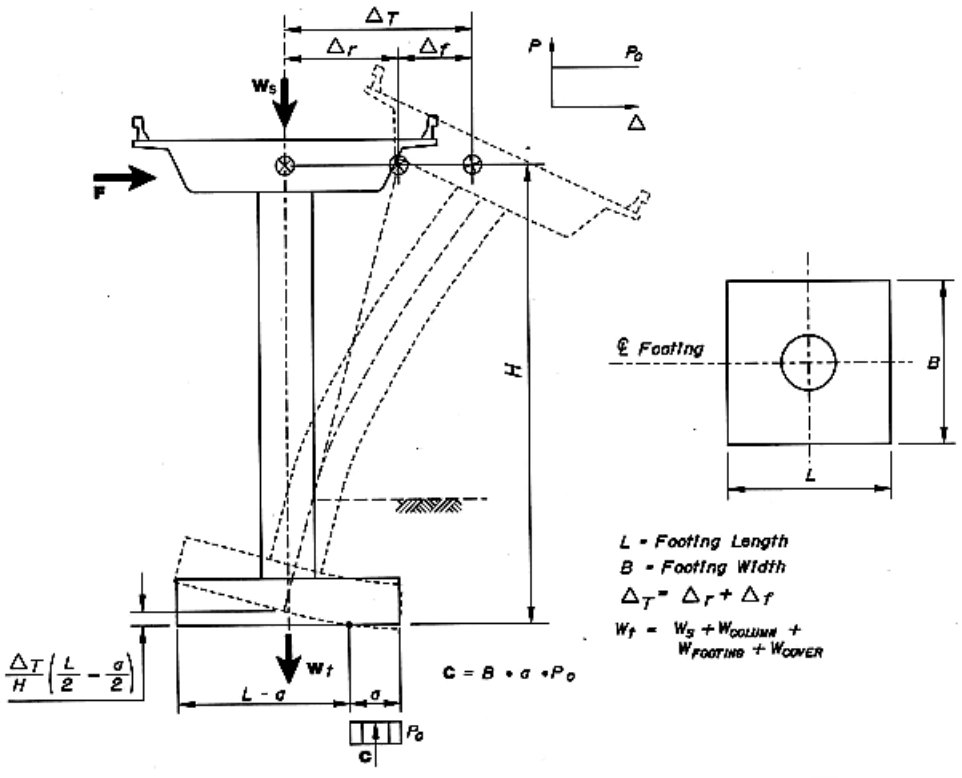

Figure 1. Rocking Equilibrium of a Single Column Bent.

"Δ" is referred to as the total displacement on top of the column.

- Iterate until convergence, otherwise the bent is shown to be unstable.

Once a converging solution is reached, the flexural displacement of a column "Δ_{flex}" is determined based on the column flexural stiffness K_{flex} and the converging force F using:

$$\Delta_{flex} = F/K_{flex} \quad (4)$$

The displacement due to rocking "Δ_{rock}" is equal to:

$$\Delta_{rock} = \Delta - \Delta_{flex} \quad (5)$$

The flexural ductility demand on the column "μ" can be calculated based on the yield displacement of the column "Δ_{yield}" using:

$$\mu = \Delta_{flex}/\Delta_{yield} \quad (6)$$

- If $\mu > 1$ then the shear capacity is assessed based on the flexural ductility demand "μ".
- If $\mu < 1$ then shear capacity is assessed with no consideration to "μ".

The above procedure was extensively used with no account for duration of an earthquake or a validation against results obtained using nonlinear procedures. The forces that result from rocking analysis can be of lesser magnitude than forces induced by column plastic hinging. Ductility demand on the column can also be smaller when compared to a fixed base analysis.

Typically, retrofits that result from a rocking analysis include:

a. casing the column for shear enhancement and confinement and / or
b. adding an overlay to enhance the footing shear and flexural capacity or increasing the size of the footing to gain stability and increase of the footing cap flexural capacity.

SCOPE OF STUDY

In order to verify the results obtained using WinRock, a group of columns representing cases encountered in the Caltrans bridge inventory is considered (see Table I). The following tasks are performed:

A/ Establish flexural drift capacity of these columns for two cases:

a. columns with lap spliced connection to the footing
b. columns having poor transverse confinement with continuous reinforcement to the footing

B/ Establish seismic hazard using a suite of six different acceleration records with one record representing low seismicity, one record representing moderate seismicity, and four records representing high seismicity.

C/ Develop typical column to footing models having dense soil characteristics.

D/ Perform a WinRock analysis on the group of columns to calculate flexural drift and total drift demands on each of the columns (see Table I).

E/ Perform nonlinear analysis using Drain 2DX [3] based on the suite of records and modeling of the rocking behavior.

TABLE I. COLUMN PARAMETERS

Column Diameter D (ft)	ρ (%)	Column Height H (ft)	Footing		
			Length (ft)	Width (ft)	Depth (ft)
3	1,2,3,4	20	9	9	3
4	1,2,3,4	20,30	12	12	3
5	1,2,3,4	20,30,40	15	15	3.5
6	1,2,3,4	30,40,50	18	18	4
7	1,2,3,4	30,40,50	21	21	5

F/ Examine the validity of the linear simplified analysis by comparing WinRock analysis to the nonlinear analysis.

Task A (Establish Flexural Drift Capacity)

Rocking of the footing acts as a means of base isolation, limiting the seismic input to the structure. Rocking can be considered a satisfactory mode of response provided instability is prevented, and displacement demands on the bridge column do not exceed the flexural displacement capacity. Older columns have two major weaknesses:

a. lap spliced connections at the base of the column
b. poor transverse reinforcement

In order to determine the drift capacity for case (a), the displacement capacity for each of the columns in Table A is calculated equal to 1.5 times the yield displacement, assuming an allowable ductility capacity equal to 1.5.

The displacement capacity for case (b) is determined using Mander's [4,5]unconfined concrete model. The results for both cases are plotted against (D/H) ratios since they represent the best scatter in data. A regression analysis is performed and a lower bound curve is found for both cases (see Figure 2).

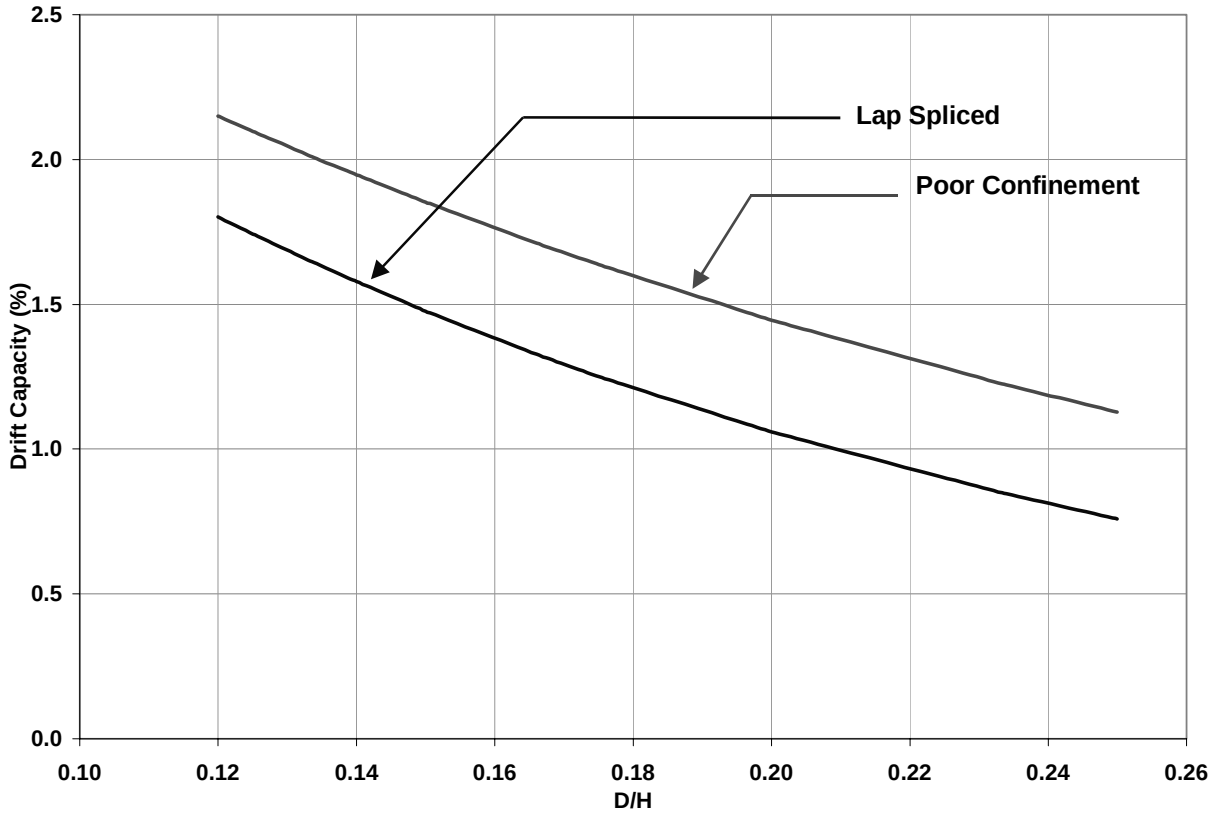

Figure 2. Drift Capacity of Lap Spliced and Poorly Confined Columns

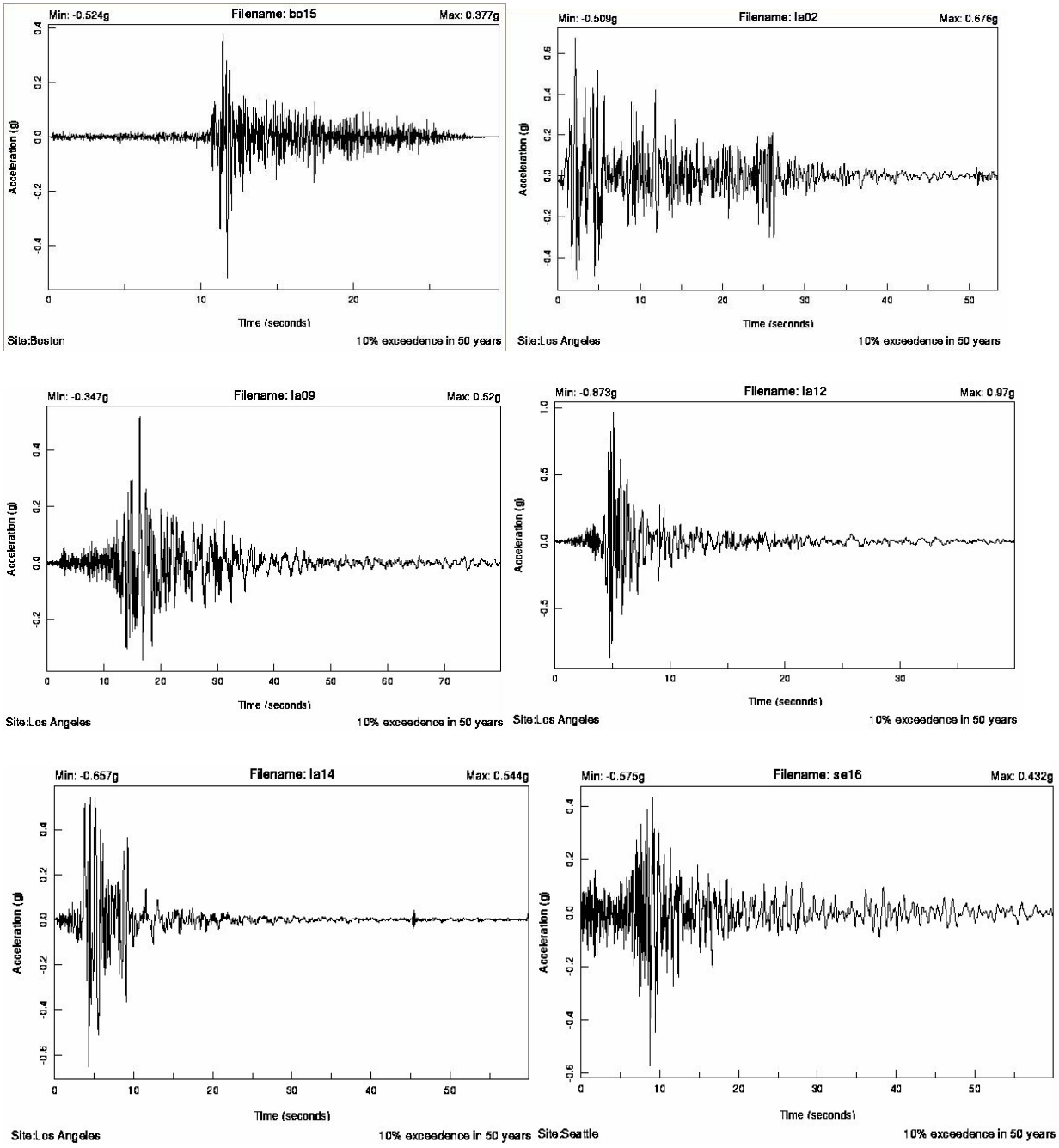

Figure 3. Acceleration Records

- For columns with lap spliced connections:

$$\text{Drift capacity (\%)} = 4.0*(.0013)^{X} \quad \text{where } x=D/H \tag{7}$$

The drift capacity ranges between 1.8% for low (D/H) ratios to 0.9% for high (D/H) ratios.

- For columns with poor confinement:

$$\text{Drift capacity (\%)} = 3.9*(.0070)^{X} \quad \text{where } x=D/H \tag{8}$$

The drift capacity ranges between 2.2% for low (D/H) ratios to 1.1% for high (D/H) ratios.

Task B (Establish Seismic Hazard)

Six records are considered in this study. These records represent acceleration time histories (see Figure 3) that have been derived from historical recordings and have been altered so that their mean response spectrum matches the 1997 NEHRP design spectrum for soil type S_D and having the same hazard of 10 % probability of exceedance in 50 years. The six records chosen for this study were picked from the SAC project [6] and are the following:

1. The Saguenay record for hazard in the Boston area corresponding to a low seismicity level.
2. the 1949 Eastern Washington, Tacoma county record for hazard in the Seattle area corresponding to a moderate seismicity level.
3. The 1940 El Centro, 1992 Landers, 1989 Loma Prieta, and 1994 Northridge records for hazard in the Los Angeles area corresponding to a high seismicity level.

Rocking dissipates energy by impact on the soil and radiation damping. Traditionally, a 10% damping level is used in rocking analysis. The same level is used for the WinRock type of analysis as well as the nonlinear analysis conducted by Drain 2DX.

Task C (Develop Typical Column to Footing Models)

- In this study, the columns are considered to be supported on a square footing with each dimension equal to three times the column diameter. This is considered to be a minimum dimension representative of older footing. Corresponding to each column diameter an average depth of footings encountered in older bridges is considered. These dimensions are reported in Table I.
- A cover depth of 2 feet is considered for all columns
- A lumped mass on top of the column equivalent to $0.1f'_cA_g$/ Acceleration g
- The soil is characterized by a rigid elastic perfectly plastic curve shown in Figure 4
- The inertia of the lumped mass on top of the column, the column, and the footing as well as the weight of the cover are all considered in the rocking analysis
- Effective properties of the column and the footing are considered
- For the nonlinear analysis, the column and the footing are discretized into beam-column elements with rigid elements at the column to footing joint. The soil is modeled with nonlinear springs with zero tension capacity.

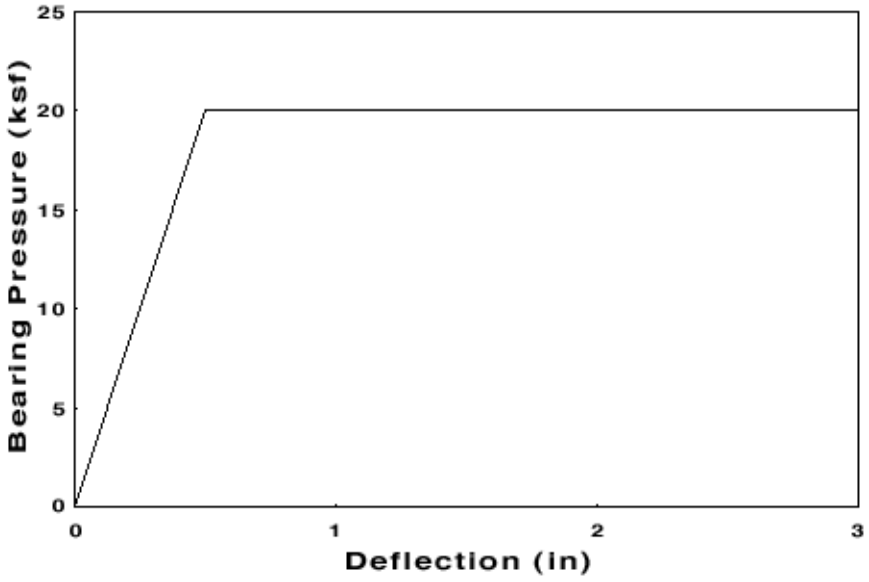

Figure 4. Soil Bearing vs. Deflection Curve

TABLE II. RESULTS OF LINEAR "WINROCK" ANALYSIS

Record	ρ = 1%		ρ = 4%				
	$(Drift_{flex})_{max}$ Large D/H	$(Drift_{flex})_{max}$ Small D/H	$(Drift_{flex})_{max}$	$Drift_{tot}$ Small D/H	$Drift_{tot}$ Large D/H	**No. of Overtuning** Small D/H	**No. of Overtuning** Large D/H
LA02	2%	3.5%	0.6%	3.7%	5.9%	3	0
LA09	2.5%	6%	0.4%	6%	9%	6	1
LA12	1.6%*	1.6%*	0.6%	2.5%*	2.5%*	1	1
LA14	4%	5%	0.5%	5%	6.8%	4	0
SE16	2.3%	1.5%	0.6%	2.5%*	2.5%*	3	0

*No definite pattern for drift vs D/H ratios

Task D (Perform WinRock Analysis)

Using WinRock, the 24 column cases were run for the 10% damped spectrum of each of the six records representing three levels of seismicity.

a. Results for low level seismicity:

Regardless of the reinforcement percentage, the flexural drift did not exceed 1.3% for small D/H ratios (i.e. D/H<.2) and 0.7% for large D/H ratios with virtually little or no rocking for all cases.

b. Results for moderate and high levels of seismicity:

The columns with 1% reinforcement showed no rocking with the flexural drift being equal to the total drift while the columns with 4% reinforcement showed rocking with the rocking drift dominating the response. Overturning cases were dominant for the 4% reinforcement columns with small D/H ratios. A summary of the analysis results is shown in Table II.

Task E (Nonlinear Analysis)

Using Drain 2DX, the 24 columns cases were run for each of the six records with the following results:

a. Results for low level seismicity.

Regardless of the reinforcement percentage or D/H ratios, the maximum flexural drift reported for all cases did not exceed 0.4% while the maximum total drift did not exceed 0.6%. Both drifts are relatively small and show little flexural demands and relatively minor rocking response.

b. Results for high and moderate level seismicity

The results for the 1% and 4% reinforcement columns are reported in Tables III and IV respectively. Table III shows the maximum ratio of flexural drift from Drain 2DX "FDD" compared to the flexural drift from WinRock "FDW". This ratio can be as large as 10.3, which reveals the unreliability of predicting flexural ductility levels using WinRock. The higher ratios of $(FDD/FDW)_{max}$ are usually associated with low D/H ratios while the low ratios $(FDD/FDW)_{max}$ are associated with high D/H ratios. Thus, the unreliability of results is generally emphasized for low D/H ratios. The flexural drift predicted by Drain 2DX can be as large as 9%, which is quite excessive for flexural elements. Flexural ductility levels are consistently greater for high D/H ratios than for low D/H ratios.

TABLE III. COMPARISON OF LINEAR AND NONLINEAR ANALYSIS FOR COLUMNS WITH ρ = 1%

ρ = 1% Record	$\left(\frac{FDD}{FDW}\right)_{min}$	$\left(\frac{FDD}{FDW}\right)_{max}$	$(FDD)_{max}$	μ_{flex} Small D/H Drain	μ_{flex} Large D/H Drain	Total Drift Range
LA02	0.62	1.1†	3.4%	3	4	1.8%-4.6%
LA09	0.52	2.25†	9%	8	12	1.8%-12%
LA12	0.60	3.4†	1.6%	0.4	0.9	0.9%-2.2%
LA14	0.55	10.3†	6%	2	2	2.1%-8%
SE16	0.53	3.46†	1.6%	1	1	1.0%-2.3%

† Low D/H
Scattered over D/H

Table IV reports the maximum ratio of flexural drift from Drain 2DX compared to WinRock. This ratio is shown to be as large as 2.5 which reveals inaccurate prediction of flexural ductility levels using WinRock. However, it can be seen at the highest flexural drift found using Drain 2DX does not exceed 0.9% with flexural ductility at or below 1.0. These results show that the uncertainty or inaccuracy in predicting the flexural ductility for the 4% reinforcement columns does not change the general trend of negligible column flexural demand and dominance of the footing rocking on the response of the column to footing model.

Task F (Examine the Validity of Linear Analysis)

A comparison between the results of the simplified "WinRock" analysis and the nonlinear analysis is performed. The findings that can be drawn from this study that are relevant to practicing engineers are as follows:

a. For older bridge columns on spread footings in areas of low seismicity level, the flexural and the total drifts demands seem to be small relative to the drift capacity. The only major concern for earthquake resistance would be checking the shear capacity for these low drift demands. The footprint size need not to be of concern except that the shear and the flexural capacities of the existing footing should be checked for the rocking response resulting from the column to footing system leaning against the toe of the footing.
b. For moderate or high seismic levels, the columns with 1% reinforcement exhibit different response than columns with 4% reinforcement. The columns with 1% reinforcement showed high flexural demands while columns with 4% reinforcement showed high rocking response with low flexural demands on the columns. For all records, there are multiple cases where flexural demands predicted by Drain 2DX significantly exceeded flexural demands predicted by WinRock especially for low (D/H) ratios. However the magnitude of flexural demand (i.e. ductility) was quite significant for the 1% reinforcement columns, and negligible for the 4% reinforcement columns.

In all cases, the size of the footprint was not a cause of instability. Taking into consideration that 3 times the column diameter footing dimension is a minimum, it is deemed that a retrofit that aims at enlarging the footing is usually not warranted and should only be seldom used.

Several cases for columns with 1% and 4% reinforcement were run using Drain 2Dx for two 150% scaled records. The two records were chosen because they induce the largest drift demands out of the six records described previously (see Table V). The results show that instability occurred in the 1% reinforcement columns that had previously high flexural demands. The 4% reinforcement columns did not show instability because of the size of the footing.

TABLE IV. COMPARISON OF LINEAR AND NONLINEAR ANALYSIS FOR COLUMNS WITH ρ = 4%

ρ = 4% Record	$\left(\frac{FDD}{FDW}\right)_{min}$	$\left(\frac{FDD}{FDW}\right)_{max}$	$(FDD)_{max}$	$(\mu_{Drain})_{max}$	$(\mu_{Drain})_{min}$	Total Drift Max
LA02	1.31	1.73	0.9%	0.3	0.2	4.6%
LA09	1.4*	1.9*	0.9%	0.4	0.1	7.2%
LA12	0.34	1.8†	0.7%	0.3	0.8	2.7%
LA14	0.18	2.5	0.9%	0.3	1.0	5.2%
SE16	0.33	1.81	0.8%	0.2	0.4	2.8%

† Low D/H
Scattered over D/H

Implications of Linear Analysis Practice

The results of the parametric and comparative study between linear and nonlinear analysis suggest the following implications on the state of the practice linear type of analysis (ie. WinRock type of analysis):

- The flexural drift calculated using WinRock and Nonlinear analysis differ greatly for the case where restoring moment is close to the overturning moment.
- The rocking mechanism can not be used inadvertently as a form of isolation where restoring moment is close to overturning moment. The minimum recommended ratio of the column overstrength plastic moment capacity to the restoring moment should be equal to 1.5 in order to ensure column isolation from the flexural ductility mechanism.
- The linear WinRock analysis results in a larger number of cases of system instability.
- The scatter of the magnitude of the total drift for a rocking dominant system calculated using the linear WinRock analysis is between 90% and 130% of magnitude calculated using nonlinear analysis. This scatter range is consistent with the state of the practice "Equal Displacement (5% damping)" rule used in the linearization of system response [7].

In summary, the major checks for assessing the column to footing system should target the column flexural and shear capacities. Results show that column retrofit is definitely needed on older columns with low transverse reinforcement ratios as well as columns with lap splices. The footing shear and flexural capacities should be checked against demands under the rocking response (i.e. the total dead load of the system bearing against the toe of the footing). Enlargement of footings resting on dense soil is not typically warranted as shown by the results described above and based on the 3 times column diameter minimum dimension of the footing.

TABLE V. NONLINEAR ANALYSIS RESULTS FOR MAGNIFIED ACCELERATION RECORDS

Acceleration Record	Column Data			Total Drift (%)
	Diameter (ft)	Reinforcement (%)	Height (ft)	
1.5 x LA09	4	4	20	10.84
1.5 x LA09	5	1	40	Overturned
1.5 x LA09	6	4	30	6.09
1.5 x LA14	4	1	20	Overturned
1.5 x LA14	4	4	20	7.45

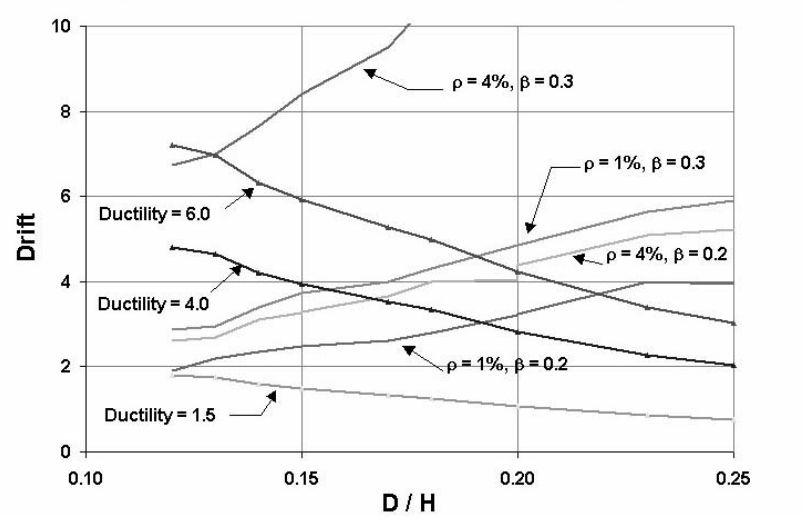

Figure 5. Drift Capacity at Various Limit States for 3D Footing Dimension.

PROPOSED ANALYSIS AND LIMIT STATES FOR ROCKING

Based on the premise of possible change or modification in site condition, it is recommended not to rely on the rocking mechanism to limit displacement demands on the column. In conformance with the state of the practice, this recommendation should be complied with more closely for the design of new bridges than for the assessment of existing bridges. Thus the design of a new column should conform with current established ductility requirements regardless of the possible mechanism that might end governing. Figures 5 and 6 show governing drift capacity at different limit states for column cases utilized in this study using a 3 times the column diameter and a 4 times the column diameter as the footing width. Figures 7 and 8 show a recommended flowchart for the assessment of an existing column/footing system or the design of a new system. The linear procedure mentioned in the Introduction is used to establish the displacement demand "Δ", based on equations (1) to (3). The restoring moment is calculated based on the equilibrium of forces of the deformed column/footing system shown in Figure 1.

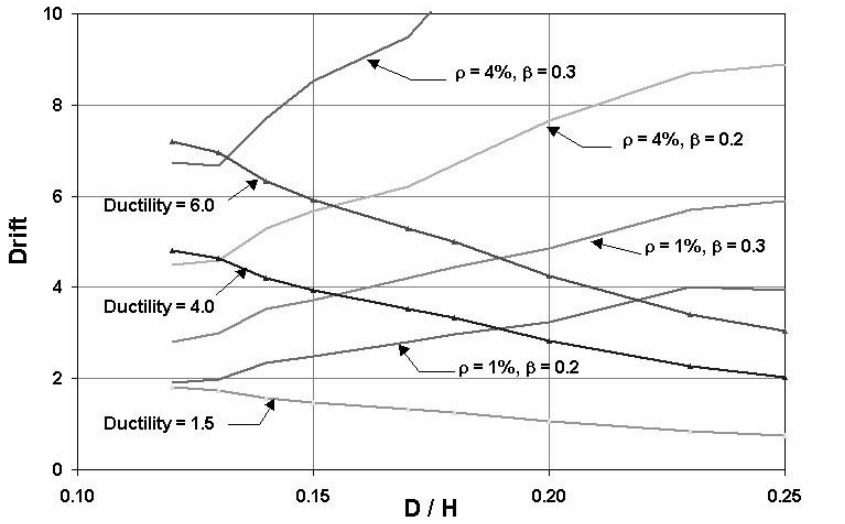

Figure 6. Drift Capacity at Various Limit States for 4D Footing Dimension.

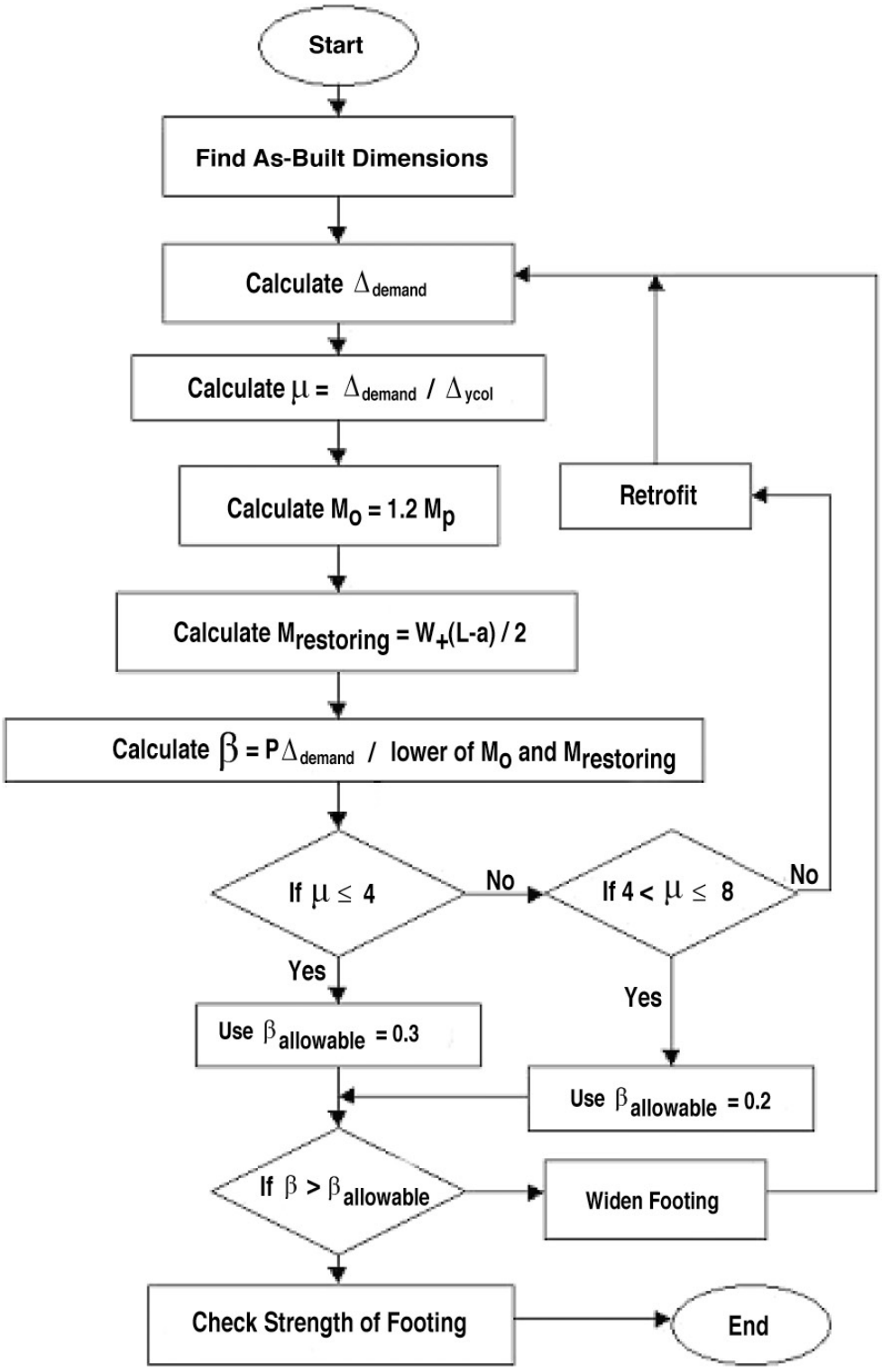

Figure 7. Flowchart for Assessment of an Existing Column/Footing System.

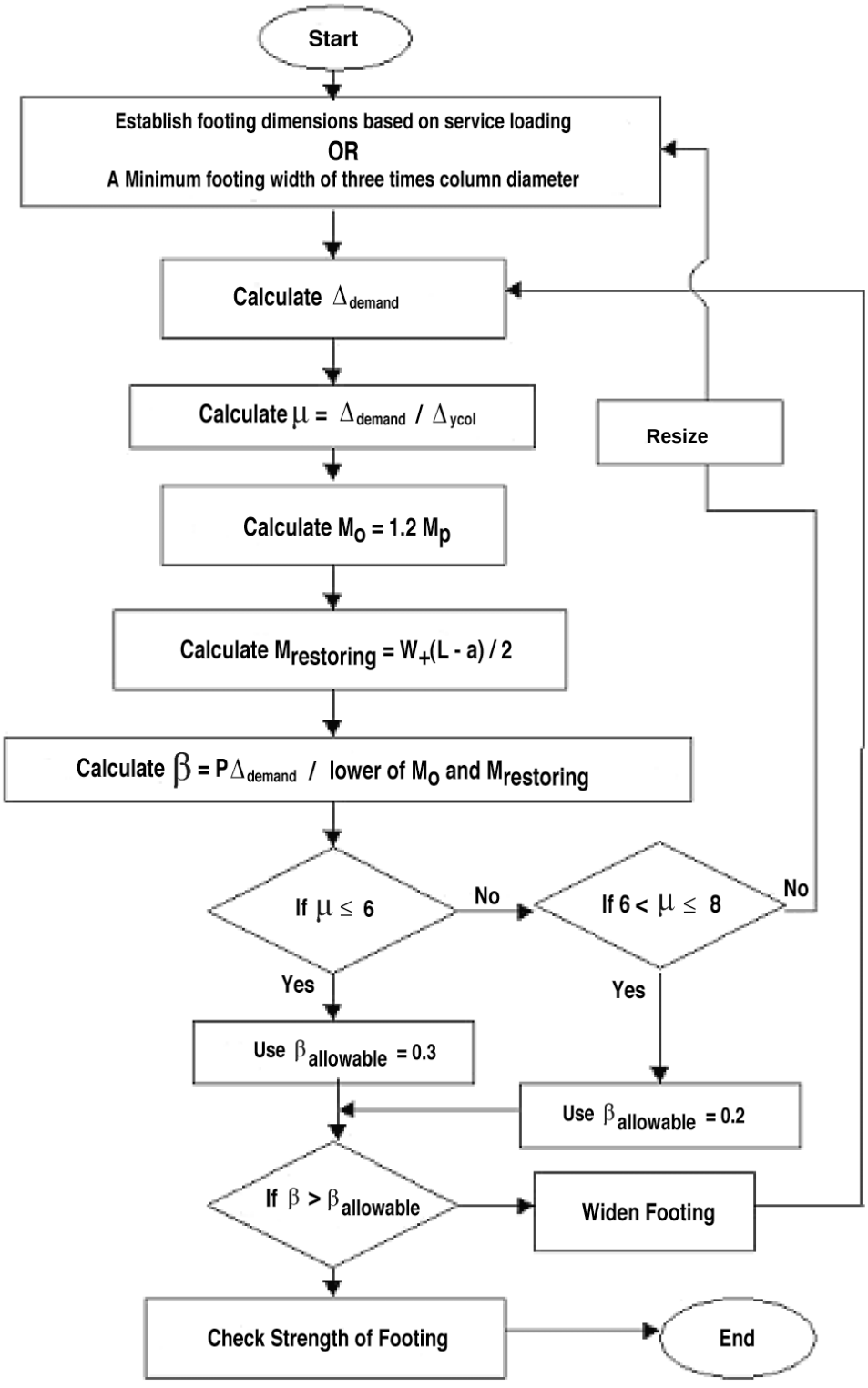

Figure 8. Flowchart for Design of a New Column/Footing System.

CONCLUSIONS

Results of linear and nonlinear analysis are presented and correlated. A simplified method consistent with state of the practice linearization techniques in seismic analysis is presented for the assessment of an existing column/footing system or the design of a new system.

ACKNOWLEDGEMENTS

The authors would like to thank Doug Menzmer and Abhijit Naik of the California Department of Transportation for their contribution to this paper.

REFERENCES

[1] Housner, George W., February 1963. "The Behavior of Inverted Pendulum Structures During Earthquakes," *Bulletin of the Seismological Society of American*, Vol. 53, No.2, pp. 403-417.

[2] Priestley, M.J. Nigel, Frieder Seible, July 1991. "Seismic Assessment and Retrofit of Bridges," *University of California San Diego*, Report No. SSRP-91/03.

[3] Prakash, V., Powel, G.H., and Fillippou, F.C., 1992. "Drain-2DX Base Program User Guide," *University of California Berkeley*, Report No. UCB/SEMM-92/29.

[4] Mander, J.B., M.J.N. Priestley, and R. Park, 1988a. "Theoretical Stress-Strain Model for Confined Concrete," *Journal of Structural Engineering, ASCE,* Vol. 114, No. 8, pp. 1804-1826.

[5] Mander, J.B., M.J.N. Priestley, and R. Park, 1988b. "Observed Stress-Strain Behavior of Confined Concrete,"*Journal of Structural Engineering, ASCE,* Vol. 114, No. 8, pp. 1827-1849.

[6] Somerville, Paul, 1998. "Develop Suites of Ground Motions," *SAC Steel Project Task Number 5.4.1,* Richmond, California.

[7] Mazzoni, Silvia, Jamison Smith and Gregory Fenves, 2001. "Consistent Linearization in Seismic Design," *Progress work for California Department of Transportation.*

Legacy Parkway Seismic Design

STRATEGIES FOR DEVELOPING A HIGH PERFORMANCE STRUCTURE WITH TYPICAL BRIDGE DESIGN FEATURES ON A DESIGN-BUILD PROJECT

Thomas R. Cooper, P.E. and Joseph I. Showers, P.E.

ABSTRACT

The legacy Parkway Project in Salt Lake City, Utah requires that the structures be designed to perform as "essential" structures and therefore perform under seismic loads such that they can be used soon after the design seismic event. The project is at a site with relatively high ground acceleration (0.6g) and soft soils. This results in applied spectral coefficients of 1.2g.

While this type of performance criterion is usually achieved through rather extravagant and costly designs, the Legacy Parkway design and construct team has achieved such seismic performance of the structures using solutions typical to more common bridges. The initial phase of the design-build process provided an opportunity to complete seismic evaluation and design of typical structures considering a variety of factors such as steel and concrete superstructures, single and multiple column bent configurations, and multiple site soil conditions.

This paper will discuss the approaches used to achieve a high level of seismic performance using typical bridge design elements, and also will discuss some of the value engineering concepts that were developed to achieve the high level of performance using typical, off-the-shelf bridge construction elements.

Thomas R. Cooper, P.E., Senior Supervising Engineer, Parsons Brinckerhoff, 3840 Rosin Court, Suite 200, Sacramento, CA 95834

Joseph I. Showers, P.E., Asst. Vice President, Parsons Brinckerhoff, Denver, CO 80264

INTRODUCTION

The legacy Parkway Project in Salt Lake City, Utah requires that the structures be designed to perform as "essential" structures and therefore perform under seismic loads such that they can be used soon after the design seismic event. This paper discusses the seismic design approaches used to achieve this level of performance while using traditional and common bridge components.

Project Description

The Legacy Parkway will be a four-lane, limited-access, divided highway extending approximately 21 kilometers (13 miles) from Interstate 215 (I-215) at 2100 North in Salt Lake City, Utah, northward to Interstate 15 (I-15) and U.S. 89 near Farmington City, Utah. The project will be located in flat topography between the existing I-15 and Union Pacific Railroad corridors and the wetlands east of the Great Salt Lake. The Fluor Ames Kramer Joint Venture began construction of the $330 Million design-build project in the summer of 2001.

The project includes 26 bridges with a combined deck area in excess of 64,000 square meters. All bridges on the project will be constructed with either prestressed concrete girders with maximum spans of 49 meters, or welded steel plate girders for spans of up to 76 meters. The structure type selected for a specific location depended on the bridge geometry, aesthetic considerations, and constraints on construction operations. Both of these structure types are relatively conventional types of construction in the Utah market, and have a proven track record with UDOT.

Substructure components, such as columns and bent caps, are of a standardized design to the maximum extent possible to provide for a maximum economy of repetition to design and construction. Bents are of two types:

- Single column bents with single 2.5 meter octagonal columns and post tensioned bent caps. This type of bent can accommodate cap widths of up to 15 meters.
- Multiple column bents with 1.82 meter octagonal columns and a reinforced concrete bent cap. This type of bent can accommodate cap widths between 15 and 30 meters.

Pot bearings are used on steel plate girder bridges while neoprene bearings are used on prestressed concrete girder bridges. The only exceptions to this are three bents where integral concrete bent caps were used with steel plate girders due to limited vertical clearance over I-15.

Integral abutments are used on all bridges with a total length of 125 meters or less, and seat-type abutments are used on bridges with greater overall lengths.

During the preliminary design of the bridges, efforts were made to eliminate skews on bridges wherever possible. A majority of the abutments and bents are normal to the bridge centerline or have skew angles of less than 15 degrees.

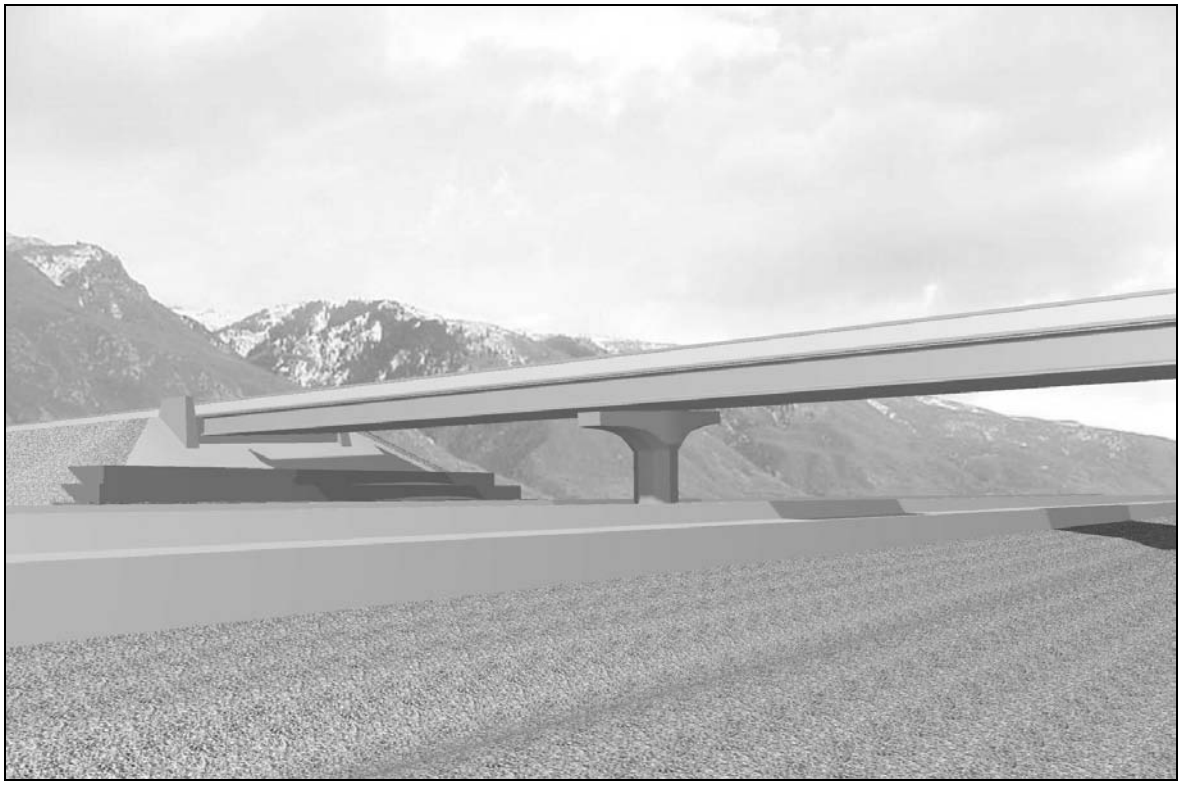

Figure 1. Typical two-span precast I-girder structure on the Legacy Parkway project.

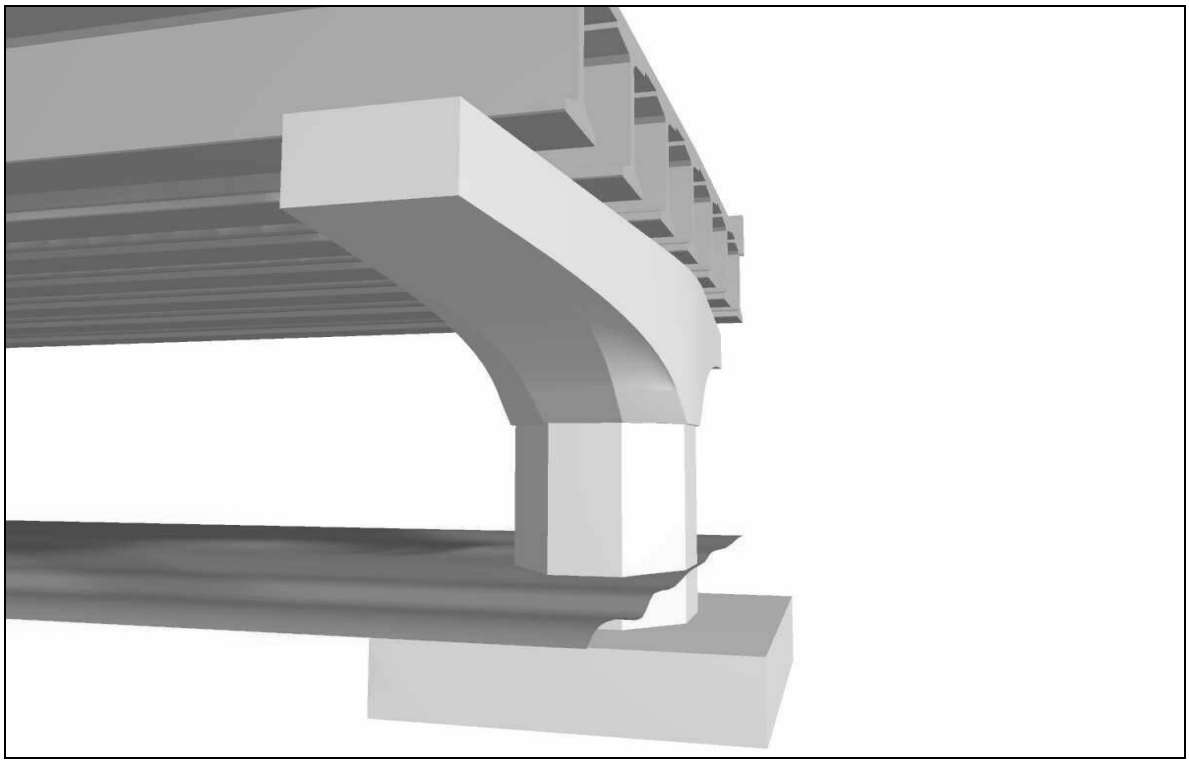

Figure 2. Typical Single column bent supporting continuous precast I-girder superstructure.

Level of Performance

All of the structures are designed as "Essential Bridges" under the definition provided by AASHTO (Division 1-A). The seismic performance level of the structures is "Serviceability", following minor repairs, which may be required, after the event of the "Design Level Earthquake".

Seismicity

The structures are designed for PGA = 0.6g. AASHTO curves for Type III soil are used to account for soil amplification.

Seismic Design Strategies

Seismic design of the bridges for the Legacy Parkway project is primarily based on AASHTO, amended by project specific design criteria, which addresses issues not specifically accounted for by the AASHTO code.
In order to achieve the level of performance required three primary seismic design strategies were used:

1. For fixed-end simple span structures the piles were kept essentially elastic. This was achieved through a combination of seismic resistance by the piles and also by the soil at the abutments. In order to develop reliable lateral resistance of the soil in the transverse direction, abutment "fin walls" were incorporated.
2. For multiple span single column structures, a combination of sliding and minor, repairable column damage was permitted.
3. For multiple span, multi-column bent structures, sliding on standard bearing types was used as the fusing device to avoid damage to columns. This was used on structures that are relatively short, and therefore subjected to high shear loads in the columns and foundations if the superstructure to substructure connection is fixed or pinned.

These strategies were applicable in large extent because of the fundamental approach to have all continuous girder superstructures, hence displacements can occur without the possibility of a drop-off failure. The strategies are discussed further in the following brief case histories of some of the typical structures.

CASE HISTORIES

Case History 1: Bridge 29 – Multi-Span Precast I-Girder on Multi-Column Bents

General Structure Description

The bridge is a 110.3-m long three-span (42.3-m - 34.0m – 34.0-m) multi-girder "regular" (no high skew) bridge with integral abutments that is 25.686-m wide. The superstructure consists of 12 Pre-cast Pre-stressed Concrete "I–Girders" made composite with a concrete deck, pier diaphragm and abutment end diaphragms. The superstructure is integral with the abutments and supported on 2-three-column reinforced concrete bents (see Figure 3).

The abutments are made integral with the superstructure and are supported on a single row of concrete filled steel pipe (406mm x 10mm) Piles. The abutment diaphragms feature fin walls (3.6-m x 3.72-m x 0.915-m with chamfers 0.38-m x 0.610-m at connection with diaphragm) to activate the passive resistance of the embankment during transverse EQ motions (max. pressure= 7.7ksf).

The approach slabs (15.44-m x 24.7-m x 0.580-m) are connected to the bridge deck at each end by reinforcing bar. The connection between the deck and approach slab allows in-plane rotation.

Seismic Behavior

The seismic design strategy for this structure is to allow limited displacements at the piers (displacement and/or movement of the bearings before engaging shear keys), thus limiting the loads that can be transferred to the columns, and controlling seismic load distribution between bents and abutments. Overall displacement of the structure will be controlled by (1) mobilizing backfill soil behind the abutments in the longitudinal direction, and (2) mobilizing backfill soil in the transverse direction via fin walls. Gapped shear keys will be provided for the girder bearings at the pier cap, which will be engaged during higher-level seismic events.
The seismic design strategy for this structure consists of:

- Fused lateral load transfer to piers, via bearings
- Superstructure sliding over support seats

The strategy includes strength design of bearing connections to resist service loads such as wind, and braking forces, as well as a qualitative assessment for more frequent seismic loadings. In the event of design level earthquakes, the bearing connections are designed to fail and therefore act as a fuse limiting force transfer to the substructure.
Upon failure of the bearing connections, the load transfer through the bearings is through friction until the shear keys are engaged. The structure uses the bearing initial stiffness to take advantage of the softening effect of the bearings. This establishes the upper bound of expected seismic loads applied to the substructure, which is within the “essentially elastic” capacity of the pier columns. The “fused” bearing behavior results in superstructure sliding over the girder seats. Shear keys are provided at the bents to lock-up the columns after the superstructure has displaced far enough to use the available longitudinal resistance of the abutment, and as a failsafe mechanism.

Influence of Approach Slabs on System Damping

Energy will be dissipated at the abutments from pushing the soil as well as dragging (pulling or pushing) the approach slabs, thus increasing the damping in the structural system. The viscous damping ratio for this type of behavior varies between 8% and 20%.

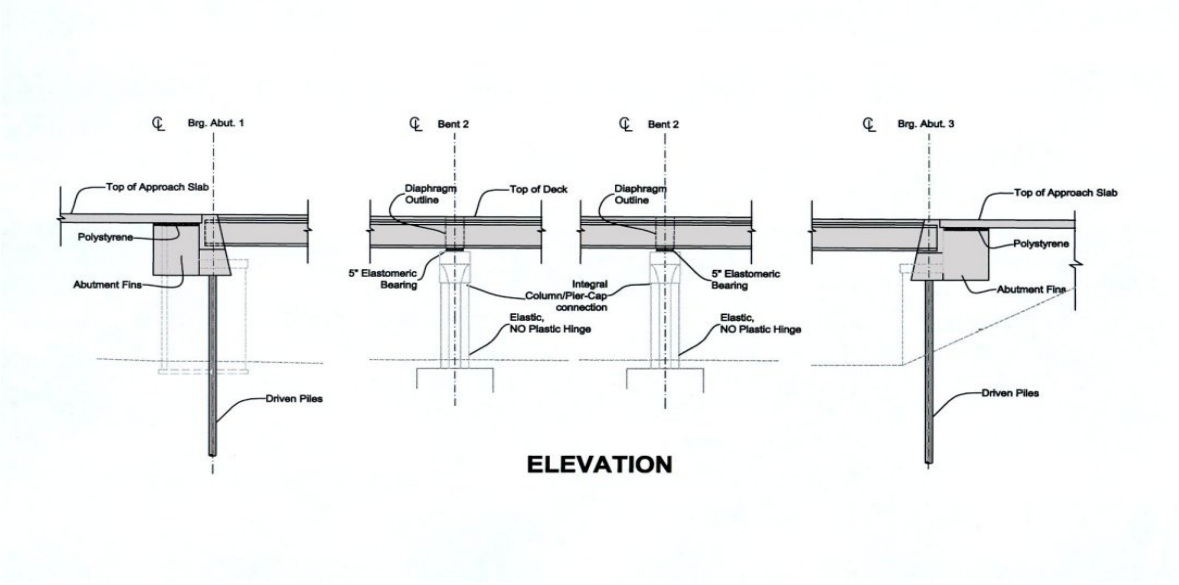

Figure 3. Typical multi-span multi-column bent supporting continuous precast I-girder superstructure.

The spectral acceleration for the range of likely natural periods for this structure resides on the plateau of the response spectrum and represents the maximum value. The results of the multi-modal dynamic analysis showed that the response was typical of that for a regular bridge. The primary response modes were the transverse and longitudinal. The effective seismic weight comprised the superstructure, abutment diaphragm & fin walls and the approach slabs (see Figure 3).

System Capacity

The capacity of the system is understood to be the sum of the following resisting elements.

- Abutment Piles
- Back Wall and fin-wall Passive Pressure
- Approach Slab Friction
- Column-foundation strength (after bearing-key engagement)

Expected Damage Under Design Event

The following are descriptions of the types of damage to be expected for Bridge 29.

Bearings	Minimal damage. May require repositioning.
Superstructure	Essentially elastic response. May require repositioning.
Columns	Minimal repairable post-elastic response
Column Foundations	Piles remain essentially elastic
Exp. Joints	No expansion joints on the structure
Abutment	Potential settlement, piles remain essentially elastic.

Figure 4. Seismic behavior to be expected for Bridge 29.

Case History 2: Bridge 26 – Multi-span Steel Plate Girders on Multi-Column Bents

General Structure Description

The structure is 168.8 m long with three-spans (43.5 m – 67.3 m – 58.0 m). Three of the supports are highly skewed, with a maximum skew of 55 degrees at Bent 3. The substructure consists of short seat type abutments and multi-column bents with non-integral caps. The abutments are supported by two rows of concrete filled steel pipe (406 mm diameter x 10 mm) piles. The columns are octagonal with a long dimension of 1820 mm. Each column is supported on piled footings, using concrete filled steel pipe piles. The superstructure consists of built up steel girders made composite with a concrete deck. Superstructure girders are supported on pot bearings.

Seismic Behavior

The seismic design strategy for this structure consists of:

- Fused lateral load transfer to piers, via bearings
- Superstructure sliding over support seats, including the abutment

The strategy includes strength design of bearing connections to resist service loads such as wind, and braking forces, as well as a qualitative assessment for more frequent seismic loadings. In the event of design level earthquakes, the bearing connections are designed to fail and therefore act as a fuse limiting force transfer to the substructure.
Upon failure of the bearing connections, the load transfer through the bearings is accomplished through friction. This essentially establishes the upper bound of expected seismic loads applied to the substructure, which is well within elastic capacity of the pier columns, with a 1.5% longitudinal reinforcement ratio.
The "fused" bearing behavior results in superstructure sliding over the girder seats, for which adequate width is provided to prohibit unseating at the abutment. Shear keys in the transverse direction are provided at the bents. At the abutments, and primarily in the longitudinal direction, the backfill soil could provide additional resistance strength to limit the extent of superstructure movement. The backfill can contribute to resistance in the longitudinal as well as the transverse directions (i.e. through interaction with wing-walls). However, the seismic design for substructure forces and superstructure displacements has conservatively ignored this backfill resistance.

Expected Damage Under Design Event

Due to the expected fuse at the superstructure – substructure interface, the majority of damage will be localized to the bearing elements. Damage to the abutments will be limited to expansion joint damage. While the entire superstructure is expected to displace at the supporting abutments and bents, unseating will not occur.

While the bridge can be opened to traffic following the immediate repair tasks, follow-up repairs can be performed to replace damaged bearings and connections.

The expected inspection and immediate repair which may be required, following a design level earthquake, will be centering the bridge near it's original position, and temporary repairs over bridge joints to allow for traffic.

Abutment Piles	Essentially elastic pile response
Bearings	Expected elastic response with gapped shear key stoppers in the longitudinal and transverse directions. Bearings will break free from restraint system and slide on the top of the pier cap. .
Superstructure	Essentially elastic response. May require repositioning.
Columns	Minimal repairable post-elastic response
Column Foundations	Piles remain essentially elastic
Expansion Joints	Some Expansion Joint Damage
Abutment	Backwall damage/failure

Figure 5. Seismic behavior to be expected for Bridge 26.

VALUE ENGINEERING CONCEPTS

As a part of the seismic analysis and foundation design of the bridge for the Legacy Parkway project, the project team has undertaken activities that examine the potential options for savings in construction of the bridge foundations (Value Engineering). These areas of potential modification to standard designs are discussed herein:

Pile Tension Capacity

A pile testing program was developed and conducted to evaluate the possibility of using higher axial (tension) pile capacities being used on the designs than is typically allowed by AASHTO. In both tests that were conducted, significantly larger tension capacities were documented than is currently permitted by AASHTO. Once concurrence had been obtained from UDOT to substantiate the validity of the tests, the results were incorporated into the design criteria and design process.

This VE study was successful in developing a design standard for the project that significantly increased the allowable tension capacity of piles for typical bent foundations. This resulted in a relatively large reduction in the number of piles required for bent foundations.

Example of Potential Savings from the Pile Load Testing

In order to demonstrate the savings that have resulted from the pile load testing, a foundation design has been prepared that ignores the results of the vertical pile load testing conducted by FAK for this project and instead uses the standard AASHTO value for tension capacity of 55% of the compression capacity.

Bent	Footing size w/ Testing Results	Number of Piles w/ Testing results	Footing size without Testing Results	Number of Piles without Testing results
2	8.5m x 8.5m x 2.6m	32	8.5m x 8.5m x 2.6m	49
3	8.5m x 8.5m x 2.6m	32	8.5m x 8.5m x 2.6m	49
4	8.5m x 8.5m x 2.6m	32	8.5m x 8.5m x 2.6m	49
5	18m x 5.5m x 2.6m	34	20m x 6.1m x 2.6m	56
6	8.5m x 8.5m x 2.6m	32	8.5m x 8.5m x 2.6m	49
Total	**-**	**162**	**+28.6cu-m**	**252**

Figure 6. Comparison of foundation designs with and without pile tension testing.

Based on the pile compression capacity provided by the geotechnical engineer for typical footing piles, the results from the analysis of the effect of reducing pile tension capacity are summarized above.

Use of 65ksi Steel for Piles

Potential savings from the use of 65ksi steel instead of the traditional 50ksi steel was identified and evaluated for both bent and abutment foundations. This approach was significantly more effective than adding more piles in providing an elastic foundation. This VE study was successful in developing a design standard for the project that significantly decreased the number of piles for integral abutments and also worked in concert with the pile tension testing program to reduce the number of piles required to resist tension loads in the bent foundations.

Fused Bearings

Fused sliding bearing strategies, particularly for the stiffer structures, provided several benefits:

- Reduced the seismic lateral loading due to softening effect on the dominant modes of vibrations
- Reduced the strength and reinforcement required at the fixed ends of columns
- Reduce the bending demands on pile group foundations at the base of the columns, and therefore, reduce the number of required piles.

For the 0.6g PGA loading, majority of the structures with periods of vibration less than 0.8 seconds, draw the maximum 1.2g spectral acceleration. The traditional force and deformation control methods provided minimal options to favorably alter the structure dynamic characteristics.

Seismic performance of stiffer structures, which converge at higher ranges of code-permitted “repairable damage”, was considerably improved by fused bearing strategies. (Note: While use of this approach using traditional bearing types proved to be effect for this application, if the required level of performance was for “no damage”, then use of true isolation devices would be a more appropriate design strategy.)

Results of Fused Bearing Evaluation

As noted above, the seismic performance of some of the bridges, as well as their design and construction complexities and cost can considerably be improved using fused bearings.

	Non-Fused	**Fused Bearings**
Bearing properties	Pinned	Fuse at 40%g
Governing Column Moment demands (kips-ft)	38,000	8400
Column Plastic Moment Capacity (1.5% rebar, Kips-ft)	13249	13249
Foundation Size (footing, no. of piles) **Seismic Load Design**	21.3 ‘ x 21.3 ‘ 25-150 Ton Piles	20’ x 20’ 12-150 Ton Piles
Foundation Size (footing, no. of 150 ton piles) **Service Load Design**	18’ x 18’ 8 - 150 ton piles	18’ x 18’ 8 – 150 ton piles

Figure 7 – Comparison of column response of fused vs. non-isolated strategies for a typical bent of a multi-span, multi-column structure on the Legacy Parkway Project.

Figure 7 shows how column base moment demands will be reduced by 30%, relative to AASHTO permitted design, based on allowed elastic force-reduction factors. For this case, foundation strength was reduced up to 30% (e.g. less piles), and the column remained essentially elastic (e.g. no damage and fully serviceable).

The fused bearing strategy essentially allows for placement of a “weak-link fuse”, by design, in the seismic load path. It should be noted that the bridge structures within this project, the strategy of “weak-link fuse” is part of the design by use of traditional elastomeric bearing or pot bearing, in combination with shear keys with limited strength. This strategy benefits from the advantages of isolation design strategies at no additional cost for specialty devices.

CONCLUSION

Seismic design strategies that use traditional, off-the-shelf bridge elements have been used to develop designs that result in serviceable behavior following the design seismic event. The designs cover a wide breadth of structure types and also address the difficult and often costly impacts of constructing highway structures in soft soil sites, where seismic loads are high.

Plastic Hinge Length of Reinforced Concrete Bridge Columns

Robert K. Dowell and Eric M. Hines

ABSTRACT

The displacement capacity of a reinforced concrete bridge column is a function of the curvature capacity of the critical section, column height and equivalent plastic hinge length. Capacity design philosophy requires the column displacement capacity to be greater than the maximum displacement demand from seismic loading. Therefore, the plastic hinge length is of critical importance in determining the seismic safety of reinforced concrete bridge structures. The UCSD plastic hinge length expression has been used extensively in California and elsewhere and has worked well for typical circular and rectangular bridge columns. However, recent column tests at UCSD, comprised of highly confined boundary elements separated by a shear wall and similar to the new East Bay Spans of the San Francisco-Oakland Bay Bridge (SFOBB), Second Benicia Martinez Bridge and Third Carquinez Strait Bridge indicate that the plastic hinge length for unusual section geometries may be more than twice the length from the current expression. This increase is due to additional tension shift associated with the wider columns and demonstrates an overly conservative design using the existing expression.

The UCSD plastic hinge length expression is empirically based and is a function of the column length and longitudinal rebar size. Aspect ratio, axial load ratio, longitudinal steel ratio and transverse steel ratio are not included in the hinge length determination. In the paper a new plastic hinge length expression is derived from the idealized moment-curvature response and the diagonal shear crack angle in the hinge region, found from the 3-component UCSD shear equation. The new plastic hinge length expression is derived from basic principles, which allows it to be used for any section shape. Longitudinal steel and axial load ratios influence the plastic hinge length indirectly by changing the idealized moment-curvature response. The amount of transverse steel and the aspect ratio also affect the plastic hinge length by modifying the shear crack angle and the amount of tension shift. It is a simple expression intended for design and analysis. The new approach results in more economical designs for wide bridge columns and has been used for prediction analysis of the Longitudinal Column Test of the SFOBB at UCSD .

Robert K. Dowell, Principal, Dowell-Holombo Engineering, Inc., 6264 Rockhurst Drive, San Diego, CA 92120 and Lecturer, University of California, San Diego, La Jolla, CA 92093-0085
Eric M. Hines, Graduate Student, University of California, San Diego, La Jolla, CA 92093-0085

INTRODUCTION

The equivalent plastic hinge length is a useful engineering concept for the seismic design of reinforced concrete (RC) bridge columns, allowing displacement capacity to be determined from curvature capacity of the critical section and member length. Curvature capacity is found from moment-curvature analysis of the critical section and is terminated when either the extreme tension reinforcing bar or extreme confined concrete compression fiber exceed limiting strain values.

For typical RC bridge columns a plastic hinge length expression was developed at UCSD [1], which is a function of the cantilever length L and strain penetration, given as

$$L_p = 0.08L + 0.15 f_y d_b \qquad (f_y \text{ in ksi})$$

With Grade 60 steel and probable yield stress of 66 ksi, this may be approximated as

$$L_p = 0.08L + 10 d_b$$

The two terms allow for (1) nonlinear curvature distribution along the member length and tension shift due to diagonal shear cracking as well as (2) strain-penetration of the vertical column reinforcement into the footing or superstructure. The UCSD plastic hinge length expression has been used extensively in California for the seismic design of new bridges and seismic retrofit design of older existing bridges, as well as for prediction and post-test analyses of large-scale structural tests at UCSD and elsewhere. It has worked well for typical column design with circular or rectangular section geometry.

Recent tests at UCSD of more unusual column shapes [2], comprised of highly confined corner elements separated by a shear wall ("barbell" column tests) and representative of several new toll bridge column designs, such as the East Bay Spans of the San Francisco-Oakland Bay Bridge, Second Benicia Martinez Bridge and the Third Carquinez Strait Bridge, indicate that the UCSD plastic hinge length expression may not work as well for columns with complicated section geometry. The test results clearly demonstrate that the plastic hinge length is a function of both the cantilever length and the section width. With a wider section, the tension shift effect increases with greater spread of plasticity. The degree that tension shift increases the plastic hinge length depends on the section width and the diagonal shear crack angle in the plastic hinge region, which is influenced by the amount of transverse shear reinforcement and the curvature ductility demand. From typical moment-curvature analysis, the amount of transverse shear reinforcement has no effect on the force-deformation results. However, test results in [2] demonstrate that the amount of transverse shear reinforcement has an effect on the plastic hinge length and should be included in determining the displacement capacity of the member.

In the paper, a new plastic hinge length expression is proposed for RC bridge columns that allows for variations in section shape, axial load level and longitudinal and transverse reinforcement levels. Rather than an empirical approach, as presented in [1], a closed form expression is derived directly from the idealized moment-curvature response and diagonal shear crack angle. The UCSD shear equation [1, 3] is used in conjunction with the moment-curvature

program ANDRIANNA [4] to determine the shear crack angle θ and ratio η of shear resisted by transverse steel V_s to the ultimate shear force V_u.

Plastic hinge lengths determined from the proposed equation are compared to "measured" plastic hinge lengths that were back-calculated from results of 5 "barbell" column tests reported in [2]. The new approach results in a plastic hinge length expression that is a function of both the column length and width, as well as the critical shear crack angle. The effects of section shape, axial load level, longitudinal steel ratio and confinement steel on the plastic hinge length are indirectly considered through their influence on the shape of the idealized moment-curvature response. As mentioned above, the amount of transverse shear reinforcement can be an important contributor to the plastic hinge length and is included in the proposed expression through its effect on the diagonal shear crack angle associated with tension shift.

The diagonal shear crack angle is determined from simple hand methods at ultimate moment, which has shown good agreement with the Modified Compression Field Theory [5] and measured test results. As the proposed approach includes the amount of transverse shear reinforcement to determine the diagonal shear crack angle, a reduction in transverse shear reinforcement results in a longer plastic hinge length, in agreement with the findings reported in [2].

SPREAD OF PLASTICITY WITH NO TENSION SHIFT

Typical moment-curvature and idealized moment curvature results are given in Figure 1. The first branch of the idealized moment-curvature response goes through first yield and extends until nominal moment is reached, which defines the idealized yield point or curvature ductility 1. The first yield point is defined by the moment and curvature where the extreme tensile rebar first reaches yield. Nominal moment is defined as the moment where either the extreme compression concrete strain reaches 0.004 or the extreme rebar tensile strain reaches 0.015. Ultimate moment and curvature are based on the ultimate compressive strain capacity of the confined concrete, defined by the Mander Model [6] or the ultimate tensile strain capacity of the reinforcing steel. The second branch of the idealized moment-curvature response is defined by the idealized yield point and the ultimate curvature point, with its slope being extremely important to the spread of plasticity and the plastic hinge length.

Figure 2 shows four inter-related graphs that share axes at their boundaries, clearly demonstrating the shaded plastic hinge region in the lower right graph (with all curvatures in the shaded region exceeding the idealized yield curvature). The horizontal axis to the right of the origin represents section curvature and the horizontal axis to the left of the origin defines the position *x* along the member length, measured from the critical section. The vertical axis above the origin represents section moment and the vertical axis below the origin defines the position *x* along the member length, measured from the critical section.

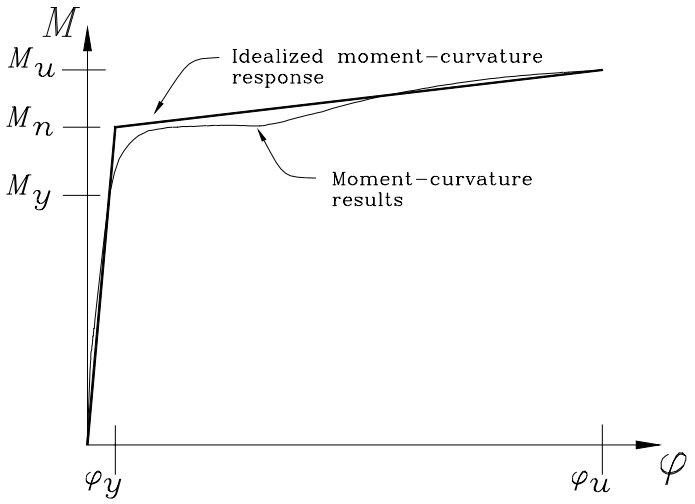

Figure 1. Idealized moment-curvature response of RC column

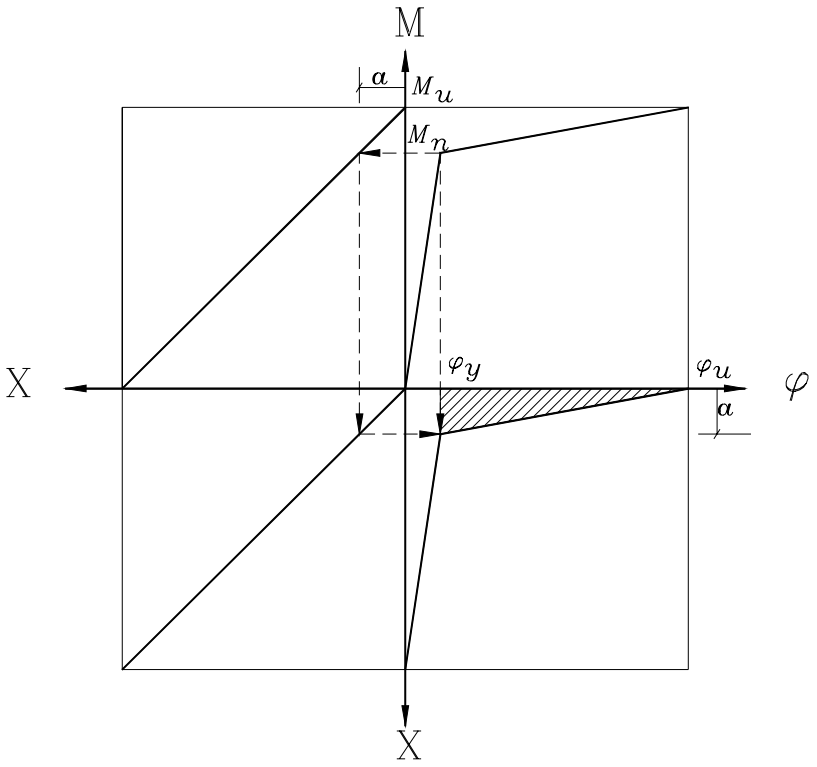

Figure 2. Spread of plasticity for cantilever column at ultimate (no tension shift)

The top right graph of Figure 2 is the idealized moment-curvature response, the top left graph is the moment diagram along the member length, the bottom left graph represents the position *x* versus position *x* along the member length and will, therefore, always be diagonal (used to reflect results from the moment diagram graph to the curvature distribution graph), and the bottom right graph is the desired curvature distribution along the member length, which is required to determine the plastic hinge length. As demonstrated in Figure 2, the curvature

distribution along the member length is found by extending horizontal and vertical lines from points along the idealized moment-curvature graph, and finding their intersections in the curvature-*x* graph.

TENSION SHIFT

The spread of plasticity shown in Figure 2 includes the ratio of ultimate to nominal moment, which is known to be an important factor in the spread of plasticity. Not considered in Figure 2 is the tension shift effect, which also has an important influence on the spread of plasticity and on the plastic hinge length. The tension shift phenomenon results in larger than expected flexural rebar stress and is due to diagonal shear cracking, as discussed in many books on RC, such as [1] and [5]. This is also the reason that the ACI code [7] requires reinforcement to extend a distance *d* beyond where it is needed based on flexure alone. The tension shift *k* multiplied by the applied shear force *V* equals the additional moment that the reinforcement is associated with. In the development of the plastic hinge length expression, the moment diagram in the upper left graph of Figure 3 is modified to account for tension shift. In the critical region, tension shift varies as a function of the distance *x* from the column base, given as

$$k = \left(x - \frac{\eta}{2a_1} x^2 \right) \qquad (x \le w\tan\theta) \qquad (1)$$

with $\eta = V_S/V_U$ and $a_1 = w\tan\theta$. This expression shows that with $x = 0$ there is no tension shift at the column base, which is consistent with observed horizontal cracks and the limiting moment at the critical interface section. With $x = a_1$ the tension shift from Eq. (1) is

$$k = a_1\left(1 - \frac{\eta}{2}\right) = a_2 = w\tan\theta\left(1 - \frac{\eta}{2}\right) \qquad (x \ge w\tan\theta) \qquad (2)$$

The increased spread of plasticity due to tension shift is evident in the bottom right graph of Figure 3 (shaded area), compared against the graph with no tension shift included (Figure 2). The same graphical procedure used to develop Figure 2 was employed in the development of Figure 3, with the moment diagram (upper left graph) shifted by *k* from Eqs. (1) and (2) to allow for the tension shift phenomenon. Also shown in Figure 3 is the original linear moment diagram, and thus the tension shift *k* is the horizontal distance between original and shifted moment diagrams. In the following section, the plastic hinge length expression is derived for a RC bridge column with tension shift included. As discussed previously, tension shift can be an important contributor to the plastic hinge length and displacement capacity of a member, especially for wide columns.

PLASTIC HINGE LENGTH

The plastic hinge length is derived in the following for a RC bridge column with tension shift included. Plastic rotation is found by integrating plastic curvatures over the length *a* shown in Figure 3. At any location *x* beyond *a* the member remains elastic and, therefore, there is no

need to integrate curvatures over the entire member length. Plastic rotation is defined as the summation of plastic curvatures over the extent of plasticity *a*, which is longer than the plastic hinge length.

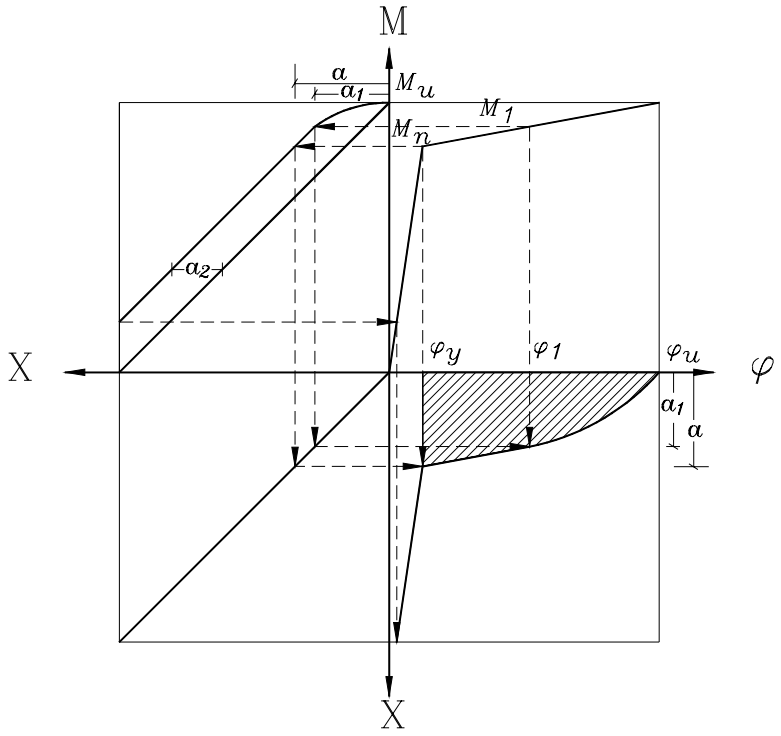

Figure 3. Spread of plasticity for cantilever column with tension shift included

As Figure 3 demonstrates, with tension shift included there are two distinct regions to integrate curvatures over, namely, from zero to a_1 and from a_1 to a. Therefore, the plastic rotation integral is defined with two terms as

$$\theta_p = \int_0^a \phi_p dx = \int_0^{a_1} \phi_p dx + \int_{a_1}^a \phi_p dx \tag{3}$$

The first limit a_1 in Eq. (3) is given as $w\tan\theta$, and the second limit a represents the total spread of plasticity as found in the following. Limit a is the distance from the critical section to a member location x where no further yielding or plasticity develops (based on idealized yield). This is found from Figure 3 as

$$a = w\tan\theta\left(1-\frac{\eta}{2}\right)+\mu L \tag{4}$$

where the overstrength ratio is

$$\mu = \left(1-\frac{M_n}{M_u}\right)$$

The 1st and 2nd terms of Eq. (4) are related to tension shift and overstrength, respectively. The plastic rotation defined in Eq. (3) is written, with limits, as

$$\theta_p = \int_0^{w\tan\theta} \phi_p dx + \int_{w\tan\theta}^{w\tan\theta\left(1-\frac{\eta}{2}\right)+\mu L} \phi_p dx \tag{5}$$

Plastic curvature is a function of the idealized moment-curvature response and the shifted moment demand m_x, at any location x along the member length. The plastic curvature expression is given as

$$\phi_p = \left(\phi_u - \phi_y\right)\left(\frac{m_x - M_n}{M_u - M_n}\right)$$

where the moment demand m_x is shifted or modified due to tension shift (see top left graph of Figure 3). There are two distinct regions of tension shift. Within limit a_1, tension shift is

$$k = \left(x - \frac{\eta}{2a_1}x^2\right) \qquad (x \le a_1 = w\tan\theta) \tag{6}$$

allowing the moment demand to be defined as the section moment m_{sec} plus tension shift k multiplied by the shear force V, or

$$m_x = m_{\text{sec}} + Vk \tag{7}$$

The section moment along the member length is defined in terms of the ultimate moment M_u and the distance from the critical base section x as

$$m_{\text{sec}} = M_u\left(1 - \frac{x}{L}\right) \tag{8}$$

Thus the shifted moment is found by substituting Eqs. (6) and (8) into Eq. (7), resulting in

$$m_x = M_u\left(1 - \frac{x}{L}\right) + V\left(x - \frac{\eta}{2a_1}x^2\right) \tag{9}$$

Replacing shear force V in Eq. (9) with the ultimate moment M_u divided by the cantilever length L, and simplifying, results in the shifted moment m_x at location x of

$$m_x = M_u\left(1 - \frac{x}{L}\right) + \frac{M_u}{L}\left(x - \frac{\eta}{2a_1}x^2\right) = M_u\left(1 - \frac{\eta}{2a_1 L}x^2\right)$$

With a_1 given as $w\tan\theta$, the moment m_x in the critical region is written in its final form as

$$m_x = M_u\left(1-\frac{\eta}{2Lw\tan\theta}x^2\right) \qquad (x \le w\tan\theta) \qquad (10)$$

Similarly, for the remainder of the member length ($x \ge w\tan\theta$) the shifted moment is given as the section moment plus the shear force V multiplied by the maximum tension shift a_2. The tension shift for this portion of the member is constant as shown in Figure 3, given as

$$k = a_2 = w\tan\theta\left(1-\frac{\eta}{2}\right) \qquad (11)$$

Thus the shifted moment is written below as the section moment from Eq. (8) plus the shear force V multiplied by the constant tension shift k from Eq. (11).

$$m_x = M_u\left(1-\frac{x}{L}\right)+Vk$$

Replacing the shear force V with the ultimate moment divided by the column length, and replacing tension shift k with Eq. (11) gives

$$m_x = M_u\left(1-\frac{x}{L}\right)+\frac{M_u}{L}w\tan\theta\left(1-\frac{\eta}{2}\right)$$

which, upon simplifying, results in

$$m_x = M_u\left(1-\frac{x}{L}+\frac{w}{L}\tan\theta\left[1-\frac{\eta}{2}\right]\right) \qquad (x \ge w\tan\theta) \qquad (12)$$

The plastic rotation is given as

$$\theta_p = \int_0^{w\tan\theta}\phi_p\,dx + \int_{w\tan\theta}^{w\tan\theta\left(1-\frac{\eta}{2}\right)+\mu L}\phi_p\,dx$$

which is written in terms of the tension-shifted moments m_x as

$$\theta_p = \int_0^{a_1}\left(\phi_u-\phi_y\right)\left(\frac{m_x-M_n}{M_u-M_n}\right)dx + \int_{a_1}^{a}\left(\phi_u-\phi_y\right)\left(\frac{m_x-M_n}{M_u-M_n}\right)dx \qquad (13)$$

With the shifted moment m_x in Eq. (13) replaced by Eq. (10) in the first term and Eq. (12) in the second term, the plastic rotation is written

$$\theta_p = (\phi_u - \phi_y)\int_0^{a_1}\left(\frac{M_u\left[1-\frac{\eta x^2}{2Lw\tan\theta}\right]-M_n}{M_u-M_n}\right)dx + (\phi_u - \phi_y)\int_{a_1}^{a}\left(\frac{M_u\left[1-\frac{x}{L}+\frac{w}{L}\tan\theta\left(1-\frac{\eta}{2}\right)\right]-M_n}{M_u-M_n}\right)dx$$

Plastic rotation is also defined in [1] as

$$\theta_p = (\phi_u - \phi_y)L_p$$

By equating plastic rotations from the above two expressions, ultimate and yield curvatures cancel from both sides of the equation and the plastic hinge length is written

$$L_p = \int_0^{a_1}\left(\frac{M_u\left[1-\frac{\eta x^2}{2Lw\tan\theta}\right]-M_n}{M_u-M_n}\right)dx + \int_{a_1}^{a}\left(\frac{M_u\left[1-\frac{x}{L}+\frac{w}{L}\tan\theta\left(1-\frac{\eta}{2}\right)\right]-M_n}{M_u-M_n}\right)dx$$

which reduces to

$$L_p = \int_0^{a_1}\left(1-\frac{\eta x^2}{2\mu Lw\tan\theta}\right)dx + \int_{a_1}^{a}\left(1-\frac{x}{\mu L}+\frac{w}{\mu L}\tan\theta\left[1-\frac{\eta}{2}\right]\right)dx \qquad (14)$$

By integrating Eq. (14), and simplifying, the final plastic hinge length is given as

$$L_p = \frac{\mu L}{2} + w\tan\theta\left(1-\frac{\eta}{2}\right) + \frac{w^2\tan^2\theta}{\mu L}\left(\frac{\eta^2}{8}-\frac{\eta}{6}\right) \qquad (15)$$

Or as a ratio of the column length

$$\frac{L_p}{L} = \frac{\mu}{2} + \lambda\tan\theta\left(1-\frac{\eta}{2}\right) + \lambda^2\frac{\tan^2\theta}{\mu}\left(\frac{\eta^2}{8}-\frac{\eta}{6}\right) \qquad (16)$$

Note that λ is the member aspect ratio *w/L* and *w*, θ, μ and η are the distance between tension and compression centroids, diagonal crack angle, overstrength ratio and transverse steel shear force ratio, respectively. The 1st term in Eq. (15) is from overstrength, the 2nd term is associated with constant tension shift and the 3rd term reduces the constant tension shift due to the flattening shear cracks near the critical section. This 3rd term is responsible for the varying curvature distribution within the critical distance a_1 in the lower right graph of Figure 3. It is of interest to note that the aspect ratio λ of the member is clearly represented in the 2nd and 3rd terms of the plastic hinge length expression given in Eq. (16).

COMPARISONS TO MEASURED PLASTIC HINGE LENGTHS

Five RC "barbell" cantilever columns were tested at UCSD [2], each consisting of a shear wall with highly confined boundary end regions. The section geometry was identical for the five columns, with the exception of a reduced wall thickness from 6 inches to 4 inches for Column 2C. Columns 1A and 1B were flexural columns with a height of 16 ft, while Columns 2A, 2B and 2C were shear columns with a height of 8 ft. Vertical wall and boundary reinforcement, as well as boundary confinement steel were identical for all five columns. The only difference between the two flexural columns was that Column 1B had minimal transverse shear reinforcement in the wall that connects confined boundary elements, whereas Column 1A had enough transverse wall reinforcement to resist the entire shear force associated with column plastic hinging. Shear Columns 2A and 2B had the same difference in transverse wall reinforcement as Columns 1A and 1B, with minimal transverse wall reinforcement for Column 2B and enough transverse wall reinforcement in Column 2A to resist the entire shear force from column plastic hinging. Due to the reduced wall thickness of 4 inches and the least amount of transverse wall reinforcement, Column 2C had the most severe shear damage of the 5 test specimens.

For each of the five tests, "measured" plastic hinge lengths were back-calculated from the experimental test data and reported in [2]. Values of the critical shear crack angle θ and shear ratio $\eta\ (V_s/V)$ are found from the UCSD shear equation [1, 3] in conjunction with moment-curvature results from ANDRIANNA [4] at ultimate. Measured day-of-test concrete strengths and measured reinforcement material properties were used in the moment-curvature analyses. The plastic hinge length results show fairly close agreement between calculated and measured, using the derived hinge expression given in Eq. (15), (see Figures 4 and 5) in conjunction with calculated shear crack angles. Note that a strain penetration term is added to the plastic hinge lengths calculated from Eqs. (15 and 16), consistent with the 2nd term of the UCSD plastic hinge length expression [1]. Thus, calculated plastic hinge lengths presented in Figure 4 include a strain penetration value of 4.95 inches, which is approximately 10 bar diameters. If the total calculated plastic hinge length is less than twice the strain penetration, then the plastic hinge length is equal to two times the strain penetration value, as suggested in [1].

The bar charts in Figures 4 and 5 show the improvement of the proposed method of calculating the plastic hinge length for bridge columns with unusual cross-section shape, compared to the original UCSD plastic hinge length expression [1]. For Columns 2A, 2B and 2C the UCSD expression results in less than ½ the measured plastic hinge length. Figure 4 shows two results from the new approach; data labeled *New Model, derived shear angle* are results from the proposed plastic hinge length expression given in Eq. (15) with the shear crack angle calculated from the UCSD shear equation. Data labeled *New Model, measured shear angle* are results from the same expression given in Eq. (15) with the average shear crack angle measured from the column tests. This demonstrates that differences between measured and calculated plastic hinge lengths can be attributed to variations in the shear crack angle used in Eq. (15), with the two sets of calculated values typically bounding the "measured" plastic hinge lengths.

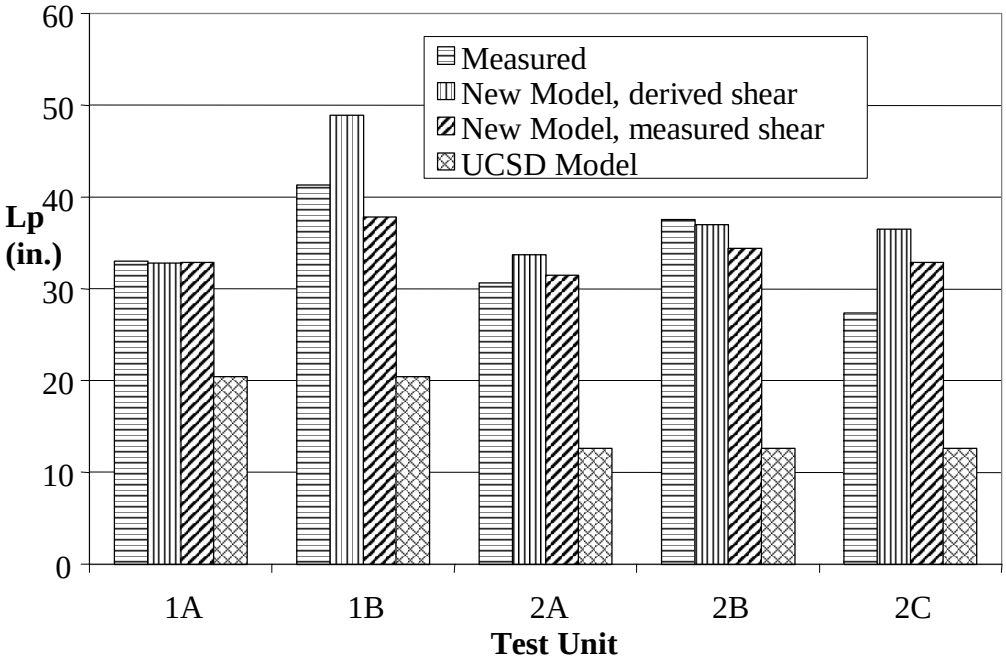

Figure 4. Comparison of measured and calculated plastic hinge lengths.

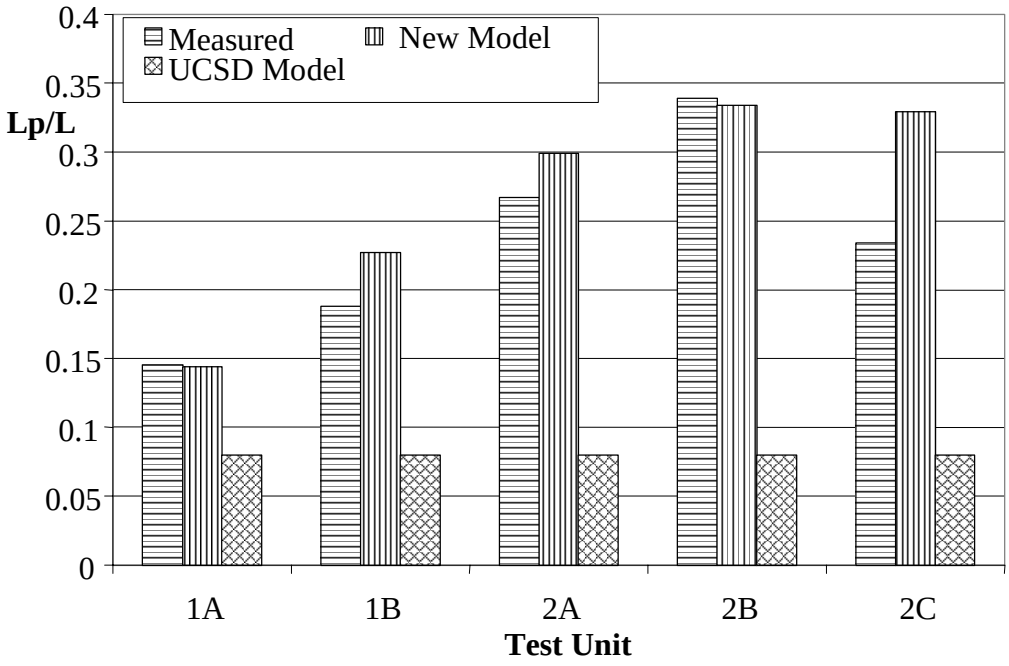

Figure 5. Experimental and calculated plastic hinge length ratios.

Figure 5 compares measured and calculated [Eq. (16)] plastic hinge length ratios (without strain penetration included) for the five "barbell" column tests. Results are presented in this form to

allow direct comparison to the well-known UCSD plastic hinge length ratio of 0.08. The results show that the measured plastic hinge length ratio can be more than 4 times the UCSD coefficient, whereas the new method follows the experimental results fairly closely for all tests considered. Results from the new plastic hinge length expression in Figure 5 are based on derived shear crack angles. As was shown in Figure 4, closer results are possible with improved knowledge of the average shear crack angle, giving further confirmation of the new plastic hinge length expression.

CONCLUSIONS

A new plastic hinge length expression has been developed for RC bridge columns. Compared to other plastic hinge length expressions that are based on specific test results, the proposed expression is derived from first principles and is therefore applicable to a wider variety of column types, as demonstrated in the paper. Comparisons to "measured" plastic hinge lengths from structural tests at UCSD have shown that the new approach gives closer results than the original UCSD expression for bridge columns of unusual section shape and similar results for the more typical circular columns. Plastic hinge length expressions typically give the hinge length as a proportion of either the member length or the member width. In reality, the plastic hinge length is a function of member depth and length, as well as the diagonal shear crack angle. A rational method has been proposed for determining the plastic hinge length of RC bridge columns that is applicable for typical and more unusual column shapes.

REFERENCES

1. Priestley, M.J.N., Seible, F., and Calvi, G.M., *Seismic Design and Retrofit of Bridges*, John Wiley & Sons, New York, 1996.
2. Hines, E.M., Seible, F., Priestley, M.J.N., *Cyclic Tests of Structural Walls with Highly-Confined Boundary Elements*, UCSD Report, June 11, 2000.
3. Kowalsky, M.J., and Priestley, M.J.N., *Improved Analytical Model for Shear Strength of Circular Reinforced Concrete Columns in Seismic Regions*, ACI Structural Journal, V. 97, No. 8, May-June, 2000.
4. Dowell, R.K., *ANDRIANNA User's Manual*, Version 1, 2001.
5. Collins, M.P., and Mitchell, D., *Prestressed Concrete Structures*, Prentice-Hall, Inc., Englewood Cliffs, New Jersey, 1991.
6. Mander, J.B., *Seismic design of bridge piers*, University of Canterbury, Christchurch, Ph.D. Dissertation, 1984.
7. ACI Building Code Requirements for Structural Concrete (ACI 318-95), American Concrete Institute, Detroit, Mich., 1995.

Applicability of the Pushover Based Procedures for Bridges

Matej Fischinger and Tatjana Isaković

ABSTRACT

Introducing new performance-based design procedures, pushover analysis has become increasingly popular. However, many of these procedures are simply extrapolated from buildings, not taking into account specific characteristics of the bridge structures. The specific and complex response of the bridge may preclude the use of the static, pushover based analysis. Thus, the objective of the reported research has been to identify the cases where the pushover analysis is acceptable and the cases where more rigorous inelastic time-history analysis is required for viaduct structures.

Several cases of a three span single column bent viaducts were analyzed in the transverse direction. The stiffness of piers, the eccentricity of mass, the boundary conditions at the abutments, and the reinforcement of columns were varied. The N2 method, which combines inelastic static (push-over) analysis of the MDOF system and inelastic spectrum analysis of an equivalent SDOF system, was used. The results of the N2 procedure were compared by the inelastic time-history analysis.

Although the N2 method frequently yielded similar results as the inelastic time-history analysis, there were several cases, where the two methods yielded significantly different results, not only quantitatively but also qualitatively. Qualitative differences were found in cases where the torsional structural stiffness was smaller than the flexural one. Other important parameters that influence the seismic response of viaducts in the transverse direction include the ratio of the stiffness of the deck and piers, eccentricity, boundary conditions at the abutments, and the relative strength of the columns.

A “regularity index” has been proposed as a numerical measure to help the designer to decide about the suitability of the pushover analysis for bridges. The index is defined as a relative difference between the areas bounded by the normalized displacement lines obtained within the first and second iteration of the N2 method.

A general conclusion has been that the pushover based procedures for bridges should be used with care. In a case of rather complex bridges, time-history analysis may be more suitable solution.

Matej Fischinger, Professor, Tatjana Isaković, Assistant Professor, both
University of Ljubljana, Faculty of Civil and Geodetic Engineering, Institute of Structural Engineering and Earthquake Engineering, Jamova 2, Ljubljana, SI-1000 Slovenia

INTRODUCTION

It has been widely recognized that standard elastic seismic analysis procedures may not always yield adequate results. A single parameter (seismic response reduction factor) is often not enough to correctly account for the energy dissipative capacity of certain structural systems, in particular in the case of irregular structures and non-standard structural solutions. Therefore a wide consensus has been reached (i.e. [1]) that new inelastic procedures are needed.

In principle, the inelastic time-history analysis is the correct approach. However, at the present it may not be feasible or at least practical for everyday design use, since the additional requirements include (but are not limited to) the knowledge and data about ground motions and hysteretic behavior of structural elements, materials and mechanisms.

Nowadays the most rational analysis and performance evaluation methods for practical application appear to be simplified inelastic procedures, which combine the non-linear static (pushover) analysis and the response spectrum method [2]. In fact these methods have been around for many decades [3, 4, 5]. However the earthquake engineering community has not paid much attention to the simplified non-linear procedures until mid-1990s, when a breakthrough of such methods occurred. They have been implemented in many modern guidelines and codes (mostly for buildings) as in the ATC 40, FEMA 356 and Eurocode 8. Since than SDOF based pushover analysis has become increasingly popular. One of the authors (Fischinger) has been also promoting the N2 procedure (used in this paper for the comparative analyses) as typical representative of such methods since mid 1980s [5].

However, one should be cautious of the uncritical use of these procedures, forgetting their inherent limitations, in particular in the case of structural systems for which such methods have been not originally developed and tested enough. Bridges, especially viaducts with continuous deck, typically used in Europe, may belong to such category of structures. First of all it should be realized that all the above-mentioned procedures, guidelines and codes have been developed primarily for buildings and consequently any extrapolation without taking into account specific characteristics of the bridge structures may be questionable [6].

The specific and complex response of a bridge (viaduct) in the transverse direction may result from the fact that the superstructure of the viaduct is often very flexible in its own plain (while slabs in buildings are practically infinitely rigid). Consequently, many modes can be excited during the response. Several authors have addressed the problem of higher modes in the frame of the simplified SDOF methods for buildings (i.e. [7]). However, the problem was seldom discussed in the case of bridges [8].

Also, in bridges the structural elements resisting lateral load are usually situated in one plain only. Therefore, quite complex torsional (in the case of the roller supports at the abutments) and distorsional (in the case of the pinned supports at the abutments) response modes can be excited.

All these may preclude the use of the static, SDOF based analysis. Thus, the objective of the reported research has been to identify the cases where the pushover analysis is acceptable and the cases where more rigorous inelastic time-history analysis is required for typical European viaduct structures.

ANALYZED STRUCTURES AND SEISMIC LOAD

Analyzed Structures

In the parametric study, the response in the transverse direction of several idealized viaducts (see Figure 1) was investigated. The typical viaduct had a 200-metre long deck, and three single-column bents. The heights of the individual columns were varied (h_c = 7 m, 2 x 7 m, 3 x 7 m, and 4 x 7 m). Any particular combination is defined by V_{ijk}, where i, j, and k denote the heights of the first, second and third columns, respectively, expressed in multiples of the unit height of 7 m. For example, V213 (see Figure 1c) denotes a viaduct with a first column height of

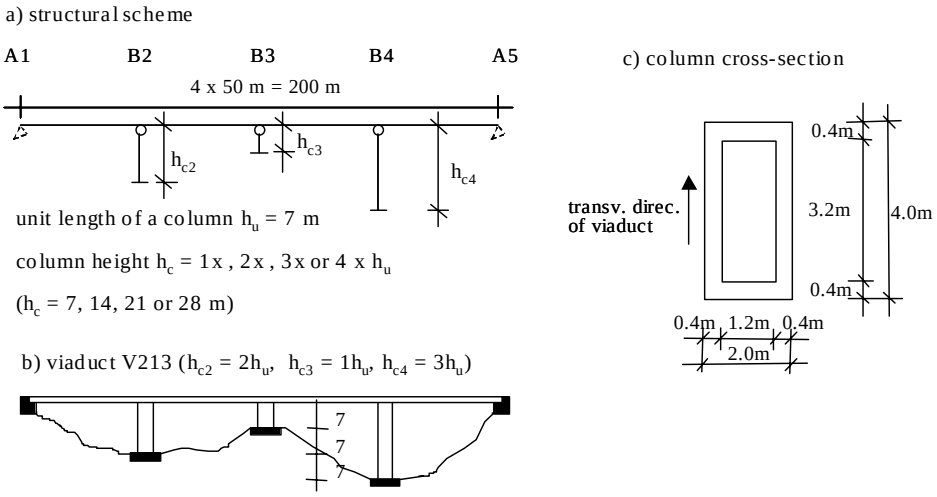

Figure 1. Layout of the investigated viaducts

two units (2 x 7 = 14 m), a second column height of one unit (1 x 7 = 7 m), and a third column height of three units (3 x 7 = 21 m). For each combination, two extreme boundary conditions at the abutments were considered. In the first case it was assumed that the abutments were pinned in the transverse direction (in the paper these viaducts are denoted as P viaducts), whereas in the second case roller supports at the abutments were assumed (R viaducts).

The 24 typical structures (of both P and R type) were analyzed using inelastic methods of analysis (see section "Methods of analysis"). For each structure two different amounts of column reinforcement ("strong" and "weak") were taken into consideration. Since the length of the end spans was found to be a very important parameter, strongly influencing the response of R-type viaducts, six additional structures with end spans of reduced length (i.e. 35 m) were also analyzed.

Seismic Load

In the simplified inelastic method (the N2 method), inelastic spectra derived from the EC8/2 design spectrum were used. A peak ground accelerations of 0.35g was first considered. After that the peak ground acceleration was doubled (a_g = 0.7g), since it was realized the intensity of seismic load could affect the regularity of the response.

In the inelastic dynamic analysis two artificial earthquake records were used (see Figure 2). They were generated on the basis of the Eurocode 8/2 design spectrum. Average of the results obtained with these two records were considered in the presented study.

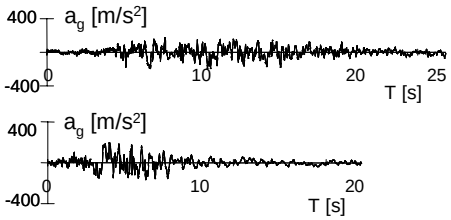

Figure 2. Accelerograms, used in the inelastic time-history analysis

METHODS OF ANALYSES

The N2 method (see more detailed explanation in [2]) has been chosen as a typical representative of the simplified inelastic procedure. The method, which has been developed at the University of Ljubljana [2], makes use of pushover analysis of the MDOF model of the structure in order to estimate seismic capacity, and inelastic dynamic analysis of the equivalent SDOF system to estimate the global seismic demand. Inelastic spectra are typically used in this step. Using pushover analysis, a characteristic non-linear force-displacement relationship of the MDOF system is first determined. At this stage the displacement shape of the structure has to be assumed, since it determines the distribution of the lateral load. In the present study a parabolic shape was assumed for P viaducts, and uniform distribution of displacements for the R viaducts [9].

The results of the N2 procedure were compared against the results obtained by the inelastic time-history analysis of a MDOF system (IA). In the presented study the response was calculated using the modified program DRAIN-2DX [10]).

QUANTITATIVE CRITERION, DEFINING THE SCOPE OF APPLICATION FOR SDOF METHODS (REGULARITY INDEX)

It was supposed that the N2 method could be used for the analysis only if the response obtained by this method did not differ significantly from that obtained by the IA. The comparison was based on the relative difference (D) between the areas bounded by the envelopes of the displacement lines obtained by the N2 and IA. However, in practice one would never perform both types of analysis. Therefore a relatively simple numerical index was introduced to help the designer to estimate the applicability of the N2 method (or any similar method). This index has been called “regularity index” (RI), alluding that simplified methods can be used only in the case of reasonably regular structures. The index represents relative difference between the areas bounded by the normalized displacement lines of the first and second iteration of the N2 method (see Figure 3). So, in practice one can always choose the simpler procedure (N2) from the beginning and than decide about the appropriateness of the decision by repeating the relatively simple step of calculating displacements.

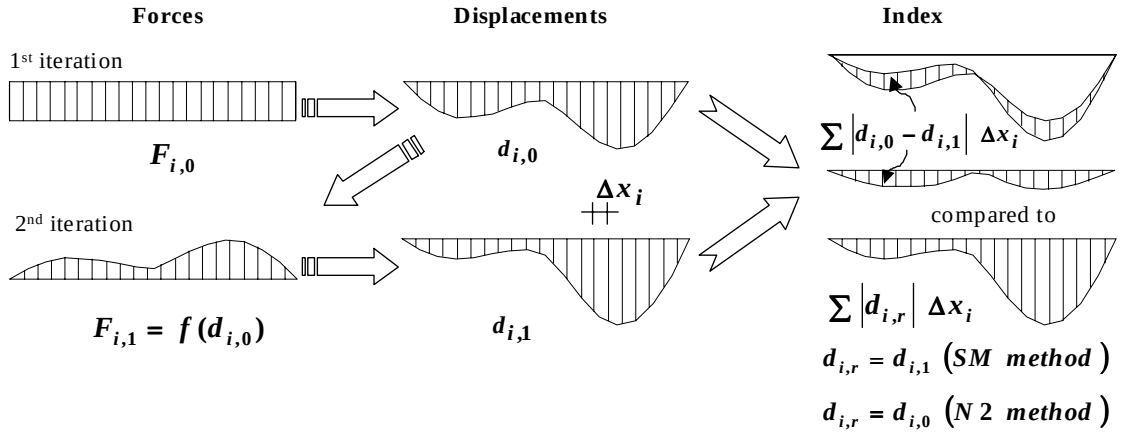

Figure 3. Definition of the proposed index

a) P viaducts b) R viaducts

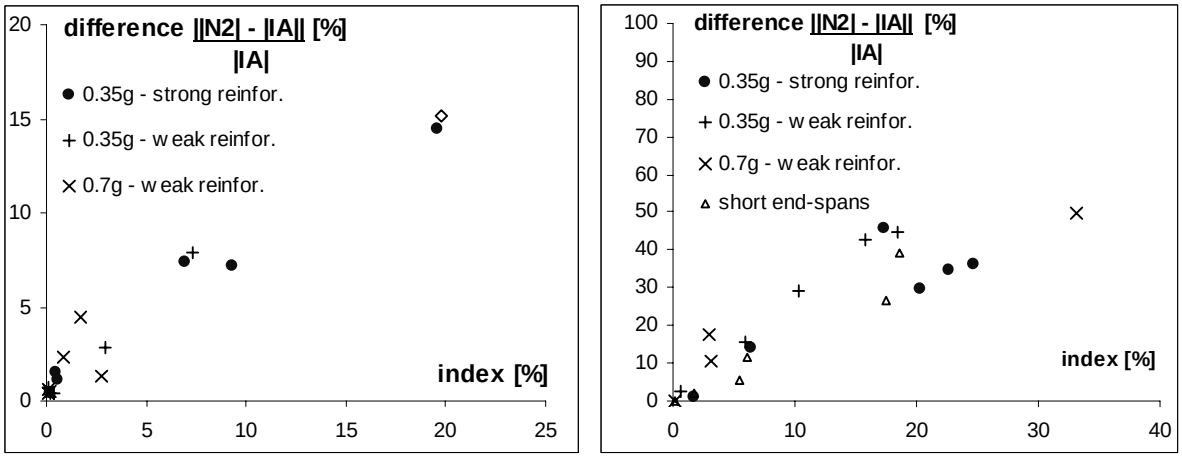

Figure 4. The difference between the N2 and IA method as a function of the proposed index

The D and RI were correlated (see Figure 4) to check the efficiency of the proposed index. The correlation coefficient was very good (more than 0.9), although the result should be considered by care, since the number of the analyzed viaducts was relatively small. Based on the comparison of the D an RI in Figure 4 one can roughly estimate that all viaducts having RI less than 5% could be analyzed with the N2 and similar simplified inelastic procedures.

"N2" VERSUS "IA" – TYPICAL EXAMPLES

Analyzing the differences between the results obtained with the N2 and IA method some important parameters that influence the response of viaducts have been identified. They are:

- the ratio between the stiffness of the deck and that of the piers,
- eccentricity (defined by distance between the center of mass and stiffness),
- the ratio between the torsional and flexural stiffnesses of the viaduct (definition can be found elsewhere [6]),
- the type of constraints at the abutments, and
- the relative strength of the columns.

The influence of these parameters on the response is briefly summarized in the next two subsections. A detailed analysis of some of the important parameters has been covered fully elsewhere [6]. Various types of structures, which cannot be analyzed using the N2 method are identified in the next two subsections. Since the type of the constraints at the abutments changes the response drastically (compare Figures 5 and 6, where an example is shown), the response of: a) viaducts with pinned supports at the abutments (P viaducts), and b) viaducts with roller supports (R viaducts) at the abutment is discussed separately.

Some representative examples including a typical European viaduct (real structure) are also discussed in more detail in the following subsections. For these viaducts the differences between results of the N2 and IA method are quantified using the proposed index (RI). In the last subsection a possibility to consider higher modes in N2 method is briefly presented.

In general it can be concluded that N2 method has to be used with care, particularly for the analysis of R viaducts. In these viaducts a large influence of higher modes can be expected in many cases. For example the average value of the regularity index (RI) for all analyzed R viaducts was 12.3%, while the value of 3.1% was obtained for the same structures but with the pinned supports at the abutments (P viaducts).

Viaducts with Pinned Supports at the Abutments (P Viaducts)

The N2 methods cannot be used for the next three types of P viaducts:

a) Viaducts where the eccentricity is large (e.g. larger than 5%),
b) Viaducts where eccentricity is small (e.g. smaller than 5%), the torsional stiffness is smaller than flexural stiffness and the relative strength of the columns is relatively large,
c) Viaducts where the eccentricity is small (e.g. smaller than 5%), where the deck is flexible, columns are stiff and their strength is large.

Viaducts with Large Eccentricity

It is well known that the large influence of higher modes can be expected in viaducts of this type. Consequently, in such cases N2 method fails to predict the response correctly. Since this is well known case it is not further discussed.

Viaducts with Small Eccentricity, Large Strength of Columns and Small Torsional Stiffness

Structures, where the torsional stiffness was smaller than flexural were found to be "irregular" even if the eccentricity was small. The very stiff central columns are typical for these types of viaducts. An example is presented in Figure 5.

The level of "irregularity" of these viaducts is influenced by the relative strength of the columns, too. The regularity of the viaduct strongly depends on the ratio between the stiffness of the deck and that of the piers [6]. The deck is usually designed to respond elastically during strong earthquakes. However, columns are usually designed to withstand significant plastic deformations during strong earthquakes. Their stiffness may therefore be significantly reduced. The reduction of column (pier) stiffness depends on the properties of the columns as well as on the intensity of the earthquake load. The weaker the reinforcement in the column is, and the

stronger the earthquake, the larger is the reduction in column (pier) stiffness. Consequently, the superstructure has a more important role and the viaduct responds more "regularly".

The influence of the relative strength is illustrated in Figure 5. In viaduct V213P the value of regularity index was 7.3% in the case of "weak" reinforcement and 19.6% for structure with "strong" reinforcement of columns (see Figure 5a). When the same structure with the "weak" reinforcement was subjected to the earthquake load of doubled intensity (a_g = 0.7g), the value of index was reduced to 1.7% only (see Figure 5b).

Viaducts with Small Eccentricity, Large Strength of Columns, Flexible Deck and Stiff Columns

In viaducts with very stiff and relatively strong end columns the influence of higher modes can be expected even if they are symmetric. Such an example is viaduct V121P (see Figure 7), where end columns are very stiff in comparison with the deck. In this viaduct, for example, the value of the regularity index is RI = 9.3%. Note that the difference between the shapes of the deflection lines obtained with the N2 and IA method is largest between the abutment and stiff column.

a) a_g = 0.35g b) a_g = 0.7g

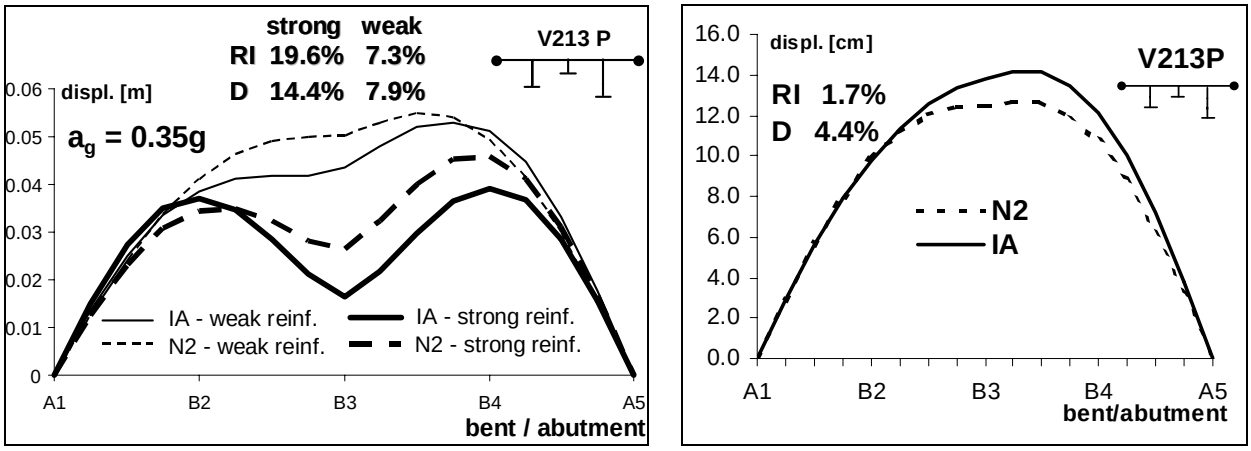

Figure 5. Response of the torsionaly sensitive viaduct V213P

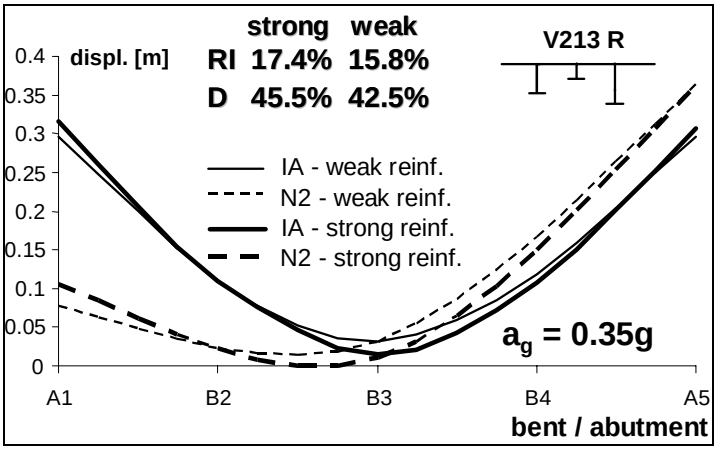

Figure 6. Response of "irregular" torsionaly sensitive viaduct V213R (a_g = 0.35g)

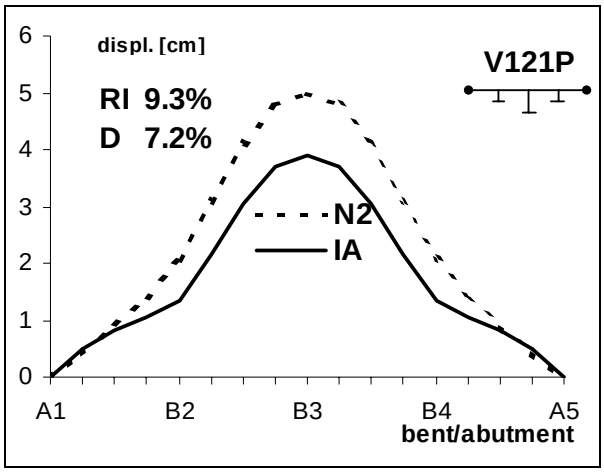

Figure 7. Response of viaduct with strong end columns

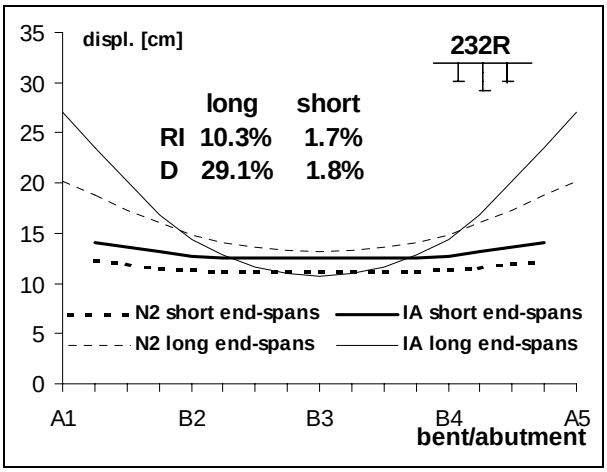

Figure 8. Influence of the length of the end spans on regularity

Viaducts with Roller Supports at the Abutment (R Viaducts)

The N2 methods cannot be used for the next types of R viaducts:

a) Viaducts where the eccentricity is large (e.g. larger than 5%),
b) Viaducts where eccentricity is small (e.g. smaller than 5%) and the torsional stiffness is smaller than flexural stiffness,
c) Viaducts where the eccentricity is small (e.g. smaller than 5%), the deck is flexible and columns are stiff.
d) Some viaducts with stiff deck, flexible columns and large end spans.

First three types of viaducts are not further discussed, since the reasons for "irregularity" are the same as in the case of P viaducts. However, there are some slight differences between P and R viaducts of these types. They are summarized below.

It is worth to mention again that the "irregularity" of R viaducts is much higher than "irregularity" of P viaducts. The R viaducts are torsionaly more sensitive than P viaducts. The influence of the relative column strength on the regularity is not so large as in the case of P viaducts. For example, in the viaduct V213R (see Figure 6), the value of the regularity index was RI = 17.4% and RI = 15.8% for "strong" and "weak" reinforcement of columns, respectively.

Viaducts with Very Large End Spans

R viaducts with very long end-spans can respond irregularly even if they are symmetric [6]. However, when the length of the end-spans in symmetric R structures is reduced (the more realistic and usual case) their behavior is significantly more regular (see Figure 8). For example in the viaduct V232R the value of regularity index RI = 15.6% is obtained, when the length of the end spans were the same as the length of the central spans. When the length of the end-spans was reduced (0.7 of the length of central spans) the response was "regular" and the value of regularity index of RI = 2.4% was obtained.

Asymmetric R structures are, in general, irregular. For this type of structure the N2 method has to be used with care.

Real Viaduct

The applicability of the N2 method and the efficiency of the proposed regularity index, were tested on several real viaducts, too. An example is shown in Figure 9. This is a typical European viaduct, which appears to be quite "regular". However the results of the N2 and IA method were quite different (see Figure 10). The reasons for the "irregularity" of this viaduct are very stiff end columns (B2, B3, B4 and B14). The value of regularity index was in this case RI = 19.8%, therefore the viaduct can be classified as the "irregular".

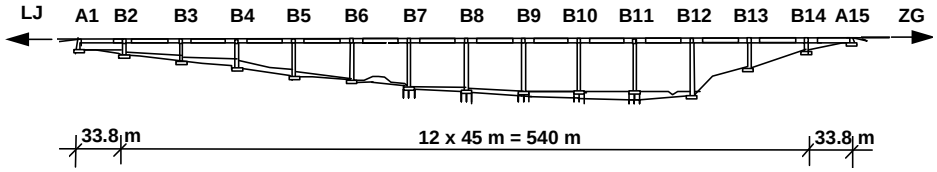

Figure 9. A typical European viaduct, which appears to be quite "regular"

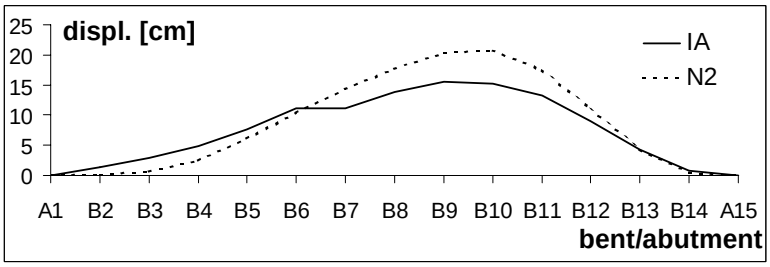

Figure 10. Response of the typical viaduct

Possible Way to Consider Higher Modes with the N2 method

It was shown in the previous subsections, that N2 method has to be use with care, since it fails to account for higher modes in so called "irregular" structures. However, based on some very limited experiences [8] it was concluded that assuming more than one displacement shape, applying the N2 method for each shape, and enveloping the results may obtain an acceptable solution. Although this observation cannot be generalized at the present, it is certainly worth of further investigation. Nevertheless, since the object of the N2 method is to provide a simplified alternative to inelastic time-history analysis, it is doubtful that this may be accomplished by the assumption of numerous deformed shapes in order to carry out several pushover analyses for the purpose of enveloping results.

CONCLUSIONS

The specific and complex response of the bridge may preclude the use of the static, pushover based analysis. In the paper the cases where the pushover analysis (using N2 method) is acceptable and the cases where more rigorous inelastic time-history analysis is required are identified.

The most important parameters influencing the response of viaducts were summarized. They are: the ratio between the stiffness of the deck and that of the piers, eccentricity, the ratio

between the torsional and flexural stiffnesses of the viaduct, the type of constraints at the abutments, and the relative strength of the columns.

A "regularity index" has been proposed as a numerical measure to help the designer to decide about the suitability of the pushover analysis for bridges.

It has been demonstrated that, even if the geometry of a viaduct appears to be regular and almost symmetric, the response can still be quite complex, with the important influence of higher modes. It was concluded that viaducts with pinned supports at the abutments (P viaducts) are, in general, less sensitive to the influence of the higher modes than similar viaducts with roller supports at the abutments (R viaducts). The scope of applicability of the pushover analysis is therefore wider for P viaducts than for R viaducts. The pushover based procedures should not be used in the analysis of torsionaly sensitive viaducts and viaducts with short stiff columns. The smaller the relative strength of the columns is, more applicable are these methods.

A general conclusion has been that the pushover based procedures for bridges should be used with care. In a case of rather complex bridges, time-history analysis may be more suitable solution.

REFERENCES

[1] Fajfar, P. and H. Krawinkler (eds). 1997. *Seismic Design Methodologies for the Next Generation of Codes*, Balkema.

[2] Fajfar, P. 2002. "Structural Analysis in Earthquake Engineering – A Breakthrough of Simplified Non-Linear Methods," to be presented as a keynote lecture at the 12th European Conference on Earthquake Engineering, September 9-13, 2002.

[3] Freeman S.A., J.P. Nicoletti, and J.V. Tyrell. 1975. "Evaluations of Existing Buildings for Seismic Risk – A Case Study of Puget Sound Naval Shipyard, Bremerton, Washington," in Proc. of the 1st U.S. National Conference on Earthquake Engineering, Berkeley, EERI, pp. 113-122.

[4] Saiidi M., and M.A. Sozen. 1981. Simple Nonlinear Seismic Analysis of R/C Structures. *Journal of Structural Engineering, ASCE*, (107): pp. 937-952.

[5] Fajfar P., and M. Fischinger M. 1989. "N2 – A Method for Non-Linear Seismic Analysis of Regular Buildings," in Proc. of the 9th World Conference on Earthquake Engineering, Tokyo, Kyoto 1988, Maruzen, Vol.5: pp. 111-116.

[6] Isaković, T., M. Fischinger, and P. Fajfar. 1999. The Seismic Response of Reinforced Concrete Single-Column-Bent Viaducts Designed According to Eurocode 8/2. *European earthquake engineering*, 13(1): 3-18.

[7] Chopra A.K., and R.K. Goel. 2002. A Modal Pushover Analysis Procedure for Estimating Seismic Demands for Buildings. *Earthquake Engineering and Structural Dynamics*, 31: 561-582.

[8] Fischinger, M., T. Isaković, and R. Moore. 1999. RC Viaducts: "Pushover Versus Inelastic Time-History Analysis," in Proc. IIEES, Tehran, pp. 961-968.

[9] Gašperšič, P. 1996. *A method for the seismic damage analysis of building and bridge structures.* Ph. D. Thesis (supervised by P. Fajfar). University of Ljubljana, Faculty of Civil and Geodetic Engineering, Ljubljana, Slovenia (in Slovenian).

[10] Prakash, V., G.H. Powell, and S. Campbell. 1993. *Drain-2DX; Version 1.10; Users Guide*, UCB/SEMM 93/17, University Of California, Berkeley.

Seismic Performance of Reinforced Concrete Bridge Columns

David Sanders, Patrick Laplace, Saiid Saiidi and Saad El-Azazy

ABSTRACT

Eight columns were tested under multiple El Centro earthquake motions until failure using a shake table. Four columns were detailed using pre-1971 Caltrans guidelines while four used new current details. The four older columns were flexural columns while the new columns consisted of two designed for flexural failure and two for shear failure. The first column (as-built) failed due to severe lap-splice failure at very low ductility. The second and third columns were retrofitted with a steel jacket while the fourth used a carbon wrap. The columns performed well based on ductility but the lap-splice did not reach yielding as per design. The carbon wrap performed significantly better than the steel jacket retrofits, providing higher lap-splice bar strains and larger ductility.

The flexurally dominated new columns had the same configuration as the older style column with the addition of more confining reinforcement. These columns had an aspect ratio of 6.5. Columns preformed well with significant spalling and bar buckling at the end of the test. The two shear dominated columns had an aspect ratio of 3. The shear columns were tested in double curvature using a unique dual link system. The two sets where subjected to different loading paths. In the shear column, a severe shear failure followed by total collapse occurred at 3.25 x El Centro. The collapse was significantly affected by axial load. Current shear capacity equations were used to compare measured versus calculated capacity. Strain rate was shown to be significant for the columns.

David Sanders, Associate Professor, Dept. of Civil Engineering/258,Univ. of Nevada, Reno, NV 89557
Patick Laplace, Research Assistant Professor, Dept. of Civil Eng./258,Univ. of Nevada, Reno, NV 89557
M. “Saiid” Saiidi, Professor, Dept. of Civil Engineering/258,Univ. of Nevada, Reno, NV 89557
Saad El-Azazy, Senior Bridge Engineer, Caltrans, 1801 30th Street, Sacramento, CA 95816

INTRODUCTION

Caltrans has conducted a comprehensive bridge retrofit program that involved the retrofitting of deficient bridge columns. A majority of these columns had low transverse steel ratios and lap splices at the base of the columns. The performance of these columns under earthquake excitation was marginal at best, with premature failure of the lap splices and low displacement ductilities. Although many studies were performed on as-built and steel jacket retrofitted columns, a limited number were performed using earthquake loading on shake tables. There have also been few earthquake loading tests on the newer carbon fiber retrofitted columns, which have been tested using typical quasi-static procedures. The objective of this study was to compare the performance enhancement of steel and carbon fiber jacket retrofits applied to deficient as-built columns. A total of four columns were tested in this portion of the study.

With the Caltrans retrofit program being completed, the second objective was to investigate new design. Columns were designed to be either flexural or shear dominated. A total of four columns were tested in this portion of the study. Shear failures in bridge columns are undesirable due to the sudden and brittle failure of a shear dominated column, potentially followed by complete collapse due to gravity loads. Current design procedures generally provide for a ductile flexural response. Accurate assessment of shear capacity is still a necessity. No previous shear dominated columns have been tested under earthquake loading on a shake table system.

COLUMN PROTOTYPE

The prototypes were 48 inch diameter circular columns. They were not based on a specific bridge in the Caltrans inventory, but were either modeled using typical pre-1971 details or 1998 details. The older bridge columns had lap splices lengths at the footing-column interface ranging between $20d_b$ to $30d_b$ typical for #11 Grade 40 bars (where d_b is the longitudinal bar diameter). A lap splice length of $24d_b$ was chosen for the prototype. Typical transverse steel was #5 hoops spaced at 12 inches while longitudinal steel ratios were 2% on average. Aspect ratios ranged between 4 and 6, while axial load ratios were 10% or less. An aspect ratio of 4.5 was chosen for the prototype with an axial load ratio of 10%, based on typical column dimensions.

For the current design columns all the dimensions were the same except increased development length of longituindal bars and increased confinement. The prototype flexural column had #5 spirals at a 3-inch pitch with an aspect ratio of 4.5 while the shear column had #5 spiral at a 4-inch pitch with an aspect ratio 1.5. The longitudinal steel was #11 Grade 60 bars with no lap splices at the base of the column. The longitudinal steel ratio was 2% for the flexural columns and 3.5% for the shear columns. The axial load ratio chosen was 10%.

SCALE MODELS

A scale factor of 1/3rd was chosen based on shake table and mass-rig capacities. Table I shows the data for the scale models. Specimen names with a “6” in the front were design based 1960 criteria, while those with a “9” were desined based on 1998 criteria [1]. The “F” and “S”

stand for flexure and shear respectively. 6F is the as-built pre-1971's specimen. 6FS and 6FC are the retrofitted speicmens with steel and carbon sheet shells respectively. 9F1 and 9F2 are two identical 1998 style flexural columns. 9S1 and 9S2 are identical 1998 shear based columns. The 0.176 inch diameter wire used in pre-1971 columns had a yield strength of 65 ksi. To match the typical steel used prior to 1971, an annealing procedure was developed to reduce the yield stress from 65 ksi to 46.3 ksi. The hoops were constructed using a 7-inch lap. Rigid footings were designed and constructed to post-tension the columns to the shake-table deck for all specimens.

The flexural test setup shown in Figure 1 uses the mass rig inertial system developed in a previous study [2,3]. Axial load is applied by rams on the top of the column while the inertial load come from the mass rig. An array of strain gages were placed on the longitudinal and transverse steel while displacement instruments were placed along the column height to measure curvature. Acceleration was measured at the top of the specimen, on the mass and on the link between the mass and the specimen. Specimen displacement and link force were also measured. All data was sampled at 160 Hz. The flexural columns were loaded in single curvature, while the shear columns were loaded in double curvature. The footing and top stub for the shear specimens were designed using similar details to provide for a symmetric response in the column. Figure 2 shows the shear test setup.

Flexural Steel Jacket Retrofit Columns 6FS1 and 6FS2

Both columns were retrofitted with steel jackets to improve confinement in the plastic hinge zone and prevent premature lap splice failure. The steel jacket design was based on the Caltrans Memo To Designers, 1998 [1]. The confinement stress (σ_c) and maximum jacket strain

TABLE I: SPECIMEN DETAILS

Details	**Pre-1971 Flexural Columns**	**1998 Flexural Columns**	**2000 Shear Columns**
Column Height	72 in.	72 in.	48 in.*
Column Diameter	16 in.	16 in.	16 in.
P/f'cAg	7%	10%	10%
Concrete Strength	5900 psi - 6F 5650 psi - 6FS1 5720 psi - 6FS2 5990 psi - 6FC	5428 psi - 9F1 5523 psi - 9F2	5360 psi - 9S2 5325 psi - 9S2
Long. Reinf. Ratio	2.0%	2.0%	3.5%
Long. Reinf.	20 #4 Grade 40	20#4 Grade 60	16#6 Grade 60
Long. Yield Stress	50.9 ksi	65 ksi	65 ksi
Trans. Reinf. %	0.15%	0.92%	0.92%
Transverse Reinf.	0.176 inch dia. wire hoops @ 4.5 inches	¼-in. diameter wire spiral @ 1.5"	¼-in. diameter wire spiral @ 1.5"
Transverse Yield Stres	46.3 ksi	57.6 ksi	57.6 ksi
Cover to Transverse	0.82	0.75	0.75
Loading Setup	Single Curvature Pinned at Top	Single Curvature Pinned at Top	Double Curvature Held Top and Bottom

* Clear Height

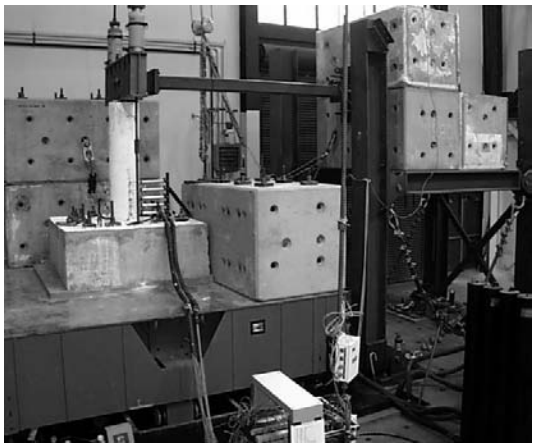

Figure 1. Carbon-fiber retrofit setup

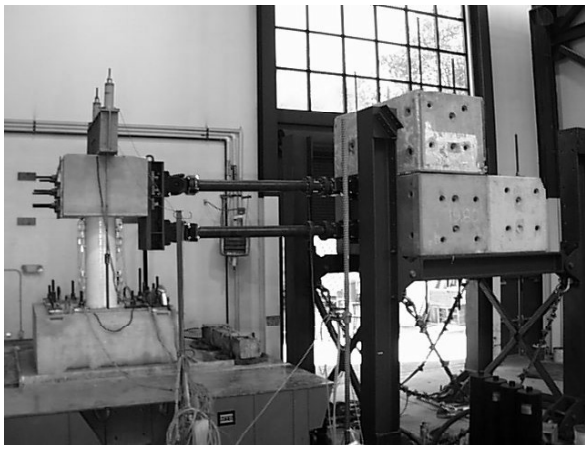

Figure 2. Shear column test setup

(ε_{max}) were 300 psi and 0.001 respectively. The required thickness of the steel jacket shell, t_j is ρ_j D/4 and the jacket volumetric ratio ρ_j is set to equal $\sigma_c/E\varepsilon_{max}$ where *E* is the steel jacket elastic modulus. The required jacket thickness based on a column diameter of 16 inches and grout thickness of 1/2 inch was 0.044 inches (approximately 18 gauge steel). This small thickness requirement was impractical for fabrication as a circular steel shell. The steel jacket thickness was increased to 0.125 inch to improve fabrication and weldability.

A 1.0-inch gap was required at the base of the jacket to prevent concentrated stresses due to large column rotations. A ½-inch gap was formed between the shell and the column surface to allow for the application of the non-shrink grout. The original length of the steel shell was based on covering a portion of the column equal to 2 times the column diameter (32 inches). After initial testing of the first steel jacketed column and a premature failure of the top column connection, the steel jacket height was increased to cover the full length of the column.

Flexural Carbon Fiber Jacket Retrofit Column 6FC

The design of the carbon fiber retrofit was based on the Caltrans Memo To Designers, 1998. The design requirements for the carbon fiber jacket for the plastic hinge zone were the same as the steel jacket retrofit. The design requirements for the non-plastic hinge zone for the confinement stress and maximum jacket strain were 150 psi and 0.004 respectively. The jacket modulus *E* is the carbon fiber elastic modulus in the primary fiber direction (the circumferential direction). The number of layers of carbon fiber was found from t_j/t_f where t_f is the individual dry fiber sheet thickness (0.0065 inches), specified in the Caltrans Memo to Designers and t_j is defined above. The number of layers required in the plastic hinge zone are based on the elastic modulus *E*, measured as 31700 ksi. For the plastic hinge zone, 6.3 layers were required but 7 layers were used. The non-plastic hinge zone region required 0.79 layers but 1 layer was used. The 7 layers were applied to the column up to a height of *1.5 D* (24 inches) where *D* is the column diameter. The remaining height was wrapped with 1 layer as per the non-plastic hinge zone requirement. A gap of 1 inch was created at the base of the column to prevent the carbon fiber wrap from contacting the footing surface under high rotations.

LOADING PROTOCOL

The test motions are shown in Table II The El Centro [7], Imperial Valley Earthquake, N-S component was used for all the motions. The values shown in the table are the acceleration amplitude scale factors multiplied against the full scale El Centro motion (0.35 g PGA, 13.4 in/sec PGV and 3.1 inch PGD). The earthquake was time scaled at 0.58 times the full-scale motion (54 seconds) to maintain similitude in response between the full scale and model column. The time scale requirement is due to the stiffness and mass scaling between the prototype and model, which reduces to a time scale factor equal to sqrt(l_s) where l_s is the length scale factor of 1/3. Throughout the tests, pulse motions/square waves were used to produce a free vibration response to determine stiffness and damping characteristics of the columns.

OBSERVED PERFORMANCE

As-Built Column 6F

The as-built column has a capacity envelope that drops at a very low ductility due to the failure of the lap splice at the base of the column (see Fig. 3 & Table III). It is essentially elastic performance for the 1/4 and 1/3 scale El Centro motions. The 2/3 x El Centro produced the first vertical splitting cracks along the lap splice at the base of the column. The flexural cracking increased and the crack at the top of the lap splice propagated around the circumference of the column. The peak lateral capacity for column 6F was recorded during the 1.0 x El Centro. The splitting cracks along the lap splice were well defined and slippage likely occurred during this motion (see Fig. 4). There was little increase in damage to the column during the 1.25 x El Centro motion due to lower measured force levels and a concentrated rotation at the top of the lap splice. No spalling was observed for any of the motions.

TABLE II. LOADING MOTIONS
(# x El Centro Amplitude)

As-Built	**6FS1**	**6FS2**	**6FC**	**9F1**	**9F2**	**9S1**	**9S2**
0.25	0.25	3.0	0.15	0.33	0.17	0.25	0.15
0.33	0.33	2.5	0.25	0.66	3.5	0.33	3.0
0.50	0.5	3.5	0.33	1.0	2.5	0.66	3.25
0.66	0.66	4.0	0.50	1.5	3.5	1.0	1.0
1.00	1.0		0.66	2.0		1.5	
1.25	1.5		1.0	2.5		2.0	
	Repair		1.5	3.0		2.5	
	0.5		2.0	3.5		3.0	
	0.25		2.5	4.0		3.25	
	1.5		3.0				
	2.0		3.5				
	2.5		4.0				
	3.0						

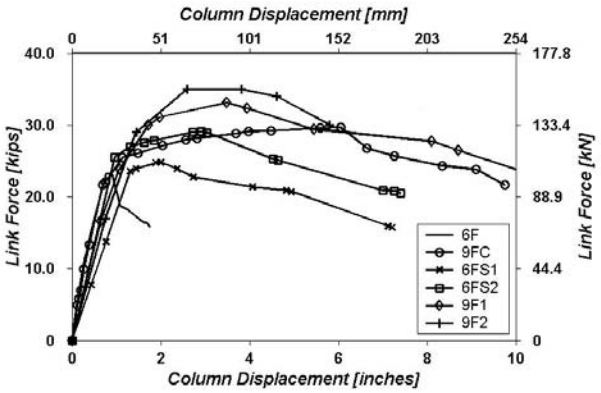

Figure 3. Measured force-displacement envelopes for flexure columns

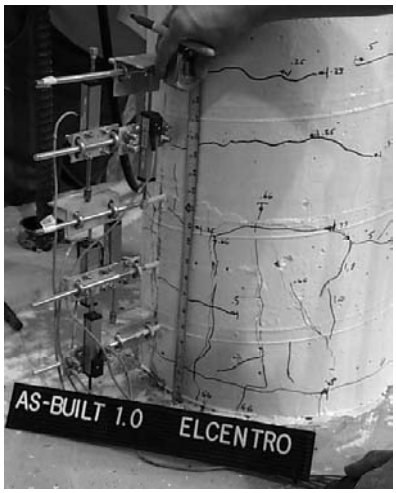

Figure 4: As-built after 1.0 El Centro

Figure 5: New design (9F1) after 4.0 El Centro

TABLE III. MEASURED RESPONSE

Column	Motion	Peak Load (kips)	Yield Displ. (in)	Peak Displ.* (in)	Drift* (%)	Ductility*
As-built – 6F	1.0	23.2	0.5	1.8	2.4	3.5
6FS1	3.0	24.8	0.96	5.3	7.4	5.6
6FS2	4.0	25.3	1.0	7.0	9.7	7.0
6FC	4.0	29.7	0.91	9.10	13.9	10.0
9F1	4.0	33.1	1.0	8.70	12.1	8.7
9F2**	3.5	32.0	1.2	5.97	8.3	5.0
9S1	3.25	94.1	0.73	2.78	5.8	3.8
9S2	3.25	92.1	0.47	1.77	3.7	3.8

*@ 80% Max Load ** Not taken to complete failure, to be repaired

Steel Jacketed Column: 6FS1 and 6FS2

There was a significant difference in the capacity envelopes between the two identical steel jacket columns (see Fig. 3 & Table III). The steel jacket column subjected to the initial high amplitude earthquake motion (6FS2) showed significantly higher capacity throughout the deformation than the steel jacket column subjected to the incremental motions (6FS1). This may be due to more bars slipping in column 6FS1 due to the interaction of more low level motions as compared to column 6FS2. Both steel jacketed columns show a similarity in the deflection at which they began yielding and degrading in strength. The lower stiffness of column 6FS1 may also be due to the sensitivity of the lap splice to multiple low-level cyclic motions from the initial earthquakes, in effect degrading the bond between the lap splice.

For 6FS1, 1.5 x El Centro produced minor spalling at the base of the column. The column began to spall some of the grout between the steel shell and the column surface during the 2.0 x El Centro motion. The cover concrete at the base of the column between the gap and footing surface spalled during 2.5 x El Centro. The cover at the lap splice completely spalled after the final 3.0 x El Centro motion. There was no significant core damage visible, but two longitudinal bars were visible. No buckling or fracture of the bars were visible. The test was stopped due to the low lateral capacity measured during the last motion and before complete column collapse could occur.

In 6FS2, the first motion caused spalling of the footing surface at the base of the column. No bars or core damage were visible within the 1 inch gap. The 2.5 x El Centro motion caused no further damage to the column. An increase in the footing surface spalling due to 3.5 x El Centro was observed. Slight column damage was visible in the gap region and 2 longitudinal bars were visible. The final motion of 4.0 x El Centro produced severe damage in the gap region at the base of the column. The longitudinal bars buckled in this region and core damage was visible.

Carbon Fiber Jacketed Column 6FC

The carbon jacket column showed similar elastic and yielding capacities as the steel jacketed 6FS2 column, but diverged significantly past a deflection of 3 inches (see Fig. 3 & Table III). The peak capacity of the carbon jacket column was close to the peak capacity of the 6FS2 steel jacket column, supporting the similarity of the initial confining effects of the steel shell and carbon jacket relative to each other. While the capacity of the steel jacket columns dropped, the carbon jacket column continued to show an increase in capacity and peaked at 6 inches of deflection, versus peaks at 3 and 2 inches for the steel jacketed columns. This difference may be due to the improved confinement effect of the carbon fiber wrap versus the steel jacket shell.

Minor cracking at the base of the column occurred during 1.0 x El Centro. The 2.5 x El Centro response was the first motion where minor circumferential cracking occurred at the top of the lap splice. Spalling in the gap region started to occur after this motion. The footing surface spalled after 3.0 x El Centro. The surface spalled more severely after 3.5 x El Centro. Longitudinal bar buckling occurred during 4.0 x El Centro. The column strength dropped significantly after the 4.0 motion so the test was stopped.

Flexure Columns: 9F1 and 9F2

For 9F1, small spalling occurred at 2.0 x El Centro. Spalling extended up the column approximately 2 inches. After 3.0 x El Centro, the spalling extended to 7 inches. After the 3.5 x El Centro, spalling expanded to approximately 9 inches in height. At this point, initial deterioration of core concrete had begun but confinement steel had not yielded. In addition there was a permanent displacement of 1.5 inches. As soon as the 4.0 x El Centro motion was applied, P-) effects became substantial. The capacity of the column dropped quickly until column failure at which point the mass rig reached its maximum allowed deflection of 17 inches. The final condition of the column is shown in Fig. 5. See basic performance data in Table III.

The initial motion for 9F2 was 3.5 x El Centro. As in specimen 9F1, the motion caused a spalling height of 8 inches. A qualitative comparison of the spalling region indicated that the extent of damage was less in specimen 9F2 than specimen 9F1. This is primarily stated since the concrete core was undamaged. In addition, there was a permanent displacement of 0.5 inch with no confinement steel yielding versus 1.5 inches for 9F2. During the 2.5 x El Centro earthquake, the strains in the confinement increased slightly, but little visible change in spalling was realized. The impact of the second 3.5 earthquake was to cause confinement steel yielding and a permanent displacement of 1.2 inches. There was a significant increase in the amount of damage in the plastic hinge region with separation occurring between the longitudinal bars and core concrete. The peak force dropped between the first run of 3.5 x El Centro and the second run, 34 kips to 30 kips.

The force-deformation envelopes in Fig. 3 show the ductility improvement of the carbon fiber retrofit compared with the performance of the new designs (9F1), but the lack of full lap splice development and lower grade longitudinal steel in the retrofits prevent them from achieving the higher capacities of the new designs.

Shear Columns: 9S1 and 9S2

The displacement envelopes for the shear columns are given in Figure 6. Basic measured data is given in Table III. For 9S1, essentially elastic response was observed through 2/3 x El Centro. There was minor flexural cracking along the column height. No spalling or shear cracks were visible. The 1.5 x El Centro motion produced the first shear cracks near the lower portion of the column. The shear cracks were inclined at an approximate angle of 45 degrees. There was a significant increase in shear cracking along the 45 degree plane and an increase in vertical cracking along the column height after 2.5 x El Centro. Severe shear cracking occurred over the majority of the column surface during 3.0 x El Centro but the columns was still carrying gravity loads and was intact. The column completely collapsed during 3.25 x El Centro (see Fig. 7).
For 9S2, significant shear cracking at 45 degree inclinations occurred during 3.0 x El Centro. There was no significant spalling. There was significant diagonal and vertical shear cracks along the column height. After the 3.25 x El Centro motion, there was severe spalling and shear cracking along the column. A large portion of the longitudinal and spiral steel was visible. Severe degradation occurred through the core at the center of the column (see Fig. 8). There were no spiral fractures or bar buckling due to the relatively low flexural demand. The final 1.0 x El Centro motion was used to test the stability of the column. The column did not sustain any additional damage after this motion and remained stable, but it was felt that any larger motion would have caused complete collapse.

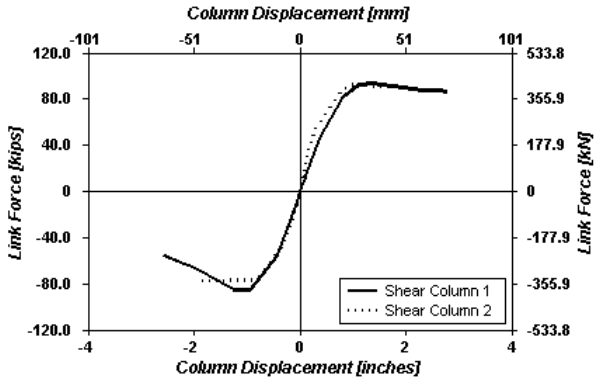

Figure 6. Measured force-displacement envelopes

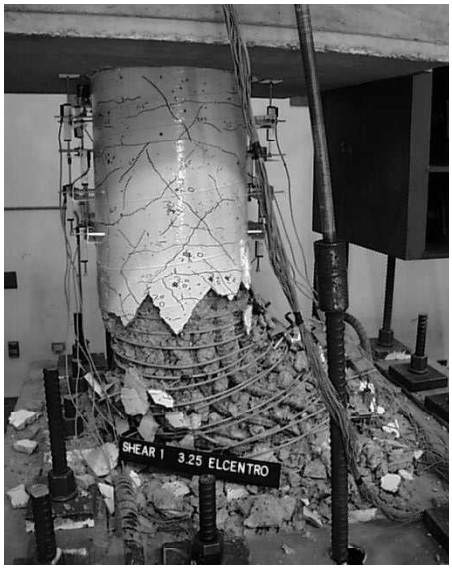

Figure 7. Column 9S1
after 3.25 x El Centro

Figure 8. Column 9S2
after 3.25 x El Centro

CALCULATED PERFORMANCE

Force-Displacement Envelopes

A program called X- Section [9] used by Caltrans was used for the moment curvature analysis. Three points on the moment-curvature curve are needed: cracking, yield, and ultimate moment and curvature, respectively. X-Section can idealize the moment curvature by an elastic-perfectly plastic procedure. X-Section passes the elastic idealized curve through the point of first bar yield, then uses an equal area method to determine the idealized yield curvature. The results of the idealization are part of the X-Section output. A procedure for further idealizing the moment-curvature envelope for un-retrofitted lap-spliced columns was presented by Priestley et.

al.[5] and was used for this analysis. This idealization takes the lap splice failure into account, whereas X-Section assumes full lap development. X-Section calculated the confined concrete properties internally using the Mander model [4] for concrete. A stress-strain model developed by Xiao[8] for carbon fiber wrapped concrete was used in this study. A program called SPE-MC [6] was used since it allowed text file input of the material stress-strain curves.

Two shear equations were used to calculate the shear capacity of the columns; Caltrans and UCSD. The Caltrans equation was outlined in the Memo to Designers while the UCSD equation used was from Priestley et. al. UCSD recommends using a 30 degree shear crack inclination angle, but since the observed shear cracks were 45 degrees for both columns, the UCSD equation was also used with 45 degrees to form a better comparison to the Caltrans equation. The effects of strain rate were quantified in a previous study [2] and applied for the shear columns. Strain rate was calculated by differentiating the strain measurement in the transverse steel and using the rate occuring at the point of effective yield. This rate was used to calculate the corresponding increase in yield stress and applied to the transverse steel component in the shear equations. This provided a reasonable estimate of the increase in shear capacity due to the measured strain rate at effective yield of the column. Both shear equations were solved for capacity versus column displacement to produce force-displacement envelopes. This was achieved by varying the ductility factor in the Caltrans equation and the *k* factor[5] in the UCSD equation. The Caltrans shear equation provided a better approximation of the shear capacity than the UCSD equation using 45 degree shear crack inclination. The UCSD equation using the recommended 30 degree shear crack inclination had a calculated capacity 1.5 times greater than measured.

Time History Analysis

The program, called RCShake [3,4], used a trilinear hysteretic model developed for this study. The measured and calculated peak displacements per motion from RCShake are plotted in Figure 9 for the as-built and retrofitted columns. Due to the lap splice slippage observed in all the columns, it is difficult to calculate the higher displacements using simple hysteretic models that do not incorporate lap splice bond models. By assuming no strain hardening in the longitudinal steel and calculating the force-deformation envelope from a moment-curvature analysis, the ductility calculations from the hysteretic model can be improved with a better

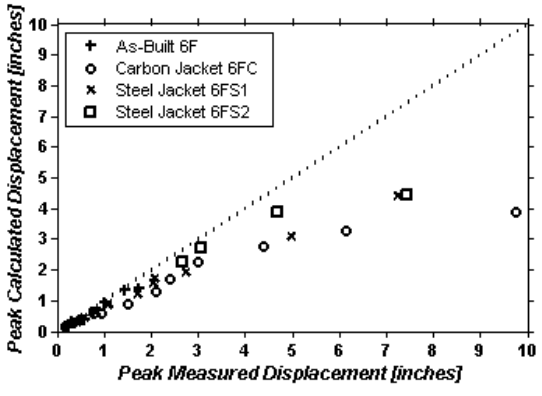

Figure 9. RCShake Response Comparison

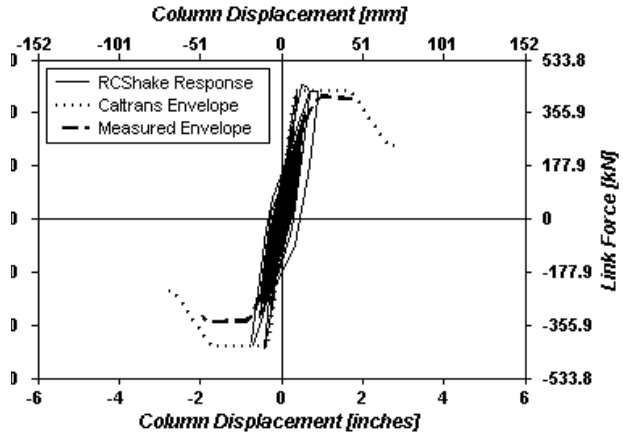

Figure 10. RCShake Response For Column 9S2

representation of the slipping lap splice. Even so, the ultimate displacements and failure mode due to lap-splice degredation and pull-out were not predicted with sufficient accuracy. Force predictions compared well with measured for all the columns using RCShake.

The calculated force-displacement envelopes using the Caltrans and USCD shear equations were used as input into the program. The calculated response from RCShake is shown in Figure 10. Although the trilinear hysteretic model could capture the lateral forces with sufficient accuracy, the model could not achieve the collapse displacement and mechanism. This is likely due to the brittle and sudden failure typical in shear dominated columns which is difficult to capture with simple hysteretic models.

CONCLUSIONS

1) Although overall performance of the steel jacket retrofit was good, the longitudinal bars in the steel jacket retrofits did not reach strains much higher than yield. The first steel jacketed column subjected to incremental motion showed a sensitivity to lap splice degradation due to low level incremental motions. Some longitudinal bar strains for this column only reached a peak of 50% of yield. This suggests the steel jacket retrofits provide enhancement of the lap splice but not equivalent to the level of a non-lapped column. The carbon jacketed column showed a marked improvement with the longitudinal bar strains near or above yield, due to the improvement in confinement.

2) The steel jacketed column subjected to the incremental motion did not show a significant improvement (7% increase) in capacity versus the as-built column. The steel jacketed column subjected to the high initial motion showed marked improvement (25% increase) in capacity versus the as-built. The column lap splice was not as degraded and reached slightly higher longitudinal bar strains. The carbon jacketed column also had a significant increase in lateral column capacity (28% increase) and maintained this level at significantly higher displacement than the steel jacketed columns. This was due to the improved confinement effect of the carbon fiber retrofit. For the shear specimens,the Caltrans shear equation including the effects of strain rate accurately predicted the peak capacity of both shear columns. The Caltrans shear equation was used to calculate a force-displacement envelope based on ductility. This calculated envelope based on this procedure compared well with the measured force deformation envelope of the shear columns. Current methods for predicting the capacity of new flexural columns did well especially when including strain rate effects.

3) The design strain for the steel jacket and carbon fiber was 0.001, which is the lower bound at which slippage in the lap splice would occur. The steel jacket radial strains did not reach this level of strain and only achieved a peak strain of 0.0005, or 50% of the design strain. The carbon jacket radial strains reached a peak strain above the design strain of 0.001, with some jacket locations achieving a peak strain of 0.002 to 0.006. The carbon jacket was more effective at confining the concrete than the steel jackets.

4) The as-built failed at a ductility of 1.25 due to the poor confinement and lap splice failure. The steel jacketed columns failed at a ductility of 5 and 6 respectively. They did not achieve the high levels of ductility expected for a steel jacket retrofit column. The carbon jacketed column reached a high displacement ductility of 10 which was a significant improvement over the steel jacketed columns. This high ductility was achieved through higher jacket radial strains and higher longitudinal bar strains. A good ductility level (8.7) was achieved

for the new design flexural column tested to failure.

5) The greatest effect of load path was the premature lap splice failure and lower capacity of the steel jacket column subjected to the multiple incremental motion. The lap splice degraded more severely than the column subjected to the initial high amplitude motion. The stiffness was significantly less for the column subjected to the incremental motion, again due to the higher quantity of cycles in the load history and degradation of the lap. The large aftershocks subjected to the second 6FS2 column showed the column could still perform well after a first large initial motion. Once several large aftershocks were place on the column, the level of performance was very similar to the 6FS1 column subjected to incremental motion. The effect of load path was not significant between the measured shear column capacities. The only measurable effect was the difference in collapse points between the columns. The first column subjected to incremental motion collapsed at 3.25 x El Centro while the second shear column survived the 3.25 and following 1.0 x El Centro without collapse. Collapse would have been imminent if a slightly larger aftershock would have occurred. In the case of the new flexural designs, load path had an effect on the initial stiffness. The effect of load path dimishes after damage levels increased.

6) Analysis methods such as X-Section and RCShake do a very good job of predicting capacity but have a harder time predicting displacements at higher levels of excitation. Programs tend to underestimate the ultimate displacements. Including strain rate effects improves the predition of capacity.

ACKNOWLEDGEMENTS

The authors would like to thank the California Department of Transportation for their support of this research project. Conclusions and opinions reported in this paper are those of the authors only, and should not be construed to be endorsed by the sponors. Thanks are also extended to design engineers within Caltrans that assisted with the project.

REFERENCES

1. Caltrans Memo To Designers, 1998.
2. Laplace, P., D. Sanders, M. Saiidi, B. Douglas, *Shake Table Testing of Flexure Dominated Reinforced Concrete Bridge Columns*, Report No. CCEER-99-13, University of Nevada, Reno, 1999.
3. Laplace, P., D. Sanders, M. Saiidi, Experimental Study and Analysis of Retorfitted Flexure and Shear Dominated Circular Reinforced Concrete Bridge Columns Subjected to Shake Table Excitation, Report No. CCEER- 01-6, University of Nevada, Reno June 2001, pp 452.
4. Mander, J. B., M. J. N Priestley, and R. Park, "Theoretical Stress Strain Curve for Confined Concrete Columns", *ASCE Journal of Structural Engineering*, Vol. 114, No. 8, August 1988, pp. 1804-1826.
5. Priestley, M. J. N., F. Seible, G. M. Calvi, *Seismic Design and Retrofit of Bridges*, John Wiley and Sons, New York 1996.
6. *SPE-MC*, Seismic Performance Engineering, Moment Curvature Analysis Software by Thomas Ballard, www.seismicperformance.com.
7. *Strong Motion Earthquake Accelerograms, Digitized and Plotted Data*, Volume II, Part A, EERL 71- 50, Earthquake Engineering Research Laboratory, California Institute of Technology, Pasadena, California, 1971.
8. Wu, Hui, Yan Xiao, "Compressive Stress-Strain Behavior of Concrete Confined by Carbon Fiber Jackets", ICCI 1998, Second International Conference on Composites in Infrastructure.
9. *X-Section*, VER. 2.40, MAR-14-99, Moment-Curvature Analysis Software by Mark Seyed, Caltrans.

Emerging Seismic Design and Retrofit Technologies

Chair: Mark Reno

Seismic Design of Concrete Towers of the New Carquinez Bridge

Ravi Mathur, Mark A. Ketchum and Greg Orsolini

Precast Segmental Bridge Superstructures: Seismic Performance of Segment-to-Segment Joints

Sami Megally and Frieder Seible

In-situ Tests of As-is and Retrofitted RC Bridges with FRP Composites

Chris Pantelides, Jeff Duffin, Jon Ward, Chris Delahanty and Lawrence Reaveley

Calibration of Strain Wedge Model Predicted Response for Piles/Shafts in Liquefied Sand at Treasure Island and Cooper River Bridge

Mohamed Ashour, Gary Norris and J.P. Singh

Seismic Performance of a Concrete Column/Steel Cap/Steel Girder Integral Bridge System

Sri Sritharan, Robert E. Abendroth, Lowell F. Greimann, Wagdy G. Wassef and Justin Vander Werff

Seismic Design of Concrete Towers of the New Carquinez Bridge

Ravi Mathur[1], Mark A. Ketchum[2] and Greg Orsolini[3]

ABSTRACT

The new Carquinez Strait suspension bridge was designed to meet stringent seismic performance standards. Meeting these standards in the San Francisco Bay seismic environment required innovative design and analysis. The approach to achieving seismic performance is discussed, focusing on global issues, design of the 125-m tall concrete towers, and the 90-m deep drilled shaft foundations.

[1] Principal Bridge Engineer, Parsons Transportation Group, 120 Howard Street, #850, San Francisco, CA 94105
[2] Vice President, OPAC Consulting Engineers, 315 Bay Street, San Francisco, CA 94133
[3] Senior Project Manager, Parsons Transportation Group, 120 Howard Street, #850, San Francisco, CA 94105

INTRODUCTION

Long span suspension bridges with spans over 700 m have not been built in the United States for the past 38 years when the 1,300 m main span Verrazano Narrows bridge opened to traffic in 1964. Since the Verrazano Narrows, which had the distinction of having the world's longest span at that time, the Carquinez Bridge would be the first long span suspension bridge with a main span of 728 m to be opened to traffic in the year 2003.

The bridge, which spans the Carquinez straits, about twenty miles northeast of San Francisco is located within a few miles of several active faults. While other famous suspension bridges like the Golden Gate Bridge and the San Francisco-Oakland Bay-Bridge are undergoing major seismic retrofit, Carquinez Bridge is the first bridge in the United States, located in a potentially high seismic risk area, to be designed to present day stringent seismic design standards. This paper discusses the seismic design of some of the key elements of the bridge with an emphasis on the concrete towers and tower foundations.

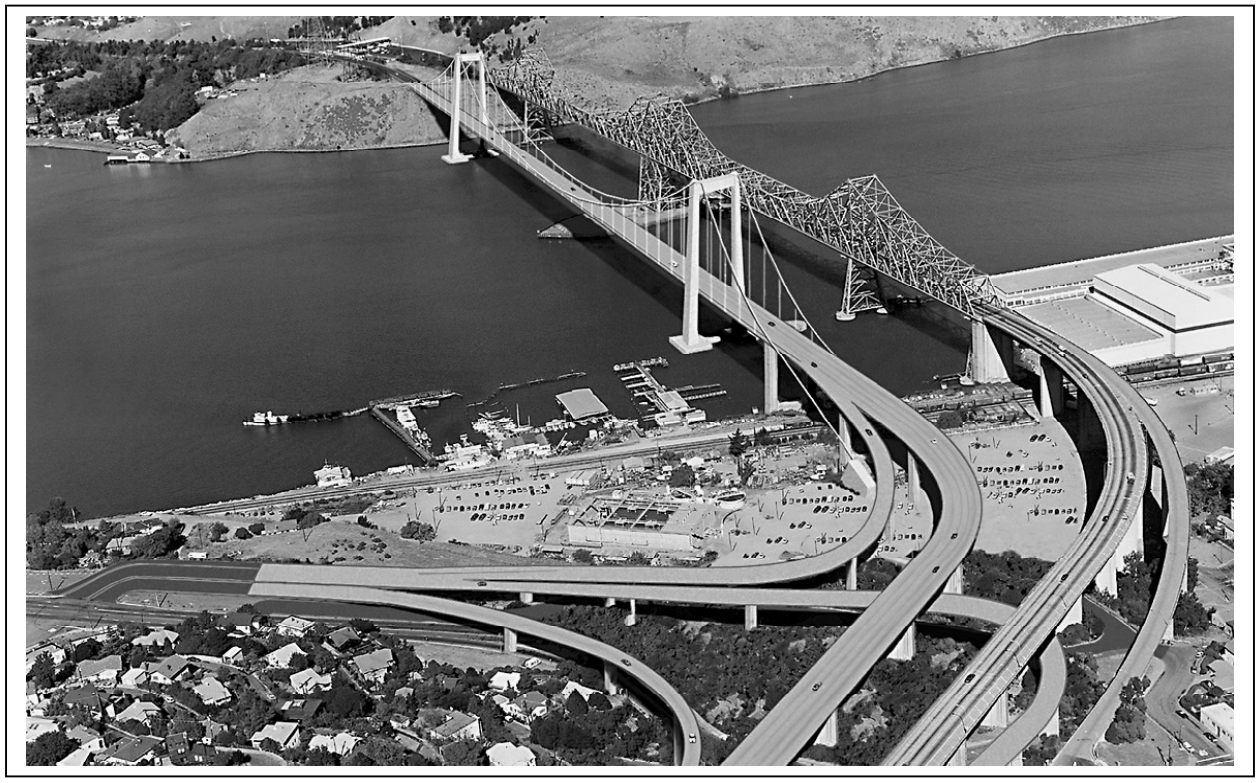

Figure 1 – Rendering of the New Carquinez Bridge

The first Carquinez Bridge, designed by David Steinman and Charles Derleth, was built in 1927 by the American Toll Bridge Company. It replaced a heavily used ferry service and cleared a bottleneck on the highway between San Francisco and Sacramento. The State of California acquired the bridge in 1941 and in the face of growing traffic needs designed and constructed a second Carquinez Bridge in 1958. Completion of the second bridge was part of an ambitious project that transformed a two-lane road into the modern eight-lane interstate highway of today. Both bridges are multi-span cantilever truss bridges with maximum spans of about 360 m.

Considering the potential for seismic activity in the Carquinez straits, safety initiatives prompted the California Department of Transportation (Caltrans) to commission retrofit studies of the existing structures. These studies were carried out by a joint venture team of HNTB and CH2M Hill. As a result of these studies, replacement over retrofit was considered the best "Overall Value" for the 1927 bridge due to several reasons; the bridge had severe seismic deficiencies, its main members required rehabilitation due to fatigue and corrosion, the concrete deck required replacement and the lane width were substandard with no shoulders. The study thus concluded that retrofitting the 1927 bridge to current seismic safety standards could be nearly as costly as replacement. Consequently, the State chose to replace the 1927 bridge. The 1958 bridge was considered for seismic retrofit for continued service.

Caltrans chose the joint venture team of De Leuw, Cather & Co., OPAC Consulting Engineers and Steinman Boynton Gronquist & Birdsall (De Leuw and Steinman are now part of Parsons Transportation Group) to design the replacement bridge. A type selection study was undertaken by the Consultants to choose between a cable stayed and suspension bridge alternatives. The study concluded that a two-tower suspension bridge would cost about the same as a three-tower cable stayed bridge. However, for reasons of better seismic performance, shorter construction schedule, better aesthetics and less construction risk, the suspension bridge alternative was chosen for final design.

The design of the bridge was completed in 1999 and the bridge is presently under construction with completion expected to be in late 2003.

BRIDGE DESCRIPTION

The new Carquinez Bridge with a main span of 728 m has a total length of about 1060 m between the North Anchorage and the Transition Pier as shown in Figure 4. The bridge will carry 4 lanes of westbound traffic along Interstate 80 in addition to a pedestrian/bike lane. See Figure 5. The overall width of the bridge deck between the main cables is 27.2m.

Towers - Two reinforced concrete towers of the bridge rise about 125 m above the water level. Each tower leg consists of a hollow box section with spirally reinforced corner pilasters about 1.0 m in diameter. The long walls connecting these pilasters are 500 mm thick. The short walls are 650 mm between the foundation and lower strut due to the high shear forces in the walls below the strut. Above the lower strut, the short walls have been reduced in thickness to 500 mm. The lower legs have a constant 3.75 m width transversely and are inclined at approximately 1 in 40 towards each other. In the longitudinal direction, the tower legs are tapered at approximately 1 in 100 from 5.8 m at the tower top to 8.25 m at the base. This hollow cellular section has been shown to provide superior seismic performance as well as agreeable aesthetics. See Figure 2.

The tower legs have been designed to behave elastically under the most severe design earthquake forces with limited inelasticity being permitted at the tower base. They have been detailed to have ductility capacities in considerable excess of their demands and exceed the Design Criteria requirement of minimum displacement ductility capacity of 4.

Two reinforced concrete struts connect the two tower legs. Both struts are post-tensioned concrete boxes. The lower strut is 6.0 m deep by 5.0 m with a 3.0 m square void. The upper strut is 4.5 m deep by 3.0 m with a 2.5 m square void. The struts have been designed to remain elastic. The strut nominal capacity is 20% greater than the plastic moment capacity of the tower legs. This design ensures that any inelasticity will occur in the more ductile tower leg rather than the post-tensioned struts.

Two different concrete strengths have been specified for the tower leg construction. Between the foundation and the lower strut, the tower leg concrete has a specified minimum compressive strength f_c' of 56 MPa. From the lower strut upwards the tower legs have a specified concrete compressive strength of not less than 35 MPa. Both the post-tensioned concrete tower struts have a specified compressive strength of 42 MPa.

Tower Piles - Each tower leg is supported on six 3 m diameter drilled shaft piles. 45 mm thick steel casings with an average length of about 47 m for the south tower and about 38 m for the north tower are driven to bedrock. The rock sockets are about 43 m long at the south tower and about 24 m long at the north tower. See Figure 4. The piles are detailed to provide adequate ductility and confinement to withstand the large seismic forces. The axial load demands are resisted by the pile skin friction alone. End bearing is not considered due to the wet construction of the piles.

Tower foundations posed one of the biggest construction challenges of the project. Construction of the north tower piles involved driving the casings to the specified tip. The casings were then cleaned out and an 2.7 m diameter rock socket was drilled beyond the tip of the casing. Polymer slurry with 6 percent salt concentration was used to stabilize the hole and to minimize softening and swelling of soft claystone and siltstone present in the rock. Once the rock socket tip elevation was reached, the rebar cage was lowered and concrete placed using a tremie pipe displacing the slurry. The rebar cage was then lowered in the casing and lapped with the rock socket cage. Concrete was then poured into the casing to complete the pile construction.

The rock mass at the south tower piles is highly fractured and polymer slurry was not able to stabilize the rock socket hole. Thus, a different construction method was employed here. Once the casing was in place, a 3.3 m

diameter under-reamer was used to drill about 7.5 m deep segments, which were stabilized using polymer slurry. A lean concrete mix was then placed by tremie. Once the concrete hardened, a 2.7 m diameter hole was cored through the concrete ensuring a stable hole for the rock socket. Thus, proceeding in segments of about 7.5 m, the rock socket tip was reached. Pile construction was then completed using the same procedure that was used at the north tower piles.

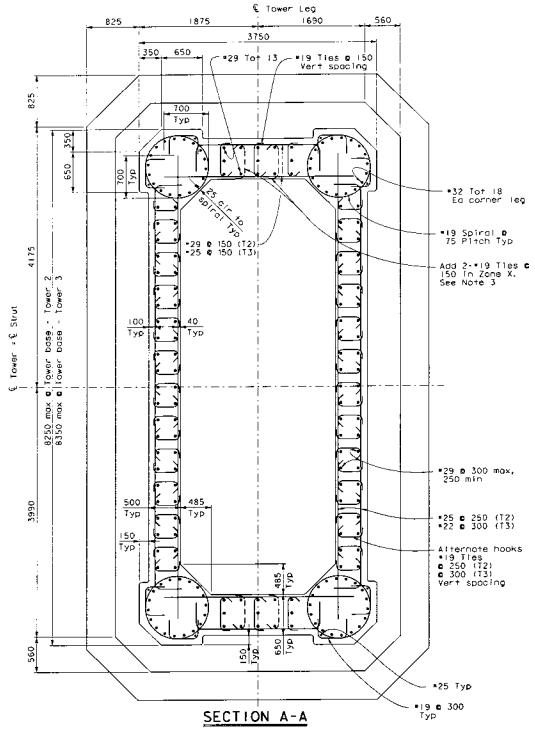

Cross-section Tower Leg

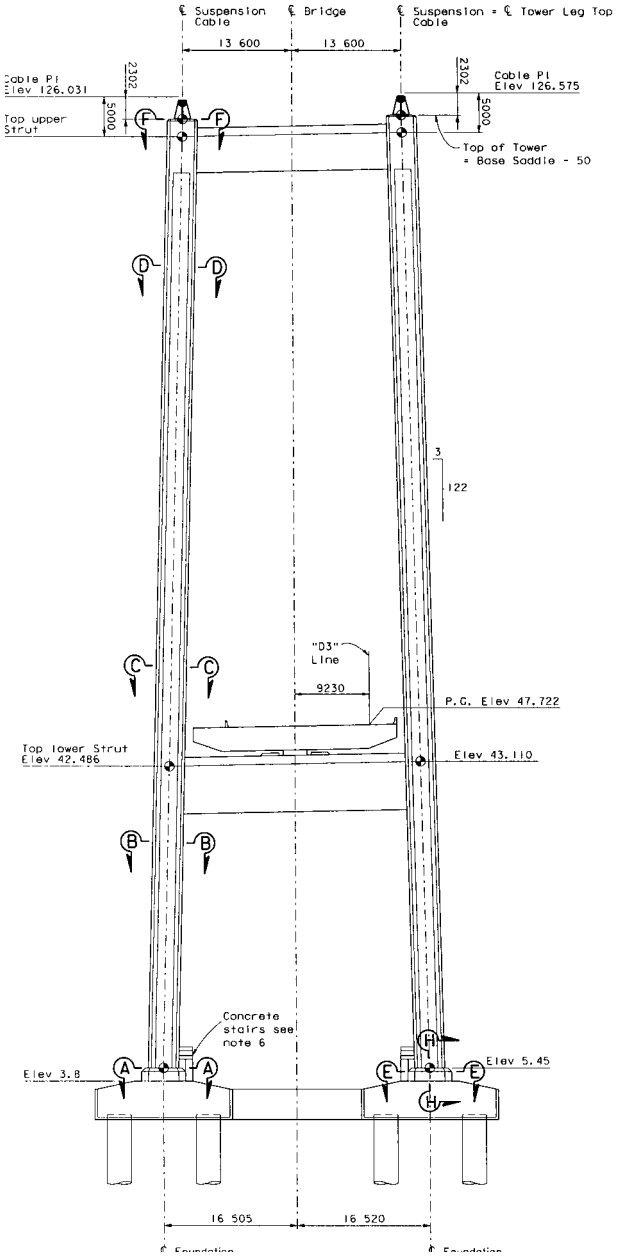

Tower Elevation

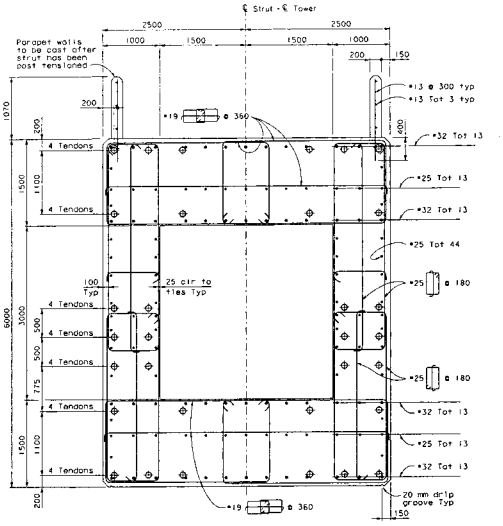

Cross-section Tower Lower Strut

Figure 2 – Reinforced Concrete Tower and Cross-sections

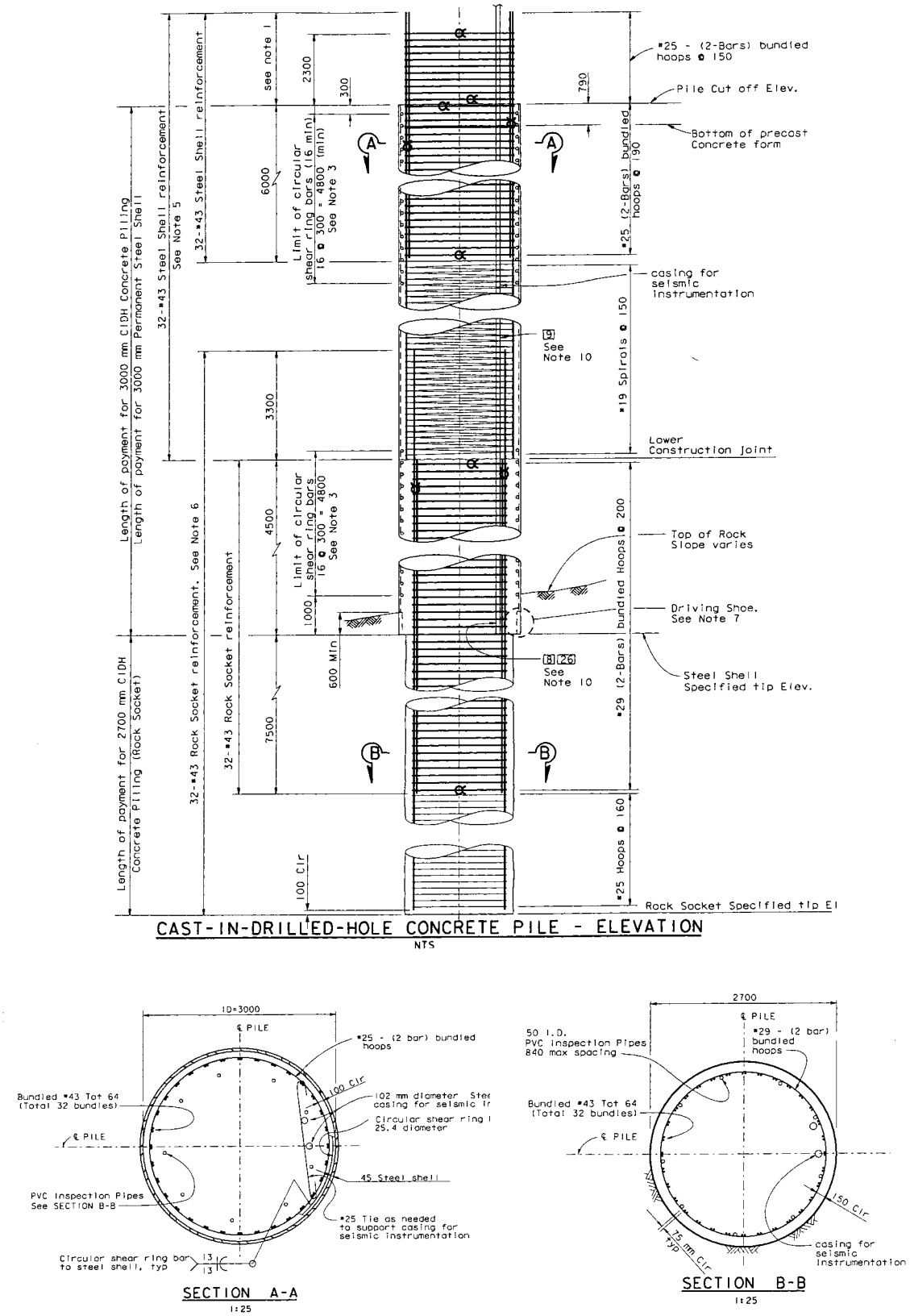

Figure 3 – Piles supporting the Tower Leg

Tower Foundations and Footing Forms - The tower foundations are about 2.3 m below the mean sea level. To avoid construction of the footings under water, the designers envisioned the use of precast footing forms. These forms were to be cast in the dry and floated to the site. They were to be positioned in place at the exact location and elevation over an erection frame supported on temporary piles. The precast form would now act as a cofferdam for the construction of the footing and also act as a template for driving the tower piles (drilled shafts).

However, the contractor chose to modify this construction method. Since the construction of the drilled shafts was on the critical path, the contractor started the construction of the shafts sooner while the precast forms were still being fabricated. Once the drilled shafts were constructed and the footing forms fabricated, the forms were floated in place at high tide and lowered on top of the piles. The contractor used a positioning system for the drilled shafts that allowed tight tolerances on the horizontal position of the steel casings, and thereby, ensured proper mating of the precast footing forms to the casings.

This construction technique will now be used on two other San Francisco Bay area bridges which use large diameter drilled shaft piles and footings which are below water: the new Benicia Martinez Bridge and the San Francisco Oakland Bay Bridge east span replacement project.

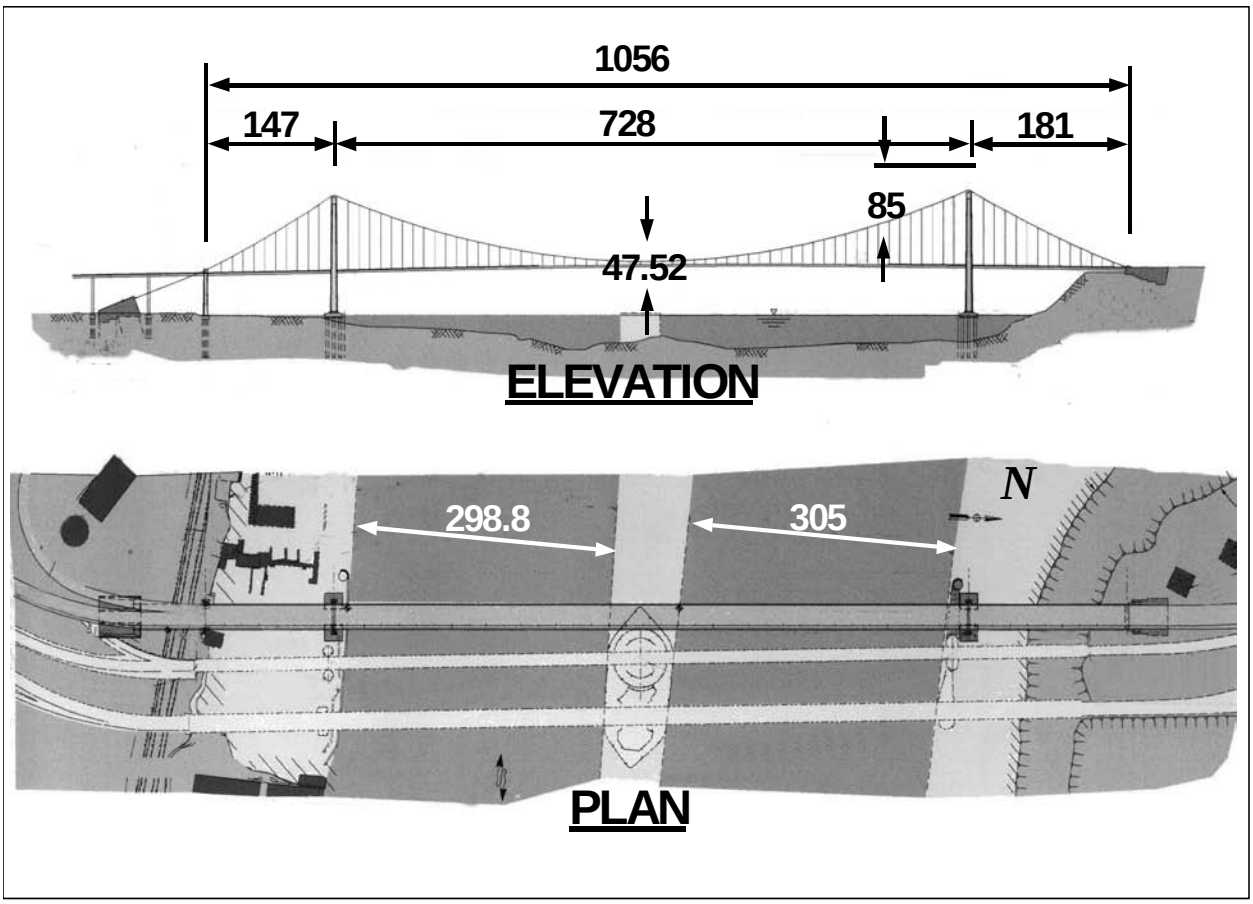

Figure 4 Bridge General Plan

Transition Pier - The Pier is located at the south end of the suspension bridge where it transitions to a steel girder supported span of the approach viaduct. The approach viaduct is designed by Caltrans and the real challenge in designing the structure was to mate the two bridges with vastly different dynamic response during an earthquake. The suspension bridge is much more flexible than the approach viaduct. Thus the steel box girder superstructure of the viaduct is designed as an isolation structure to accommodate up to 1.5 m of differential movement longitudinally between the two bridges, providing a flexible link.

The Pier column cross-section is a hollow rectangular box with spirally tied corner pilasters. The bent cap supports the suspension bridge loads through tall rocker links and also loads from the approach viaduct girders. In keeping with the Caltrans philosophy, the Pier is designed with a strong cap/weak column with plastic hinges forming at the column top and bottom in a transverse earthquake.

In addition to supporting loads from the bridge decks, Pier P1 also supports cable tie-down loads. The tie-down sections pass through the hollow columns and are anchored into the footings. To prevent the tie-down forces from being transferred to the columns, tie-down anchor rods are grouted in the solid sections at the base of the columns and the cap only after the superstructure box girder is erected and its load transferred to the footing. Each column is supported on 25-760 mm cast-in-steel-shell concrete (CISS) pile. Because of the high tensile load from the tie-down, the net compression force on the footing is considerably reduced.

Deck - The new Carquinez Bridge will be the first major suspension bridge in the United States to use a closed steel orthotropic box girder deck. This design is particularly effective in resisting bending stresses because of the large flange area. At the same time the closed box shape provides adequate torsional rigidity against wind, seismic and other unsymmetrical loads. In cross section, the box girder is 3 m deep and 29 m wide. The edge plate and side plates are shaped to provide an aerodynamically stable cross section.

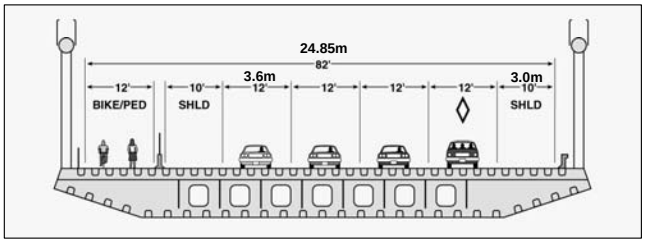

Figure 5 - Section - Steel Orthotropic Box Girder Deck

The suspended superstructure is designed as a continuous element with expansion joints only at the extreme ends of the girder resulting in a total girder length of 1,056 m. The box girder offers many advantages over truss-stiffened suspension spans including lower steel costs and lower maintenance costs, since much of the steel surface is sheltered within the section. The design of the deck incorporated several advances in fatigue endurance and innovative use of groove welded connections. These innovative modifications were made and validated as part of full-size physical testing for the Williamsburg bridge deck replacement in New York City.

Longitudinal bulkheads are provided to improve the vertical shear carrying capacity of the box and to accommodate seismic demands resulting in large bending moments about the vertical axis of the girder. The bulkheads also act as longitudinal distributing member along the box girder between two transverse bulkheads. Transverse bulkhead spacing is determined by the spacing of the suspenders, which is 12.4 m. Coincident with each suspender, a transverse bulkhead is provided with an intermediate bulkhead between each of them. The steel box girder remains essentially elastic under all loading conditions.

Initial fabrication of the bridge deck is being carried out by the Japanese firm Ishikawajima-Harima Heavy Industries Co. Ltd. (IHI) at their plant in Japan. The fabricated box girder segments will be transported across Pacific Ocean to the Carquinez Bay and lifted directly onto the span in their final position.

Cable System - Each main cable is comprised of 8,584 zinc coated carbon steel wires compacted into a diameter of 512 mm. The No. 6 gage cold drawn wire has a specified minimum ultimate strength of 1,570 N/mm^2 and a minimum yield strength by the 0.2% offset method of 1180 N/mm^2. A maximum allowable working stress of 690 N/mm^2 was used.

In the splay chambers of the anchorages the main cables each splay into 37 individual strands, with each strand secured around strand shoes of conventional design. This design approach considers that the cables will be constructed by air spinning, which reflects the contractor's selected method of cable erection. Each strand shoe is connected to a pair of anchor rods that extend to the rear of the gravity anchor block and attach to a series of steel anchor girders embedded in the concrete anchorage.

The main cable center tie to the box girder consists of a rigid built-up steel triangular frame connected to the main cable via a steel casting. The cable tie restrains the longitudinal movement of the deck to that of the main cable. A modest inelasticity was found in the cable center tie under large transverse demands.

Anchorages - The subsurface condition at the two cable anchorages is significantly different. As a result their geometry as well as their foundations are different.

North Anchorage - This is a gravity type anchorage, which is located high up on a rock buff overlooking the Carquinez Strait. The anchorage is combined with the bridge abutment, which supports the bridge deck through tall rocker bearings. The underlying rocks are folded and fractured with the strike and dip varying across the site. Geologic mapping and subsurface exploration identified a series of shear zones and faults though there was no evidence to suggest that these features were of tectonic origin. To reduce the pressure on the rock buff, the anchorage is located about 35 m from the face.

The top of the buff will be benched to allow the bridge girder to span to the abutment. The heel of anchor blocks for each cable is embedded about 20 m in the rock and rises in steps up to the abutment seat. Resistance to the large cable forces is provided by base friction as well as the passive resistance against the embedded structure. To enhance the resistance of the anchor blocks against block failure of the buff, the two blocks are connected by a massive grade beam. This helps to mobilize a much larger block of rock mass providing increased factor of safety against failure.

South Anchorage - Unlike the North Anchorage, the South Anchorage is located on fill underlain by soft clay, loose sand and weathered rock. With high ground water, the sand was found to be susceptible to liquefaction. The lateral resistance to the cable pull is thus provided by 380-762 mm CISS piles. 171 of these piles are vertical and the rest are driven at a batter of 3:1, with the batter being in the direction of the cable pull. The cable splay chambers and part of the anchor blocks are above ground with the remaining anchor block embedded below grade. The anchorage is located well south of the transition pier and below the approach viaduct. Its location was partly determined by the presence of Union Pacific tracks, which were to be cleared by the main cables.

SEISMIC DESIGN CRITERIA

The bridge is being designed for two levels of earthquake, the Safety Evaluation Earthquake (SEE) corresponding to a maximum credible event with a 1000 to 2000-year mean return period and the lower level Functional Evaluation Earthquake (FEE) with a 300-year mean return period. Under a SEE, any damage to the bridge has to be readily repairable without limiting traffic on the bridge. Under a more frequently occurring FEE the damage would not require repair or cause any permanent offsets. As much as possible, the Important Bridge criteria as required by Caltrans are met. Performance criteria are set by limiting strain levels in concrete, reinforcement and steel elements.

Limiting Concrete Strain Value – When designing for FEE event a maximum concrete strain of 0.004 was used for all reinforced concrete elements. For a SEE event, the stress-strain relationships proposed by Mander for confined concrete were used. For the tower piles, this strain was limited to 75 percent of the ultimate strains determined by Mander's equations. This was done to limit the damage in the tower piles under a SEE.

Limiting Strain Values for Pile Steel Casing – ASTM A252M, Grade 3 steel casing was specified with an F_y=310 MPa and F_u=455 MPa. Limiting strains in the steel casing of pile shafts was:

Longitudinal Tension (along pile axis)	0.045
Hoop Tension	0.060
Compression	0.010

Limiting Strain Values for Reinforcement – ASTM A706M, Grade 414 reinforcement was specified. To achieve the performance goals under a FEE event, the tension reinforcement strain was limited to 0.015. Under the SEE event the strain values in column reinforcement were limited to ε_{pg} except as discussed in the following table.

Table I – Limiting Strains for Reinforcement

REINFORCEMENT	ε_u	ε_{pg}	ε_{pp}
Main Column Bars #36, #43 & #57	0.08	0.05	0.03
Main Column Bars #33 and smaller	0.12	0.06	0.045
Spirals and Hoops #25 and smaller	0.12	0.10	0.06

ε_u = Ultimate steel strain
ε_{pg} = Design level steel strain for tower "performance goals"
ε_{pp} = Design level steel strain for pile shaft "performance goals"

ROCK MOTIONS AND DESIGN RESPONSE SPECTRA

Geomatrix Consultants carried out seismic ground motion study for maximum credible earthquakes (MCE) on the governing faults. Three design earthquakes were selected for the Carquinez Bridge. See Table II.

Comparison of the response spectra of the MCE on the San Andreas, Hayward and Franklin faults indicate that the spectral values for the Franklin event are equal to or higher than the other two events over the entire period ranging from 0 to 7.5 seconds. The response spectrum for this event was selected as the design response spectrum. Three sets of multi-support rock motions based upon the Franklin event were developed for the non-linear time-history analysis of the bridge.

Table II – Source of Earthquake and Ground Motion Characteristics

EQ Source	Magnitude M_w	Distance from bridge (km)	Peak Rock Accelerations (g)	
			Horizontal	Vertical
San Andreas	8	41	0.26	0.19
Hayward	$7^1/_4$	13	0.55	0.47
Franklin	$6^1/_2$	1	1.00	0.96

Rock motions were developed at each support location of the bridge corresponding to the SEE. Near source effects were incorporated in these motions to account for directivity effects. Also included were spatial variation in the motions over the length of the bridge.

SEISMIC ANALYSIS

The seismic performance evaluation of the bridge made use of a global inelastic dynamic computer model of the entire bridge. Seismic demands obtained from the structural analysis were compared with the capacities of the respective elements to ensure that their seismic performance is consistent with the project Design Criteria.

The global analysis was supported by detailed component analysis of the steel box girder deck, tower legs and tower piles. Local component analysis helped provide insight into their performance resulting in considerable design and detailing refinement.

Modeling – A global model of the bridge was developed from the north to the south anchorage. The model included the Crockett approach viaduct on the south side of the bridge, which was designed by Caltrans. The model thus captured the interaction between the approach viaduct and the suspension bridge.

The global model accurately represented the bridge geometry, stiffness and mass and considered all important structural components including pile foundations, anchorages, main towers, transition pier, cables, suspenders and orthotropic deck. To start with, a linear elastic model was used, but this was refined during the analysis as geometric non-linearity was introduced in the cables and material non-linearity was introduced in concrete elements found to experience inelastic behavior.

Discussed here are the methods and assumptions used to model the towers and the tower piles.

Towers – The tower legs and struts were modeled with two-node frame elements, which include the axial, bending, and torsional stiffness. Minor inelastic deformations were permitted at the base of the tower legs and below the lower strut. Moment-curvature (M-ϕ) relationships were developed and used at these locations to model the material non-linearity.

Each of the two tower legs is supported on 6 piles through a pile cap. Since the pile cap and the 6 piles have the same magnitude of stiffness, a rigid pile cap assumption was found invalid and 4-node isoparametric shell elements were used to model the cap.

Tower Piles – The drilled shafts including the 3 m diameter permanent steel shells and the 2.7 m diameter rock sockets were modeled explicitly using 2-node frame elements including axial, bending and torsional stiffness.

Nonlinear M-ϕ relationships were used to model the material behavior over the full length of the piles. The M-ϕ curves varied over the height of the piles with variation in reinforcement and confinement provided by the cap, the shell and the rock.

Additional hydrodynamic mass and soil mass is added to the pile elements through discrete lumped mass at the nodes. The hydrodynamic mass was assumed to be equal to the volume of water displaced by the piles. The soil mass tributary to the tower piles was assumed to be the volume of soil contained within a "doughnut" of a radius equal to 1.5 times the pile radius.

The soil stiffness along the height of the piles is considered to be non-linear and is based on p-y and t-z curves. These rock/soil springs were spaced at approximately 3 m intervals over the height of the pile. Rock motions were applied through these points representing the soil.

Analysis Results – The nonlinear time history analyses of the bridge were performed using ADINA program. Results obtained from this analysis were used to design the various bridge components. Results for the towers and the tower piles are discussed here.

Towers – Minor inelastic deformations were obtained at the base of the tower legs and below the strut. M-ϕ relationships were developed at these sections under varying axial loads. In evaluating the curvature capacity, the maximum concrete and reinforcement strains were limited to the value defined in the Design Criteria. From the lower strut upwards, the tower legs have been designed to essentially remain elastic.

For the purpose of determining the shear stresses induced into the tower legs, the legs were assumed to act as four columns bounding four connecting shear walls. Since the shear in the tower legs below the lower strut is controlled by the plastic moment of the tower legs at the base and below the lower strut, and since the nonlinear M-ϕ relationship for flexural hinging at these locations is incorporated into the analysis, the shear and torsion demands are taken directly from the analysis for design of these elements. Above the lower strut, the tower legs are to remain elastic and the elastic shear demands are used to design for shear and torsion.

The tower struts, which are post-tensioned boxes, have been designed to remain elastic during the SEE. The upper strut has been designed to have a flexural capacity 1.2 times the tower leg plastic moment capacity. This ensures inelastic deformations are limited to the legs. The lower strut has not utilized the same criteria, since designing the strut for combined plastic moments above and below the strut would be unrealistically conservative. The lower strut has been designed for a nominal moment of 1.2 times the elastic demands found from the global analysis.

Tower Piles – For the purpose of evaluation, the tower piles are assumed to have 3 distinct sections.

1) Piles at the pile cap where the rebar cage extends into the cap.
2) Piles below the cap and above the rock socket where it is confined by a permanent casing 45 mm thick. Casing contributes to both lateral confinement and flexural strength.
3) Piles within the rock socket.

Pile flexural capacity was obtained from a M-ϕ analysis for varying axial loads. The capacity was based either on the limiting compressive strains in the confined concrete or tensile strains in the reinforcement or the permanent casing. In determining the capacity of the pile section with casing the shell thickness was reduced to account for corrosion.

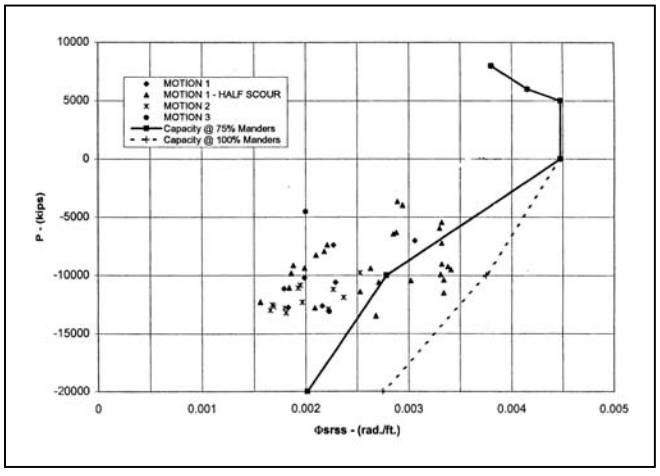

Figure 6 - Tower Pile Curvature Demand vs. Capacity Curve at the Rock Socket

Concrete compressive stress-strain relationship was based on Mander's equations. As stated in the project design criteria, maximum concrete strains are limited to 75% of ultimate strains determined by Mander to limit damage in the piles. However, for rock sockets, where the rock provides additional confinement which is not modeled in the evaluation of curvature capacity, concrete strains up to ultimate strains of confined concrete are allowed.

The adequacy of the pile sections under seismic loads was determined by plotting the curvature capacity of

each section at varying loads. Seismic curvature demands and the corresponding axial load on the piles at various time steps was plotted on this same graph. If the capacity curve envelopes the data points obtained from the seismic demands, the section design was assumed to be adequate. See Figure 6 for example plot.

Critical sections to evaluate the shear were at the rock socket. Plot of shear capacity envelopes vs. shear demands were plotted similar to flexure envelopes. Based on detailed study of soil-structure interaction between the sockets and the surrounding rock, it was determined that the shear results in the sockets found by the global analysis were unrealistically high. Shear results from the global analysis were thus reduced by a factor determined from the detailed study.

It is worth mentioning here that essentially all the inelastic excursions in the tower legs and piles were due to the near-field pulse generated due to the proximity of the Franklin fault to the bridge site.

Local Modeling – Local structural models were developed to support seismic analysis and design. Models of the tower bases, piles, and pile cap were developed to verify design capacities, section ductilities, and evaluate compliance with the seismic performance criteria. This advanced analysis work was performed by Anatech Consulting Engineers and SCSolutions Inc.

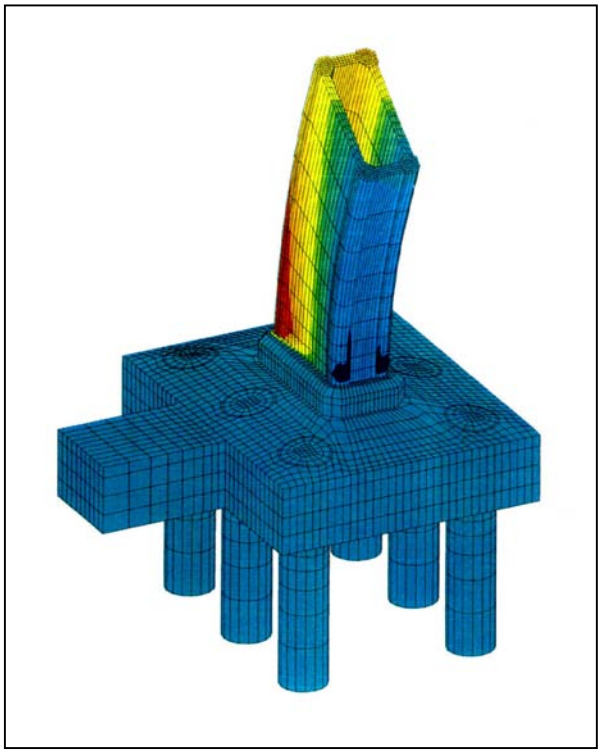

Figure 7 - Vertical Strain Contours – Longitudinal Pushover (Developed by Anatech Consulting)

In the preliminary design, a three-dimensional model of a hollow "tied-corner" tower cross section was compared to a hollow rectangular cross section, and the "tied-corner" scheme was chosen for final design.

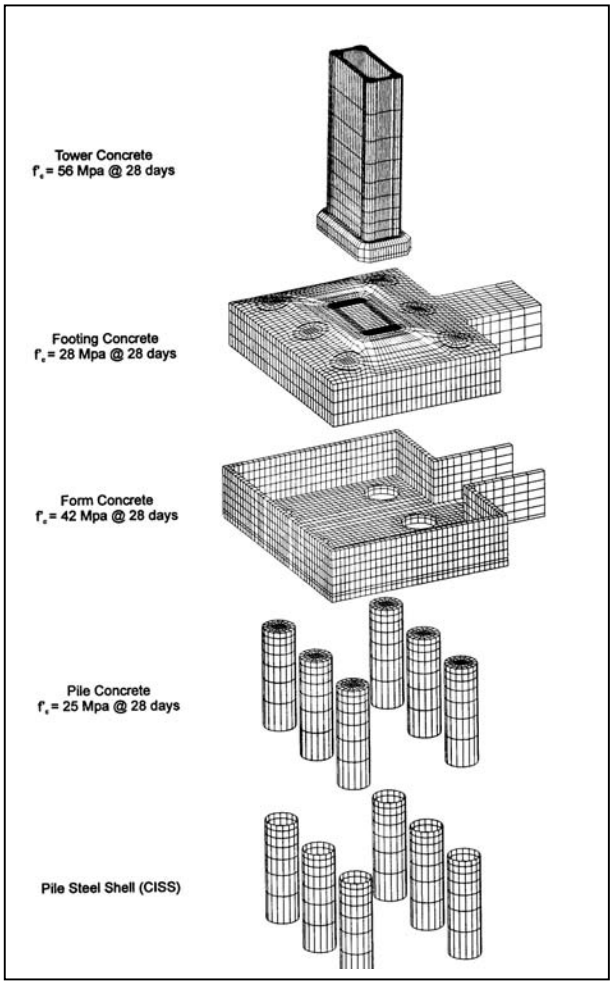

Figure 8 - Pile-cap Model – Finite Element Geometry (Developed by Anatech Consulting)

Other local continuum analytical studies were performed for lower/upper strut to column joint region and for the tower base/pile-cap/pile system to verify this system's seismic performance. Figure 7 shows the vertical strain contours during a longitudinal pushover indicating regions of concrete cracking and rebar yielding. Figure 8 shows components of the finite element model of the tower base/pile-cap/pile region.

CONCLUSIONS

The New Carquinez Bridge was designed for forces and deformations obtained using state-of-the-art analysis methods. Rock motions at each support were developed corresponding to the SEE incorporating the near-source effects. The three-dimensional model of the bridge incorporated geometric non-linearity in the cables and material non-linearity in the concrete elements which show inelastic behavior. Soil-structure interaction at the tower piles was considered using non-linear springs to represent the p-y and t-z characterizations of the soil/rock. This paper focused on modeling and seismic behavior of the concrete towers and the drilled shaft piles.

Seismic studies demonstrated that the bridge design meets the Seismic Design Criteria adopted for the project. During a SEE event minimal damage is expected in the tower legs and tower piles, which could result in cover concrete spalling and limited yielding of the reinforcement. During a FEE event, no damage is expected to these bridge elements.

The design of the bridge was completed in June 1999 when the 100% PS&E package was submitted to Caltrans. The bids were opened in January 2000 and the lowest bid of $188 million and 1,000 days was submitted by a 65-35 joint venture of FCI Constructors Inc. and U.K. based Cleveland Bridge. The bridge is under construction with construction progressing simultaneously on the two towers and south anchorage. Construction of the tower foundations, transition pier, and the north anchorage is already complete or nearing completion. Fabrication of the bridge deck is being carried out by the Japanese firm Ishikawajima-Harima Heavy Industries Co. Ltd. (IHI), that of the main cables is being carried out by Bridon International at their UK plant and the suspenders are being fabricated by Changqing Wonderbridge Cable Co Ltd in China.

Suspension bridges are inherently flexible structures with the suspended superstructure and tall towers resulting in long periods of vibration and therefore smaller seismic forces. Thus, these bridges are well suited in areas of high seismicity. The New Carquinez Bridge should therefore ride out the next big earthquake without suffering major damage.

ACKNOWLEDGEMENTS

The design of this bridge was funded by Caltrans. It took a cooperative team effort between several design firms, Caltrans and the Peer Review Panel to accomplish the task of designing such a major bridge. The authors would like to acknowledge the contribution of all individuals who worked on this project including Sheila Apte and Shawn Marlow who worked on the design of the towers and tower foundations and C.-Y. Chang of Geomatrix Consultants who was responsible for the geotechnical design of the tower foundations. Special thanks go to Mike Marquez, Caltrans Project Manager for his timely assistance and overall support during the entire design effort. Caltrans is also acknowledged for providing overall supervision of the design and making key decisions based upon consultant recommendations.

REFERENCES

[1] Marquez, M., G. Orsolini, M. Ketchum and T. Spoth. June 2000. “Suspension Solution”, *ASCE Civil Engineering Magazine*.
[2] De Leuw – OPAC – Steinman. February 1999. “Third Carquinez Strait Bridge Seismic Report.”
[3] De Leuw – OPAC – Steinman. March 1999. “Carquinez Bridge & Overhead Design Report.”
[4] Geomatrix Consultants & Earth Mechanics. August 1999. “Foundation Report Volumes-1-3.”
[5] Anatech Consulting Engineers. February 1999. “Seismic Performance Evaluation for Tower Leg Sections of the Third Carquinez Straits Bridge” a Report.
[6] Anatech Consulting Engineers. February 1999. “Detailed Analysis of the Foundation Pilecap and Tower Base – Pilecap-Pile Connection for the Third Carquinez Straits Bridge” a Report.
[7] Mander, et. al. 1988. “Theoretical Stress-Strain Model for Confined Concrete”, *ASCE Journal of Structural Engineering*.

Precast Segmental Bridge Superstructures: Seismic Performance of Segment-to-Segment Joints

Sami Megally and Frieder Seible

ABSTRACT

Precast segmental bridges are not commonly constructed in high seismic zones because of lack of information on their seismic performance. A research program is currently in progress at the University of California, San Diego (UCSD) to investigate the seismic performance of precast segmental bridges. The research program consists of three phases, which involve large-scale laboratory tests and finite element analyses. This paper presents results of the first two phases of the experimental program. The objective of these experiments was to investigate the seismic performance of segment-to-segment joints of precast segmental bridge superstructures with different ratios of internal to external post-tensioning.

In the first phase, the seismic performance of superstructure joints close to midspan with high positive flexural moments and low shears was investigated, whereas performance of joints close to the columns with high negative flexural moments combined with high shears was investigated in the second phase.

Four large-scale test units were tested in each of the two phases with a total of eight test units. The joints of the first, third and fourth test units in each of the two research phases were epoxy bonded with no mild steel reinforcement crossing the segment-to-segment joints. The second test unit had reinforced cast-in-place deck closures at locations of segment-to-segment joints with the remaining portions of the joints connected by epoxy. In each of the two phases, the first and second test units were post-tensioned with internally bonded tendons, whereas the third test unit was post-tensioned with external tendons. Internally bonded tendons achieved half of the post-tensioning of the fourth test unit, whereas external tendons achieved the other half. Test units of the first phase were subjected to fully reversed cyclic loads simulating earthquake vertical motions, whereas cyclic loading of the second phase tests simulated earthquake longitudinal motions.

The experiments showed that segment-to-segment joints could undergo significant opening and closure before failure. The experiments also showed that post-tensioning of the superstructure with external tendons only would result in higher displacement and ductility, minimum residual permanent displacements and minimum loss of the effective prestressing force after earthquake occurrence.

Sami Megally, Assistant Project Scientist, Department of Structural Engineering, University of California at San Diego (UCSD), 9500 Gilman Drive, La Jolla, CA 92093-0085
Frieder Seible, Executive Associate Dean of Engineering and Professor of Structural Engineering, University of California at San Diego (UCSD), 9500 Gilman Drive, La Jolla, CA 92093-0085

INTRODUCTION

Despite the well-known advantages of precast segmental bridges, they are not currently constructed in high seismic zones such as California because of lack of information on their seismic performance. Current design guidelines [1] permit the use of precast segmental bridges in high seismic zones only if the precast segments are epoxy bonded and at least 50 percent of the superstructure post-tensioning is achieved by internally bonded tendons. In other words, external tendons should achieve no more than 50 percent of the superstructure post-tensioning.

Because of the current practice restrictions and the lack of information on seismic performance of precast segmental bridges, a research program was initiated by the American Segmental Bridge Institute (ASBI) and funded by Caltrans (California Department of Transportation) to investigate the seismic performance of precast segmental bridges. This research program is currently in progress at the University of California, San Diego (UCSD). The research project consists of the following three phases:

- **Phase I:** To investigate the performance of superstructure segment-to-segment joints under fully reversed cyclic loading. Only joints close to midspan with high bending moments and low shears were considered in this phase.
- **Phase II:** To investigate the performance of superstructure joints close to the columns where the joints are subjected to high bending moments combined with high shears.
- **Phase III:** To investigate the seismic performance of superstructure-column systems under longitudinal seismic loading.

The first two phases were completed and the major experimental results are presented in this paper. Finite element models of the test units of both phases were developed. However the finite element analyses results are not presented here due to space limitations.

PROTOTYPE STRUCTURE

The test units of the first two phases were designed based on the prototype structure shown in Fig. 1. The prototype structure is a five span bridge with three interior spans of 100 ft and two exterior spans of 75 ft. The tendon profile in the superstructure has a harped-shape with harping points at 1/3 locations of the span (see Fig. 1). The prototype structure is constructed using the span-by-span method. The cross section of the superstructure consists of a single cell box girder. Horizontal continuity tendon near the bottom soffit of the prototype superstructure was also included in design of the Phase II test units.

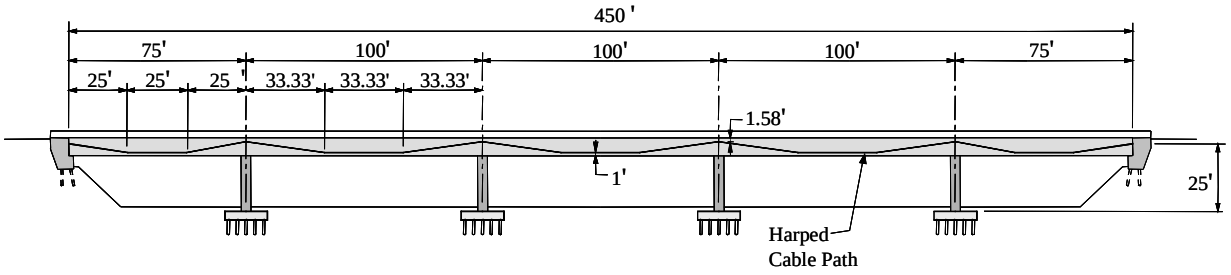

Figure 1. Prototype structure

EXPERIMENTAL PROGRAM ON JOINTS SUBJECTED TO HIGH BENDING MOMENTS COMBINED WITH LOW SHEARS (PHASE I)

Description of Test Units

The test variables in Phase I were: (1) the ratio of internal to external post-tensioning of the superstructure, and (2) presence of continuous mild steel reinforcement in the deck across the segment-to-segment joints. Four large-scale units with different ratios of internal to external post-tensioning were tested and the test matrix is given in Table I. It should be mentioned that the test matrix of the Phase II experiments is identical to that of the Phase I experiments (Table I). Each test unit consisted of six precast segments, which were epoxy bonded. Test Units 100INT and 100INTCIP used 100 percent internal post-tensioning (bonded tendons). Test Unit 100EXT was similar to Unit 100INT but it was post-tensioned with external tendons only (see Fig. 2). Unit 50INT/50EXT was also similar to Unit 100INT except that half of the post-tensioning was achieved by external tendons and the remaining half by internally bonded tendon (see Table I and Fig. 2). The terms 100INT, 100EXT and 50INT/50EXT in test unit designation indicate the percentages of post-tensioning achieved by internally bonded and external tendons. In designation of the second test unit, CIP stands for the cast-in-place deck closure joints.

TABLE I. TEST MATRIX (PHASE I AND PHASE II TEST UNITS)

Test Unit	Test Description
100INT	100% Internal PT (Post-Tensioning)
100INTCIP	100% Internal PT and cast-in-place deck closure joints
100EXT	100% External PT
50INT/50EXT	50% Internal PT + 50% External PT

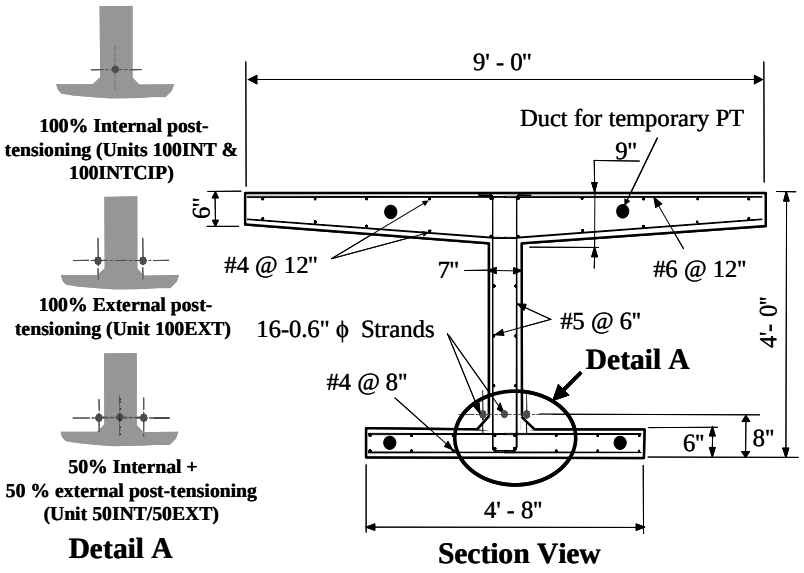

Figure 2. Cross section of the Phase I test units

In Units 100INT, 100EXT and 50INT/50EXT, no mild steel reinforcement was present across the segment-to-segment joints, whereas Test Unit 100INTCIP had reinforced cast-in-place deck closures at the locations of segment-to-segment joints. The remaining portions of the joints in Unit 100INTCIP, along the web and bottom flange, were epoxy bonded. The reinforced cast-in-place deck detail across each joint of Unit 100INTCIP was similar to the detail proposed for the new East Bay Skyway of the San Francisco-Oakland Bay Bridge. Only one half of a single cell box girder in the shape of an equivalent I-section was modeled at 2/3-scale in the experiments to simplify the test setup (see Fig. 2).

Figure 3 shows the load frame and a typical test unit simply supported at both ends. The test zone of each unit consisted of four precast segments (Segments 2 to 5 in Fig. 3). Each test unit was loaded by means of four vertical hydraulic actuators as shown in Fig. 3 in two testing stages. The first testing stage represented service load conditioning, whereas the second testing stage represented vertical seismic loading of the superstructure. In the seismic testing stage each test unit was subjected to fully reversed cyclic vertical displacements with increasing amplitude up to failure. The forces in all the four actuators were maintained equal at all times.

Experimental Results (Phase I)

Crack Development and Modes of Failure

Under downward loading of all test units, the first crack occurred at the midspan joint in the concrete cover adjacent to the epoxy-bonded joint. This was followed by cracking at the two

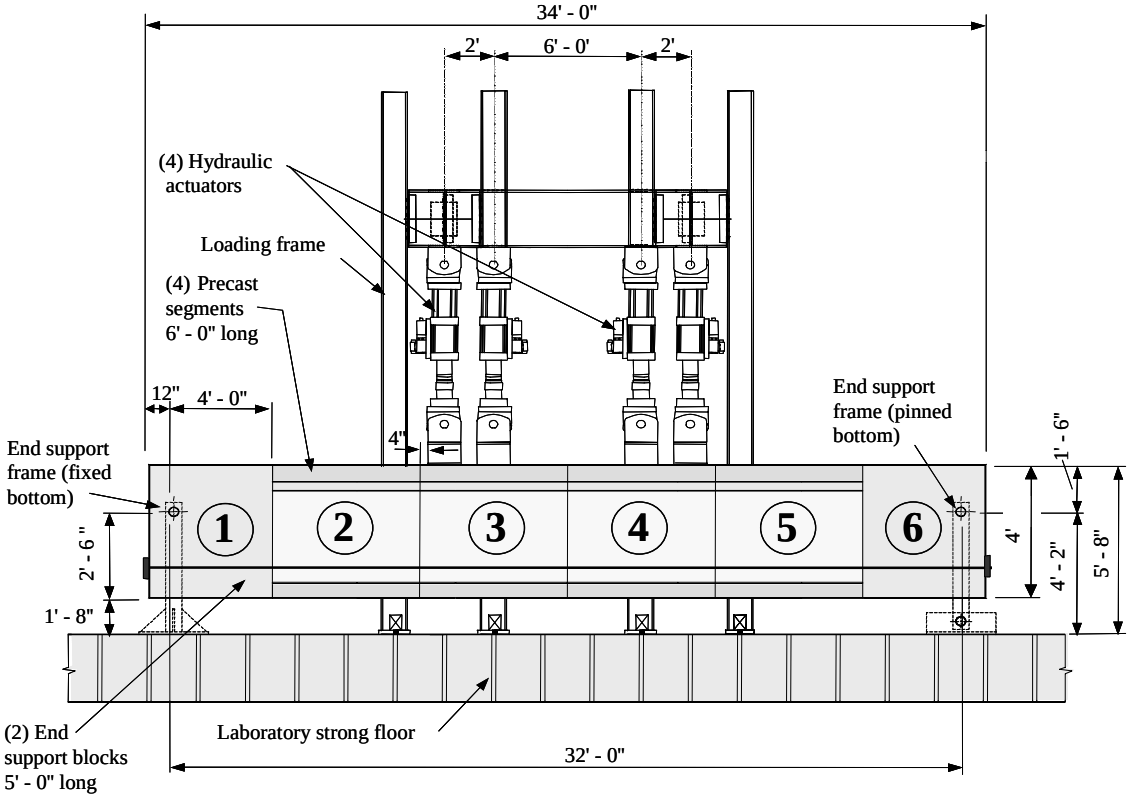

Figure 3. Test setup of Phase I experiments

joints adjacent to the midspan joint of Test Units 100INT, 100INTCIP and 50INT/50EXT, which had internally bonded tendons. The midspan joint was the only one that opened during downward loading of Unit 100EXT with 100 percent external tendons. In the upward loading direction, cracking occurred only at the midspan joint in Units 100INT, 100EXT and 50INT/50EXT, whereas several closely spaced cracks developed inside the segments of Unit 100INTCIP because of the continuity of the deck at joint locations.

Test Unit 100INT failed when the prestressing strands ruptured at the midspan joint as shown in Fig. 4, which also shows a close-up view of the ruptured prestressing strands. Failure of Unit 100INTCIP initiated by buckling of the cast-in-place deck reinforcing bars which was followed, after repeated displacement cycles, by compression failure of the deck at midspan (see Fig. 5). Failure of Test Unit 100EXT (with external tendons) initiated by crushing of the deck at the midspan joint. In contrast to the explosive failure of Units 100INT and 100INTCIP, failure of Unit 100EXT occurred gradually; the load carrying capacity dropped gradually with increased displacement in the post-peak range. Testing of Unit 100EXT was terminated when displacement capacity of the hydraulic actuators was reached. Figure 6 shows the midspan joint of Unit 100EXT at the maximum downward displacement reached during the experiment. Test Unit 50INT/50EXT failed at a relatively low displacement when the internal tendon ruptured.

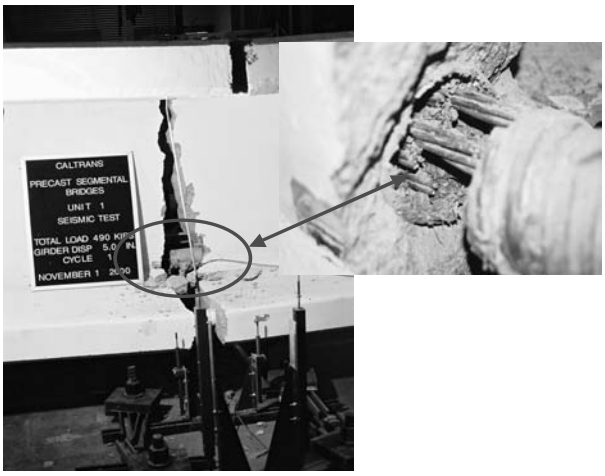

Figure 4. Test Unit 100INT at failure (Phase I)

Figure 5. Compression failure of Test Unit 100INTCIP (Phase I)

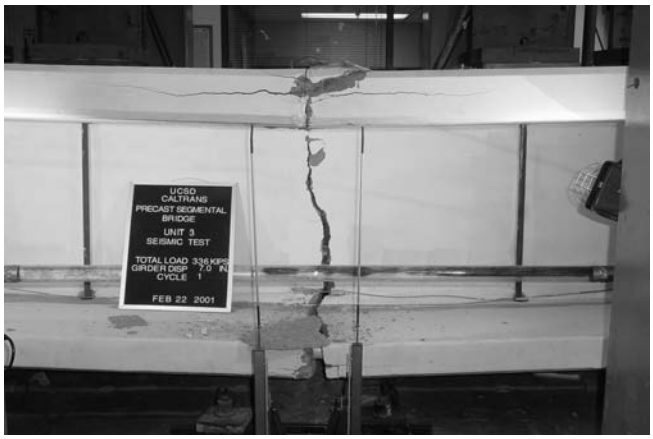

Figure 6. Test Unit 100EXT at maximum downward displacement (Phase I)

Load-Displacement Response

Figure 7 shows the history of total applied load versus vertical displacement measured at 6 inches from midspan for Test Units 100INT and 100INTCIP; the variable of these two test units was presence of mild steel reinforcement in the deck across the segment-to-segment joints. Figure 8 is similar to Fig. 7 but it shows the load versus displacement for Units 100INT, 100EXT and 50INT/50EXT with the test variable being the ratio of internal to external post-tensioning. Sign convention in Figs. 7 and 8 is positive for downward loading and displacement. The reference load level indicated by the horizontal solid lines in Figs. 7 and 8 represents the total load on each test unit before application of the fully reversed cyclic vertical displacements.

The performance of Units 100INT and 100INTCIP was similar under downward loading, however the performance of the two units was substantially different under upward loading (see Fig. 7). Unit 100INT did not have continuous deck reinforcement crossing the joints; thus once the midspan joint opened there was a large drop in the applied upward load. The yield strength of the deck reinforcing bars in Unit 100INTCIP could be developed resulting in a maximum total upward load of 327 kips, rather than 93 kips for Unit 100INT. Figure 7 also shows the enhancement in energy dissipation with the cast-in-place deck joints in Unit 100INTCIP.

Figure 9a shows the envelope of the hysteresis loops of Figs. 7 and 8 for downward loading direction only. Figure 9a indicates that 100 percent external post-tensioning significantly increases the ductility and maximum displacement reached before failure. The force in the internal tendon of Unit 50INT/50EXT was higher than the force in the external ones as evidenced from the recorded tendon strains. The measured strains in the internal tendon in Unit 50INT/50EXT were higher than the strains, at the same displacement levels, in the internal tendons of Units 100INT and 100INTCIP with 100 percent internal post-tensioning. Thus, the internal tendon in Unit 50INT/50EXT failed at a relatively small displacement compared to the other units. Thus in terms of seismic performance of joints, combination of internal and external tendons is not recommended. The maximum load carrying capacity, V_u, and the maximum displacement before failure, Δ_u, are given in Table II for all test units of Phase I.

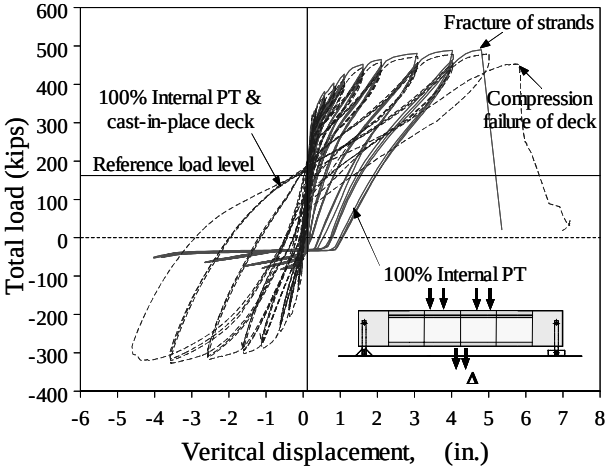

Figure 7. Load versus displacement (Phase I, Units 100INT and 100INTCIP)

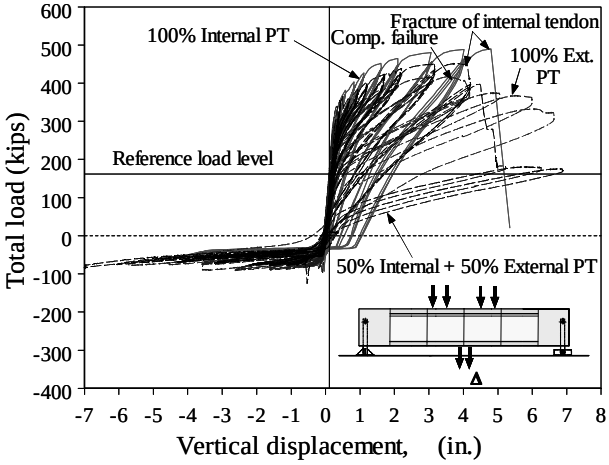

Figure 8. Load versus displacement (Phase I, Units 100INT, 100EXT and 50INT/50EXT)

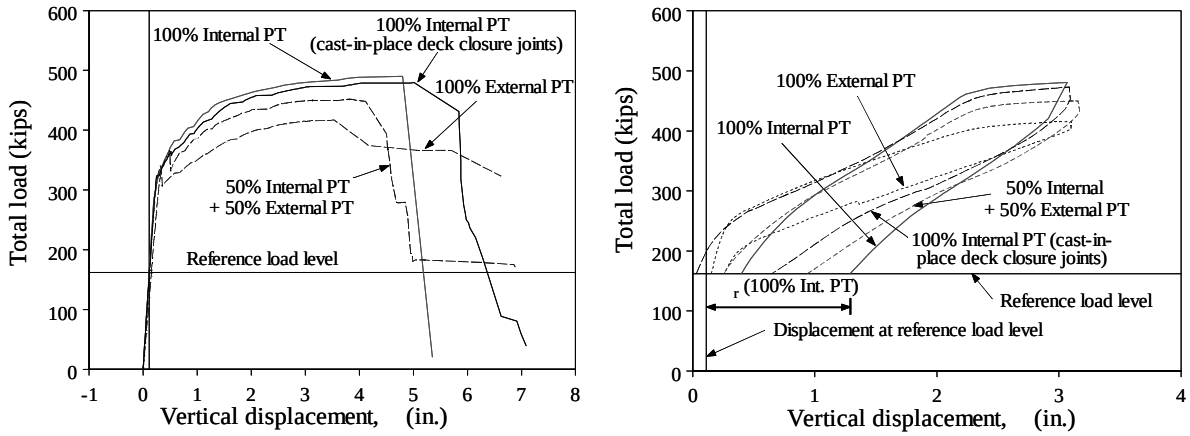

(a) Envelope of load versus displacement (downward loading)

(b) Downward load versus displacement (3 in. displacement cycle)

Figure 9. Load-displacement response of the Phase I test units

TABLE II. LIMITED TEST RESULTS (PHASE I EXPERIMENTS)

Test Unit	V_u (kip)	Δ_u (in.)	Δ_r (in.)	Δ_r/Δ_{Ref}	ζ (%)	ζ/ζ_{Ref}
100INT	490	4.8	1.17	8.36	4.21	1.60
100INTCIP	480	5.9	0.53	3.79	8.75	3.33
100EXT	417	6.6	0.14	1.00	2.63	1.00
50INT/50EXT	451	3.8	0.82	5.86	3.87	1.47

Δ_r and ζ were measured during the 3 in. displacement cycle.

Figure 9b shows the load versus displacement curve during the downward loading portion of the 3 in. displacement cycle of all test units. The displacement measured during the unloading portion of any of the curves shown in Fig. 9b at the reference load level represents the permanent residual displacement, Δ_r, after earthquake occurrence. Values of Δ_r measured after 3 in. maximum displacement of all Phase I test units are given in Table II. The values of Δ_r for all test units are normalized to the residual displacement of Unit 100EXT, Δ_{Ref} (= 0.14 in.). The ratio Δ_r/Δ_{Ref} is given in Table II for all test units. Comparison of the Δ_r/Δ_{Ref} values indicates that residual displacements can be minimized by use of 100 external post-tensioning. This is because the strains in external tendons are significantly less than the strains in internally bonded tendons. Inelastic strains in internal tendons result in loss of the prestressing force and large permanent residual displacements. Comparison of Δ_r/Δ_{Ref} values for Units 100INT and 100INTCIP also indicates that use of cast-in-place deck closure joints reduces the residual displacements.

Viscous damping coefficient, ., can be considered as a measure of energy dissipation capability of the test units. The viscous damping coefficient, as a ratio of critical damping, is determined by an equation [2] that relates the area within the hysteretic loop of the 3 in. displacement cycle to that of the elastic strain energy. The values of . are given in Table II. The viscous damping coefficients for all test units are normalized to the damping coefficient of Unit

100EXT, $\cdot_{Ref}$ (= 2.63 percent). Table II also gives values of the ratio $./._{Ref}$ for all test units. Table II indicates that segment-to-segment joints in superstructures with internally bonded tendons are able to dissipate more energy than joints in superstructures with external tendons. Also use of cast-in-place deck closure joints substantially enhances energy dissipation capability.

EXPERIMENTAL PROGRAM ON JOINTS SUBJECTED TO HIGH BENDING MOMENTS COMBINED WITH HIGH SHEARS (PHASE II)

Description of Test Units

As in the Phase I test units, the test variables in the Phase II test units were: (1) the ratio of internal to external post-tensioning of the superstructure, and (2) presence of continuous mild steel reinforcement in the deck across the segment-to-segment joints. Four large-scale units were tested and the test matrix of Phase II was identical to the test matrix of Phase I and is given in Table I. As in Phase I, only one half of the prototype box section was modeled in the experiments to simplify the test setup. The test units were constructed again at a 2/3-scale of the prototype structure shown in Fig. 1. Cross section of the test units is shown in Fig. 10. In each of the Phase II test units, only one segment-to-segment joint was modeled, which was the joint between Segments 1 and 2 (see Fig. 11a). The main objective was to study the performance of this joint under the combined effect of high bending moments and high shears. The precast Segments 1 and 2 (see Fig. 11a) were epoxy bonded.

The harped-shape tendon was modeled in the experiments by the inclined tendon shown in Fig. 11a. As mentioned earlier, a horizontal continuity tendon near the bottom soffit was included in design of the prototype structure for Phase II. The need for this continuity tendon should be based on seismic design of the structure. This horizontal tendon was also modeled in the experiments and is shown in Fig. 11a.

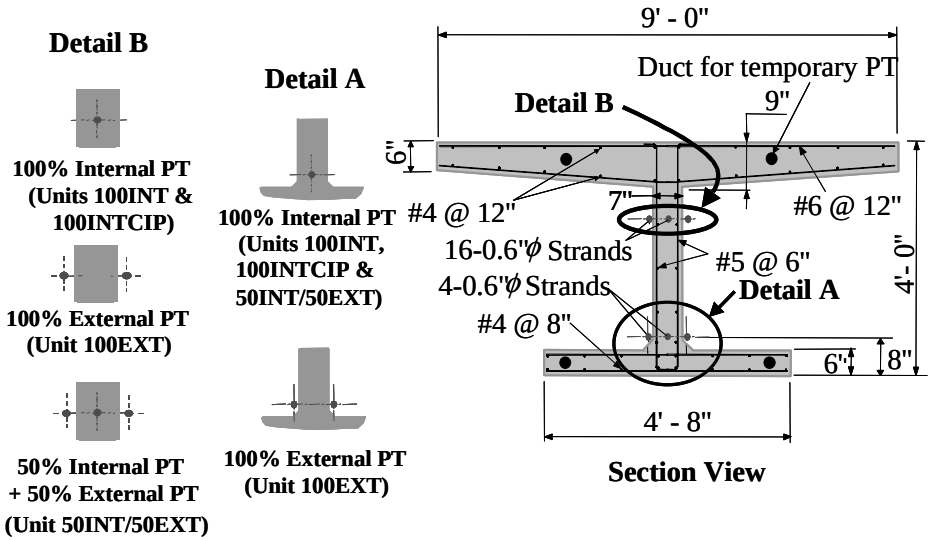

Figure 10. Cross section of the Phase II test units

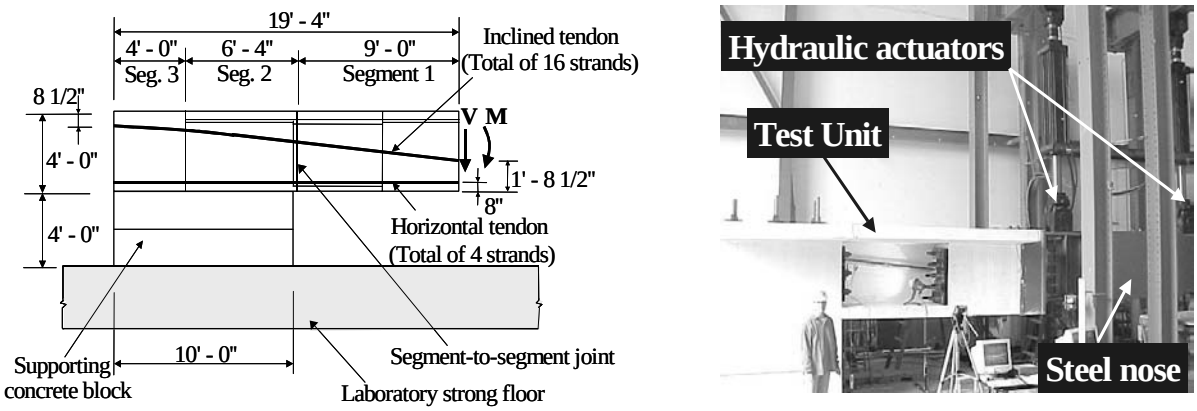

(a) Test unit and tendon layout

(b) Test setup

Figure 11. Test units and test setup of Phase II experiments

Again, Test Units 100INT and 100INTCIP used 100 percent internally bonded tendons. Test Unit 100EXT was post-tensioned with external tendons only (see Fig. 10). In Unit 50INT/50EXT, the horizontal continuity tendon near the bottom soffit was internally bonded, whereas half of the harped-shape prestressing steel consisted of external tendons and the other half consisted of internally bonded tendons (see Fig. 10). As in Phase I, Unit 100INTCIP of Phase II had a cast-in-place deck closure at location of the joint between Segments 1 and 2.

Each test unit was subject to shearing force, V, and bending moment, M, at its end (see Fig. 11a). The shearing force and bending moment were applied by means of two vertical hydraulic actuators, which were connected to a steel beam (steel nose) as shown in Fig. 11b. In the initial testing stage, each test unit was loaded to the reference load level (as in Phase I experiments). In the second testing stage, fully reversed cyclic vertical displacements were applied at the tip of the steel nose until failure of the test unit. The forces in the two actuators were related to each other by a prescribed function to obtain the correct simultaneous values of bending moment and shearing force at the segment-to-segment joint throughout the test. In determination of the prescribed function that related V to M, it was assumed that the prototype structure was subjected to gravity loads combined with longitudinal seismic forces.

Experimental Results (Phase II)

Crack Development and Modes of Failure

The first crack occurred in all test units at the segment-to-segment joint due to flexure under downward loading. As in Phase I experiments, the flexural crack occurred in the concrete cover adjacent to the epoxy-bonded joint. A similar flexural crack occurred in the bottom slab at the joint location under upward loading. These flexural cracks propagated in the web of the I-shaped cross-section until they were joined together. The flexural crack widened under further loading until failure of the test units. Because of the continuity of the deck, the first flexural crack in the deck of Unit 100INTCIP occurred under downward loading at the construction joint between the cast-in-place deck closure joint and the precast segment. The presence of mild steel reinforcement across the segment-to-segment joint controlled the widths of cracks. Other flexural cracks, with very small widths, also occurred within the precast segments in Unit 100INTCIP.

All test units failed under downward loading by compression in the bottom slab. The Phase II test units were subjected to negative bending moments and the failure mode of all test units was governed by the compressive force capacity of the bottom slab, which was relatively small compared to the compressive force capacity of the deck. It should be mentioned that Test Unit 100INT, with 100 percent internal post-tensioning, had a premature local crushing in the bottom slab at 3 in. of downward displacement (displacement measured at the steel nose tip). This premature concrete crushing was a result of aggregate segregation in a local zone of the bottom slab. Despite this premature concrete crushing, Test Unit 100INT could undergo further displacement until occurrence of compression failure at 6 in. downward displacement. Figures 12a and 12b show, respectively, Test Units 100INT and 100EXT just before failure.

Despite the high shearing force transferred at the segment-to-segment joint, no vertical slip was observed between the adjacent precast segments in all test units. The vertical slip was observed only after compression failure of the bottom slab. This indicates that no vertical slip should be expected between the precast segments before flexural failure of the superstructure.

Load-Displacement Response

Figure 13 shows the history of total applied load versus vertical displacement measured at the tip of the steel nose for Test Units 100INT and 100INTCIP; the variable of these two test units was presence of mild steel reinforcement in the deck across the segment-to-segment joint. Figure 14 is similar to Fig. 13 but it shows the load versus displacement for Units 100INT, 100EXT and 50INT/50EXT with different ratios of internal to external post-tensioning. Sign convention in Figs. 13 and 14 is positive for downward loading and displacement. The horizontal solid lines in Figs. 13 and 14 represent the reference load level.

There was no mild steel reinforcement crossing the segment-to-segment joint of Unit 100INT, whereas the yield strength of the deck reinforcing bars crossing the joint in Unit 100INTCIP could be developed. Thus the maximum total downward load of Unit 100INTCIP was 141 kips, compared to a maximum total load of 94 kips in Unit 100INT (see Fig. 13). Figure 13 shows that Unit 100INTCIP could undergo higher displacements under upward loading. Figure 13 also shows the enhancement in energy dissipation in Unit 100INTCIP.

(a) Test Unit 100INT

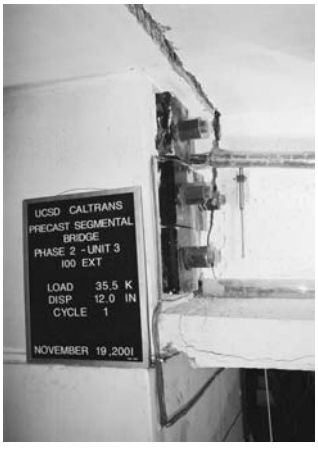

(b) Test Unit 100EXT

Figure 12. Onset of compression failure of the Phase II test units

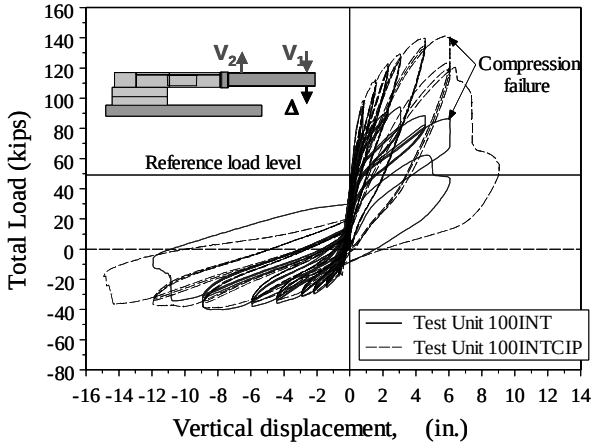

Figure 13. Load versus displacement (Phase II, Units 100INT & 100INTCIP)

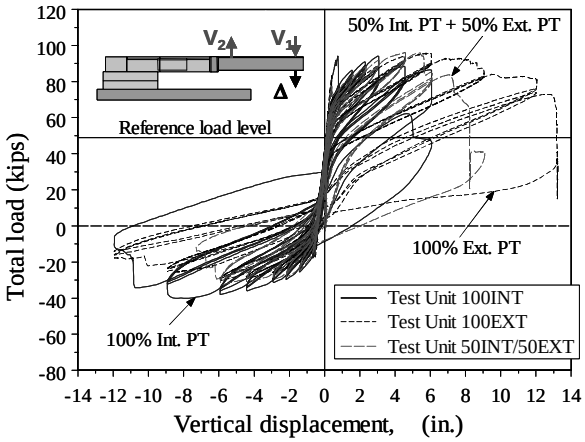

Figure 14. Load versus displacement (Phase II, Units 100INT, 100EXT and 50INT/50EXT)

Figure 15a shows the envelope of the hysteresis loops of Figs. 13 and 14. Figure 15a confirms the findings of Phase I tests that 100 percent external post-tensioning significantly increases the ductility and maximum displacement reached before failure. Values of maximum downward displacement reached before failure of Units 100INT, 100INTCIP and 50INT/50EXT were comparable despite the premature concrete crushing of Unit 100INT at 3 in. displacement. However, the maximum displacement reached before failure of Unit 50INT/50EXT under upward loading was significantly less than maximum upward displacements for the other test units (see Fig. 15a). This agrees with findings of the Phase I experiments and indicates that for optimum seismic performance of segment-to-segment joints, internally bonded and external tendons should not be combined. The maximum downward load carrying capacity, V_u, and the maximum displacement before failure, Δ_u, are given in Table III for all test units of Phase II.

Figure 15b is similar to Fig. 9b, but it is plotted for the Phase II test units. Values of the residual permanent displacement, Δ_r, measured after 4.5 in. maximum displacement of all test units are given in Table III. The values of Δ_r for all test units are again normalized to the residual displacement of Unit 100EXT, Δ_{Ref} (= 0.17 in.). Values of the ratio Δ_r/Δ_{Ref} are given in Table III.

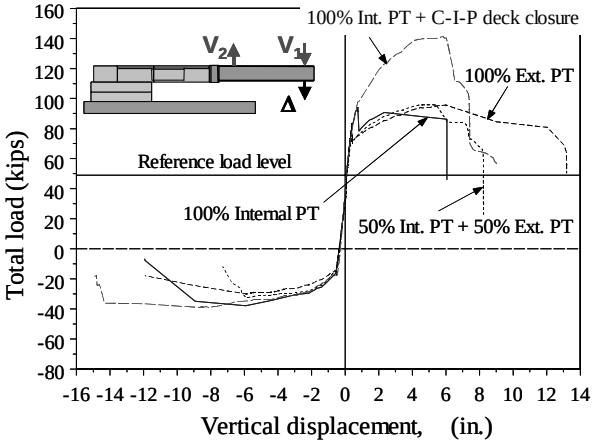

(a) Envelope of load versus displacement curves

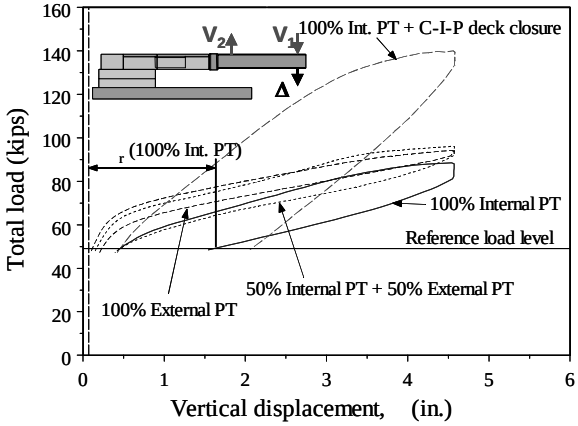

(b) Downward load versus displacement (4.5 in. displacement cycle)

Figure 15. Load-displacement response of the Phase II test units

TABLE III. LIMITED TEST RESULTS (PHASE II EXPERIMENTS)

Test Unit	V_u (kip)	Δ_u (in.)	Δ_r (in.)	Δ_r/Δ_{Ref}	ζ (%)	ζ/ζ_{Ref}
100INT	94.2	6.0	1.53	9.00	4.84	2.47
100INTCIP	141.3	6.4	1.99	11.71	5.79	2.95
100EXT	95.6	12.9	0.17	1.00	1.96	1.00
50INT/50EXT	96.0	7.2	0.39	2.29	3.70	1.89

Δ_r and ζ were measured during the 4.5 in. displacement cycle.

The Δ_r/Δ_{Ref} values indicate that residual displacements can be minimized by use of 100 percent external post-tensioning, which agrees with the findings of Phase I. The . values, given in Table III, indicate that energy dissipation is increased with internal post-tensioning (bonded tendons).

CONCLUSIONS

The following can be concluded from this study:

1. Superstructure segment-to-segment joints can undergo significant openings without failure even when subjected to high bending moments combined with high shearing forces.
2. Test units with internally bonded tendons experienced explosive failure due to rupture of strands or compression failure caused by buckling of the cast-in-place mild reinforcement. With 100 percent external post-tensioning, the failure was not explosive since the forces in external tendons were significantly less than forces in the internally bonded tendons. The ductility and maximum displacement before failure of test units could be substantially increased by use of 100 percent external post-tensioning. Also, residual displacements after earthquake occurrence can be minimized by use of 100 percent external post-tensioning.
3. Combination of internal and external post-tensioning of precast segmental bridge superstructures is not recommended in high seismic zones since the internal bonded and external tendons do not participate in the force transfer in parallel but rather sequentially with the internal bonded tendons carrying most of the loading up to their failure.
4. The use of cast-in-place deck closure joints, as proposed for the new East Bay Skyway of the San Francisco-Oakland Bay Bridge, improves the energy dissipation capability but complicates the precast segmental construction concept.
5. Vertical sliding between precast segments may occur only after their flexural failure.

ACKNOWLEDGMENT

Caltrans is acknowledged for funding of this research under contract No. 59A0051.

REFERENCES

[1] AASHTO, 1999. *Guide Specification for Design and Construction of Segmental Concrete Bridges*. American Association of State Highway and Transportation Officials, 2nd Edition, Washington, DC, 78 pp.

[2] Chopra, A.K., 1995. *Dynamic of Structures*. Prentice Hall, Inc., New Jersey, 729 pp.

In-situ Tests of As-is and Retrofitted RC Bridges with FRP Composites

Chris Pantelides, Jeff Duffin, Jon Ward, Chris Delahanty, and Lawrence Reaveley

ABSTRACT

The paper presents the results of three in-situ quasi-static tests performed on three reinforced concrete bridge multi-column bents. The bridge was built in 1963 but the design did not consider earthquake-induced forces or displacements since wind loads governed the design. The tests comprised of the following: a test of Bent #4 with the deck removed; a test of Bent #5 with half the deck load; and a test of Bent #6 with half of the deck load and retrofitted with a carbon FRP composite seismic retrofit. All three bents were strengthened with a reinforced concrete grade beam connecting the pile caps under each of the columns. The lower bound of performance was exhibited by Bent #4, followed by Bent #5; Bent #6 performed exceptionally well as compared to the other two bridge bents, reaching a drift of 6%. The paper describes an analytical model of the bents including soil-structure interaction and the FRP composite seismic retrofit design. In addition, the paper describes the damage sequence, and a comparison of observed behavior and the behavior predicted by finite element models.

Chris Pantelides, Lawrence Reaveley, Prof., Dept. of Civil & Envir. Engrg., Univ. of Utah, Salt Lake City, UT 84112
Jeff Duffin, Jon Ward, Chris Delahanty, Grad. Res. Assist., Dept. of Civil and Envir. Engrg., Univ. of Utah, Salt Lake City, UT 84112

INTRODUCTION

In-situ tests of bridges allow verification of design methods and establishment of capacities for loads up to failure. This knowledge contributes to better designs for new bridges and better retrofit techniques for existing bridges. The lateral load capacity of bridges is of interest due to potential catastrophic failures in large earthquakes. Recent earthquakes such as the 1989 Loma Prieta, 1994 Northridge, and 1995 Kobe, have repeatedly demonstrated the vulnerabilities of older reinforced concrete bridges to seismic deformation demands. While experimental validation of retrofit concepts for the columns of such bridges exists [1], [2], [3], in-situ tests of retrofitted bridge bents are not common. An in-situ verification of retrofit and rehabilitation of reinforced concrete bridges under simulated seismic loads was performed in 1998 [4]. In that study, two new concepts of strengthening and confinement of beam-column joints with Carbon Fiber Reinforced Polymers (CFRP) were implemented, that of the "U-strap" and "ankle-wrap". The tests included a lateral quasi-static cyclic test of a reinforced concrete bridge bent, a test of a bridge bent retrofitted with CFRP composites, and a test of a damaged bridge bent rehabilitated with epoxy injection and CFRP composite jackets. In 2000, three additional in-situ tests were performed on three bridge bents of the Southbound lanes of the South Temple Bridge, at Interstate 15 before their demolition: (a) test of a bent in the as-built condition retrofitted with a grade beam but without the deck (Bent #4), (b) test of a bent in the as-built condition retrofitted with a grade beam but with the deck (Bent #5), and (c) test of a bent retrofitted with a grade beam and rehabilitated with FRP advanced composites (Bent #6). The objectives of the in-situ tests were to: (a) determine the lower-bound capacity of the bent in the as-built condition retrofitted with an overlay grade beam, without the deck (Bent #4); (b) determine the capacity of the bent in the as-built condition retrofitted with an overlay grade beam, with the deck spanning only one side of the span, representing half of the gravity load (Bent #5); and (c) determine the improvement in strength and ductility of the bent retrofitted with an overlay grade beam and rehabilitated with CFRP composites with half of the gravity load (Bent #6). The present paper describes the experimental findings of the three tests, all of which were performed by applying a quasi-static cyclic lateral load at the bent cap level.

BENT #4 WITH GRADE BEAM – AS-IS WITHOUT DECK

This test was carried out on Bent #4 constructed in 1963, which had been subjected to the effects of the environment, including salt degradation, and freeze-thaw cycling. This provided a unique opportunity to present a good estimate of the in-situ capacity of an existing bridge with details, which did not consider the concepts of ductility and capacity design [1]. Reinforced concrete bridges must be designed to allow ductile behavior and ultimately be either serviceable or repairable after a severe earthquake. The objective of this research was to analyze such a structure to determine: (1) existing capacity, (2) failure modes, (3) performance-based assessment and damage level criteria for verifying the adequacy of existing codes.

The South Temple Bridge was a reinforced concrete bent frame built in 1963 with the dimensions provided in Figure 1. The steel reinforcement details are shown in Figure 2. There had been severe spalling on various sections of the 37-year old structure due to concrete degradation brought on by rebar corrosion and freeze/thaw action. The original foundation consisted of three pile caps of which the exterior caps were 0.914m x 2.133m x 2.133m, and the

center pile cap was 0. 914m x 2.743m x 2.74m, and between these pile caps were 0.457m x 0.457m x 4.80m strut beams. The foundation was modified in order to develop a compression/tension load path. The dimensions of the new reinforced grade beam, which was cast monolithically around the columns, were 1.219m x 2.133m x 17.678m.

There were two different concrete strength properties associated with Bent # 4, as the cast in place grade beam was a new material, and the bent itself was older concrete. The specimen concrete strength was determined by coring the mid-span of the columns. The respective concrete strengths were as follows: Bent $f_c' = 33$ MPa; Grade Beam $f_c' = 39$ MPa. Seven different sizes of steel reinforcement were used throughout the structure. In the columns, bent cap and original strut beam, 300 MPa (Grade 40) 16mm, 25mm, and 32mm bars were used for longitudinal reinforcement. The stirrups consisted of 10mm and 13mm bars. In the new grade beam, 400 MPa (Grade 60) 25mm longitudinal bars were used, and the stirrups were 10mm bars. The actual properties of the steel reinforcement were determined as follows: Bent $f_y = 325$ MPa; Grade Beam $f_y = 455$ MPa. Deficiencies in terms of current seismic requirements included lack of confinement of column reinforcement in the plastic hinge regions, insufficient column splice length, lack of anchorage of column reinforcement, insufficient anchorage of reinforcement from

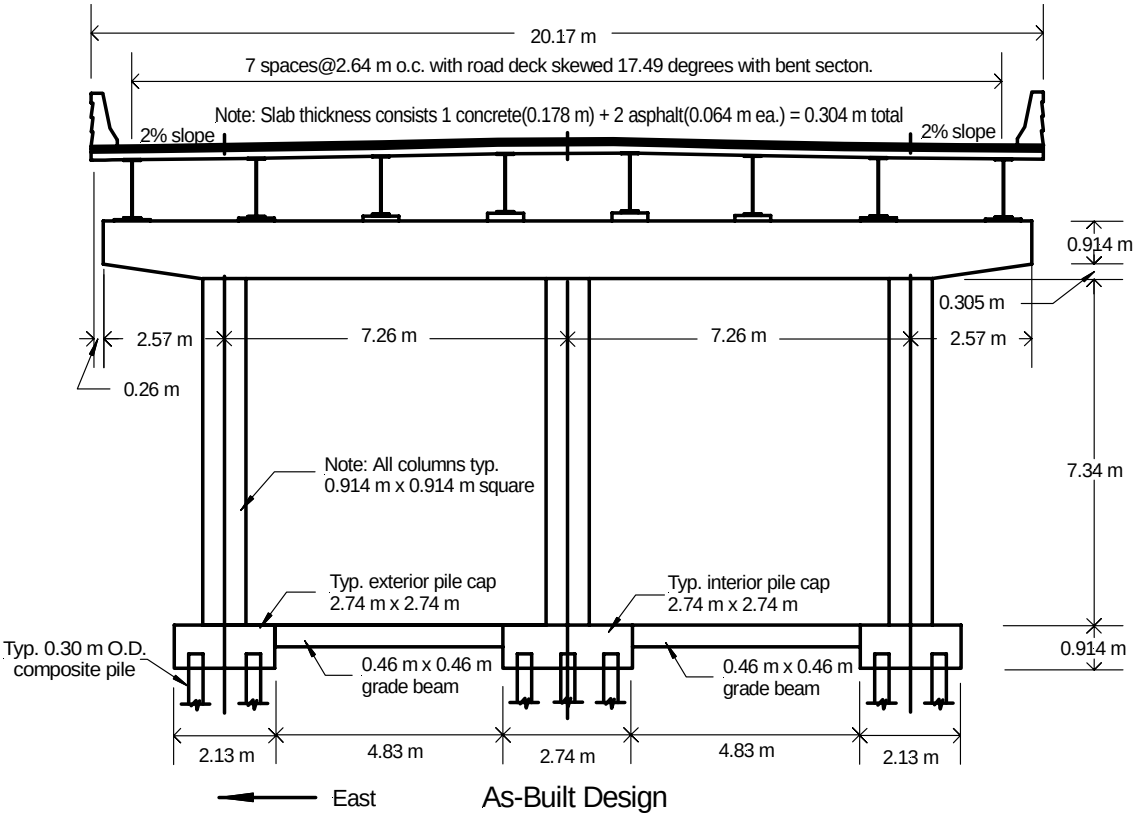

Figure 1. Dimensions of Bridge Bent #4

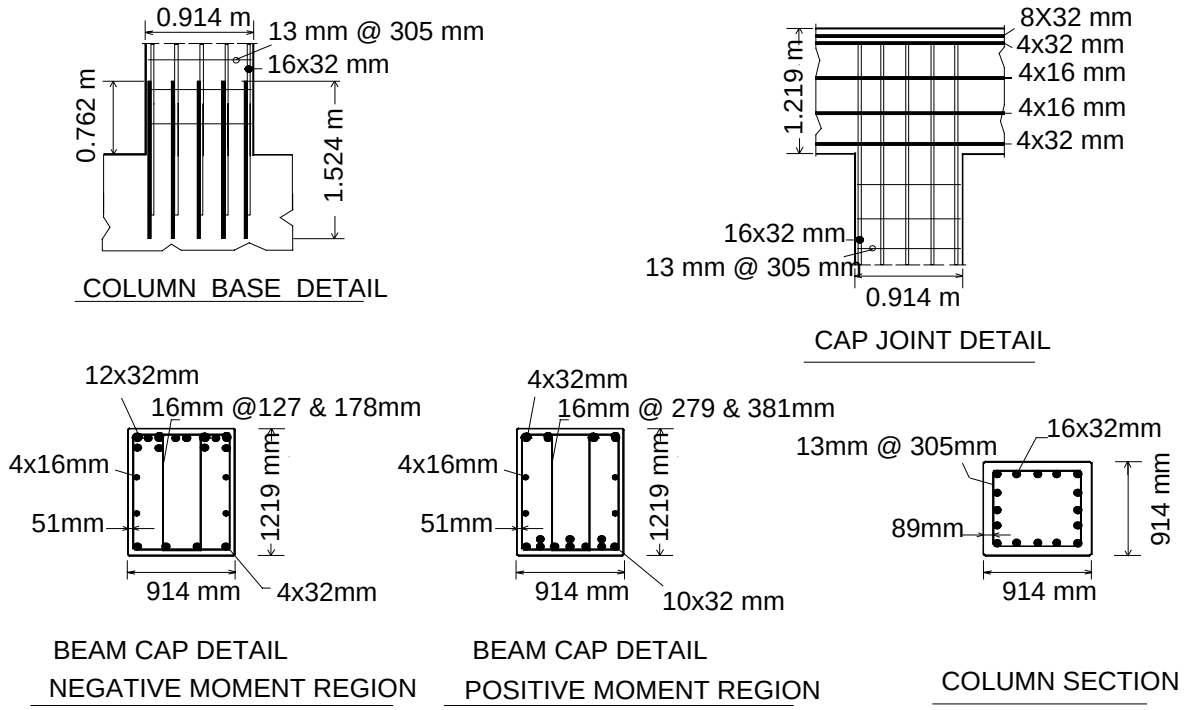

Figure 2. Steel Reinforcement Details

the piles to the pile cap, insufficient concrete area and steel in the strap beam connecting the pile caps, and inadequate shear reinforcement in the beam cap-column and pile cap-column joints.

In order to improve the deficiencies related to the strap beam and pile to pile-cap and pile cap to column connections, an overlay grade beam was constructed as shown in Figure 3. A quasi-static cyclic load was applied at the bent cap as shown in Figure 4, at increments of displacement drift: 0.5%, 1%, 1.5% etc., with three cycles per drift increment. The applied load versus time curve is shown in Figure 5(a); the maximum load applied was 1,575 kN (push) and 1,575 kN (pull). In addition, the maximum displacement applied is shown in Figure 5(b); the maximum displacement applied was 355 mm (push) and 138 mm (pull). Figure 6 shows the hysteretic behavior of the bent.

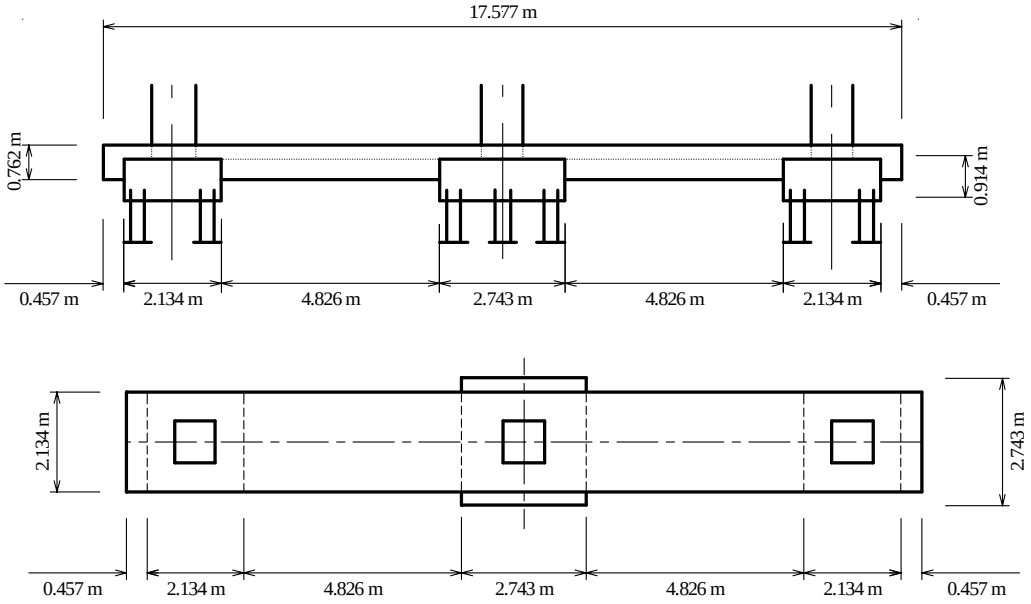

Figure 3. Grade Beam elevation and plan

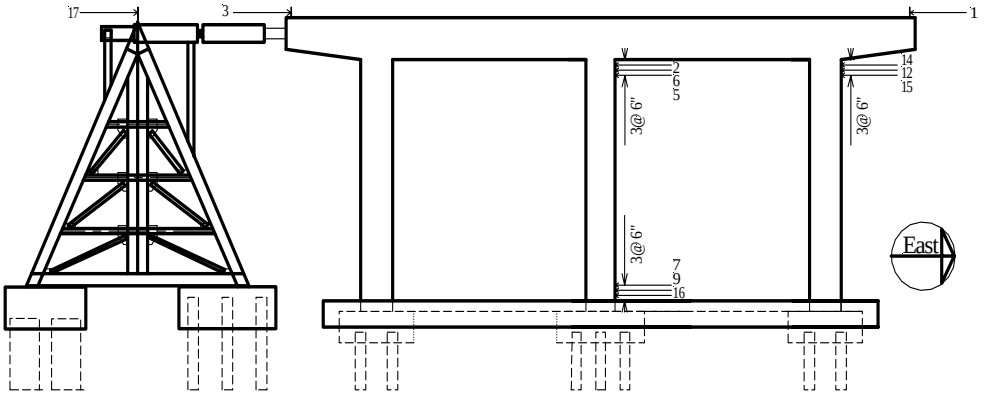

Figure 4. Lateral quasi-static load application on Bent

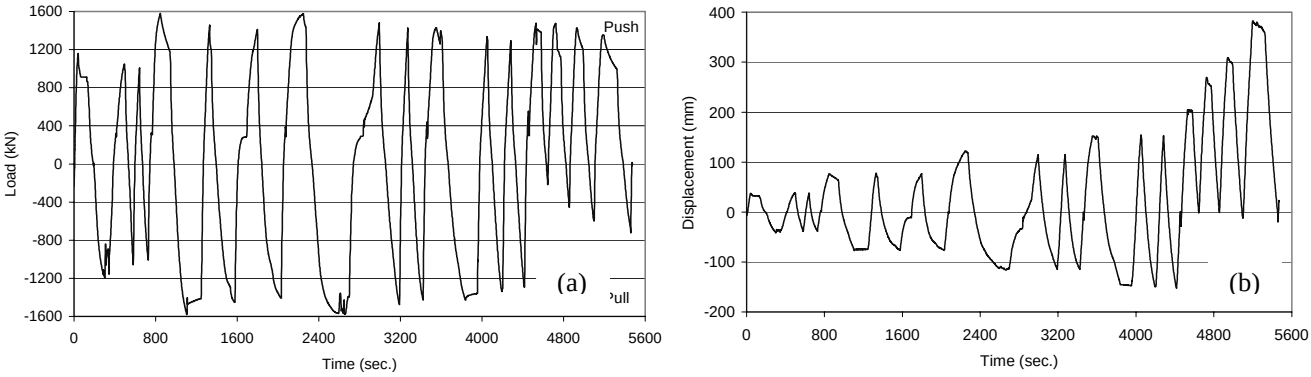

Figure 5. Bent #4: (a) load at bent cap, (b) displacement at bent cap

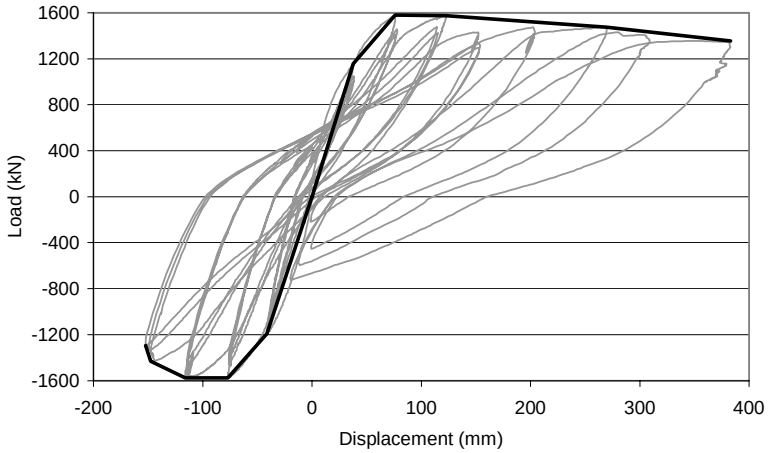

Figure 6. Bent #4 hysteretic behavior

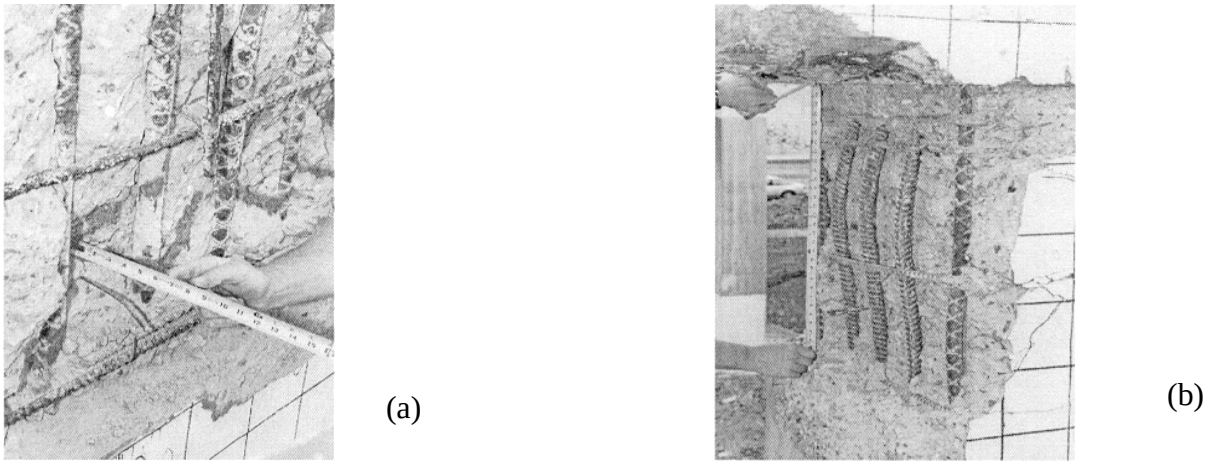

Figure 7. Bent #4 damage: (a) column/bent cap joint, (b) column top

The damage of Bent #4 at the end of the test was quite extensive. Figure 7(a) shows the damage at the east bent cap column joint, just above the column; 177 mm of concrete had spalled by the end of the test. In addition, large diagonal shear cracks spanning the depth of the bent cap-column joint were observed. The top of the center column suffered extensive damage, the concrete spalled and the longitudinal bars buckled as can be seen in Figure 7(b). Buckling of the column bars was more pronounced in the center of the column rather than the edges. Extensive shear cracking at the column base as well as failure of the lap splice region were observed.

BENT #5 WITH GRADE BEAM – AS-IS WITH DECK

The deck connecting Bent #5 and #6 was left in place. Therefore, Bent #5 had half of the original dead load when it was tested. The maximum lateral load recorded in the push direction was 2046 kN, and the last push reading was 1741 kN, as shown in Figure 8(a). The maximum displacement recorded in the push direction was 205 mm, and in the pull direction was -287 mm, as shown in Figure 8(b). The hysteresis diagram for the total system, including movement of the superstructure and grade beam, is shown in Figure 9.

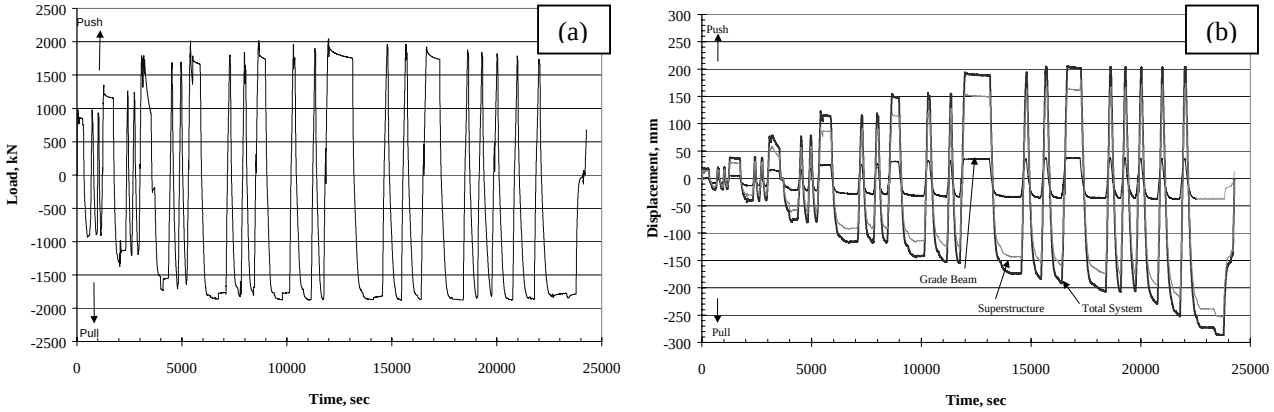

Figure 8. Bent #5 with grade beam and deck: (a) load, (b) displacement

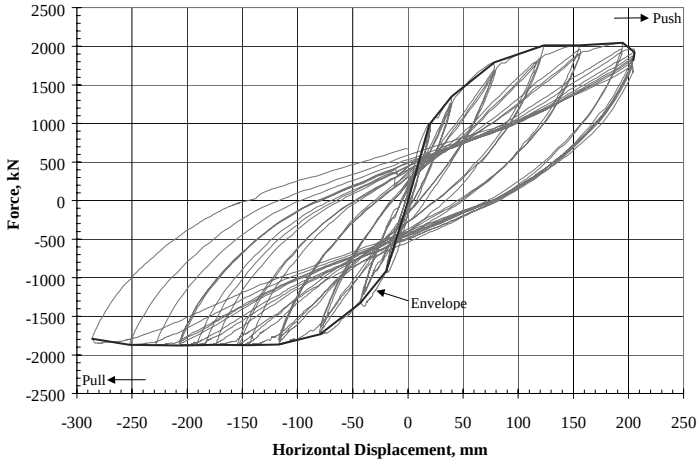

Figure 9. Hysteresis curves for Bent #5

At the end of the test, the columns were still carrying the axial load, but were severely damaged. There were flexural cracks wider than 4 mm, shear cracks wider than 2 mm, vertical cracks that were 2.13 m long, and spalling that covered approximately 30% of the column cross-sectional area. In addition, there was initial buckling of the longitudinal bars of the top of the center column. Most of the damage in the joints between the columns and bent cap was shear-induced damage. At the end of the test, there were very few cracks in the cores of the joints, but they reached 1.5 mm wide, as shown in Figure 10(a). The grade beam sustained very little damage during testing. The only damage it received occurred at 2.5% drift, or 191 mm, as shown in Figure 10(b). This damage was a set of cracks running the width and height of the grade beam at the cold joints with the already existing pile caps under each column; the width of the cracks was 1 mm.

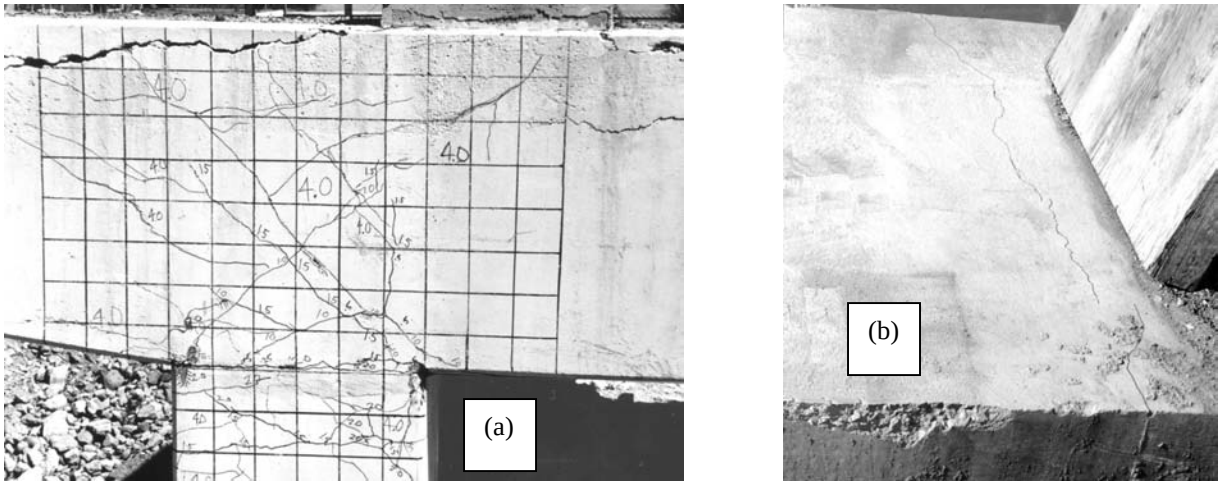

Figure 10. Damage to Bent #5: (a) top of column and joint, (b) crack in grade beam

BENT #6 WITH DECK RETROFITTED WITH CFRP COMPOSITE

The carbon fiber jacket design layout was identical to the 1998 test [5], with the following exceptions: (1) the East joint had two FRP composite layers oriented parallel to the bent cap axis (in the zero degree direction) 4.572m long, added on the North and South faces of the bent cap centered on the East column; (2) the Center joint had one zero degree oriented FRP composite layer of length 3.353m, added on the North and South faces of the bent cap centered on the Center column; (3) the number of 0.457m layers in width closest to the columns increased from two layers to four layers in thickness. The next adjacent 0.457m wide layers changed from one layer to two layers in thickness; (4) the 0.914m wide column confinement layers applied at the top of the columns next to the bent cap increased from three layers to six layers in thickness. The next lower 0.457m wide layers increased from two layers to three layers in thickness. The last 0.457m wide layers downward from the bent cap increased from one layer to two layers in thickness; (5) the 0.914m wide column confinement layers applied at the bottom of the columns next to the grade beam increased from ten layers to fourteen layers in thickness. The next adjacent 0.457m wide layer increased from two layers to three layers thickness. The last 0.457m

wide upward layers from the grade beam increased from one layer to two layers in thickness, and (6) the carbon FRP composite U-straps were applied across the full width of the column. The properties of the carbon FRP composite were determined according to ASTM D3039 as: fiber volume = 25%, elastic modulus = 70 GPa, tensile strength = 700 MPa, thickness = 1.058 mm. The final design of the carbon FRP composite is shown in Figure 11.

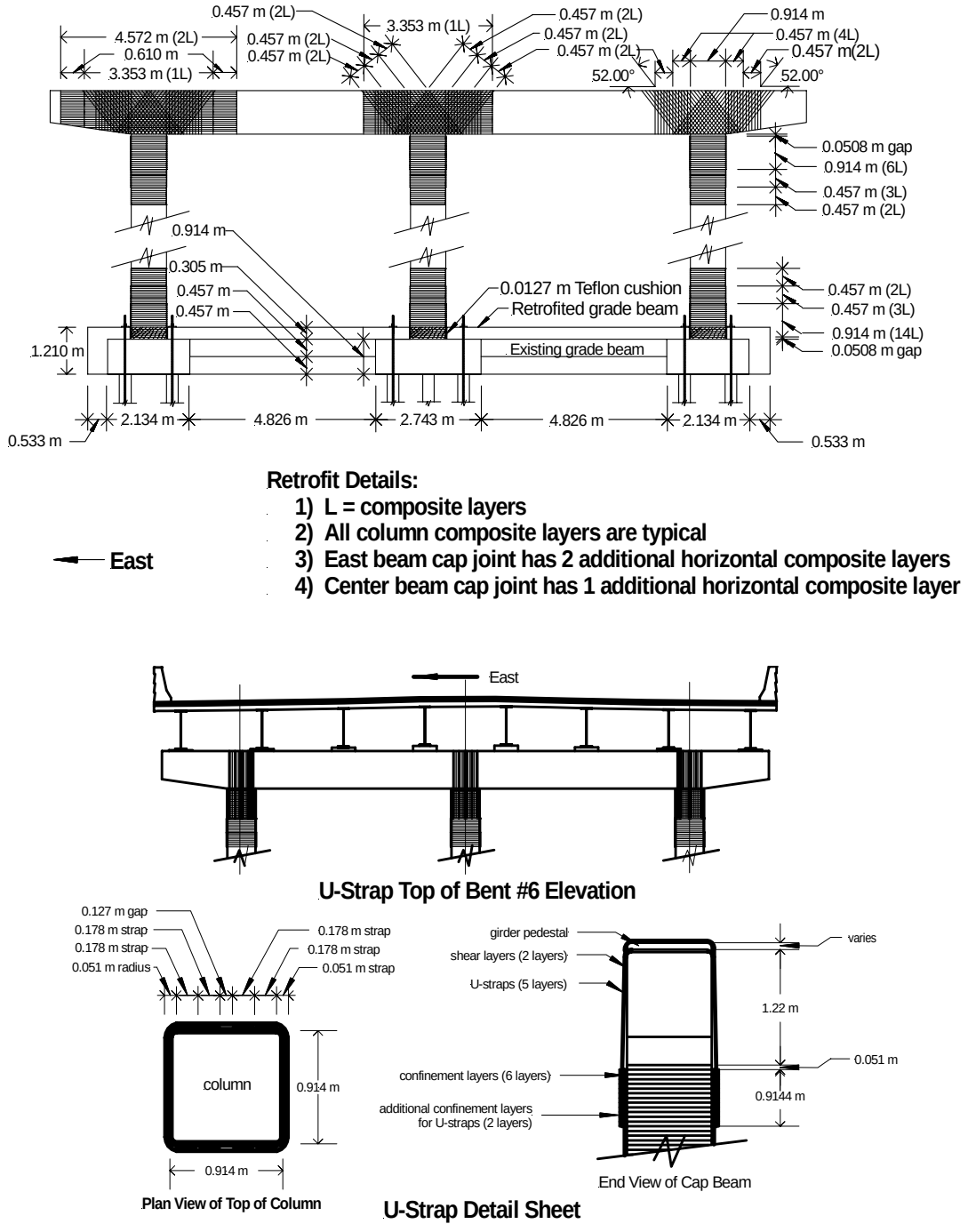

Figure 11. CFRP composite design for Bent #6

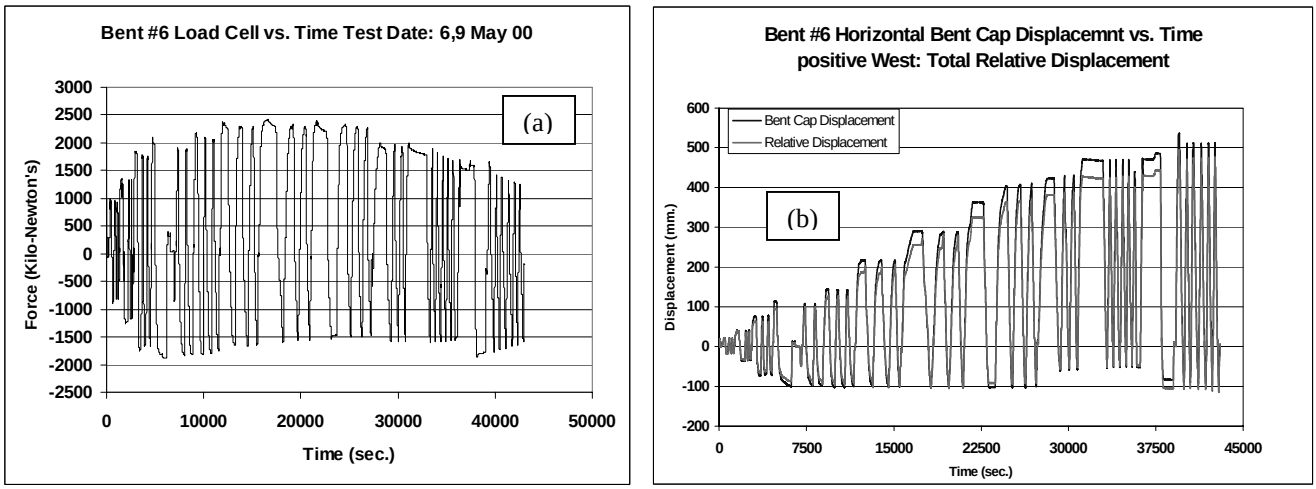

Figure 12. Bent #6: (a) applied load history, (b) bent displacement

In the 1998 test of Bent #6 (Northbound) a maximum horizontal force of 1,903 kN and displacement of 265mm were observed [4]. Also, at the maximum displacement the resistive force capacity of the total system dropped 23 %. In the present test, the maximum horizontal force in the push direction was 2,350 kN and the total horizontal displacement was observed to be 522mm for the total system. In the pull direction the maximum horizontal force was –1868 kN and the maximum horizontal displacement was observed to be –113mm for the total system. The load history and displacement for Bent #6 during the 2000 test is shown in Figure 12. In the push direction, at the maximum horizontal displacement, the force capacity of the total system dropped 47 % and in the pull direction at the horizontal maximum displacement the load capacity dropped – 17 % for the total system. The hysteretic behavior is shown in Figure 13 for the total displacement of the system, including that of the grade beam-pile-soil interaction. It can be observed that the bent has an unsymmetrical hysteresis, due to the fact that the actuator displacement capacity was reached early in the pull direction because of the horizontal displacement of the load frame foundation.

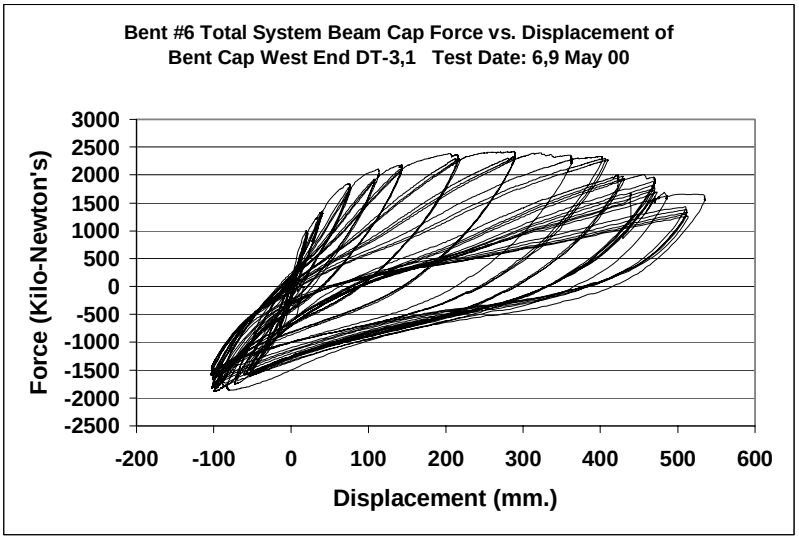

Figure 13. Hysteresis curve for Retrofitted Bent #6

The analytical model used to predict the performance of Bent #6 was DRAIN-2DX [6]. However, in order to input the correct fiber section properties of the confined concrete, the program ANSYS [7] was used to determine the stress-strain curves for the confined concrete with CFRP composite for the cross-sectional properties; these are shown in Figure 14 for different cases depending on the number of CFRP composite layers (L). The results of the analytical model correlate well with the experimental results, as shown in Figure 15.

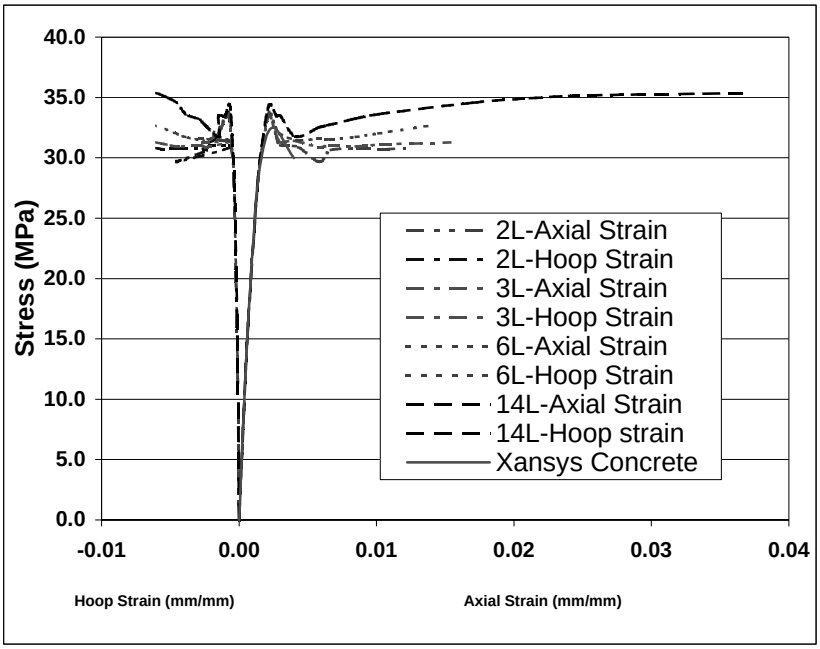

Figure 14. Stress strain curves for confined concrete with CFRP composite jackets

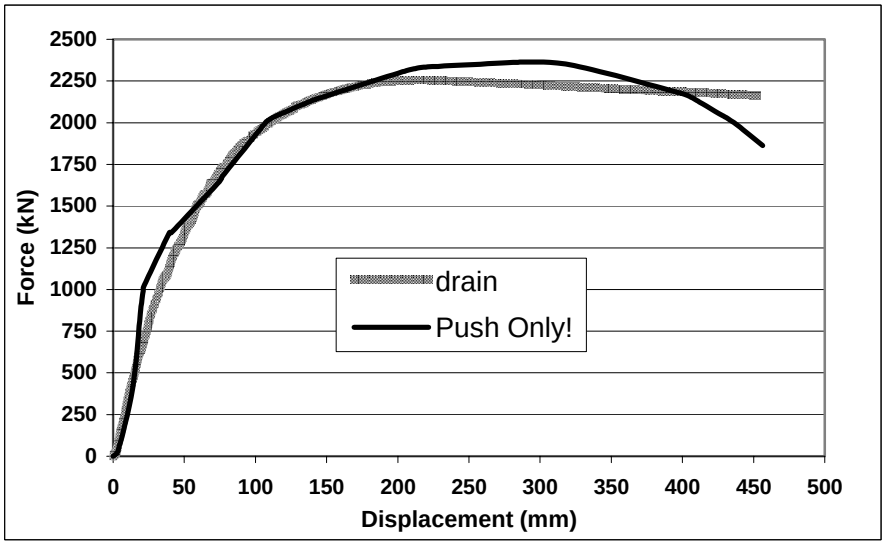

Figure 15. Experimental versus analytical results for Bent #6 retrofitted CFRP composites

Figure 16. Bent #6 retrofitted with CFRP composites: (a) damage, (b) condition at 6% drift

Damage to Bent #6 at the completion of the test was extensive. At a displacement drift of approximately 6%, large flexural cracks appeared in the CFRP composite, as shown in Figure 16. At about the same time the FRP composite U-straps failed in tension. The failure surface was close to the bent cap-column interface. In addition to the failure of the CFRP composite, a large shear crack appeared in the bent cap. This shear crack, which was present on three of the four faces of the beam had a maximum width of 1.25 mm and formed in the vicinity of where the carbon CFRP composite was terminated near the west joint.

The condition of the east column after removal of the concrete cover, underneath the CFRP composite jacket, revealed continuation of the surface concrete cracks to the underlying concrete core. These cracks were significant, of average width ranging from 0.6 mm to 3.5 mm. In addition, bar debonding was observed at the top bars in the negative moment region, above the joint. The vertical longitudinal column bars in the same area showed significant bar pullout from the concrete of the order of 2 mm. The damage observed was anticipated, since the test was successful and the bent was pushed a total distance of 522 mm in the transverse direction, which is a large displacement that could not have been achieved if the seismic retrofit with CFRP composites were not in place. As Figure 16 shows, the structure became a mechanism and was rather unstable but was carrying a gravity load equal to half of the originally present gravity load.

CONCLUSIONS

The experimental results of three in-situ lateral load tests on three R/C bents of an existing bridge were described. From the results shown in Table 1, it is obvious that the lower-bound of the overall performance belongs to Bent #4, the as-is bent with no gravity loads; however, it must be emphasized that the grade beam played a beneficial role even in this case. Comparing the results for the as-is Bent #5 and the CFRP composite-retrofitted Bent #6 it can be observed that Bent #5, achieved only half the drift of Bent #6 but performed well in terms of peak load; this is due largely to presence of the grade beam, which prevented premature failure of the foundation at the piles, and allowed the superstructure to perform. The behavior of the

TABLE 1. OVERALL PERFORMANCE OF BENTS #4, #5 AND #6 IN IN-SITU TESTS

Bent #	Description	Peak Load (kN)	Peak System Displacement (mm)	Peak Superstructure Drift (%)
4	As-is: No Gravity	1575	381	4.6
5	As-is: ½ Gravity	2046	287	3.1
6	CFRP: ½ Gravity	2350	522	6.0

CFRP composite-retrofitted bent clearly was superior to the other two bents, reaching a drift of 6%, which was a very high drift for bents constructed with such inadequate seismic resistant details. The load capacity was 15% higher than that of Bent #5 in the as-is condition. Overall, it must be stated that the grade beam had a significant beneficial effect in the performance of the three bents, and that the CFRP composite retrofit was successful. The new element in the CFRP composite retrofit was the use of fibers parallel to the axis of the bent cap, which proved to be very beneficial in resisting the joint principal tensile stresses developed at high drifts.

REFERENCES

[1] Priestley, M.J.N., Seible, F., and Calvi, G.M. 1996. *Seismic Design and Retrofit of Bridges.* John Wiley & Sons, Inc., New York.

[2] Seible, F., Priestley, M.J.N., Hegemier, G., and Innamorato, D. 1997. "Seismic retrofitting of RC columns with continuous carbon fiber jackets." *J. of Compos. Constr.*, 1(2), 52-62.

[3] Sexsmith, R., Anderson, D., and English, D. 1997. "Cyclic behavior of concrete bridge bents." *ACI Struct. J.*, 94(2), 103-113.

[4] Pantelides, C.P., Gergely, J., and Reaveley, L.D. 2001. "In-situ Verification of Rehabilitation and Repair of Reinforced Concrete Bridge Bents under Simulated Seismic Loads." *Earthq. Spectra*, EERI, 17(3), 507-530.

[5] Pantelides, C.P., and Gergely, J. 2002. "Carbon-Fiber-Reinforced Polymer Seismic Retrofit of RC Bridge Bent: Design and In Situ Validation." *J. Compos. Constr.*, 6(1), 52-60.

[6] Prakash, V., Powell, G.H., and Filippou, F.C. 1992. "DRAIN-2DX Base Program User Guide." *Rep. No. UCB/SEMM-92/29*, Univ. of California, Berkeley, Calif.

[7] ANSYS 6.0. User's Manual, 2001. Ansys Inc., Canonsburg, Pa.

ACKNOWLEDGEMENTS

Financial support for this research was provided by the Utah Department of Transportation and the Federal Highway Administration. The authors would like to thank Wasatch Constructors for their assistance in the project. The authors would like to thank Samuel Musser, Dr. Steve Bartlett, and Doug Anderson of the Research Division of the Utah Department of Transportation for their support and encouragement; Dr. Larry Cercone of Navlight Composites; Mr. Scott Isaac of Sika Corporation; Dr. Evert Lawton of the University of Utah, and Dr. Kyle Rollins of Brigham Young University. In addition, the authors would like to thank the following students from the Department of Civil and Environmental Engineering, University of Utah for their assistance: Danny Alire, Chandra Clyde, Curtis Cook, Jon Hansen, Nicole Marriott, Paul McMullin, Jason Rapich, Morgan Sandall, and Yasuteru Okahashi.

Calibration of Strain Wedge Model Predicted Response for Piles/Shafts in Liquefied Sand at Treasure Island and Cooper River Bridge

Mohamed Ashour, Gary Norris and J.P. Singh

ABSTRACT

This paper describes the calibration of the Strain Wedge Model (SWM) response using the Treasure Island and Cooper River bridge test measured data. The SWM, initially developed to assess the relationship between one-dimensional beam on elastic foundation (BEF) or so called "p-y" curve behavior and three dimensional soil pile interaction, has been extended to include laterally loaded piles/shafts in liquefiable soil. Because the SWM relies on the undrained stress-strain characterization of the soil as occurs in the triaxial test, it is capable of treating one or more layers of soils that experience limited or full liquefaction. This paper provides a methodology to assess the post-liquefaction response of an isolated pile/shaft in sand under an applied pile/shaft head load/moment combination assuming undrained conditions in the sand. The degradation in soil strength due to the free-field excess porewater ($u_{xs,ff}$), generated by the earthquake that results in developing or full liquefaction, is considered along with the near-field excess porewater pressure ($u_{xs,\ nf}$) generated by lateral loading from the superstructure.

Current design procedures assume slight or no resistance for the lateral movement of the pile in the liquefied soil which is a conservative practice. Alternatively, if liquefaction is assessed not to occur, some practitioners take no account of the increased $u_{xs,ff}$, and none consider the additional $u_{xs,\ nf}$ due to inertial interaction loading from the superstructure; a practice that is unsafe in loose sands. The paper characterizes the reduction in pile response and the changes in the associated p-y curves due to a drop in sand strength and Young's modulus as a result of developing liquefaction in the sand followed by inertial interaction loading from the superstructure.

Mohamed Ashour, Research Assistant Professor, Civil Engineering Dept., University of Nevada, Reno, NV 89557.
Gary Norris, Professor, Civil Engineering Dept., University of Nevada, Reno, NV 89557.
J.P. Singh, Principal, J.P. & Associates, 23 Red Arrow Court, Richmond, CA 94803

INTRODUCTION

The potential of soil to liquefy is one of the critical research topics of the last few decades. Several studies and experimental tests have been conducted for better understanding on the potential of soil to liquefy in both the free- and/or near-field soil regions. However, predicting the response of pile foundations in liquefied soil or soil approaching liquefaction is very complex.

The procedure presented predicts the post-liquefaction behavior of laterally loaded piles in sand under developing or fully liquefied conditions. Due to the shaking from the earthquake and the associated lateral load from the superstructure, the free field $u_{xs,ff}$ and near-field $u_{xs,nf}$ develop and reduce the strength of loose to medium dense sand around a pile. The soil is considered partially liquefied or experiencing developing liquefaction if the excess porewater pressure ratio (r_u) induced by the earthquake shaking (i.e. $u_{xs,ff}$) is less than 1, and fully liquefied if $r_u = 1$. Therefore, the stress-strain response of the soil due to the lateral push from the pile as the result of superstructure load (and $u_{xs,nf}$) can be as shown in Fig. 1. The full-scale load tests on the post-liquefaction response of isolated piles and a pile group, performed at Treasure Island and Cooper River bridge [1 and 12], are the most significant related tests. However, the profession still lacks a realistic procedure for the design of pile foundations in liquefying or liquefied soil.

The most common practice employed is that presented by [2] in which The traditional p-y curve for clay is used but based on the undrained residual strength (S_r) of the sand. As seen in Fig. 2 [3], S_r can be related to the standard penetration test (SPT) corrected blowcount, $(N_1)_{60}$. However, a very large difference between values at the upper and lower limits at a particular $(N_1)_{60}$ value affects the assessment of S_r tremendously. Even if an accurate value of S_r is available, S_r occurs at a large value of soil strain. In addition, a higher peak of undrained resistance is ignored in the case of the partially liquefied sand, while greater resistance at lower strain is attributed to the sand in the case of complete liquefaction. Such clay-type modeling can, therefore, be either too conservative (if $r_u < 1$) or unsafe (if $r_u = 1$). Furthermore, the p-y curve reflects soil-pile-interaction, not just soil behavior. Therefore, the effect of soil liquefaction (i.e. degradation in soil resistance) does not reflect a one-to-one change in soil-pile or p-y curve response.

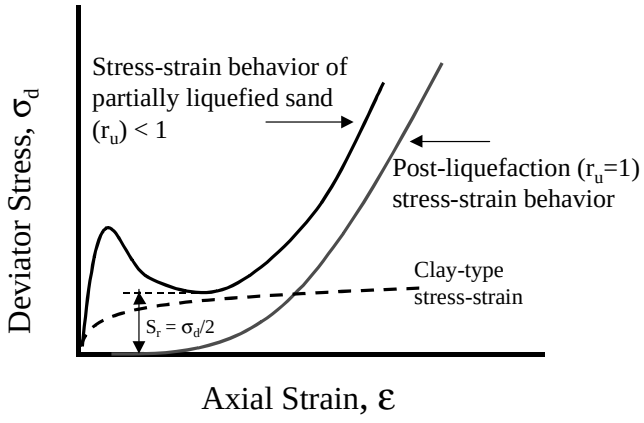

Figure 1. Subsequent undrained stress-strain behavior of sand that has experienced partial (r_u <1) or complete (r_u =1) liquefaction

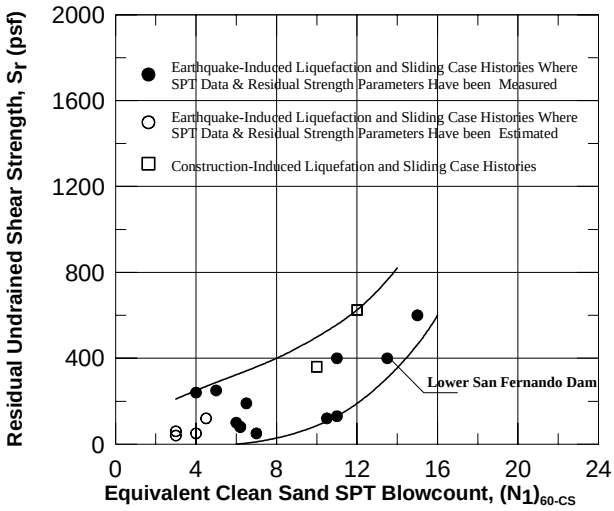

Figure 2. Corrected blowcount vs. residual strength [3]

The post-liquefaction stress-strain characterization of a fully or partially liquefied soil is still under investigation by several researchers. The current assessment of the resistance of a liquefied soil carries a lot of uncertainty. This issue is addressed experimentally [4 and 5] showing the varying resistance of saturated sands under undrained monotonic loading after being liquefied under cyclic loading corresponding to the free-field shaking of the earthquake (Fig. 4).

With lateral loading from the superstructure following full liquefaction or partial liquefaction with a significant drop in the confining pressure, the sand responds in a dilative fashion. However, a partially liquefied sand with small drop in confining pressure may experience contactive behavior followed by dilative behavior under a compressive

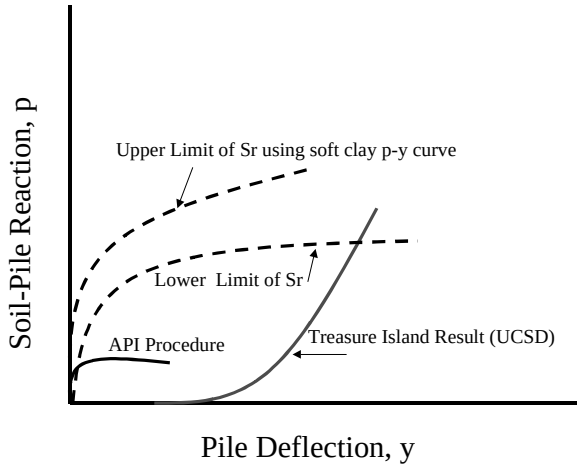

Figure 3. Undrained p-y curve in liquefied soil

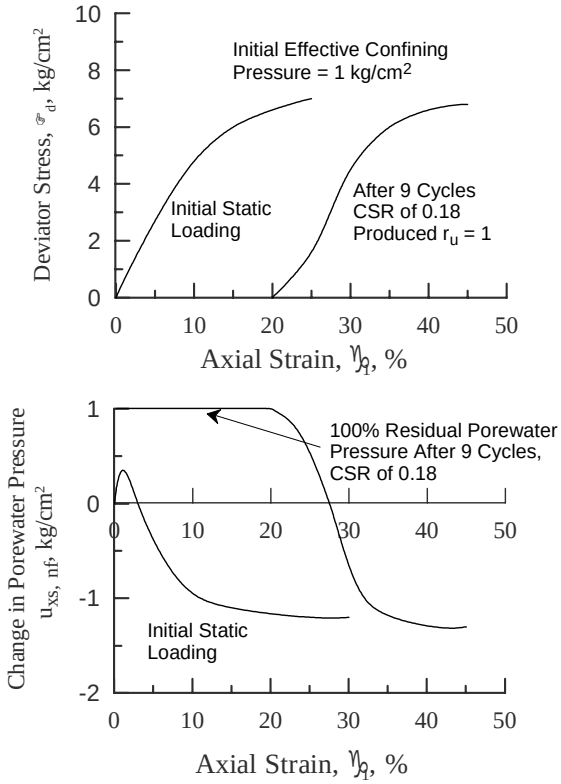

Figure 4. Undrained behavior of fully liquefied Sacramento sand [4]

monotonic loading. The postcyclic response of sand, particularly after full liquefaction, reflects a stiffening response, regardless of its initial (static) conditions (density or confining pressure).

As seen in Fig. 3, there is no particular technique that allows the assessment of the p-y curve and its varying pattern in a partially or fully liquefied sand. Instead, the soil's undrained stress-strain relationship should be used in a true soil-pile interaction model to assess the corresponding p-y curve behavior. Because the traditional p-y curve is based on field data, a very large number of field tests for different pile types in liquefying sand would be required to develop a realistic, empirically based, p-y characterization.

PROPOSED ANALYSIS PROCEDURE OF A LATERALLY LOADED PILE IN SAND UNDER DEVELOPING LIQUEFACTION CONDITIONS

The degradation in soil resistance due to earthquake shaking and the induced $u_{xs,ff}$ is based on the procedures proposed in [6]. This $u_{xs,\,ff}$ reduces the effective stress and, therefore, the corresponding soil resistance for subsequent (postcyclic) undrained load application. This is followed by the assessment of the $u_{xs,\,nf}$ in the near-field soil region induced by the lateral load from the superstructure. The variation in soil resistance (undrained stress-strain relationship) around the pile (near-field zone) is evaluated based on the undrained formulation for saturated sand presented in [7 and 8].

The assessed value of the free-field excess porewater pressure ratio, r_u, induced by the earthquake is obtained using Seed=s method [6]. $u_{xs,\,ff}$ is calculated conservatively at the end of earthquake shaking corresponding to the number of equivalent uniform cycles produced over the full duration of the earthquake. Thereafter, the lateral load (from the superstructure) is applied at the pile head that generates additional porewater pressure ($u_{xs,\,nf}$) in the soil immediately around the pile, given the degradation in soil strength already caused by $u_{xs,\,ff}$. Note that $u_{xs,\,ff}$ is taken to reduce the vertical effective stress from its pre-earthquake state ($\bar{\sigma}_{vo}$), to $\bar{\sigma}_v = (1 - r_u)\ \bar{\sigma}_{vo}$. Thereafter, the behavior due to an

inertial induced lateral load is assessed using undrained stress-strain formulation in the SWM [7, 8 and 9]. The technique presented yields the p-y curves in liquefied soil (undrained p-y curves) along the deflected length of the pile, showing a distinct change from the corresponding drained soil-pile interaction response. The undrained SWM takes into account the effect of pile properties as well as the properties of the sand on the resulting nonlinear p-y curves and, hence, the pile head response. The analysis considers the developing or mobilized wedge of resisting soil as part of its nonlinear deflection compatible evaluation.

FREE-FIELD EXCESS POREWATER PRESSURE, $u_{xs,\,ff}$

A simplified procedure for evaluating the liquefaction potential of sand for level ground conditions [6] is developed based on the sand=s corrected SPT blow count, $(N_1)_{60}$. The $u_{xs,\,ff}$ in sand or silty sand soils due to the equivalent history of earthquake shaking can likewise be assessed. The procedure requires knowledge of the total and effective overburden pressure (σ_{vo} and $\overline{\sigma}_{vo}$, respectively) in the sand layer under consideration, the magnitude of the earthquake (M), the associated maximum ground surface acceleration (a_{max}) at the site, and the percentage of fines in the sand. The cyclic stress ratio, CSR [$(\tau_h)_{ave}$ / $\overline{\sigma}_{vo}$], induced by the earthquake at any depth is computed. If N cycles of CSR are induced, but N_L cycles are required to liquefy the sand at this same stress ratio, then the excess porewater pressure ratio (r_u) generated is given as a function of N/N_L. Given r_u, the $u_{xs,\,ff}$ generated and resulting reduced vertical effective stress are expressed as

$$u_{xs,ff} = r_u \overline{\sigma}_{vo} \quad and \quad \overline{\sigma}_v = (1 - r_u)\overline{\sigma}_{vo} \tag{1}$$

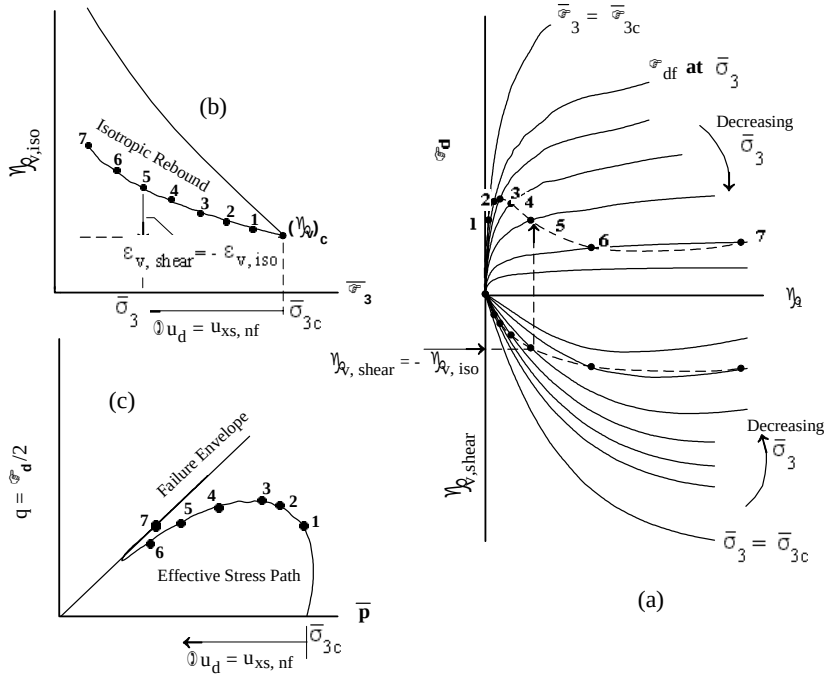

Fig. 5 Interrelationships among (a) Drained and undrained stress-strain behavior
(b) Isotropic consolidation rebound, and
(c) Undrained effective stress path [10].

NEAR-FIELD EXCESS POREWATER PRESSURE, $u_{xs,\,nf}$

The technique for assessing undrained response developed in [10] and formulated in [7] employs a series of drained tests (with volume change measurements) on samples isotropically consolidated to the same confining pressure, σ_{3c} (= $\overline{\sigma}_{vo}$), and void ratio, e_c, to which the undrained static loading test is to be subjected (no prior cyclic loading). However, the drained tests are rebounded to different lower values of effective confining pressure, $\overline{\sigma}_3$, before being sheared (Fig. 5).

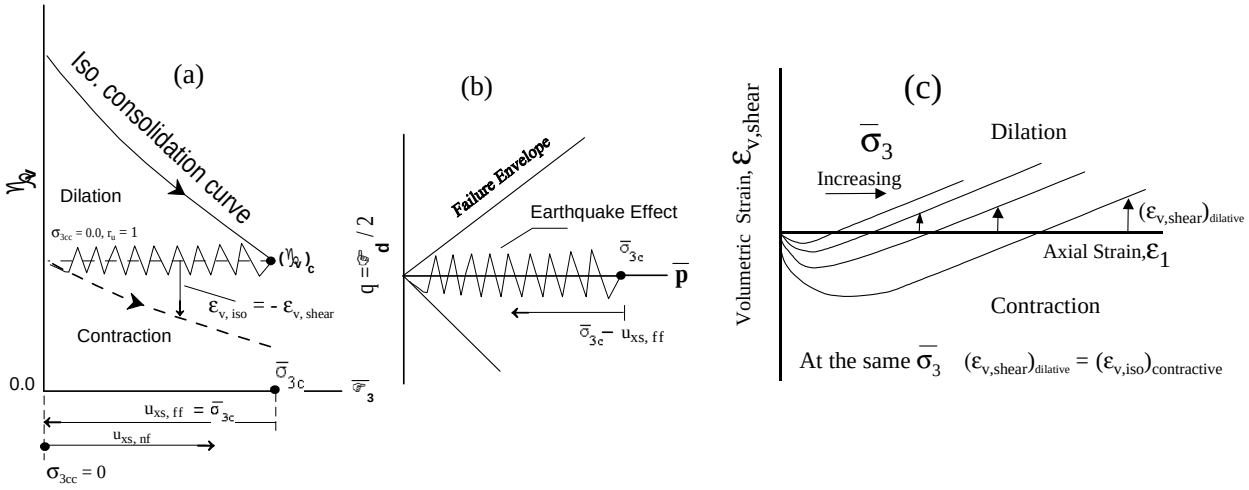

Figure 6. Fully liquefied sand interrelationships among
(a) Isotropic consolidation followed by cyclic loading
(b) Undrained effective stress path, and
(c) Drained stress-strain behavior under different values of $\overline{\sigma}_3$

During an isotopically consolidated undrained (ICU) test, which represents the state in the saturated sand around the pile, the application of a deviatoric stress, σ_d, produced by the lateral load from the superstructure causes $u_{xs,\,nf}$ to build up, which results in a reduced effective confining pressure, $\overline{\sigma}_3$ (Figs. 5b and 5c), as given by Eqn. 2. In order to simulate the effect of $u_{xs,\,ff}$ combined with $u_{xs,\,nf}$, the confining pressure is reduced from σ_{3c} under undrained conditions, for free-field excitation ($u_{xs,\,ff}$), before the pile load induced σ_d and $u_{xs,\,nf}$ are taken to occur [8]. Accordingly, Figs. 5b and 5c are modified as seen in Figs. 6 and 7 and expressed in Eqn. 3.

$$\overline{\sigma}_3 = \sigma_{3c} - u_{xs,nf} \qquad (near\text{-}field\ porewater\ pressure\ only) \tag{2}$$

$$\overline{\sigma}_3 = (\sigma_{3c} - u_{xs,ff}) - u_{xs,nf} = \sigma_{3cc} - u_{xs,nf} \qquad (effect\ of\ u_{xs,ff}\ and\ u_{xs,nf}) \tag{3}$$

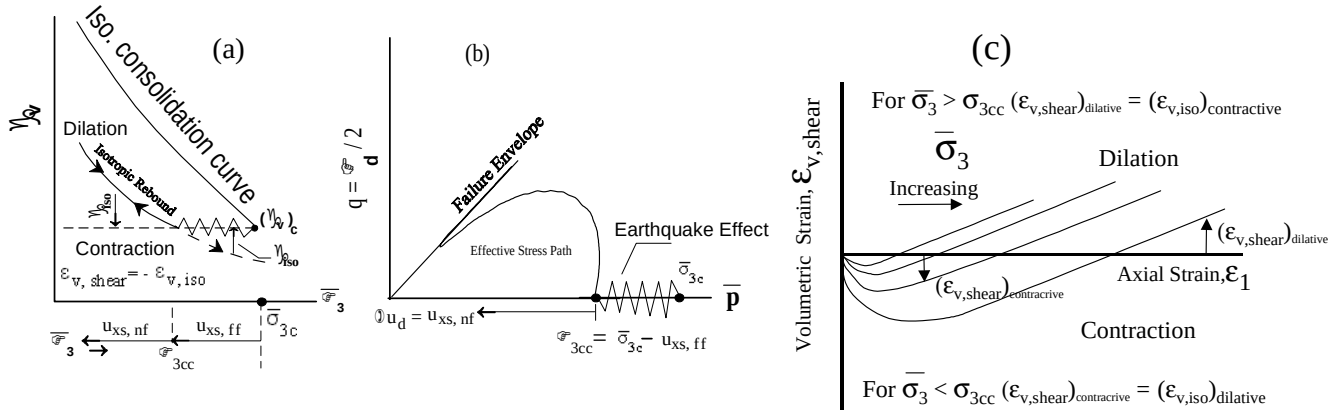

Figure 7. Limited liquefied sand interrelationships among
(a) Isotropic consolidation followed by cyclic loading (r_u <1)
(b) Undrained Effective stress path, and
(c) Drained stress-strain behavior under different values of $\bar{\sigma}_3$

If $u_{xs,\,ff}$ is equal to σ_{3c} (i.e. $r_u = 1$), the sand will experience a fully liquefied state ($\sigma_{3cc} = 0$) due to the earthquake shaking (Fig. 6). However, the sand is subjected to limited liquefaction when $r_u < 1$ (Fig. 7). Due to σ_d, caused by the load from the superstructure, a reduction in the confining pressure occurs (Eqn. 3) and an isotropic volumetric strain ($\varepsilon_{v,\,iso}$) develops, the same as recorded in an isotropically rebounded drained triaxial test (Fig. 5b for $u_{xs,\,nf}$, Figs. 6a and 7a for $u_{xs,\,ff} + u_{xs,\,nf}$). At the same time, a compressive volumetric strain component ($\varepsilon_{v,\,shear}$) develops due to this superstructure-pile induced deviatoric stress, σ_d. However, in the undrained test, the volumetric change or volumetric strain must be zero. Therefore, the shear related volumetric strain, $\varepsilon_{v,\,shear}$, must be equal and opposite to $\varepsilon_{v,\,iso}$, (i.e. $\varepsilon_{v,shear} = -\varepsilon_{v,\,iso}$) so that the total volumetric strain, $\varepsilon_v = \varepsilon_{v,\,iso} + \varepsilon_{v,shear}$, in undrained response is zero.

In the isotropically consolidated-rebounded drained triaxial test, $\varepsilon_{v,\,iso}$ and then $\varepsilon_{v,\,shear}$ (to match $\varepsilon_{v,\,iso}$) are obtained separately and sequentially; in the undrained test, they occur simultaneously, but with the same end results [10]. The corresponding effective stress path ($\bar{p} = \bar{\sigma}_3 + \sigma_d /2$ versus $q = \sigma_d /2$) can also be plotted as shown in Figs. 5c, 6b and 7b. A group of equations established by [7 and 8] and based on readily assessed properties of sand that yield all the relationships presented in Figs. 5 through 7, is employed in this paper.

The SW model representation of deformation in the soil is predicated based upon undrained triaxial test stress-strain response at constant confining pressure ($\bar{\sigma}_{3c}$) corresponding to the initial effective overburden pressure ($\bar{\sigma}_{vo}$). Therefore, the appropriate predicted undrained stress-strain curve (Fig. 1) is employed in the SW model analysis to analyze the response of a laterally loaded pile in liquefiable sand. The calculated undrained response of sand is function of the relative density of sand at consolidation pressure (σ_{3c}); the shape of the grains of sand; the angle of internal friction (v); the drained axial strain at a deviatoric stress level of 50% (ε_{50}); the original vertical effective stress in sand ($\bar{\sigma}_{vo}$), the magnitude of the earthquake and the maximum ground acceleration (a_{max}).

UNDRAINED STRAIN WEDGE MODEL (SWM) FOR LIQUEFIED SAND

The basic purpose of the SWM is to relate stress-strain-strength behavior of the soil in the wedge to one-dimensional Beam on Elastic Foundations (BEF) parameters. The SW model is, therefore, able to provide a theoretical link between the more complex three-dimensional soil-pile interaction and the simpler one-dimensional BEF characterization. The SWM is based on the mobilized passive wedge in front of the pile (Fig. 8) which is characterized by base angle, β_m, the current passive wedge depth, h, and the spread of the wedge via the fan angle, ν_m (the mobilized effective stress friction angle). The horizontal stress change at the passive wedge face, $\Delta\sigma_h$, and side shear, τ, act as shown in Fig. 8.

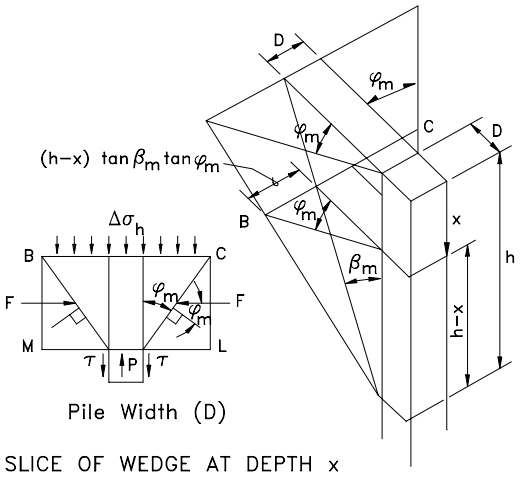

Figure 8. Basic characterization of the strain wedge model (SWM) [9].

The varying depth, h, of the deflected portion of the pile is controlled by the stability analysis of the pile under the conditions of soil-pile interaction. The effects of the soil and pile properties are associated with the soil-pile reaction along the pile by the Young's modulus of the soil (E), the stress level in the soil (SL), the pile deflection (y), and the modulus of subgrade reaction (E_s) between the pile segment and each soil sublayer [9].

The shape of the wedge in any soil layer depends upon the properties of that layer and, therefore, would seem to satisfy the nature of a set of independent Winkler Asoil@ springs in BEF analysis. However, the mobilized depth (h) of the passive wedge at any time is a function of the various soils (and their stress levels) and the bending stiffness (EI) and the head fixity conditions of the pile. This, in turn, affects the resulting p-y response in a given soil layer; therefore, the p-y response is not a unique function of the soil alone. The governing equations of the mobilized passive wedge shape are applied within each soil sublayer (i) of a given deposit. The configuration of the wedge (Fig. 8) at any instant of load is a function of the stress level in the sublayer of sand and, therefore, its mobilized friction angle, ν_m. Note that

$$(\beta_m)_i = 45 + \frac{(\varphi_m)_i}{2}, \qquad \text{and}$$

$$\left(\overline{BC}\right)_i = D + (h - x_i)\,2\left(\tan\beta_m\right)_i\left(\tan\varphi_m\right)_i \tag{4}$$

where $\overline{BC}$ is the width of the wedge face at any depth. h symbolizes the current full depth of the passive wedge in front of the pile; x_i represents the depth from the top of the pile or passive wedge to the middle of the sublayer under consideration; and D indicates the width of the pile cross-section (Fig. 8).

STRAIN WEDGE MODEL WITH LIQUEFIED SOIL (UNDRAINED CONDITIONS)

Under undrained conditions, the major principal stress change ($\Delta\sigma_h$) in the wedge is in the direction of pile movement, and it is equivalent to the deviatoric stress (σ_d) in the isotropically consolidated undrained (ICU) triaxial test. Assuming that the horizontal direction in the field is taken as the axial direction in the triaxial test, the vertical stress change ($\Delta\sigma_v$) is zero and the perpendicular horizontal stress change ($\Delta\sigma_{ph}$) is taken to be the same. Corresponding to the (ICU) triaxial compression test, the deviatoric stress is increased, while the effective confining pressure decreases due to the positive induced excess porewater pressure, Δu_d. Note that Δu_d represents $u_{xs,nf}$ in the near-field region. The cycles of earthquake loading will generate excess porewater pressure in the free-field ($u_{xs,\,ff}$) that will reduce the effective stress in sand (Eqns. 1 and 2) according to its location below ground surface. Once the excess porewater pressure ($u_{xs,\,nf}$) increases due to the pile loading, the confining pressure in the sand around the pile reduces to

$$\overline{\sigma}_v = \overline{\sigma}_3 = (\sigma_{3c} - u_{xs,\,ff}) - u_{xs,nf} \qquad where \qquad \overline{\sigma}_h = \overline{\sigma}_v + \Delta\sigma_h \tag{5}$$

$u_{xs,\,nf}$ (= Δu_d) is a function of stress level. Therefore, the assessment of the mobilized resistance of the sand ($\sigma_d = \Delta\sigma_h$) as a function of the axial strain (major strain) under undrained conditions allows the determination of the sand resistance and pile deformation at the associated undrained horizontal strain, ε_u. The current value of undrained Young=s modulus in sand sublayer (i) which is associated with ε_u is given as

$$(E_u)_i = \left[\frac{\Delta\sigma_h}{\varepsilon_u} \right]_i = \left[\frac{\sigma_d}{\varepsilon_u} \right]_i \tag{6}$$

$$SL_i = \left[\frac{\Delta\sigma_h}{(\Delta\sigma_{hf})_{\overline{\sigma}_3}} \right]_i = \frac{(\sigma_d)_i}{(\overline{\sigma}_3)_i \left[\tan^2\left(45 + \frac{\varphi_i}{2} \right) - 1 \right]} = \frac{\tan^2\left(45 + \frac{(\varphi_m)_i}{2} \right) - 1}{\tan^2\left(45 + \frac{\varphi_i}{2} \right) - 1} \tag{7}$$

The major principal effective stress change, $\Delta\sigma_h$, in the passive wedge is in the direction of pile movement and is equivalent to the deviatoric stress change in the undrained triaxial test, σ_d (assuming that the horizontal direction in the field is taken as the axial direction in the triaxial test). The mobilized effective stress fanning angle, ν_m, of the passive wedge is related to the stress level or the strain in the sand. Knowing the soil strain, ε_u, the deviatoric stress, σ_d, and the associated instant effective confining pressure, $\overline{\sigma}_3$; ν_m can be determined from the associated effective stress-strain curve and effective stress path. Based on the approach presented in [7], both the stress level, SL, and the mobilized angle of internal friction, ν_m, associated with the effective stress, $\overline{\sigma}_3$, and soil strain, ε_u, under undrained conditions can be calculated. Stress level (SL) relates σ_d (= $\Delta\sigma_h$) to σ_{df} (= $\Delta\sigma_{hf}$); where $\Delta\sigma_{hf}$ is the peak of the associated drained (i.e. current $\overline{\sigma}_3$) effective stress-strain curve.

The initial and subsequent values of confining pressure are not equal along the depth of the passive wedge of sand in front of the pile. Therefore, at the same value of horizontal soil strain (ε_u), the undrained resistance of the sand surrounding the pile varies throughout the depth of the passive wedge of sand providing different values of stress level. Such behavior requires the determination of the mobilized undrained resistance of the sand along the depth of the passive wedge. The SWM provides the means to divide the sand layer into equal-thickness sublayers in order to calculate the undrained sand response at each sublayer (i) according to the location and the properties of sand of that sublayer.

SOIL-PILE INTERACTION IN THE SW MODEL UNDER UNDRAINED CONDITIONS

By applying the drained SWM procedures for sand [9], the modulus of subgarde reaction of sand under undrained conditions (E_{su}) at any sublayer (i) can be determined based on the associated values of E_u and SL. The SW model relies on calculating E_{su}, which reflects the soil-pile interaction at any level during pile loading or soil strain. By comparison with the drained E_s, in drained sand [9], E_{su} is given as in any sublayer (i) as

$$(E_{su})_i = \frac{p_i}{y_i} = \frac{D(A\,\varepsilon_u\, E_u)_i}{\delta (h - x_i)} = \frac{(A\, E_u)_i}{(h - x_i)} D(\Psi_u) \tag{8}$$

Corresponding to a horizontal slice of (a soil sublayer) at a depth x (Fig. 8) under horizontal equilibrium, the soil-pile reaction, the undrained p_i (line load) is expressed as a function of $\Delta\sigma_h$ where $\Delta\sigma_h$ represents the mobilized undrained resistance in sand sublayer (i).

$$p_i = (\Delta\sigma_h)_i \overline{BC_i}\, S_1 + 2\,\tau_i\, D\, S_2 \tag{9}$$

Shape factors S_1 and S_2 are equal to 0.75 and 0.5, respectively, for a circular pile cross section, and equal to 1.0 for a square pile; τ is shear stress along the sides of the pile. A is a parameter that governs the growth of the passive soil wedge and based on the concepts presented in [9]. Ψ_u is equal to 1.55 where the total stress Poisson's ratio for undrained sand is equal to 0.5. Equation 9 is based upon the undrained response of sand using the undrained stress-strain relationship (ε_u, σ_d and E_u). Once the values of E_{su} at any level of loading along the length of the deflected portion of the pile are calculated, the laterally loaded pile and the three-dimensional passive wedge in front of the pile can be transformed into a BEF problem and solved using a numerical technique such as the finite element method. The evaluation of E_{su} as a function of soil and pile properties is the key point to the SWM analysis.

TREASURE ISLAND FULL-SCALE LOAD TEST ON PILE IN LIQUEFIED SOIL

A series of full-scale field tests in liquefied soil was performed at Treasure Island in San Francisco Bay [1]. The soil properties employed in the SWM analysis for the test site are described in Table 1 based on the data reported [11]. In this analysis, the sand is assumed to contain 10% fines. The soil was liquefied by carrying out controlled blasts at that site without densifying the soil in the test area. Drained and undrained lateral loading tests were performed on a long isolated pipe pile of 0.324 m diameter, a CISS (cast in steel shell) pile of 0.61 m diameter, and a 0.310-m wide H-pile. All tested piles exhibited free-head conditions and were laterally loaded 1.0 m above ground surface. The test piles had different values of bending stiffness (EI) which are calculated and presented with each test as shown in the following figures.

The predicted and observed drained response of the three piles compare favorably as seen in Fig. 9. While the pipe pile (0.324-m diameter) exhibits a bending stiffness less than that of the H-pile, both piles experienced approximately the same (observed) drained responses. The procedures followed in the Treasure Island test (liquefying the soil around the pile and then loading the pile laterally) are similar to those presented in this paper. The assessed post-liquefaction undrained behavior of the tested piles is based on the procedures presented herein, and includes the effect of ($u_{xs,ff} + u_{xs,nf}$).

TABLE I. SOIL PROPERTIES EMPLOYED IN THE SWM ANALYSIS FOR TREASURE ISLAND TEST

Soil Layer Thick. (m)	Soil Type	Unit Weight, $\bar{\gamma}$ (kN/m^3)	$(N_1)_{60}$	φ (degree)	ε_{50} %	*S_u kN/m^2
0.5	Brown, loose sand (SP)	18.0	16	33	0.45	
4.0	Brown, loose sand (SP)	8.0	11	31	0.6	
3.7	Gray clay (CL)	7.0	4		1.5	20
4.5	Gray, loose sand (SP)	7.0	5	28	1.0	
5.5	Gray clay (CL)	7.0	4		1.5	20

* Undrained shear strength

The piles were cyclically loaded after the first blast at the site. The observed (field) undrained points [1], which are shown in Fig. 9, represent the peaks of the cyclic undrained response of these piles. It should be mentioned that the good agreement between the measured and predicted undrained response (Fig. 9) is based on an assumed maximum ground acceleration, a_{max}, of 0.1g. This value of a_{max} generates high excess porewater pressures ($u_{xs, ff}$) in most of the sand layers. It should be noted that the value of a_{max} employed in the analysis causes an excess porewater pressure ratio (r_u) equal to unity in most of the sand and the best match with the measured free-field excess porewater pressure pattern induced in the field [1].

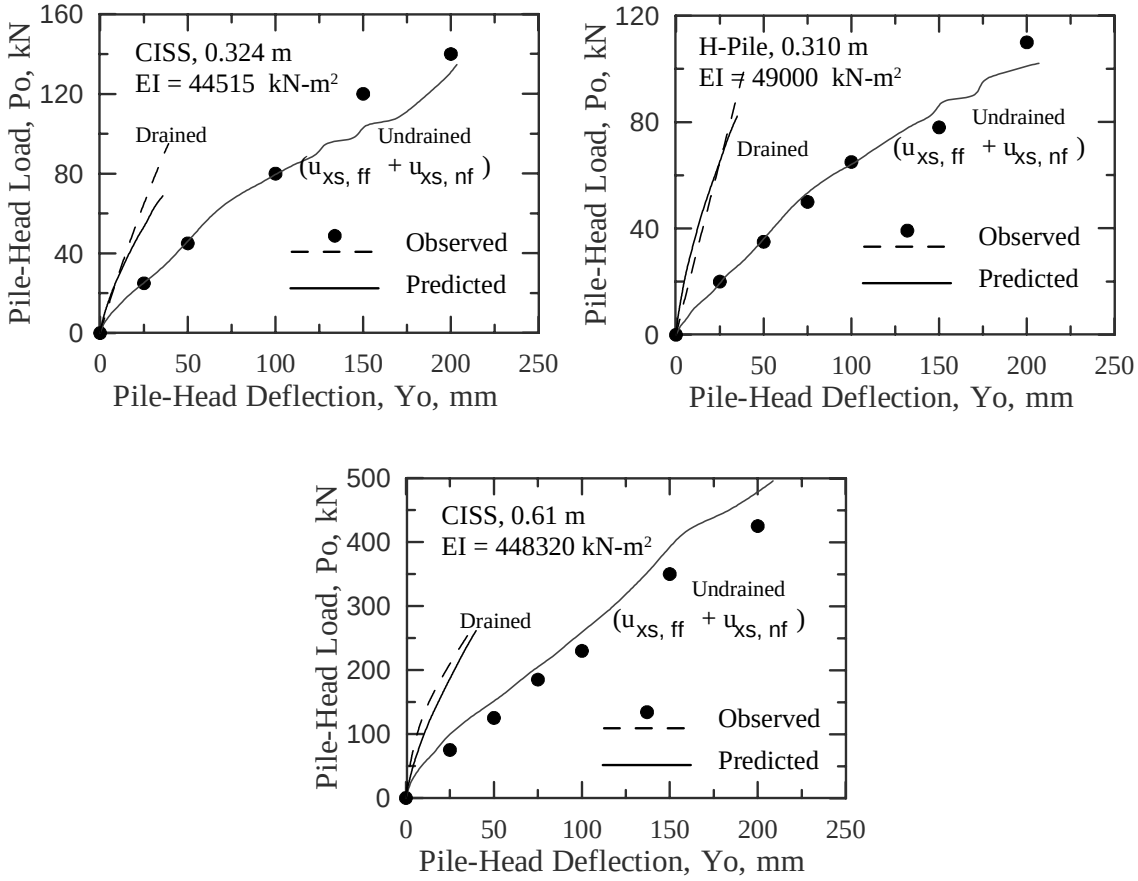

Figure 9. Post-liquefaction Pile head response at Treasure Island test

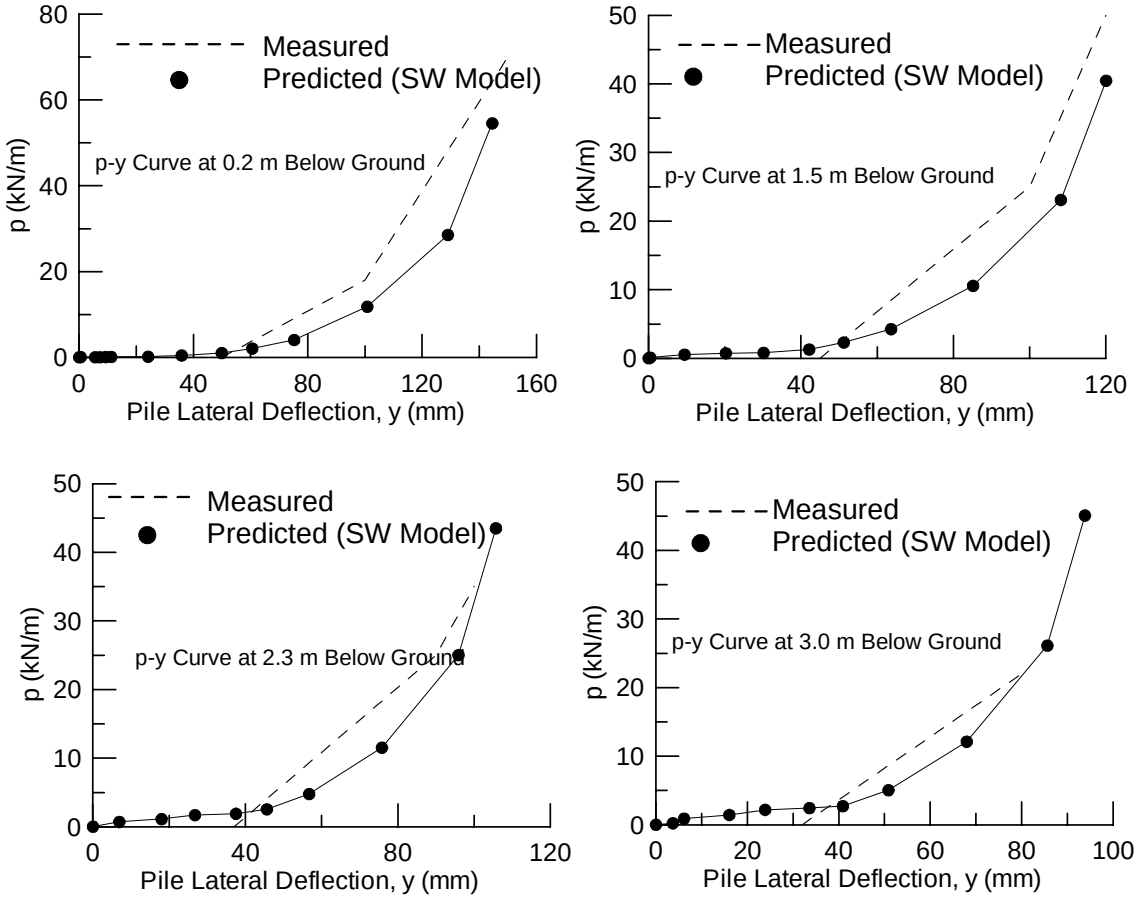

Figure 10. Predicted p-y curves using the SWM vs. the observed ones for Treasure Island test.

The p-y curve comparisons shown in Fig. 10 proves the capability of the SWM for predicting the p-y curve of a pile/shaft in fully or partially liquefied soils. The back-calculated p-y curves at different depths for a 0.61-m CISS pile [11] are presented in Fig. 10. It was not possible for any other technique, such as the traditional p-y curve with a reduction multiplier, to allow the assessment of a p-y curve comparable to the pattern or values of the observed one. It was obvious from the $u_{xs,\,ff}$ distribution measured along the depth of the pile right after the blast that the upper 4.6 m was a almost fully liquefied.

COOPER RIVER BRIDGE TEST AT THE MOUNT PLEASANT SITE, SOUTH CAROLINA SITE

Cyclic lateral load tests were performed on two large diameter long shafts at the Mount Pleasant site. Shaft MP-1 (Cast-in-Steel-Shell, CISS, and bending stiffness (EI) = 2 x 10^8 kip-ft^2) was 8.33-ft diameter and the shaft MP-2 (Cast-in-Drilled Hole, CIDH, and EI = 1.38 x 10^8 kip-ft^2) was 8.5-ft diameter with one-inch-thick steel shell. The lateral load in both cases was applied at a point 43-inches above the ground surface. The Mount Pleasant site soil profile consists of 40 ft of loose to medium dense, clean or silty or clayey sands overlaying a thick layer of the Cooper Marl [12]. Table II summarizes the basic properties of the soil profile at the Mount Pleasant site used in the SWM analysis. Lateral static load tests were carried out in as is conditions, and liquefied conditions induced by controlled blasting (Figs. 11 and 12) [12]. The blast successfully generated high porewater pressure (r_u =1) within most of the upper 38 ft as indicated by the piezometer data.

LPILE analysis for the load test for the project were carried out using (1) traditional p-y curve for the 38 feet thick overburden consisting of sandy deposits for $\varphi = 35^o$ and $\gamma = 60$ pci and (2) the back calculated p-y curves for

Cooper Marl from the O-cell tests as no traditional p-y curves representative of the Cooper Marl conditions were available. The LPILE results for pre- and post-liquefaction conditions are based on the back-calculated p-y curve from the O-cell tests are shown in Figs. 11 and 12. In contrast, SWM predicted p-y curve for the Cooper Marl showed good agreement with the back-calculated p-y curve from the O-cell tests. The SWM results shown in Figs. 11 and 12 are based on the p-y curves predicted from the SWM analysis.

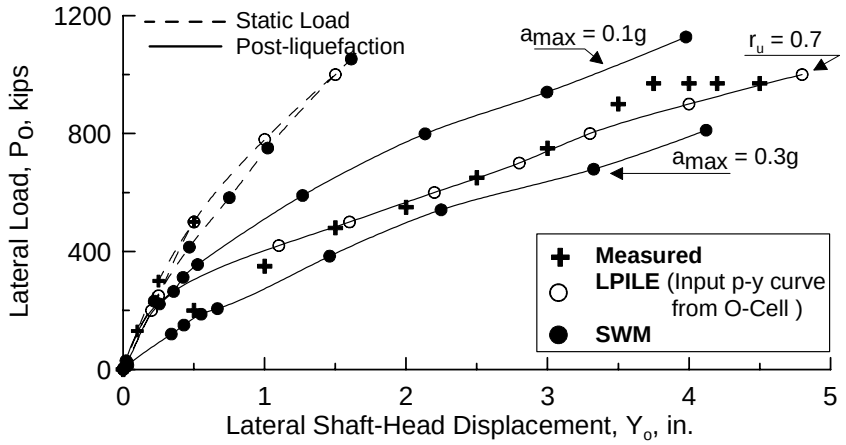

Figure 11. Lateral response of shaft MP-1 at Mount Pleasure test site (Cooper River Bridge)

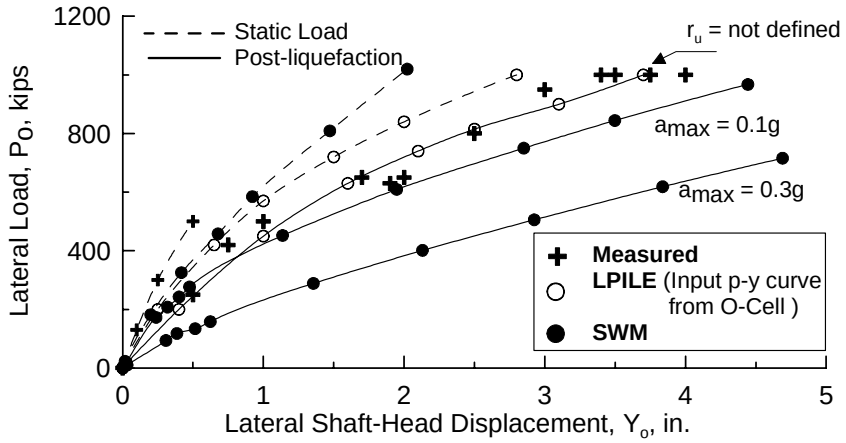

Figure 12. Lateral response of shaft MP-2 at Mount Pleasure test site (Cooper River Bridge)

TABLE II. SOIL PROPERTIES EMPLOYED IN THE SW MODEL ANALYSIS FOR COOPER RIVER BRIDGE TEST AT MT. PLEASANT

Soil Layer Thick. (ft)	Soil Type	Unit Weight, $\bar{\gamma}$ (pci)	$(N_1)_{60}$	φ (degree)	ε_{50} %	*S_u psf
4	Slightly clay sand (SP-SC)	120	19	34	0.004	
9	Sandy clay (CH)	62	7	30	0.008	
16	Very clayey sand (SC-CL)	62	10	32	0.006	
9	Silty sand (SM)	62	7	30	0.008	
80	Cooper Marl	65	20		0.002	4300

LPILE shaft responses for liquefied conditions computed for various values of r_u (trials) were compared to the measured shaft responses tested under liquefaction conditions in order to come up with a reasonable shaft response agreement with the field results. A constant value for r_u =0.7 for the upper 38 ft of overburden used in the LPILE analysis (for shaft MP-1) showed reasonable agreement with the field results Fig. 11). It should be noted that (1) r_u measured in the field was very close or equal to one and (2) use of r_u in the LPILE analysis only reduces the bouyant (effective) unit weight of soil thereby producing a softer shaft responses. r_u used with shaft MP-2 in LPILE analysis was not defined in the report [12].

The SWM analysis for shaft in liquefied soil depends on several factors to include earthquake magnitude, peak ground acceleration (a_{max}), and the soil properties to determine the values of r_u and the additional excess porewater pressure resulting from the superstructure lateral loading. Earthquake magnitude of 6.5 and a_{max} of 0.1g and 0.3g are used in the SWM analysis to obtain the shaft responses shown in Figs. 11 and 12. It should be noted that a_{max} of 0.3g develops complete liquefaction in the upper 38 ft of soil. Despite the diameter and EI of shaft MP-1 were larger than those of shaft MP-2, shaft MP-2 experienced a post-liquefaction lateral response stiffer than that of shaft MP-1 as observed in the field test (Figs. 11 and 12). The use of different values of a_{max} in the SWM analysis is to exhibit the varying shaft response. Knowing the seismic zone (i.e. M and a_{max}) and soil and shaft properties at a particular site, the designer will be able to assess the lateral response of a shaft/pile in liquefiable soils using the SWM computer program.

SUMMARY

The procedure presented yields the undrained response of a laterally loaded pile in liquefiable soil incorporating the influence of both the developing excess porewater pressure in the free-field $u_{xs, ff}$ (due to ground acceleration) and the additional $u_{xs, nf}$ (due to the lateral load from the superstructure). The technique reflects the effect of soil liquefaction on the assessed (soil-pile reaction) p-y curves based on the reduced soil-pile interaction response (modulus of subgrade reaction). The capability of this procedure will (1) reduce the uncertainty of dealing with the behavior of laterally loaded piles in liquefiable soils and (2) allow estimation of realistic responses of laterally loaded piles in liquefiable soils based that properly account for local site conditions and shaft properties as demonstrated by the predictions for the Treasure Island and Cooper River Bridge load tests.

REFERENCES

[1] Ashford, S. A., and Rollins, K. 1999. AFull-scale behavior of laterally loaded deep foundations in liquefied sands.@ Report No. TR-99/03, Struct. Engg Dept., University of Calif., San Diego.

[2] Wang, T. and Reese, L. C. 1998. ADesign of pile foundations in liquefied soil.@ Pub. No. 75, ASCE, Geotech. Earthquake Engg. and Soil Dynamics Conf., Seattle, WA, Vol. 2, Aug., 1331-1343.

[3] Seed, R. B. and Harder, L. F. 1990. ASPT-based analysis of cyclic pore pressure generation and undrained residual strength.@ Vol. 2, BiTech Publishers Ltd, Vancouver, B. C., Canada.

[4] Seed, H. B. 1979. “Considerations in the earthquake-resistance design of earth and rockfill dams.” Geotechnique 29, No. 3, pp. 215-263.

[5] Vaid, Y. P. And Thomas, J. 1995. “Liquefaction and post-liquefaction of behavior of sand.” J. of Geotech. Engg, ASCE, Vol. 121, No. 2, pp. 163-173.

[6] Seed, H. B., Idriss, I.M. and Arango, I. 1983. AEvaluation of liquefaction potential using field performance data.@ Journal of Geotechnical Division, ASCE, Vol. 109, No. 3, pp. 458-482.

[7] Ashour, M. and Norris, G. 1999. ALiquefaction and undrained response evaluation of sands from drained formulation.@ J. of Geotech. Engg, ASCE, Vol. 125, No. 8, pp. 649-658.

[8] Ashour, M. (2002) “Post Liquefaction Response of Liquefied Soils.” Proceeding 37th Engineering Geology and Geotechnical Engineering Symposium, March 27-29, 2002, Boise, Idaho.

[9] Ashour, M., Norris, G., and Pilling, P. 1998. ALateral loading of a pile in layered soil using the strain wedge model.@ J. of Geotech. Engg, ASCE, Vol. 124, No. 4, pp. 303-315.

[10] Norris, G., Siddharthan, R., Zafir, Z., and Madhu, R. 1997. ALiquefaction and residual strength of sands from drained triaxial tests.@ J. of Geotech. Engg, ASCE, Vol. 123, No. 3, pp. 220-228.

[11] Weaver, T. J., Ashford, S. A. and Rollins, K. M. 2001. “Development of p-y curves for a 0.6-m CISS pile in liquefied sand.” The 6th Caltrans Seismic Research Workshop Program, June 12th-13th, Paper No. 5-104.

[12] S&ME Inc. 2000. “Cooper River Bridge replacement project, Charleston, South Carolina.” Report prepared by S$ME, Inc., 840 Low Country Blvd, Mt. Pleasant, SC 29464.

Seismic Performance of a Concrete Column/Steel Cap/Steel Girder Integral Bridge System

Sri Sritharan, Robert E. Abendroth, Lowell F. Greimann,
Wagdy G. Wassef, and Justin Vander Werff

ABSTRACT

This paper presents an overview of a research project that investigates integral concrete pier and steel girder bridge systems for seismic regions. The major aspects of this research are to design an integral connection for a two-span, prototype bridge that consists of a single column bent, steel girders and a steel cap beam; to perform experimental verification of the connection details; and to establish the overall seismic performance of the bridge system. Two test units at 1/3-scale were planned for the experimental component of this study. Testing of the first unit has recently been completed, which exhibited satisfactory seismic performance by developing the plastic moment capacity in the column, as intended in the design. The superstructure response was elastic, confirming the adequacy of the girder-to-cap and column-to-cap connections details. The design approach, connection details, observed behavior, and preliminary test results for the first test unit are also included in the paper.

INTRODUCTION

Integral concrete pier and steel girder systems for bridges, as shown in Fig. 1, have several advantages over conventional integral and non-integral bridge structures consisting of only concrete or steel. However, integral concrete pier, steel girder bridges are seldom used in seismic regions because of the lack of research and insufficient design information available for this type of system. Engineers with the consulting firm of Modjeski and Masters, Inc. (MM) and researchers at Iowa State University (ISU) are jointly investigating the seismic design of integral concrete pier connections for steel girder bridges. This research is sponsored by the National Cooperative Highway Research Program (NCHRP) as Project 12-54. The main objectives of this investigation are to: (a) develop integral connection details that can withstand seismic loading, (b) perform experimental validations of the proposed connection details from (a), and (c) establish suitable design recommendations and specifications for integral bridges having concrete substructures and steel superstructures.

CONCEPTS

Following a review of the current design practice of various integral pier bridges, several initial concepts for integral pier bridge systems suitable for seismic resistance were initially developed using concrete columns, steel girders, and steel or concrete cap beams [1,2]. Some of these concepts are presented in Fig. 2.

Sri Sritharan, Assistant Professor, Dept. of Civil and Construction Eng., Iowa State University, Ames, IA 50010
Robert Abendroth, Assoc. Professor, Dept. of Civil and Construction Eng., Iowa State University, Ames, IA 50010
Lowell Greimann, Professor and Chairman, Department of Civil and Construction Engineering, Iowa State University, Ames, IA 50010
Wagdy Waseff, Associate, Modjeski and Masters, Inc., 4909 Louise Drive, Mechanicsburg, PA 17055
Justin Vander Werff, Graduate Research Assistant, Dept. of Civil and Construction Eng., Iowa State University, Ames, IA 50010

Fig. 1 An integral concrete pier bridge with steel girders.

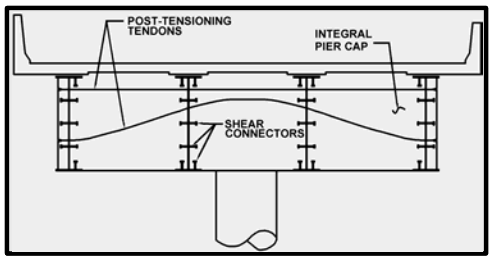

(a) Concept No. 1 – with a concrete cap beam

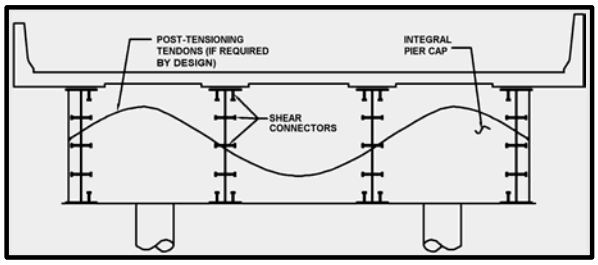

(b) Concept No. 2 – with a concrete cap beam

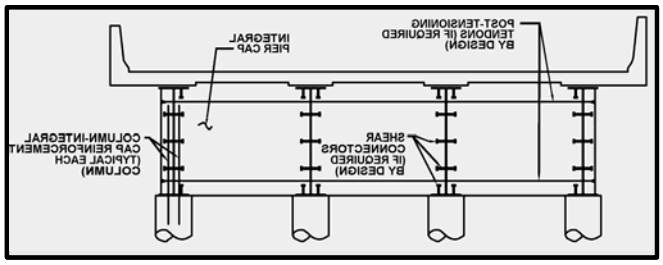

(c) Concept No. 3 – with a concrete cap beam

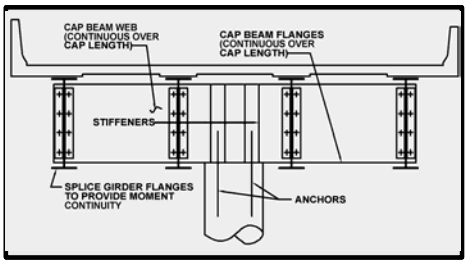

(d) Concept No. 4 – with a steel cap beam

Figure 2. Different concepts for integral bridge systems with concrete piers and steel girders.

Considering the potential benefits and constructability issues associated with the different systems, a modified version of concept No. 4 in Fig. 2 was selected for further investigation. The selected concept employs a single column bent; a steel, box-shaped, cap beam; steel girders; and a cast-in-place concrete deck. Another reason for selecting a steel cap beam in this investigation was that a parallel study undertaken jointly by the University of California at San Diego and the California Department of Transportation examines the design of concrete cap beams in similar bridge systems [3].

BENEFITS

From a survey conducted as part of this research study, it was determined that the main motivation for using an integral bridge system in non-seismic regions is due to a significant reduction in the height of the structure when compared to that for a bridge system with simply supported details between the superstructure and the piers [1]. This reduces the costs of the bridge approach embankment. For seismic loading conditions, bridge systems incorporating integral piers offer several advantages. A moment-resisting connection between the column and the pier cap will (a) increase redundancy in the structure, (b) enhance energy dissipation potential by increasing the number of plastic hinges, and (c) enable pin-connections at the column base in multi-column configuration which will significantly reduce the substructure cost [4].

In addition, the integral bridge concept with steel girders and steel cap beams chosen for the investigation, reported in this paper, will provide several other benefits. By allowing prefabrication of girders, cap beams, and girder-to-cap connections, this concept for bridges will improve quality, minimize falsework, reduce field labor, and accelerate construction of the bridge, resulting in reduced structure and maintenance costs. The proposed system will require the girders to be field spliced at locations away from cap beam, which can be readily accomplished. Although prefabrication of components is feasible when concrete girders and concrete cap beams are used as part of an integral bridge system [5,6], the connection between the girders and cap beams will be established mostly likely in the field. Also this connection may require cast-in-place construction for the cap beams, eliminating the prefabrication option (see examples in Refs. [3,5]). Cast-in-place construction for the cap beams will increase formwork and labor costs. Furthermore, if the girders are terminated at the vertical faces of the concrete cap beam (rather than extending through the beams), the girders need to be supported by temporary falsework that does not experience settlement. Structural steel has a desirable strength-to-weight ratio. Using steel for the girders and cap beams as in the current study, the dead weight, as well as the seismic mass, is minimized for the bridge.

DETAILED INVESTIGATION

To facilitate a detailed investigation of the proposed bridge system under seismic conditions, a symmetric, continuous, two-100-ft span, two-lane highway bridge, with a total width of 37.5 ft (including the shoulders), as depicted in Fig. 3 was selected as a prototype structure. The prototype structure was analyzed using a grillage model that was subjected to different load combinations, including several service-level load conditions. Based on the analysis results, the column longitudinal reinforcement ratio was determined. By using the estimated column overstrength moment resistance and the capacity design philosophy, the critical force conditions for the connections were established.

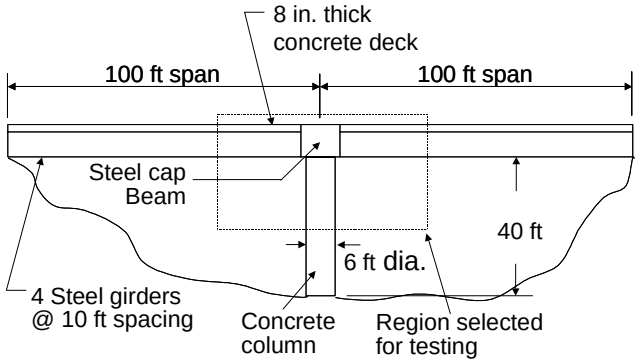

Figure 3. The prototype bridge structure.

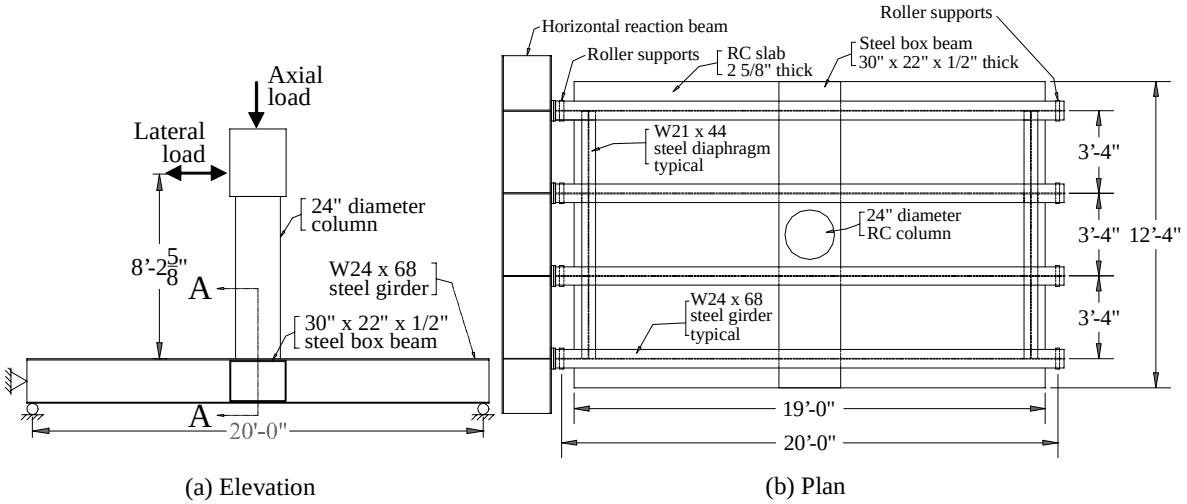

(a) Elevation (b) Plan

Figure 4. Overall dimensions and test setup of SPC1.

The experimental part of the study involves the design of the bridge including the connections at the pier and the verification of the critical details using 1/3-scale test models. As identified in Fig. 3, only the center portion of the prototype structure is modeled in the experiment. The column clear height for the model was chosen as the distance between the inflection point that is located at about the column mid height and the bottom of the cap beam in the prototype bridge. This enables the use of cantilever columns in the test models. The setup of a test model in the laboratory is shown in Fig. 4, in which the test unit is inverted for convenience and the girders are simply supported at their ends. Two separate integral bridge designs are investigated in the study, with the corresponding test units being referred to as SPC1 and SPC2. The testing of SPC1 has been completed, while the alternative concepts for SPC2 are currently under review. The connection details of SPC1 and its seismic performance, as well as a brief summary of different options under consideration for SPC2, are presented in the remainder of this paper.

TEST UNIT SPC1

Design Approach and Connection Details

As expected, the analysis of the grillage model confirmed that the design of the bridge was governed by the combination of dead and seismic loads. Using existing seismic design guidelines [7,8] and considering the need to subject integral connections to sufficient demand during testing, a 2-ft diameter column with a longitudinal reinforcement ratio of 2% was established for SPC1; this column size corresponds to a 6-ft diameter column in the prototype structure. Assuming that the plastic moment capacity would be fully developed in the column adjacent to the cap beam, integral connection details were designed so that the superstructure of the bridge would remain essentially elastic during seismic loading. This design approach is consistent with the current seismic design practice [4,8].

In developing the connection details between the cap and girders, a continuous cap beam without any splices was considered necessary to ensure satisfactory torsional resistance. As a result, the girders were dimensioned such that the cap beam could be placed between the girder flanges as shown in Fig. 5. To simplify construction, each girder was terminated at the face of the cap beam. The girder flanges near the cap beam were coped to permit the installation of splice plates, which, together with diaphragm plates, provided continuity of the girders through the cap beam. The splice plates were bolted to the top and bottom plates of the cap beam and welded to the girders positioned on both sides of the cap beam. As

indicated in Fig, 5, the connection between each girder and the cap beam consisted of three different details; a bolted connection along the depth between the girder web and face of the cap beam, a fillet welded connection between the top and bottom edges of the cope in girder web and splice plates, and a full-penetration weld between the flanges of the girders and splice plates. The fillet welds between the web and the splice plate were dimensioned to resist the shear flow between the web and the flanges, while the bolted connection between the splice plates and the cap beam was designed to resist the maximum moment transferred from the longitudinal girders to the pier cap. The diaphragm plates located inside the cap beam were bolted to all four plates composing the box-shaped cap beam. The anchorage length of the column longitudinal bars into the cap beam-to-column joint and detailing requirements for the intersection of the cap beam through girder webs controlled the dimensions of the cap beam and girders.

The design of the connection between the concrete column and the steel cap beam was performed using a strut-and-tie model with an objective of minimizing the amount of joint shear reinforcement. This design technique was proven to be very effective in recent seismic testing of bridge joints [4,6]. Relying on two mechanisms with equal capacity, as illustrated in Fig. 6, the total tension force (T_c) corresponding

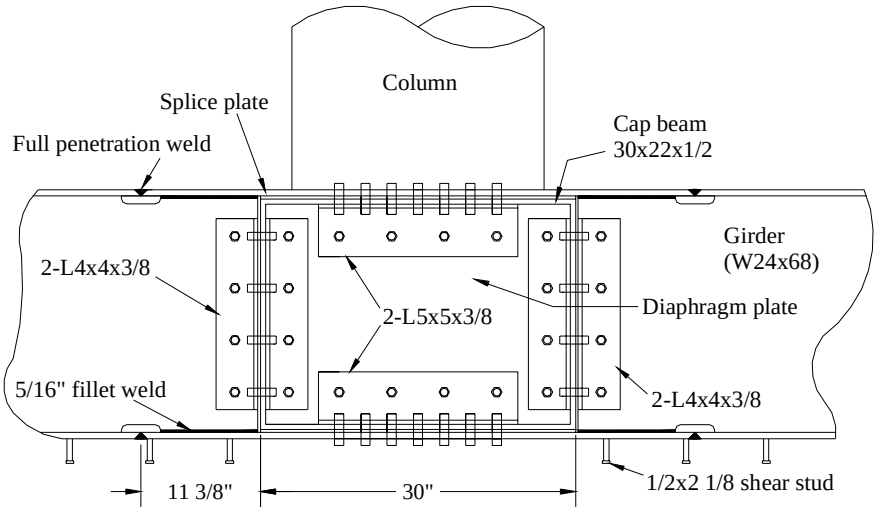

Figure 5. The connection details between the steel girder and steel cap beam.

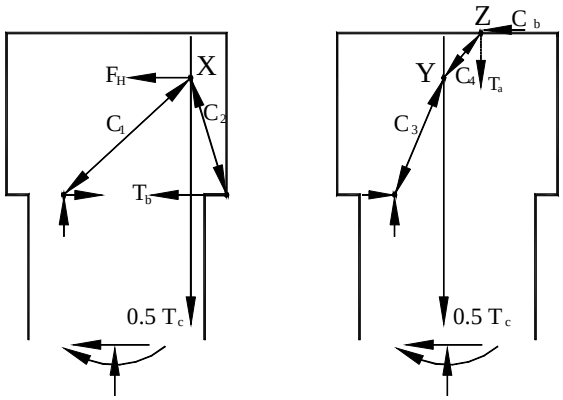

(a) Mechanism 1 (b) Mechanism 2

Figure 6. The force transfer mechanisms for the concrete column to steel cap beam connection.

to the column overstrength moment was anchored into the joint so that the moment capacity could be fully developed in the column plastic hinge adjacent to the cap beam. Estimating the forces in struts and ties of the two mechanisms enabled appropriate beam-to-column connection details, shown in Fig. 7, to be established using joint spiral reinforcement and shear studs on the inside surfaces of the cap beam. The amount of joint spiral reinforcement was quantified based on the magnitude of the tension force F_H to sustain Mechanism 1 depicted in Fig. 6, assuming that the vertical steel plates of the cap beam would not effectively resist this tension force. Also, the use of spiral reinforcement was preferred because it ensures adequate confinement for the joint core concrete. The cap beam was assumed to not adequately confine the joint concrete. Since spalling of joint concrete was not possible, the spiral within the cap beam did not have to be tied to the column main reinforcement. Therefore, the spiral reinforcement was dimensioned to provide a one-inch wide gap between the joint spirals and column longitudinal reinforcement. This clearance permitted the column reinforcement cage to be easily installed through the holes in the cap beam plate.

Terminating the column longitudinal reinforcement bars inside the pier cap would have provided adequate development length. However, except for two of these bars, the column bars extended two inches into the concrete deck. Comparable longitudinal strains were monitored on both lengths of column reinforcing bars, which are referred to as long and short bars in this paper.

Construction

Paxton & Vierling Steel Co. of Carter Lake, Iowa, was subcontracted to fabricate the portion of the superstructure consisting of the cap beam, girders and girder-to-cap connections. The spiral reinforcement was placed inside the cap beam during fabrication and the superstructure steel assembly was shipped to ISU's main structural laboratory. Following construction of the formwork for the deck and placement of the slab reinforcement, the prefabricated portion of the superstructure was erected and then the column reinforcement cage was dropped into place. Concrete was then placed for the deck, cap beam-to-column connection and column in three different castings. A four-inch diameter access hole was placed on the top plate (as constructed in the laboratory) of the cap beam to pump the concrete into the column-to-cap beam connection. Although the joint concrete in the prototype structure could be placed relatively easily, the casting of the concrete through the access hole for the steel compartment within the cap beam of SPC1 was extremely difficult. As a result, voids developed at the top corners of the steel compartment, which were filled with a flowable grout after casting of the column. Based on the observed performance of SPC1, a concept to improve construction of the cap beam-to-column connection is suggested under the section titled *Additional Test Results*.

Seismic Performance

Figure 8 shows the lateral cyclic-load sequence and the corresponding axial load applied to the column end of test unit SPC1. The axial load simulated the gravity effects, while the cyclic load with full reversals replicated the seismic effects. Although the calculated axial load in the column at one-third scale was 102 kips, a lower load of 60 kips was applied to the test unit throughout most of the cyclic load testing to more accurately model the bending moments in the girders at the vertical faces of the cap beam. However, a higher axial load of 130 kips was applied to the column during the third lateral load cycle at a system ductility (μ_Δ) of 4. This larger axial load value was more appropriate for developing the critical shear forces in the girders of the test specimen.

The observed force-displacement response of SPC1 is shown in Fig. 9, in which the lateral displacement corresponding to $\mu_\Delta = 1$ is 1.35 inches. The shape and dependability of the hysteresis loops obtained under repeated loading confirmed that the seismic behavior of the test unit was satisfactory. During the second load cycle at $\mu_\Delta = 4$, slight buckling of an extreme column longitudinal reinforcing bar was first observed adjacent to the cap beam. The buckling of at least three extreme longitudinal bars on each side of the column was apparent in the next loading cycle with the higher axial load in the test

specimen, and a sequential fracture of these bars due to high-amplitude, low-cycle fatigue ensued in the first load cycle at $\mu_\Delta = 6$. For this ductility, testing was started with a column axial force of 60 kips and terminated at the end of the first load cycle since the lateral load resistance of the system was reduced by about 30%. The force-displacement data obtained during testing at $\mu_\Delta = 6$ was omitted from Fig. 9 for clarity.

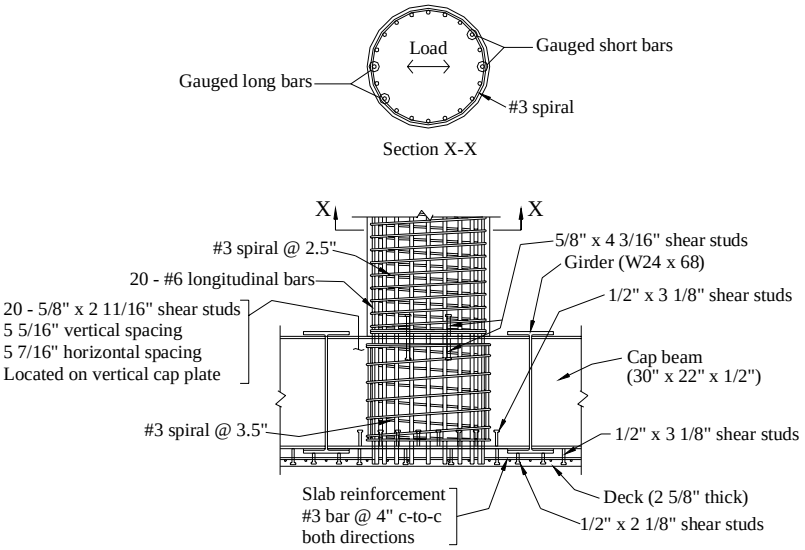

Figure 7. The concrete column to steel cap beam connection details.

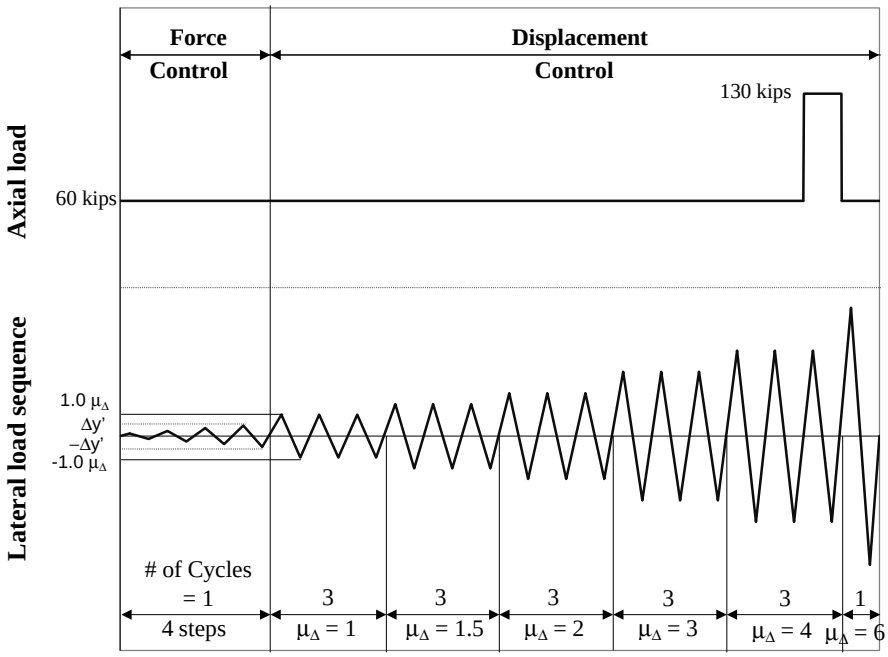

Figure 8. Load sequence applied to test unit SPC1.

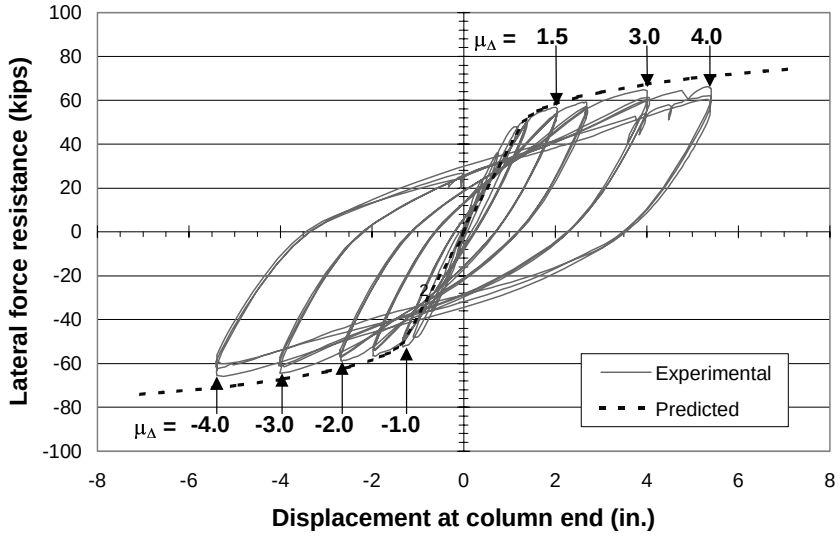

Figure 9. Force-displacement response of test unit SPC1.

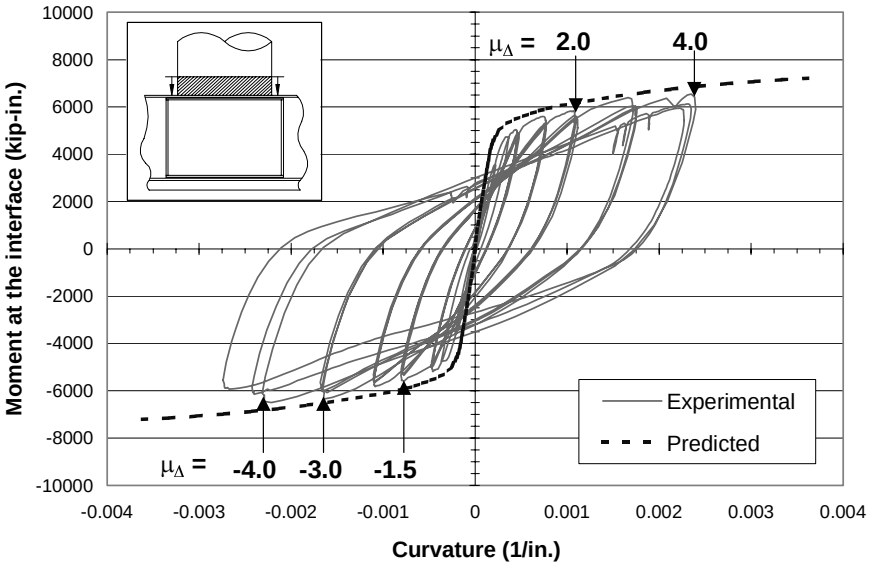

Figure 10. Moment-curvature response of the column adjacent to the cap beam in SPC1.

Buckling of the column bars was not anticipated at $\mu_\Delta = 4$, and appears to have been partially triggered by insufficient anchorage of the spiral reinforcement adjacent to the cap beam. As previously shown adequate in reinforced concrete bridge bent tests (e.g., Ref. [6]), the column spirals in SPC1 was anchored adjacent to the cap beam with two turns. In comparison to those tests where a concrete cap beam and a concrete column were used, the damage to the cover and core concrete of the column immediately adjacent to the cap beam appeared to be more severe in SPC1. This could have affected the anchorage of the spiral reinforcement in the plastic hinge region. Improving anchorage of the spiral reinforcement with a hook at the end or replacing column spirals with welded hoops may be desirable for the proposed bridge system.

The response of superstructure in SPC1 was elastic during the entire test. No distress was observed in the connections between the steel girders and the steel cap beam and between the concrete column and the steel cap beam. As anticipated, flexural cracks, including three cracks that extended across the entire width, developed in the deck on both sides of the column, indicating that the entire bridge width was effective in resisting the combined lateral and axial loads applied to the column. One of these full-width flexural cracks formed at the girder-to-cap interface while the other cracks were located at about two feet spacing away from the interface. The deck experienced some additional tension cracks, radiating from the column perimeter.

Figure 9 also shows a predicted response envelope for SPC1 based on a grillage model that incorporated a rotational spring to account for plastic action of the column hinge and strain penetration effects into the cap beam-to-column connection. An initial prediction, which was completed using estimated concrete strengths and measured steel properties prior to testing of SPC1. This prediction was revised to account for the measured material properties. As seen in Fig. 9, the predicted response envelope is in satisfactory agreement with the observed behavior for SPC1.

Additional Test Results

In addition to the force-displacement response discussed above, other selected test results are presented in this section. Figure 10 shows the moment-curvature response of the column adjacent to the cap beam up to the third cycle at $\mu_\Delta = 4$, accompanied by the predicted response envelope obtained using the measured material properties. The stability of the moment-curvature response and satisfactory agreement between the measured and the predicted envelopes confirm that the behavior of the column-to-cap connection was satisfactory. This observation, as well as the force-displacement response of the system presented in Fig. 8, also indicates that extending the column longitudinal bars into the deck for improving anchorage is unnecessary.

The measured strain in the joint spiral reinforcement did not exceed 200 microstrain, indicating that the spiral reinforcement was not mobilized during the transfer of forces through the joint. In contrary to the design assumption, this observation might have been due to the steel plates of the cap beam and/or tension capacity of the joint concrete providing the tension force necessary for supporting the joint mechanism. As a measure of action in the joint, the dilation measured at the joint center parallel to the lateral loading direction is plotted in Fig. 11 as a function of the horizontal load applied to the column. The joint dilations shown in this figure correspond to the first cycle at each load step in the push and pull directions, which were limited to 0.01 inches. Dilations of up to 0.014 inches were measured in the second and third loading cycles in the ductility range from 2 to 4. These values are considerably small and are consistent with strains measured in the joint spirals. However, it is important to observe the steep increase in the dilation plot in Fig. 11 as load increases from that corresponding to the column theoretical yield strength.

Since detailing requirements governed the cap beam and girder dimensions and that the buckling of the column longitudinal bars could be delayed as discussed previously, a similar bridge system could be designed with higher lateral load resistance. As the lateral load increases, larger joint dilations and more participation of the spiral reinforcement in the force transfer would be expected. Therefore, the elimination of the spirals within the joint would not seem to be appropriate. However, reducing the spiral reinforcement or replacing the spirals and concrete inside the steel compartment with fiber-reinforced grout may provide a satisfactory connection between the steel cap beam and the concrete column. The second alternative is attractive in that it will significantly improve constructablity of the connection.

Tensile strain profiles established for a short and a long extreme column bar, located on opposite sides of the column, are compared in Fig. 12 for loadings up to the column theoretical yield strength. This strain profile plot and a similar profile plot (not shown here) established for a pair of bars located at an angle of 36° to the lateral load direction confirm that the maximum bond stresses developed along the embedded portions of the short and long column bars are comparable. Furthermore, the data indicate that the bond stress developed along the portion of the long bars that extended beyond the cap beam and into

the deck is negligible and that the maximum bond stress had not been developed over the last six inches of the column short bars. From these observations, it is concluded that the column longitudinal bars in this type of an integral bridge system do not need be extended into the concrete deck. However, the column bars should be provided with adequate anchorage length and should be extended as close as possible to the top plate of the cap beam in the upright position.

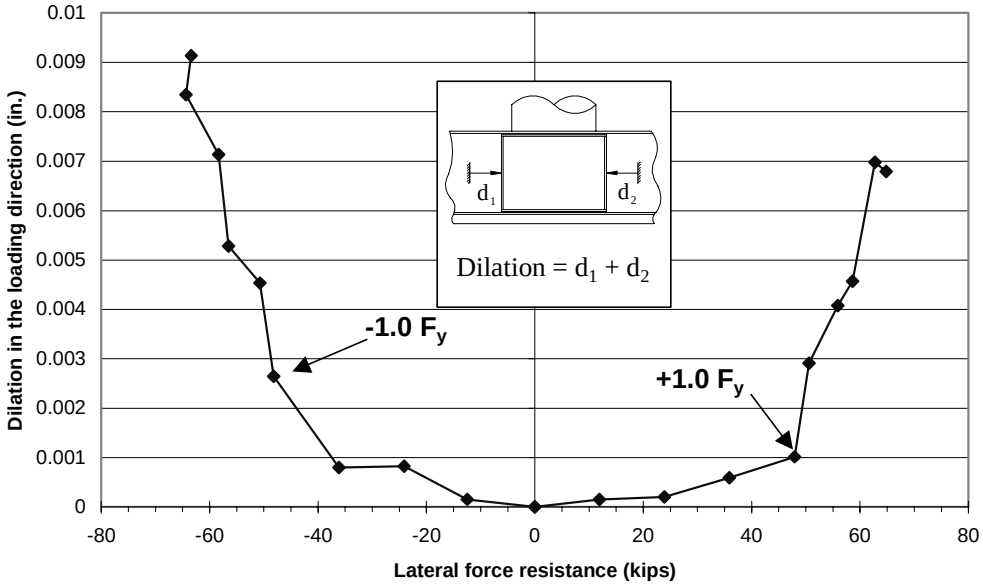

Figure 11. Measured dilation at the joint center in test unit SPC1.

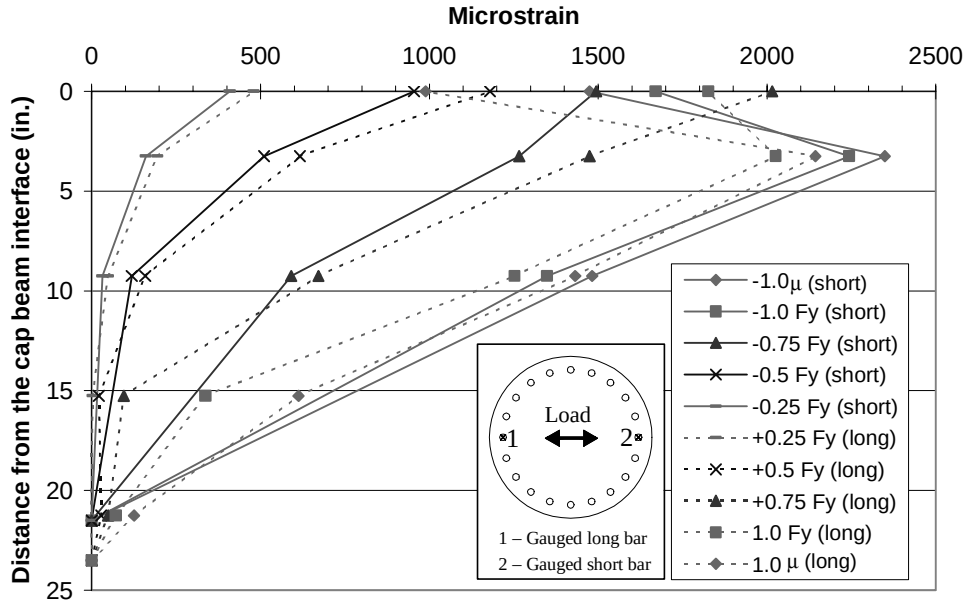

Figure 12. Strain profiles along the embedded portions of two extreme column longitudinal bars.

TEST UNIT SPC 2

The project team has suggested five alternatives for test unit SPC2. An NCHRP research advisory panel, that oversees Project 12-54, is currently reviewing the alternatives. Based on the panel's recommendations, the concept and connections detail for SPC2 will be finalized. The five alterative concepts that are under considerations are:

1. A system similar to SPC1, but with a shallower cap beam. To satisfy the anchorage requirement, the column bars need to be extended into the deck due to the reduced cap beam depth. Alternatively, the column bars may be mechanically anchored to the cap beam.
2. A system similar to SPC1 with completely eliminating the joint spirals and shear studs. This option is likely to cause a cap beam-to-column joint failure, but the response will be useful in understanding the force transfer mechanism across the joint.
3. A combination of alternatives 1 and 2.
4. Replace the box-shaped cap beam in SPC1 with an I-shaped plate-girder pier cap.
5. A test specimen identical to SPC1, with the column longitudinal reinforcement increased from 2% to 2.5% and appropriate modifications to the cap beam-to-column connection based on the test data obtained from SPC1.

Construction of test unit SPC2 is expected to take place in the Spring of 2002, followed by testing in the Summer of 2002.

CONCLUSIONS

The research presented in this paper is an investigation of integral concrete pier bridges with steel girders and steel cap beams for seismic loading conditions. When compared to existing integral bridge systems, there are several benefits associated with these bridges, which will result in reduced construction and maintenance costs. Using a two-span, continuous, prototype bridge, integral connection details were designed for a 1/3-scale bridge model that consisted of a two-foot diameter concrete column, steel girders and a box-shaped steel cap beam. When the bridge model was subjected to simulated seismic loading, dependable hysteresis performance was obtained. Satisfactory seismic behavior was observed for the girder-to-cap and column-to-cap connections.

Based on the recorded data from this test unit, it was found that the column longitudinal bars could be sufficiently anchored into the steel cap beam, without extending them into the deck. The joint spiral reinforcement, which was designed as a part of the joint mechanism, was not significantly involved in the joint force transfer. However, the joint dilation measurements indicated that the amount of joint spiral reinforcement might be reduced, but this reinforcement should not be completely eliminated. Alternatively, the spirals and joint concrete within the steel cap beam may be replaced with a non-shrink, fiber-reinforced, grout, which would improve constructability of the cap beam-to-column connection as well. The test also revealed that the end of the column spiral reinforcement adjacent to the steel cap beam should be detailed with a hook that is anchored in the core concrete of the column.

ACKNOWLEDGEMENTS

The research project described in this paper is funded by the Transportation Research Board as NCHRP Project 12-54. The authors gratefully acknowledge the advice and assistance provided by an NCHRP panel that is chaired by Mr. Mark Reno and coordinated by Mr. David Beal. From Modjeski and Masters, Inc., Dr. John Kulicki serves as the administrative officer for this research project, and Mr. Dustin Davis performed grillage analysis of the prototype bridge. Testing of Unit SPC1 was conducted in

the Structural Engineering Laboratory at ISU with extensive help from Mr. Doug Wood, the laboratory manager, and Mr. Ryan Staudt, an ISU graduate student.

REFERENCES

[1] Modjeski and Masters, Inc. in association with Iowa State University. December 1999. "Integral Connections of Steel Bridge Structures Interim Report", NCHRP Project 12-54.

[2] Sritharan, S., R. E. Abendroth, L. F. Greimann, and W. G. Wassef. October 2001. "Integral Concrete Piers for Steel Girder Bridges in Seismic Regions," presented at the 5th NSF Workshop on Bridge Research in Progress, Minneapolis, Minnesota.

[3] Patty, J., F. Seible, and C-M. Uang. June 2001. "Longitudinal Seismic Response of Concrete Substructure to Steel Superstructure Integral Bridge Connections," presented at the 6th Caltrans Seismic Research Workshop, Sacramento, California.

[4] Priestly, M. J. N., F. Seible, and G. M. Calvi. 1996. *Seismic Design and Retrofit of Bridges.* New York: John Wiley and Sons, Inc.

[5] Holombo, J., M. J. N. Priestley, F. Seible. March-April 2000. "Continuity of Precast Prestressed Spliced-Girder Bridges Under Seismic Loads," *PCI Journal*, 45(2):40-63.

[6] Sritharan, S., M. J. N. Priestley, F. Seible. 1999. "Enhancing Seismic Performance of Bridge Cap beam/Column Joints Using Prestressing," *PCI Journal*, 44(4):74-91.

[7] AASHTO. 1998. *LRFD Bridge Design Specifications*, Second Edition, American Association of State Highway and Transportation Officials, Washington, D. C.

[8] ATC. 1996. *Improved Seismic Design Criteria for California Bridges: Provisional Recommendations*. ATC-32, Applied Technology Council, Redwood City, CA.

Development and Testing of the New LRFD Seismic Design of Highway Bridges

Chair: Ian M. Friedland

Recommended LRFD Guidelines for the Seismic Design of Highway Bridges

Ronald L. Mayes, Ian M. Friedland and ATC Project Team

Recommended Design Approach for Liquefaction Induced Lateral Spreads

Geoffrey R. Martin, M. Lee Marsh, Donald G. Anderson, Ronald L. Mayes and Maurice S. Power

Application of the New LRFD Guidelines for the Seismic Design of Highway Bridges

Derrell A. Manceaux

Cost Impact Study for a Typical Highway Bridge Using Different Return Period Seismic Design Maps

Jeffrey Ger, David Straatmann, Suresh Patel and Shyam Gupta

Testing of the LRFD Bridge Seismic Design Provisions Through a Comprehensive Trial Design Process

M. Lee Marsh, Richard V. Nutt, Ronald Mayes and Ian M. Friedland

Recommended LRFD Guidelines for the Seismic Design of Highway Bridges

Ronald L. Mayes, Ian M. Friedland and ATC Project Team[1]

ABSTRACT

This paper provides an overview of the proposed seismic design provisions that have been developed to replace those currently in use throughout the United States. The proposed provisions include two-level design procedures, advanced analytical tools such as push-over, updated ground motion data, new site characterizations, simplified methods for lower seismicity regions, and more comprehensive liquefaction provisions. Many of the developments that have followed in the wake of recent earthquakes have been incorporated into the proposed provisions. The effort has been conducted and overseen by broad-based and nationally recognized teams. The proposed provisions are now being used in trial designs around the country and will be considered for adoption in Guide Specification form in 2002 by AASHTO.

Ronald Mayes, Staff Consultant SGH 220 Sutter St. Suite 300, San Francisco Ca. 94108
Ian Friedland, Associate Director for Development, Applied Technology Council, Washington, D.C.
ATC Project Team, Donald Anderson CH2M Hill, Michel Bruneau University of New York at Buffalo, Gregory Fenves University of California at Berkeley, John Kulicki Modjeski and Masters, John Mander University of Canterbury, Lee Marsh Berger/Abam Engineers, Geoffrey Martin University of Southern California, Richard Nutt Bridge Consultant, Maurice Power Geomatrix Consultants, Andrei Reinhorn University of New York at Buffalo.

BACKGROUND

In the fall of 1998, the AASHTO (American Association of State Highway and Transportation Officials)-sponsored National Cooperative Highway Research Program (NCHRP) initiated a project to develop a new set of seismic design provisions for highway bridges, compatible with the AASHTO *LRFD Bridge Design Specifications* (AASHTO, 2000). NCHRP Project 12-49, which was conducted by a joint venture of the Applied Technology Council and the Multidisciplinary Center for Earthquake Engineering Research (the ATC/MCEER Joint Venture), had as its primary objectives the development of seismic design provisions that reflected the latest design philosophies and design approaches that would result in highway bridges with a high level of seismic performance.

NCHRP Project 12-49 was intended to reflect experience gained during recent damaging earthquakes and the results of research programs conducted in the United States and elsewhere over the prior 10 years. The primary focus of the project was on the development of design provisions which reflected the latest information regarding: design philosophy and performance criteria; seismic hazard representation, loads and displacements, and site effects; advances in analysis and modeling procedures; and requirements for component design and detailing. The new specification is intended to be nationally applicable with provisions for all seismic zones, and all bridge construction types and materials.

The current provisions contained in the AASHTO *LRFD Bridge Design Specifications* are, for the most part, based on provisions and approaches carried over from Division I-A, "Seismic Design," of the AASHTO *Standard Specifications for Highway Bridges* (AASHTO, 1996). The Division I-A seismic provisions were originally issued by AASHTO as a Guide Specification in 1983 and were subsequently incorporated with little modification into the *Standard Specifications* in 1991. Thus, the current *LRFD* (Load and Resistance Factor Design) provisions are based on seismic hazard, design criteria and detailing provisions, that are now considered at least 10 years and in many cases nearly 20 years out-of-date. Because AASHTO is in the process of transitioning from the *Standard Specifications* to the *LRFD* specification, it made sense to comprehensively update the seismic provisions.

NCHRP Project 12-49 developed a preliminary set of comprehensive specification provisions and commentary intended for incorporation into the AASHTO *LRFD* specifications. However, due to the amount of detail in the new provisions and the general view that the new provisions were significantly more complex than the existing provisions, the AASHTO Highway Subcommittee on Bridges and Structures recommended that the new provisions be adopted by AASHTO first as a Guide Specification (MCEER, 2001). This would then allow bridge designers the opportunity to become familiar with the proposed new specifications, and for any problems such as omissions and editorial or technical errors in the new provisions to be identified and rectified, prior to formal adoption into the AASHTO *LRFD* specifications.

BASIC CONCEPTS

The development of these specifications was predicated on the following basic concepts.

- Loss of life and serious injuries due to unacceptable bridge performance should be minimized.

- Bridges may suffer damage and may need to be replaced but they should have low probabilities of collapse due to earthquake motions.
- The function of essential (critical lifeline) bridges should be maintained even after a major earthquake.
- Upper level event ground motions used in design should have a low probability of being exceeded during the approximate 75-year design life of the bridge.
- The provisions should be applicable to all regions of the United States.
- The designer should not be restricted from considering and employing new and ingenious design approaches and details.

In comparison to the current AASHTO *Standard Specifications for Highway Bridges* and the AASHTO *LRFD Bridge Design Specifications*, the recommended Guide Specifications contain a number of new concepts and additions as well as some major modifications to the existing provisions. These are discussed in this paper.

NEW SEISMIC HAZARD MAPS

The national earthquake ground motion map used in the existing AASHTO provisions is a probabilistic map of peak ground acceleration (PGA) on rock that was developed by the U.S. Geological Survey (USGS) in 1990. The map provides contours of PGA for a probability of exceedance (PE) of 10% in 50 years, which corresponds to approximately 15% PE in the 75-year design life assumed by the *LRFD* specifications for a typical highway bridge.

In 1993, the USGS embarked on a major project to prepare updated national earthquake ground motion maps. The result of that project was a set of probabilistic maps first published in 1996 that cover several rock ground motion parameters and three different probability levels or return periods. The maps are available as large-scale paper maps, as small-scale paper maps obtained via the Internet, and as digitized values obtained from the Internet or a CD-ROM published by USGS (Frankel et al., 2000). Parameters of rock ground motions that have been contour mapped by USGS include peak ground acceleration (PGA) and elastic response spectral accelerations for periods of vibration of 0.2, 0.3, and 1.0 second. Contour maps for these parameters have been prepared for three different probabilities of exceedance (PE): 10% PE in 50 years, 5% PE in 50 years, and 2% PE in 50 years (approximately 3% PE in 75 years). In addition to these contour maps, the ground motion values at any specified latitude and longitude in the U.S. can be obtained via the Internet for the aforementioned three probability levels for PGA and spectral accelerations for periods of vibration of 0.2, 0.3, and 1.0 seconds. In addition, the published data contains not only the PGA and spectral acceleration values at three probability levels but also the complete hazard curves (i.e., relationships between the amplitude of a ground motion parameter and its annual frequency of exceedance at each grid point location). Therefore, the ground motion values for all of the aforementioned ground motion parameters can be obtained for any return period or probability of exceedance from the hazard curves. These maps formed the basis for seismic design using these new provisions. Upper bound limits of 1.5 times the median ground motions obtained by deterministic methods have been applied to limit probabilistic ground motions in the western United States.

DESIGN EARTHQUAKES AND PERFORMANCE OBJECTIVES

The existing AASHTO provisions have three implied performance objectives for small, moderate and large earthquakes with detailed design provisions for a 10% PE in 50 year event (approximately 15% PE in 75 year event) to achieve the stated performance objectives. The new provisions provide more definitive performance objectives and damage states for two design earthquakes with explicit design checks for each earthquake to ensure the performance objectives are met (Table 1). The upper-level event, termed the 'rare earthquake' or Maximum Considered Earthquake (MCE), describes ground motions that, for most locations, are defined probabilistically and have a probability of exceedance of 3% in 75 years. However, for locations close to highly active faults, the MCE ground motions are deterministically bounded so that the levels of ground motions do not become unreasonably high. Deterministic bound ground motions are calculated assuming the occurrence of maximum magnitude earthquakes on the highly active faults and are equal to 1.5 times median ground motions for the maximum magnitude earthquake but not less than 1.5g for the short-period spectral acceleration plateau and 0.6g for 1.0-second spectra acceleration. On the current MCE maps, deterministic bounds are applied in high-seismicity portions of California, in local areas along the California-Nevada border, along coastal Oregon and Washington, and in high-seismicity portions of Alaska and Hawaii. In areas where deterministic bounds are imposed, ground motions are lower than ground motions for 3% PE in 75 years. The MCE earthquake governs the limits on the inelastic deformation in the substructures and the design displacements for the support of the superstructure.

The lower level design event, termed the 'expected earthquake', has ground motions corresponding to 50% PE in 75 years. This event ensures that essentially elastic response is achieved in the substructures for the more frequent or expected earthquake. This design level is similar to the 100-year flood and has similar performance objectives. An explicit check on the strength capacity of the substructures is required. Parameter studies performed as part of the development of the provisions show that the lower level event will only impact the strength of the columns in parts of the western United States. Background on the choice of the two design events is provided in Appendix A of the Guide Specification.

DESIGN INCENTIVES

The provisions contain an incentive from a design and construction perspective for performing a more sophisticated "pushover analysis." The R-Factor increases approximately 50% when a pushover analysis is performed, primarily because the analysis results will provide a greater understanding of the demands on the seismic resisting elements. The analysis results are assessed using plastic rotation limits on the deformation of the substructure elements to ensure adequate performance.

NEW SOIL FACTORS

The site classes and site factors incorporated in the new provisions were originally recommended at a site response workshop in 1992 and subsequently were adopted in the

Seismic Design Criteria of Caltrans (1999), the 1997 NEHRP Provisions (BSSC, 1998), the 1997 Uniform Building Code (UBC) (ICBO, 1997), and the 2000 International Building Code (IBC) (ICC, 2000). This is one of the most significant changes with regard to its impact on the level of seismic design forces. It should be noted that the recommended soil factors affect both the peak (flat) portion of the response spectra as well as the long-period descending portion of the spectra (Figure 1). The increase in site factors with decreasing accelerations is due to the nonlinear response effects of soils. Soils are more linear in their response to lower acceleration events and display more nonlinear response as the acceleration levels increase. The effects of soil nonlinearity are also more significant for soft soils than for stiff soils.

NEW SPECTRAL SHAPES

The long period portion of the current AASHTO acceleration response spectrum is governed by a spectrum shape that decays as $1/T^{2/3}$. During the development of this decay function for the existing provisions, there was considerable massaging of the factors that affect the long period portion of the spectra in order to produce a level of approximately 50% conservatism in the design spectra when compared to the ground spectra beyond a one-second period. The new provisions remove this conservatism and provide a more correct spectral shape that decays as 1/T for periods below three seconds. Guidance is also provided for the spectral shapes beyond a period of three seconds.

EARTHQUAKE RESISTING SYSTEMS AND ELEMENTS (ERS AND ERE)

The provisions provide a mechanism to permit the use of some seismic resisting systems and elements that were not permitted for use in the current AASHTO provisions. Selection of an appropriate ERS is fundamental to achieving adequate seismic performance. To this end, the identification of the lateral-force-resisting concept and the selection of the necessary elements to facilitate the concept should be accomplished in the conceptual design or Type, Selection, and Layout (TS&L) phase of the project. Seismic performance is typically better in systems with regular configurations and evenly distributed stiffness and strength. Thus, typical geometric configuration constraints, such as skew, unequal pier heights, and sharp curves, conflict, to some degree, with the seismic design goals. For this reason, it is advisable to resolve potential conflicts between configuration and seismic performance early in the design effort. The classification of ERS and ERE into the categories of (1) permissible, (2) permissible with owner's approval, and (3) not recommended is done to trigger due consideration of seismic performance that leads to the most desirable outcome — that is, seismic performance that ensures wherever possible post-earthquake serviceability. It is not the objective of this specification to discourage the use of systems that require owner approval. Instead, such systems may be used, but additional design effort and consensus between the designer and owner are required to implement such systems.

NO ANALYSIS DESIGN CONCEPT

The no analysis design procedure is an important new addition to the recommended provisions. It applies to regular bridges in the lower seismic hazard areas, including the expanded areas now requiring more detailed seismic design. The bridge is designed for all non-seismic loads and does not require a seismic demand analysis. Capacity design procedures are used to determine detailing requirements in columns and in the connection forces of columns to the footing and superstructure. There are no seismic design requirements for abutments, except that integral abutments need to be designed for passive pressure.

CAPACITY SPECTRUM DESIGN PROCEDURE

The capacity spectrum design method is a new addition to the provisions and is conceptually the same as the new Caltrans' displacement design method. The primary difference is that the capacity spectrum design procedure begins with the non-seismic capacity of the columns and then assesses the adequacy of the resulting displacements. At this time, the capacity spectrum method may be used for very regular bridges that respond essentially as single-degree-of-freedom systems, although future research should expand the range of applicability. The capacity spectrum approach uses the elastic response spectrum for the site, and this is reduced to account for the dissipation of energy in the earthquake resisting elements. The advantage of the approach is that the period of vibration does not need to be calculated, and the designer sees the explicit trade-off between the design forces and displacements. The method is also quite useful as a preliminary design tool for bridges that may not satisfy the current regularity limitations of the approach.

DISPLACEMENT CAPACITY VERIFICATION ("PUSHOVER") ANALYSIS

The pushover method of analysis has seen increasing use since the early 1990's, and is widely employed in the building industry and by some transportation departments including the Caltrans seismic retrofit program. This analysis method provides additional information on the expected deformation demands of columns and foundations and, as such, provides the designer with a greater understanding of the expected performance of the bridge. The method was used for two different purposes in these new provisions. First, it provided a mechanism under which the highest R-Factor for preliminary design of a column could be justified, because there are additional limits on the column plastic rotations that the results of the pushover analysis must satisfy. Second, it provided a mechanism to allow incorporation of earthquake resisting elements (ERE) that require owner's approval. The trade-off was the need for a more sophisticated analysis so that the expected deformations in critical elements could be assessed. The ERE could then be used, provided that the appropriate plastic deformation limits were met.

FOUNDATIONS

The new provisions are an update of the existing AASHTO LRFD provisions incorporating explicit material that was referenced in the existing specifications and to

incorporate recent research. The changes include specific guidance for the development of spring constants for spread footings and deep foundations (i.e., driven piles and drilled shafts.), as well as approaches for defining the capacity of the foundation system under overturning moments. The capacity provisions specifically address issues such as uplift and plunging (or yield) limits within the foundation. Procedures for including the pile cap in the lateral capacity and displacement evaluation are also provided. The implications of liquefaction of the soil, either below or around the foundation system, are also described. This treatment of liquefaction effects is a major technical addition to the provisions.

ABUTMENTS

The new provisions incorporate much of the research that has been performed on abutments over the past 10 years. Current design practice varies considerably on the use of the abutments as part of the ERS. Some agencies design a bridge so that the substructures are capable of resisting all of the seismic loads without any contribution from the abutment. Other agencies use the abutment as a key component of the ERS. Both design approaches are permitted in these provisions. The abutments can be designed as part of the ERS and become an additional source for dissipating the earthquake energy. In the longitudinal direction, the abutment may be designed to resist the forces elastically utilizing the passive pressure of the backfill or, in some cases, passive pressure at the abutment is exceeded, resulting in larger soil movements in the abutment backfill. This requires a more refined analysis to determine the amount of expected movement, and procedures are provided herein to incorporate this nonlinear behavior. In the transverse direction, the abutment is generally designed to resist loads elastically. These provisions therefore recognize that the abutment can be an important part of the ERS and considerable attention is given to abutment impacts on the global response of the bridge. For the abutments to be able to effectively contribute to the ERS, a continuous superstructure is required.

LIQUEFACTION

Liquefaction has been one of the most significant causes of damage to bridge structures during past earthquakes. Most of the damage has been related to lateral movement of soil at the bridge abutments. However, cases involving the loss of lateral and vertical bearing support of foundations for central piers of a bridge have also occurred. Considerable research and development have occurred over the past decade in the areas of liquefaction potential and effects, and much of this information has been incorporated in these new provisions. For example, the new provisions outline procedures for estimating liquefaction potential using methods developed in 1997, as part of a national workshop on the evaluation of liquefaction. Procedures for quantifying the consequences of liquefaction, such as lateral spreading of approach fills and settlement and potential flow of liquefied soils, are also given. The provisions also provide specific reference to methods for treating deep foundations extending through soils that are spreading or flowing laterally as a result of liquefaction.

Consideration of liquefaction is based, in part, on the mean earthquake magnitude at a site, and mean magnitudes are found in the same USGS database that is used to obtain spectral accelerations. For sites with mean earthquake magnitudes less than 6.0, the effects of

liquefaction on dynamic response can be neglected. When liquefaction occurs, vibration and permanent movement occur simultaneously during a seismic event. The recommended methodology in these provisions is to consider the two effects independently; i.e., de-coupled.

If lateral flow or spreading occurs, significant movement of the abutment and foundation systems can result and this can be a difficult problem to mitigate. The range of design options include (1) designing the piles for the flow forces to (2) an acceptance of the predicted lateral flow movements, provided inelastic hinge rotations in the piles remain within a specified limit. The acceptance of plastic hinging in the piles is a deviation from past provisions in that damage to piles is accepted when lateral flow occurs, thereby acknowledging that the bridge may need to be replaced if this option is selected.

Assessment techniques for determining post-earthquake conditions of deep foundations, such as piles and drilled shafts are expected to be developed in the future. Currently, such techniques as down-hole inclinometers are available. Additionally, video assessment techniques are emerging, but are not in use in the U.S. If appropriate sensing devices and access types can be developed, then practical assessment damage to deep foundations can become a tool for engineers to evaluate foundation condition and the need for repair or replacement.

Structural or soil mitigation measures to minimize the amount of movement to meet higher performance objectives are also outlined in the new provisions. Due to the concerns about the potential cost impact of liquefaction coupled with the impact of higher level design events, two detailed case studies on the application of the recommended design methods for both liquefaction and lateral flow design were performed (NCHRP, 2001). The results are also summarized in Appendix H of the provisions. These examples demonstrated that for some soil profiles application of the new provisions would not be significantly more costly than the application of the more conservative current provisions.

STEEL DESIGN REQUIREMENTS

The existing AASHTO Specifications do not have seismic requirements for steel bridges, except for the provision of a continuous load path to be identified and designed (for strength) by the engineer. Consequently a comprehensive set of special detailing requirements for steel components expected to yield and dissipate energy in a stable and ductile manner during earthquakes were developed, including provisions for ductile moment-resisting frame substructures, concentrically-braced frame substructures, and end-diaphragms for steel girder and truss superstructures. These provisions now provide a complete set of guidance on steel structures, drafts of which have been well reviewed by a wide range of engineers knowledgeable in steel design and construction practice.

CONCRETE DESIGN REQUIREMENTS

There are no major additions to the concrete provisions, but there are important updates for key design parameters based on research conducted over the past decade. The minimum amount of longitudinal steel was reduced from 1% to 0.8%, which will result in cost savings when used with the capacity design procedures. An implicit shear equation was also added where no

seismic demand has been determined. Modifications to the explicit shear equation and confinement requirements were made, and a global buckling provision was added, as were plastic rotation limits for the pushover analysis.

SUPERSTRUCTURE DESIGN REQUIREMENTS

Detailed design requirements are not included in the current AASHTO seismic design provisions, other than those required by the generic load path requirement. Therefore, for the higher hazard levels, explicit design requirements have been added since the current provisions result in a wide discrepancy in their application.

BEARING DESIGN REQUIREMENTS

One of the significant issues that arose during development of the steel provisions, and was subsequently endorsed by the NCHRP Project Panel and the ATC/MCEER Joint Venture Project Team (PT) and Project Engineering Panel (PEP), was the critical importance of bearings as part of the overall bridge load path. The 1995 Kobe, Japan earthquake (and other more recent earthquakes) clearly showed the very poor performance of some bearing types and the disastrous consequence that a bearing failure can have on the overall performance of the bridge. Three design options are included to address the issue; these are (1) testing of the bearings, (2) ensuring restraint of the bearings, and (3) a design concept that permits the girders to slide on a flat surface if the bearings fail.

SEISMIC ISOLATION PROVISIONS

The *Guide Specifications for Seismic Isolation Design* were first adopted by AASHTO in 1991; they were significantly revised and reissued in 1999. Under the NCHRP 12-49 project, the 1999 Guide Specification provisions were incorporated into the recommended LRFD provisions. This resulted in the addition of a new chapter, Chapter 15, for the recommended NCHRP 12-49 LRFD provisions, based on issues related to seismic isolation design. That new recommended chapter is included in this Guide Specification as Section 15, and it is essentially the same as the 1999 AASHTO *Guide Specifications for Seismic Isolation Design* (AASHTO, 1999).

COST IMPLICATIONS

A parameter study was performed as part of the project. In brief, the study shows that the net effect on the cost of a column and spread footing system is on the average 2% less than the current Division I-A provisions for multi-column bents and 16% less than Division I-A provisions for single column bents. These cost comparisons are based on the use of the more refined method for calculating overstrength factors and 2400 different column configurations including the seismic input of five different cities.

One factor that caused a cost increase in some of the lower period configurations was the short period modifier, which accounts for the increased ductility demands inherent in short period structures. Since this provision needs to be a part of any new code and is not part of the current Division I-A provisions, the cumulative effect of all the other charges (including the 3% PE in 75 year/1.5 mean deterministic event, new soil factors, new spectral shape, new R-Factors, new phi-factors, cracked section properties for analysis, etc.) would likely have resulted in lower average costs had the short period modifier been a part of the current specification, Division I-A.

ACKNOWLEDGMENTS

Development of the original NCHRP Project 12-49 provisions (from which the Guide Specification was generated) was by the ATC/MCEER Joint Venture. Ian Friedland of ATC (and formerly MCEER) was the project principal investigator and Ronald Mayes was the project technical director. Christopher Rojahn of ATC was the project administrative officer on behalf of the ATC/MCEER Joint Venture. The Project team members for NCHRP Project 12-49 included:

- Donald Anderson, CH2M Hill, Inc.
- Michel Bruneau, University at Buffalo
- Gregory Fenves, University of California at Berkeley
- John Kulicki, Modjeski and Masters, Inc.
- John Mander, University of Canterbury (formerly with the University at Buffalo)
- Lee Marsh, BERGER/ABAM Engineers
- Ronald Mayes, Simpson Gumpertz and Heger
- Geoffrey Martin, University of Southern California
- Andrzej Nowak, University of Michigan
- Richard Nutt, bridge consultant
- Maurice Power, Geomatrix Consultants, Inc.
- Andrei Reinhorn, University at Buffalo

The project also included a distinguished advisory committee through ATC (the Project Engineering Panel); Ian Buckle, of the University of Nevada at Reno, co-chaired this committee with Christopher Rojahn of ATC. The NCHRP Project Panel C12-49, under the direction of NCHRP Senior Program Officer David Beal and chaired by Harry Capers of the New Jersey Department of Transportation, also provided significant input and guidance during the project. Three drafts of the specifications and commentary were prepared and reviewed by these panels and the AASHTO Highway Subcommittee on Bridges and Structures seismic design technical committee (T-3), which was chaired by James Roberts of Caltrans.

REFERENCES

AASHTO (2000) *LRFD Bridge Design Specifications,* American Association of State Highway and Transportation Officials, Second Edition with Interims, Washington, D.C. www.aashto.org.

AASHTO (1999) *Guide Specifications for Seismic Isolation Design,* Association of State Highway and Transportation Officials, Washington, D.C.

AASHTO (1996) *Standard Specifications for Highway Bridges*, American Association of State Highway and Transportation Officials, Sixteenth Edition with Interims, Washington, D.C. www.aashto.org.

BSSC (1998) *NEHRP Recommended Provisions for Seismic Regulations for New Buildings and Other Structures,* Report FEMA 302, Building Seismic Safety Council, Washington, D.C.

Caltrans (1999) *Seismic Design Criteria*, Version1.1, California Department of Transportation, Sacramento, CA. July.
Frankel, A.D. and Leyendecker, E.V. (2000) Uniform Hazard Response Spectra and Seismic Hazard Curves for the United States: CD-ROM Published by the U.S. Geological Survey National Seismic Hazard Mapping Project, March. http://geohazards.cr.usgs.gov/eq/
ICBO (1997) *Uniform Building Code*, Structural Engineering Design Provisions, Volume 2, International Conference of Building Officials, Whittier, CA.
ICC (2000) *International Building Code*, International Code Council, Inc. Falls Church, VA.
MCEER (2001) *Recommended LRFD Guidelines for the Seismic Design of Highway Bridges*, Multidisciplinary Center for Earthquake Engineering Research, NCHRP Project 12-49, MCEER Highway Project 094, Task F3-1, Buffalo, NY.
NCHRP (2001) *Liquefaction Study Report*, National Cooperative Highway Research Program, Project 12-49, Transportation Research Board, National Research Council, Washington, D.C.

Table 1 Design Earthquakes and Seismic Performance Objectives

		Performance Level[1]	
Probability of Exceedance For Design Earthquake Ground Motions[4]		**Life Safety**	**Operational**
Rare Earthquake (MCE) 3% in 75 years	Service[2]	Significant Disruption	Immediate
	Damage[3]	Significant	Minimal
Expected Earthquake 50% in 75 years	Service	Immediate	Immediate
	Damage	Minimal	Minimal to None

Notes:

(1) Performance Levels

These are defined in terms of their anticipated performance objectives in the upper level earthquake. Life safety in the MCE event means that the bridge should not collapse but partial or complete replacement may be required. Since a dual level design is required the Life Safety performance level will have immediate service and minimal damage for the expected design earthquake. For the operational performance level the intent is that there will be immediate service and minimal damage for both the rare and expected earthquakes.

(2) Service Levels*:

- *Immediate* – Full access to normal traffic shall be available following an inspection of the bridge.
- *Significant Disruption* – Limited access (Reduced lanes, light emergency traffic) may be possible after shoring, however the bridge may need to be replaced.

(3) Damage Levels:

- None – Evidence of movement may be present but no notable damage.
- Minimal – Some visible signs of damage. Minor inelastic response may occur, but post-earthquake damage is limited to narrow flexural cracking in concrete and the onset of yielding in steel. Permanent deformations are not apparent, and any repairs could be made under non-emergency conditions with the exception of superstructure joints.
- Significant – Although there is no collapse, permanent offsets may occur and damage consisting of cracking, reinforcement yield, and major spalling of concrete and extensive yielding and local buckling of steel columns, global and local buckling of steel braces, and cracking in the bridge deck slab at shear studs on the seismic load path is possible. These conditions may require closure to repair the damage. Partial or complete replacement of columns may be required in some cases. For sites with lateral flow due to liquefaction, significant inelastic deformation is permitted in the piles, whereas for all other sites the foundations are capacity-protected and no damage is anticipated. Partial or complete replacement of the columns and piles may be necessary if significant lateral flow occurs. If replacement of columns or other components is to be avoided, the design approaches producing minimal or moderate damage such as seismic isolation or the control and repairability design concept should be assessed.

(4) Earthquake Ground Motions:

The upper-level earthquake considered in these provisions is designated the Maximum Considered Earthquake, or MCE. In general the ground motions on national MCE ground motion maps have a probability of exceedance of approximately 3% in 75 years. However, adjacent to highly active faults, ground motions on MCE maps are bounded deterministically as described in Appendix A of the Guide Specification. When bounded deterministically, MCE ground motions have a probability of exceedance higher than 3% in 75 years. The performance objective for the expected earthquake is either explicitly included as an elastic design for the 50% in 75 year force level or results implicitly from design for the 3% in 75 year force level.

Recommended Design Approach for Liquefaction Induced Lateral Spreads

Geoffrey R. Martin, M. Lee Marsh, Donald G. Anderson, Ronald L. Mayes, and Maurice S. Power

ABSTRACT

In support of the recent NCHRP 12-49 study to develop the next generation of seismic design guidelines for new bridges, a detailed study of design approaches to evaluate and mitigate liquefaction-induced lateral spread deformations was undertaken. The motivation for this study was the recommended increase in design return period for the "Maximum Considered Earthquake" (MCE) to 2475 years (probability of exceedance of 3% in 75 years) in contrast to the current AASHTO Division 1-A value of 475 years (probability of exceedance of 15% in 75 years). Prior to the study, concerns had been expressed by representatives of several state transportation agencies that costs could be significantly increased for mitigation of impacts from liquefaction-induced lateral spread on a bridge structure.

In this paper, the design approach developed in the study, as documented in the Recommended LRFD Guidelines for the Seismic Design of Highway Bridges, is summarized. The approach described offers a method for evaluating lateral spread potential, and if required, optimizing mitigation requirements. The method is simple to use and is within the capabilities of a normal team of geotechnical and bridge engineers.

Case studies of two liquefaction-prone sites and their respective bridges (one in Washington State and one in Missouri) are briefly outlined to demonstrate the approach. The scope of the study included simplified and non-linear effective stress liquefaction analyses, estimation of lateral spread deformations, evaluation of structural and ground modification mitigation options, and evaluation of impacts. The study focused on design differences between the recommended MCE design provisions and the current AASHTO design provisions, and led to a recommended design approach for liquefaction induced lateral spreads.

The conclusions from the study indicate that for the Missouri site, no additional costs were necessary to address the recommended MCE event versus the current AASHTO event, while for the Washington site, costs were only slightly increased. In drawing these conclusions, the importance of pile pinning effects in reducing lateral ground deformations was identified, together with the need to recognize that mobilization of moment ductility in piles should be acceptable in MCE collapse prevention events. While the effects of the proposed change in return periods were small for the two selected cases, other specific sites could possibly be affected to a greater degree, depending on the particular combination of soil conditions and bridge type.

Geoffrey R. Martin , Professor, University of Southern California, Department of Civil and Environmental Engineering, Los Angeles, CA 90089-2531

M. Lee Marsh, Senior Project Manager, Berger/ABAM Engineers, 33301 Ninth Ave. South, Suite 300, Federal Way, WA 98003-6395

Donald G. Anderson, Principal Geotechnical Engineer, CH2M Hill, 777 108th Ave. NE, Bellevue, WA 98004-5118

Ronald L. Mayes, Simpson Gumpertz & Herger, Inc., 222 Sutter Street, Suite 300, San Francisco, CA 94108

Maurice S. Power, Principal Engineer, Geomatrix Consultants, Inc., 2101 Webster Street, 12th Floor, Oakland, CA 94612

INTRODUCTION

The vulnerability of highway bridges to earthquake-induced ground failures arising from liquefaction has been clearly demonstrated by the extensive damage observed in past earthquakes. Damage has been primarily associated with large translational flow slides and related embankment deformations (when static factors of safety against slope failure drop below 1.0 due to low residual undrained strengths of liquefied soil layers) or progressive but limited lateral spread embankment deformations of the order of feet, driven by earthquake ground shaking subsequent to liquefaction, with deformations ceasing at the end of the earthquake.

Damage modes associated with such lateral deformations are related to displacement demands on abutments and piers leading to possible pile damage and/or span collapse. Representative damage in the 1964 Alaska and Niigata earthquakes and the 1991 Costa Rica earthquake has been documented by Youd, [1]. Damage in the 1995 Kobe earthquake is described by Tokimatsu and Asaka [2]. Two specific examples of lateral spread pile damage are noted below.

The first example is that of the performance of the Landing Road Bridge in the 1987 Edgecumbe earthquake (New Zealand) documented by Berrill et. al. [3]. The bridge approach spans to a riverbank were supported by concrete wall piers founded on battered prestressed concrete piles. Liquefaction induced lateral spreads in the liquefiable sand layer of the order of 6 feet were estimated. Observations from back analyses and excavations, indicated that the piles successfully resisted the passive pressures mobilized against the piers, albeit cracks in the piles suggested plastic hinges in the piles were on the verge of forming as shown schematically in Figure 1.

In the Kobe earthquake, field investigations using borehole cameras and slope indicators, showed that failures of piles in lateral spread zones concentrated at the interfaces between liquefied and non-liquefied layers, as well as near pile heads. Also lateral pile analyses using p-y interface springs together with pile deformations induced by estimated ground displacement profiles, were consistent with observed pile performance, (Tokimatsu and Asaka, [2]), as shown for example in Figure 2.

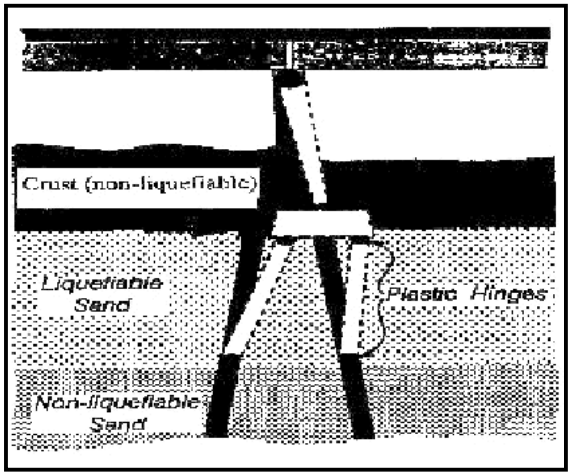

Figure 1 Landing Road Bridge Lateral Spread (after Berrill et al., 1997)

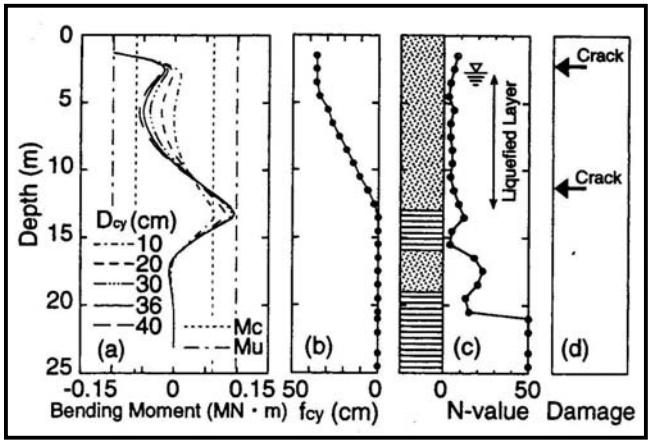

Figure 2 Site and Damage Characteristics for a Precast Concrete Pile Subjected to a Lateral Spread in the Kobe Earthquake (after Tokimatsu and Asaka, 1998)

Whereas the evaluation of the mode and magnitude of liquefaction induced lateral ground deformations involves considerable uncertainty and is the subject of on-going research, in many cases the current state of the practice utilizes the Newmark sliding block approach on an assumed dominant failure plane at the base of a liquefied zone, as discussed further in the case study presented below. Hence free field displacements are defined by an estimated lateral displacement on a failure surface, as shown in Figure 3.

Where highway bridge site liquefaction problems are identified in relation to potential earthquake induced bridge damage modes associated with lateral spreads, mitigation methods need to be addressed. Apart from relocating the bridge to another less vulnerable site, two basic options are normally considered.

1. Foundation/bridge structural retrofit to accommodate the predicted liquefaction and related ground deformation demands. This requires soil-foundation structure interaction analyses to determine if the deformation and load capacity of the existing foundation/bridge system is adequate to accommodate the ground deformation demands without collapse or can meet prescribed performance criteria. If not, mitigation methods focused on strengthening the structural foundation system can be evaluated, and costs compared to the ground modification mitigation option noted below.
2. The use of site remediation techniques, where stabilizing measures or ground modification and improvement approaches are undertaken to prevent liquefaction and/or minimize ground displacement demands. Such methods include for example, the use of vibro-stone columns to form an embankment or buttress through the liquefiable zone.

The design approach for evaluating and mitigating the effects of liquefaction induced lateral spreads documented in the recently published Recommended LFRD Guidelines for the Seismic Design of Highway Bridges (MCEER, [4]) is summarized below. Case studies utilizing the approach are then described.

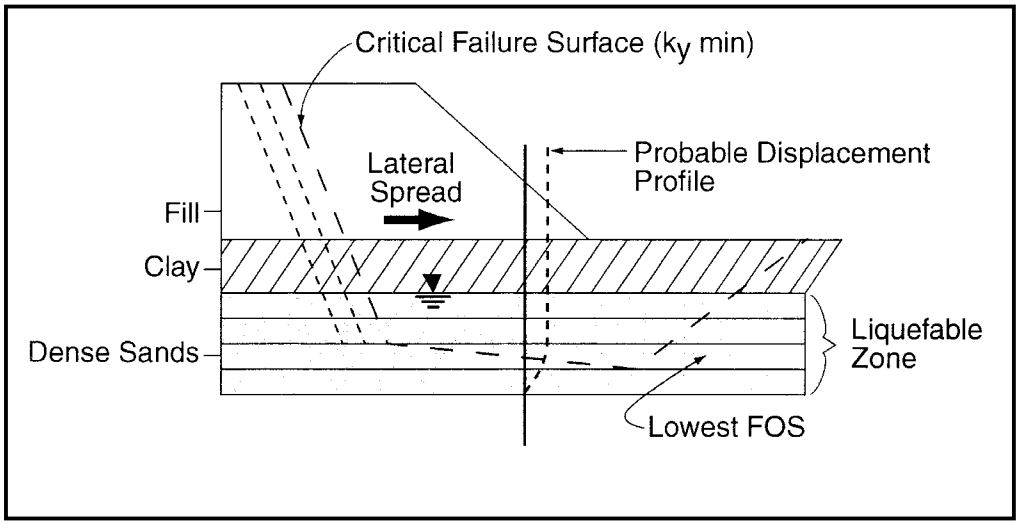

Figure 3 Newmark Sliding Block Analysis

RECOMMENDED LRFD GUIDELINES: LATERAL SPREAD DESIGN APPROACH

Initial design of pile foundations would normally be based on the LRFD design procedures for static loading. The determination of the liquefaction potential at a site follows the widely recognized simplified procedures based on SPT blowcounts or CPT data, as documented in Appendix D, of the recommended LRFD Guidelines. If liquefaction occurs, bridge inertial loading and associated foundation design is first checked for two conditions:

1. Nonliquefied configuration – use of appropriate spectrum for site soil conditions.
2. Liquefied configuration – softened pile-foundation stiffness in liquefied layer and same site soil spectrum is used unless special studies are undertaken.

If liquefaction-induced lateral flow or spreading of the ground is predicted during a seismic event, piles that would be loaded by the deforming ground need to be checked and possibly re-designed to withstand the loads from the moving soil. The recommended approach for evaluating this condition involves the following four basic steps:

1. Slope stability analyses are conducted to determine the minimum yield acceleration and the associated failure surface (normally associated with the deepest soil layer showing liquefaction potential). This step may include the pinning effects of the piles or the increased resistance of soil that has been improved by some type of ground improvement method.
2. Newmark sliding block analyses are performed to estimate displacements of the soil-pile system.
3. The passive force that can ultimately develop against a pile or foundation as soil movement occurs is estimated, and
4. The likely plastic mechanisms that may develop in the foundations and substructure due to lateral spread are evaluated.

It is assumed that the effects of ground displacement can be decoupled from the effects of structural inertial loading. In most cases, this is reasonable as peak vibration response is likely to occur in advance of maximum ground displacement, and displacement induced maximum moments and shear will generally occur at deeper depths than those from inertial loading.

The rationale behind the proposed method is to assess the ability of the structure to both accommodate this movement and/or potentially limit the movement. The concept of considering a plastic mechanism in the foundation under the action of spreading forces is tantamount to accepting substantial damage in the foundation. This is a departure from seismic design for vibration alone, as it is unlikely that the formation of a hinge mechanism in the foundation will lead to structure collapse. The reasoning behind this is that lateral spreading is essentially a displacement-controlled process. Thus the estimated soil displacement represents a limit on the structure displacement excluding the phenomenon of buckling of the piles or shafts below grade and the continued displacement that could be produced by large P-Δ effects. Buckling should be checked, and methods that include the soil residual resistance should be used. Meyersohn et al. [5] provide a method for checking buckling as an example.

The magnitudes of moment and shear induced in pile foundations by ground displacements may be computed using soil-pile interaction programs such as; LPILE (Wang and Reese [6]), where the assumed displacement field is applied to interface springs whose properties are represented by p-y curves. Examples of such analysis approaches are given by Jakura and Abghari [7], O'Rourke et al. [8], Soydemir et al., [9], and Ishihara and Cubrinovski [10]. In the liquefied zone, the soil is normally treated as a soft cohesive soil when calculating lateral spring characteristics (or p-y

curves), where the maximum soil cohesion is assumed equal to the undrained residual strength of liquefied soil. In some cases, large ground deformations may slide past the foundation system, exerting full passive pressures in the process. However, foundations may remain intact without failure in a state of limiting equilibrium, as in the case history reported by Berrill et al. [3].

The reinforcing or pinning effects the piles or pile group have on the lateral displacements may be considered by representing the pile shear forces at the location of the failure plane as an equivalent shear strength in the calculation of yield accelerations used in the Newmark analyses. This becomes an iterative approach as shear forces are a function of displacements which, in turn, are reduced as shear forces increase.

In the event that the pile foundations cannot accommodate the displacement demands, one option is to install additional foundation piles (using a pilecap overlay in a retrofit case) to increase the pinning action and, hence, reducing the displacement demands. Another option is the use passive piles driven through the liquefiable layer and failure surface, to provide additional pinning action without physically attaching to the bridge structure, often referred to as "pinch" piles. The former option is particularly relevant if additional piles are required because of retrofit needs to accommodate high overturning moments or to minimize down drag effects. Where additional piles are required, the costs of mitigation should be compared with the costs of ground remediation to reduce lateral spread displacements.

The framework of the simplified approach to the design problem using the above concepts and presented in the LRFD Guidelines, is outlined in the flow chart shown in Figure 4. The steps involved are described as follows:

Step 1: Identify the soil layers that are likely to liquefy

Step 2: Assign residual undrained strengths to layers that liquefy. Conduct pseudo-static seismic stability analyses to determine the minimum yield acceleration k_y. This defines the depths of soil likely to move and the extent of the likely-soil failure block. Impacts to a bridge structure can be by considering the proximity of the failure block to the foundation system. Static factor of safety FOS values < 1 (k=0) will define uncontrolled flow failures.

Step 3: Estimate the maximum lateral spread displacement of the soil (static FOS > 1). This may be accomplished using Newmark displacement charts (MCEER [4]) or a site-specific Newmark time history analysis.

Step 4: Assess whether the soil will continue to displace or flow around a stable foundation or whether movement of the foundation will occur in concert with the soil. This assessment requires a comparison between the estimated passive soil forces that can be exerted on the foundation and the ultimate structural resistances that can be developed by the structure. In cases where a crust of non-liquefied material may exist at the ground surface, the full structural resistance may be less than the displacement-induced passive forces and, in such cases, the foundation is likely to continue to move with the soil. In many cases, it may be immediately obvious which condition is more likely to occur. Schematic illustrations of the two cases are shown in Figure 5.

Step 5: If the soil continues to displace around a stable foundation, the foundation is designed to withstand the passive pressures created by the flowing soil. The induced forces are effectively the largest forces that the structure will experience and, for this reason, it is conservative to design a structure for such forces.

Step 6: If the assessment indicates that movement of the foundation is likely to occur in concert with the soil, then the structure must be evaluated for adequacy at the maximum expected displacement. The implication of this assessment is that for relatively large ground movements, soil displacements are likely to induce similar magnitude movements of the foundation. In this context,

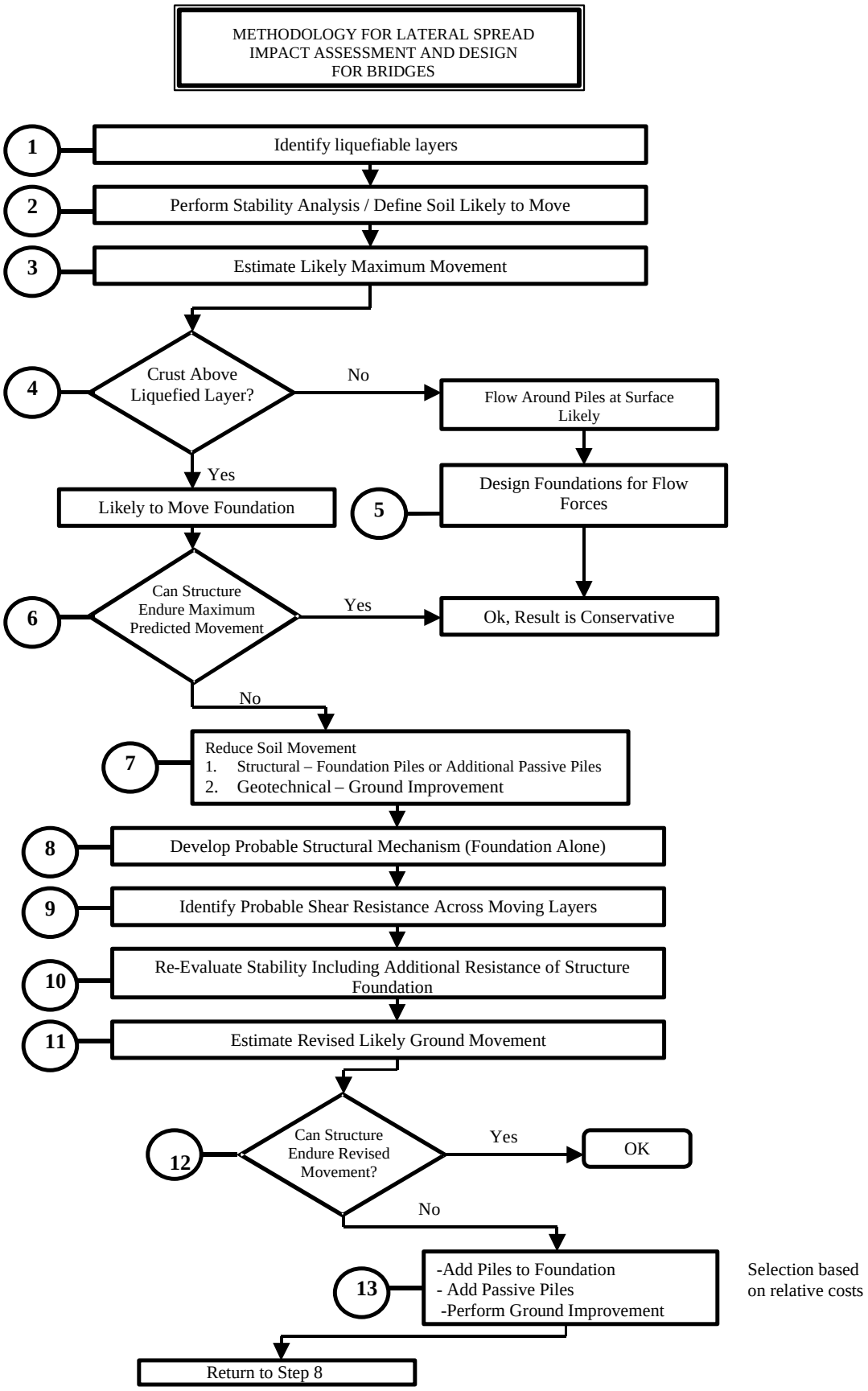

Figure 4 Lateral Spread Design Flow Chart (MCEER 2001)

"large" is taken relative to the structural yield resistance. The resulting induced movements of the foundations may produce substantial plasticity or hinge zones in the foundations, and may induce relatively large reactions in the superstructure. For an upper level event, a plastic rotation of 0.05 radians is the recommended acceptance criteria, although values determined by rational cross section analyses are also acceptable and preferred in many cases.

Step 7: If the deformations determined in Step 6 are not acceptable, two ways to restrict the foundation and substructure forces to values less than yield can be considered. The first method is to design or retrofit the foundations to resist the forces that would accompany passive flow of the soil around the foundations. The second method would be to limit the ground movement by providing either ground or structural remediation. It is the structural option that provides a potential first path, and this makes use of the "pinning" or dowel action that pile or shaft foundations contribute as they cross the potential failure plane of the moving soil mass. This can effectively reduce the magnitude of lateral displacement.

Step 8: Determine the plastic mechanism that is likely to occur in the presence of spreading. This should be done in a reasonable manner. Due to the range of inherent uncertainties, great precision in the determination may not produce more accuracy. Simple estimates of the mechanism and its corresponding lateral resistance capability may be adequate. Such estimates could be based on hinge development in stable or firm soil zones above and below (by say 2 pile diameters) the liquefiable layer. Maximum "pinning" shear could then be assumed equal to 2Mp/L, where Mp is the plastic moment and L *is* the distance between hinges -this assumes that the load transfer in the liquefied zone is negligible. The lateral shear that produces the plastic mechanism can be adjusted downward to account for the driving influence of the P-Δ effect. A more precise method of determining the plastic mechanism would be to use an approach that ensures compatibility of deformations between the soil and piles (e.g., one that is similar to LPILE) and which accounts for plastic deformations in the piles themselves (e.g., the program BSTRUCT by O'Rourke et al., [8]).

Step 9: Assess the system for a prescribed displacement field to represent the likely soil spreading deformation. From this analysis, an estimate of the likely shear resistance that the foundation will provide is determined, which can then be incorporated back into the stability analysis.

Step 10: If substantial resistance is provided, then its effect on limiting the instability driven movement of the soil block should be accounted for. This step is typically not included in current assessments of potential foundation movements, although inclusion of such resistance may often improve the structure's expected performance.

Step 11 and 12: Recalculate the overall displacement on the basis the revised resistance levels. Once a realistic displacement is calculated, the foundation and structural system can be assessed for this movement. It is at this point that more permissive displacements than those allowed for substructure design can be relied upon. This implies that plastic and potentially large rotations may be allowed to occur in the foundation under such conditions.

Step 13: If the structure's behavior is acceptable, then the liquefaction design is complete. If not, assess whether or not adequate behavior can be achieved by providing additional piles or shafts. Note that these may not need to connect to the foundation (passive piles) or the cap. Alternately, ground improvement approaches may be considered such as stone columns. The selection of structural or geotechnical methods is based on the relative economy of the system being used.

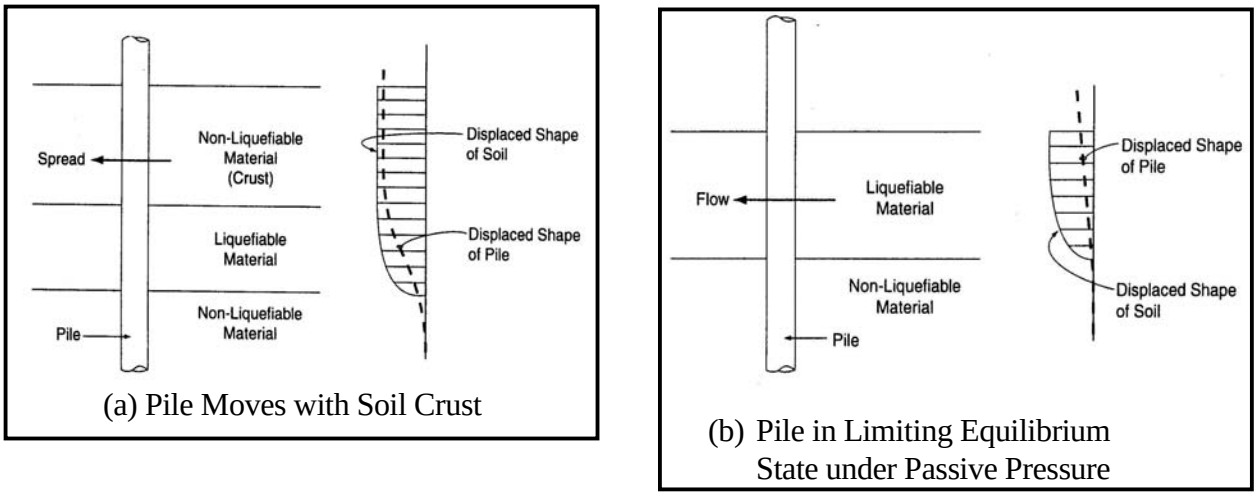

Figure 5 Pile Deformation Models

CASE STUDIES

The approach in the Recommended LRFD Guidelines was developed as part of the recent NCHRP 12-49 study to develop seismic design guidelines for highway bridges. During the course of the project, concerns were expressed that the adoption of the proposed "Maximum Considered Earthquake" (MCE) in contrast to the current AASHTO Division 1-A earthquake, could significantly increase the costs of mitigation of liquefaction induced lateral spreads. The MCE is defined as earthquake ground motions having a probability of exceedance of 3% in 75 years (2475 year return period), except that near highly active faults, MCE ground motions are deterministically bounded to lower values. The AASHTO Division 1-A earthquake ground motions have a probability of exceedance of 15% in 75 years (475 year return period).The two case studies described below were undertaken to evaluate the potential for significant cost increases if the recommended MCE was adopted.

West Coast Site-Washington

Figure 6 shows the simplified site soil profile of an actual Washington State Department of Transportation (WSDOT) bridge site used for analyses. Seismic hazard analyses of the site (assumed located near Olympia) generated a peak acceleration of 0.42g (site class E) for the proposed 2475 year return period and corresponds to a 6.5 mean magnitude event. For the 475 year return period in the existing AASHTO LRFD specification, a peak acceleration of 0.24 g corresponding to a magnitude 6.5 event was computed.

The 500 ft long box girder bridge structure is continuous between the overhanging stub abutments. The intermediate piers are two column bents supported on pile caps and concrete-filled 24 in. steel pipe piles, embedded in till at elevation -200 ft. Soils between elevations of 0 to -100ft comprise interlayered medium-dense sands and soft clays (shear strength 1000 psf). Stiff clays (shear strength 2000 psf) were assumed between elevations –100 to –200 ft.

Evaluations of liquefaction potential (step 1 of the design procedure) using the Seed Simplified Procedure (Youd and Idriss, [11]) for the 2475 year event, show liquefaction in all sands without overlying fill, and with overlying fill for layers at elevations –10 to –15 ft, –30 to –35 ft and – 45 to – 50 ft. For the 475 year event, liquefaction occurs in sands at elevations –30 to –35 ft and – 45 to –50 ft with overlying fill, but does not occur for sands below the fill.

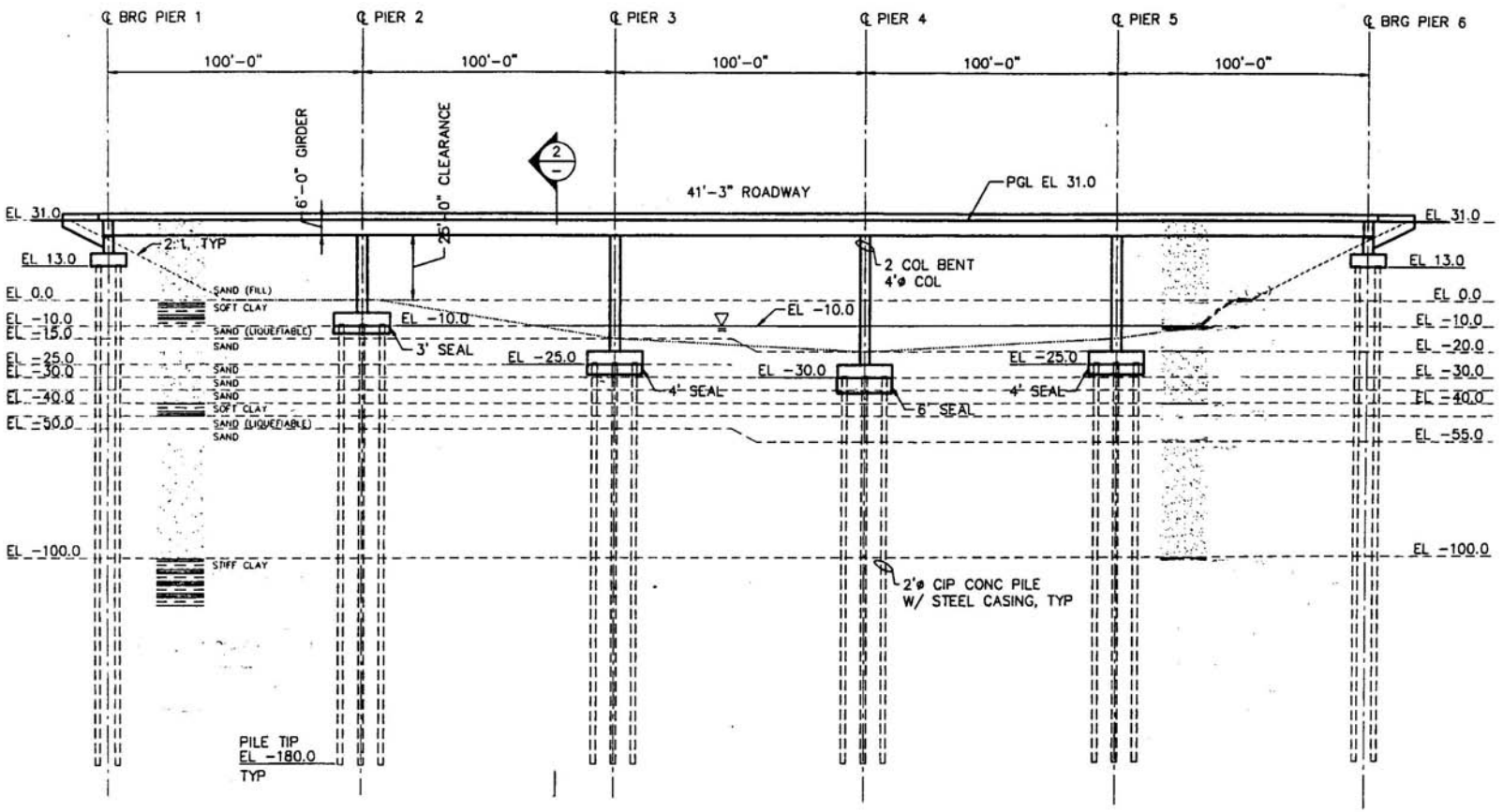

Figure 6 Site Profile and Structure Elevation, Washington Bridge

One dimensional nonlinear effective stress site response analyses were also conducted (using the program DESRA-MUSC (Qiu, [12]), to evaluate time histories of pore pressure increases and site liquefaction characteristics. Acceleration time histories were developed from records consistent with the hazard levels and site conditions, and modified to match design response spectra. The results were generally consistent with the above factor of safety calculations. However, a key conclusion from these studies was the strong likelihood that lateral spread deformations would be controlled by a failure zone in the layer at elevations of between –45 ft to –50 ft. In general, effective stress site response analyses show high post-liquefaction shear strains focus on the deepest layer susceptible to liquefaction.

Once liquefaction has been determined to occur, a post-liquefaction stability analysis is performed as indicated in Step 2 of the procedure. Pre-liquefaction analyses indicate static FOS values for embankment slopes were greater than 1.5. However, when post liquefaction residual undrained strengths of 300 psf were assigned to the sand layer at elevations –45 to –50 ft, FOS values dropped to a minimum of approximately 0.8 as shown in Figure 7, indicating the potential for an unconstrained flow failure. Both the deep (elev. –50 ft) and shallow (elev. -15 ft) flow failures were evaluated for the 475 and 2475 year events.

Given the large unconstrained lateral spreading, the next step (step 7) was to evaluate the beneficial pinning action of the pile foundations. The deep failure mechanism for lateral spread at the right abutment shown in Figure 8 is used as an example. Given the high passive pressure forces which could be generated by the embankment moving against the abutment and piles, it is clear in this case that limiting equilibrium associated with flow around foundations could not develop, and the foundation will move with the soil.

The maximum pinning forces that could be developed are now considered to see if they are sufficient to provide static slope stability. Figure 8 illustrates the pinning forces acting on a soil block sliding on the lower liquefiable layer. In this case, abutment and Pier 5 piles each contribute about 90 kips, the abutment about 400 kips (passive resistance provided by backfill acting against end diaphragm), and the columns at Pier 5 about 420 kips. The total abutment pile resistance is 1080 kips and corresponds to the approximate plastic mechanism shear with 30 ft between points of assumed fixity in piles. This comprises of 10 feet of liquefiable material and a conservatively assumed 5D versus 2D (D = pile diameter) to fixity above and below that layer. This conservatism allows for softening in adjacent layers. The upper portion of the soil block is assumed to move essentially as a rigid body, and therefore the piles are assumed to be restrained by the integrity of this upper block. The pile resistance at Pier 5 is determined in a similar manner, and the shear that the Pier 5 piles contribute is 1440 kips.

These forces (3360 kips total) represent maximum values that occur only after significant plasticity develops. In the case of Pier 5, the approximate displacement limit is 22 ins., which comprises 4 inches to yield and 18 inches of plastic drift. The plastic drift limit is taken as 0.05 radians, which is reasonable for well detailed ductile piles. Because the piles of Pier 6 are the same, their limits are also 22 ins. of displacement.

The total 3360 kip resistance calculated above, represents 70 kips/ ft width, and was introduced into the slope stability analysis as an equivalent shear strength (530 psf) along the shear plane in the liquefied zone. This was sufficient to increase the FOS to greater than 1.0, hence negating the potential flow failure. Similar pinning analyses for the upper failure surface led to a FOS of 1.0 indicating a potential flow failure was still a problem. For the lower surface, the lateral spread displacement due to inertial forces remains to be evaluated (step 3), by calculating a yield

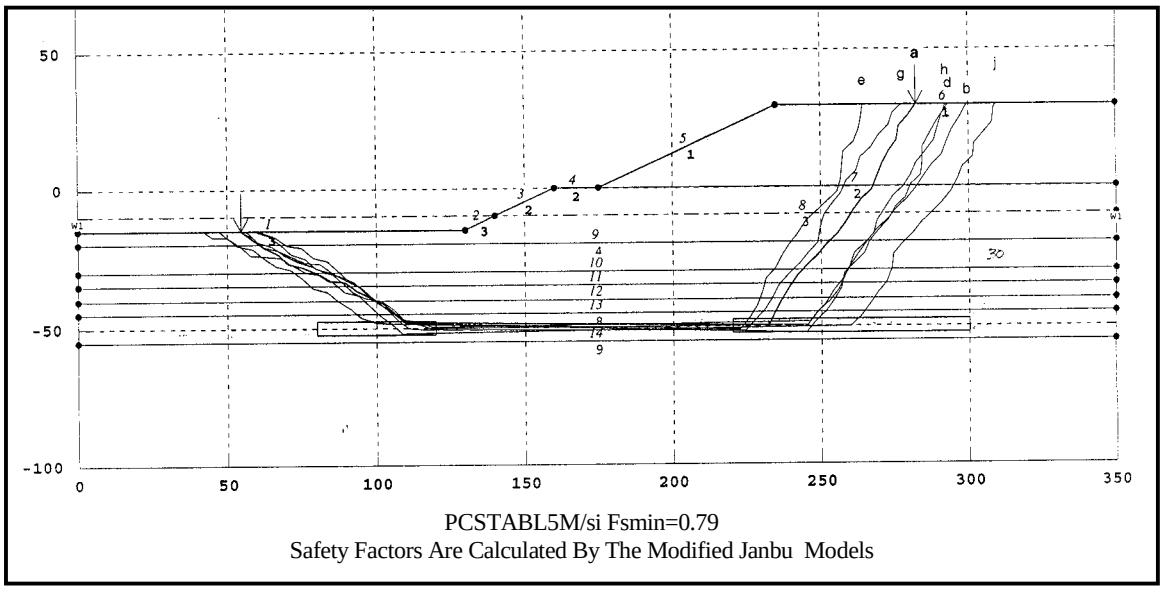

Figure 7 Typical Sliding Mechanism for Flow Failure

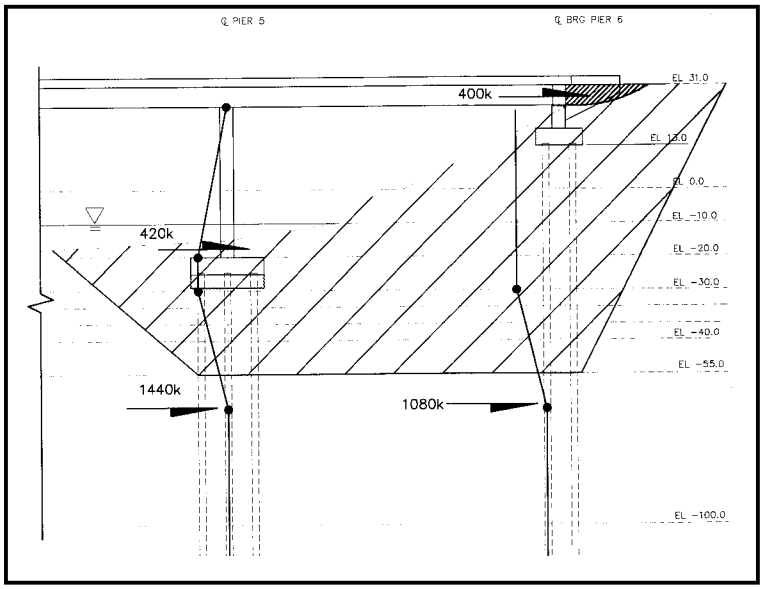

Figure 8 Forces Provided by Bridge and Foundation Piles for Resisting Lateral Spreading

acceleration and estimating resulting lateral displacements using available charts based on the Newmark sliding block method. For the calculated yield acceleration of 0.02g, a displacement of about 22 ins. results for the 475 year event and 36 inches for the 2475 year event. The 22 in. displacement is within the plastic capacity of the piles, whereas for the 2475 year event, either additional "pinch" piles could be added or ground remediation considered. For the latter case, assuming the installation of a 30 ft wide stone column toe buttress extending through the liquefied zones to an elevation of –55 ft, leads to a yield acceleration of 0.12g and estimated lateral displacements of less than 5 ins. for the 475 year event and 8 ins. for the 2475 year event. For the upper failure surface, stone column remediation would be required to a depth of about 30 ft. to prevent shallow flow failures. For this case history, remedial work is required for both the 475 and 2475 year events. The stone column option over a 30 ft length appears a reasonable option, and would cost about $120,000 for both sides or about 4% of the likely bridge cost.

Mid America Site – Missouri

The second bridge site considered in the study was located in the New Madrid earthquake source zone in southeast Missouri. Figure 9 shows the simplified site soil profile and bridge structure provided by the Missouri Department of Transportation (MODOT). Based on site hazard analyses, a peak ground acceleration of 0.53g corresponding to a M7.5 earthquake was adopted for the 2475 year event and 0.17g, corresponding to a M 6.6 earthquake, for the mean 475 year event

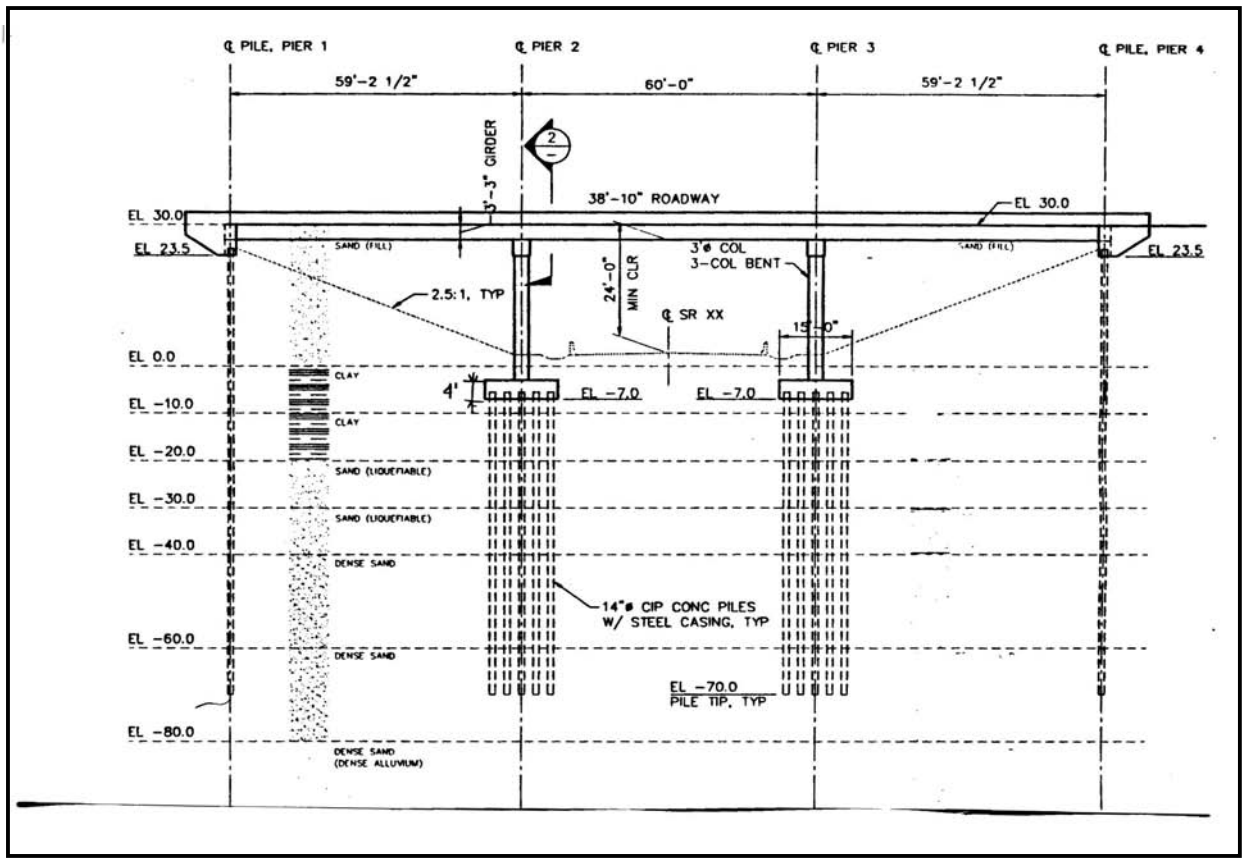

Figure 9 Elevation and Ground Profile for the Mid-America Bridge

The bridge is a three span structure comprised of AASHTO prestressed girders supported on three column bents. The pile caps for each column are supported on 14 inch diameter steel pipe piles. Integral end diaphragm abutments are supported by nine 14 in. diameter pipe piles.

Evaluations of liquefaction potential using the Seed Simplified Procedure show that liquefaction will occur in the sand layer between elevations –20 to –40 ft for the 2475 year event but will not occur for the 475 year event unless higher magnitude events of 7.0 to 7.5 are assumed. Post liquefaction static stability analyses where undrained shear strengths of 300 psf were assigned to the liquefied soil layers, indicated FOS values greater than 1.0, negating the potential for flow slides. Yield accelerations without consideration of pile pinning effects were estimated as 0.02g for a deep seated lateral spread failure seated at elevation –40 ft. Resulting lateral displacements based on the Newmark sliding block method, were about 30 ins. for the 2475 year event and 8 in. for the 475 year event (if liquefaction occurred). For the 2475 year event, mitigation involving utilization of pile or ground improvement need consideration.

In a similar manner to that described for the Washington Bridge, maximum shear forces associated with plastic hinge development in the piles were computed. For a deep soil wedge involving abutment piles and Pier 3, and assuming 32 ft. between hinge locations, a maximum shear force resisting lateral movement of 1372 kips develops and corresponds to 18 ins. of displacement for 0.05 radians of plastic drift at pile hinges. This resisting force when added to the stability analysis, increased the yield acceleration to 0.10g and reduced the corresponding displacement estimate to about 5 ins., which would be acceptable. Hence, no mitigation at this site would be necessary if pile pinning effects are accounted for.

CONCLUSIONS

The approach for assessing the impact of liquefaction-induced lateral spreads on bridge foundation design in the Recommended LFRD Guidelines, provides a systematic and practical methodology to a complex problem. The beneficial effects of considering the resistance that the bridge substructure offers to lateral displacements of soil via a “pinning” action can be significant and should be considered in predictions of lateral soil movements. In addition, the benefit of allowing inelastic behavior of pile foundations under the action of lateral ground spread, is that relatively large displacements of the ground may be accommodated by the structure without collapse. If pile foundations cannot tolerate the predicted displacements (including pile pinning effects), then either structural or ground improvement remediation options should be used.

For the two case studies considered, cost impacts for 475 versus 2475 earthquake events were evaluated. In the case of the Washington State Bridge, ground remediation was considered necessary for both events, with a cost estimate of roughly 4% of the bridge cost. For the Mid-America Bridge, the beneficial effects of pile pinning led to the conclusion that a foundation design for the 475 year event would perform satisfactorily for the 2475 year event.

The results from this study do not necessarily mean that changing from a 475-year return period to a 2474-year return period will have minimal-to-no effect on bridge design for liquefiable sites in every case. The change in design return period will result in some sites having to consider the potential for liquefaction, where liquefaction may not have been an issue with the 475-year return period by virtue of the large areas being affected or deeper liquefiable layers. However, by following the methods described in the recommended approach, it will often be found that the beneficial effects from pile pinning will significantly reduce or eliminate the consequences of liquefaction under the recommended provisions. Where liquefaction-induced spreads are found to

be an issue, the recommended approach provides a simple method for optimizing the method of mitigation. This recommended approach involves the use of simple computational methods available to every geotechnical and bridge engineer. The results are also intuitively reasonable, allowing the designer to do a "reality check."

ACKNOWLEDGMENTS

The studies described in this paper formed part of the National Cooperative Highway Research Program Sponsored Project 12-49, to develop a new set of seismic design provisions for highway bridges comparable with the AASHTO LRFD Specifications. The project was conducted by a joint venture of the Applied Technology Council and the Multidisciplinary Center for Earthquake Engineering Research, Buffalo. The bridge and geotechnical groups at the Washington State and Missouri Departments of Transportation provided valuable support to this effort through the identification of site conditions and bridge types. This support was appreciated.

REFERENCES

[1] Youd, T.L. 1993. "Liquefaction-Induced Damage to Bridges," Transportation Research Record No. 14311, National Research Council, *National Academy Press*, Washington, D.C. 35-41.

[2] Tokimatsu, K. and Asaka, Y. 1998. "Effects of Liquefaction-Induced Ground Displacements on Pile Performance in the 1995 Hyogoken-Nambu Earthquke," *Special Issue of Soils and Foundation*, pp. 163-177

[3] Berrill, J.B., Christensen, S.A., Keenan, R.J., Okada, W. and Pettinga, J.R. 1997. "Lateral-spreading Loads on a Piled Bridge Foundation," *Seismic Behavior of Ground and Geotechnical Structures, Proc. Special Technical Session on Earthquake Engineering*, 14th ICSMFE, A.AA. Balkema, Rotterdam, 173-183.

[4] Multidisciplinary Center for Earthquake Engineering Research (MCEER), Report on "Recommended LRFD Guidelines for the Seismic Design of Highway Bridges," Part I: Specifications, Part II: Commentary and Appendices, April 9, 2001.

[5] Meyersohn, W.D., O'Rourke, T.D., and Miura, F. 1994. 'Lateral Spread Effects on Reinforced Concrete Pile Foundations, *Fifth U.S.-Japan Workshop on Earthquake Disaster Prevention for Lifeline Systems*, Tsukuba, Japan.

[6] Wang, S.T. and Reese, L.C. 1998. "Designing Pile Foundations in Liquefied Soils," *Geotechnical Earthquake Engineering and Soils Dynamics III*, ASCE Geotechnical Special Publication, No. 75, Vol. 2, pp. 1331-1343. (Code documentation – LPILE Plus Version 4.0m, ENSOFT Inc., Austin, Tx)

[7] Jackura, K.A. and Abghari, A. 1994. "Mitigation of Liquefaction Hazards at Three California Bridge Sites," *Proc. 5th U.S.-Japan Workshop on Earthquake Resistant Design of Lifeline Facilities and Countermeasures Against Soil Liquefaction*, Technical Report NCEER-94-0026, NCEER, Buffalo, N.Y., 195-513.

[8] O'Rourke, T.D., Meyersohn, W.D., Shiba, Y. and Chaudhuri, D. 1994. "Evaluation of Pile Response to Liquefaction-Induced Lateral Spread," Proc. *5th U.S.-Japan Workshop on Earthquake Resistant Design of Lifeline Facilities and Countermeasures Against Soil Liquefaction*, Technical Report NCEER-94-0026, NCEER, Buffalo, N.Y., 457-478.

[9] Soydemir, C., Zoli, T., Le Plant, K., Kramer, S., Davidson, W. and McCabe, R. 1997. "Seismic Design of Central Artery Bridges Across Charles River in Boston: Geotechnical/Substructure Aspects," *Proc. 2nd Nat. Seismic Conference on Bridges and Highways*, FHWA/Caltran, Sacramento, CA., pp 1235-1246.

[10] Ishihara, K. and Cubrinovski, M. 1998. "Problems Associated with Liquefaction and Lateral Spreading During Earthquake," *Geotechnical Earthquake Engineering and Soil Dynamic III*, ASCE Geotechnical Special Publication, No 75, Vol. 1, pp. 301-312.

[11] Youd, T.L. and Idriss, I.M 1997. *Proceedings of the NCEER Workshop on Evaluation of Liquefaction Resistance of Soils*, National Center for Earthquake Engineering Research, Technical Report NCEER-97-0022, December, 276p.

[12] Qiu, Ping 1997. "Earthquake Induced Nonlinear Ground Deformation Analyses," Ph.D. Thesis, Department of Civil Engineering, University of Southern California.

Application of the New LRFD Guidelines for the Seismic Design of Highway Bridges

Derrell A. Manceaux, P.E.

ABSTRACT

In July 1996 the National Highway Institute presented Course No. 13063, titled "Seismic Design of Highway Bridges". This course provided step-by-step guidelines for the seismic design and analysis of bridges using the AASHTO, Division IA design specifications. In conjunction with the course, seven seismic design examples of common bridges were published.

Recently, new "Recommended LRFD Guidelines for the Seismic Design of Highway Bridges" have been developed based on NCHRP Project 12-49, FY '98. Since the new Guide Specifications differ significantly from the AASHTO, Division IA Specifications, an example illustrating use of the new Guide Specifications will help bridge engineers learn the new guidelines more quickly.

This paper will utilize Design Example #1 from the set of design examples previously published and apply the new seismic guidelines to the example. It will provide a discussion on the designers' perspective on using of the new LRFD Guide specifications by comparing a structure designed with both specifications. Since the design examples have been widely distributed and used by many practicing bridge engineers, this comparison may help designers to understand the application of the new methods along with any resulting differences from the previous method, Division IA-Seismic Design, for the example selected.

Derrell Manceaux, Special Projects Engineer, FHWA-Federal Lands Highway Division, 555 Zang Street, Room 259, Lakewood, CO 80228

INTRODUCTION

The advancement of bridge specifications for seismic analysis and design has been evolving over the past forty years. During the early sixties, the AASHTO requirements for an earthquake load applied to a structure was calculated by a single equation involving the structure dead load modified with a foundation coefficient. The force generated was small and did not represent the true seismic forces applied to a structure. During the mid seventies, the seismic code evolved considerably. While the seismic force was still calculated from one single equation, this equation accounted for important seismic items such as ground acceleration, soil properties, and different coefficients to adjust the force based on the importance of the component being considered.

During the early nineties, Division IA of the AASHTO Specifications (Division IA) was adopted for seismic design. This specification provided significant improvement on the application of seismic loads, analysis requirements and design methods of important structural components. The focus of the code was to require seismic loads to be carried in a ductile or elastic manner and to prevent brittle failures.

Since the adoption of Division IA over ten years ago, it is felt that revised provisions could better capture the latest knowledge gained. Recent earthquakes and research programs conducted have helped gain this new experience.

The latest advancement of seismic specifications is the "Recommended LRFD Guidelines for the Seismic Design of Highway Bridges" (LRFD Guide), which are based on NCHRP Project 12-49, FY '98 [1]. The LRFD Guide focuses on design philosophy and performance criteria, seismic hazard representations, loads and displacements, site effects, advances in analysis, modeling procedures, and new requirements for design and detailing.

The LRFD Guide requires that designers recognize paths for seismic loads. It requires a predetermined structural behavior be established so damage or failure will be predictable. It also requires owners be notified if any assumption is made that would permit significant damage to occur in inaccessible locations. However, although many formulas are very different from Division IA, certain analysis and design methods are unchanged in moderate seismic regions from the previous specifications. The LRFD Guide provides increased guidance to ensure that no element in a structure carrying a seismic load is overlooked. The new LRFD Guide has made a significant improvement over the previous specifications, including Division IA.

This paper discusses the application of the new LRFD Guide to a structure that was previously designed under Division IA. It discusses the designers' perspective on the use of the LRFD Guide and it explains major differences noted between the two specifications.

The reader may obtain a copy of this paper and of the design calculations used for this document at the web site: http://www.cflhd.gov/sdhb/

OVERVIEW OF STRUCTURE

The structure being studied is the same structure as in the "Seismic Design of Bridges Design Example No. 1-Two Span Continuous CIP Concrete Box Bridge" [2]. The structure

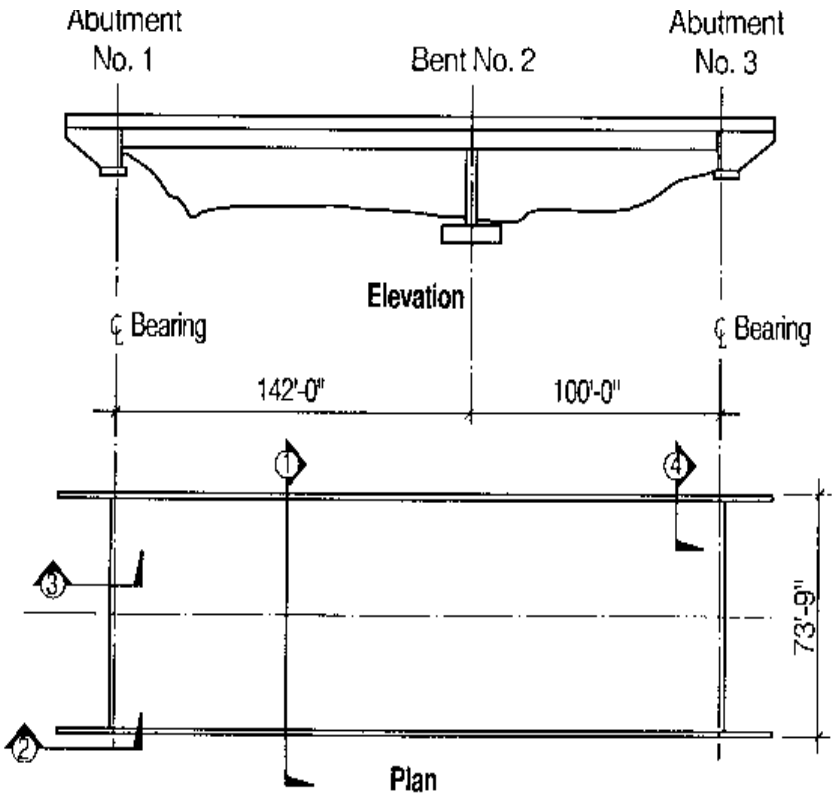

Figure 1. Plan and Elevation

consists of a two span, cast-in-place concrete box girder. [Figure 1] The pier is a three column, integral bent and the abutment is a seat-type, stub base. The structure is founded on spread footings with a “fixed” base.

The abutments are assumed to provide restraint in the transverse direction. Since a six-inch expansion joint exists at the abutment, longitudinal restraint is not considered at the abutments. The superstructure is assumed to allow free rotation about a vertical axis at each of the abutments.

Due to cracking and possible plastic hinging in the pier columns, it is felt that the cracked section properties should be used to obtain more realistic results. However, in order to allow the results to be comparable to the original design, the same gross section properties for the column are used as in the benchmark design example.

PROCEDURE

Under Division IA, preliminary data required before any seismic design is started includes the ground acceleration (A), importance of the structure (I), and soil characteristics (S). With this information, the designer is able to build a response spectrum, obtain the Seismic Performance Category (SPC) of the structure, and determine the minimum analysis procedures required.

Preliminary data required under the new LRFD Guide is similar. Ground accelerations are required. The Performance Level (Life Safety or Operational) of the structure and soil information is required. Similarly, this information is used to generate a response spectrum, to determine a Seismic Hazard Level (SHL), to find the Seismic Design Requirements (SDR) and to find the Seismic Design and Analysis Procedure (SDAP).

The SDR is one of six categories of minimum detailing requirements based on the seismic hazard level and performance objective. The SDAP is one of five procedures defined for conducting seismic design and analysis. The SDAP is based on the seismic hazard level, performance objective, structural configuration, and the type of defined load path for the seismic forces.

Design and Analysis Requirements

Division IA requires initial data for the design example. The minimum ground acceleration is 0.28g. The Importance Classification (IC) of this bridge is taken to be II. It is assumed not to be essential for use following an earthquake. From this information, the Seismic Performance Category (SPC) is determined to be "C". The minimum analysis method for this structure is a single mode, or a uniform load analysis. Higher levels of analysis may be utilized. The soil profile for this location is Type II, deep cohesionless soil, which requires the Site Coefficient (S) to be 1.2. Calculations from these values provide a response spectrum with a maximum acceleration of the structure equal to 0.7g [Figure 2].

The LRFD Guide requires four ground accelerations to generate the response spectrum shown [Figure 2]. These will be used to generate two response spectrum curves, a Maximum Considered Earthquake (MCE) and a frequent design earthquake. The Performance Level of the bridge is assumed to be Life Safety. The soil profile for this location has a Site Class of "D". This is a stiff soil. From this information the Seismic Hazard Level is determined to be IV, the highest value available. For this Hazard Level, the Life Safety Seismic Design and Analysis Procedures (SDAP) is determined to be "C/D/E" and the Seismic Design Requirements (SDR) is found to be "4". For the SDAP of "C/D/E", class "C" may not be used since transverse restraint is required at the abutments. The simpler method, Class "C", only requires a design for non-seismic loads and a manual check for deflections with seismic loads. Class "D" requires a Uniform Load or Multimode analysis. This example will use a multimode analysis. Calculations from the initial data provide a response spectrum with a maximum spectrum acceleration of the structure equal to 0.975g for the MCE and a maximum spectrum acceleration of 0.264g for the frequent earthquake [See Figure 2]. After plotting the different response spectra, the reader can observe that even though the accelerations are different, the actual shapes are all similar. For this reason, there is little difference required in design effort from the engineer.

Following determination of Response Modification Factors (R), in order for the designer to have an approximate idea of the controlling spectrum, the LRFD Guide suggests dividing each response spectrum by the R factor [Figure 3]. For this example, the MCE acceleration controls over the Division IA spectrum and the frequent earthquake spectrum. The designer should not use the modified response spectrum to determine seismic forces on the structure. This is only a guide to determine the controlling spectrum.

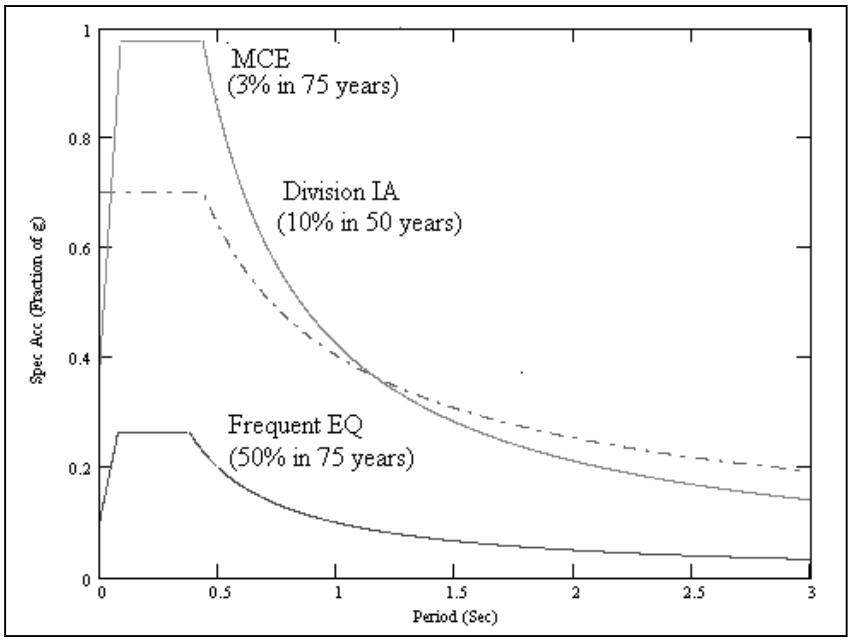

Figure 2. Design Response Spectrum

Seismic Load Path

Unlike the Division IA specifications, the LRFD Guide has criteria that requires the designer to define a load path to carry the inertial forces from the superstructure into the substructure and through the foundations.

The inertial loads in the transverse direction that originate from the superstructure are carried into the integral pier cap beam and abutment diaphragms by the rigid deck. The forces are then transferred into the shear key at each end of the abutment. The integral pier cap provides transverse restraint, as the forces are transferred into the pier cap. Once the load is in either of the substructure units, it is carried into the footings and dissipates into the soil.

The inertial loads in the longitudinal direction that originate from the superstructure are carried into the integral pier cap beam by the rigid deck. The forces are then transferred into the columns and into the footing only at the pier. The stresses dissipate into the soil through the footings. Since the expansion joint at the abutments is assumed and verified not to close, soil behind the endwall cannot help carry any longitudinal force.

Stiffness and Strength

Division IA does not provide guidance on modifying substructure properties to account for cracked sections due to high seismic activity. This subject is discussed in the LRFD Guide. Based on the LRFD Guide, cracked sections should be used for analysis in this example.

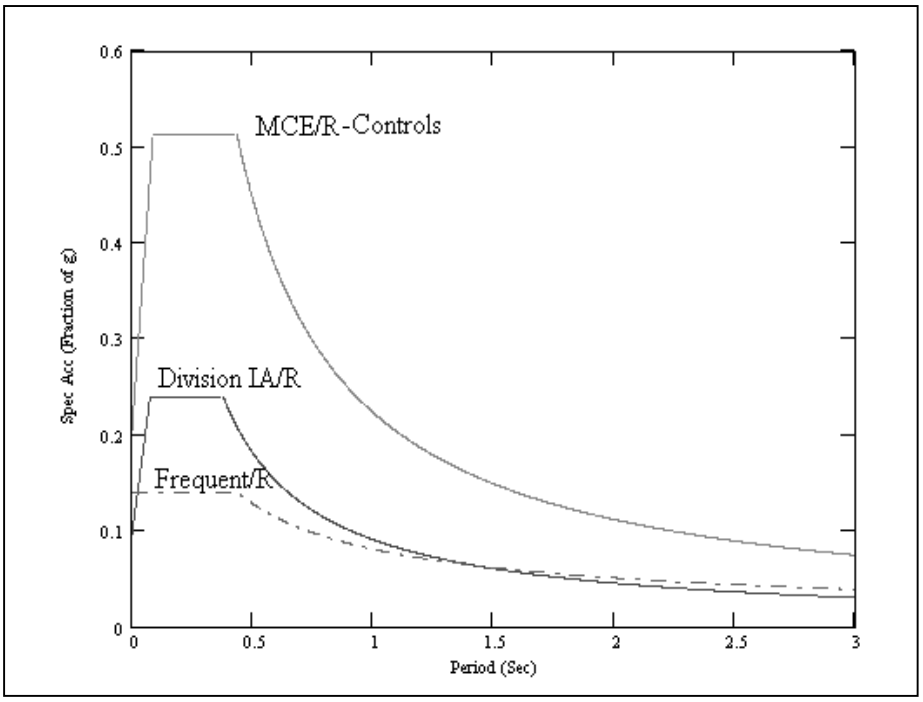

Figure 3. Controlling Response Spectrum

The reader should note that the analysis in Division IA should have also utilized cracked section properties since large deflections do occur. In order to provide results that are comparable to the original example, the same section properties, I_{gross}, will be used for the substructure. Any differences that occur will be comparable and will not affect the results of this comparison.

Foundations Support

The LRFD Guide has requirements to indicate when foundation springs should be used. It is felt that this section of the LRFD Guide is helpful. However, extra tedious work is required to determine if the foundation springs are needed. For this example, since springs were utilized in the original design example as a comparison to a fixed base, the difference in deflection does not contribute more than 20% difference and springs can be neglected as suggested by the LRFD Guide.

Response Modification Factors

Division IA recognizes that a properly detailed structure can displace “R” times the yield displacement. For this reason, it permits use of a Response Modification Factor (R) of 5 be used for multi-column bents to account for ductility in the substructure.

The LRFD Guide also permits the use of a Response Modification Factor (R). However, the LRFD Guide realizes that the stiffness of a structure is dependant on the natural period. For this reason, the natural period is used in calculate the “R” factor by modifying a base “R” factor.

When performing the calculations for "R", the designer must be aware that the shortest period of the structure (stiff direction) should be used. The Base Response Modification Factor (R_B) is 4 for a multi- column bent. However, when modified to account for structure stiffness, the "R" value for the MCE is found to be 1.9 (See Equation 1). The "R" value for the frequent earthquake is 1.1.

$$R: = 1 + (R_B - 1)\ \frac{T}{1.25T_s} \quad R_B \tag{1}$$

R_B is the base response modification factor, T is the short period of the structure, and T_S is the period at the end of constant design spectral acceleration plateau.

The difference in the Response Modification Factors is significant from Division IA. Since each code permits certain elastic forces to be divided by the Ductility Factor, "R", to determine the design forces, these factors significantly affects the final design of this structure.

Multimode Analysis-Pier Design Forces

Following a multimode analysis, the controlling moments are plotted in Figure 4. They are compared to the results from the original design. The earthquake moments shown are reduced with the Response Modification Factors, R, and corresponding dead load moments are added to the results. These moments include the separate load cases to account for the uncertainty of the earthquake direction. In addition to an earthquake being applied in one direction, Division IA requires an additional 30% applied to an earthquake in the transverse. The LRFD Guide has similar requirements, but has increased the additional transverse load to 40%.

The strength reduction factor, phi, is approximately 0.6 with Division IA. The LRFD Guide permits use of a phi value of one. These have also been in included in the results shown in Figure 4.

The reader should note that since the "R" value for the MCE earthquake is less than used in Division IA, the moments fall outside the allowable moment interaction diagram and the structure is considered over stressed. The pier columns require redesign. Figure 5 shows a moment interaction diagram for the redesigned of the column. The new column requires forty five #11 bars (3.9%). This doubles the reinforcing steel shown in the original design if the same cross section is maintained. The amount of reinforcing is excessive and a new column dimension should be considered. The LRFD Guide restricts the maximum longitudinal steel to 4%. However, in order to provide a continued comparison to the original design, the same column dimensions will be maintained.

Column Shear and Transverse Reinforcement

For a Seismic Hazard Level of IV, the LRFD Guide requires an Explicit Approach to designing transverse reinforcing. This is Method 2 in the LRFD Guide. The method at first appears laborious, however, after reading the requirements, it is realized that the method is the same as that which should be used in Division IA to calculate the shear forces.

This method requires that shear which will occur due to plastic hinging in the piers be accounted for in the design. The plastic moment forces are increased by an over strength factor of 1.5 to account for unanticipated strength gains that may not be anticipated in the design. This is an increase from the over strength factor in Division IA of 1.3

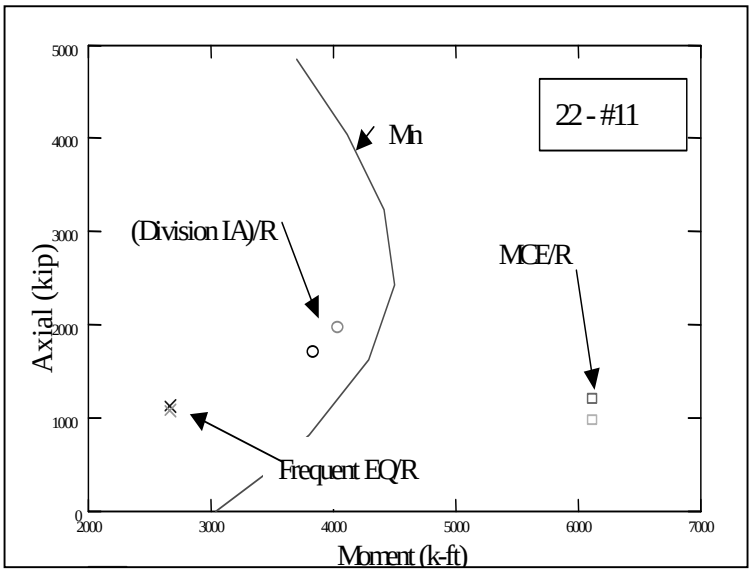

Figure 4.Controlling Moments -Original Design

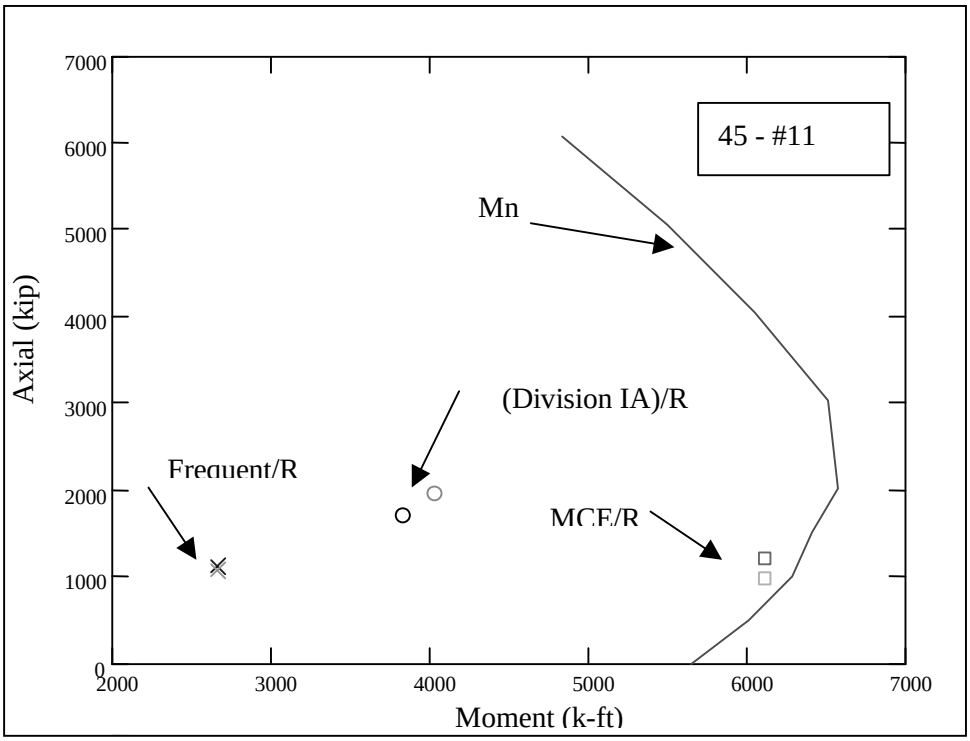

Figure 5. Controlling Moments-Redesign

The resulting plastic shear from the corresponding plastic moments can be calculated by hand since the structure is determinate. If a redesign of the pier had not been required, the plastic shears would have been similar to the original design. However, since the redesigned column has significant increase in strength, the corresponding shears also increased. This increase of shear requirement must be considered

The original design required a #5 spiral with a pitch of 3.5 inches in the end zones to confine the concrete. However, the controlling calculations from the LRFD Guide requires a #5 spiral with a pitch of one inch in the end regions. This pitch appears unreasonable, but the reader should remember that the column cross section was not modified to maintain uniformity in the design comparison. If the column had been proportioned differently to maintain approximately 2% longitudinal reinforcing for the design for moments, the concrete shear capacity would have increased and the shear requirement for reinforcing steel would have relaxed.

Reinforcing for the shear requirements in the LRFD Guide has change considerably from Division IA. The new procedure requires several very tedious calculations. With experience, it is hoped that a trend for the controlling spiral calculations will be observed. This should help reduce the design effort required in calculating the reinforcing for shear.

Minimum Seat Width Requirements

Similar to Division IA, minimum seat width requirements exist. The calculations are very similar to each other. Division IA requires a seat width of 1.9 feet. This should be compared to a requirement of 2.3 feet with the LRFD Guide.

Other Considerations

This paper has covered several of the major aspects of comparing a design performed with the new LRFD Guide and one performed with the current Division IA specifications. There are many additional considerations that should not be overlooked in completing the seismic design.

Since the structure utilizes transverse restraint at the abutment, a shear key must be designed. This key must not be permitted to fail since it is defined in the load-carrying path. The plastic moments and shears should be applied to the footings to obtain foundation pressures. This is the same requirement as Division IA. The designer should be aware that the “no splice” locations be observed. Splice lengths and development length requirements should be followed.

Also, this example only utilized a small portion of the LRFD Guide. There are other significant differences between the two codes that are not required for this example but should be addressed in other projects. Some of these differences include liquefiable soils, battered piles, soil springs, and the design of the superstructure to account for plastic moments occurring in the substructure connections.

CONCLUSION

In conclusion, two major considerations should be addressed concerning the comparison of the new LRFD Guide to Division IA. The first is how the LRFD Guide affects the actual

design of the structure. The second is the amount of effort required to perform the engineering calculations that the LRFD Guide requires.

Structural Requirements

The structural design requirements for the design example are larger than the original design using Division IA. Since the Base Response Modification Factors are modified by formulas using the shortest primary structural period, the "R" values return low values and the elastic moments do not reduce as expected for a ductile, and redundant pier for this particular example. Since the "R" values are low, the elastic forces do not reduce significantly and additional longitudinal reinforcing steel must be placed in the columns. In addition, the shear requirements increased since the plastic capacity of the column increases.

Since the capacity for the columns are greater than the capacity in the original design, all components that are required to be design as a function of the plastic moments of the substructure will also be modified to carry this increased demand.

The LRFD Guide requires that if lateral restraint is utilized at the abutments for the frequent earthquake, then this restraint must be removed for the MCE. However, since the structure is a two-span, the pier cannot be permitted to carry a torsion mode and the transverse restraint is defined in the primary load-carrying path. Since the transverse restraint is required, SDAP "C" could not be utilized and the next higher category, "D", was required.

A comparison of results is shown in Table I. This table tabulates the Division IA requirements to the corresponding LRFD Guide requirements for the seismic design of the structure discussed. A copy of this paper and all design calculations used for this document may be obtained at the web site: http://www.cflhd.gov/sdhb/

Engineering Effort

Following the comparative design using each of the two seismic specifications, there are new formulas used in the LRFD Guide that are not in Division IA. These formulas have been revised based on experience learned from recent earthquakes and from current research.

Table I. Comparison of Results

Item	Division IA	LRFD Guide	
	Design EQ	MCE	Frequent EQ
Maximum Spectrum Acc. Coefficient	0.70 g	0.97g	0.26g
Seismic Performance Category	C	-	-
Seismic Hazard Level	-	IV	IV
Seismic Design & Analysis Procedure	-	C/D/E	C/D/E
Seismic Design Requirements	-	4	4
Importance Classification	II (Other)	-	-
Performance Level	-	Life Safety	Life Safety
Site Effects	II (S=1.2)	-	-
Site Classification	-	D	D
Vertical Acceleration	Neglect	Neglect	Neglect
Response Modification Factor (R)	5	R_B=4 (column)	R_B=1.3
	-	R=1.9	R=1.1
Design Moment/phi (k-ft)	4000	6100	2800
Plastic-Design Shear (kip)	426	769	-

The formulas return differing results than before, however, once the designer becomes familiar with the different requirements, there is little additional effort required from the designer to utilize many of the formulas.

The LRFD Guide also requires two levels of earthquakes be considered, a Maximum Considered Earthquake (MCE) and a frequent earthquake. Since two different earthquakes must be considered, this requires additional effort from the designer. However, the intent of this new requirement should help produce structures that remain serviceable during a frequent earthquake event and perform as required by the LRFD Guide during a MCE. This new requirement is a significant improvement over Division IA.

The most significant difference observed between the two specifications is that the LRFD Guide offers much more guidance than Division IA. This guidance will help designers recognize proper seismic design methods and find answers to many questions that have occurred with Division IA. The LRFD Guide will help produce designs across the country that should be much more uniform than previous seismic codes has ever offered.

ACKNOWLEDGEMENTS

The writer would like to acknowledge Myint Lwin, Structural Design Engineer, from the FHWA Western Resource Center and Bonnie Klamerus, Structural Engineer, from the FHWA Central Federal Lands Highway Division for helping review the documents and offer advice in the preparation of this paper.

REFERENCES

[1] “Recommended LRFD Guidelines for the Seismic Design of Highway Bridges” based on NCHRP Project 12-49, FY ’98, “Comprehensive Specifications for the Seismic Design of Bridges” by ATC/MCEER Joint Venture
[2] R. Mast, L. Marsh, C. Spry, S. Johnson, R. Griebenow, J. Guarre, and W. Wilson. 1996. “Seismic Design of Bridges Design Example No. 1”, Publication No. FHWA-SA-97-006

Cost Impact Study for a Typical Highway Bridge Using Different Return Period Seismic Design Maps

Jeffrey Ger[1], and David Straatmann[2], Suresh Patel [3], and Shyam Gupta[4]

ABSTRACT

This paper compares the costs of a typical three-span P/S I-girder bridge designed for seismic categories A, B, C, and D based on the current 1996 AASHTO Standard Specifications for Highway Bridges for a 500-year return period earthquake (i.e. 10% probability of exceedance in 50 years) as well as for different spectral response accelerations specified in the current USGS map (1997 NEHRP Provisions) for a 2500-year return period earthquake (i.e. 2% PE in 50 years) which is being considered for future AASHTO Seismic Design Guidelines for Highway Bridges. For both 500-year and 2500-year design earthquakes, the mitigation of potential ground spreading due to abutment slope instability associated with liquefaction potential of soil using stone columns and deep mixed (cement-soil mix) columns are included in the cost estimation. The foundation flexibility is also taken into account in the bridge analysis and design.

The cost comparison of this study can provide a general guideline on the bridge preliminary cost estimation, which can be very helpful for the preparation of the budget for highway projects. It also provides the cost impact on the significance of designing a bridge in the New Madrid seismic zone from a 500-year return period design earthquake to a 2500-year design earthquake. It indicates that the cost impact of changing from 10% PE design earthquake map to 2% PE design earthquake map is not significant for bridges at locations being classified as the current seismic categories B and C, if some conservative design provisions in the current AASHTO seismic design specifications are not adopted. However the cost may increase 19%, if a bridge located in the current seismic category D is designed using 2% PE design earthquake map instead of 10% PE design earthquake map. It also indicates that the improvement of abutment slope stability may increase bridge cost significantly if 2% PE earthquake is used.

BRIDGE DESCRIPTION

A three-span (68'-68'-68') prestressed concrete I-girder bridge with a 32'-0" roadway width is considered in this study (Figure 1). It is a square bridge designed for AASHTO HS20-44 load. The bridge consists of integral end bents and two intermediate bents. Each intermediate bent has two 3.5' diameter concrete circular columns. All bents have pile foundations with 40' long steel H-piles. The foundation soil is considered as dense sand in the study with the friction angle of ϕ = 38 degrees. For the abutment design, an intermediate wing is also considered if it is needed for the bridge designed. The AASHTO Groups I through VI load combinations were also considered in the bridge design.

SEISMIC MAPS

Figure 2 compares the current AASHTO map with 10% PE in 50 years and the USGS peak ground acceleration map with 2% PE in 50 years. Four locations corresponding to seismic performance categories A, B, C, and D are chosen for the seismic analysis and design of the bridge. These locations are designated as locations A, B, C, and D as shown in Figure 2. The peak accelerations of soft rock due to 10% PE earthquake are 0.16g, 0.26g, and

[1] Structural Engineer, FHWA, Florida Division, 227 N. Bronough Street, Suite 2015, Tallahassee, FL 32301.
[2] Structural Designer, Missouri Depart of Transportation, Bridge Div., P.O. Box 270, Jefferson City, MO 65102.
[3] Structural Engineer, MoDOT, P.O. Box 270, Jefferson City, MO 65102.
[4] State Bridge Engineer, MoDOT, P.O. Box 270, Jefferson City, MO 65102

0.36g for the locations B, C, and D, respectively. Location A is chosen so that the seismic analysis is not required. From the figure, it can be seen that the USGS 2% map accelerations corresponding to these locations are approximately 0.55g, 1.4g, and 1.6g. The ratios of peak acceleration due to 2% PE earthquake to that due to 10% PE earthquake are 3.4, 5.4, and 4.4 at locations B, C, and D, respectively. It shows that the acceleration coefficients are very high at locations C and D if 2% PE map is considered. In fact the New Madrid seismic zone cuts right across south-eastern Missouri area. Soil type III is used for the development of the design response spectrum based on the current AASHTO 10% PE map. Site class D (equivalent to soil type III) is used for the development of 2% PE design response spectrum based on the 1997 NEHRP Provisions [1]. Figures 3a and 3b show the response spectra generated based on the AASHTO 10% PE map and USGS 2% PE map, respectively. The site classes associated with the new soil factors (Figure 3b), F_a and F_v, described in the 1997 NEHRP Provisions were also adopted in the 2000 International Building Code, and this is one of the most significant changes with regard to its impact on the level of seismic design forces. The first and second natural periods of the bridge are between 0.3 to 0.5 seconds.

BRIDGE ANALYSIS AND DESIGN

The seismic response spectrum analysis was used in the analysis. Flexibility due to soil-foundation interaction was also considered in the analysis. The stiffness matrix of the foundation was generated using the design charts developed by PoLam, etc [4]. The flexural capacity of a pile is limited to its plastic moment with consideration of pile axial load-biaxial moments interaction effect using the computer program "COM624P". For 10% PE earthquake, the allowable pile capacity is equal to 70 tons for HP 12x53 pile as described in the Missouri Bridge Design Manual. However, for a 2% PE earthquake, the allowable pile capacity is 86.6 ton for HP 12x53 obtained by dividing the ultimate pile capacity of pile by a factor of safety of 2 although AASHTO allows using full ultimate pile capacity in seismic design. The ultimate pile capacity is calculated using the "SPILE" computer program. For the 10% PE earthquake, a foundation is designed based on the elastic seismic moment divided by half of the R factor (i.e. 0.5R=2.5) for seismic category B and R=1 for seismic categories C and D, where R is the response modification factor. For the 2% PE earthquake, a foundation is designed for 1.3 times the column ultimate moment capacity (i.e. 1.3 Mp) with consideration of axial load effect. For the 10% PE earthquake, a column is designed based on the current AASHTO Div. I-A with a reduction factor, ϕ, of 0.5 when the stress due to the maximum axial load for the column exceeds $0.2 f_c^{'}$ and the value is increased linearly from 0.5 to 0.9 when the stress due to the maximum axial load is between $0.2 f_c^{'}$ and 0. For the 2% PE earthquake, a column is designed based on the proposed LRFD seismic design guidelines [1] with the resistance factor, ϕ =1.0. Therefore, the conservative column and foundation design provisions in the current AASHTO seismic design specifications are not considered for bridges designed based on 2% PE earthquake in this study. The force-displacement relationship at bridge abutments is a highly complex nonlinear problem affected by the abutment design. The iterative technique associated with the rigid body transformation (RDT) is adopted for the analysis [2, 3]. The abutment passive capacity of 7.7 kip/ ft^2 is used here.

ABUTMENT SLOPE STABILITY ANALYSIS

The abutment slope stability analysis was conducted using the computer program "PC-STABLE5M". The spill slope of 2:1 is used at each abutment for bridge located at location A. For bridges located at locations B, C, and D, a 3:1 spill slope is used. A factor of safety (FOS) of slope stability is considered acceptable if it is greater than or equal to 1.5 for non-seismic load and 1.1 for seismic load. If FOS for seismic load is less than 1.1 at location A, then a 3:1 spill slope is used. In order to investigate the applicability of in-situ ground stability improvement for earthquake, two approaches are considered in the slope stability analysis. They are stone column and deep mixed (DM, cement-soil mix) column applications. Both sand and clay backfill materials are considered in this study.

Without Consideration of Liquefaction

Several assumptions made in the slope stability calculations are: 1) the effect of the water table was not taken into account, 2) liquefaction was not investigated, 3) minimum diameter of stone column and DM column used are 3 feet with 7' center-to-center spacing, 4) soil characteristics used for PC-STABLE5M program are: for sand, γ_s = 110 pcf, ϕ = 38°, c = 0 psf; and for clay, γ_s = 110 pcf, ϕ = 20°, c = 400 psf , 5) stone column characteristics used for program, γ_c = 130 pcf, ϕ = 45°, c = 0 psf, 6) deep mixed column characteristics used for program, γ_c = 130 pcf, ϕ = 0°, c = 8000 psf, and 7) the unit prices are \$20/ft and \$85/ yd^3 for stone column and DM column, respectively. A pseudo-static seismic coefficient is applied to the abutment slope to represent the inertial forces within the soil. This seismic coefficient is assumed to be 2/3 of the peak ground acceleration to define an average cyclic loading condition [1].

For sand backfill, the slope stability safety factors for 10% PE earthquake are 1.6, 1.2, 0.9, and 0.85 for bridge locations A, B, C, and D, respectively. The safety factors for bridge locations C and D can be improved to 2.01 and 1.87, respectively, if seven DM columns are installed. Using stone column approach doesn't meet the minimum safety factor criteria of 1.1 at bridge locations C and D. The slope stability safety factors for 2 % PE earthquake are 1.4, 0.81, 0.46, and 0.38 at bridge locations A, B, C, and D, respectively. The safety factors for locations B, C and D can be improved to 1.8, 1.14, and 1.22 respectively if 7, 7, and 14 DM columns are installed at locations B, C, and D, respectively. Similarly, the stone column approach can't meet the minimum safety factor criteria of 1.1at locations C and D.

For clay backfill, the slope stability safety factors for 10% PE earthquake are 2.95, 1.82, 1.41, and 1.32 for bridge locations A, B, C, and D, respectively. The slope stability safety factors for 2 % PE earthquake are 2.04, 1.27, 0.81, and 0.71 for bridge locations A, B, C, and D, respectively. The safety factors for locations C and D can be improved to 1.14, and 1.12 respectively if fourteen DM columns are installed.

With Consideration of Liquefaction

For the slope stability analysis with consideration of liquefaction, it is assumed that the water table was taken at a constant depth of 5 feet below the bottom of the slope and the residual stress of 400 psf is used in this study. The safety factor of 1.1 for liquefaction potential based on the stress ratio method [5] is adopted here.

For sand backfill, the slope stability safety factors for 10% PE earthquake at bridge locations B, C and D are 1.23, 1.215 and 1.12, respectively, if seven DM columns are installed (Figure 8). The slope stability safety factors for 2 % PE earthquake are 1.49, 1.20, and 1.27 at bridge locations B, C, and D, respectively if 14, 21, and 28 DM columns are installed at locations B, C, and D, respectively, as shown in Figure 9.

For clay backfill, the slope stability safety factors for 10% PE earthquake are 1.68, 1.28, and 1.19 for bridge locations B, C, and D, respectively if seven DM columns are installed. The slope stability safety factors for 2 % PE earthquake are 1.14, 1.25, and 1.31 for bridge locations B, C, and D, respectively if 7, 21, and 28 DM columns are installed at locations B, C, and D respectively.

COST COMPARISONS

Without Consideration of Liquefaction

10% PE Earthquake

The analysis results show that the bridge total costs without consideration of abutment slope stability check are \$358,157, \$403,309, \$446,738, and \$457,180 for bridge locations A, B, C, and D, respectively. The percent increases from location A are 12.61%, 24.73%, and 27.65% for bridge locations B, C, and D, respectively. Figure 4 shows the foundation sizes and details of intermediate bent based on bridges located at A, B, C, and D. Figure 5 shows the abutment details based on bridges located at A, B, C, and D. The slope stability analyses indicated that DM columns are needed for bridge locations C and D with sandy backfill. The cost of DM column installation at each abutment is \$5793 for location C and \$5793 for location D. Therefore the bridge total costs with consideration of DM columns are \$358,157, \$403,309, \$458,324, and \$468,766 for bridge locations A, B, C, and D, respectively.

The percent increases from bridge location A are 12.61%, 28%, and 31% for bridge locations B, C, and D, respectively. For bridges with clay backfill, soil reinforcement (i.e. DM columns or stone columns) is not required at locations A, B, C, and D due to sufficient FOS.

2% PE Earthquake

The seismic spectrum acceleration coefficient of 1.0g, 1.6g, and 2.5g corresponding to 0.2 second period and the soft rock acceleration coefficient of 0.2g, 0.5g, and 0.8g corresponding to 1.0 second period were used to develop the design response spectrum for bridge locations B, C, and D, respectively, in accordance with the 1997 NEHRP Provisions (Figure 3). The analysis results show that the bridge total costs without consideration of abutment slope stability check are $358,157, $409,771, $453,778, and $505,461 for bridge locations A, B, C, and D. The percent increases from bridge location A are 14.41%, 26.70%, and 41.13% for bridge locations B, C, and D, respectively. It shows that the cost for a bridge located at location D is significantly greater than that at location C. This is due to 1) the abutment passive pressure reaches to the passive capacity of 7.7 ksf. After several iterations [2,3], two intermediate wings are required at each abutment; and 2) column longitudinal reinforcement is controlled by the AASHTO minimum reinforcement criteria (i.e. 1% of column cross-sectional gross area) at bridge location C, but it is controlled by the seismic load at bridge location D (i.e. elastic seismic demand moment divided by R=5). These cause the column longitudinal reinforcement increases from 18-#8 to 24-#10 for bridge location D and the foundation thickness increases from 3'-9" to 4'-0" at intermediate bents due to peripheral shear force increase. Figure 6 shows the foundation sizes and details of intermediate bent based on the bridges at locations A, B, C, and D. Figure 7 shows the abutment details based on the bridges at locations A, B, C, and D. As mentioned previously, the slope stability analyses indicated that DM columns are needed for bridge locations B, C and D. The costs of DM column installation at each abutment are $5793, $5793, and $12,488 for locations B, C, and D, respectively, for sand backfill. Therefore the bridge total costs with consideration of DM columns are $358,157, $421,357, $465,364, and $530,437 for bridge locations A, B, C, and D, respectively. The percent increases from location A are 18%, 30%, and 48% for bridge locations B, C, and D, respectively, for sand backfill. For clay backfill, the costs of DM column installation are $9345 and $9483 at locations C and D, respectively. Therefore the bridge total costs with consideration of DM columns are $358,157, $409,771, $472,468, and $524,427 for bridge locations A, B, C, and D, respectively. The percent increases from location A are 14%, 32%, and 46% for bridge locations B, C, and D, respectively.

With Consideration of Liquefaction

10% PE Earthquake

For sand backfill, the cost of DM column installation at each abutment is $4673, $6557, and $6515 at locations B, C, and D respectively as shown in Figure 8. Therefore the bridge total costs with consideration of DM columns are $358,157, $412,655, $459,852, and $470,210 for bridge locations A, B, C, and D, respectively. Figure 11 shows the cost ratios at locations A, B, C, and D. The cost ratio is defined as the cost at location A, B, C, or D to the cost at location A. The percent increases from bridge location A are 15%, 28%, and 31% for bridge locations B, C, and D, respectively. For clay backfill, the costs of DM column installation are the same ($6401) at locations B, C and D. Therefore the bridge total costs with consideration of DM columns at each abutment are $358,157, $416,111, $459,540, and $469,982 for bridge locations A, B, C, and D, respectively. The percent increases from location A are 16%, 28%, and 31% for bridge locations B, C, and D, respectively (Figure 11).

2% PE Earthquake

The slope stability analyses indicated that DM columns are needed for bridge locations B, C and D. The costs of DM column installation at each abutment are $13,190, $19,735, and $26,306 for locations B, C, and D, respectively, for sand backfill (Figure 9). Therefore the bridge total costs with consideration of DM columns are $358,157, $436,151, $493,248, and $558,073 for bridge locations A, B, C, and D, respectively. The percent increases from location A are 22%, 38%, and 56% for bridge locations B, C, and D, respectively, for sand backfill (Figure 11). For clay backfill, the costs of DM column installation are $6401, $19,735 and $26,306 at locations B, C and D, respectively. Therefore the bridge total costs with consideration of DM columns are $358,157, $422,573,

$493,248, and $558,073 for bridge locations A, B, C, and D, respectively. The percent increases from location A are 18%, 38%, and 56% for bridge locations B, C, and D, respectively (Figure 11). It can be seen that the cost increases significantly from location C to location D based on 2% PE earthquake. However the cost increase is less significant if 10% PE earthquake is considered. Figure 10 shows the cost of DM column installation in terms of percentage of bridge construction cost without and with consideration of liquefaction. At location D, the cost of slope improvement is about 2.5% of the bridge construction cost for 10% PE earthquake (Figure 10a). However it increases to 11% for 2% PE earthquake (Figure 10b).

Cost Comparison Between 10% and 2% PE Earthquakes

For sand backfill, the ratios of the cost for 2% PE earthquake to the cost for 10% PE earthquake are 1.0, 1.04, 1.02, and 1.13 for bridge locations A, B, C, and D, respectively, with consideration of DM columns but without consideration of liquefaction, and 1.0, 1.06, 1.07, and 1.19 with consideration of liquefaction (Figure 12). For clay backfill, the ratios are 1.0, 1.02, 1.06, and 1.15 for bridge locations A, B, C, and D, respectively, with consideration of DM columns but without consideration of liquefaction, and 1.0, 1.02, 1.07, 1.19 with consideration of liquefaction (Figure 12).

CONCLUSIONS

If the slope stability associated with liquefaction potential is considered in the design, it shows that the bridge cost estimation in terms of percent increase from bridge location A are 16%, 28%, and 31% for bridge locations B, C, and D, respectively, due to 10% PE earthquake, and the percent increases from bridge location A are 22%, 38%, and 56% for bridge locations B, C, and D, respectively, due to 2% PE earthquake. The cost comparison between 10 % and 2 % PE earthquakes shows that the ratios of the cost for 2 % PE earthquake to the cost for 10 % PE earthquake are 1.0, 1.06, 1.07, and 1.19 for bridge locations A, B, C, and D, respectively, with sand backfill, and 1.0, 1.02, 1.07, and 1.19, respectively, with clay backfill. It indicates that the cost impact of changing from 10% PE design earthquake map to 2% PE design earthquake map is not significant for a bridge located at B and C. However the cost may increase 19%, if a bridge is located at D using 2 % PE design earthquake map instead of 10 % PE design earthquake map. This is due to some conservative design provisions in the current AASHTO seismic design specifications for the 10% PE design earthquake and higher cost of slope instability mitigation for the 2% PE design earthquake. It also indicates that the improvement of abutment slope stability may increase bridge cost significantly if 2% PE earthquake is used.

This study does not consider the effect of soil liquefaction and ground spreading on the structural response. Further investigation is needed to include the pile deformations and stresses due to lateral spreading around piles.

REFERENCES

[1] MCEER Highway Project 094, Task F3-1, “Recommended LRFD Guidelines for the Seismic Design of Highway Bridges”, based on NCHRP 12-49, 2001.

[2] Ger, Jeffrey, Mike Nop, and Anousone Arounpradith, “Seismic Analysis of Skewed Bridges with Soil-Foundation Interaction”, Proceedings of Mid-America Highway Seismic Conference, St. Louis, Missouri, 1999.

[3] Priestley, M. J. N., F. Seible, and G.M. Calvi, *Seismic Design and Retrofit of Bridges*, John Wiley & Sons, Inc., 1996.

[4] Polam, I., M. Kapuskar and D. Chaudhuri, “Modeling of Pile Footings and Drilled Shafts for Seismic Design”, MCEER Report MCEER-98-0018, December 1998.

[5] American Association of State Highway and Transportation Officials (AASHTO), Standard Specifications for Highway Bridges, 16th Edition, 1996.

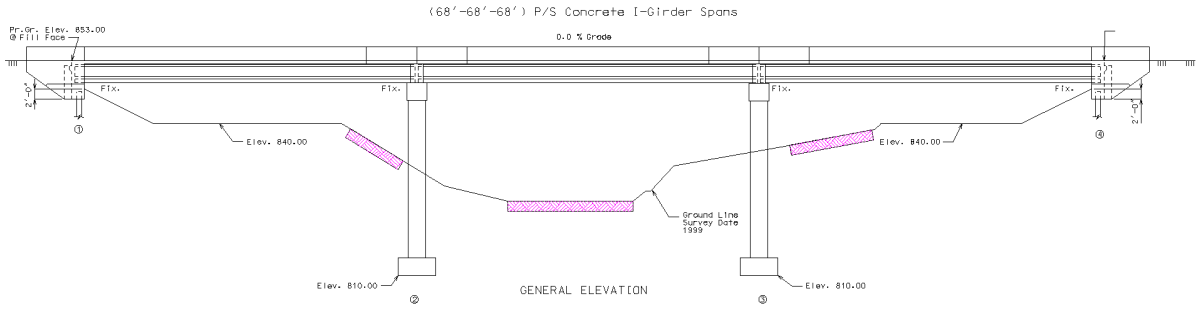

Figure 1. Three-span (68'-68'-68') Prestressed I-girder Bridge

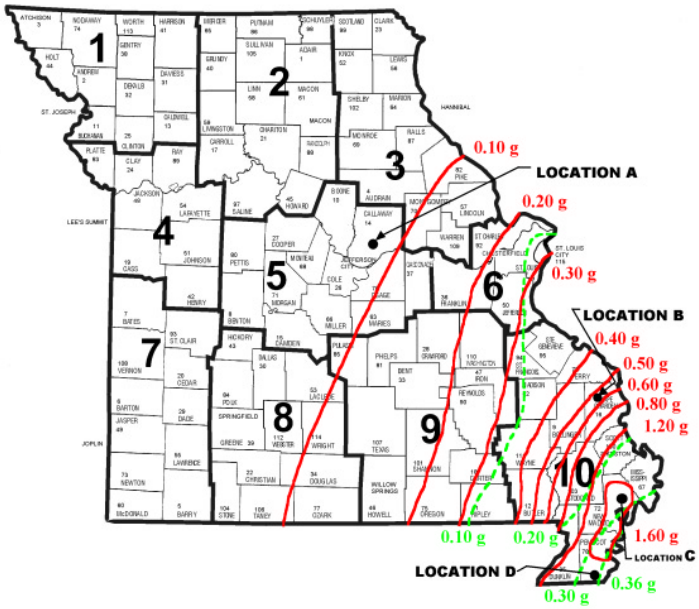

_____: New U.S. Geological Survey Map (2%)

- - - - - : Current AASHTO Map (10%)

Figure 2. Seismic Map Comparison

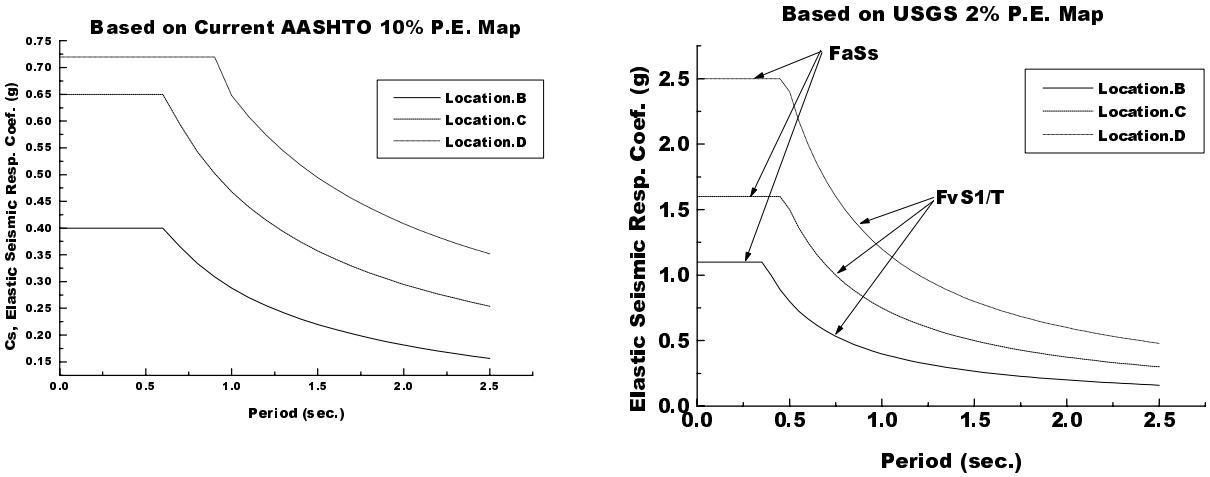

(a) (b)

Figure 3. Response Spectra Based on 10% and 2% P.E. Maps

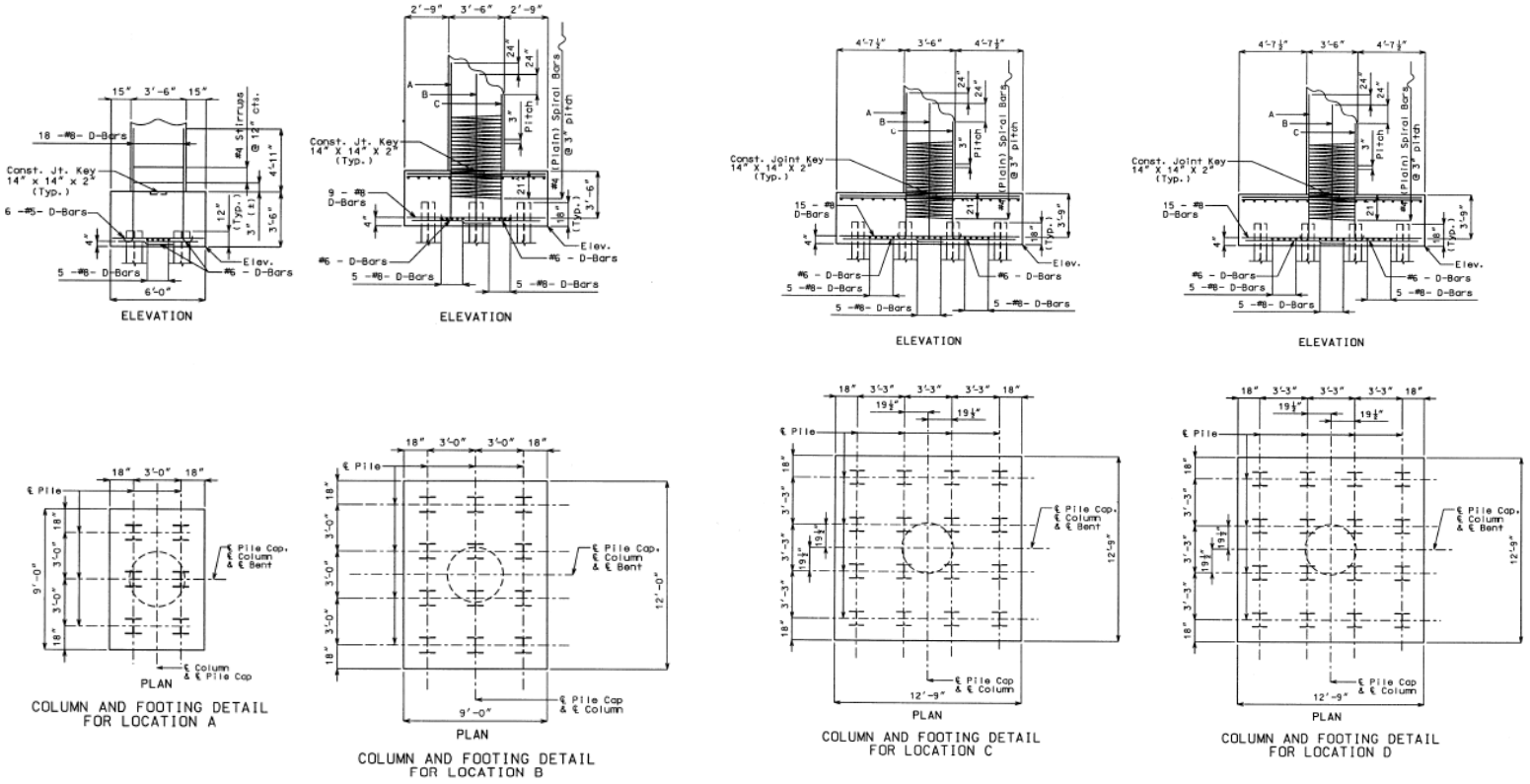

Figure 4. Foundation Details for Intermediate Bent (10% PE earthquake)

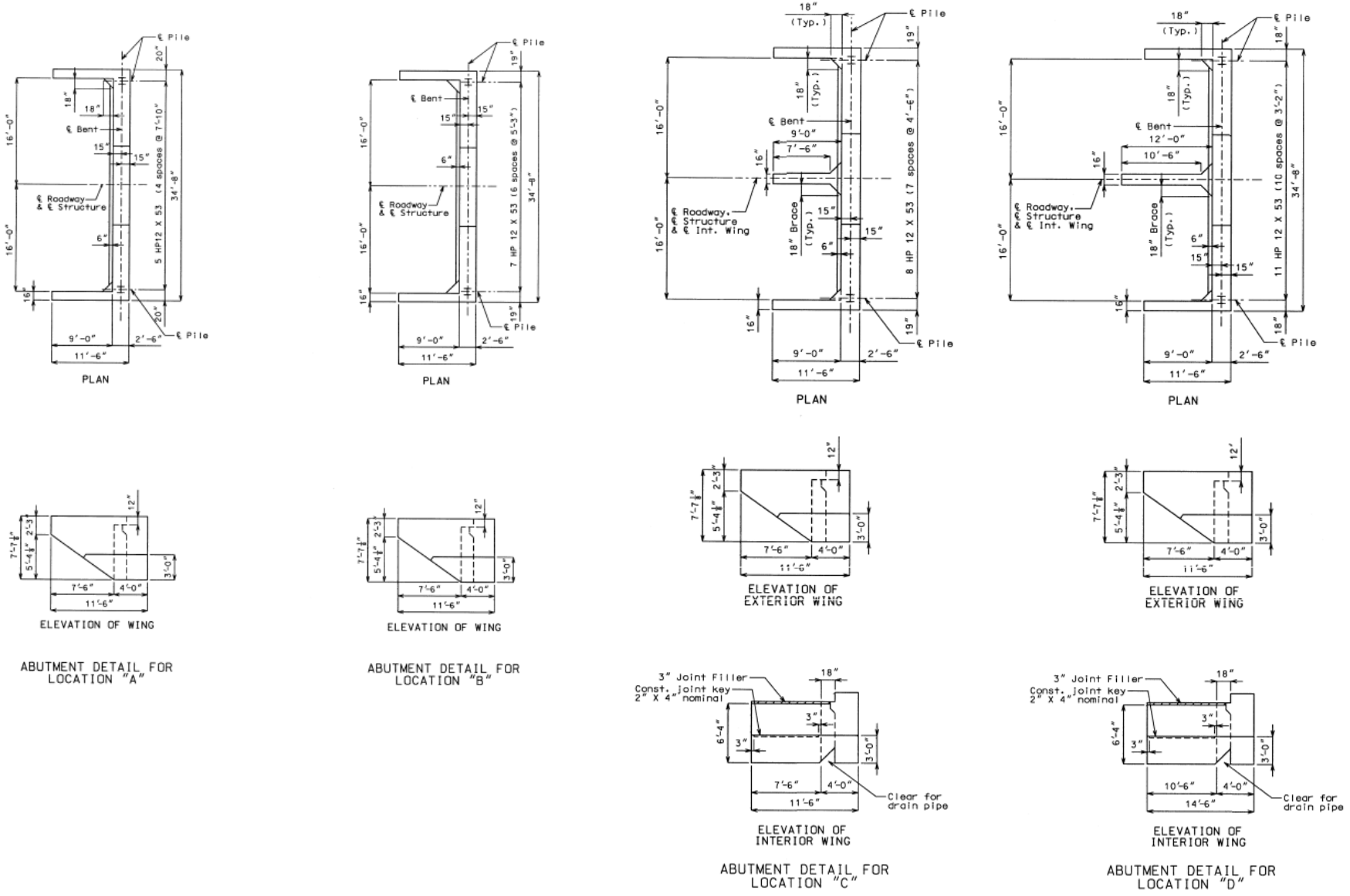

Figure 5. Abutment Details (10% PE earthquake)

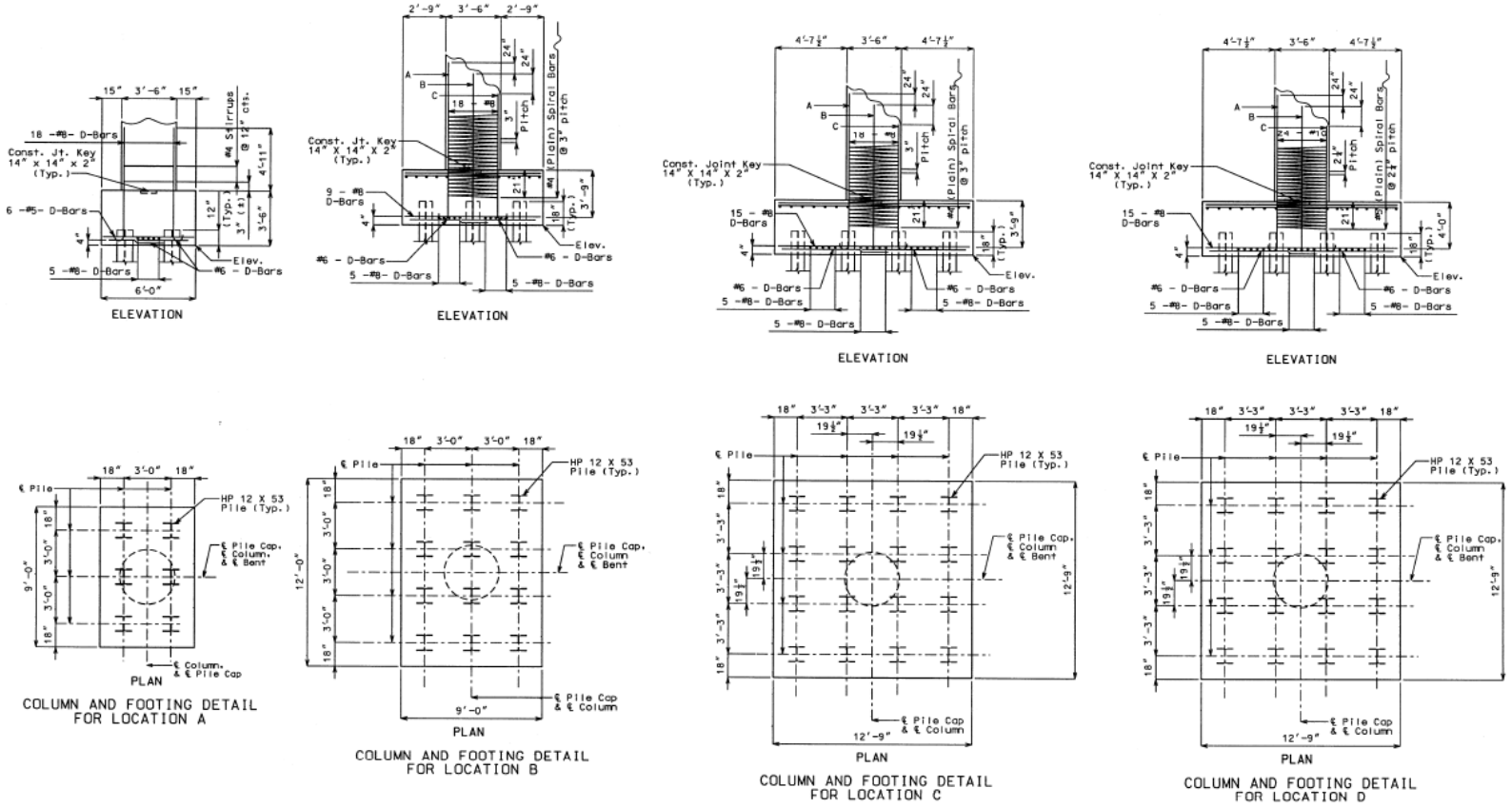

Figure 6. Foundation Details for Intermediate Bent (2% PE earthquake)

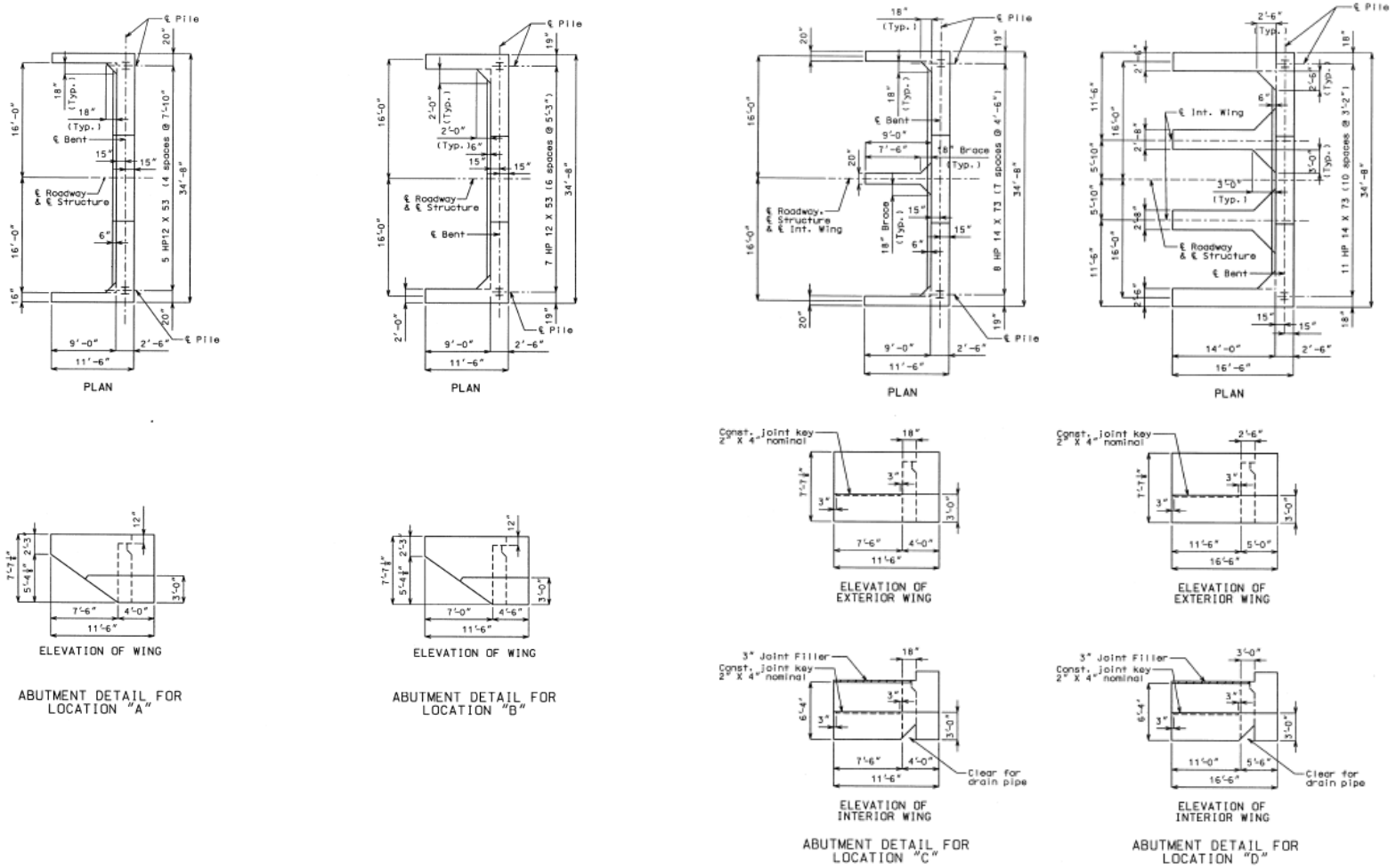

Figure 7. Abutment Details (2% PE earthquake)

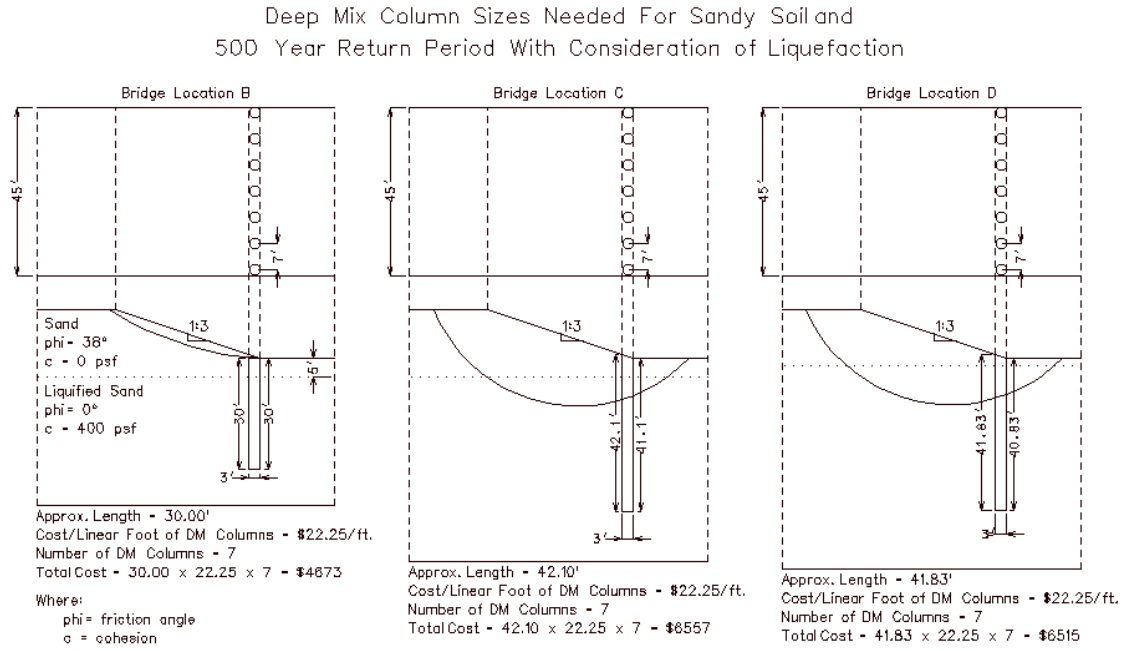

Figure 8. Slope stability improvement for sandy soil backfill (10% PE earthquake)

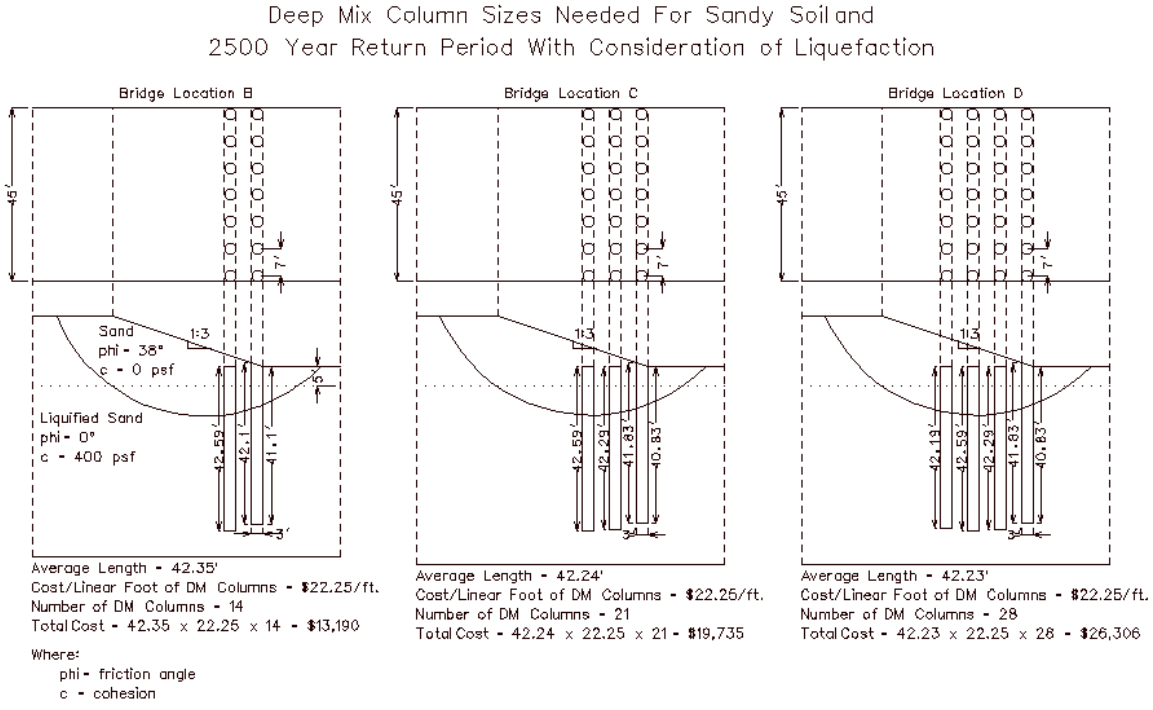

Figure 9. Slope stability improvement for sandy soil backfill (2% PE earthquake)

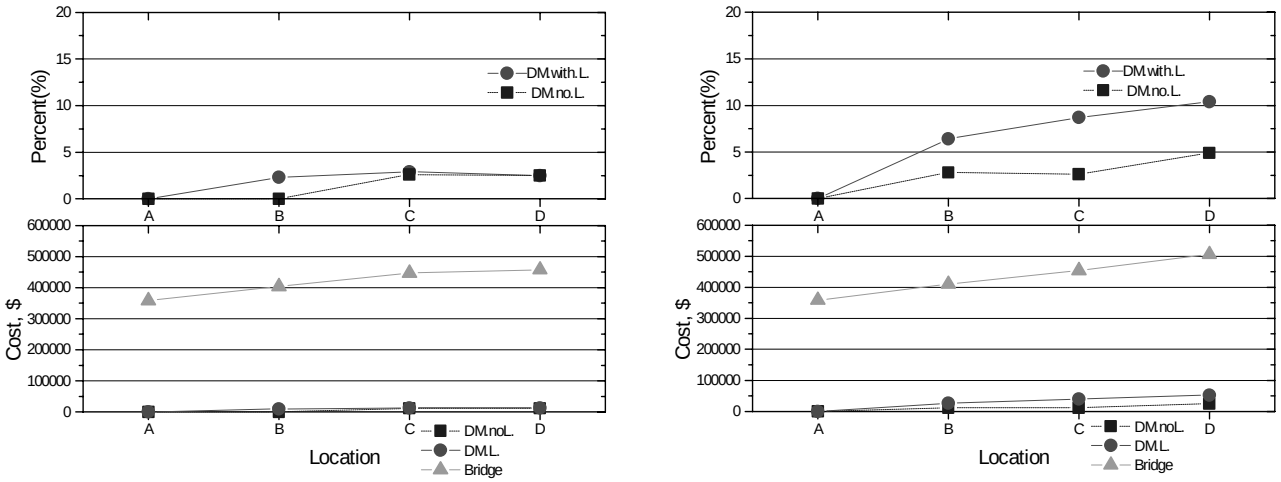

(a) (b)

Figure 10. Cost of slope stability improvement, (a) 10% P.E. and (b) 2% P.E.

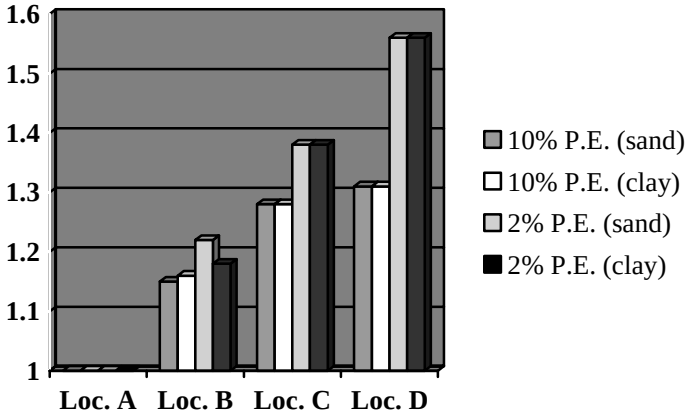

Figure 11. Cost Ratio w/ consideration of slope stability improvement and w/ liquefaction

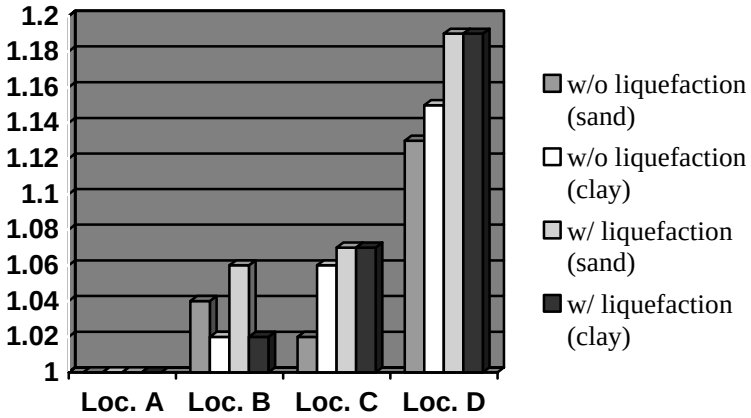

Figure 12. Cost Comparison between 10% and 2% P.E. earthquakes

Testing of the LRFD Bridge Seismic Design Provisions Through a Comprehensive Trial Design Process

M. Lee Marsh, Richard V. Nutt, Ronald Mayes and Ian M. Friedland

ABSTRACT

The Multidisciplinary Center for Earthquake Engineering Research (MCEER), with funding from the Federal Highway Administration (FHWA), has organized and is conducting a trial design program using the "Recommended LRFD Guidelines for the Seismic Design of Highway Bridges." The "Recommended LRFD Guidelines" were prepared by MCEER and the Applied Technology Council (ATC), on the basis of the results of the AASHTO-sponsored NCHRP Project 12-49, "Comprehensive Specification for the Seismic Design of Bridges."

The majority of States represented on the AASHTO Bridge Committee's T-3 technical committee (Seismic Design) are participating in the trial design program, as are several other States and the Central Federal Lands division of the FHWA. Each participating agency is preparing at least one complete design using the "Recommended LRFD Guidelines," in order to assess and quantify the impacts if and when the Guidelines are implemented and adopted by AASHTO as a Guide Specification. The results of the program will also assist in identifying any significant problems with the provisions contained in the Guidelines themselves.

Due to the variety of bridge types, construction practices, and seismic hazard and soils conditions found throughout the United States, the trial design program will exercise the majority of provisions contained in the "Recommended LRFD Guidelines." It is anticipated that the AASHTO Bridge Committee will make a decision regarding adoption of the Guidelines as an AASHTO *Guide Specification* in 2002 based, in large part, on the results of this program.

The trial design program was initiated in December 2001, and will be completed in April 2002. This presentation will provide an overview of the program, and summarize some of the key findings from it.

M. Lee Marsh, /ABAM Engineers, Inc.
Richard V. Nutt, Consultant
Ronald Mayes, Simpson Gumpertz & Heger
Ian M. Friedland, Applied Technology Council

Poster Session

Coordinator: Myint Lwin

Cyclic Testing of Truss Pier Braced Latticed Members
Michel Bruneau, Kangmin Lee, and John Mander

Caltrans/CSMIP Bridge Strong Motion Instrumentation Project
Pat Hipley, Tony Shakal and Moh Huang

Seismic Retrofitting Challenges Stimulate New Innovations for the Benicia-Martinez Bridge
Roy A. Imbsen and Moe Amini

West Anchorage Design of San Francisco - Oakland Bay Bridge Main Span for Seismic Loads
John Sun, Rafael Manzanarez and Marwan Nader

Seismic Retrofit of the US 40/I-64 Double Deck Bridge
Mark R. Capron

Bridge Abutment Model Sensitivity for Probabilistic Seismic Demand Evaluation
Kevin Mackie and Bozidar Stojadinovic

Dynamic Response of Bridge Structures Supported on Extended Reinforced Concrete Pile Shafts
T.C. Hutchinson, C.J. Curras, R.W. Boulanger, Y.H. Chai, and I.M. Idriss

Proportioning Substructure Columns of Short Bridges for Improved Seismic Performance
Mehmet Inel and Mark A. Aschheim

Near-Field Ground Motions and their Implications on Seismic Response of Long-Span Bridges
George P. Mavroeidis and Apostolos S. Papageorgiou

Shake Table Response of Flexure-Dominated Bridge Columns with Interlocking Spirals
Juan Correal, M. Saiid Saiidi, David Sanders and Saad El-Azazy

Expansion Joints for Seismic Isolated Bridges
Efthymios Tim Delis

Development of Analytical Fragility Curves for Highway Bridges Considering Strong Motion Parameters
Kazi R. Karim and Fumio Yamazaki

State Street Bridge: CFRP Composite Seismic Rehabilitation and Specifications
Chris Pantelides, Fadel Alameddine, Thomas Sardo, Roy A. Imbsen, Larry Cercone, and Frederick Policelli

Recommendations on Experimental Procedures for Bridge Column Testing
Jerry J. Shen, W. Phillip Yen, and John O'Fallon

Implementation of Seismic Isolators and Supplemental Dampers in Cable-Stayed Bridges
Michael J. Wesolowsky and John C. Wilson

Seismic Isolation of Bridges Subject to Strong Earthquake Ground Motions
Victor A. Zayas, Stanley S. Low, and Anoop S. Mokha

Behavior of Ductile Steel Retrofitted Deck-Truss Bridges
Majid Sarraf and Michel Bruneau

Cyclic Testing of Truss Pier Braced Latticed Members

Michel Bruneau, Kangmin Lee, and John Mander

ABSTRACT

Analytical and experimental research is conducted to investigate the behavior of bridge truss pier brace members. The objective is to generate knowledge and results that can be broadly applicable to evaluate the seismic capacity of steel truss bridges of the type built during the first half of the 1900's throughout the United States. They were typically designed to resist wind forces, but not earthquakes. From a review of past practices, commonly used shapes and details that have been historically used for built-up members in steel truss bridge braced pier substructures were selected, and an experimental program has been devised whereby several cross-sectional shapes and geometric configurations of X-bracing are explored to ascertain the inelastic deformation capability of these critical elements. These tests are underway at the time of this writing. Knowledge from this experimental and analytical study will be also be used to develop retrofit measures for members that are seismically vulnerable

Michel Bruneau, Professor, Department of Civil, Structural and Environmental Engineering, University at Buffalo, 130 Ketter Hall, NY 14260
Kangmin Lee, Ph.D. Candidate, Department of Civil, Structural and Environmental Engineering, University at Buffalo, 210 Ketter Hall, NY 14260
John Mander, Professor, Department of Civil Engineering, University of Canterbury, Christchurch, New Zealand

INTRODUCTION

A large number of steel truss bridges have been built throughout the United States, many in zones of moderate to high seismicity. These bridges have typically been designed to resist wind forces, but not earthquakes. Structural analyses of such bridges often reveal that many key structural members along the load path followed by the seismically induced forces may buckle or suffer brittle fracture of their non-ductile connections. However, seismic evaluation remains difficult due to the lack of knowledge on the cyclic inelastic behavior of built-up members of the type typically found in these bridges, and on their riveted connections. Although some testing of bridge-specific latticed members has been conducted by other researchers, results to date have mostly been project specific. Consequently, it is difficult to draw general conclusions from those studies. The objective of this research is therefore to provide theories and results that can be broadly applicable to many steel truss bridges that share similar structural characteristics and details.

RESEARCH APPROACH

A survey was conducted to investigate those commonly used shapes and details that have been historically used for built-up members used in steel truss bridge braced pier substructures. This survey showed that braces in these bridges almost universally consist of latticed built-up members with riveted connections. Common cross-sectional shapes have been identified. Their potential failure modes are global buckling (in-plane or out-of-plane of the frame) or local buckling. To this end, based on representative details, an experimental program has been devised whereby several cross-sectional shapes and geometric configurations of X-bracing are explored to ascertain the inelastic deformation capability of these critical elements. These tests are underway at the time of this writing. Results from these tests will be used to develop simple strength and deformation models based upon rational mechanics and able to predict strength and displacement limit states. Knowledge from this experimental and analytical study will be also be used to develop retrofit measures for members that are seismically vulnerable.

PRELIMINARY RESULTS

Drawings were obtained for a few existing bridges having truss substructures (bents, towers, etc.) with latticed members. Design provisions in the literature, particularly in steel design textbooks published at the turn of the century (Ketchum, 1920, Wells, 1913, and Kunz, 1915), were also reviewed, along with recent research work conducted for the major crossings in California (Uang and Kleiser, 1997, and Dietrich and Itani, 1998 and 1999). This allowed to extract a range of parameters typically encountered for such members, including typical built-up member configurations and lacing geometry, typical b/t and KL/r ratios for the built-up members and their lacings, connection details, and other lacing characteristics.

As a result of this work, parameters worthy of experimental consideration (and their range) have being identified (Table 1 and Figure 1). While some bridges were observed to have members having b/t ratios in excess of 16, it was decided to restrict testing to specimens having b/t values of 8 and 16 on the basis that this would allow to compare the cyclic performance of members having considerably different expectations in terms of local buckling behavior. Note that the AISC recommended maximum b/t value for ductile seismic design is 7.6 for grade 50 steel.

Likewise, it was judged that testing braces having slenderness (KL/r) of 60 and 120 would encompass the range of member slenderness observed in bridges, while allowing to compare the cyclic inelastic behavior of members expected to have significantly different levels of inelastic buckling. The resulting specimens designed based on these considerations are listed in Table 2 and section shapes are detailed in Figure 2. Note that only built-up members constructed of angles are considered.

Specimens with section shape A (Ay8-60, Ay8-120, Ay16-60, and Ay16-120) were instrumented with displacement and strain gages and tested. The test set-ups are shown in Figures 3 to 6 for these specimens. Note that the set-up for Ay8-60 was used to test two specimens having the same section type and b/t ratio, but two different values of the KL/r ratio (60 and 120). This was achieved by using the same members, and testing first in an X-bracing (KL/r of 60) configuration (but without connecting the upper end of one brace, as shown in the circle in Figure 7), and second, in a single brace (KL/r of 120) configuration.

Axial gravity loads were applied at the top of the frame for specimens Ay16-60 and Ay16-120 to reduce slippage in the hinges in the set-up and reduce the global frame horizontal displacements observed during testing of the other two specimens. Also note that for Ay16-60 (in the X-bracing configuration), a dummy member was used instead of the previously used approach of using a specimen brace unconnected at its upper end to prevent damage to the member to be used as a slender specimen (i.e. Ay16-120).

Figures 8 and 10 show the axial force–displacement curve experimentally obtained for the specimens with section shape A. These hysteretic curves exhibit the typical behavior of bracing members observed from the previous studies. The Ay16-60 and Ay16-120 specimens locally bucked instead of globally buckling, because of their large width-to-thickness ratio (b/t = 16). Repeated buckling and straightening of the braces (reversed cyclic loading) at the local buckling location led to failure by fracture.

Figures 11 and 12 show the different buckled shapes at the maximum compressive deformations of the braces for the Ay8-60 and Ay16-60 specimens respectively. The Ay8-60 specimen globally bent (Figure 11), while the Ay16-60 specimen remained almost straight (except at the location of local buckling) (Figure 12).

To investigate fracture life of the bracing member under cyclic loading, the test results of the Ay8-120 specimen were compared with fracture life models of bracing members suggested by Goel (Hassan and Goel, 1991) and Tremblay (Archambault et al., 1995). Results are summarized in Table 1. Although the fracture life models used have been developed for structural tubular sections, it appears based on the preliminary results obtained so far that these models predicted the fracture life of the Ay8-120 specimen well (results not available for other specimens at time of writing).

CONCLUSIONS

Because this research program is only mid-course, firm conclusions would be premature. However, preliminary results suggest that fracture life prediction models developed by others for tubes might also work for the built-up members typically used in truss bridges. This would be a most valuable model to assess the seismic resiliency of these type of bridges, if subsequent tests validate this finding. Toward that same goal, another outcomes of this research program is expected to be detailed information on the maximum cyclic ductility and maximum energy dissipation capacity of built-up braces, using hysteretic curves of the type presented in this paper to generate this quantitative information.

ACKNOWLEDGEMENTS

This research was conducted by the University at Buffalo and was supported by the Federal Highway Administration under contract number DTFH61-98-C-00094 to the Multidisciplinary Center for Earthquake Engineering Research.

REFERENCES

[1] Ketchum, Milo Smith (1920), “The Design of Highway Bridges of Steel, Timber and Concrete”, McGraw-Hill Co., New York, New York.

[2] Wells, Melville Backer (1913), “Steel Bridge Designing”, The Myron C. Clark Publishing Co., Chicago, Illinois.

[3] Kunz, F. C. (1915), “Design of Steel Bridges; Theory and Practice for use of Civil Engineers and Students”, McGraw-Hill Co., New York, New York.

[4] Uang, C.-M. and Kleiser, M. (1997), “Cyclic performance of latticed members for the San Francisco-Oakland Bay Bridge”, *Report No. SSRP-97/01*, Division of Structural Engineering, University of California, San Diego, La Jolla, California.

[5] Adrianne M. Dietrich, and Ahmad M. Itani (1998), “Cyclic Behavior of Built-up and Steel Members and Their Connections”, *Report No. CCEER 98-10*, Department of Civil Engineering, University of Nevada, Reno, Nevada.

[6] Adrianne M. Dietrich, and Ahmad M. Itani (1999), “Cyclic Behavior of built-up and Perforated Steel Members on the San Francisco-Oakland Bay Bridge”, *Report No. CCEER 99-9*, June, Department of Civil Engineering, University of Nevada, Reno, Nevada.

[7] Hassan, O. F. and Goel, S. C. (1991), “Modeling of Bracing Members and Seismic Behavior of Concentrically Braced Steel Structures”, *Report No. UMCE 91-1*, January, Department of Civil Engineering, The University of Michigan, Ann Arbor, Michigan.

[8] Archambault, Marie-Helene, Tremblay, Robert, and Filiatrault, Andre (1995), “Etude du Comportment Seismique des Contreventements Ductiles en X Avec Profiles Tubulaires en Acier”, *Rapport No. EPM/GCS-1995-09*, Departement de Genie Civil Section Structures, Ecole Polytechnique de Montreal, Montreal, Canada.

TABLE 1. SUMMARY OF EXPERIMENTAL PARAMETERS TO BE CONSIDERED

Built-up Members			Lacings		
Configuration	B/t ratio	KL/r ratio	Type	Angle	KL/r ratio
Type "A" Type "B"	8 – 16	60 – 120	Single Lacing	60^o	100 – 120

TABLE 2 GIVEN SPECIMEN NAMES

Name	Section Shape	Bucking Axis	b/t ratio	KL/r
Ay8-60, Ay8-120	A	Y	8	60 and 120
Ay16-60, Ay16-120	A	Y	16	60 and 120
By8-60, By8-120	B	Y	8	60 and 120
By16-60, By16-120	B	Y	16	60 and 120
Bx8-60, Bx8-120	B	X	8	60 and 120
Bx16-60, Bx16-120	B	X	16	60 and 120

TABLE 3 FRACTURE LIFE OF SPECIMEN AY8-120

Fracture Life	Fracture of one angle*	Entire Fracture*	Goel Model Case 1**	Goel Model Case 2**	Tremblay Model Case 1**	Tremblay Model Case 2**
	36.26	40.72	38.64	62.74	29.23	43.07

* For that built-up shape, entire fracture of the specimen required the application of more cycle of inelastic deformations than fracture of a single angle.

** Case 1 was calculated considering actual width-to-depth ratio of the specimen. Case 2 was calculated assuming that the four angles created an equivalent square tube.

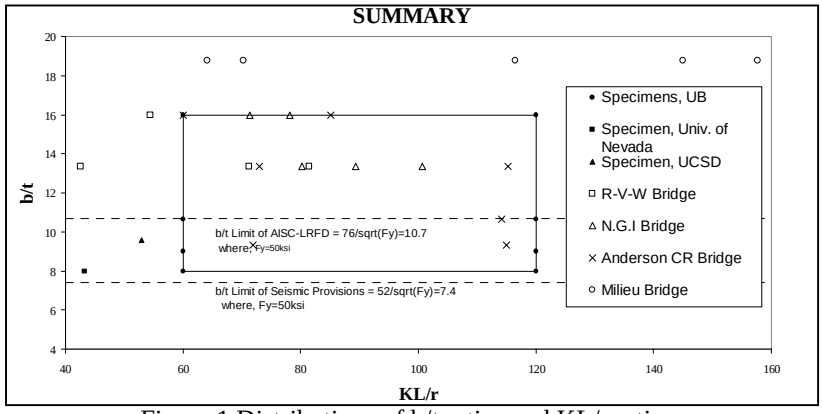

Figure 1 Distributions of b/t ratios and KL/r ratios

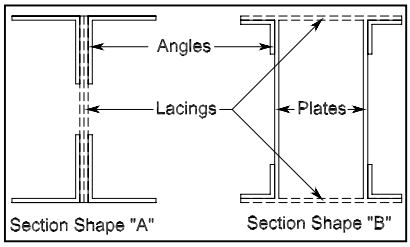

Figure 2 Section shapes

Figure 3 Test Set-up for Ay8-60 Specimen

Figure 4 Test Set-up for Ay8-120 Specimen

Figure 5 Test Set-up for Ay16-60 Specimen

Figure 6 Test Set-up for Ay16-120 Specimen

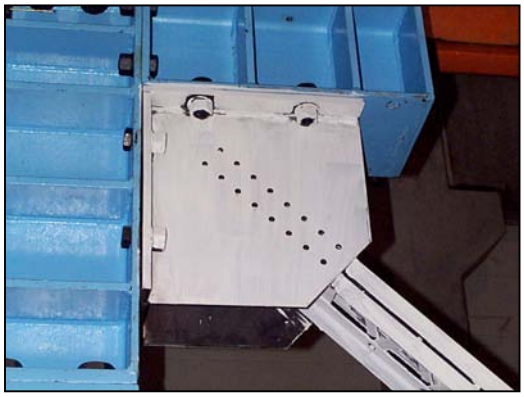

Figure 7 Unconnected end of a brace (Ay8-60)

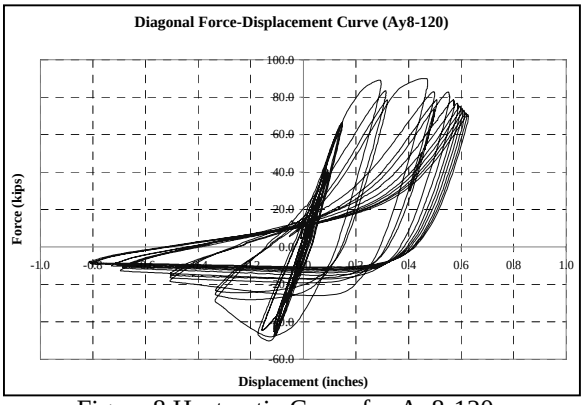

Figure 8 Hysteretic Curve for Ay8-120

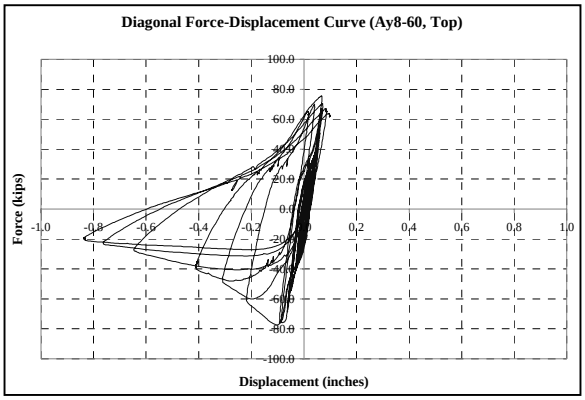

Figure 9 Hysteretic Curve for Ay8-60

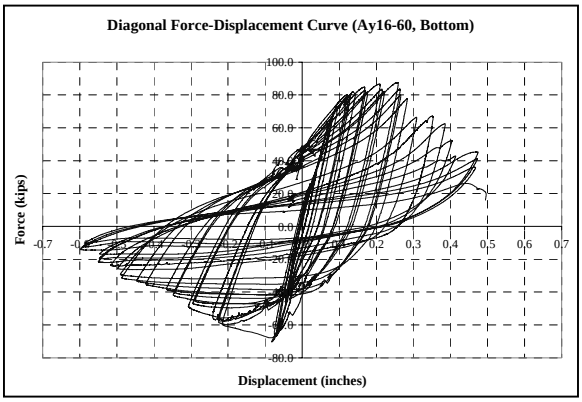

Figure 10 Hysteretic Curve for Ay16-60

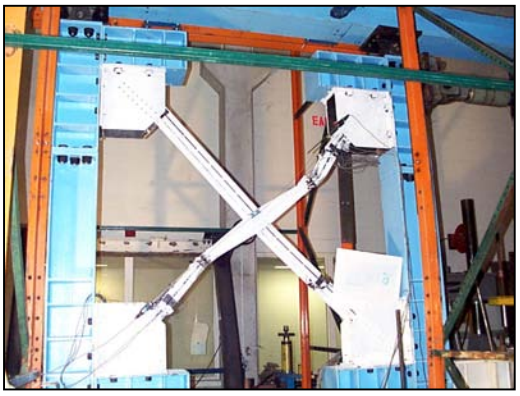

Figure 11. Buckled shape Specimen Ay8-60

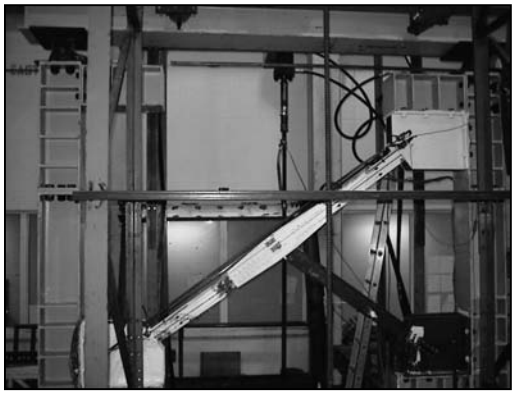

Figure 12. Buckled shape Specimen Ay16-60

Caltrans / CSMIP Bridge Strong Motion Instrumentation Project

Pat Hipley, Tony Shakal and Moh Huang

ABSTRACT

The California Department of Transportation (Caltrans) has been working with the California Strong Motion Instrumentation Program (CSMIP) of the Department of Conservation's California Geological Survey (CGS) for many years to place strong-motion sensors on various bridge structures and ground sites. The bridge instrumentation project encompasses both regular highway bridges and toll bridges. As of January 2002, 65 bridges ranging from small two span overcrossings with monolithic abutments to large seven-mile long toll structures have been instrumented for strong motion. This poster session will present the current status of the bridge instrumentation project and discusses the sensor layouts for the three new large toll bridge structures to be built in the San Francisco Bay area. Along with conventional instrumentation, many new and challenging placements of the sensors are in the works. Some new uses include placing sensors near the bottom of large diameter piles, instrumentation of suspension cables, recording pile cap rocking and translation, and using relative displacement sensors. Most of the new installations will have a phone connection and will be triggered at a set threshold by earthquakes. The records will be downloaded and automatically processed in the Sacramento office. This near-real-time data will be used for post-earthquake response including notification of emergency personnel. If there is a major earthquake, the data can be useful in determining which piers of large toll bridges should be inspected first. The data will also be used to verify current dynamic modeling techniques for bridge super- and sub-structures.

Presently, nine downhole arrays are operational and are located in various regions around the State. These downhole arrays will record the subsurface motion of the soil at different geologic levels and this data will be used to substantiate vibration theories and soil modeling techniques.

Pat Hipley, California Department of Transportation, Office of Earthquake Engineering, 1801 30th Street, MS 9-2/5i, Sacramento, CA 95816

Tony Shakal, California Geological Survey, California Strong Motion Instrumentation Program, 801 K Street, MS 13-35, Sacramento, CA 95814-3531

Moh Huang, California Geological Survey, California Strong Motion Instrumentation Program, 801 K Street, MS 13-35, Sacramento, CA 95814-3531

INTRODUCTION

Placing strong motion instruments to simultaneously record the movements of the ground and bridge structures during seismic events is imperative to advancing our understanding of how these structures respond to earthquake motions. There are 65 bridges instrumented as of January 2002 and some large installation projects are currently in the works for the San Francisco Bay area's toll bridges (see Figure 1).

Installing sensors on structures that will be close to the epicenters of large earthquakes is the goal of this project. There are many locations in California where a big earthquake could occur and many candidate bridge structures. No earthquake is the same and each earthquake will produce a unique waveform that will shake each structure in different ways. Most locations selected are near major faults or are in potentially high seismic zones. Another project objective is to monitor both small and massive bridge structures. The majority of the bridges in California are small two and three span structures. Some of these smaller bridges will need to be monitored, but on the other hand, the great bridges, such as our toll bridges, represent a huge investment to the public and are critical to the state's transportation system.

UNDERTAKING THE INSTALLATIONS

Strong motion sensors tell us whether the motion of a particular structure, excited by seismic ground movement, is what we would expect and what we are designing for. Until there are actual readings during large earthquakes to compare the data to our theories of structural dynamics, we can only speculate as to what this movement will be. Some sensors are placed on the ground away from any structural influences (freefield sensors) to measure the ground motion and this motion will be used as the input data for analysis. Multiple sensors are placed on the structure to give sufficient readings to determine the relative displacements and mode shapes. For large structures, this requires monitoring the foundations and the superstructure simultaneously. Much can be learned from these readings and the data will be crucial for advancing modeling techniques.

Sensors are placed on a bridge to record displacements in both the longitudinal and the transverse directions. Vertical sensors are used to compare midspan deflections to the vertical movement of the piers and are used to determine if spread footings are "rocking" during an earthquake. Some new designs will incorporate conduits tied to the pile reinforcement cages that are lowered into the ground and cast in place with concrete. Downhole instruments are then placed into the piles at depth to record the underground pile movements. At the Interstate 5/ Route 14 Interchange in Los Angeles, one bent (a single column pile extension pier), has sensors at 100' (bottom of pile), 33' (the plastic hinge zone), ground level, and at the roadway 100' above the ground. This will give us motion readings from the top to the bottom of that bridge support system during an earthquake. The toll structures will also incorporate sensors into the piles as part of the existing bridge retrofitting effort and as part of the construction of the new replacement structures.

An important aspect of structural dynamics gained from the strong motion readings is how fast these structures come to rest after forced vibration (damping). How well a bridge structure damps out the movements of an earthquake will be valuable information to the earthquake engineering community.

Much of the effort in the past few years has been to place instruments on the toll structures as part of the seismic retrofitting work. Eight of the ten Caltrans toll bridges have been or are currently being retrofit for earthquake induced motions. Some of the toll structures are being completely replaced to bring those crossings up to our current seismic standards. In all these contracts, seismic system installation work has been included in the plans.

For large toll bridges, fragility models can be developed for various members (such as the towers) that provide the relative movement that can occur before the safety of the structure is compromised. As an example, if a tower deflects a few inches, it may be well inside the elastic range of that system, but if it deflects many feet, it may require a bridge closure until further investigation is performed. These new seismic monitoring systems will quickly make data available to local maintenance personnel so they can make judgements as to the structural integrity of these important bridges after an earthquake.

Seismic monitoring systems have also been designed and will be incorporated into the three new toll crossings being built in the San Francisco bay area. These bridges are; the new Bay Bridge, the new Carquinez Strait Bridge, and the new Benicia/Martinez Bridge. Large amounts of accelerometers are required to achieve meaningful data for these long bridge structures. For all of the California toll bridges combined, close to 1000 channels will need to be maintained after the installation efforts are completed. These significant structures represent billions of dollars worth of investment to California's taxpayers and having seismic response data available will be invaluable.

DOWNHOLE ARRAYS

Data recorded by downhole arrays with sensors installed at different depths provide critical information for studies of site amplification effects. As of January 2002, nine downhole arrays are operational, and the installation of many new arrays is planned for the near future.

For each borehole there is a triaxial accelerometer package installed at the bottom of the drilled hole to record the ground motion in three directions. Subsurface downhole arrays are installed at bridges in different geologic areas throughout the State. These arrays represent deep soft alluvium sites (except for the Tunitas Creek array in Half Moon Bay) with sensors located a few yards down to 800 feet in the ground. Downhole arrays allow the study of the response of different geologic stratum for a variety of seismic motions.

Data recorded at the in-place downhole arrays so far represents mostly low amplitude motions. This allows representative studies of linear response of the soil profiles caused by seismic activity. Long-period (up to 8 seconds) large amplitude (up to 4 inches) displacements were recorded at a few downhole arrays in southern California during the October 16, 1999 Hector Mine earthquake at distances of 125 to 145 miles from the epicenter. These slow moving, large displacement motions were the same in magnitude and phase from deep in the ground all the way up to the ground surface.

Caltrans drilling crews bore the holes and install the conduits for the downhole instruments and Caltrans Geology and Geophysics personnel log the holes (lithology, P-S suspension, E-logs, etc.) for future reference. This logged data is also used to determine the exact level at which to place the instrument packages. Acquiring actual data as to how various soil types respond to the underlying rock motion will advance our knowledge regarding what ground motions to expect at

our structures. We are noticing that the same sites react very uniquely to different earthquakes. Soil vibration models can be refined using the downhole data and more accurate soil models will be the building block for more realistic seismic bridge design.

NEW USES FOR STRONG MOTION SENSORS

In the city of Eureka, the Humboldt Bay bridges (3 total) are augmented with seismic gates. The seismic retrofit design for these structures is still underway and the gates are an interim measure that will be in place until the retrofit construction is completed. These gates are similar to railroad crossing gates and will close the bridge in the event of strong ground shaking. The closure of the structures will prevent public use of these bridges until a thorough inspection can be completed. When the gates are activated, local traffic control personnel and the bridge maintenance crews are notified immediately. Along with the installation of gates at Humboldt Bay, there are permanent seismic gate systems on two bridges located near the town of Leggett. These two large concrete arch bridges are instrumented with accelerometers that will activate the gates if there is a strong earthquake in this very rural location.

In the early part of the 1990's, CGS developed an automated alphanumeric paging system that was used to alert Caltrans emergency response personnel in the event of an earthquake in near real time. If the ground shaking at an instrumented site reaches a set threshold, the system will download the data via a phone line, process the data, and send a page out to selected individuals. The message would include wording as to the estimated intensity of the shaking (light, moderate, strong, severe), and would give spectral response data points (example: 1.0 g @ 1.0 sec. period) for engineering use. This early warning system evolved into the Tri-net system that is similar in scope but is a cooperative effort between several state agencies and universities. These group are also developing a system to plot "shake maps" displaying lines of intensity of ground shaking in the region for quick use by emergency response organizations. The data from the systems installed under this strong motion instrumentation project will be made available for use by these organizations.

SUMMARY

The California Department of Transportation and the California Geological Survey are committed to developing and maintaining seismic motion detection systems for California's bridges. This data will be used to further our understanding of how the soil and the bridges react to large earthquakes. The recordings will be utilized to verify design assumptions and to update seismic codes. It is imperative that these systems are in place when a large earthquake occurs in California to record the response of these bridge structures. This data represents an invaluable tool to the development of our theories of system dynamics during earthquakes and will be important for rapid assessment of the stability of large structures after a major event. Until there are actual recordings displaying the movements of large civil structures caused by earthquakes, there will only be speculation and conjecture as to what this motion will be.

BRIDGE AND DOWNHOLE SITE MAP
CALIFORNIA STRONG MOTION INSTRUMENTATION PROGRAM

CALIFORNIA DEPARTMENT OF TRANSPORTATION
CALIFORNIA DEPARTMENT OF CONSERVATION

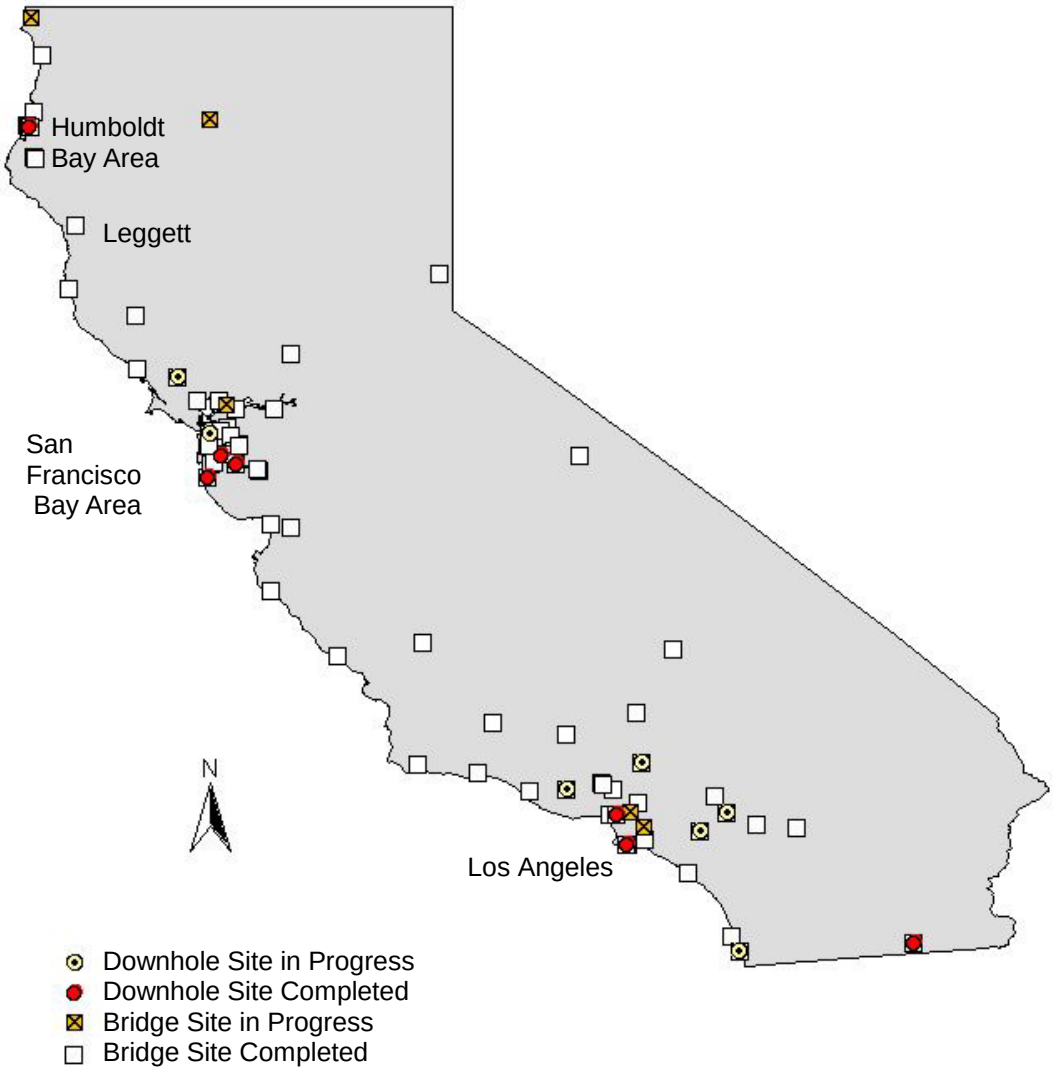

Figure 1

Seismic Retrofitting Challenges Stimulate New Innovations for the Benicia-Martinez Bridge

Roy A. Imbsen and Moe Amini

ABSTRACT

The seismic upgrading of the Benicia-Martinez Bridge, now in the final stages of construction, is an excellent example of how a teaming approach spurs innovation to solve engineering challenges. The Benicia-Martinez Bridge is a high-level, deck-type, welded truss bridge with welded girder approach spans. This 6,215 foot-long structure carries traffic over Carquinez Strait between cities of Benicia and Martinez. New innovations to be shared with the profession in this presentation include:

1. Implementation of the friction pendulum bearing into the retrofit of long span bridges, which includes design, testing, fabrication and installation.
2. Anchorage of existing caissons by core drilling 150-feet down through the caissons into bedrock using innovative monitoring and coring equipment.
3. Load testing of a drilled shaft and pipe piling anchorage using the Osterberg test method.
4. Rocking by allowing axial elongations of the foundation piles.
5. Use of the world's largest friction pendulum isolation bearing.

The concept of seismic isolation is combined with other strategies (e.g., strengthening, ductility, force limitation, etc.) to achieve critical lifeline performance for a maximum credible earthquake at a lower cost than could be achieved without isolation. If the bridge were strengthened without isolation, the full seismic inertia would be developed and transferred from the deck down through the truss system and bearings and reach to the substructure piers and foundations.

Roy A. Imbsen, President, Imbsen & Associates, Inc., 9912 Business Park Drive, Suite 130, Sacramento, CA 95827
Moe Amini, Contract Manager, Caltrans Office of Structure Contract Management, 1801 30th Street MS 12, Sacramento, CA 95816.

BACKGROUND

Following the 1989 Loma Prieta earthquake and resultant damage to the transportation system in San Francisco and the surrounding region, the California governor appointed a Board of Inquiry to assess seismic design criteria used for the California highway system. The board recommended that important transportation structures be designed not only to prevent collapse but in addition remain serviceable in the aftermath of a major earthquake.

Also, following the Loma Prieta quake, the California Department of Transportation (Caltrans) expanded their seismic retrofit program, which had been started in response to the 1971 San Fernando earthquake. Under this program, Caltrans undertook seismic vulnerability studies and prioritized retrofit designs for all bridges statewide. In 1993, Benicia-Martinez Bridge became the first state-owned toll bridge selected for a seismic vulnerability study, which was awarded to Imbsen & Associates, Inc. (IAI).

Following the 1994 Northridge earthquake, Caltrans accelerated their seismic retrofit program for all major toll bridges. Caltrans immediately designated the Benicia-Martinez Bridge a *lifeline* bridge, providing the critical north-south transportation along San Francisco's East Bay area and access to Travis Air Force Base. Lifeline bridges must provide immediate service for emergency vehicles and to the general public following a major earthquake event. This new standard was a significant increase in the, then current bridge design specifications included in the American Association of State Highway and Transportation Officials (AASHTO).

The Benicia-Martinez Bridge is a high-level, welded deck trussbridge, as shown in Figure 1, that carries Interstate 680 over the eastern end of Carquinez Strait between the cities of Benicia, in Solano County, and Martinez, in Contra Costa County. The main bridge consists of seven 528-ft. spans, two 429-ft. spans, and one simply supported 330-ft. span. The contract for the retrofitting of the main truss spans was awarded in 1998 to a joint venture between FCI and Interbeton, for a bid total of nearly $90 million. The most significant and challenging aspect of the contract was the requirement that normal service be maintained in this heavily traveled lifeline structure while construction work was carried out. Only a very limited lane closure schedule was permitted.

Figure 1. Benicia-Martinez Bridge

SEISMIC HAZARD

To meet the seismic performance goals for a lifeline bridge, the retrofit design must keep the structure essentially elastic during a *functional evaluation earthquake* event, having a 40% probability of occurring during the useful lifetime of the bridge (i.e., an earthquake expected to occur once in 300 years). Additionally, the design must allow the structure to provide service to normal traffic immediately following a *safety evaluation earthquake* event, a quake likely to occur once in 1,000 years.

The seismic hazard at the bridge location is contributed mainly by three sources: the San Andreas Fault, 30 miles away, which could give rise to an event with a magnitude (M_W) of 8 or greater and a duration of 40 seconds; the Hayward Fault, 12 miles distant and the potential source of a 20-second, 7.25 magnitude event; and the Green Valley Fault, less than 2 miles away and capable of producing a 13-second, 6.75-magnitude event, as shown in Figure 2.

Recordings obtained from recent earthquakes show that the long-duration pulses generated by near-source earthquakes produced the most damaging effects. The Green Valley Fault is located close to the site and will induce the highest shaking intensity verns the seismic lateral loads. This motion governs the seismic retrofit design.

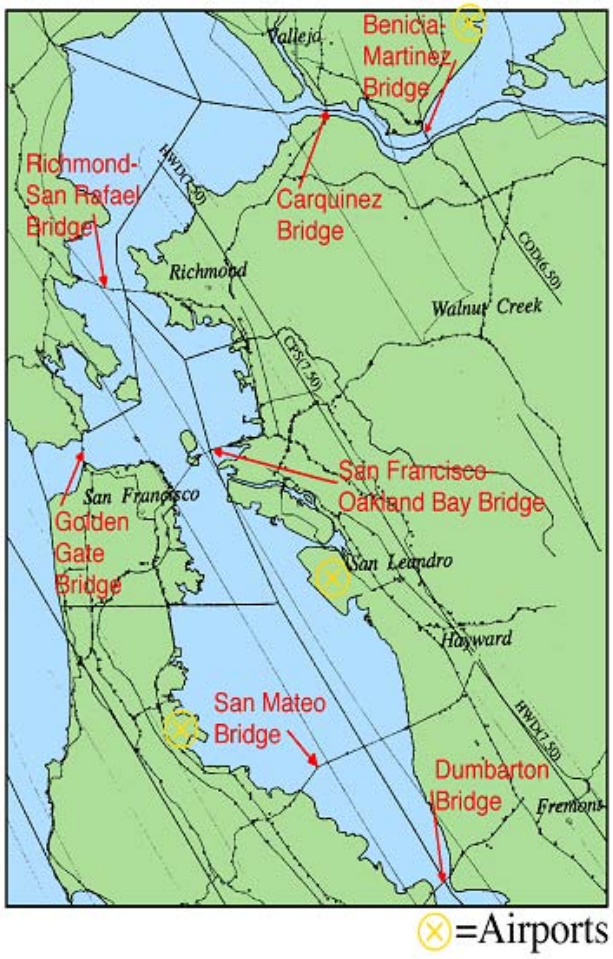

Figure 2. Seismic Hazard Map

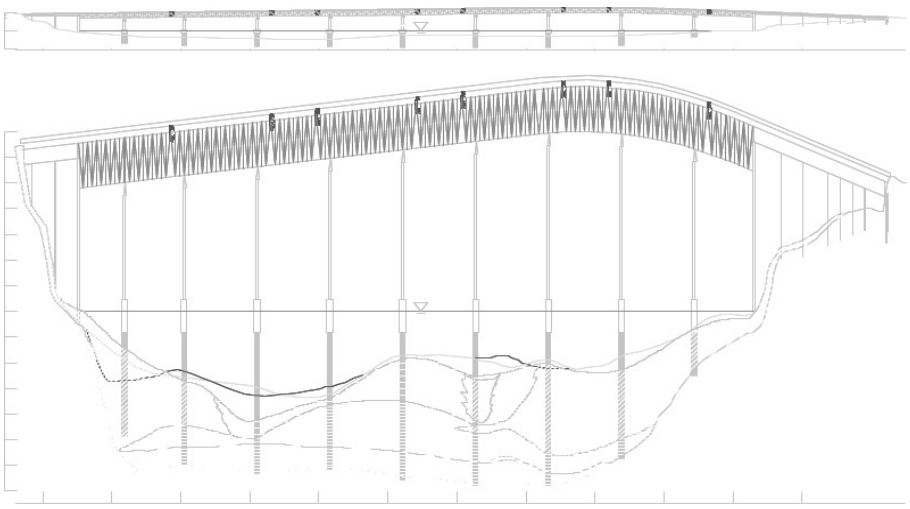

Figure 3. Soil Profile

SEISMIC DESIGN CRITERIA

To meet the new performance goal set for the lifeline bridge and the severe ground motion at the site, a truly ***performance based design*** was implemented. The main design parameters for the Benicia-Martinez retrofit were structural displacements and local deformations for individual components. To accomplish these design objectives, the design was based on *nonlinear seismic analysis* (rather than the conventional force-based, linear approach to design). Minor inelastic flexural deformations and uplifting in the foundation piles were allowed. Caltrans' Seismic Peer Review Panel was actively involved in reviewing and approving the design criteria. The unique construction requirements for the foundation retrofit included drilled shaft and pipe anchorage load testing, and a drilling operation through the existing caissons to install a steel pipe insert.

EXISTING BRIDGE

All bridge piers are set in the water, with the exception of two that are founded on land-based spread footings, as shown in Figure 3. The base section of the water piers consists of four in-line reinforced concrete cells (see Figure 4). The top 40 ft. consists of two split cellular columns (each 15 ft. by 15 ft.) spaced 42 ft. center-to-center. The 25-ft.-deep footings are also of reinforced concrete cellular construction, each with 18 cells.

Four separated continuous spans are supported on fixed bearings. Between these continuous spans, "drop-in" truss spans are suspended by fixed and expansion hinges (see Figure 3). Two trusses, at a spacing of 42 ft. center-to-center, are braced with top and bottom lateral bracing, end sway frames at piers, and intermediate swayframes. All truss bearings are steel rocker bearings, measuring 3 ft. 8 in. from the top of the rocker to the base of masonry plate. Chords and diagonals have an H-type cross section. High-strength bolts are used for truss connections.

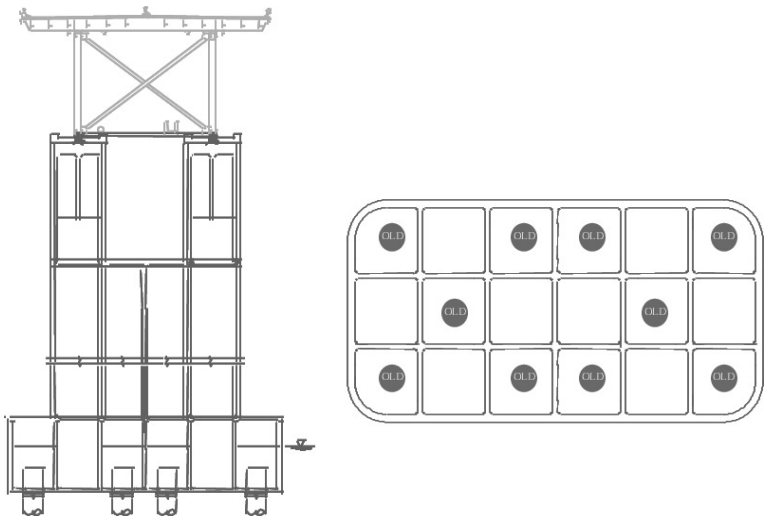

Figure 4. Typical Pier and Footing

Steel caissons 6 ft. in diameter are sunk into bedrock—eight caissons at piers 4 and 12, and 10 at the other piers. At the caisson tips, shown in Figure 3, 60-in.-diameter "rock-sockets" are drilled at least 5 ft. deep into bedrock to anchor the caissons. Spiral reinforcements are provided in the lower 20 ft. of caisson and socket. The caissons are filled with concrete to a depth of 8 ft. into the footing, and the footing cells (where caissons were located) are filled to a total depth of 15 ft. from the bottom of footing. A 12-in. slab rests over the entire footing.

In 1980, cable earthquake restrainer units were placed at the water piers to restrain the trusses vertically and horizontally. Support blocks of reinforced concrete were also placed under the lower chord members of the trusses near the pier faces, as shown in Figure 5.

In addition to the heavy tributary weights of the truss superstructure itself—approximately 6,000 kips per span, the weight of each pier, including the 25 ft. footing, ranges from 10,000 kips to 15,000 kips. It is important to recognize that the seismic inertia loads on the foundations come not only from the truss superstructure but also from the massive piers.

SEISMIC RETROFIT STRATEGY

For deep foundations at the water piers, the cost of achieving fully elastic foundation response could be prohibitively high. Thus, it was cost-effective to allow limited nonlinear ductile behavior in the form of restrained uplift and limited flexural yielding of individual caissons. The uplift and yielding of individual caissons are limited such that the overall caisson group foundation is still essentially elastic. To account for the variability in nonlinear response to ground motion, three sets of ground motions with distinctly different characteristics were selected for the design scenario earthquake; the seismic retrofit design was based on the maximum values of the three ground motion sets.

Figure 5. Truss Span - Bearings

To meet the required performance goals with minimum cost both **strengthening** and **isolation** strategies were considered.

Conventional Strengthening Approach --- If the bridge were strengthened, using fixed rocker bearings, as shown in Figure 6, the full seismic inertia force would be developed and transferred from the deck, through the truss system and bearings, down to the substructure piers and foundations. The truss bearings—the most critical link in the lateral load path—are also the most vulnerable in terms of both strength and stability. The strength capacity of various bearing components (e.g., pintles, anchor bolts, pins, bearing plates, keeper plates) is an order of magnitude lower than the expected earthquake demands. In addition, strengthening the bearings would mean that all connected members (above and below) would be subjected to the full seismic load. Connected members include bracing members, truss chords at the panels adjacent to the bearing supports, and non-redundant expansion hinge hangers that were not designed to transfer transverse earthquake loads or the torsional response of the drop-in spans.

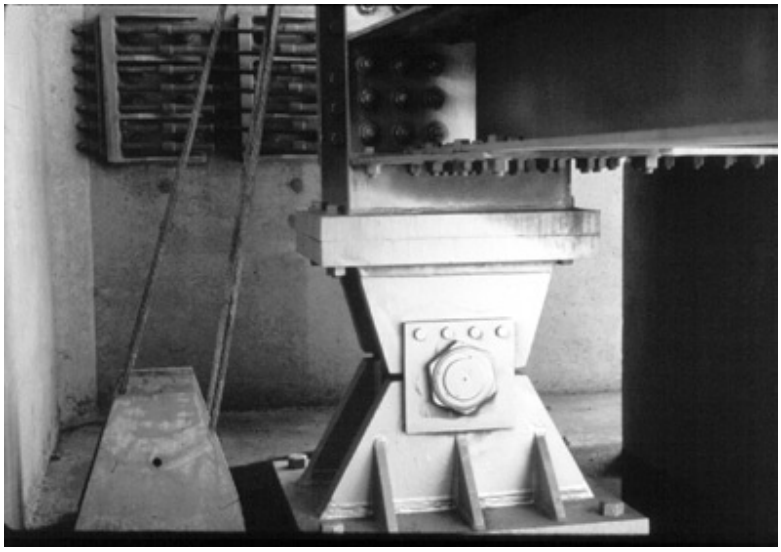

Figure 6. As-Built Bearing

Finally, because of the substantial inertia in the substructure pier and foundation footing, the strengthening approach would expose numerous existing vulnerabilities in the substructure, which include:

- The hollow concrete pier columns lack sufficient flexural and shear capacity and are not ductile.
- The cellular concrete footings transfer load from the piers to the caissons, but the footing blocks are not strong enough to transfer the horizontal shear.
- The axial tension capacity of each caisson at the 5-ft.-deep "rock-socket" is minimal relative to the expected seismic loads.
- Further, the substructure piers would be deficient even under the lower-intensity functional evaluation earthquake event.

All these vulnerabilities must be retrofitted to obtain the required strength.

Seismic Isolation Strategy --- Cost and complexity associated with using strengthening as the primary retrofit method, seismic isolation was adopted as a primary strategy to provide *reliable and predictable performance* under future earthquake excitations. Seismic isolation will decouple the superstructure and substructure dynamic responses, as shown in Figure 7, reducing the seismic loads considerably for both superstructure and substructure. To support the high vertical load at each bearing (more than 3,000 kips), and to accommodate the large seismic horizontal displacement expected (3 to 4 ft.), frictional pendulum isolation bearings were incorporated into the final design, as shown in Figures 8 and 9.

With the seismic isolation bearings incorporated, most truss members and bracing are able to resist the reduced seismic demands elastically. Remaining deficient top lateral members and connections along the load path were identified and strengthened with cover plates or replaced. Hanger elements in the expansion and fixed hinges were strengthened. Adding new vertical and diagonal members to the drop-in spans introduced new load paths for truss torsional demands, reducing the forces in the hangers. New transverse shear keys at the top chord level were also installed at the truss hinges to control relative motion between the drop-in spans and the adjacent fixed spans. Expansion joints at Piers 3 and 13 were designed to minimize deck damage and to facilitate immediate use following an earthquake.

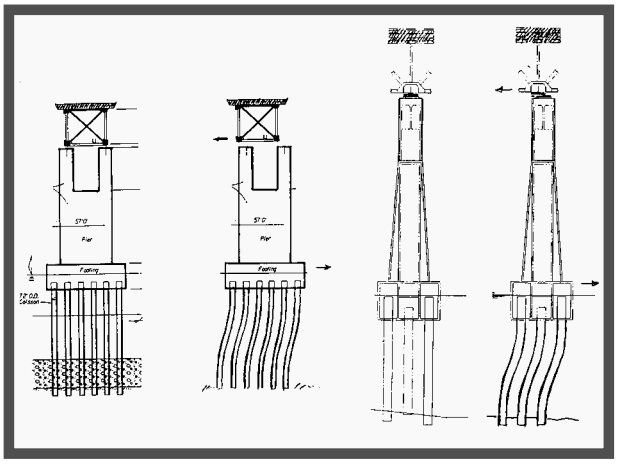

Figure 7. Relative Transverse and Longitudinal Displacemnt at the Isolation Bearing

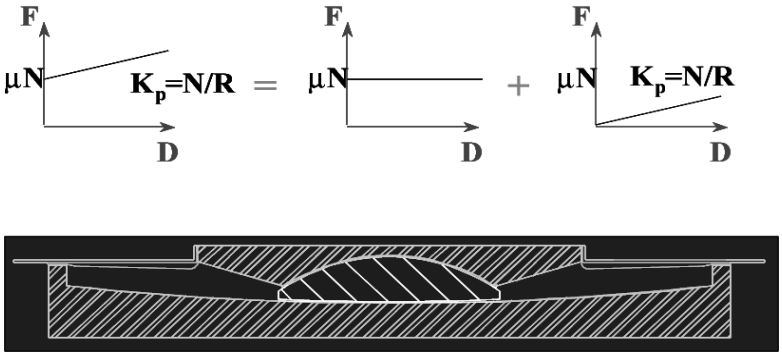

Figure 8. Friction Pendulum Bearing

Foundation retrofit for the substructure piers included adding new caissons, installing pipe tie-downs within the existing caissons, and strengthening the footing boxes to distribute seismic forces to all caissons, as shown in the schematic included in Figure 10. Four new caissons were added to the void cells of the footing boxes at each pier. The new caissons have sufficient anchorage to minimize the uplifting and rocking responses of the foundations. The reinforced rock-sockets were driven to greater depths—50 ft. to 70 ft. into the bedrock—to develop the necessary uplift capacity and to apply compressive forces to the deeper and thus better-quality rock.

Although the new caissons are the main source of resistance to the foundation seismic loads, the existing caissons continue to support service loads. To ensure the existing caisson connections are not damaged during an earthquake, Steel pipe piles, 1 in. thick and 12.75 in. in diameter, were installed in drilled holes inside existing caissons. The pipes are anchored into the rock to produce the required uplift capacities. At the top of the existing caissons, new, stronger connections transfer tension and shear between the caissons and the footing box. Within the upper 10 ft. of the voided footing box , internal reinforced concrete cap beams are provided to establish connections to the new caissons as well as to the new pipe inserts in the existing caissons. This rigid internal cap beam will distribute seismic loads among all caissons during a seismic event.

Footings for the two land piers were enlarged and tie-down anchors added to restrain the rocking response of the footing. Additionally, the footing was keyed to the rock to enhance shear force transfer.

All piers were strengthened such that they will remain elastic under seismic lateral loads. However, the existing cellular reinforced concrete piers have low ductility that can not be easily enhanced. Therefore, the pier retrofit incorporated interior stiffener walls as well as external sloping walls. The geometry of the sloping walls was designed to significantly increase the stiffness of the existing piers such that the base reactions along the external rows of existing and new caissons can be mobilized. Pier wall reinforcements are developed into the newly added internal footing caps. These retrofit measures are intended to ensure elastic response of the pier shafts and footings during the safety evaluation earthquake event. Minor yielding is restricted only to the top of the concrete-filled steel caissons. For deep soft soil site, it is crucially important to prevent flexural yielding of caissons occurring at some distance below the mudline.

Figure 9. Installed Friction Pendulum Bearing

RETROFIT CONSTRUCTION

Replacement of existing bearings with isolation bearings under traffic is delicate work. At Benicia-Martinez, the pier columns supporting the bearings measure 15 ft. by 15 ft. The replacement strategy had to allow for removal of the rocker bearings and placement of the largest bridge isolation bearings ever used—up to 12 ft. by 12 ft. Due to the recent development of these bearings, quality control and manufacturing specifications were important ingredients of the contract. The effects of aging, service load movements, temperature-related movements, rusting, and maintenance on the bearings are thoroughly evaluated during the design process.

The varying soil profile along the bridge alignment contributes to the significantly different seismic responses at various pier locations. The elevation of the bedrock, as shown in Figure 3, consists of intermingled claystone, siltstone, and sandstone. The bedrock varies from the ground surface at both ends of the bridge to 120 ft. below the mean sea level in the channel. Similarly, the mudline elevation ranges from 90 ft. to 40 ft. below mean sea level. Local scouring has occurred around the piles at all piers. Logs of test borings (LOTB) revealed considerable material variability in the rock layers under the channel. The test results also showed fairly steep orientations of rock layer formations with respect to the horizontal plane. This resulted in considerable material variation across any given elevation.

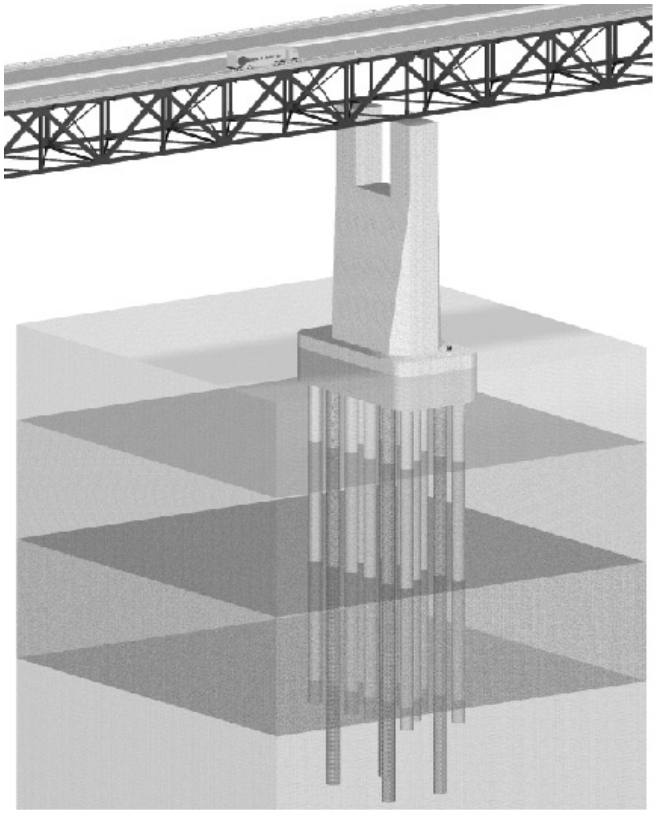

Figure 10. Typical Pier Foundation

These logs formed the basis for determining the required design anchorage length for drilled shafts (for new caissons) and pipe inserts (for existing caissons). Due to the high design loads (up to 12,500 kips for the drilled shaft) as well as the uncertainties arising from the rock property variation, pile anchorage load testing program was the first order-of-work. This allowed project engineers to take necessary corrective actions up front by increasing or decreasing tip elevation.

At approximately mid-height of the anchorage, load cell devices were installed to test the upper anchorage strength against the lower anchorage strength. Compressible material was placed at the base of the test anchorage to prevent end bearing contribution to the lower segment and thus allow accurate reading of the anchorage strength. All tests successfully confirmed the design strength for rock anchorage.

Holes were drilled in the existing caissons, for the placement of the 12-3/4 in.-diameter steel pipe. Since the existing caissons continued to support the service loads during construction, the drilling operation was extremely critical and required significant quality control measures. Contractual specifications called for monitoring the relative position of the drilled hole with respect to the center of the caissons at intervals of 20 ft. (in the upper zone) to 45 ft. (in the lower zone).

The monitoring system measured the thickness of concrete around each hole in different directions to establish the relative deviation of the center of the hole with respect to the center of the caisson. A maximum deviation of 12 in. was specified over the entire length of the caissons (up to 145 ft.). This safety measure minimized the chances of damaging existing steel casings during drilling operations. Although a single source of error could have fallen within the tolerance of the drilling operation, imperfection of existing caissons could also have resulted in drilling offsets.

An impact echo monitoring system was used to measure the travel for sound waves and to establish the eccentricity of the drilled hole with respect to the center of the existing caissons. Excessive deviations were then corrected by either filling the hole and re-drilling or by altering the direction of the drilling for the remainder of the work.

CONCLUSIONS

The seismic retrofit of the Benicia-Martinez Bridge proceeded smoothly to completion on budget and within schedule. In response to the successful use of large friction pendulum seismic isolation bearings in this project, bearings of similar and bigger sizes are being used for seismic retrofit design on other major bridges nationwide—making the structural response during seismic events much more predictable and greatly improving bridge serviceability following an earthquake. This is particularly important for the transportation network in major metropolitan areas.

Because a large portion of the bridge's structural weight lies in its substructure piers and footings, significant strengthening of these foundation components is required during the seismic retrofit. But the Benicia-Martinez retrofit project demonstrated that even for the highest level of seismic performance requirements, it is not necessary to require that the foundations remaining elastic, as required in conventional seismic design practices. Limited nonlinear behavior in the form of flexural yielding of the concrete-filled steel caissons and the restrained uplift of caissons were allowed in this project, resulting in significant reduction of the retrofit construction cost.

Using innovative seismic isolation technology, engineers completed a seismic retrofit on the Benicia-Martinez Bridge – located in the most hazardous earthquake zone in California.

West Anchorage Design of San Francisco – Oakland Bay Bridge Main Span for Seismic Loads

John Sun, Rafael Manzanarez and Marwan Nader

ABSTRACT

Located at the rocky edge of the Yerba Buena Island, the west anchorage of the San Francisco – Oakland Bay Bridge suspension span serves as the anchor for this single tower self-anchored suspension bridge.

With extensive comparative studies on numerous alternatives, the new looping cable anchorage system is recommended for the final design of the west anchorage of the self-anchored suspension span. The looping cable Anchorage system essentially consists of a prestressed concrete portal frame, a looping anchorage cable, deviation saddles, a jacking saddle, independent tie-down systems, and gravity reinforced concrete foundations. This anchorage system is chosen for its dimensional compactness and structural efficiency as well as reliability under static and seismic loads. This paper describes the major design issues, design philosophy, and key structural elements of this innovative suspension cable anchorage system.

John Sun, Senior Bridge Engineer, T.Y. Lin International, 825 Battery Street, San Francisco, CA 94111, Phone: (415) 291-3700, Fax: (415) 433-0807, E-mail: jsun@tylin.com

Rafael Manzanarez, Vice President, T.Y. Lin International, 825 Battery Street, San Francisco, CA 94111, Phone: (415) 291-3700, Fax: (415) 433-0807, E-mail: rmanzanarez@tylin.com

Marwan Nader, Associate, T.Y. Lin International, 825 Battery Street, San Francisco, CA 94111, Phone: (415) 291-3700, Fax: (415) 433-0807, E-mail: mnader@tylin.com

INTRODUCTION

In May 1998, the Bay Area Metropolitan Transportation Commission selected the self-anchored, single tower suspension alternative as the signature span of the San Francisco-Oakland Bay Bridge East Span Seismic Safety Project (SFOBB). The rendering of the bridge is shown in Figure 1.

While the single tower asymmetric suspension bridge satisfies the aesthetic preference of the bridge type selection committee, the concept of "self-anchored" is dictated by the geotechnical condition, shown in Figure 2. At the east anchorage pier, the combined depth of young bay mud, old bay mud, and sand layers reaches over 100 meters above the Franciscan rock formation. Such soil conditions make construction of the conventional earth anchorage undesirable in both technical and economic terms. The deck anchorage system becomes the natural choice for the east anchorage, and consequently for the west anchorage.

Figure 1. Rendering of the East Bay Suspension Span

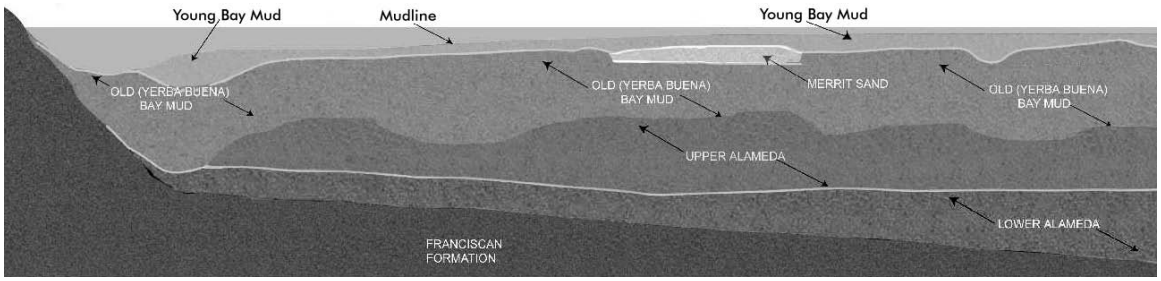

Figure 2 East Bay Bridge Soil Profile

Looping Cable Anchorage System

Among all the key structural components in this suspension system, the west anchorage is one of the most critical elements for several considerations:

- The west anchorage piers also take up to 70% of the total base shear in the critical longitudinal direction under critical seismic loads. This requirement results from the limited shear capacities of a very flexible tower and the east anchorage pier being founded on a flexible pile foundation system in the bay mud.
- The post-yield behavior of the west anchorage pier columns has a significant effect on the residual displacement, or "permanent set" of the main suspension span.
- The 17400 5.4-mm diameter wire cable is capable of developing up to 700 MN of (or 70,000 metric tons, cable-breaking capacity) cable force with about 280 MN (or 28,000 metric tons) uplift at deck level.
- The west anchorage structural system must resist longitudinal compression thrusts from the orthotropic deck without significant local effects, such as bending or shear lag.

- The anchorage must also satisfy all geometry requirements, such as roadway clearance, minimum saddle radius, the single plane requirement of the anchorage cable layout, and roadway elevation differential.
- The west anchorage shall be compact and clean so that it is a natural part of the grace that the bridge has.

A number of anchorage systems may be used to deliver the requirements. Among the alternatives studied are:

- *Box-side Cable Splay Anchorage System I*
- *Box-Side Splay Anchorage System II*
- *Box-side Anchorage with Mid-Air Floating Saddle*
- *Loop Cable Anchorage*
- *Giant Block Anchorage System*
- *Integrated Pier Anchorage*

Based on extensive comparative studies, the ***Looping Cable Anchorage*** is chosen for final design for its dimensional compactness and its structural efficiency as well as reliability to resist static and seismic loads.

As shown in an isotropic view of looping cable at west anchorage in Figure 3, unlike the conventional cable anchorage system, the main cable is not splayed at the west piers, instead, is continuously looped around the west anchorage cap beam. This looping of the cable is achieved by using a pair of deviation saddles at the outer edges of both roadways, and a jacking saddle located at the center-line of the cap beam.
While the deviation saddles provide bearing resistance for the looping cable, the jacking saddle ensures the balance of the cable forces in the "live cable" and anchorage cable.

3a. Looping Cable Geometry 3b. West Anchorage Key Elements

Figure 3. Looping Cable Anchorage Layout

Essentially, the looping cable anchorage system has major elements: the looping cable and companion saddles, and the flexible anchorage prestressed concrete frame system. In the following sections, design issues of layout, the looping cable geometry, and the design concept of the flexible anchorage frame as well as its effects on the global bridge behavior will be discussed.

Loop-cable anchorage geometry layout

Design of the looping cable anchorage starts with the anchorage cable geometry layout. Following factors have been accounted for in setting anchorage cable geometry:

- The overall looping anchorage cable must be placed on a single plane to keep the out-of-plane bending on cable saddles to a minimum.
- The longitudinal compression resultant thrust developed within the west anchorage cap beam joint should be at the same elevation as the centroid of each main box girder to avoid locked-in bending of the deck under dead load.
- The minimum possible saddle radius should be used to keep the anchorage dimension compact.
- The roadway layout, overhead clearance for the most outer lanes, and cable geometry at dead and service loads near the west anchorage are among the other factors considered in the design.

The determination of the loop cable geometry is the result of an interactive optimization procedure.

West Anchorage Portal Frame

As shown in Figure 3b, the west anchorage flexible frame consists of two multi-column reinforced concrete (RC) piers, a prestressed concrete cap beam monolithically connected to the piers, independent cable tie-down systems, and reinforced concrete gravity foundations. The design philosophy of this prestressed concrete flexible frame is reflected in the designated structural functions of its sub-structural elements, which are described individually in the following sections.

Cap Beam

The west anchorage cap beam has several structural functions. First, together with the deviation saddles and the jacking saddle, it anchors the main cable to the cap beam-pier joints of the anchorage frame. The massive cable force is then redistributed in the transverse, longitudinal and vertical directions through the cap beam. Secondly, as the most important "joint of the bridge," it connects the main cable, the west anchorage piers, the main span box girders, the west approach span hinges, and the expansion joint. Thirdly, it serves as a counterweight for the main span for design service loads.

Multi-Column Piers

Since the east pier of the bridge is on a flexible piled foundation with piles of more than 100 meters in length, and the multi-shaft tower of 160 meters in height is very flexible, the overall structural stiffness, especially in the longitudinal direction, is dictated by that of the west piers.

A number of pier cross-sections for concrete, steel, and concrete-steel composite materials are considered at the preliminary design phase. These alternatives include a single hollow rectangle with four corner columns, a twin-column, and a four-column pier section. The four-column pier is recommended for the final design for the following considerations:

- The lateral flexibility of the four-column piers increases the fundamental period of the bridge to more than 3.5 seconds, thus significantly improving the bridge global response.
- The multi-reinforced concrete columns have adequate vertical stiffness to limit the first vertical mode period less than 0.1 seconds, away from the peak vertical response period of 0.15 seconds.
- The reinforced concrete columns have proven displacement capacity when adequately confined.
- The concept ensures consistency in use of the reinforced concrete material from cap beam to pier, then to foundation, consequently reducing the difficulties in connection details, resulting in a more reliable structural system.
- It maintains the aesthetic harmony between the flanking piers and the tower.
- It is also an economical alternative.

Another key issue of the pier design is connectivity between the pier and cap beam. Theoretically, there can be three types of pier-cap beam connections, namely, bearing connection, monolithic connection – I/full moment transfer, and monolithic connection – II/partial moment transfer.

The concept of a "pin" seems attractive since it eliminates the bending moment transfer to the deck girder from the piers. However, it proves to be difficult to achieve due to the large vertical force under combined dead and critical seismic loads. The "pinned bearing" is also undesirable for erection loading conditions considering a flexible tower and sliding bearing at the east pier. Furthermore, the condition of a theoretical "pin" is also questionable within the 150 years of bridge service life.

A "fully fixed" versus a "partially fixed" monolithic connection is also studied and compared. The idea of a "partially fixed" connection is to design a pier column section so that it functions as the "fixed" joint during erection, service, and functional earthquake loads, and functions as a hinge when designed moment capacities are exceeded under Safety Evaluation Earthquakes (SEE). It is important to note that this connection concept works only when there is a large enough differential between the design moment for erection and service load, and that for the safety evaluation seismic loads. Since the "partially fixed" hinge near the cap beam requires that section moment

capacity within the hinge is significantly smaller than that of adjacent column sections, dimensional narrowing at the hinge sections are required to achieve this design objective. Another concern about the "partially fixed" concept is that it will experience more frequent damages and repairs than that of a "fully fixed" connection. This may have a negative psychological impact on commuters.

After overall considerations, the design team recommended a full monolithic connection between the pier and cap beam.

In addition, two performance requirements guide the effort of the west anchorage pier seismic design:

(a) Minimal Damage Criteria for Functional Evaluation Earthquakes (FEE)

Minimal damage implies essentially elastic response, and is characterized as minor inelastic response/narrow cracking in concrete/no apparent permanent deformation. This requirement is represented by limiting the maximum concrete compression strain to less than 0.004, and maximum tensile strain for the reinforcement to 0.001 under FEE loads.

(b) Repairable Damage Criteria for Safety Evaluation Earthquakes

Repairable damage is characterized as yielding of reinforcement (not necessarily for replacement)/spalling of concrete/small permanent deformation. Repairable damage is ensured by limiting the maximum concrete compression strain to less than 2/3 of the ultimate concrete strain derived from Mander's model, and the maximum tensile strain in the reinforcement to less than 2/3 of the defined ultimate steel tensile strain. In addition, the permanent displacement must be less than 300 mm for both the flanking piers and the tower.

The reinforcement design of a pier column is shown in Figure 21. The critical pushover analysis in bridge longitudinal direction, shown in Figure 22, clearly demonstrates the adequacy of the pier design.

Tie-Down System Design

The tie-down system is designed to take the additional uplift action at the west anchorage under seismic events and to ensure the integrity of the vertical load carrying system of the bridge.

It is also important to note that the tie-down cables are not attached to pier columns so that these cables are kept from being damaged when the pier columns experience large lateral displacement, even failure, under a major seismic event.

CONCLUSIONS

The loop cable anchorage system provides an efficient, reliable, and compact cable anchorage solution for the west anchorage of the east Bay Bridge suspension span. It is developed to meet the challenges imposed by the unique bridge structural layout and aesthetic requirement.

ACKNOWLEDGEMENT

The authors would like to acknowledge the invaluable discussions with Dr. Man-Chung Tang, Mr. Charles Seim of T. Y. Lin International, Mr. Paul Mueller of Mueller Industries, Inc., Mr. Herb Rothman of Weidlinger Associates, Mr. Jackson Durkee, Mr. Hajime Hosokawa of Nippon Steel, and Dr. Frieder Seible of UC San Diego. Our sincere thanks also go to Dr. Brian Maroney, Mr. Ade Akinsanya, and Mr. Vong Toan of California Department of Transportation for the comments made during the bridge's final design phase.

REFERENCES

[1] Man-Chung Tang, Rafael Manzanarez, Marwan Nader, Sajid Abbas and George Baker, "Replacing the East Bay Bridge," J. of Civil Engineering, Sept. 2000, pp. 38 – 43

[2] John Sun, Rafael Manzanarez, "Cable Report," Submitted to California Department of Transportation for the San Francisco – Oakland Bay Bridge East Span Seismic Safety Project, April 28, 2000.

Seismic Retrofit of the US 40/I-64 Double Deck Bridge

Mark R. Capron, P.E.

ABSTRACT

This paper presents a summary of the seismic retrofit of the US40/I-64 Double Deck Bridge Complex in St. Louis, Missouri. This complex includes some 15,700 feet of elevated roadway with details typical of 1960's design standards. The discussion includes development of the retrofitting strategy for the over 65 million dollar project and a number of non-seismic issues that have been encountered on the project.

Mark R. Capron, P.E., Project Manager and Structures Fellow, Jacobs Civil, 501 North Broadway, St. Louis, Missouri, 63102

INTRODUCTION

This paper presents a summary of the design and construction of the seismic retrofit of the US 40/I-64 double deck bridge complex in St. Louis, Missouri. This complex provides the Missouri approaches to the Poplar Street Bridge over the Mississippi River, and with over 130,000 vehicles per day, is one of the most critical transportation links in the state. Jacobs Civil (formerly Sverdrup Civil) has provided seismic evaluation and retrofit design for this important bridge complex. The following paragraphs present a description of the bridge, the seismic evaluation and retrofitting strategy, non-seismic issues, and conclusions for the project.

DESCRIPTION OF THE BRIDGE

The US 40/I-64 double deck complex includes more than 15,700 feet of side-by-side and double deck elevated roadway. The project is located in downtown St. Louis, and the land beneath and adjacent to the structure is heavily used for buildings, parking, access roads, and active rail lines. The superstructure consists of reinforced concrete deck supported on multi-girder and two-girder steel framing. The steel girders are three to five span continuous construction with discontinuity for thermal expansion provided by steel bearing supported hinges located within the spans and about five feet from the bents, as shown in Figure 1. The superstructure is supported on the bents by steel rocker type and fixed type bearings. A total of 270 steel bearings are used in the expansion hinges and some 764 steel bearings are located on the bents. The substructure consists of 139 reinforced concrete bents (see Figure 2) with rectangular, circular, and elliptical columns and reinforcement lap splice details typical of mid-1960 design standards. The majority of bents are supported on battered steel H-piles driven to rock at depths of 14 to 83 feet, while 21 of the bents are supported on 42-inch to 60-inch diameter drilled shafts that are founded on rock at depths of 24 feet or less.

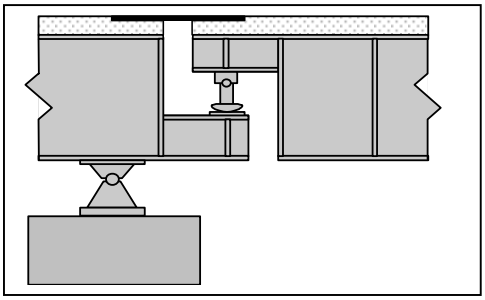

Figure 1. Typical Expansion Hinge

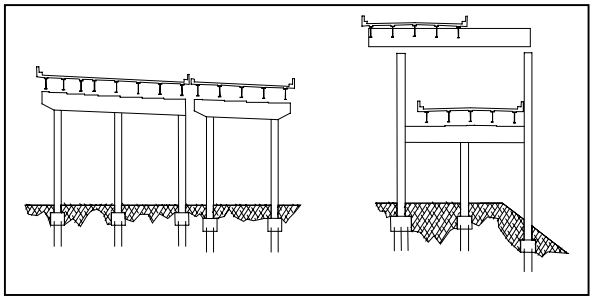

Figure 2. Typical Bents

SEISMIC EVALUATION AND RETROFITTING STRATEGY

Seismic evaluation of the complex was based on [1, 2]. Key seismic parameters included Acceleration Coefficient, A=0.10, Soil Type II, and the AASHTO design spectra [3]. Due to the size of the project, the evaluation was conducted with a series of tasks, each of which was intended to progressively define the seismic vulnerabilities of the structure and then to develop a seismic retrofitting strategy for the complex. Initially, typical bents and details were evaluated for the empirical demands given in [1, 2]. Next, multi-mode response spectra dynamic analysis was performed for the entire complex with both seismic isolation bearings and conventional bearings, and detailed Capacity Demand (C/D) ratios were evaluated for 13 representative bents [4]. Then C/D ratios were evaluated for all of the bents and a retrofitting strategy involving a seismic isolation system along with retrofits of the column splices and restraint of the expansion hinges was adopted. As final design of the retrofit was developed, the cost and complexity of replacing the existing bearings was identified as a major construction risk, and a strategy for competitive procurement of an isolation system that encouraged retention of many critical existing bearings was developed and implemented [5]. During final design, additional studies of the vulnerabilities of critical components were performed and 83 foundations, the cross frames at the bent lines, and the rocker type bearings at the expansion hinges were identified as requiring retrofits. Also, both of the two proposals that were developed for the isolation system recommended replacement of all 764 of the existing bearings at the bents. Upon evaluation of the isolation system proposals, and the construction risks of replacing all of the bearings, the project team elected to terminate selection of an isolation system, and to investigate alternatives to bearing replacement.

The studies of alternatives to bearing replacements concluded that the seismic performance objectives for the project could be satisfied by retrofit strategies that minimized bearing replacement through strengthening of critical structural components, as well as strategies that required replacement of most of the bearings with seismic isolation bearings along with less extensive structural modifications. Based on evaluation of the estimated cost and construction risk of the various alternatives, a retrofitting strategy was adopted that focused on structural modifications and minimized bearing replacement. Final design of the adopted retrofitting strategy included the following components:

- Replacement of the bearings at 14 bents with PTFE sliding bearings,
- Replacement of the cross frames at all of the bents,
- Strengthening of the cross girders that support the upper deck,
- Longitudinal and transverse bumpers at the bent bearings,
- Conventionally reinforced and prestressed modifications to the bent caps,
- Steel and prestressed concrete confinement jackets for the columns,
- Modification of the footings with the addition of groups of 30-inch diameter drilled shafts,
- Replacement of the expansion hinge bearings with PTFE sliding bearings and restrainers, and
- Seat extensions and PTFE sliding bearings at the abutments.

NON-SEISMIC ISSUES

During development of the project, issues were encountered with the cost and the size of the project. Preliminary estimates of the project cost were on the order of 25 million dollars while the estimated cost at completion of the final design phase was about 65 million dollars. The primary areas of cost increase included the cost of modifications to the superstructure cross frames and cross girders to accommodate seismic forces, the cost of removing lead paint and repainting the structure, and the cost of replacing the lighting system on the structure, and the cost of replacing a large retaining wall along a portion of the structure. MoDOT initially planned to issue a single contract for retrofit of the complex; however, feedback from potential contractors revealed concern for unacceptable cost risk with a single contract. Based on input from the contractors, MoDOT divided construction of the project into a number of smaller packages.

Because the project is located in a congested urban area, construction of the project has been complicated by the following factors:

- The land beneath the bridge is owned by a number of different owners, which required multiple agreements to obtain temporary right-of-way for construction of the project. Because of the difficulties in obtaining and maintaining these agreements, MoDOT is currently evaluating obtaining permanent right-of-way for the project.
- Access through and around the construction areas must be maintained during construction to provide for continued operation of the businesses adjacent to the structure. This has presented a number of safety related issues, as well as complicated construction operations.
- There are multiple underground utilities in the area of the footing modifications, many of which are unknown until encountered during construction. These utilities have required redesign of a number of footing modifications to clear buried pipes and cables that can not be economically relocated.
- The close proximity to aboveground structures and utilities has restricted access to placing reinforcement in the bentcaps and drilled shafts. Based on feedback from the contractor, several of the details in the bentcap reinforcing steel were modified to simplify construction.
- Limited headroom beneath the bridge has required a number of specialized drill rigs to install the drilled shafts. This issue was extensively reviewed with the contractors prior to beginning construction and has been resolved.
- The need to maintain traffic during construction of the retrofit has greatly restricted the times available to install connections to the roadway slabs.

CONCLUSION

This paper has presented a summary of the development of the seismic retrofit of a major double deck bridge project. Development of the retrofitting strategy considered alternatives that replaced all of the bearings with seismic isolation devices, as well as strategies that minimized bearing replacement through structural modifications. Based on evaluation of estimated cost and construction risk, a strategy that minimized bearing replacement was selected for the project. The estimated construction cost of the project was greater than initially planned due to the cost of strengthening superstructure components, repainting the structure, replacing the lighting system, and replacement of a large retaining wall along the structure. Construction was complicated by a congested urban site and the need to interface with multiple land owners and users of the land beneath the bridge.

ACKNOWLEDGEMENT

The author wishes to acknowledge the contributions to the project of a number of engineers at MoDOT, FHWA, and Jacobs Civil.

REFERENCES

[1] Federal Highway Administration (FHWA) 1983, *Seismic Retrofitting Guidelines for Highway Bridges*, Report No. FHWA/RD-83/007, Springfield, Virginia, National Technical Information Service (NTIS).

[2] FHWA 1995, *Seismic Retrofitting Manual for Highway Bridges*, Publication No. FHWA-RD-94-052, Springfield, Virginia, NTIS.

[3] American Association of Highway and Transportation Officials (AASHTO) 1996, *Standard Specifications for Highway Bridges, Division IA Seismic Design*, Washington, D.C, AASHTO.

[4] Capron, M. R. 1999, *Modeling and Analysis for Seismic Retrofit of the US40/I-64 Double-Deck Complex in St. Louis, Missouri*, St. Louis, Missouri, Proceedings Mid-America Highway Seismic Conference.

[5] Capron, M. R. 1997, *An Approach to Competitive Procurement of Seismic Isolation Systems*, Sacramento, California, Proceedings National Seismic Conference on Bridges and Highways.

Bridge Abutment Model Sensitivity for Probabilistic Seismic Demand Evaluation

Kevin Mackie[1] and Bozidar Stojadinovic[2]

INTRODUCTION

Modeling the contribution of bridge abutments to overall bridge seismic response has been the focus of a significant research effort in the past decade. Many recent studies have shown how that abutment response significantly influences the response of short-and medium-length bridges. Some of these studies are based on sensitivity analyses using deterministic bridge models with varying abutment characteristics and capacities, and a relatively small number of earthquake ground motions.

In this paper, a comparison of Probabilistic Seismic Demand Models (PSDMs) obtained using Probabilistic Seismic Demand Analysis (PSDA) is used to conduct a sensitivity study on how bridge abutment models affect seismic demand for short- and medium-length bridges. The advantages of this method are in a large number of earthquake ground motions used in the sensitivity analysis, and in a probabilistic interpretation and comparison of bridge demand. Abutment capacity is not considered at this point because of a shortage of reliable abutment capacity data. PSDMs are a part of a performance-based seismic design framework developed by the Pacific Earthquake Engineering Research (PEER) Center. This design framework is based on the principle of de-aggregation of uncertainties that define probabilistic performance-based seismic design. Given a class of structures, such as typical highway overpass bridges, PSDMs define the relation between seismic hazard and structural demand. They are typically used to compute the probability of exceeding an Engineering Demand Parameter (EDP), such as drift, given the value of a seismic hazard Intensity Measure (IM), such as Arias intensity. Comparison of PSDMs for bridges with systematically varied abutment models gives a probabilistic characterization of the effect of abutments and their importance in the overall seismic demand for a bridge.

[1]Kevin Mackie, Graduate Student, Dept. of Civil & Env. Engineering, University of California, 721 Davis Hall #1710, Berkeley, CA 94720-1710
[2]Bozidar Stojadinovic, Assistant Professor, Dept. of Civil & Env. Engineering, University of California, 721 Davis Hall #1710, Berkeley, CA 94720-1710

PROBABILISTIC SEISMIC DEMAND MODEL

The PSDM is the outcome from a Probabilistic Seismic Demand Analysis (PSDA) [1]. The procedure used to formulate the PSDMs of interest involves five steps. First, a set of ground motions is selected and categorized according to Intensity Measures (IMs) descriptive of their content and intensity. Secondly, the class of structures to be investigated is defined, along with a suite of Engineering Demand Parameters (EDPs) that can be measured during analysis to assess structural performance. Thirdly, a finite element analysis model is generated to model the class of structures selected, with specific allowances for varying the abutments through parameters. Fourthly, nonlinear dynamic analyses are performed until all motions and abutment model combinations have been exhausted. Finally, a demand model is formulated between resulting IMs and structural EDPs. The PSDA process, IM and EDP definitions, and application to various PSDMs are detailed elsewhere [2].

In this study, the IMs were limited to Peak Ground Velocity (PGV), Cumulative Absolute Displacement (CAD), and Arias Intensity only. The bridge EDPs used are strictly displacement based, including global drift ratio (Δ) and column section displacement ductility (μ_Δ). Nonlinear models were generated for each bridge configuration and analyzed using the PEER OpenSees (www.opensees.org) platform. The EDPs are assumed to follow a log-normal distribution [3]. As a result, each of the following PSDMs is plotted in log-log space, with the EDP on the abscissa and the IM on the ordinate. Coefficients of a linear, or piecewise-linear regression then yield linear equations. The dispersion values for each regression analysis are listed in each corresponding figure. Each demand model is constructed in the longitudinal and the transverse direction independently.

Class of Structures and Analytical Model

Typical new California highway overpass bridges are selected as the class of structures. The bridges presented in this paper are designed according to Caltrans specifications [4] for reinforced concrete bridges. Configurations in this study are limited to two-equal-span overpasses with seat-type abutments on either end. Common to all bridges is a single column bent continuing below grade into a Type I integral pile foundation.

The base bridge configuration includes two 60 ft spans, a single-column bent 30 ft above grade, with a 5.25 ft diameter circular column, 2% longitudinal perimeter bar reinforcement, and 0.7% transverse spiral reinforcement. The base bridge is on a NEHRP C soil site. Bridge columns and pile shafts are modeled using three-dimensional flexibility-based beam-column elements. This element is limited to axial-flexural interaction, hence no shear failure is modeled. P-Δ effects were included for the column, but no other methods of softening were incorporated into the model. Soil-structure interaction was modeled using bilinear *p-y* springs placed at varying depths along the length of the pile shafts. The bridge deck was designed as a typical reinforced concrete box girder section for a three-lane roadway. The deck was assumed to remain elastic, therefore input into the model using elastic elements with cracked stiffness properties. Each abutment model comprises a five-element array of gap-spring elements in the transverse direction, two gap-spring elements in the longitudinal direction, and five gap-spring elements in the vertical direction. Different bridge instantiations were generated by varying parameters as described below.

Abutment Models

Bounds for abutment stiffness and mass variation are based on existing abutment methods. First group of methods is based on the Caltrans procedure for determining longitudinal and transverse stiffness' and strengths of an abutment [4,5]. Longitudinal direction values are formulated by combining passive backwall pressure, shear strength of the wall itself, and strength and stiffness of the pile groups

supporting the abutment. These stiffness and strength values have been validated in large-scale abutment tests [6]. Transverse direction values are computed assuming a seat-type abutment with resistance from the wing walls, shear keys, and pile group. Obtained transverse stiffness and strength values are smaller than those obtained using Caltrans procedure. An idealized trilinear backbone force-displacement response curve was used to model the abutments, with varied stiffness and strength values shown in Table 1. These values were used as input parameters for the gap-spring elements in the OpenSees bridge model, described above.

A second group of methods involves deriving the response of the soil embankments in the transverse direction. Assuming a symmetric embankment with defined cross-section geometry, soil shear moduli and unit weight, Wilson and Tan determine the stiffness per unit length of the embankment [7]. The total stiffness is then derived from an estimated wing wall length. This length is purposely underestimated to make the transverse stiffness conservatively low. Wilson and Tan assume that abutment longitudinal stiffness is the same as transverse and calculate the vertical stiffness using the same cross-section approach. Using a similar procedure, Zhang and Makris generalize to any embankment geometry and calculate transverse and vertical stiffness and damping values for dynamic abutment response calculations [8]. Only the stiffness value is used herein. As in Wilson, longitudinal and transverse stiffness' are assumed the same.

TABLE 1. ABUTMENT STIFFNESS AND MASS PARTICIPATION VALUES

Proposed by	**Longitudinal Ka_l (k/in)**	**Transverse Ka_t (k/in)**	**Vertical Ka_v (k/in)**	**Participating mass (k s^2/in)**
Caltrans [4, 5]	2215	627	NA	7.4
Maroney [6]	1080, 168	487	NA	5.7 [9]
Wilson & Tan [7]	587	587	1643	7.4
Zhang & Makris [8]	1006	1006	2817	12.6

The other fundamental factor governing abutment response is the inertial force it generates during an earthquake. This force is included in the analysis using a concentrated mass at the abutments. Coupled with the stiffness quantities defined above, the abutment becomes a single degree of freedom oscillator attached to each end of the bridge. Determining the mass participating in abutment response is highly uncertain and is usually approximated by a critical length of the embankment. Different researchers have proposed participating lengths that best match recorded data [8, 9] as shown in Table 1. As suggested Wissawapaisal and Aschheim [10], this critical length may vary with earthquake intensity. Hysteretic damping is not included in any of the abutment models, but 2% Rayleigh system damping is.

ABUTMENT MODEL SENSITIVITY

Sensitivity studies were performed by varying, in turn, longitudinal stiffness, transverse stiffness, and participating mass of both abutments. Stiffness values range from 0 (no abutment case, only rollers) to 1000 k/in. Mass values range from 0 to 8 ks^2/in. To differentiate between the effect of increasing abutment stiffness and mass, longitudinal stiffness' are varied for the cases of no mass and a median mass. The resulting PSDMs shown below are not necessarily the optimal PSDMs for the given IM-EDP combinations. Optimal models utilize first mode spectral acceleration for the IM. Period independent IMs have been used in order to isolate the affect of abutment stiffness change on the response.

Longitudinal Stiffness

Longitudinal response in the presence of varying stiffness is difficult to evaluate in the case of bridges with seat-type abutments. Abutment stiffness is only activated once sufficient column deformations have caused the gap to close. Several studies were therefore performed. To evaluate stiffness only, response with the case of 0 abutment mass was performed first. For cases of large gaps (6"), response is identical in all except the high intensity region. In this study there is insufficient data in this range to assess sensitivity. Therefore, the gap was reduced to 2" to better assess stiffness sensitivity. Fig. 2 shows the response at varying stiffness levels. After gap closure, stiffer abutments reduce response. Even the lower stiffness bound provides improved response over the no abutment case. Finally, a median value of mass was added to the abutments and the 6" gap study repeated. The added inertia at the abutments is sufficient to cause significant gap closure. However, the mass appears to dominate the response as there is no appreciable difference between stiffness levels. At very high intensities, the 1000 k/in stiffness median response begins to decrease.

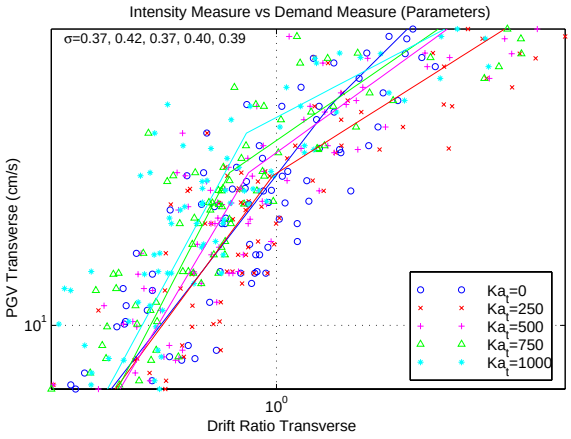

Figure 1. Ka_t sensitivity, PGV-Δ PSDM.

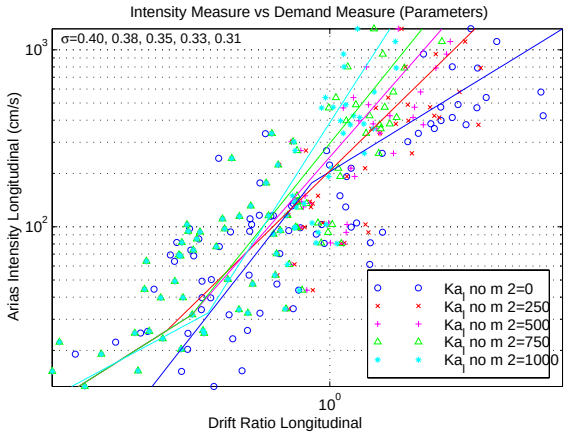

Figure 2. Ka_l (2") sensitivity, Arias-Δ PSDM.

Transverse Stiffness

The effects of increasing abutment stiffness are more readily investigated in the transverse direction as there is no gap before mobilizing the total abutment stiffness. The increase in transverse stiffness in the presence of embankment inertia has little effect on the response (Fig. 1). As expected, stiffer abutments reduce median response at all intensity levels. Excluding abutments from the model yields similar results as a low stiffness abutment in the presence of inertial forces, especially for smaller intensities. Making this assumption, however, is highly non-conservative in the high intensity region.

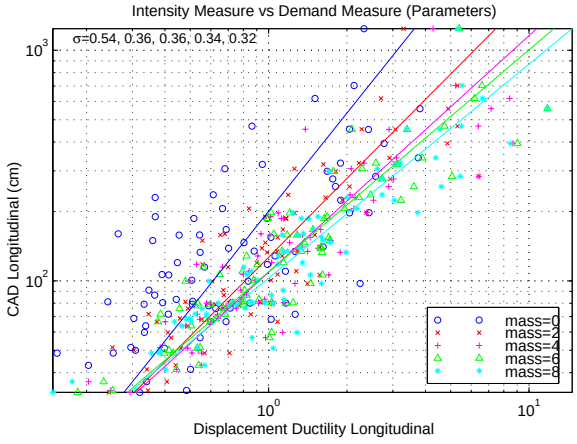

Figure 3. Mass sensitivity, CAD-μ_Δ PSDM.

Participating Mass

As indicated by the stiffness sensitivities in the presence of mass, the participating mass is more critical to bridge response. Fig. 3 shows the increasing contribution of participating mass to the total response at higher intensities. This verifies the observations in Aschheim [10], as reduced mass in required to maintain a response level as intensity is increased. Similarly, at constant intensities, the response increases with more participating mass.

CONCLUSION

As demonstrated, PSDMs can be used as a tool to assess the sensitivity of highway bridge overpass response to abutment parameters. Specifically, the participating length of the embankment, and hence the mass associated with the abutment, is the most critical parameter. Neglecting to include mass in the analysis under-predicts the response, even if large longitudinal or transverse stiffness' are applied. In the absence of inertia forces also, global response is insensitive to the selection of longitudinal stiffness. Therefore, any of the methods discussed are sufficient for approximating the longitudinal stiffness. Transverse stiffness values have a larger affect in the absence of inertia, however, given the predominance of mass, transverse stiffness sensitivity is also reduced to the point where calculated values are sufficient. Further studies are needed to investigate the dependence of the participating embankment length on bridge length, intensity and other factors.

As a simplified model, it is possible to conservatively analyze a given bridge with only rollers at the abutments. This assumption is valid only at lower intensities due to the trade-off introducing stiffness and mass to the abutment incurs. However, introduction of more complex abutment models do not necessarily improve the accuracy of the solution when improperly calibrated.

ACKNOWLEDGEMENT

This work is supported by the Earthquake Engineering Research Center's Program of the National Science Foundation under Award EEC-9701568 as PEER Project #312-2000 "Seismic Demands for Performance-Based Seismic Design of Bridges." The opinions presented in this paper are solely those of the authors and do not necessarily represent the views of the sponsors.

REFERENCES

[1] Luco, N., C.A. Cornell, and G.L. Yeo. 2001. "Annual limit-state frequencies for partially-inspected earthquake-damaged buildings," presented at 8th International Conference on Structural Safety and Reliability, Denmark.

[2] Mackie, K., and B. Stojadinovic (Nov/Dec 2001). "Probabilistic Seismic Demand Model for California Highway Bridges," *J. Bridge Engrg*., 6(6): 468-481.

[3] Shome, N., and C.A. Cornell. 1999. "Probabilistic seismic demand analysis of nonlinear structures," Reliability of Marine Structures Report No. RMS-35, Dept. of Civ. and Envir. Engrg., Stanford Univ.

[4] Caltrans. July 1999. *Seismic Design Criteria 1.1*. California Department of Transportation.

[5] Goel, R.K., and A. Chopra. 1997. "Evaluation of bridge abutment capacity and stiffness during earthquakes." *Earthquake Spectra*, 13(1): 1-23.

[6] Maroney, B., B. Kutter, K. Romstad, Y.H. Chai, and E. Vanderbilt. 1994. "Interpretation of Large Scale Bridge Abutment Test Results," presented at 3rd Annu. Seismic Research Workshop, Sacramento, CA.

[7] Wilson, J.C., and B.S. Tan. August 1990. "Bridge Abutments: Formulation of Simple Model for

Earthquake Response Analysis," *J. Engrg. Mechanics*, 116(8): 1828-1837.

[8] Zhang, J. and N. Makris. March 2001. "Seismic Response Analysis of Highay Overcrossings Including Soil-Structure Interaction," PEER Report 2001/02, College of Engrg., University of California Berkeley.

[9] Werner, S.D. 1994. "Study of Caltrans' seismic evaluation procedure for short bridges," presented at 3rd Annu. Seismic Research Workshop, Sacramento, CA.

[10] Wissawapaisal, C., and M. Aschheim. 2000. "Modeling the transverse response of short bridges subjected to earthquakes." Mid-America Earthquake Center CD release 00-05, Univ. of Illinois, Urbana-Champaign.

DYNAMIC RESPONSE OF BRIDGE STRUCTURES SUPPORTED ON EXTENDED REINFORCED CONCRETE PILE SHAFTS

T.C. Hutchinson[1], C.J. Curras[2], R.W. Boulanger[3], Y.H. Chai[3], and I.M. Idriss[3]

ABSTRACT

This paper describes results from a numerical study of the seismic performance of bridge and viaduct structures supported on extended, large-diameter, cast-in-drilled-hole (CIDH) pile shafts. The study included consideration of ground motion characteristics, site response, lateral soil resistance, structural parameters including geometric nonlinearity, and performance measures. The nonlinear dynamic analyses used a beam on nonlinear Winkler foundation (BNWF) framework to model the soil-pile interaction, nonlinear fiber beam-column elements to model the reinforced concrete section, and one-dimensional site response analyses for the free-field soil profile response. Earthquake ground motions with different frequency contents, intensities, durations and permanent displacements were used as rock outcrop motions in this study. The dynamic analyses were limited to the transverse response of a regular structural system such that a single bent could be analyzed independently. Results presented herein focus on how variations in the ground motion, structural and soil characteristics affect the overall system performance.

INTRODUCTION

Near-fault ground motions with strong velocity pulses can subject bridge and viaduct structures to very large displacement and ductility demands. For bridge and viaduct structures supported on extended cast-in-drilled-hole (CIDH) pile shafts, plastic hinging in the pile shaft can develop below the ground surface. Residual deformations in these types of structures after an earthquake are an important concern, and may be increased by the presence of strong, uni-directional pulses in the ground motion. The magnitude of inelastic deformation demands in the structure will depend on the ground motion characteristics (including the amplitude, period and shape of any large pulses), the lateral strength and period of the structure, and the hysteretic characteristics of the yielding elements (structural and soil). The seismic performance of these structures will be inherently coupled to the subsurface soil conditions through their influence on site response, foundation stiffness, and energy dissipation.

Although the implications of large lateral displacements on the overall response of extended pile shaft supported bridge structures is well recognized, a quantitative assessment of such effects on their performance has not yet been thoroughly carried out. Such an evaluation requires analytical models capable of capturing the nonlinearity of the soil and pile under dynamic reversed cyclic loading conditions. Moreover, there is a need to evaluate the performance of these generally long period structures under strong ground motions with long duration and/or long period characteristics, in accord with current design motion scenarios. This paper describes a portion of results from a larger numerical study of the seismic performance of bridge and viaduct structures supported on extended, large-diameter, CIDH pile shafts [5]. The study included consideration of ground motion characteristics, site response, lateral soil resistance, structural parameters, geometric nonlinearity, and performance measures. Results described herein focus on how variations in the ground motion, and the structural and soil characteristics affect the performance measures important for evaluating the inelastic seismic response of these structures.

DYNAMIC FINITE ELEMENT (FE) ANALYSES

The system considered consists of a fairly regular multi-span bridge or viaduct structure with individual bents supported on a single large diameter extended reinforced concrete pile shaft. The transverse response of such a system may be characterized by the response of a single bent if the bridge structure has a fairly uniform distribution of strength and stiffness between bents. The superstructure was assumed monolithically constructed with the extended pile shaft.

[1] (TCH) Dept. of Civ. and Env. Engrg., Univ. of California, Irvine, CA 92697-2175
[2] (CJC) Dept. of Civ. and Env. Engrg., Univ. of Wisconsin-Platteville, WI 53818
[3] (RWB, YHC, IMI) Dept. of Civ. and Env. Engrg., Univ. of California, Davis, CA 95616

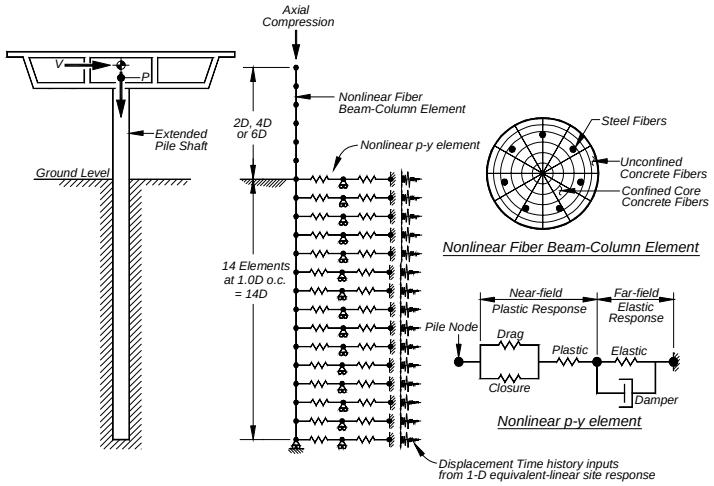

Figure 1. Details of the finite element model for the dynamic BNWF analysis showing the nonlinear beam-column fiber element and the nonlinear p-y element.

The FE approach used to model the soil-pile interaction is based on a beam-on-nonlinear-Winkler foundation (BNWF) framework, where the soil medium is modeled by a series of closely spaced nonlinear p-y elements. The model is discretized into nonlinear beam-column elements and nonlinear p-y elements as shown in Figure 1. The soil-structure system was modeled using the finite element analysis platform FEAP [1]. The CIDH pile and extension are modeled using the flexibility-based fiber beam-column element from the FEDEAS element library [2]. Gravity loading was simulated by applying a constant vertical load to the center of mass of the superstructure. The pile tip was assumed vertically constrained, but rotationally and horizontally unconstrained. The nonlinear p-y elements, which account for gapping effects and radiation damping, are described in [3]. Parameters for the p-y elements were based on common US design procedures [4]. Additional details regarding the constitutive laws and modeling assumptions may be found in [5]. Horizontal free-field soil motions obtained from one-dimensional site response calculations, performed using the equivalent-linear program SHAKE96 [6, 7], were input to the free-field ends of all p-y elements to represent dynamic earthquake loading. Structural rayleigh damping was set at 5% of the equivalent elastic yield period of the soil-pile systems.

Rock Outcrop Motions

Twelve earthquake motions with different frequency contents, intensities, durations and permanent displacements were used as rock outcrop motions in this study. Each motion was input as a rock outcrop at the base of the site and the peak rock outcrop acceleration (a_{max}) was scaled to produce several intensities. Six of these motions were categorized as near-fault recordings and have a strong long period pulse component. Two of the motions selected were synthetic motions with a particularly long duration of shaking. The baseline soil profile selected for this parameter study was modeled after the Gilroy 2 site in California. The site consists of predominantly loamy soils but may be classified more generally as a mix of dense sand and stiff clays. Shear wave velocities at the site range from 200 to 500 m/s in the upper 30 m.

Structural systems

Twelve different bridge structures supported on large-diameter extended CIDH pile shafts were modeled. Consistent with standard construction detailing, the extended pile shafts have an above-ground cross-section that is slightly smaller than their below-ground cross-section. These structures have above-ground heights L_a = 2D, 4D, and 6D, where D (below-ground pile diameter) was taken as both D = 1.5 m and D = 3.0 m. The embedded pile length was set at 14D for each case based on providing reasonable axial load carrying capacities. Two different axial loads were used in the study, $0.05f'_cA_g$ and $0.1f'_cA_g$, where f'_c = unconfined compressive strength of the concrete and A_g = gross area of the pile shaft. Longitudinal and transverse reinforcement ratios were about 1%.

DYNAMIC FINITE ELEMENT ANALYSES RESULTS

Maximum and Residual Drift Ratios

For near-fault ground motions, the inelastic response of a bridge structure tends to be associated with a biased response in one direction, which may result in a large permanent displacement and rotation. The biased lateral response of the structure is often worsened by the combined effects of high axial force, low lateral strength, and increased flexibility due to soil compliance, which collectively increase the importance of geometric nonlinearity or "P–Δ effects". Subsequent to the 1995 Hanshin earthquake, design guidelines for highway bridges in Japan [8, 9]

specified an allowable residual drift ratio of 1% for important bridge structures. For the structures considered herein, the permanent or residual drift ratio γ_{res}, defined as the slope (from vertical) of the above-ground pile extension after the earthquake, is used to quantify the magnitude of the permanent deformation in the bridge structure. Figure 2 shows the residual drift ratio γ_{res} versus the maximum drift ratio γ_{max} for the structures supported on 3.0 m diameter pile shafts, with an axial load of $0.05 \cdot f'_c A_g$. As expected, the residual drift ratio γ_{res} generally increases with the maximum drift ratio γ_{max}, and although there is considerable scatter in Figure 2, the increase appears to be exponential. The exponential fit to the data indicates that if maximum drift ratios are less than 8%, residual drift ratios will generally be less than 1% (based on the mean trend in the data) and at most 1.75%. A higher degree of confidence in keeping residual drift ratios less than 1% may be achieved by using the upper bound relation between γ_{max} and γ_{res}, in which case, maximum drift ratios would be limited to less than 6%. However, it is recommended that the ability of the FE model to specifically capture residual displacements has not been fully explored and thus warrants calibration against experimental data.

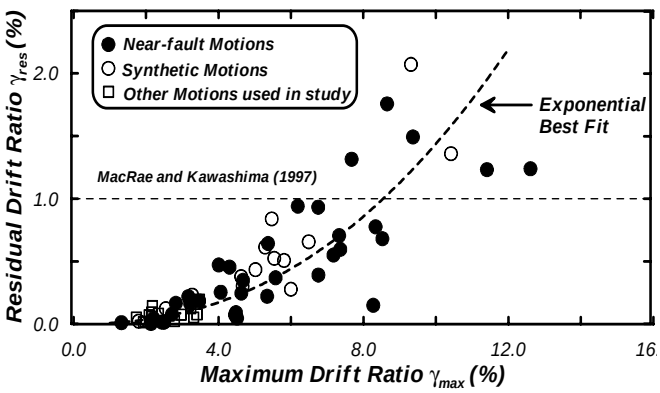

Figure 2. Residual drift ratio γ_{res} as a function of the maximum drift ratio γ_{max} in the superstructure.

P-Δ Effects

For bridge structures supported on extended pile shafts, the extension of the supporting foundation below ground level increases the flexibility of the system and decreases its lateral strength, thus increasing its susceptibility to amplification of displacement demands and/or collapse due to the combined effects of gravity loading acting through large lateral displacements (P-Δ effects). The sensitivity of these structures to second-order effects was evaluated by analyzing the 3.0 m diameter pile shafts with and without P-Δ effects incorporated in the time history analysis. Current bridge design codes [e.g. 10, 11] suggest avoiding the possible adverse effects associated with dynamic P-Δ demands by minimizing the ratio of the axial load times the lateral displacement demand to the section flexural capacity. In this paper, this has been termed the secondary-moment-strength-ratio $SMSR \equiv P\Delta^o_{max} / M_p$, where P = axial load, Δ^o_{max} = maximum displacement calculated from the FE analysis (without P-Δ effects) and M_p = plastic moment capacity of the section where inelastic action occurs. Figure 3 shows the *SMSR* evaluated for the 3.0 m diameter pile shafts, where (a) shows the difference in maximum displacements with and without P-Δ effects ($\Delta_{max} - \Delta^o_{max}$) and (b) shows the displacement amplification ratio (*DAR*). The displacement amplification ratio *DAR* is defined as $DAR \equiv \Delta_{max} / \Delta^o_{max}$, where Δ_{max} = maximum displacement calculated from the FE analysis (with P-Δ effects). The mean *DAR*, for $SMSR \leq 20\%$ was fairly close to unity (1.03) with a coefficient of variation (COV) of 0.08. Overall, the analyses results indicate that the current practice of limiting the secondary-moment-strength-ratio *SMSR* to avoid detrimental P-Δ effects is acceptable, although it is noted that the consequences of exceeding *SMSR* = 20% were not very significant in many cases (up to *SMSR* ~ 30%).

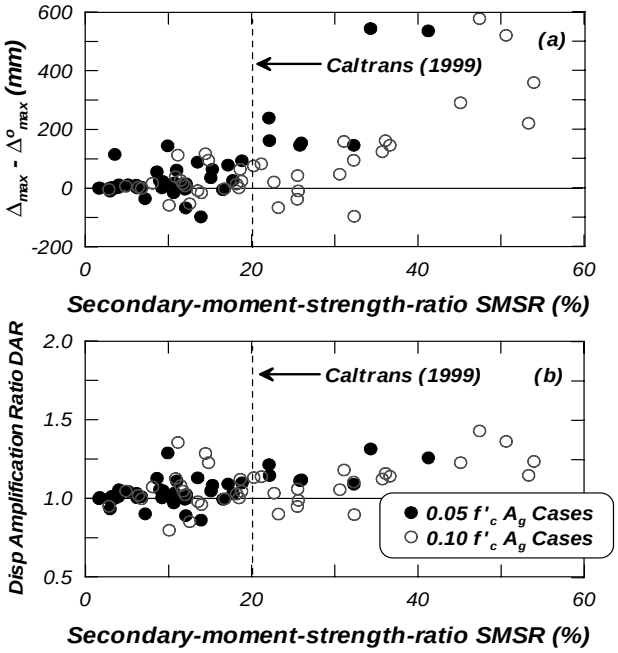

Figure 3. Change in maximum displacement ($\Delta_{max} - \Delta^o_{max}$) and ratio of maximum displacements *DAR* as a function of the secondary-moment-strength-ratio *SMSR* for 3.0 m diameter pile shafts.

Curvature Ductility Demands μ_ϕ

Structural Variation

The local curvature ductility demand μ_ϕ in the yielding pile shaft is an important performance measure because it is related to the damage in the pile imposed during the earthquake (e.g. spalling of cover concrete, crack widths, potential for buckling or fracture of longitudinal reinforcement). The association between global displacement ductility μ_Δ and local curvature ductility demands μ_ϕ allows for an understanding of the magnitude of local damage to the pile for a given global deformation level. Figure 4 shows the relation between global displacement and local curvature ductility's for the 3.0 m diameter pile shaft structures supporting an axial load of $0.05f'_cA_g$ – as determined from the FE analysis and using a simplified kinematic model [12]. To minimize local demands in accord with [10] (i.e., $\mu_\phi \leq 13$), allowable global displacement ductility's would range from $\mu_\Delta = 5.2 – 6.1$ for the 1.5 m diameter pile shafts and from $\mu_\Delta = 4.8 – 5.5$ for the 3.0 m diameter pile shafts (for the range of above-ground heights and soil type considered). Alternatively, if a design displacement ductility of $\mu_\Delta = 3.0$ is used, for these large diameter pile shafts, local curvature ductility demands were fairly small and range from $\mu_\phi = 5.1 – 6.9$ for the 1.5 m diameter pile shafts and from $\mu_\phi = 6.9 – 7.2$ for the 3.0 m diameter pile shafts. From these and other results, it is evident that the ratio of ductility's (μ_ϕ/μ_Δ) will vary for different structural configurations (pile diameter, above-ground height, etc.) and soil conditions.

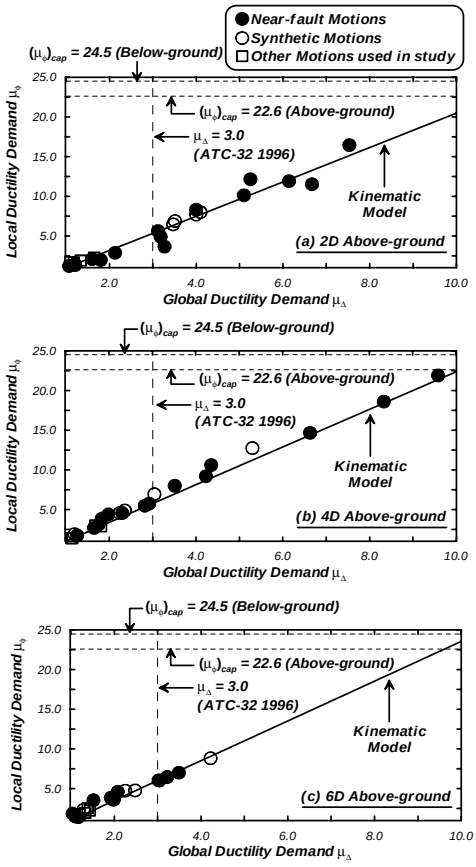

Figure 4. Local versus global ductility factors for 3.0 m diameter pile shafts with $0.05f'_cA_g$ with above-ground heights of: (a) 2D, (b) 4D and (c) 6D.

Soil Parameter Variation

The potential variability in p-y parameters (due to factors such as installation effects, soil variability, and soil property uncertainty) was evaluated by re-analyzing a set of full-scale load tests [4]. Analyses were performed to determine a range of initial stiffness and ultimate strength scaling factors to reasonably match measured pile response. Scaling factors on p-y ultimate strength (m_p) and stiffness (m_s) of 2.0, either up or down ($m_p = m_s = 2.0$ and $m_p = m_s = ½$), were chosen as being representative of reasonable ranges of variability at sites with relatively thorough subsurface characterizations. The effect these p-y parameter variations had on the local curvature ductility μ_ϕ demands were studied for a subset of structures and ground motions [4]. These results indicate that the soil variation generally had a smaller effect on the local curvature ductility than it did on the other performance measures studied. When softer, weaker p-y parameters ($m_p = m_s = ½$) were assumed the following trends were observed: (1) yield displacement Δ_y increased, (2) equivalent elastic period T_e increased, (3) maximum displacement demand Δ_{max} increased, (4) global displacement ductility μ_Δ demand decreased, and (5) the ratio of local to global ductility's factors μ_ϕ/μ_Δ increased. These factors were observed to combine and cause the local curvature ductility demand μ_ϕ to be relatively unaffected.

CONCLUSIONS

Nonlinear static and dynamic numerical analyses were used to evaluate the inelastic seismic response of bridge and viaduct structures supported on extended cast-in-drilled-hole (CIDH) pile shafts. Results presented herein are part of a more complete study [5]. Although many design issues must be considered for bridge structures supported on extended pile shafts, results of the numerical studies indicate three measures particularly important to the overall seismic performance evaluation of this class of structures:

(1) Maximum and residual drift ratios (γ_{max} and γ_{res}) - The dynamic FE analyses of CIDH pile-supported structures, indicates that if maximum drift ratios are less than about 8%, residual drift ratios will generally be less than 1% (based on the mean trend in the data) and at most 1.75%. A higher degree of confidence in keeping residual drift ratios less than 1% may be achieved by using the upper bound relation between γ_{max} and γ_{res}, in which case

maximum drift ratios would be limited to less than about 6%. However, it is recommended that the ability of the FE model to specifically capture residual displacements has not been fully explored and thus warrants calibration against experimental data.

(2) Secondary-moment-strength-ratios (*SMSR*) – Limiting the secondary-moment-strength-ratio (*SMSR*) of the extended pile shaft system generally provides a means for minimizing the effects P-Δ moments have on these structures (e.g., excessive displacement amplification and/or subsequent collapse). Analytical cases presented in this study suggest that current design guidelines (i.e. *SMSR* ≤ 20%) are acceptable in terms of their ability to minimize dynamic P-Δ sensitive behavior; however, the consequences of allowing *SMSR* up to 30% are not very significant.

(3) Kinematic relation between curvature ductility (μ_ϕ) and displacement ductility (μ_Δ) – For the pile shafts considered in this study, embedded in a fairly dense sand, limiting the local demands to $\mu_\phi \leq 13$, would allow displacement ductility's ranging from $\mu_\Delta = 5.2 - 6.1$ for the 1.5 m diameter pile shafts and from $\mu_\Delta = 4.8 - 5.5$ for the 3.0 m diameter pile shafts. Alternatively, limiting $\mu_\phi \leq 10$ (to minimize damage to the pile shaft below ground level), would allow displacement ductility's ranging from $\mu_\Delta = 4.0$ to 4.7 for the 1.5 m diameter pile shafts and from $\mu_\Delta = 3.7$ to 4.2 for the 3.0 m diameter pile shafts. However, for pile shafts embedded in loose sand or softer clay, the local curvature ductility demand is expected to increase, resulting in design displacement ductility factors smaller than that of dense sand.

ACKNOWLEDGEMENTS

This work was supported in part by the Pacific Earthquake Engineering Research Center through the Earthquake Engineering Research Centers Program of the National Science Foundation under Award number 2081999. T.C. Hutchinson was also supported on a fellowship provided by the Earthquake Engineering Research Institute (EERI) for the last year of this research. Any opinions, findings, and conclusions in this paper are those of the authors and do not necessarily represent a policy of either agency or endorsement by the State or Federal government.

REFERENCES

[1] Taylor, R.L. 1998. "FEAP – A finite element analysis program." Dept. of Civil and Envir. Engrg., University of California, Berkeley.

[2] Filippou, F.C. 1999. "FEDEAS: Finite Elements for Design, Evaluation, and Analysis of Structures." On-line manual: Univ. of California, Berkeley, CA. http://www.ce.berkeley.edu/~filippou/Research/fedeas.html

[3] Boulanger, R.W., Curras, C. J., Kutter, B.L., Wilson, D.W., and Abghari, A. 1999. "Seismic soil-pile-structure interaction experiments and analyses." *Journal of Geotechnical and Geoenvironmental Engineering*, ASCE, 125(9): 750-759.

[4] Curras, C.J., Hutchinson, T.C., Boulanger, R.W., Chai, Y.H., and I.M. Idriss. 2001. "Lateral loading and seismic response of CIDH pile supported bridge structures." *Foundations and Ground Improvement, T.L. Brandon ed., Geotechnical Special Publication No.113* ASCE, 260-275.

[5] Hutchinson, T.C., Boulanger, R.W., Chai, Y.H. and Idriss, I.M. 2001. "Inelastic seismic response of extended pile shaft supported bridge structures." Final report to Pacific Earthquake Engineering Research Center.

[6] Schnabel, P.B., Lysmer, J. and Seed, H.B. 1972. SHAKE: a computer program for earthquake response analysis of horizontally layered sites. *UCB/EERC-72/12, EERC*, University of California, Berkeley, 102 pp.

[7] Idriss, I.M., and Sun, J. 1991. User manual for SHAKE91. Center for Geotechnical Modeling, Dept. of Civil and Envir. Engrg., University of California, Davis, California.

[8] Japan Road Association. 1996. *Design Specifications of Highway Bridges. Part V: Seismic Design.* Japan.

[9] MacRae, G.A. and Kawashima, K. 1997. "Post-earthquake residual displacements of bilinear oscillators." *Earthquake Engineering and Structural Dynamics*, 26: 701-716.

[10] Applied Technology Council. 1996. "Improved Seismic Design Criteria for California Bridges: Provisional Recommendations ATC-32." June.

[11] Caltrans. 1999. Caltrans Seismic Design Criteria – Version 1.1. California Department of Transportation, Division of Structures. Sacramento, California. July.

[12] Chai, Y.H. 2002. "Flexural strength and ductility of extended pile-shafts - analytical model." *Journal of Structural Engineering*, ASCE, (in press).

Proportioning Substructure Columns of Short Bridges for Improved Seismic Performance

Mehmet Inel[1] and Mark A. Aschheim[2]

ABSTRACT

Empirical observations and analysis of the recorded response of two California bridges show that the flexibility of the bridge embankments has a significant effect on the displacement demands sustained by the substructure columns of short bridges responding to earthquake excitations. Computation indicates that the stiffness of the columns has little effect on peak displacement responses of short bridges, and bridges with flexible columns will transfer most of the lateral inertial force to the embankments via the deck and abutments. Because the deck and abutments provide a capable load path, the columns only need to maintain gravity load support while accommodating the lateral displacement demands. This understanding leads one to select columns with smaller diameters than typically result using the conventional *R* (or *Z*) factor design approach. Several benefits result from the use of smaller diameter columns: (1) damage to the columns is reduced or avoided, (2) the columns are less vulnerable to shear failures, and (3) the reduced size of the columns and foundations reduces construction costs.

This paper suggests a new displacement based approach for design of the substructure columns for improved seismic performance to meet the specified seismic performance objectives. Strategies to determine the number of columns are discussed for cases in which seismic loading is the governing load combination. A case study compares the dynamic response of a short bridge designed according to the conventional and proposed approaches. The comparison illustrates that although the bridges with small diameter columns may have slightly larger displacement demands compared to bridges with conventional large diameter columns, the curvature and displacement ductility demands on the small diameter columns are either similar to or smaller than those in conventional columns. Designs using conventional columns were found to violate the Caltrans requirement for target displacement ductility under even moderate ground shakings, while the smaller diameter columns satisfied this requirement for all the ground motions considered.

[1] Graduate Research Asst., Mid-America Earthquake Center, University of Illinois at Urbana-Champaign.
[2] Asst. Professor, Mid-America Earthquake Center, University of Illinois at Urbana-Champaign.

INTRODUCTION

Considering economic constraints and uncertainty in earthquake loading, it usually is not feasible to design a structure to behave elastically under severe earthquakes. Conventional seismic design approaches rely on ductile behavior to permit design for reduced seismic forces using a strength reduction factor, *R*, or ductility and risk assessment factor, *Z*. Elastic strength demands are established using a suitable response spectrum (e.g., ARS spectrum used by Caltrans Seismic Design Criteria [1]), and these demands are divided by a factor, *R* or *Z* to account for inelastic behavior. In the conventional design approaches, bridge columns are major components of lateral load resistance. The relatively high lateral force demands obtained using *Z* factor approach results in large diameter columns in high seismic zones (i.e. California).

The large diameter columns have a small yield curvature and thus a small yield displacement. Therefore, to accommodate a given displacement demand may require large curvature and displacement ductilities be sustained by the columns in the design earthquake. The displacements generated in earthquakes of varied intensities may cause column damage to exceed the levels associated with the design performance objectives. The large diameter columns also have relatively squat aspect ratios. Such columns have relatively high shear demands associated with flexural hinging and have performed poorly in past earthquakes.

This paper focuses on bridges with relatively stiff decks that lack intermediate joints for thermal movement, termed “short” bridges. The Meloland Road Overcrossing (MRO) and Painter Street Overcrossing (PSO) are two such bridges that were instrumented by the California Strong Motion Instrumentation Program (CSMIP). The reinforced (MRO) or prestressed (PSO) concrete decks of these bridges are relatively stiff for transverse deformations. The recorded response of the MRO and PSO has been studied by numerous investigators (e.g., [2, 3]). These studies underscore that for small intensity motions, displacements in the transverse (or skew) direction have significant components represented by deck deformations, while for moderate or strong intensity motions, the decks move nearly as a rigid body with displacements in the transverse (or skew) direction being dominated by the response of embankments. This implies that the bent column deformation demands are dominated by the response of the embankments, particularly for stronger motions.

Bridges with flexible columns will transfer most of the transverse inertial force to the embankments via the relatively stiff deck and the abutments. Thus, a capable load path that does not rely on the substructure columns is available for resisting lateral loads. This differs from the case of buildings responding to lateral load, for which the response depends entirely on the characteristics of the structural framing. Because the deck and abutments provide a capable load path, the columns only need to maintain gravity load support while accommodating the lateral displacement demands. This suggests that compatibility of the column displacement capacities with the demands of the bridge system is more important than the contribution of columns to lateral load resistance or their ductility capacities. Substructure columns need only have enough flexibility and confinement to accommodate the displacement demands while maintaining gravity load carrying capacity. Because the strength and stiffness of the columns have relatively minor influence on the response of the bridge, the use of *R* or *Z* factors for their design is inappropriate. Instead, a new design approach is needed for proportioning the columns of short bridges.

PROPOSED DESIGN APPROACH

This paper proposes the use of flexible substructure columns that have smaller diameters than typically result using the conventional *R* (or *Z*) factor approach. [1] The smaller diameter columns have larger yield displacements relative to those of larger diameter columns, and thus can tolerate a greater range of displacements without damage, have reduced damage in larger earthquakes. The relatively slender aspect ratios associated with smaller diameter columns reduce or eliminate their vulnerability to shear failure. In addition, the smaller diameter columns and smaller flexural strengths reduce the costs of the constructing the columns and foundations.

The use of smaller diameter columns can cause computed displacement demands to increase to some degree. However, because the smaller diameter columns have larger yield displacements, the increased displacement demands generally can be accommodated with less damage than occurs to conventional large diameter columns. A subsequent example explores these issues further.

Various configurations may be used to provide flexible columns. For example, the same number of columns may be used, but with smaller diameters, resulting in higher axial load ratios, or a larger number of smaller diameter columns may be used, to keep axial load ratios similar to those used in current practice. Inel [2] found experimental evidence to suggest that deformation capacities of rectangular section columns were not strongly influenced by axial load when ATC-32 [4] recommended confinement was used. Well-confined circular columns are expected to have larger deformation capacities.

For the proposed approach to be successful, it is necessary to be able to estimate column displacement demands accurately. Neglecting or accounting for embankment flexibility has a significant effect on the expected damage to the substructure columns. Inel [2] provides a simple technique to estimate deformation demands on the substructure columns of short bridges that account for embankment flexibility. This technique makes use of an "equivalent" SDOF model of the bridge and accounts for embankment flexibility using normalized capacity curves. The embankment capacity curves are presented for common embankment fill properties and dimensions. In this paper, the technique suggested by Inel [2] is used to estimate displacement demands of substructure columns.

An example is considered to illustrate the influence of different column designs on the behavior of an example bridge. Two bent configurations (Figure 1) were considered for the PSO: (1) the as-built configuration with two 1.52-m diameter columns, and (2) an alternative, with four 0.61-m diameter columns. For both configurations, the columns are assumed as fixed at the base and integrally connected to the bent cap at the top. A concrete strength of 27.5 MPa (4 ksi) and steel strength of 420 MPa (60 ksi) were used in the modeling. Longitudinal column reinforcement of 2% was assumed for the columns. Transverse reinforcement was provided per ATC-32 provisions [4]. The estimated yield displacement of each bent, Δ_y, is given in Table 1.

In the analyses, embankment flexibility was taken into account by using the "equivalent" SDOF model developed by Inel [2], with an effective embankment length of 2 m. The bridge was subjected to three earthquake motions: 1940 El Centro (N180), 1994 Northridge Earthquake recorded at Newhall LA County Fire Station (N360), and 1995 Kobe Earthquake recorded at Takatori-kisu (N360).

[1] In this paper, typical Caltrans columns of 1.5- to 1.8-m (5- or 6-ft) diameter columns are termed "larger" diameter columns while 0.6- to 1-m (2-ft to 3.5-ft) columns are termed "smaller" diameter columns.

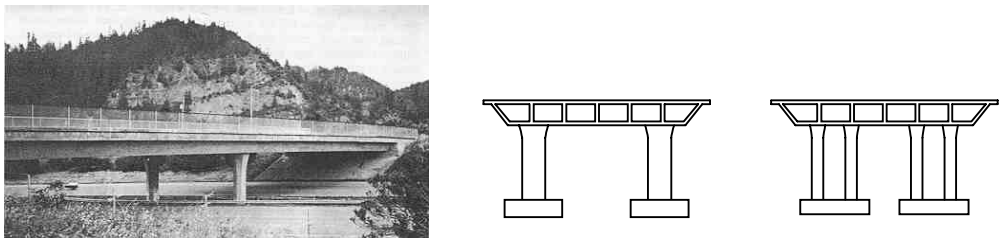

(a) (b) (c)

Figure 1. (a) PSO bridge photo (McCallen and Romstad [3]), (b) as-built configuration w/two 1.52-m diameter columns, and (c) alternative configuration w/four 0.61-m diameter columns.

The peak displacement, displacement ductility, and curvature ductility demands are reported in Table 1. Although the peak displacements of the bridge with smaller diameter columns sometimes exceed those of the conventional bridge, their greater flexibility and larger yield displacement result in smaller curvature and displacement ductility demands. Caltrans Seismic Design Criteria [1] recommends that column displacement ductilities be limited to 5 for multi-column bents. In the current example, the smaller diameter columns satisfied this limit for all three motions, while displacement ductility demands as high as 10.4 developed in the conventional columns.

Table 1. Performance comparison of the PSO with small diameter columns and conventional large diameter columns

Central Bent Configuration	Δ_y (mm)	$P/(A_g f_c')$	El Centro			Newhall			Takatori-kisu		
			Δ_{peak} (mm)	μ_Δ	μ_ϕ	Δ_{peak} (mm)	μ_Δ	μ_ϕ	Δ_{peak} (mm)	μ_Δ	μ_ϕ
Four 0.61 m Diameter Columns	80	0.27	40	<1	<1	192	2.4	5.2	390	4.9	12.5
Two 1.52 m Diameter Columns	29	0.11	50	1.7	3.2	179	6.2	16.4	302	10.4	29.0

This example shows that the use of smaller diameter columns can improve the performance of "short" bridges. An approach for proportioning the columns of short bridges follows:

1. Identify earthquake hazard levels and associated ground motions for the design performance objectives.
2. Compute displacement demands of the bridge bent accounting for embankment flexibility and assuming no column contribution to lateral resistance, using the L_2 values of Table 2.
3. Determine the limiting yield displacement for the substructure columns based on the computed displacement demands and the allowable displacement ductility or plastic rotation demands associated with the performance levels. Select the largest of these yield displacements for each column or bent.
4. Select column diameters to obtain a yield displacement greater than the estimate of Step 3 (e.g. $\Delta_y = \phi_y L^2 / 3$ for a cantilever column).
5. Select the number of columns to provide adequate resistance to gravity load combinations and considering the proportioning of the bent cap and foundations.

6. Verify adequacy of design by ESDOF analysis using the L_1 values of Table 2, accounting for the bent and embankment contributions to the bridge capacity curve. If performance limits are not satisfied, either select smaller diameter column than the one selected in Step 4 or change boundary conditions to increase flexibility of column and go to Step 5.
7. Detail the transverse reinforcement per ATC-32 [4].

Table 2. Recommended embankment lengths for different level of ground motions.

Ground Motion Intensity*	L_1 (m), lower bound embankment length	L_2 (m), "best" fit embankment length
Low	4	8
Moderate or Strong	2	4

* Low intensity shaking is defined as that which causes peak deformations in the embankment not exceeding 0.2 to 0.5% of the height of the embankment; moderate and strong shakings are defined as causing larger peak deformations.

CONCLUSIONS

Empirical observations and analytical studies conducted on the recorded response of two short bridges indicate that the conventional design approach (that uses *R* or *Z* factors) is not applicable to the design of substructure columns of short bridges with nearly rigid decks. The existence of a capable load path involving the relatively stiff deck, abutments, and embankments allows substructure columns to function primarily as gravity load-carrying columns while sustaining the imposed lateral displacements due to the deck and embankment movements. This understanding leads to the use of more flexible columns to reduce damage and improve seismic performance. This paper proposes the use of columns that have smaller diameters than typically result using the conventional *R* (or *Z*) factor approach. Several benefits result if the smaller diameter columns are used, relative to the use of large diameter columns: (1) the increased flexibility of the smaller diameter columns reduces the damage that occurs in moderate or strong earthquakes; (2) the larger aspect ratio (length to diameter) reduces or eleminates their vulnerability to shear failures; and (3) the smaller diameter columns and smaller flexural strengths reduce the costs of the constructing columns and foundations.

A case study was conducted using Painter Street Overcrossing. Two bent configurations were considered, representing the conventional and proposed approaches. Comparison of the computed response of the two bridges demonstrated that the use of smaller diameter columns improves the seismic performance of short bridges when embankment flexibility is considered. A step-by-step procedure for proportioning the substructure columns was provided.

REFERENCES

[1] Caltrans SDC. 1999. *Caltrans seismic design criteria version 1.1*, California Department of Transportation, Sacramento, California.

[2] Inel, M. 2002. Displacement-based strategies for the performance-based seismic design of short bridges considering embankment flexibility, *Ph.D. Thesis*, University of Illinois at Urbana-Champaign (in preparation).

[3] McCallen, D. B., and K. M. Romstad. 1994. "Dynamic analyses of a skewed short-span, box-girder overpass," *Earthquake Spectra*, Vol. 10, No. 4, pp. 729-755.

[4] ATC-32. 1996. *Improved seismic design criteria for California bridges: Provisional recommendations*, Report No. ATC-32, Applied Technology Council, Redwood City, California.

Near-Field Ground Motions and their Implications on Seismic Response of Long-Span Bridges

George P. Mavroeidis and Apostolos S. Papageorgiou

ABSTRACT

Progress achieved over the last few decades in computer technology and in numerical techniques has enabled engineers to address complicated, properly posed, boundary value problems associated with the seismic response of long-span bridges with relatively small requirements in calculation time and equipment. Such problems may involve a variety of structural elements, complex geometries and loading conditions, as well as soil-structure interaction effects. However, this progress has helped in solving only one part of the engineer's work, the implementation of efficient numerical algorithms and the study of realistic structural models. The other equally important part is the generation of reliable synthetic ground motions (incorporating near-source effects) for realistic simulations of the seismic response of long-span bridges.

Near-fault strong ground motions are characterized by long-period velocity pulses, as well as by displacement time histories exhibiting an impulsive character and/or significant permanent displacements associated with the tectonic deformation that the site experienced during the earthquake. The waveforms of these near-source time series depend on the fault type (e.g., strike-slip, reverse, etc), the direction of ground motion component with respect to the strike direction of the causative fault (i.e., strike-normal, strike-parallel), as well as on the type of the rupture (i.e., dislocation-like versus crack-like rupture).

These near-field ground motions can be detrimental for long-period structures such as long-span bridges, high-rise buildings, base isolated buildings or bridges, and should be systematically considered and studied in the seismic hazard characterization of flexible structures. Until recently however, the importance of the long-period ground motion components for the seismic response of long-span bridges was underestimated. The gradually increasing number of near-fault ground motion seismograms recorded by broadband digital strong motion instruments has recently enabled seismologists to understand and analyze the character of the near-source ground motions, and engineers to reevaluate and reconsider the design practices of long-span bridges.

Despite the progress that has been accomplished, the recorded near-source strong ground motions should be complemented by analytical and numerical techniques that generate reliable synthetic ground motions appropriate for the engineering design of long-span bridges. In this direction, a modeling approach that combines (depending on the simulated frequency range) both deterministic and stochastic in nature methodologies can be employed. Alternatively, simple and reliable analytical models that adequately describe the nature of the impulsive near-fault motions both qualitatively and quantitatively may be used. Such mathematical models should be able to analytically represent empirical observations that are based on available near-field records. Furthermore, the input parameters of these models should have a clear physical meaning and be related to basic physical parameters of the fault rupture.

In this study, we discuss the main characteristics of the near-source ground motions, as well as their importance for the seismic response of long-span bridges. In addition, we present a simple mathematical expression for the representation of near-fault ground motions that fulfills the requirements and serves the purposes addressed above.

George P. Mavroeidis, Graduate Research Assistant, Department of Civil, Structural & Environmental Engineering, 212 Ketter Hall, State University of New York at Buffalo, Buffalo, NY 14260.

Apostolos S. Papageorgiou, Professor, Department of Civil, Structural & Environmental Engineering, 212 Ketter Hall, State University of New York at Buffalo, Buffalo, NY 14260.

INTRODUCTION

It is widely accepted nowadays that near-fault strong ground motions greatly affect the seismic response of long-period structures such as long-span bridges. Until recently however, there was a widespread belief that the long wavelength modes of a long-span bridge do not significantly participate in the dynamic response of the structure when subjected to a seismic excitation. This argument was mainly based on the observation that the energy content of actual strong ground motion records was not significant for periods larger than 3 seconds. While this remark is in general true for far-field earthquake recordings, it is not valid for near-field strong ground motion records dominated by intense long-period velocity and displacement pulses. In the latter case, the flexible bridge deck cannot react as fast as the stiff towers and therefore lags behind the tower motion. As the towers begin to move towards their original position following the reversal of the ground displacement, the deck has just started to respond and flings through the towers in the opposite direction. This behavior is effectively illustrated through numerical simulations in [1].

The gradually increasing number of near-fault ground motion seismograms recorded by broadband digital strong motion instruments has enabled seismologists to understand and analyze the character of the near-source ground motions, and engineers to reevaluate and reconsider the design practices of long-span bridges. These accelerograms, when properly processed to preserve the displacement information, reveal useful details associated with the physics of the rupture process and give an accurate picture of the actual ground motion that the site experienced during the earthquake. On the other hand, time histories recorded by analog instruments (or by digital instrument without applying a correction scheme that retains the long-period information) are not representative of actual situations; thus, caution should be employed when displacement time histories of near-fault records are compared to choose the most appropriate for reliable aseismic design of long-span bridges.

Despite the progress that has been accomplished by seismologists and engineers, there is a clear need to complement the recorded near-source ground motions by simple and reliable analytical models that adequately describe the nature of the impulsive near-fault motions both qualitatively and quantitatively. Such mathematical models should be able to analytically represent empirical observations that are based on available near-field records. In addition, the model input parameters should have a clear physical meaning and be directly or indirectly related to basic physical parameters of the fault rupture. These models, together with appropriate scaling laws of the input parameters, will provide seismologists and engineers with a tool to generate synthetic near-fault ground motions appropriate for engineering design and applications. Furthermore, this progress will enable engineers to study the response of long-span bridges subjected to near-fault seismic excitations more effectively, as a function of the input parameters of the analytical models.

NEAR-FAULT STRONG GROUND MOTION DATABASE

The *near-fault strong ground motion database* that we have compiled consists of a large number of processed near-field strong ground motion records from a variety of tectonic environments worldwide, including those generated by the recent 1999 Izmit, Turkey, 1999 Chi-Chi, Taiwan and 1999 Duzce, Turkey earthquakes. Approximately 165 recorded ground motion time histories from different fault types (i.e., strike-slip, reverse, oblique, normal) and earthquake magnitudes (i.e., M_w=5.6 to 8.1) recorded at various distances (i.e., 0 to 20 km) from the causative fault have been gathered from well known and extensively studied seismic events that have occurred in the USA, Canada, Mexico, Japan, Greece, Turkey, Romania, USSR, Iran, India and Taiwan. Additional information regarding the compiled database is provided in [2, 3]. Although all stations included in the database are located in the vicinity of their respective causative faults, velocity pulses characterize less than half of the database recordings. Typical near-source velocity time histories that exhibit *"distinct"* pulses are illustrated in Figure 1.

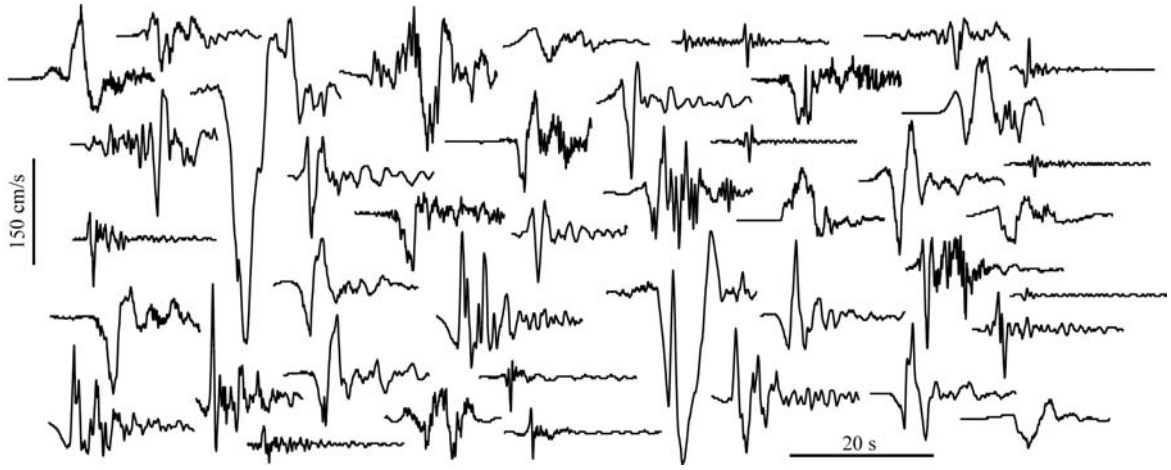

Figure 1. Strong ground motion records with distinct velocity pulses included in the compiled database.

CHARACTERISTICS OF NEAR-FAULT GROUND MOTIONS

In general, *forward directivity* and *fling* are the two main causes for the velocity pulses observed in near-field regions, even though other conditions (e.g., surface P-wave, supershear rupture velocity, special geometrical conditions) may also give rise to intense velocity pulses [2].

Forward Directivity Effect

Forward directivity occurs when the fault rupture propagates toward a site with rupture velocity approximately equal to the shear wave velocity. In this case, most of the energy arrives in a single large long-period pulse at the beginning of the record representing the cumulative effect of almost all the seismic radiation from the fault. The phenomenon is even more pronounced when the direction of slip on the fault plane points toward the site as well [4].

Fling Effect

The *fling* effect is related to the permanent tectonic deformation of the ground at a specific site due to an earthquake [5]; it appears in the form of step displacement and one-sided velocity pulse in the strike-parallel direction for strike-slip faults (e.g., stations YPT and SKR from the 1999 Izmit, Turkey earthquake) or in the strike-normal direction for dip-slips faults (e.g., stations TCU052 and TCU068 from the 1999 Chi-Chi, Taiwan earthquake).

Shear Dislocation vs. Crack-Type Rupture

A *constant stress-drop crack model* and a *uniform dislocation model* can be distinguished from the waveform of the *transverse displacement* [6]; that is from the waveform of the displacement perpendicular to the fault-surface (i.e., vertical component for low-dip faults and strike-normal component for vertical strike-slip faults). This statement is directly applicable to actual seismic events. Namely, the observed transverse displacement waveforms of low-dip earthquakes are characterized by a simple smooth ramp with a very slight overshoot as shown in Figure 2 for the 1985 Michoacan, Mexico and 1999 Chi-Chi, Taiwan earthquakes. On the other hand, the recorded transverse displacement waveforms of vertical strike-slip earthquakes display a strongly impulsive shape as illustrated in Figure 2 for the 1992 Landers, California and 1999 Izmit, Turkey earthquakes.

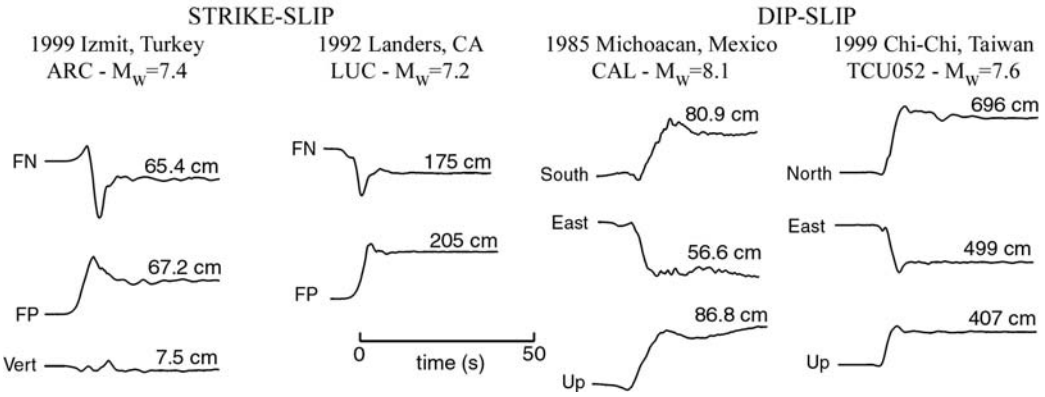

Figure 2. Typical sets of near-source displacement time histories for strike-slip and dip-slip earthquakes where significant displacement offsets were observed.

In general, dislocation models can adequately simulate strike-slip earthquakes, while large overthrust events, such as those in shallow-dipping subduction zones, require crack-like slip functions. This is an important remark related to the mechanics of rupture and results in significant waveform differences in the near-fault ground motions (see [2] and references therein).

Pulse Waveform Characteristics

The *pulse duration* (or *period*), the *pulse amplitude*, as well as the *number* and *phase of half cycles* are the principal parameters that define the waveform characteristics of near-field pulses. A more detailed discussion regarding these parameters is provided in [2].

A MATHEMATICAL EXRESSION FOR NEAR-FAULT GROUND MOTIONS

We have proposed a simple mathematical expression that effectively describes the nature of the impulsive near-source ground motions both qualitatively and quantitatively [2, 3, 7]. It generates synthetic signals as the product of a harmonic oscillation and a bell-shape envelope (i.e., shifted haversed sine function). That is:

$$v(t)=\begin{cases} A\dfrac{1}{2}\left[1+\cos\left(\dfrac{2\pi f_P}{\gamma}(t-t_0)\right)\right]\cos\left[2\pi f_P(t-t_0)+\nu\right], & t_0-\dfrac{\gamma}{2f_P}\le t\le t_0+\dfrac{\gamma}{2f_P} \quad with \quad \gamma>1 \\ 0, \quad otherwise \end{cases} \tag{1}$$

where A is the *amplitude* of the signal, f_P is the frequency of the amplitude-modulated harmonic (or the *prevailing frequency* of the signal), ν is the *phase* of the amplitude-modulated harmonic (i.e., $\nu=0$ and $\nu=\pm\pi/2$ define symmetric and anti-symmetric signals, respectively), γ is a parameter defining the *oscillatory character* of the signal (i.e., for small γ the signal approaches a delta-like pulse, for larger γ more oscillations appear), and t_0 specifies the *epoch* of the envelope's peak. The inverse of the prevailing frequency (f_P) provides an "*objective*" definition of the pulse duration (T_P).

The input parameters of the proposed mathematical expression coincide with the key features that determine the waveform characteristics of the near-source ground velocity pulses (i.e., amplitude, pulse duration, phase and number of half cycles). It is important that all input parameters have an *unambiguous physical interpretation*.

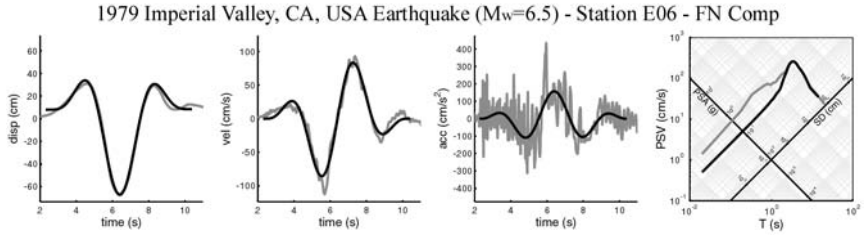

Figure 3. Proposed mathematical expression (i.e., black line) fitted to recorded ground motions (i.e., gray line).

We have calibrated our analytical model using a large number of near-fault records with distinct velocity pulses included in the compiled database. We have simultaneously fitted the displacement, velocity and acceleration time histories, as well as their corresponding elastic response spectra. A typical example is illustrated in Figure 3. Detailed analysis regarding the proposed analytical model, as well as a technique to synthesize reliable near-source ground motions are presented in [3].

CONCLUSIONS

We have addressed the importance of near-fault ground motions for the seismic response of long-span bridges. The factors that influence the character of the near-source ground motions have been presented. In addition, we have proposed a simple mathematical expression for the representation of near-field ground motions. This analytical model enables engineers to generate reliable near-source time histories appropriate for engineering design and applications.

ACKNOWLEDGEMENTS

This work was supported by FHWA Contract DTFH61-98-C-00094, Task C2-1, under the auspices of the Multidisciplinary Center for Earthquake Engineering Research.

REFERENCES

[1] McCallen, D. B. and A. Astaneh-Asl 2000. "An Explicit Integration Framework for Nonlinear Analysis of Suspension Bridges," *Journal of Seismology and Earthquake Engineering*, 2(4):19-41.

[2] Mavroeidis, G. P. and A. S. Papageorgiou 2002. "Near-Source Strong Ground Motion: Characteristics and Design Issues," *Proceedings of the Seventh National Conference on Earthquake Engineering (7NCEE)*, Boston, MA, July 21-25, 2002.

[3] Mavroeidis, G. P. and A. S. Papageorgiou 2002. "An Analytical Model for Near-Fault Ground Motions," (submitted for publication).

[4] Somerville, P. 2000. "New Developments in Seismic Hazard Estimation," *Proceedings of the Sixth International Conference on Seismic Zonation (6ICSZ)*, Palm Springs, CA, November 12-15, 2000.

[5] Abrahamson, N. A. 2000. "Near-Fault Ground Motions from the 1999 Chi-Chi Earthquake", *Proceedings of the U.S.-Japan Workshop on the Effects of Near-Field Earthquake Shaking*, San Francisco, CA, March 20-21, 2000.

[6] Aki, K. and P. G. Richards 1980. *Quantitative Seismology: Theory and Methods.* W. H. Freeman and Company, San Francisco, CA.

[7] Mavroeidis, G. P. and A. S. Papageorgiou 2002. "A Simple Mathematical Expression for the Representation of Near-Fault Ground Motions," presented at the 97th Annual Meeting of the Seismological Society of America, Victoria, Canada, April 17-19, 2002. [Abstract in *Seismological Research Letters*, 73(2).]

Shake Table Response of Flexure-Dominated Bridge Columns with Interlocking Spirals

Juan Correal[1], M. Saiid Saiidi[2], David Sanders[3] and Saad El-Azazy[4]

ABSTRACT

Interlocking spirals as transverse reinforcement in bridge columns are being used especially in large rectangular cross sections not only because they provide more effective confinement than rectangular hoops but also because interlocking spirals make the column fabrication process is easier. The behavior of columns with interlocking spirals has been studied only to a limited extent. The University of Nevada, Reno is conducting a study on the seismic behavior of interlocking spirals columns. The study is funded by the California Department of Transportation (Caltrans).

The study consists of experimental and analytical parts. The UNR shake table system is being used to test six large-scale models with interlocking spiral columns in the experimental part of the study. Two ¼ scale flexure-dominated oval columns have already been tested in the strong direction. The spacing between center to center of the spirals (1.0 and 1.5 times the spiral radius) was the principal variable studied in the first two specimens. Preliminary analytical studies of the columns have been conducted. The bond slip and shear deflections were included to predicted the force-displacement response. The shake table tests showed that the distance between the spirals did not adversely affect the shear capacity and that both columns failed in a very ductile manner with a displacement ductility capacity exceeding 8. Good agreement was also found between predicted and measured response enveloped.

[1] Research Assistant University of Nevada, Reno NV 89557
[2] Professor University of Nevada, Reno NV 89557.
[3] Associate Professor University of Nevada, Reno NV 89557.
[4] Senior Bridge Engineer Caltrans.

INTRODUCTION

The seismic design criteria (SDC) of the California Department of Transportation (Caltrans) [1] is the only bridge code in United States that provides specifications to design columns with interlocking spirals. Only a limited number of experimental and theoretical studies have been conducted on interlocking spiral columns. Tanaka and Park (1993) [2], Buckingham (1993) [3], Benzoni (2000) [4] and Mizugami (2000) [5] studied the performance of columns with interlocking spirals. None of these studies included dynamic loading of the column using earthquake simulation on shake tables.

The objective of the research discussed in this article is to study the seismic performance of flexure-dominated bridge columns with interlocking spirals using the UNR shake table system. The experimental results will be used in order to evaluate and to recommend any necessary refinement in the current Caltrans design provisions.

COLUMN DESIGN

Caltrans Provision

The SDC [1] denotes that a minimum element displacement ductility capacity of μ_c=3 shall be specified for columns in ductile structures. The desired level of element displacement ductility capacity is $\mu_c \geq 4$, in which μ_c is defined as:

$$\mu_c = \frac{\Delta_c}{\Delta_{y^{col}}} \tag{1}$$

The member displacement capacity, Δ_c, is determined from moment-curvature (M-ϕ) analysis with result idealized by an elasto-plastic relationship. Δ_y^{col} is the idealized effective yield displacement of the column. In the SDC [1], Δc of a cantilever member fixed at the base is defined as follows:

$$\Delta c = \Delta_y{}^{col} + \Delta_p \tag{2}$$

where Δ_p is the idealized plastic displacement capacity due to rotation of the plastic hinge. Δ_y^{col} and Δ_p are defined in Eq. (3) and (4), respectively.

$$\Delta_y{}^{col} = \frac{L^2}{3}\ \phi_y \tag{3}$$

$$\Delta_p = \theta_p (L - \frac{L_p}{2}) \tag{4}$$

where L = distance from the point of maximum moment to the point of contra-flexure; ϕ_y = the idealized yield curvature defined by an elasto-plastic representation of the cross section M-ϕ curve; θ_p = plastic rotation capacity ($\theta_p = L_p \phi_p$); ϕ_p = idealized plastic curvature capacity ($\phi_p = \phi_u - \phi_y$); ϕ_u = curvature capacity at the failure limit state. L_p = equivalent analytical plastic hinge length is defined as:

$$L_p = 0.08L + 0.15 f_{ye} d_{bl} \rangle 0.3 f_{ye} d_{bl} \tag{5}$$

where f_{ye}= expected yield stress for reinforcement; dbl = nominal bar diameter of longitudinal column reinforcement.

Large-Scale Models

Two ¼ scale columns with interlocking spirals were designed and constructed. The Seismic Design Criteria (SDC) [1], described above, was used to design the specimens. A target displacement ductility (μ_c) of 5 was selected. The distance between the centers of adjacent spirals was set to 1.0 and 1.5 times the radius of spirals, R, in specimens ISL1.0 and ISL1.5, respectively. These are the upper and lower limits in Caltrans SDC. A larger distance could affect the interaction between the spirals and could compromise the shear strength of the columns. The objective of the tests was to determine if the upper limit of 1.5R could still lead to satisfactory response.

The overall dimensions of the columns are shown in Figure 1. The specified concrete compressive strength of the columns was 34.5 Mpa (5000 psi) and the reinforcement was grade 60. The level of average shear stress under the maximum lateral load was $3\sqrt{f'c}$ for both specimens.

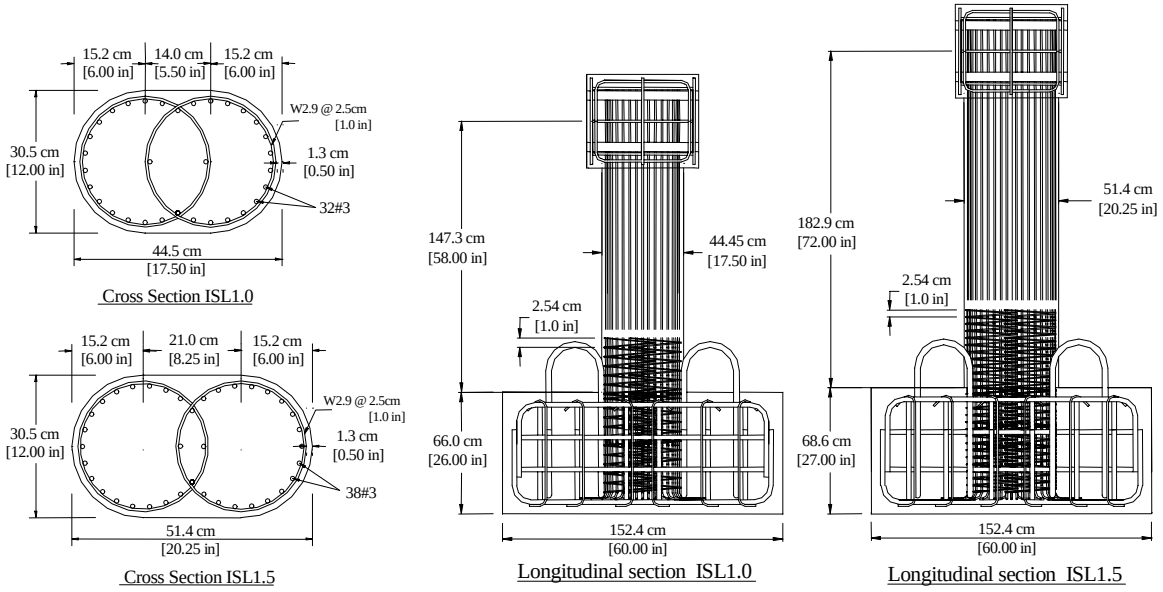

Figure 1. Test specimens dimensions

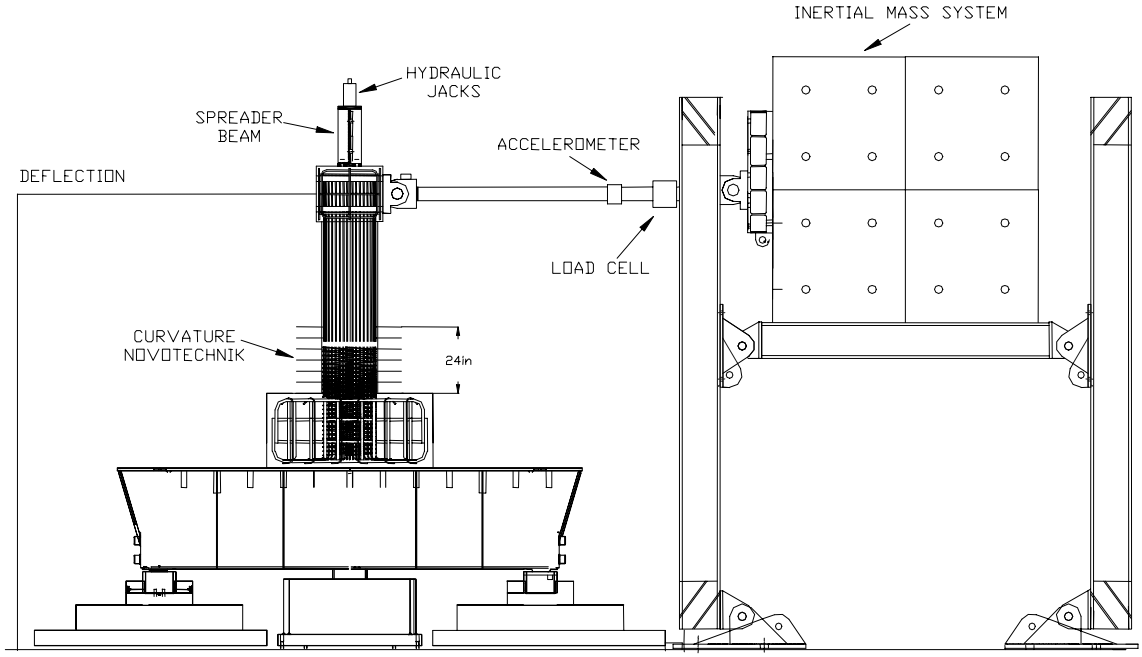

Figure 2. Test setup

TEST SETUP AND LOADING PROCEDURE

The test setup is shown in Figure 2. The axial load of $0.1f'_cA_g$ was imposed through a steel spreader beam by prestressed bars to hydraulic jacks. The lateral load was applied through the inertial mass system off the table for better stability. Strain gages were used to measure the strains in the longitudinal and transversal steel. A series of curvature measurement instruments were installed in the plastic hinge zone. Load cells were used to measure both the axial and lateral forces. An additional measurement of the lateral force was taken by an accelerometer. Displacements transducers measured the lateral displacements of the columns.

The nonlinear time history analysis of the columns subjected to a variety of input earthquakes was performed using the program RCShake [6]. The Sylmar record of the Northridge, California 1994 earthquake, was selected as the input motion based on the higher displacement ductility demand. A time compression of 0.51 and 0.50 were applied to the original Sylmar record in order to account for the ¼ scale factor of the models and adjustment due to inertia mass in ISL1.0 and ISL1.5, respectively. The earthquake was simulated in successive runs with increasing amplitudes starting with 0.1 x Sylmar. The full scale Sylmar motion has a peak acceleration of 0.606g. Intermittent free vibration tests were conducted the measure the changes in frequency and damping ratio of the columns.

EXPERIMENTAL RESULTS

General Performance

Flexural cracks were observed in specimen ISL1.0 during the first three runs and in specimen ISL1.5 during the first six runs. First spalling and shear cracks were formed in specimen ISL1.0 at 0.5xSlymar and specimen ISL1.5 at 1.25xSlymar. Shear cracks were located in the interlocking region near to the lower portion of the column. Considerable spalling, as well as propagation of flexural and shear cracks was observed after 1.25xSlymar in specimen ISL1.0. At 1.5xSlymar and 1.75xSlymar spirals were visible in specimens ISL1.0 and ISL1.5, respectively. There was no visible core damage until these motions. Longitudinal bars were exposed after 1.75xSlymar in specimen ISL1.0. Specimens ISL1.0 and ISL1.5 (Figure 3) failed during 2.0xSlymar (1.21g PGA) and 2.125xSlymar (1.29g PGA), respectively. The failure in both columns was due to fracturing of the spirals and buckling of the longitudinal bars.

Predicted and Measured Force-Displacement Relationships

A comparison of the predicted lateral force versus displacement and the measured hysteretic curves is made in Figure 4. The predicted force and displacement capacity was calculated based on the plastic moment capacity of the columns obtained from the M-ϕ curves. The program SPMC [7] was used in the M-ϕ analysis with an elastic perfectly plastic response. The bond slip and shear deflections were included in the predicted displacements. These deflections decrease between 23 and 26 percent the stiffness of the columns. In general, the predicted forces and displacements show a good agreement with experimental results.

Figure 3. Specimens ISL1.0 and ISL1.5 After Collapse.

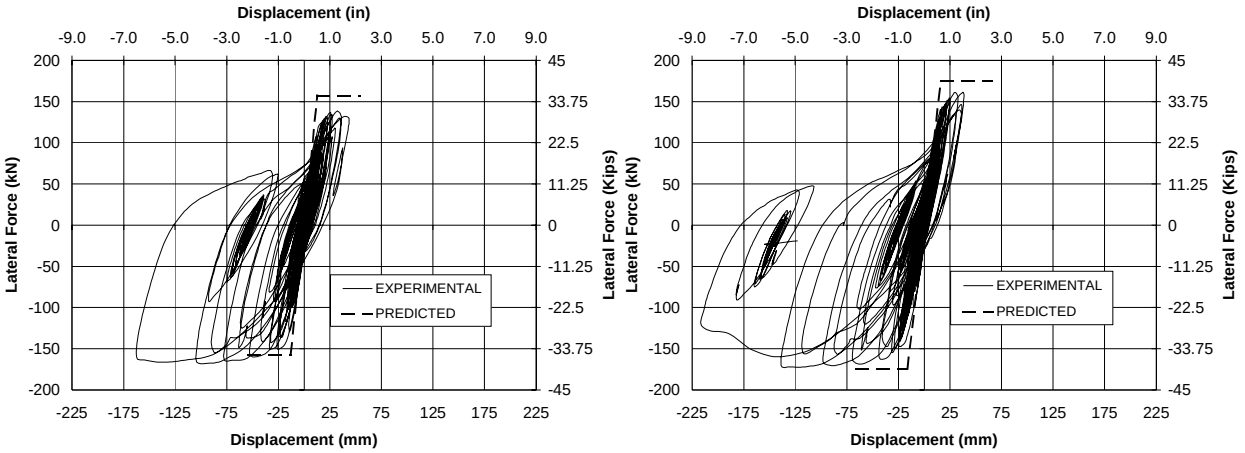

Figure 4. Hysteretic Curve and Predicted Response Specimen ISL1.0 and Specimen ISL1.5.

CONCLUSIONS

Based on the preliminary interpretation of the experimental results and preliminary analytical studies presented in this article the following conclusions were made for flexure-dominated columns:

1. Seismic performance of two flexural-dominated columns was similar and satisfactory. The measured displacement ductility capacity 8 or more in both columns, which exceeded the target ductility of 5.
2. The larger distance between the centers of the spirals in ISL1.5 did not appear to lead to excessive shear cracking or a reduction of the shear capacity. The Caltrans provision of allowing the distance to reach 1.5R is satisfactory.
3. Close agreement between the envelopes of the measured hysteresis loops and the calculated load-displacement responses indicates that the analytical method is a reliable tool to estimate the initial stiffness and the effective yield moment. The close agreement was realized only after the bond slip and shear deformations were included in the analysis.

ACNOWLEDGEMENT

The research present in this paper was sponsored by the California Department of Transportation. However, the opinions and conclusions reported in this paper are those of the authors only and not necessarily reflect the views of the sponsor.

REFERENCE

[1] Caltrans, 1999, Seismic Design Criteria, California Department of Transportation, Sacramento, California.

[2] Tanaka, H., Park, R. 1993. "Seismic Design and Behavior of Reinforced Concrete Columns with Interlocking Spirals", ACI Structural Journal March-April 1993. pp192-203.

[3] Buckingham, G.C. 1992. "Tests of Concrete Bridge Columns with Interlocking Spirals Reinforcement", presented at the Transportation Research Board 72nd annual meeting, January 11-17, 1993.

[4] Benzoni, G., Priestley, M.J.N.,Seible, F.2000. "Seismic Shear Strength of Columns with Interlocking Spiral Reinforcement", 12th World Conference on Earthquake Engineering, Auckland, New Zealand, 2000.

[5] Mizugami, Y. 2000. "Efficiency of Lateral Reinforcement in interlocking Spirals Re-bar", presented at the 16th US-Japan Bridge Engineering Workshop, October 2-4, 2000.

[6] RCShake, VER 2.31, August 2000, Dynamic Time History Analysis for the UNR Shake Table and Mass Rig System by Patrick Laplace, Department of Civil Engineering, University of Nevada, Reno.

[7] SPMC, VER. 10, July 2001, Moment-Curvature Analysis for Interlocking Spirals by Wehbe Nadim, Assistant Professor Of Civil Engineering, South Dakota State University, Brookings.

Expansion Joints for Seismic Isolated Bridges

E. Delis Ph.D., P.E.[1]

SUMMARY

Much emphasis has been given to the analysis and design of bearings in seismically isolated bridges however, not much research or effort has been made to the design of joints that can accommodate seismic movements. Until recently, the prevailing design philosophy was to accept damage at joints during a seismic event, which could be repaired or replaced at a later date. In shifting the seismic performance criteria from safety to functional approach, expansion joints have to tolerate not only large longitudinal and transversal movements but also vertical settlements. At the same time, they have to maintain full access to regular traffic almost immediately following the maximum considered earthquake. This paper presents recent designs and applications of seismic expansion joints in California bridges.

[1] Senior Bridge Engineer, Joint Seals & Bearings Specialist, Caltrans, Division of Engineering Services, P. O. Box 168041, Sacramento, CA 95816, email: Tim_Delis@dot.ca.gov

INTRODUCTION

Highway bridges are in a continuous state motion due to loads created by temperature, wind, traffic, creep and other forces [1]. Expansion joints are the connecting links of these structures to their surrounding environment. They provide deck continuity at superstructure hinges and at connections between bridge and abutments. This continuity is achieved by designing the expansion joints to accommodate the differential displacements and rotations of two adjacent bridge segments or between bridge deck and abutments. Until very recently, expansion joints were only designed to accommodate service loads. Joint damage during a seismic event and subsequent repair or replacement was anticipated. This was not an easy task however. Joint repair or replacement could take many days, weeks or even months in some special cases with severe disruption of the traffic and at an enormous cost to the local economy. Over the last three decades many local and state agencies in earthquake prone areas have invested heavily to improve and upgrade their infrastructure so it can meet higher seismic standards. As a result a number of "*important*" and "*ordinary*" bridges, new or existing, have been seismically isolated. Seismic isolating has been the preferred method due to its cost-effective way of substantially reducing the seismic-induced forces in a structure. However, this results in increased displacement and rotation demands at the expansion joints. In addition, state and local authorities have identified several structures as "*important*." In other words, these structures are expected to be fully operational after a major seismic event. Consequently, the design philosophy of the expansion joints has been changed and in many cases the joints are required to meet not only service but also seismic criteria.

Service joint requirements and desirable features in California include that the joint shall 1) accommodate longitudinal translation and rotation about the vertical axis while the other translations and rotations may be very limited, 2) provide passage of the traffic across the joints safely and comfortably, 3) be low or free of maintenance, 4) be designed and constructed so that they are water tight and prevent damage to the substructure from water, deicing chemicals, automobile fluids and other passing through foreign materials, 5) be designed to support the ASSHTO HS20-44 loading with 100 percent impact and each joint component in contact with tires shall support a minimum of 80 percent of the AASHTO HS20-44 loading with a 100 percent impact, 6) provide a maximum permissible gap in the direction of vehicular traffic of 100 mm and 75 mm in single (strip joint) and multiple openings (modular assembly) respectively, 7) be designed with tire contact area of 244 mm, measured normal to the joint, by 508 wide, 8) made of durable materials and all metal parts shall be either hot dip galvanized or painted with inorganic zinc coating, 9) not allow any component to translate or rotate due to direct application of wheel loads, 10) neither vibrate nor amplify traffic generated noise, 11) be easily accessible for inspection, 12) accommodate any future deck widening and 13) not exert any additional stresses to the bridge beyond the intent of the design.

Seismic joint requirements include those of service plus the following: The joint shall 1) provide translations and rotations in the three directions, 2) be prototype and proof tested on full sized specimen under dynamic conditions (simultaneous high velocity longitudinal and transversal displacements with vertical offset), 3) not be damaged during the design earthquake and 3) not be damaged during the maximum considered earthquake; a minor damage to the joint

could be tolerated but this shall not directly or indirectly affect the traffic and that the repair work could be performed without major disruption of traffic.

Three seismic joint systems (Swivel, Wabo Seismic Modular and Sliding) are described briefly below. As of today, the Sliding Joint has been successfully applied to several "*important*" and "*ordinary*" California bridges, while the other two systems are serious considered as viable alternatives in future projects. All three seismic joint systems allow large longitudinal and transversal movements and large rotation about the vertical axis but their capacity in accommodating large translation and rotation demands in the remaining three degrees of freedom is lower and varies for each system.

SWIVEL EXPANSION JOINT

The swivel joint consists of center and edge beams, steel brackets/stirrups, support bars, sliding plates, springs and bearings (Fig.1). The joint is designed and fabricated using fatigue-resistant connection details. The center beams are able to slide freely on swiveling support bars through the stirrups. The stirrups are attached to the support bars through pre-stressed sliding bearings in such a way that any lifting of the center beams due to traffic is prohibited. One end of the support bar is pivoted and prevents the bar from moving while the other end is allowed to rotate and slide. Because of their diagonal arrangement and their load transmitting function, the support bars control the position of the center beams and their openings thus, ensuring equidistant between center beams and edge beams. It is the geometry that maintains the equidistant function not any conventional mechanical system like springs. The joint has been successfully undergone extensive dynamic testing at the University of California at Berkeley [2] and is being currently considered for the New Carquinez Bridge and the New Bay Bridge in the San Francisco Bay area. Among the U.S. installations the swivel expansion system includes the 3rd Lake Washington Bridge (1987) [3] and the Lacey V. Murrow Floating Bridge (1992) in Washington State and the Jefferson Barracks Bridge in Illinois (1989).

WABO EXPANSION JOINT

The Wabo expansion joint is another geometry driven system and is made of edge and center beams, a control unit, support bars, transverse and longitudinal support boxes, springs and bearings (Fig.2). The support bars are connected to the beams with sliding stirrups and transfer the load to the support boxes through sliding bearings. The longitudinal support boxes house the support bars and allow them to slide in the longitudinal direction. Similarly, the transverse support boxes permit bar sliding in the transverse direction. The control unit is an adjustable hinge mechanism that is pin-connected to the center beams. As the joint opens or closes the control unit forces the center beams to maintain equal spacing between center beams and edge beams at all operation stages [4]. The joint is currently being tested under dynamic conditions at the University of California at Berkeley and the final report is expected to be released soon.

SLIDING SEISMIC JOINT

The sliding joint includes a channel assembly and a deck and a sliding steel plates (Fig.3). The assembly is anchored in the superstructure with welded studs. The channel includes i) two rows of rubber springs and ii) steel stiffeners that provide extra stiffness in the transverse direction. The rubber springs are essential elements of the sliding joint since they hold the deck plate down in case of a bridge settlement, bearing failure and/or a seismic event. The deck plate is very rigid (min. 70 mm thickness) and carries the traffic with a minimum deflection. Its upper surface is V-grooved for better traction and reduced traffic generated noise. One of its end seats on the channel assembly and is secured with two 25 mm dia. HS bolts spaced at 250 mm. A 6 mm neoprene sheet between channel and deck plate facilitates stress distribution and improves bearing. The other deck plate end is attached to a strip expansion joint. One of the edge beams of the strip is welded to the deck plate, while the other is anchored in the polyester concrete. The premixed polyester concrete is selected because it provides excellent chloride protection, smooth roadway profile, high-durability, fast cure time and ease-of-placement. The slide plate is anchored to the abutment or to the adjacent bridge segment in the case of a deck hinge. For maximum corrosion protection all metal parts of the sliding joint including the anchor studs are hot dip galvanized. The strip joint and the silicon seal placed at the ends of the deck plate provide water tightness. For the same reason, silicon seal is poured between deck plates in the transverse direction.

For service and low seismic loads, the sliding joint is able to accommodate movements up to 100 mm in the strip seal area. All horizontal forces resulting from braking and acceleration are resisted by friction and mainly by the HS bolts of the channel assembly. However, during severe earthquake conditions some of the bolts may shear off, the strip joint is expected to be damaged and the deck plate may crash into the polyester concrete or go over it. The repairs are expected to be minor, all parts are readily available and no specialized equipment or personnel are needed. Overall the sliding joint is a very attractive alternative solution due to its impressive design and construction simplicity, performance and cost effectiveness. Various versions of the sliding joint have been successfully used in California for several years now. The applications include the Golden Gate, the Benicia Martinez and the Rio Hondo [5] bridges.

CONCLUSION

Three expansion joint systems of various design, complexity and performance have been presented here. These joints enable highway bridges to meet service as well as seismic criteria and therefore providing post-earthquake life safety and minimizing economic impact.

ACKNOWLEDGEMENT

The author wants to acknowledge Roberto Lacalle, Supervising Bridge Engineer, for his valuable input. The findings, conclusions and recommendations are those of the author and do not necessarily represent those of Caltrans.

REFERENCES

[1] Caltrans, Bridge Memo to Designers Manual, 1994. Vol. 1, 7-10.

[2] Clyde D. and Whittaker A., 2000. “Full-Scale Dynamic Testing of Expansion Joints for Seismically Isolated Bridges,” EERC 2000-01, Univ. of California at Berkeley.

[3] Brown S. and Haerle U., 1986. “Design of a Sealed Expansion Joint for the 3rd Lake Washington Bridge,” Vol. 2, SP-94, ACI, Detroit, MI.

[4] Watson Bowman Acme literature.

[5] Delis E., Tokas C., Madani, M., Thompson K., 1997. "Analytical Studies for Seismic Isolation in Highway Bridges," Proceedings ASCE Structures Congress, Portland, OR.

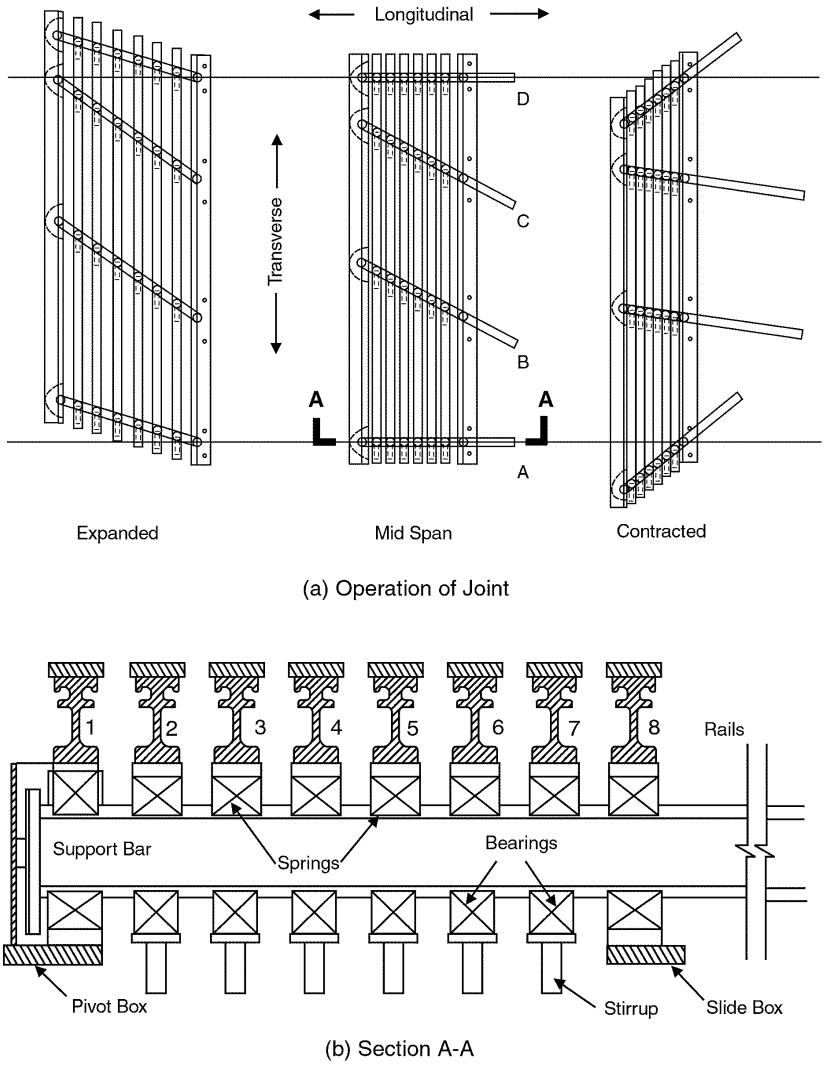

Figure 1. Swivel Expansion Joint

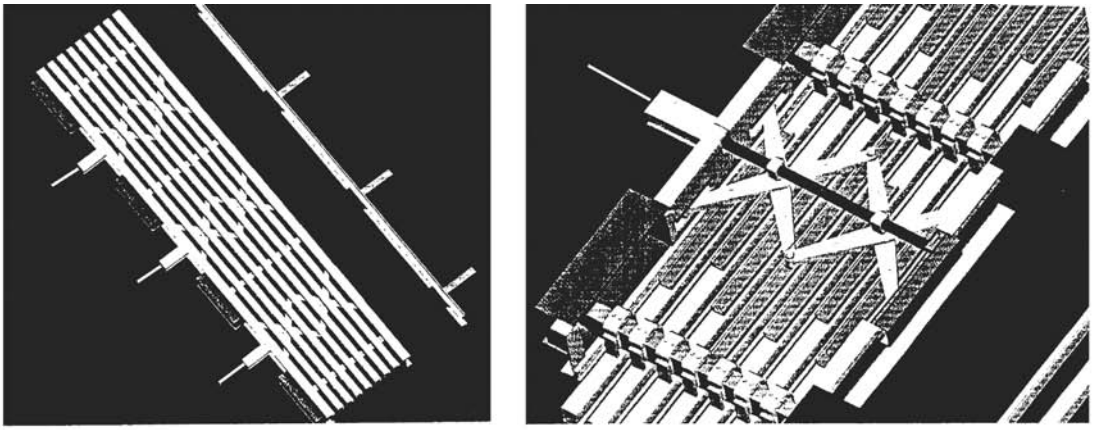

Figure 2. Wabo Expansion Joint

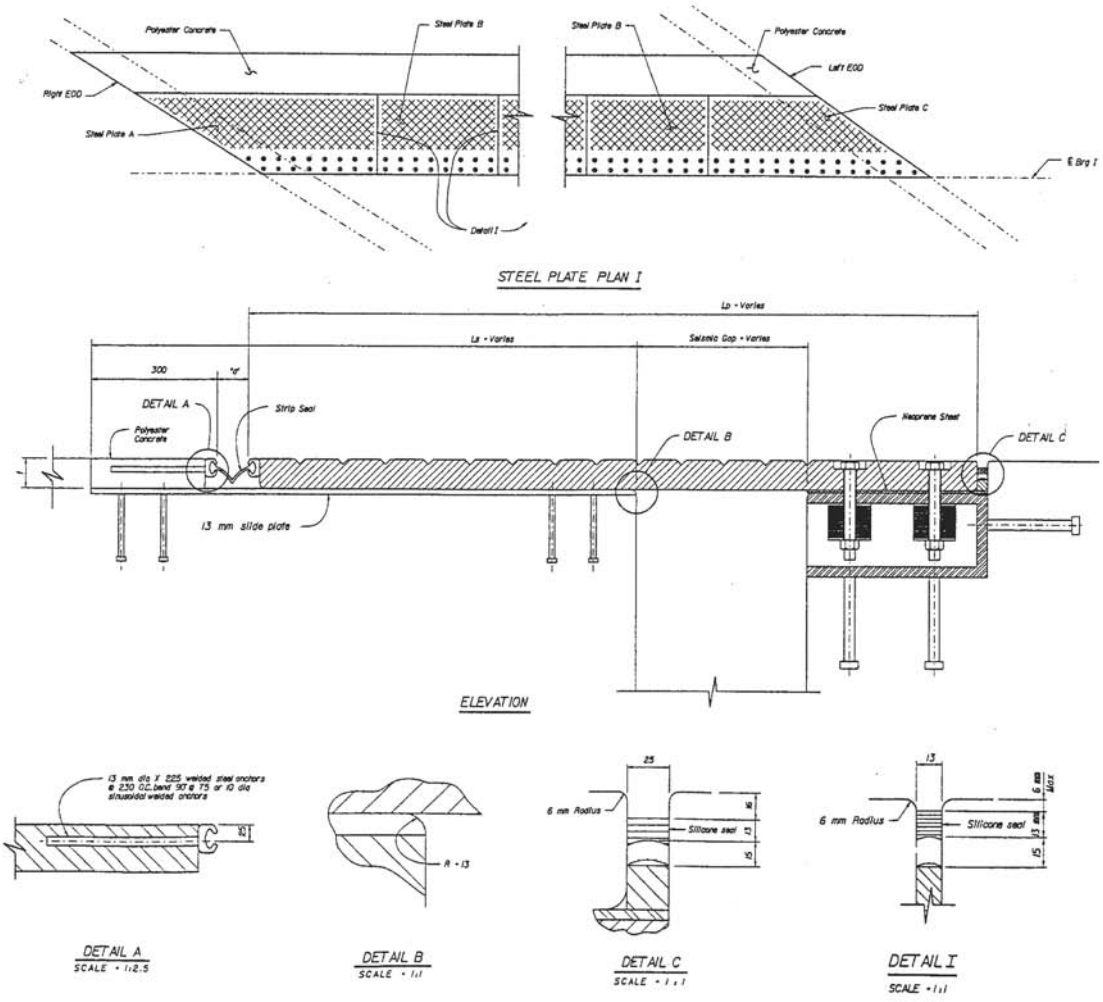

Figure 3. Sliding Seismic Joint

Development of Analytical Fragility Curves for Highway Bridges Considering Strong Motion Parameters

Kazi R. Karim and Fumio Yamazaki

ABSTRACT

The actual damages to highway systems from recent earthquakes have emphasized the need for risk assessment of the existing highway transportation systems. Due to earthquakes, highway bridges may experience sort of damages, e.g., slight, moderate, extensive, and complete. This damage information is useful for seismic retrofitting decisions, disaster response planning, estimation of direct monetary loss, and evaluation of loss of functionality. To predict the extent of probable damages, fragility curves are found to be useful tools. It shows the probability of highway structure damages as a function of strong motion parameters. They allow estimating a level of damage probability for a known ground motion parameter. In this study, an analytical approach was adopted to develop the fragility curves for highway bridges based on numerical simulation. Four typical RC bridge piers and two RC bridge structures were considered of which one is non-isolated system and the other one is isolated system, and they were designed according to the seismic design codes in Japan. A total of two hundred and fifty (250) strong motion records were selected from Japan, Taiwan and the United States. Using the selected acceleration records, nonlinear time history analyses were performed, and the damage indices for the bridge structures were obtained. Using the damage indices and ground motion parameters, fragility curves for the four bridge piers and two bridge structures were constructed assuming a lognormal distribution. The relationship between the fragility curve parameters and over strength ratio of the structures was also obtained performing a linear regression analysis. It was found that there is a significant effect on the fragility curves due to the variation of structural parameters. A strong correlation was also observed between the fragility curve parameters and over strength ratio of the structures. The relationship between the fragility curve parameters and the over strength ratio of the structures may a very useful tool to construct the fragility curves for the bridge structures knowing the over strength ratio only. The fragility curves obtained by following this approach may be useful for earthquake damage assessment of highway bridges in Japan.

Kazi R. Karim, Graduate Student, Institute of Industrial Science, the University of Tokyo, 4-6-1 Komaba, Meguro-ku, Tokyo 153-8505, Japan.
Fumio Yamazaki, Professor, School of Advanced Technologies, Asian Institute of Technology, P.O.Box.4, Klong Luang, Pathumthani 12120, Thailand.

INTRODUCTION

The 1995 Kobe earthquake, which is considered as one of the most damaging earthquakes in Japan, caused severe damages to expressway structures in Kobe area. Based on the actual damage data from the earthquake, Yamazaki *et al*. [1] developed a set of empirical fragility curves. However, the empirical fragility curves do not specify the type of structure, structural performance (static and dynamic) and variation of input ground motion, and may not be applicable for estimating the level of damage probability for specific bridge structures.

The objective of this study is to develop analytical fragility curves for highway bridges based on numerical simulation considering both structural parameters and variation of input ground motion. Karim and Yamazaki [2] developed a set of analytical fragility curves for highway bridge piers based on numerical simulation, and it was found that there is a significant effect of earthquake ground motions on fragility curves. In this study, four typical RC bridge piers and two RC bridge structures are considered, and the fragility curves are obtained based on numerical simulation [2] as a function of strong motion parameters.

DEVELOPMENT OF FRAGILITY CURVES

Yamazaki *et al*. [1] developed a set of empirical fragility curves based on the actual damage data from the 1995 Kobe earthquake, and details for constructing the empirical fragility curves can be found elsewhere [1]. Karim and Yamazaki [2] developed a set of analytical fragility curves for highway bridge piers based on numerical simulation. The procedures adopted for constructing the analytical fragility curves are briefly described below while details can be found elsewhere [2].

1. Selection of the earthquake ground motion records and normalization of PGA of the selected records to different excitation levels.
2. Performing static pushover and nonlinear dynamic response analyses using the selected records.
3. Obtaining the damage indices of the structure for each excitation level and calibrating them to get the damage ratio for each damage rank.
4. Constructing the fragility curves using the obtained damage ratio and the ground motion indices for each damage rank assuming a lognormal distribution.

BRIDGE MODELS AND INPUT GROUND MOTIONS

Four typical RC bridge piers [3] and two RC bridge structures are considered of which one is non-isolated and the other one is isolated. The piers are designed according to the 1964, 1980, 1990, and 1995 seismic design codes [4] assuming that only the size and reinforcement of the piers can be changed with other conditions such as the height of substructure (11.8m), length (35m) and weight of superstructure (23627 kN), ground condition (class II), and nominal design strength of concrete (14.7 MPa) and reinforcement (294 MPa) being unchanged. The elevation and cross-sections of the four piers are shown in Figure 1. In case of the two bridge models, they are designed according to the seismic design code in Japan [4] assuming that the size and reinforcement of the piers, height of the substructure, length and weight (W) of superstructure, ground condition, and nominal design strength of concrete and reinforcement being unchanged. Note that the parametric values for the two bridge systems are taken as that of the 1980 pier except the height, which is taken as 12m. For non-isolated bridge system, the piers are rectangular, pin-jointed to the superstructure and fixed to the base, and the superstructure is assumed to slide on ordinary frictionless bearings at the abutments. For isolated bridge system, a Lead-Rubber Bearing (LRB) is used as isolation device. The yield strength and yield stiffness of the LRB are taken as 5% W and 5% W/mm, respectively [5]. The advantage of LRB is that it has low yield strength and sufficiently high initial stiffness that results higher energy dissipation. The substructure stiffness for the whole bridge system is given as the sum of the stiffness of all piers. The physical models of the non-isolated and isolated bridge systems are shown in Figure 2. The natural period for the

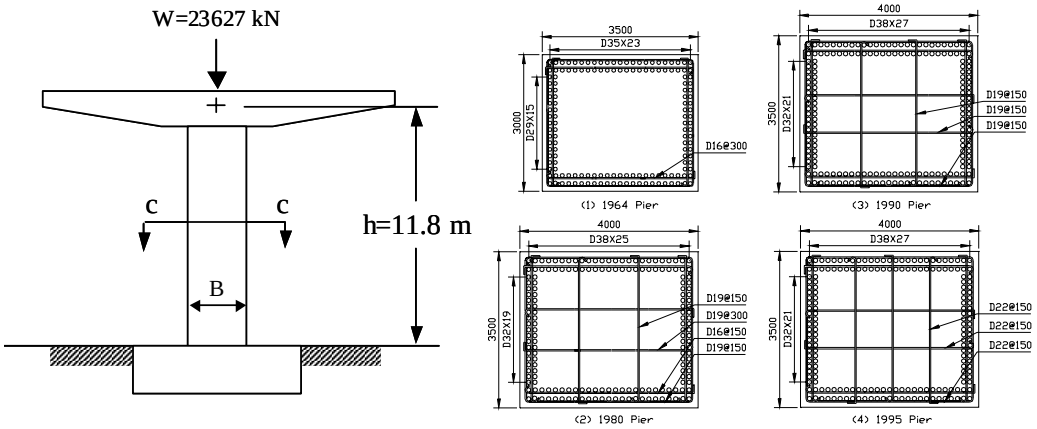

(a) Elevation of a typical bridge pier (b) Cross-sections at c-c

Figure 1. Elevation and sectional views for the four bridge piers used in this study.

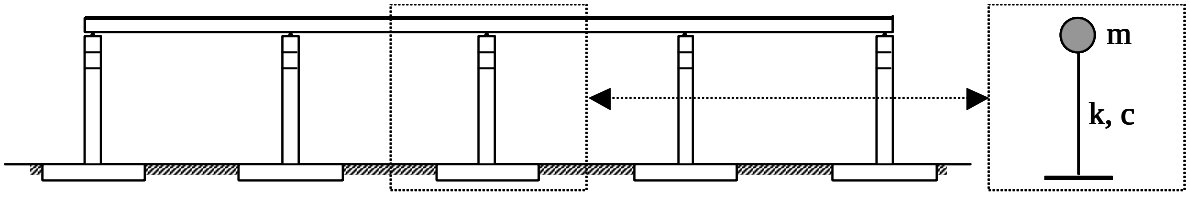

(a) Physical model of a non-isolated bridge system

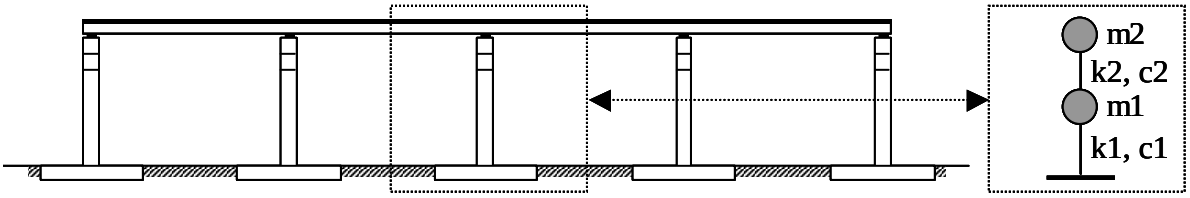

(b) Physical model of an isolated bridge system

Figure 2. Physical models of the non-isolated and isolated bridge systems used in this study.

non-isolated system to the longitudinal direction is 0.41s, and it shifts to 1.24s for the isolated system, which falls within the practical range of natural period for isolated system. For a nonlinear dynamic response analysis and to get a wider range of the variation of input ground motion, a total of two hundred and fifty (250) records were selected from the 1995 Kobe, the 1994 Northridge, the 1993 Kushiro-Oki, the 1987 Chibaken-Toho-Oki, and the 1999 Chi-Chi earthquakes.

DAMAGE ANALYSIS AND FRAGILITY CURVES

For the damage assessment of the bridge structures, Park-Ang [6] damage index was used in this study. The damage index DI is expressed as

$$DI = \frac{\mu_d + \beta \cdot \mu_h}{\mu_u} \tag{1}$$

where μ_d and μ_u are the displacement and ultimate ductility of the bridge structure, β is the cyclic loading

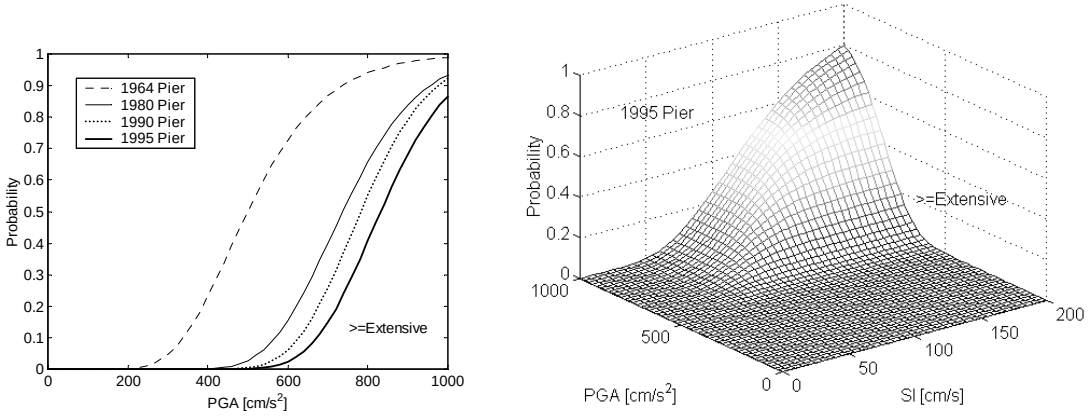

(a) Fragility curves with respect to PGA (b) Fragility surface with respect to PGA and SI

Figure 3. (a) Comparison of the fragility curves for the four bridge piers with respect to PGA, and (b) fragility surface for the 1995 pier with respect to PGA and SI.

factor taken as 0.15, and μ_h is the cumulative hysteretic energy ductility. The obtained damage indices for the selected input ground motions are then calibrated to get the damage ratio for each damage rank, which are used to construct the fragility curves [2]. Selection of input motion parameters to correlate with the structural damage is important, however, is not an easy task. Similar to the JMA instrumental seismic intensity [7], from the regression analysis between *DI* and ground motion parameters ($y = ax^b z^c$), it is also found that *DI* shows the highest correlation with both PGA and SI (R^2=0.850). Hence, fragility curves are constructed with respect to both single and multiple ground motion parameters considering PGA, PGV, and SI as the amplitude parameters. For the cumulative probability P_f of occurrence of the damage equal to or higher than rank *R* is given as

$$P_f(\geq R) = \Phi\left[\frac{\ln X - \lambda_x}{\zeta_x}, \frac{\ln Y - \lambda_y}{\zeta_y}, \rho_{xy}\right] \tag{2}$$

where Φ is the standard normal distribution, X and Y are the ground motion indices (e.g., PGA and SI), λ_x, λ_y and ζ_x, ζ_y are the mean and standard deviations of $\ln X$, $\ln Y$, respectively, and ρ_{xy} is the correlation coefficient between $\ln X$ and $\ln Y$. It should be noted that to construct the fragility curves from single ground motion parameter, only one variable should be considered in Equation (2).

Figure 3(a) shows the plots of the fragility curves for the four bridge piers for "extensive" damage with respect to PGA only, and the fragility surface for the 1995 pier for "extensive" damage with respect to both PGA and SI are shown in Figure 3(b). One can see that the level of damage probability goes higher from 1995 pier to 1964 pier. As the code requirements changes from time to time (Figure 1(b)), the structure that is designed using the recent code is supposed to perform better against earthquake force than the previous one, and the evidence can be seen on the fragility curves (Figure 3(a)). Figure 4(a) shows the fragility curves for the non-isolated and isolated bridge systems, and it can be seen that the level of damage probability for the isolated system is less than that of the non-isolated one. This is because the substructure experience less lateral force due to the energy dissipation of the isolation device.

Figure 4(b) shows the relationships between the fragility curves parameters (mean) and over strength ratio (OSR), which are obtained from linear regression analysis for four damage ranks. The OSR is defined as the ratio of the ultimate strength to the design seismic force, in other words, it is a function of all the structural parameters. Note that the data for the isolated system is not included in the regression analysis. It can be seen that there is a very strong correlation between the fragility curves parameters and OSR (R^2=1.00, 0.98, 0.99,

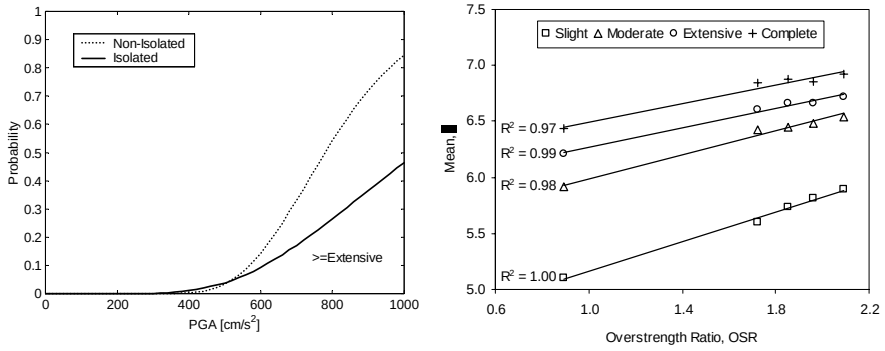

(a) (b)

Figure 4. (a) Comparison of the fragility curves for the non-isolated and isolated systems with respect to PGA, and (b) relationship between the fragility curves parameters and over strength ratio of structures.

and 0.97, for the four damage ranks, respectively). This relationship can be a very useful tool to construct the fragility curves for highway bridges knowing the OSR factor only.

CONCLUSIONS

Analytical fragility curves for the four typical bridge piers and two bridge models were obtained with respect to the ground motion parameters based on numerical simulation. It was found that there is a significant effect on the fragility curves due to the variation of structural parameters. It was also found that the level of damage probability for the isolated bridge structure is less than that of the non-isolated one. It was observed that fragility curves parameters are highly correlated to the over strength ratio of structures, and this relationship may be a very useful tool to construct the fragility curves for bridge structures knowing the over strength ratio only. However, the relationship was obtained considering only four bridge piers and one non-isolated bridge models, and to draw a solid conclusion, it is necessary to consider more bridge models for which a further research is going on.

REFERENCES

[1] Yamazaki, F., H. Motomura, and T. Hamada. 2000. “Damage Assessment of Expressway Networks in Japan based on Seismic Monitoring,” 12th World Conference on Earthquake Engineering, Auckland, New Zealand, January 30-February 4, 2000, CD-ROM, Paper No. 0551.

[2] Karim, K. R. and F. Yamazaki. 2001. “Effect of Earthquake Ground Motions to Fragility Curves of Highway Bridge Piers based on Numerical Simulation,” *Earthquake Engg. & Struct. Dyn.*, 30(12):1839-1856.

[3] Kawashima, K., J. Sakai, and H. Takemura. 1998. “Evaluation of Seismic Performance of Japanese Bridge Piers Designed with the Previous Codes,” Proc. of the 2nd Japan-UK Workshop on Implications of Recent Earthquakes on Seismic Risk, Technical Report TIT/EERG 98-6, pp. 303-316.

[4] *Design Specifications of Highway Bridges*. 1998. “Part V: Seismic Design,” Technical Memorandum of EED, PWRI, 9801.

[5] Ghobarah, A. and H. M. Ali. 1988. “Seismic Performance of Highway Bridges,” *Engg. Struct.*, 10:157-166.

[6] Park, Y. J. and A.H-S. Ang. 1985. “Seismic Damage Analysis of Reinforced Concrete Buildings,” *Journal of Struct. Engg.*, ASCE, 111(4):740-757.

[7] Karim, K. R. and F. Yamazaki. 2001. “Correlation of JMA Instrumental Seismic Intensity with Strong Motion Parameters,” *Earthquake Engg. & Struct. Dyn*, (in press).

State Street Bridge: CFRP Composite Seismic Rehabilitation and Specifications

Chris Pantelides, Fadel Alameddine, Thomas Sardo, Roy Imbsen, Larry Cercone, and Frederick Policelli

ABSTRACT

The State Street Bridge in Salt Lake City, was designed and built in 1965 according to the 1961 AASHO Specifications but the design did not consider earthquake-induced forces or displacements since wind loads governed the design. The bridge consists of four bents, each of which has four reinforced concrete columns and a bent cap supporting composite welded girders; the bents are supported on cast-in-place concrete piles and pile caps. A vulnerability analysis of the bridge was conducted and it was determined that the bridge had deficiencies in: (a) confinement of the column lap splice regions, (b) confinement of column plastic hinge zones, and (c) shear capacity of columns and cap beam-column joints. A seismic retrofit design was performed using Carbon Fiber Reinforced Polymer (CFRP) composites, which was implemented during the summer of 2000 and 2001 while the bridge was in service. The paper describes the design of the CFRP composite, which in addition to column jacketing, implemented a new "ankle wrap" for improving joint shear strength, and a new "U-strap" for improving anchorage of column bars; other rehabilitation measures included hinge restrainers. The paper also describes the specifications developed especially for the CFRP composite column jackets and the CFRP composite bent wrap; these included provisions for materials, minimum initial properties, required constructed thickness including an environmental durability reduction factor, surface preparation and finish coat requirements, as well as quality control and quality assurance provisions which included sampling and testing.

Chris Pantelides, Prof., Dept. of Civil & Envir. Engrg., Univ. of Utah, Salt Lake City, UT 84112
Fadel Alameddine, Engr., Off. of Earthq. Engrg., Calif. Dept. of Transp., Sacramento, CA 95816
Thomas Sardo, Engr., Washington Infrastructure, Irvine, CA 92614
Roy Imbsen, Principal, Imbsen & Associates Inc., Sacramento, CA 95827
Larry Cercone, President, Navlight Composites, Pasadena, CA 91107
Frederick Policelli, Principal, F. Policelli & Associates, Salt Lake City, UT 84117

BRIDGE SEISMIC RETROFIT DESIGN

The State Street Bridge at Interstate 80 in Salt Lake City, was designed in 1965 according to the State of Utah Standard Specifications for Road and Bridge Construction, 1960 Edition and Supplements, and the AASHO Specifications of 1961 and Interim Specifications. As such, the bridge was not designed to resist earthquake-induced forces or displacements because wind loads governed the design. The 55.47m-long bridge consists of two 10.82m end spans and a 33.83m middle span. The substructure consists of cast in place concrete piles, concrete pile caps, concrete columns and concrete cap beam. The dimensions and reinforcing details of one of the four bents of the bridge is shown in Fig. 1. The girders, which are not shown, are composite welded steel beams. The design spectra shown in Fig. 2 were used for the retrofit analysis and design. Design parameters for the analysis required for the seismic retrofit design were established as follows: (1) concrete compressive strength = 29 MPa, (2) maximum strain = 0.004, (3) steel yield stress: 300 MPa, (4) foundation lateral stiffness in horizontal direction = 28.3 kN/mm, (5) axial stiffness in vertical direction = 168.1 kN/mm, and (6) rotational stiffness = 45,685 kN-m/rad. Design Spectra for three design earthquakes were determined as follows: (1) 0.2 g earthquake, (2) 10% probability of exceedance in 50 years, (3) 10% probability of exceedance in 250 years.

Static pushover nonlinear analyses of the bridge bent were performed in the longitudinal and in the transverse direction using a two-dimensional model. A capacity evaluation was performed with the following criteria: (a) buckling of longitudinal column reinforcement, (b) crushing of concrete core at plastic hinge regions and maximum curvature capacity, (c) principal stresses at the bent cap to column joints, (d) shear, axial and flexural capacity of columns and bent cap, (e) lap splice failure at the column to foundation connection, and (f) principal stresses at column to pile cap connection. The CFRP composite design for a typical bridge bent is shown in Fig. 3, in which n is the number of CFRP composite layers, and the thickness of a single layer is 1.32mm. The seismic retrofit design followed recently established design procedures [1], which were confirmed by in-situ tests of bridge bents on Interstate 15 [2]. The ultimate CFRP carbon/epoxy composite tensile strength specified was 630 MPa; the material used in this application was 12,000 individual fibers per fiber bundle (tow) unidirectional carbon fibers, approximately 5 to 7 microns in diameter. The number of tows per 25mm of fabric was 19, yielding a total of 228,000 fibers per 25mm wide fabric.

CFRP COMPOSITE SPECIFICATIONS

As part of the *Supplemental Specifications* of the construction contract two special provisions were developed: (a) *Special Provision 525S* for column composite wrap, and (b) *Special Provision 526S* for bent composite wrap [3]. Several requirements of the specifications were implemented for the first time in highway bridge rehabilitation. These include: (1) utilization of “Strength Capacity” as the structural strength requirement for FRP jackets; (2) use of an environmental durability strength reduction factor to account for degradation of the CFRP composite; (3) fabrication of NOL rings during bridge site construction; (4) cooperation of the contractor with the owner in the performance of long-term health monitoring of the CFRP composite, during the CFRP composite application and while the bridge was in service; (5) requirement that the contractor procure the services of a manufacturer’s representative of the

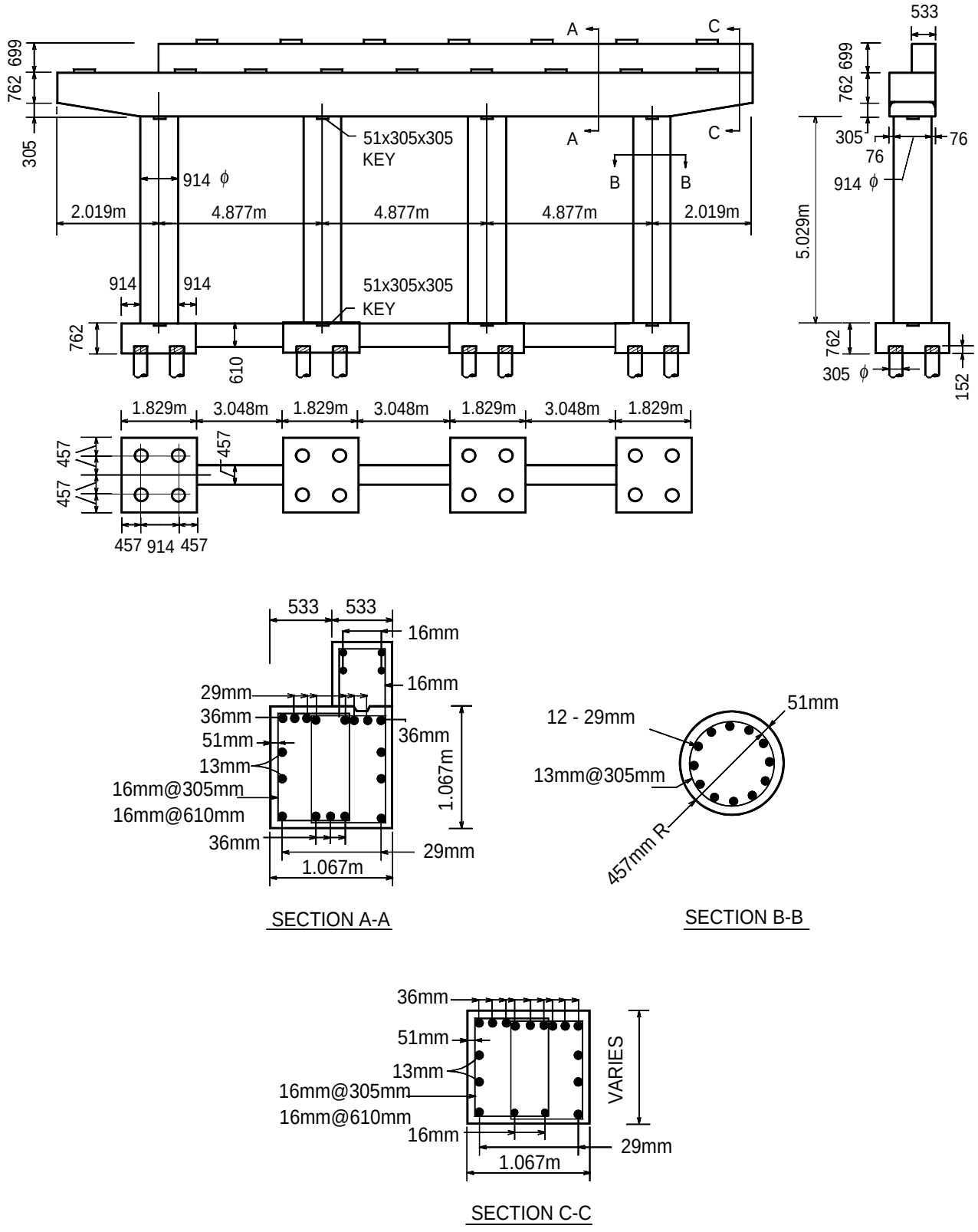

Figure 1. Dimensions and Reinforcement of State Street Bridge

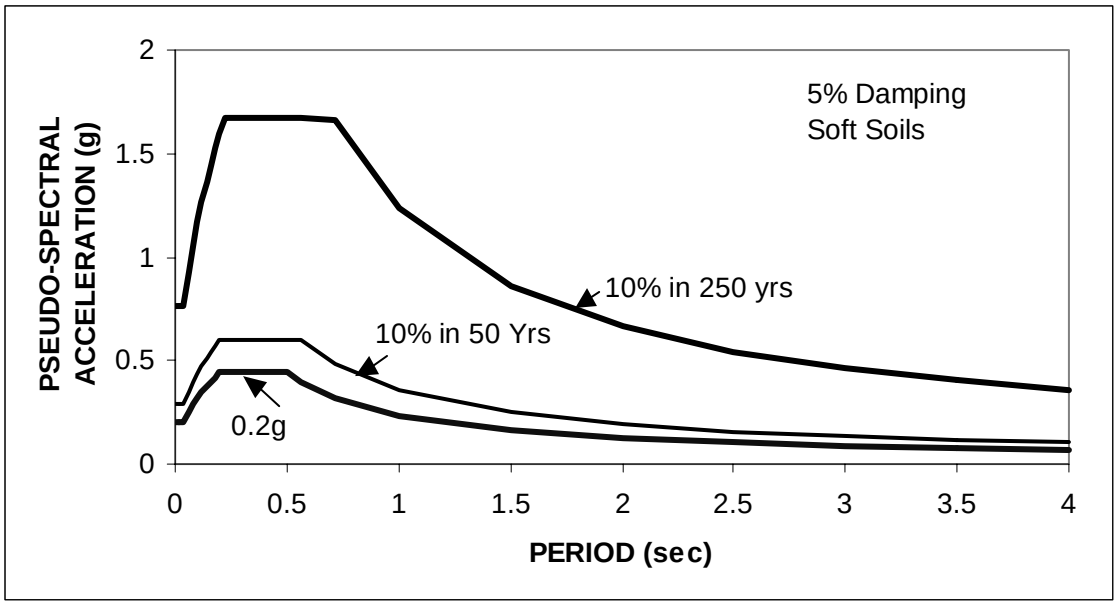

Figure 2. Design Spectra for State Street Bridge

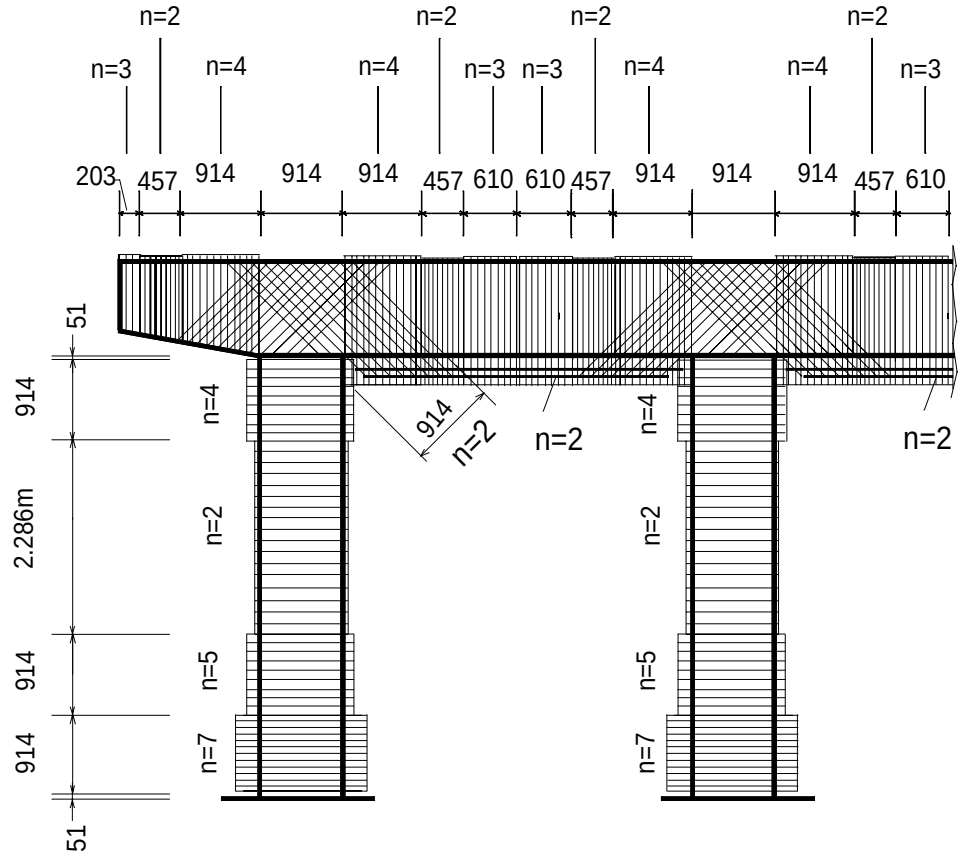

Figure 3. CFRP Composite Design for Columns, Beam Cap, and Joint "Ankle Wrap"

CFRP composite material; (6) thickness gage measurement for inspection of the finish coat; and (7) a highly organized means of carrying out the sample preparation, collection, storage, identification, and testing of the CFRP composite test samples. Strength Capacity is force per unit width or the product of the stress (S) and jacket thickness (T). The material allowable stress is defined as the mean ultimate strength, minus two standard deviations, (2σ). In addition, the ($Mean\text{-}2\sigma$) strength is multiplied by an environmental durability strength reduction factor, (ϕ), which has a value less than one. The *Supplemental Specifications* [3], required testing of 50 samples for the purpose of determining the mean and standard deviation strength values. The allowable strength, S_a, is given as:

$$S_a = \phi \ (S_{mean} - 2\sigma) \tag{1}$$

The thickness of the CFRP composite to be constructed (T_c) is related to the design strength, S_d, and design thickness, T_d, using the definition of Strength Capacity as:

$$T_c = \left(\frac{S_d}{S_a} \right) T_d \tag{2}$$

Equations (1) and (2) allow different manufacturers with different systems to proportion their designs according to the properties of their material.

CONCLUSIONS

The elements of the CFRP seismic retrofit design included the columns, bent cap and joints of the bridge, which the authors believe to be a first in North America. An evaluation of the as-built and retrofitted bridge bents showed that the retrofitted bent was functional in all three design earthquakes, whereas the as-built bent would not survive the 10% in 250 years event. The seismic retrofit of the State Street Bridge with CFRP composites, using the supplemental specifications, was implemented successfully and involved epoxy injection of voids as the only remedial action.

REFERENCES

[1] Pantelides, C.P., and Gergely, J. 2002. "Carbon-Fiber-Reinforced Polymer Seismic Retrofit of RC Bridge Bent: Design and In Situ Validation." *J. Compos. Constr.*, 6(1), 52-60.

[2] Pantelides, C.P., Gergely, J., and Reaveley, L.D. 2001. "In-situ Verification of Rehabilitation and Repair of Reinforced Concrete Bridge Bents under Simulated Seismic Loads." *Earthq. Spectra*, EERI, 17(3), 507-530.

[3] Utah Department of Transportation. 1999. "Supplemental Specifications-Special Provisions." I-80 Bridge Rehabilitation, Project No. IM-80-3(126)123, Salt Lake City, Ut.

ACKNOWLEDGEMENTS

The project and this research were funded by the Federal Highway Administration and the Utah Department of Transportation. This support is gratefully acknowledged.

Recommendations on Experimental Procedures for Bridge Column Testing

Jerry J. Shen[1], W. Phillip Yen[2], and John O'Fallon[3]

ABSTRACT

In order to make the bridge experiments more efficient in terms of providing reliable and comparable information, Federal Highway Administration has conducted a systematic study on bridge testing methods. The most common procedures and issues are identified. Proper methods on specimen construction, loading procedure, as well as measurements and data format will be established to provide experimental researchers an easy reference that makes test results comparable to results from other tests.

1 Lendis/FHWA, 6300 Georgetown Pike, McLean, VA 22101
2 Office of Infrastructure, R&D Federal Highway Administration, , 6300 Georgetown Pike, McLean, VA 22101
3 Office of Infrastructure, R&D Federal Highway Administration, , 6300 Georgetown Pike, McLean, VA 22101

INTRODUCTION

Experimental studying on bridges and components of bridges is an essential need for the improvements on design and construction techniques. As the seismic design concept for bridges gradually turns to performance-based approach, the need for a large amount of comparable tests results increases. In order to make the bridge experiments more efficient in terms of providing reliable and comparable information, the Federal Highway Administration (FHWA) has launched a systematic study on the techniques and procedures of conducting experimental bridge tests. The objective of the study is to develop the National Guidelines for Experimental Tests on Highway Structures.

A literature review covering a wide range of bridge tests were performed. Information of the major experimental research institutes was collected. Some laboratory administrative personnel were or will be interviewed to include their practical experiences. These materials will be summarized and a proposed experimental guidelines will be produced. These results will be made available for experts to review and comment.

BENEFITS FROM THE GUIDELINES

Each experimental study has its own purpose and unique setup to serve this purpose. The results from experiments always contain more information than they were designed to provide. A large part of the information is often either ignored or not comparable with other tests due to incompatible format and testing conditions. If widely adopted experiment guidelines exist, the part of an experiment that is not essential to its purpose can be conducted in the standard manner. Commonly demanded information will not be ignored. The result can be used for theoretical derivation or empirical model calibration with a solid confidence that the data were obtained from an experiment compliant to a reliable procedure. In the mean time, the tester receives additional credits and publicities because the experimental results appear in more consequent studies.

This guidelines is not similar to some of the existing testing standard such as those in ASTM testing manual. Due to the explorative origin of the tests regulated by this guidelines, making changes to the procedure in accordance to the need of the specific test does not immediately disqualify the results. The intention is to provide assistance rather than restriction to the experimental community.

COMMON METHODS AND PURPOSES FOR BRIDGE COLUMN TESTS

Dynamic structural tests are commonly divided into 3 categories. They are quasi-static tests, pseudodynamic tests, and shake table tests (Kausel, 1998; Dimig et al, 1999). Dynamic tests on bridges are carried out for either discovering element properties that were not clear to engineers or verifying the theoretical predictions. The most common goals for dynamic bridge tests are:

(1) To determine strength and ductility under strong earthquake (capacity)
(2) To determine displacement and force demand
(3) To determine effectiveness of retrofit
(4) To observe failure patterns such as cracking, buckling, etc.

(5) To observe the performance of new design or retrofit methodologies
(6) To develop and verify analytical or empirical models
(7) To inspect existing bridges

Different goal results in different test requirements and test methods. The issues being addressed in this guidelines are those shared by a number of different tests.

GUIDELINES

There are three major issues in a bridge test: specimen, loading, and data handling. The specimen is a full or reduced replica of the interested part of a real or imaginary bridge. It needs to be designed to best reflect the bridge characteristics. The loading procedure is usually a simulation of load history occurs in a real event. For random-type input such as earthquake and wind, some load histories that are different from the real load but possess certain realistic characteristics are used (e.g. cyclic load). The results of the tests need to be recorded and stored with adequate conditioning and format.

Model construction

Prototype

For general bridge studies, which may target a group of bridges, the bridge parameters, such as size, shape, designed loads, and detailing, may not be available from the original design agencies. One approach is to conduct a statistical investigation (Lowes and Moehle, 1995, Abo-Shadi et al, 2000) to determine the most representative parameters for the group of bridges. The other approach is to simply use a most common value regardless what group of bridges the test is designed for. The proper guideline provisions to these two scenarios are described below:

(1) The National Bridge Inventory (NBI) Database is a complete collection of bridge external dimensions, functions, locations, ages, etc. This information can be converted to that required by the testers (Lampe and Azizinamini, 2000). This can largely reduce the time spent on preliminary investigation and increase the representativeness of the selected parameters.

(2) When the tester only needs a general bridge model, a set of most common parameters can be provided. For example, a height of 20 ft (6 m), span of 65 ft (20 m), and width of 40 ft (12 m) can be provided. The dead load and live load can be derived from the dimensions given above. For more convenience when only one bent is involved, a dead load of 800 kip (360 ton) and a live load of 200 kip (90 ton) can be provided. The sum of dead load and live load determines the axial load of the column and the dead load alone determines the lateral loads.

Scale

A dimensionless analysis is used to find the proper scaling of each parameter (Moncarz, 1981; Bertero, 1984). In the quasi-static bridge column tests, all time-dependent parameters that relate to velocity and acceleration are ignored. The axial load and lateral load from the superstructure are reduced to an external force applied vertically and horizontally to the top of the column. The material properties, such as elastic modulus, yielding stress, and specific weight,

are kept to the same as the prototype (scale factor=1). The parameter that needs to be changed as will is the geometrical dimensions. The resultant scaling factors for quasi-static tests are listed in the 1st column of Table I.

Time and time-dependent variables need to be considered in the scaling for fast tests such as shake table tests. Because of the involvement of the gravitational acceleration (cannot be changed in large structural tests), the scaling is diverted into two courses:

(1) Gravity is insignificant:
The vertical load is either unimportant to the test or is applied externally. The self weight of the entire specimen is negligible to the purpose of the test. Supplementary vertical load (if necessary) is applied through force actuators. The input and response acceleration is allowed to be scaled without changing specific weight. The proper scaling is shown in the 2nd column of Table I.

(2) Gravity is essential:
If the gravity force from the self weight is one of the important factor in the test, the horizontal acceleration needs to be kept the same scale as the gravitational acceleration (unity) because the vertical (gravity) force and horizontal (inertia) force come from the same mass. Due to the difficulty of changing specific weight in specified proportion, the scaling of specific weight is substitute by auxiliary masses. The auxiliary mass needs to be attached to the heaviest places, which is usually the superstructures, without introducing additional stiffness. The proper scaling and auxiliary mass are listed in the 3rd column of Table I.

It has been noticed that the construction materials have different mechanical properties at different size. The mechanical properties such as elastic modulus and yielding or ultimate stress are not only difficult to change by any specific scale but also difficult to maintain constant when size is changed. There are multiple reasons that make the mechanical properties size-dependent, such as different manufacturing process and failure mechanism. Special care should be taken to ensure this does not alter the test result unexpectedly.

TABLE I SCALING FACTORS FOR DIFFERENT TESTS

Variable	Slow test	Dynamic test	
		Gravity insignificant	Gravity essential
Geometric size ℓ	S_L	S_L	S_L
Time t	N/A	S_L	$S_L^{0.5}$
Stress σ	1	1	1
Strain ε	1	1	1
Elastic modulus E	1	1	1
Yielding stress σ_y	1	1	1
Density ρ	N/A	1	1
Force P	S_L^2	S_L^2	S_L^2
Bending moment M	S_L^3	S_L^3	S_L^3
Rotation angle (Δ/L) θ	1	1	1
Curvature ϕ	S_L^{-1}	S_L^{-1}	S_L^{-1}
Displacement U	S_L	S_L	S_L
Acceleration	N/A	S_L^{-1}	1
Auxiliary mass	N/A	0	S_L^2-S_L^3
External damping	N/A	S_L^2	$S_L^{1.5}$
External stiffness	S_L	S_L	S_L

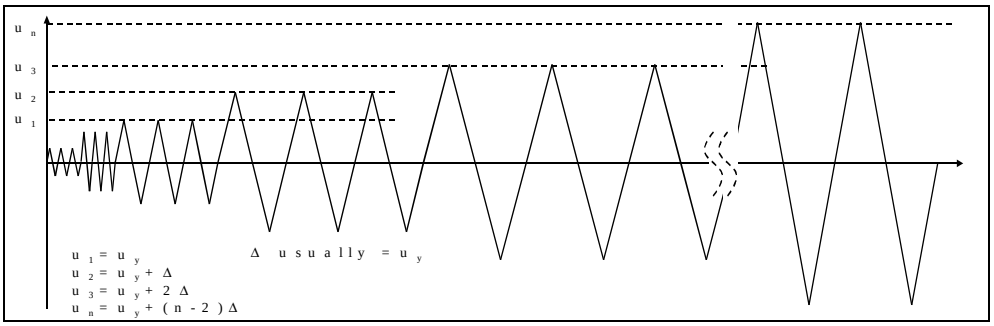

Figure 1 The progressive cyclic load history

Load histories

The cyclic loading procedure is usually considered to be a good simulation tool for earthquakes when more realistic options, i.e. true dynamic tests, are not feasible. Since it is an approximation of earthquake load, there can be numerous approaches. Most tests done to bridge columns have adopted a progressive pattern cyclic loading procedure (Figure 1). This procedure involves some pilot cycles in the elastic range that provides more accurate estimation for yielding displacement, followed by plastic cycles that contain 2-3 cycles at each deformation level and increase in multiples of yielding displacement. It is believed that two or three cycles for each displacement level is a balance between demonstration of strength degradation and avoidance of undesired early fatigue fracture (Lowes and Moehle, 1995). This procedure was evolved from the standard steel element cyclic procedures (ECCS, 1986; Stone and Cheok, 1989; ATC-24, 1992). This procedure provides a general test condition for earthquake loads.

When specific earthquake record is to be tested on the specimen, a preliminary analysis is required to estimate structural response, and consequently the displacement history of the specimen (El-Bahy et al, 1999).

The shake table test is a real dynamic test. As being more realistic, it is important to be careful controlling the test environment. The loading records need to be properly filtered and scaled. Elastic tests should be conducted prior to full-scale nonlinear tests. Modal parameters are retrieved in the elastic tests in order to well categorize the model. One or more of the hammer test, harmonic input test, and random vibration test can be used for this purpose.

Pseudodynamic tests represent the balance of actuality and test facility limit. In the slow pseudodynamic tests, the inertia force and viscous damping force are calculated in a computer that controls the loading procedure. The design of the real part and imaginary part as well as the scaling follows the specimen construction part of this guidelines.

Measurements and data acquisition

The technologies used in measurement systems evolve quickly. New issues emerge while old issues are resolved. It is not easy to setup general guidelines for all tests. However, well-configured measurement and acquisition systems share some similar principles. It is important to layout the principles to be followed.

A few fundamental values, such as lateral load, lateral displacement, and curvature, should be required by the guidelines. Some physical detail that may affect the resultant accuracy should be specified. For example, the range of the curvature measurement (with respect to section size) needs to be sufficient to cover the plastic hinge zone and part of the elastic zone.

Any potential slippage surface needs to be monitored on both sides.

The data acquisition systems have all become digital nowadays. Analog filtering is crucial for such systems. For slow static tests, the system can stop at each designated load step and allow the measurements recorded. Analog filters can be conditionally absent if several readings are made and averaged to eliminate the fluctuation from high-pitch electronic or physical noise. For high-speed tests, the analog low-pass filtering range needs to cover the highest frequency of the interested vibration component. The sampling rate should be higher than twice of the filter cut-off frequency.

The study on data format, storage, and transmission is currently one of the major efforts from many experimental institutes lead by the National Science Foundation (NSF). The progress will be closely observed and integrated with this guidelines.

SUMMARY

Most bridge column tests are either for research purpose or for specific construction or retrofit project. The uniqueness of these tests makes it difficult to set up general guidelines for all. However, as a leading agency in the highway industry, the FHWA will persevere in the effort of laying out the national testing guidelines for bridges due to the anticipated tremendous benefits to the researchers and designers in this country. The first appearance of the product is expected to take place in a short time. This project will not be able to provide premium result without the contributions from bridge testing experts. All suggestions and discussions are highly appreciated.

REFERENCES

[1] Abo-Shadi, N.; Saiidi, M.; Sanders, D. July 2000. “Seismic Response of Reinforced Concrete Bridge Pier Walls in the Weak Direction,” Technical Report MCEER-00-0006.

[2] Applied Technology Council. 1992. “Guidelines for Cyclic Seismic Testing of Components of Steel Structures,” ATC-24, Applied Technology Council, Redwood City, CA.

[3] Bertero, V. V.; Aktan, A. E.; Charney, F. A.; Sause, R. 1984. “Earthquake Simulation Tests and Associated Studies of a 1/5th-scale Model of a 7-story R/C Frame-wall Test Structures,” Report No. UCB/EERC-84/05, University of California, Berkeley.

[4] Dimig, J.; Shield, C., French, C.; Bailey, F.; Clark, A. Sept. 1999. “Effective Force Testing: A Method of Seismic Simulation for Structural Testing,” *Journal of Structural Engineering*. ASCE, 125(9), pp 1028-1037.

[5] El-Bahy, A.; Kunnath, S.; Stone, W.; Taylor, A. September 1999. ”Cumulative Seismic Damage of Circular Bridge Columns: Variable Amplitude Tests,” *ACI Structural Journal*, 96(5), pp 711-719.

[6] European Convention for Constructional Steelwork, Technical Committee 1, Structural Safety and Loadings; Working Group 1.3, Seismic Design. 1986. “Recommended Testing Procedure for Assessing the Behavior of Structural Steel Elements under Cyclic Loads,” First Edition.

[7] Kausel, E. May 1998. “New Seismic Testing Method. I: Fundamental Concepts,” *Journal of Engineering Mechanics*, ASCE, 124(5), pp 565-570.

[8] Lampe, N.; Azizinamini, A. Nov. 2000. “Steel Bridge System, Simple for Dead Load and Continuous for Live Load,” Proc. Conference of High Performance Steel Bridge, Nov. 30~Dec. 1 2000, Baltimore, Maryland.

[9] Lowes, L., N.; Moehle, J., P. Sept. 1995. “Seismic Behavior and Retrofit of Older Reinforced Concrete Bridge T-Joints,” Report No. UCB/EERC-95/09, Earthquake Engineering Research Center.

[10] Moncarz, P. D. 1981. “Theory and Application of Experimental Model Analysis in Earthquake Engineering,” Dissertation, Stanford University.

[11] Stone, W.; Cheok, G. Jan. 1989. “Inelastic Behavior of Full-Scale Bridge Columns Subjected to Cyclic Loading,” NIST Building Science Series 166.

Implementation of Seismic Isolators and Supplemental Dampers in Cable-Stayed Bridges

Michael J. Wesolowsky[1] and John C. Wilson[2]

ABSTRACT

For near-field earthquakes, significant spectral accelerations can occur in the period range from 0.5 to 1.5 seconds and longer, the same range in which many cable-stayed bridges have significant mass participation. This combination of factors can result in large tower accelerations and base shear responses. One approach to deal with this potential vulnerability is to consider the use of seismic isolators and supplemental dampers. In this study, seismic isolators were modeled for three cable-stayed bridges and the bridges were subjected to time history analyses using near-field earthquake ground motion records. The isolators were found to be successful in reducing tower accelerations, while causing larger displacements at the top of the towers. The deck displacements were successfully approximated using the design approach proposed by Naeim and Kelly. With the isolators, it was possible to achieve reductions in base shears by more than 85% in the longitudinal direction, and 25% in the transverse direction. To control seismic displacements, supplemental dampers were added which effectively reduced the tower and deck displacements to levels that approached, or were less than, their pre-isolated counterparts. These mechanisms of passive structural control demonstrated that the goal of reducing tower accelerations and base shears can be successfully accomplished by the use of seismic isolators, and that the resulting increase in tower and deck displacements due to isolation can be effectively controlled with the use of supplemental dampers.

[1] Michael J. Wesolowsky, Graduate Student, Department of Civil Engineering, McMaster University, 1280 Main St W., Hamilton, Ontario, Canada L8S 4L7; tel: 905-525-9140 ext 22552; wesolomj@mcmaster.ca

[2] John C. Wilson, Associate Professor, Department of Civil Engineering, McMaster University, 1280 Main St W., Hamilton, Ontario, Canada L8S 4L7; tel: 905-525-9140 ext 24299; jcwilson@mcmaster.ca

INTRODUCTION

Many cable-stayed bridges have long periods due to the flexibility of their cables. Since most earthquakes produce their largest spectral accelerations at lower periods (<0.5 seconds), cable-stayed bridges are able to naturally escape heavy damage due to their dynamic characteristics. However, near-field events have a tendency to produce higher accelerations at longer periods. These high accelerations can cause the bridges to experience greater seismic response. It is due to this susceptibility of cable-stayed bridges to large amplitude long-period earthquake ground motions that has led to the investigation of seismically isolating these bridges.

A modified Naeim and Kelly method [1] was used for design of the bilinear isolators in this study. Three cable-stayed bridge models were used to examine the effectiveness of these design approaches. Three isolation design cases were chosen for each bridge, which provided a range of isolated behaviour to compare across all bridges. SAP2000 was used to perform ten time-history analyses on each of the nine isolated bridge models.

Isolators can produce the negative side-effect of large deck displacements, some that are over three times higher than their non-isolated counterparts. Kasalanati and Constantinou [2] have suggested that large deck displacements incurred as a result of isolation can be controlled through the use of supplemental dampers. A supplemental damper design method was thus used which is based on the work of Clough and Penzien [3] and Priestley et al. [4]. Three damping cases were chosen for each of the nine isolation cases, which provided a range of damped behaviour to compare across all bridges. Ten time-history analyses were performed on each of the twenty-seven isolated and supplementally damped bridge models. The isolators and dampers were modeled using NLLink elements.

METHODOLOGY

The basic premise of the Naeim and Kelly isolator design method [1] is to specify a displacement (based on design code requirements and an estimated design period), then determine the required post-elastic stiffness. From this the energy dissipated per hysteretic cycle is calculated, and an iterative procedure is used to establish the required bilinear behaviour to produce the necessary energy dissipation. The basic method was modified in this study to provide for specification of a design displacement and maximum allowable force transmitted through the isolator. From these values it is possible to compute the effective stiffness of the isolator, and thus the effective period of the system (previously assumed in the basic Naeim and Kelly method). With the effective period and design displacement of the system it is possible to use any displacement design spectra to calculate the required damping of the system (also previously assumed in the basic Naeim and Kelly method). From this point, the basic Naeim and Kelly method was used to calculate the energy dissipated, and thus the hysteretic parameters of the system.

Three models, representative of various designs of cable-stayed bridges, were used in this study. The first model was of the Quincy Bayview Bridge (Quincy, Illinois), which has a main span of 247 metres, and two 134 metre side spans. The towers are H-shaped, supporting a total of 56 cables, arranged in a double fan configuration. The second model was of the Suigo Bridge (Chiba Prefecture, Japan), a relatively short two-span bridge (179 and 111 metres) supported by a monoleg tower and six cables arranged in a harp pattern. The third model (named A-1100) had A-frame towers, and was designed originally by Nazmy and Abdel-Ghaffar [5]. The main span of the bridge is 335 metres (1100 feet), with two side-spans of 146 metres. There are a total of 48 cables arranged in a fan pattern. The non-isolated periods with the greatest mass participation (longitudinal direction) were: 2.01 seconds (Quincy), 0.674 seconds (Suigo), and 1.83 seconds (A-1100).

SAP2000 was used for modeling and analysis of the bridges, and the isolators were modeled using the NLLink Plastic1 element (based on behaviour proposed by Wen [6]). These elements allow each of the six internal deformations to posses independent uniaxial-plasticity properties. Preliminary studies were done to determine effective locations for the isolators [7]. It was concluded that the optimal

isolator location in the model was at the anchor pier/deck connections. Rubber bearings having the same post-yield stiffness as the isolators were inserted at the tower pier/deck connections.

Five three-component earthquake ground motions were used to study the response of the isolated bridges. Data on these records are shown in Table I. For this study, the records were scaled to give peak horizontal ground velocities of 0.25 metres/second (representative of design level ground motions on the west coast of Canada). The pga and pgv values associated with this scaling are also shown in Table I. For this scaling, the maximum pga was 0.20*g*, from the JMANS record. Velocity scaling was used here because it is a better indicator of the frequency content and damage potential of an earthquake, especially for intermediate and long period structures [8]. Each three-component set of ground motions was applied twice to each bridge, by rotating the horizontal components 90^o for the second application. This created ten events per bridge.

Table I Earthquake Ground Motions

Record	Original				Scaled				M_w	Distance to Fault (km)
	PGA (g)		PGV (m/s)		PGA (g)		PGV (m/s)			
	NS	EW	NS	EW	NS	EW	NS	EW		
1995 Kobe, JMA	0.85	0.63	1.05	0.76	0.20	0.15	0.25	0.18	6.9	3.4
1995 Kobe, Takatori	0.42	0.79	0.64	1.76	0.06	0.11	0.09	0.25	6.9	4.3
1994 Northridge, Rinaldi	0.43	0.85	0.79	1.77	0.07	0.12	0.11	0.25	6.7	7.5
1989 Loma Prieta, LGPC	0.57	0.62	1.02	0.52	0.14	0.15	0.25	0.13	6.9	3.5
1979 Tabas Iran, Tabas	0.92	0.88	1.25	1.00	0.19	0.18	0.25	0.20	7.4	1.2

Three sets of target displacements and target forces design values were examined for each bridge. These values were selected to produce three effective periods that lengthened the dominant period of each of the bridges. In this context, the term 'dominant period' refers to the period of the mode having the largest mass participation. The isolator design criteria adopted for the bridges were aimed at reducing the average maximum non-isolated longitudinal base shear (as determined from time-history analyses using the ten sets of earthquake inputs) by factors of 4, 6 and 8. These values were selected to represent a range of moderate to large reductions in base shear, and are referred to as Cases 1, 2, and 3, respectively. The longitudinal direction was chosen as it had the largest non-isolated shears, and by using non-linear elements that had identical bi-axial properties, the transverse direction was also isolated. These reduced base shear values are used as target force values for the isolator for each of the three cases. The corresponding isolator target displacements for the three cases were specified as the average maximum non-isolated longitudinal displacement of the superstructure (as measured at the end of the deck) multiplied by factors of 2, 3 and 4.

The design procedure for supplemental dampers is described in [7]. Three supplemental damping ratios were used for each case for each bridge (9 total cases per bridge): 5%, 10% and 20%. These cases are referred to as Case Xa, Xb and Xc, where X is Case 1, 2 or 3, as described earlier. The supplemental dampers were placed at the anchor pier/deck connection in the longitudinal direction only. This configuration reduces longitudinal tower base shear and transverse mid-span deflections [7].

RESULTS

Due to space limitations, a complete description of the results of isolating and damping the three cable-stayed bridges cannot be presented. To summarize the effects of isolation and damping, isolated tower accelerations, damped tower displacements, and isolated base shears are presented.

Figure 1a shows a comparison of the normalized mean maximum accelerations of the top of the tower for all three bridges. Generally, the longitudinal average accelerations are reduced as the isolated period is lengthened (~40% reduction for Quincy, ~60% for Suigo, and ~20% for A-1100 from non-isolation to Case 3).

In the transverse direction the accelerations are decreased (~10% to ~65% from non-isolation to Case 3). For Quincy and A-1100, lengthening the period of isolation (Case 1 to Case 3) resulted in a slightly higher acceleration (up to 5%), but this was not the case for Suigo. This is due to Suigo having over 90% of the participating mass in the transverse direction in the dominant isolated period (as compared to 40% and 55% for Quincy and A-1100, respectively). This allows the bridge to respond almost exclusively at a period that is outside of the higher spectral amplitude 0.5 to 1.5 second period range, thus isolating the bridge from most of the effects of the earthquake ground motions. This effect can be seen in most computed responses of Suigo.

Figure 1b shows the effects of damping on the tower displacements for all three bridges. One advantageous result of damping is that the displacements have been reduced to values lower than their pre-isolation counterparts for all three bridges (as much as 50% of pre-isolation displacements for Suigo). This is beneficial, as the relative displacements along the height of the tower have also been reduced, providing lower stress in the tower, and ultimately, lower base shear. It can also be seen that as the isolated period increases (Case 1 to Case 3), the reduction in tower displacement increases (~50% for

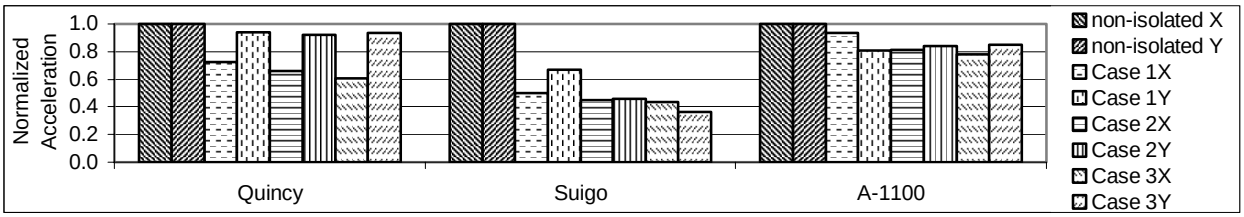

(a)

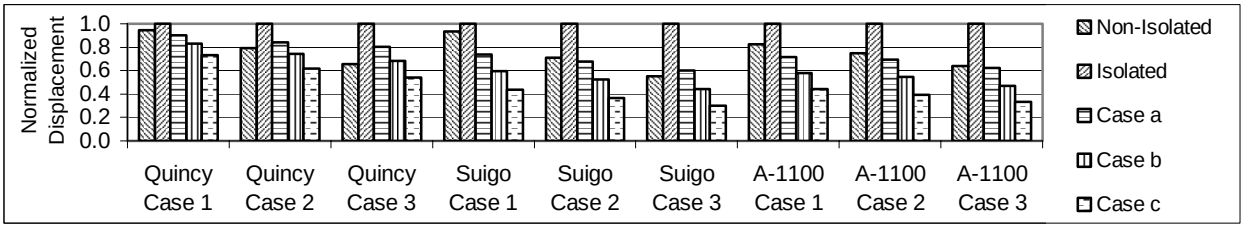

(b)

Figure 1. (a) - Effects of isolation on the normalized mean maximum tower accelerations for longitudinal (X) and transverse (Y) directions, (b) - Effects of supplemental damping on the normalized mean maximum longitudinal tower displacements.

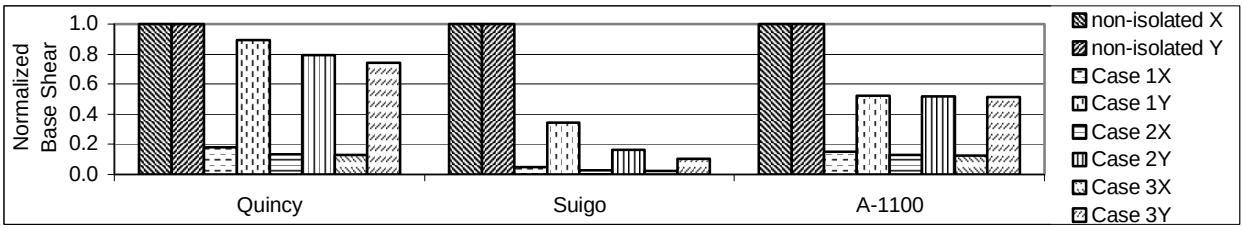

Figure 2. Effects of isolation on the normalized mean maximum base shears for longitudinal (X) and transverse (Y)

Quincy, ~70% for Suigo, and ~70% for A-1100 from basic isolation to Case Xc). This shows that isolating and damping the structure well outside of the critical period range not only reduces the base shears, but also reduces the tower displacements to levels below their non-isolated counterparts.

Figure 2 shows a comparison of normalized mean maximum tower base shears. It is clear that shears are being drastically reduced, some to less than 5% of their non-isolated counterparts. A point of note is that the percentage of total base shear being transmitted through the tower pier/deck connection has decreased with the introduction of isolation. For example, Quincy's non-isolated case has 96% of the

longitudinal base shear passing through this connection, while Case 3 has only 38%. This would mean that an increasing percentage of the lateral forces are being transferred through the cables and the tower portion of the tower pier.

CONCLUSIONS

A modified version of the Naeim and Kelly isolator design method was used to design lead-rubber type isolators for three cable-stayed bridges. Three cases were implemented into each bridge in order to present a wide range of isolated responses. Three damper cases were implemented into each isolation scheme in order to create nine total cases for each bridge. The following conclusions were drawn from all recorded responses (see [7] for a full analysis):

- Tower accelerations were decreased for all bridges by as much as 55% in the longitudinal direction and 65% in the transverse direction. Tower displacements were increased in the longitudinal direction, but decreased in the transverse direction.
- Deck displacements were increased. The isolators located at the anchor piers provided displacements that were within $\pm$45% of their target values, as predicted using the modified Naeim and Kelly method. Isolator forces were within +20 to -40% of their target values, using the same method. It can be concluded that the modified Naeim and Kelly method provided isolator designs that produced good approximations of the pre-set target values.
- Tower base shears in both directions were also reduced (more than 85% longitudinally and 25% transversely) as much of the shear was redirected to the abutment isolators. Further, the percentage of total base shear (due to the inertia of the deck) being transmitted through the tower pier/deck connection decreased with the introduction of isolation.
- Tower accelerations and displacements were decreased due to supplemental damping. This is consistent with the findings of Kelly [9] and Jangid and Kelly [10].
- Deck displacements were reduced by supplemental dampers to levels that were lower than was recorded for the pre-isolation cases. This indicated that not only base shears could be reduced though isolation, but the negative effect of displacement increases could also be effectively controlled through supplemental damping. Increased damping did not significantly reduce base shears (reductions generally less than 20%, except for Suigo which showed larger decreases (up to 70%)).

ACKNOWLEDGMENTS

The support of the Natural Science and Engineering Research Council (NSERC) of Canada is gratefully acknowledged.

REFERENCES

[1] Naeim, F., and J. M. Kelly. 1999. *Design of Seismic Isolated Structures – From Theory to Practice*. New York: John Wiley & Sons, Inc.

[2] Kasalanati, A., and M. C. Constantinou. 1999. *Experimental Study of Bridge Elastomeric and Other Energy Dissipation Systems with Emphasis on Uplift Prevention and High Velocity Near-Source Seismic Excitation*. Multidisciplinary Center for Earthquake Engineering Research (MCEER-99-0004), State University of New York at Buffalo.

[3] Clough, R. W., and J. Penzien. 1975. *Dynamics of Structures*. New York: McGraw Hill.

[4] Priestley, M. J. N., F. Seible, and G. M. Calvi. 1996. *Seismic Design and Retrofit of Bridges*. New York: John Wiley & Sons, Inc.

[5] Nazmy, A. S., and A. M. Abdel-Ghaffar. 1987. *Seismic Response Analysis of Cable-Stayed Bridges Subjected to Uniform and Multiple-Support Excitation.* Princeton University, Department of Civil Engineering.
[6] Wen, Yi-Kwei. 1976. "Method for Random Vibration of Hysteretic Systems," *Journal of the Engineering Mechanics Division*, 102(EM2):249-263.
[7] Wesolowsky, M. J. 2001. *Design and Application of Seismic Isolators and Supplemental Dampers for Cable-Stayed Bridges*. McMaster University. M.A.Sc. Thesis. Department of Civil Engineering, Hamilton, Ontario, Canada.
[8] Naeim, F. 1993. "Selection of Earthquake Records for Seismic Design of Tall Buildings," *The Structural Design of Tall Buildings*, 2(4):255-293.
[9] Kelly, James M. 1999. "The Role of Damping In Seismic Isolation," *Earthquake Engineering and Structural Dynamics*, 28(1):3-20.
[10] Jangid, R. S., and J. M. Kelly. 2001. "Base Isolation for Near-Fault Motions". *Earthquake Engineering and Structural Dynamics*, 30(5):691-707.

Seismic Isolation of Bridges Subject to Strong Earthquake Ground Motions

Victor A. Zayas, Stanley S. Low, and Anoop S. Mokha

ABSTRACT

As a consequence of the strong ground motions recorded during the Kobe, Northridge and Düzce (Turkey) Earthquakes, stronger design earthquakes are now controlling the seismic design of important structures. These stronger earthquakes include the effects of near-field pulses, fault-normal motions, and near-field deep soil site motions. It is costly to design structures to withstand these strong earthquake motions using a conventional strength approach. For non-isolated structures, structural frame drift and force demands can exceed 10 to 20 times the structure's elastic capacity, risking major structural damage. For isolated structures, the seismic isolation bearings need to have displacement capacities and isolator periods that exceed those of the rubber type isolation bearings used over the past 15 years.

The application of Friction Pendulum seismic isolation to three important bridge structures subject to strong earthquake motions is presented. The Benicia-Martinez Bridge is one of three critical lifeline bridges in the San Francisco Bay Area and the seismic design performance criteria was that it should remain functional after a major earthquake. The design earthquake included very strong near-fault ground motions, with near-fault fling and deep soil site effects resulting in ground motion spectral accelerations over 7g.

The I-40 Mississippi River Bridge in Memphis, Tennessee, is a vital defense and commerce transportation link in the Memphis area. It is situated at the southeastern edge of the New Madrid Seismic Zone. The seismic performance goal for the seismic retrofit was that the bridge should remain "operational/serviceable" after a maximum probable "Contingency Level Earthquake" (2500 year return period).

A viaduct section of the Trans-European Motorway that traverses the active Anatolian fault in northern Turkey was severely damaged in the 1999 Düzce Earthquake. A seismic assessment of the damaged viaduct was carried out and it was concluded that the viaduct could be economically repaired and retrofitted using seismic isolation. The extreme environmental conditions, coupled with the demanding performance requirements for the isolation system, which included accommodating permanent ground displacement at the fault crossing, dictated selection of Friction Pendulum bearings.

Victor Zayas, President; Stanley Low, Structural Engineer; and Anoop S. Mokha, Vice President; Earthquake Protection Systems, Inc., 2801 Giant Highway, Richmond, CA 94806

SEISMIC RETROFIT OF THE BENICIA-MARTINEZ BRIDGE

The Benicia-Martinez Bridge is a high-level, deck-type, welded truss bridge with welded girder approach spans (Fig. 1). It carries 6 lanes of traffic averaging 100,000 vehicles a day, and is essential to post-earthquake emergency response operations for the San Francisco Bay region.

The seismic retrofit was designed by Imbsen & Associates, Sacramento, for a Maximum Credible Earthquake on the Green Valley Fault [1]. The spectral accelerations of 7 and 8 g's, are more than 30 times typical seismic lateral design forces (Fig. 2). Project design criteria were developed requiring an essentially elastic response for all components, excluding foundation sub-elements for which a limited inelastic response was accepted.

The strong site-specific spectra, coupled with the tall piers and the desire to minimize the shear transfer through the bearing, necessitated the need for a long period isolation system capable of accommodating large displacements. Friction Pendulum bearings can provide both a long isolation period, and can accommodate large displacements without compromising bearing stability. Also, with the concave plate of the bearing facing up, no P-delta moments are transferred to the truss structure, eliminating the need for strengthening of the truss members. This results in significant construction cost savings.

The 22 Friction Pendulum bearings were installed at the tops of the concrete piers, directly under the roadway trusses, 2 bearings per pier. The Friction Pendulum bearings for this large toll bridge have a dynamic period of 5 seconds and a dynamic friction of 6%. The largest bearing has a displacement capacity of 53 inches, a 5 million pound design vertical load capacity, measures 13 feet in diameter, and weighs 40,000 pounds (Fig. 3). They are the largest seismic isolation bearings ever manufactured.

The large Friction Pendulum bearings for the Benicia-Martinez Bridge were the first devices tested at the Seismic Response Modification Devices (SRMD) Testing Facility at University of California, San Diego. This test facility can support 12,000 kips of vertical load and can generate peak velocities in the longitudinal and transverse directions of about 70 in/sec and 30 in/sec, respectively. The observed behavior of these large bearings is similar to other, smaller Friction Pendulum bearings that have been tested previously for many projects (Fig.4). The testing program for the Benicia-Martinez bearings was the most comprehensive and rigorous ever developed for testing seismic isolation bearings of any kind in the world.

SEISMIC RETROFIT OF THE I-40 BRIDGE OVER THE MISSISSIPPI RIVER

The I-40 Bridge is comprised of 164 spans, 160 piers, and 10 abutments. The main channel consists of five steel box girder spans, while the east approach and connecting ramps are entirely welded steel plate girder spans (Fig. 5). The bridge is a vital defense and commerce transportation link and is situated at the southeastern edge of the New Madrid Seismic Zone, one of the most active zones in the Central United States. Site conditions are characterized by deep soil deposits of up to 2500 feet. The ground acceleration for a 500-year return period (Design Level Earthquake) is 0.2g, and for a 2500 year return period (Contingency Level Earthquake) is 0.4g. The seismic performance goals dictated that the bridge must remain "operational/serviceable" following the maximum probable "Contingency Level earthquake".

A conventional retrofit strategy of increasing the capacities of the connections and piers was found to be very expensive [2]. A seismic isolation retrofit strategy was found to be

attractive because it reduced construction costs by about 40%, compared to the conventional retrofit strategy. The existing, seismically-deficient bearings were replaced by Friction Pendulum bearings. Foundation retrofit work was also minimized due to reduction of seismic forces through the bearings. The 18 Friction Pendulum bearings were installed at the tops of the concrete piers, directly under the tied arch trusses (Fig. 6). The Friction Pendulum bearings have dynamic periods of 4 or 5 seconds and a dynamic friction of 6%. The bearings have a displacement capacity of about $\pm$24 inches, and a vertical load carrying capacity of about 20 million pounds. These are the largest load-carrying bearings ever manufactured.

SEISMIC RETROFIT OF THE BOLU VIADUCT, TURKEY

The epicenter of the magnitude 7.2 Düzce Earthquake that struck Turkey on 12 November, 1999, was located very close to the 2.3 km long Trans-European Motorway (TEM) viaduct structure that was under construction in the mountainous region near Bolu, about 300km east of Istanbul. The Bolu Viaduct (Fig. 7) consists of a series of 10 span modules of a 40 m spaced precast girder/concrete slab deck system supported on about 50 m tall concrete piers. The precast/concrete deck slab system was supported on Italian-manufactured Energy Dissipation Units (EDU) and isolation bearings located on top of concrete piers. The viaduct structure suffered extensive damage during the 1999 Düzce Earthquake as a consequence of ground shaking of intensity larger than the design level and because of close proximity to the epicenter (Fig. 9). The EDU isolation system did not have a restoring force or restoring stiffness, and therefore did not satisfy the AASHTO requirement that isolation systems have a restoring force. Since the isolation system had no restoring force, the deck structure was left with a permanent offset displacement after the earthquake of about 1100 mm longitudinally and 500 mm transversely (Fig. 8). Although the EDU's were severely damaged, the deck structure and foundation suffered only minor damage.

The repair/retrofit design includes jacking the deck modules to their original position, and installation of Friction Pendulum seismic isolation bearings [3]. The return period of the (re)design earthquake was set at 2000 years corresponding to a PGA of 0.81g and included future fault rupture displacements. A prototype Friction Pendulum bearing for this project, with a displacement capacity of +/-700mm, was subjected to high-velocity testing at the SRMD facility using earthquake records that were developed to simulate the recorded Düzce Earthquake. Installation of the first bearings at the site is scheduled to begin in 2002.

REFERENCES

[1] Imbsen & Associates, Inc., "Benicia-Martinez Bridge Seismic Retrofit", Final Retrofit Strategy Report to Caltrans, 1995.

[2] Imbsen, R.A., Pecchia, D.D., Davis, G.V. & Chang, G.S., "The I-40 Mississippi River Bridge Seismic Retrofit", Structures Congress, April 18-21, 1999, New Orleans, Louisiana.

[3] Calvi, G.M., Priestly, M.J.N., and G. Germani, "Bearing and Isolation Systems for a Long Viaduct Crossing an Active Fault", 7th International Seminar on Seismic Isolation, Passive Energy Dissipation and Active Control of Vibrations of Structures, Assisi, Italy, October 2-5, 2001.

Fig. 1 Benicia-Martinez Bridge

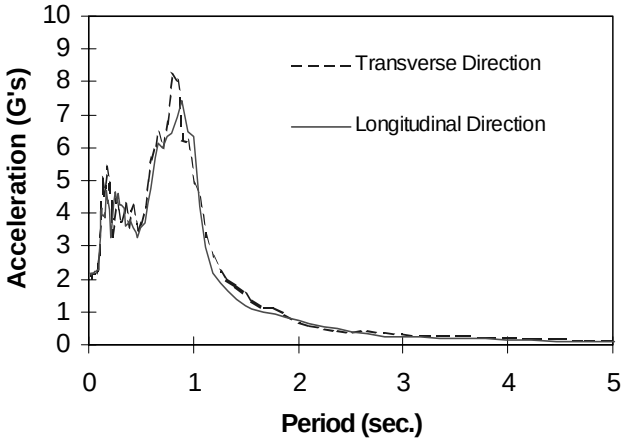

Fig. 2 Ground Motion Spectra at Pier 6

Fig. 3 Concave Plate of B-M Bearing

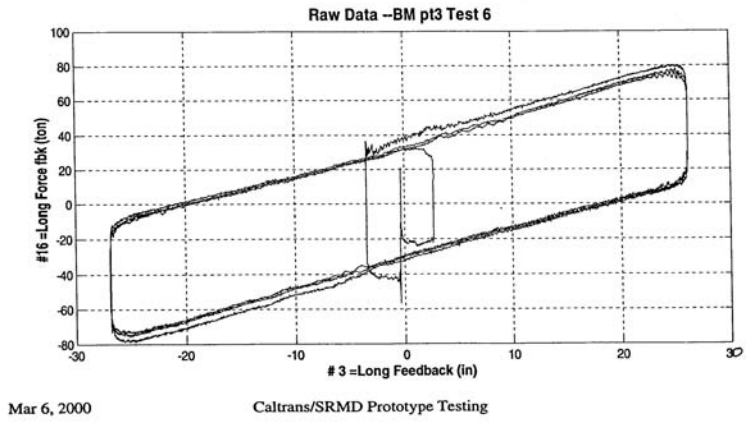

Fig. 4 Hysteretic Loop for B-M Type III bearing at 4 inches/sec (Vertical load = 473 tons)

Fig.5 I-40 Bridge over the Mississippi

Fig. 6 I-40 Bridge Bearing Installation

Fig. 7 Bolu Viaduct, Turkey

Fig. 8 Offset of Viaduct after Earthquake

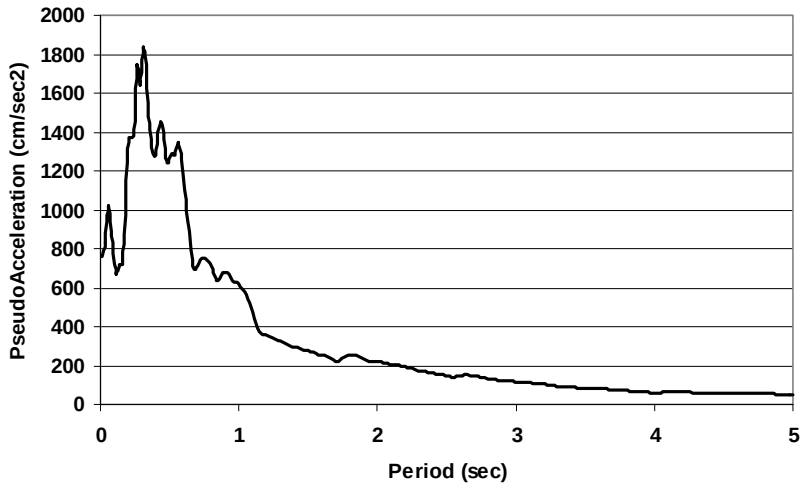

Fig. 9 Düzce Earthquake Spectrum at Bolu Station (longitudinal direction)

Behavior of Ductile Steel Retrofitted Deck-Truss Bridges

Majid Sarraf, Ph.D., and Michel Bruneau, Ph.D., P.Eng.

ABSTRACT

Seismic evaluations of many existing deck truss bridges in recent years have revealed that in the event of a major earthquake, both substructure and superstructure would suffer damage. They are typically supported on non-ductile substructures, and the superstructure lateral-load resisting system consisting of non-ductile bracing members and connections.

The proposed seismic retrofit strategy includes replacing the existing non-ductile end and lower-end panel members with ductile steel frames, which can perform as ductile fuses. These fuses limit seismically induced forces exceeding capacities of both substructure and superstructure members, therefore allowing damage and energy dissipations to take place in a well predictable and ductile manner and only at the ductile retrofit panels. A performance-based seismic design procedure was developed and used to design retrofits for a 270-ft long prototype steel deck-truss bridge. The design procedure allows a special design of eccentrically braced frames, vertical shear-link and TADAS systems used as main ductile elements of the steel retrofit panels. The results of nonlinear time-history analyses of the as-built and retrofitted bridge indicated that the retrofitted bridge suffered no damage and the earthquake energy dissipated only through ductile retrofit devices.

Series of pseudodynamic tests were performed on a 27-ft long,1/10 scale, complete 3-dimensional model of the prototype steel deck-truss bridge fabricated at the University of Ottawa, to evaluate performance of both as-built and retrofitted conditions of the bridge model. A unique testing procedure was devised and the pertaining test set-up was designed and fabricated to simultaneously apply gravity and non-uniform lateral seismic forces. Test data confirmed the vulnerability of the bridge in the end and top lateral bracings, as well as in the intermediate cross frames.

Two retrofits consisting of eccentrically braced frame and vertical shear link system were designed and implemented. Pseudo-dynamic testing of the retrofitted bridge proved the enhanced seismic performance and effectiveness of the proposed steel ductile retrofits. As the shape of hysteretic curves and test observations indicated, the steel shear-links of the retrofitted panels had a robust and ductile behavior. This paper explains the ductile steel retrofitting strategy for deck truss bridges. It presents a summary of test observations and data on seismic performance of a model deck-truss bridge in as-built and retrofitted conditions, as well as performance of ductile shear links used as main energy dissipating device in a deck-truss bridge.

Majid Sarraf, Senior Bridge Engineer, Imbsen and Associates Inc., 9912 Business Park Drive, Suite 130, Sacramento, CA 95827

Michel Bruneau, Ph.D., P.Eng., Deputy Director of Multi-Disciplinary Center for Earthquake Engineering Research 105 Red Jacket Quadrangle, SUNY at Buffalo, New York 14261-0025

INTRODUCTION

Seismic evaluations conducted on existing deck truss bridges in the recent years have revealed that these bridges could suffer damage in the event of major earthquakes ([1], [2], [3], [4] and [5]). In these structures the deck is on truss girders supported on abutments or piers. Lateral inertia forces of the earthquake applied at the deck level is indirectly transferred to the bridge supports at the end of the lower chords, imposing forces on the entire superstructure members to carry these forces. Typically, existing lateral load resisting members and their connections are not ductile and, therefore could suffer damage in the event of a major earthquake. Particularly, lateral bracings and end and intermediate cross-frames, in older truss bridges which were typically designed for wind forces or stability during construction, cannot be expected to withstand the severe cyclic inelastic deformations expected to develop during large earthquakes.

In addition to vulnerability of superstructure, these bridges are often found to be supported on unreinforced masonry or concrete substructures, which have a very non-ductile deformation characteristic. Thus, the substructure of such a bridges would also be at high risk of damage during a major seismic event. Alternative seismic retrofits, which are commonly used, are: Strengthening many non-ductile bracing and their connections, as well as strengthening the substructure, or using seismic isolation bearings. These alternatives are viable but could be costly and difficult to implement.

DUCTILE RETROFIT STRATEGY

The proposed ductile retrofit requires conversion of each end cross-frame into a ductile panels having a specially designed yielding device (i.e. a structural fuse), and conversion of the last lower end panel near each support into a similar ductile panel. In addition, stiffening of the top lateral bracing system is also needed. This stiffening has two benefits: It reduces the forces imposed on the interior cross-frames resulted from differential lateral displacement between top and bottom lateral system; second, it increases the share of the total lateral load transferred through end and top lateral system. This can be easily achieved by providing composite action between the concrete deck and the top chord system and eliminating discontinuity in the deck system.

A detailed design procedure for such ductile retrofits are described in [6]. This retrofit design is based on two main criteria: strength and stiffness. The yield strength of the ductile panels are selected to be lower than the capacity of the substructure and other superstructure to protect these components. The stiffness criteria established is based on the ductility capacity and drift limits of the superstructure. On the other hand, a very flexible device would result in large lateral displacements of superstructure and possible damage in the adjacent non-ductile members and their joints, on the other hand a very stiff device could have a substantial local ductility demand exceeding their ductility. Using the above criteria and an optimization process the end bracing and

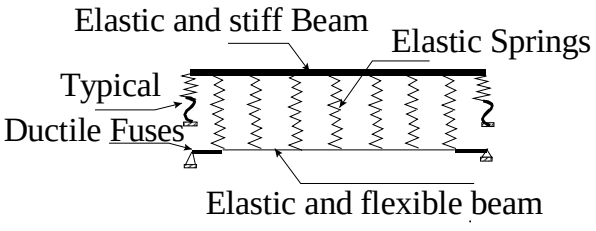

Figure 1(a). Beam analogy of ductile retrofit system

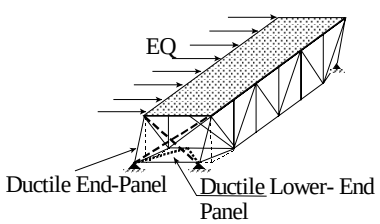

Figure 1(b). Steel ductile retrofit in a deck-truss bridge

ductile components of an eccentrically braced frame and vertical shear links were designed for a 270-ft span deck-truss bridge [7]. These ductile devices were also designed and detailed to be used as retrofits for the scale model of a deck-truss bridge.

Analytical models of the prototype truss bridge were generated using DRAIN-3DX program, in which nonlinear behavior of the ductile shear links were modeled. A series of nonlinear time-history analyses were performed for 6 different earthquakes scaled to 0.53 g (El-Centro 1940, Northridge 1994, San Fernando, 1971, at Pacoma Dam, Loma Prieta, 1989, Olympia 1949 and Taft 1952). The result of these analyses indicated that other than ductile components which yield and dissipate the induced seismic energy, no other superstructure members suffer damage. The force response of the substructure does not exceed its capacity limit, and the average global ductility for all 6 earthquakes does not exceed the global ductility capacity of ductile frames qualified for reduction factor of *R=10* in accordance with UBC. Also, the distortion angle of a shear link as required by AISC-LRFD does not exceed the 9% rotation limit.

TESTING DUCTILE RETROFITS

A 27-ft span steel deck-truss model was designed and constructed in the structures laboratory of the University of the Ottawa. It is 27-ft long, 4-ft wide and 4-ft high. Series of pseudo dynamic tests were conducted to observe the actual performance of the retrofits and confirm that other than ductile retrofit devices no damage occurs in other members of the superstructure. An innov ative loading technique was devised and used to convert a point load applied by one actuator to a distributed inertial force at the deck level. One hydraulic jack positioned vertically is used to apply the gravity loads. Figure 2 shows a general view of the completed bridge model as-retrofitted and the test set-up components.

A specially designed ductile retrofit panel including stiff bracing members and ductile links was used to replace the existing end and lower end panel conventional cross-bracing. Figure 5 shows the details of the vertical link retrofit for the end-panel. A 225-mm thick and 1100 mm wide reinforced concrete deck was cast in place. Shear studs were designed such that they could resist both forces in-plane shear force caused by both seismic loads as well as gravity loads. The end panel and lower end panel connections were high-strength bolts with minimum hole clearance which were designed to have a negligible slip. Therefore, the complete retrofit member assembly could be dismembered after testing the retrofits and the new ductile retrofit assembly would be replaced and tested. Figure 3 shows the end-panel retrofit using vertical shear link.

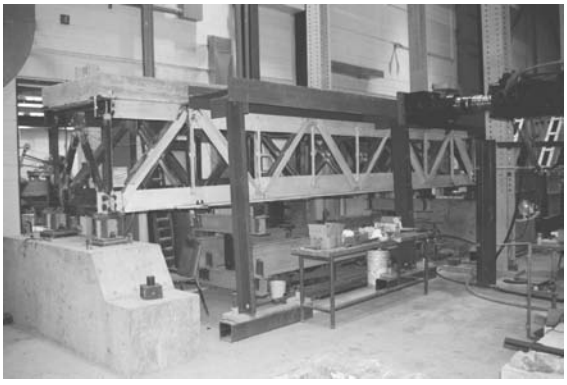

Figure 2. An overall view of the 27-ft bridge model

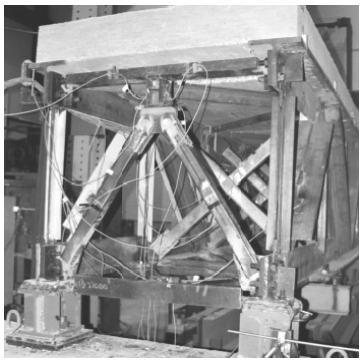

Figure 3. Steel ductile retrofit at the end panel

PERFORMANCE TESTS OF DUCTILE RETROFIT

Initial free vibration tests and cyclic loading tests were performed to determine stiffness and strength characteristic of retrofitted bridge. Subsequently, cyclic tests were performed which resulted in measured yield strength of 450 kN in the EBF retrofit, and 400 kN in VSL specimen. Yielding of both end and lower- end panel devices were detected. The measured yield strength of the retrofits were greater than predicted load of 300 kN due to a number of factors such as: actual yield strength of the steel material, resistance contribution of other components such as connections of the end panel and the last side diagonal members of the truss, as well as a small horizontal component of the applied vertical load. However, despite the additional strength in the devices, no sign of yielding or buckling of the other members of the truss was observed.

These cyclic tests were followed by pseudo-dynamic tests using El Centro earthquake ground motions scaled to peak ground acceleration of 0.5 g and 0.85 g. Overall response of the bridge was ductile with no damage observed in the cross-frames or lower lateral bracing members, considered the most vulnerable truss members. Similar ductile performance was observed for the same magnitude of El Centro Earthquake when the bridge was retrofitted with eccentrically braced frame. Figure 4 shows the force displacement curve obtained from pseudo dynamic test. The link beams exhibited strain ductilities as high as 12 and exhibited a robust hysteretic behavior (Figure 4).

Another important observation is the effect of continuity of the concrete deck and its contribution to the stiffness of top lateral bracing system. Discontinuity of the concrete deck in the as-built condition due to expansion joints does now allow the in-plane stiffness of the concrete deck to contribute to the stiffness of the top lateral system and more uniform distribution of the forces transferred to the intermediate cross bracing members. Casting composite concrete deck as part of retrofit measure also contributed to the stiffness of the top lateral bracing system. This was confirmed by the measurements of the lateral displacements along the deck and comparisons to the lateral displacements of the top chords during the as-built testing where no concrete deck was cast on the top chords. No shear failure of studs or cracking in the concrete was observed.

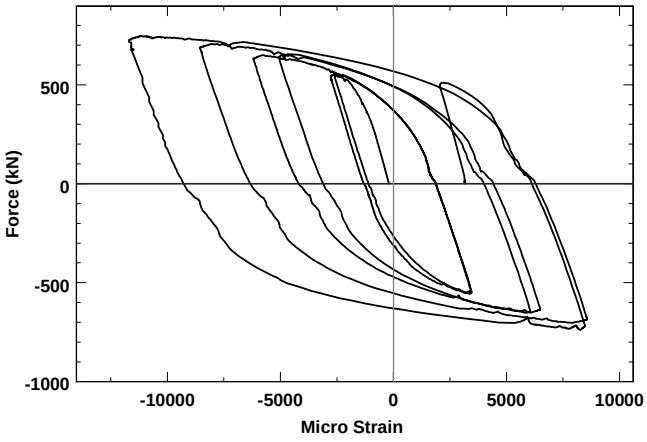

Figure 4. Hysteretic response of ductile steel retrofit link

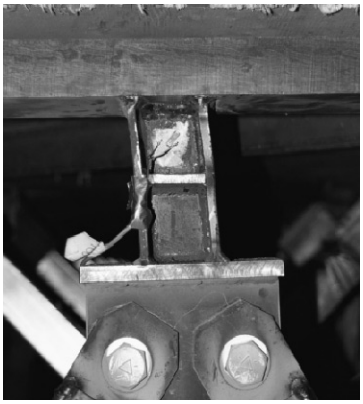

Figure 5. Inelastic deformation of vertical shear link

After successful completion of the pseudo-dynamic tests, a final cyclic test was performed for each retrofit to measure ultimate capacity of the ductile links. Both specimens exhibited substantial overstrength. Finally, the failure caused by the fracture of the welded connections to the yielding devices in the end panels, which were measured at 800 kN and 740 kN for EBF and VSL retrofitted bridge, respectively, sustaining a global displacement ductility of 3 and 2. Figure 5 shows the shear deformations of the link beam in EBF and VSL retrofits.

CONCLUSIONS

The results of pseudo-dynamic and cyclic tests performed on two different configurations of ductile energy dissipating devices (eccentrically braced frames, EBF and vertical shear link, VSL) used in a 27-ft long seismic retrofitted deck-truss bridge and for the El Centro earthquake scaled to 0.53 g, indicated that such devices can be designed and used as viable alternative seismic retrofit in deck-truss bridges.

The designed devices exhibited considerable cyclic ductility. By yielding and dissipating the induced seismic energy, these devices performed as structural fuses and protected other members of the superstructure. The devices exhibited substantial overstrength, however, which needs to be taken into account when determining the yield capacity of such protective systems to avoid overstressing other superstructural and substructural components.

ACKNOWLEDGEMENTS

The authors are grateful for the funding provided by Steel Education Foundation of Canadian Institute for Steel Construction (CISC) and the material donated by Canam Steel.

REFERENCES

[1] Imbsen, R., and Liu, W. 1993. " Seismic Evaluation of Benicia-Martinez Bridge", *Proceeding of the First U.S. Seminar, Seismic Evaluation and Retrofit of Steel Bridges*, University of California at Berkeley.

[2] Matson, D.D., and Buckland, P.G. 1995. " Experience with Seismic Retrofit of Major Bridges", *Proceedings of 1st National Seismic Conference on Bridges and Highways*. San Diego, California.

[3] The Astaneh-Asl, A., B. Bolt, K. McMullin, D. Modjtahedi, S. Cho and R. Donikian.1994. "Seismic Performance of Steel Bridges during the 1994 Northridge Earthquake," *Report number UCB/CE-Steel-94/01*, Department of Civil Engineering, University of California at Berkeley.

[4] Housner, G., Thiel, C. 1995 "The Continuing Challenge: Report on the Performance of State Bridges in the Northridge Earthquake", *Earthquake Spectra*, Vol. 11, No 4: 607-636.

[5] Bruneau, M., Wilson, J.W., Tremblay, R.1996. "Performance of Steel Bridges During the 1995 Hyogoken-Nanbu (Kobe, Japan) Earthquake", *Canadian Journal of Civil Engineering*, Vol.23, No.3, pp. 678-713

[7] Sarraf M. and Bruneau M. 1998a."Ductile Seismic Retrofit of Deck-Truss Bridges. I: Strategy and Modeling" *Journal of Structural Engineering*, ASCE, Vol. 124, No. 11, November 1998, pp. 1253-1262.

[8] Sarraf M. and Bruneau M. 1998b."Ductile Seismic Retrofit of Deck-Truss Bridges. II: Design Applications" *Journal of Structural Engineering*, ASCE, Vol. 124, No. 11, November 1998, pp. 1263-1271.

Appendix A

Conference Program

Third National Seismic Conference and Workshop on Bridges and Highways

Portland, Oregon
April 28 – May 1, 2002

Preliminary Program

MONDAY, April 29, 2002

SESSION 1 (8:00 a.m. - 9:45 a.m.)
Session Chair: Roland Nimis
Welcome and Opening Keynote Presentations

1. Gary Hamby, Director of Field Services West, FHWA
2. Frederick Wright, Executive Director, FHWA
3. Tom Lulay, Oregon DOT
4. Jim Roberts, Imbsen & Associates, Inc./Caltrans

BREAK (9:45 a.m. - 10:15 a.m.)

SESSION 2 (10:15 a.m. - 12:00 Noon)
Session Chair: Tom Post
Lessons Learned from Recent Earthquakes (Since 1998)

1. Lessons Learned from the 1999 Kocaeli, Turkey Earthquake
   Saad El-Azazy, California Department of Transportation; W. Phil Yen, Hamid Ghasemi, and James D. Cooper, FHWA; and Roy Imbsen, Imbsen & Associates, Inc.
2. Structural Movement and Damage to the Alaskan Way Viaduct Due to the Nisqually Earthquake
   George Comstock and Harvey Coffman, Washington State Department of Transportation
3. Performance of Roads and Bridges in the January 26, 2001 India Earthquake
   Bijan Khaleghi, Washington State Department of Transportation and Gary Norris, University of Nevada at Reno
4. Seismic Response of Highway Bridges Subject to Near-Fault Ground Motions
   Bulent Akbas and Jay Shen, Illinois Institute of Technology
5. Seismic Performance of Bridges in the Chi Chi Earthquake, Taiwan
   W. Philip Yen, FHWA; James Yeh, Taiwan Highway Bureau, and Liang-Hong Ho, National Expressway Engineering Bureau, Taiwan

LUNCH (12:00 Noon - 1:30 p.m.)

SESSION 3 (1:30 p.m. - 3:15 p.m. – Session Organizer: Phil Yen)
Session Chair: Michel Bruneau
Seismic Design Practices and Specifications

1. A Proposed Bridge Seismic Design Philosophy
   Brian Maroney, California Department of Transportation and Nancy McMullin Bobb, Federal Highway Administration
2. Seismic Retrofit of Bridges Using Shape Memory Alloy Restrainers
   Reginald DesRoches and Bassem Andrawes, Georgia Institute of Technology
3. Experimental Study on Seismic Behavior of Highway Bridge Foundation During Liquefaction Process
   Hiroshi Kobayashi and Keiichi Tamura, Public Works Research Institute, Japan; Naoki Sato, Eight Consultants, Inc., Japan; and Takuo Azuma, National Institute for Land and Infrastructure Management, Japan.
4. Development and Implementation of a New Seismic Design Bridge Criteria for South Carolina
   Roy Imbsen, Imbsen & Associates, Inc.; and Lucero Mesa, South Carolina Department of Transportation
5. Seismic Retrofit of the Aurora Avenue Bridge With Friction Pendulum Isolation Bearings
   Hongzhi Zhang, Washington State Department of Transportation

BREAK (3:15 p.m. - 3:45 p.m.)

SESSION 4 (3:45 p.m. - 5:30 p.m.)
Session Chair: Frieder Seible
Design of Major Bridges in High and Moderate Seismicity Areas

1. Seismic Design of the Ravanel Bridge, Charleston, South Carolina
   Michael J. Abrahams, Joseph Wang, Peter M. Wahl and John Bryson, Parsons Brinckerhoff Quade & Douglas, Inc.
2. Seismic Investigations for the Design of the New Mississippi River Bridge at St. Louis
   Thomas P. Murphy and John M. Kulicki, Modjeski & Masters, Inc.
3. Seismic Design of the Skyway Section of the New San Francisco-Oakland Bay Bridge
   Brian Maroney, Sajid Abbas, Madon Sah, Gerard Houlahan and Tim J. Ingham, T.Y. Lin International
4. Seismic Design Strategy of the New San Francisco-Oakland Bay Bridge Self-Anchored Suspension Span
   Marwan Nader, Jack Lopez-Jara and Claudia Mibelli, T.Y. Lin International
5. Seismic Design of the Metsovitokos Suspension Bridge, Pindos Mountains, Greece
   Mike Oldham, Zygmunt Lubkowski, Xiaonian Duan and Richard Sturt, Arup Advanced Technology Group, London, UK

POSTER SESSION (5:30 p.m. - 7:00 p.m.)
Session Coordinator: Myint Lwin
(Approximately 20 papers)

1. Cyclic Testing of Truss Pier Braced Latticed Members
   Michel Bruneau and Kangmin Lee, University at Buffalo; and John Mander, University of Canterbury, New Zealand
2. Caltrans/CSMIP Bridge Strong Motion Instrumentation Project
   Patrick Hipley, California Department of Transportation; Anthony Shakal and Moh Huang, California Strong Motion Instrumentation Program
3. Seismic Retrofitting Challenges Stimulate New Innovations for the Benicia-Martinez Bridge
   Roy A. Imbsen, Imbsen & Associates, Inc. and Moe Amini, Caltrans
4. West Anchorage Design of San Francisco-Oakland Bay Bridge Main Span for Seismic Loads
   John Sun, Rafael Manzanarez, Marwan Nader, T.Y. Lin International
5. Seismic Retrofit of the US 40/I-64 Double Deck Bridge
   Mark R. Capron, Jacobs Civil, Inc.
6. Bridge Abutment Model Sensitivity for Probabilistic Seismic Demand Evaluation
   Kevin Mackie and Bozidar Stojadinovic, University of California, Berkeley
7. Dynamic Response of Bridge Structures Supported on Extended Reinforced Concrete Pile Shafts
   Tara C. Hutchinson, University of California, Irvine; Christina J. Curras, University of Wisconsin-Platteville; Ross W. Boulanger, Y.H. Chai and I.M. Idriss, UC/Davis
8. Proportioning Substructure Columns of Short Bridges for Improved Seismic Performance
   Mehmet Inel and Mark Aschheim, Mid-America Earthquake Center, University of Illinois at Urbana-Champaign
9. Vertical to Horizontal Spectral Ratios for Seismic Design and Retrofit of Bridges in Western and Eastern United States
   B.S.-J. Chiou, California Department of Transportation; W.J. Silva, Pacific Engineering Analysis; and M.S. Power, Geomatrix Consultants
10. Practice-Oriented Design Tools for Assessing Permanent Deformations
    S.E. Dickenson and Nason J. McCullough, Oregon State University
11. Fragility of R/C Bridge Columns Under Pulse-Type Loading Through Simulation Methods
    Charles H. Hamilton and Gerard C. Pardoen, University of California, Irvine
12. Near-Field Ground Motions and Their Implications on Seismic Response of Long-Span Bridges
    George P. Mavroeidis and Apostolos Papageorgiou, University at Buffalo
13. Shake Table Response of Flexure-Dominated Bridge Columns with Interlocking Spirals
    Juan Correal, M. Saiid Saiidi and David Sanders, University of Nevada, Reno; and Saad El-Azazy, Caltrans
14. Expansion Joins for Seismic Isolated Bridges
    E. Delis, California Department of Transportation
15. Health Monitoring of Bridges
    Michael S. Higgins, Pure Technologies
16. Development of Analytical Fragility Curves for Highway Bridges Considering Strong Motion Parameters
    Kazi R. Karim and Fumio Yamazaki, Institute of Industrial Science, University of Tokyo, Japan
17. State Street Bridge: CFRP Composite Seismic Rehabilitation and Specifications
    Chris P. Pantelides, University of Utah; Fadel Alameddine, Caltrans; Thomas Sardo, Washington Infrastructure; Roy Imbsen, Imbsen and Associates; Larry Cercone, Navlight Composites and Frederick Policelli, F. Policelli & Associates

18. Seismic Assessment and Retrofitting of Reinforced Concrete Bridge Piers
    Alessandro Rasulo, Politecnico di Milano
19. Recommendations on Experimental Procedures for Bridge Column Testing
    Jerry J. Shen, W. Phillip Yen and John O'Fallon, Federal Highway Administration
20. Implementation of Seismic Isolators and Supplemental Dampers in Cable-Stayed Bridges
    Michael Wesolowsky and John C. Wilson, McMaster University, Canada
21. Seismic Isolation of Bridges Subject to Strong Earthquake Ground Motions
    Victor A. Zayas, Stanley S. Low and Anoop S. Mokha, Earthquake Protection Systems, Inc.
22. Behavior of Ductile Steel Retrofitted Deck-Truss Bridges
    Majid Sarraf, Imbsen and Associates, Inc. and Michel Bruneau, University at Buffalo

TUESDAY, April 30, 2002

SESSION 5 (8:00 a.m. - 9:45 a.m.)
Session Chair: Jim Roberts
Effects of Near Field Earthquakes on Bridges

1. Characterizing Near Fault Ground Motion for the Design and Evaluation of Bridges
   Paul Somerville, URS Corporation
2. Designing Ordinary Bridges for Ground Fault Rupture
   Stewart Gloyd and Raymond Fares, Parsons Brinckerhoff; Anthony Sanchez, T.Y. Lin International and Vinh Trinh, W. Koo and Associates
3. Design of the Lytle Creek Wash Bridge to Survive Permanent Ground Displacements Due to Surface Fault Rupture
   Gregory V. Brown, DMJM Harris
4. Seismic Retrofit of the Bolu Viaduct
   S.W. Park, Lendis Corporation; Hamid Ghasemi, Federal Highway Administration; J.D. Shen, Lendis Corp.; W.P. Yen, FHWA; and M. Yashinsky, Caltrans
5. PEER-Lifelines Research in Design Ground Motions
   Clifford Roblee and Brian Chiou, California Department of Transportation Office of Research; and Michael Riemer, Pacific Earthquake Engineering Research Center

BREAK (9:45 a.m. - 10:15 a.m.)

SESSION 6 (10:15 a.m. - 12:00 Noon – Session Organizer: Roland Nimis)
Session Chair: Jim Cooper
International Forum

1. Revised Design Specifications for Highway Bridges in Japan and Design Earthquake Motions
   Keiichi Tamura, Ground Vibration Team, Public Works Research Institute, Japan
2. The Challenge of the Rion – Antirion Bridge
   J.P. Teyssandier, Gefyra S.A., Greece
3. Effect of Near-Fault Earthquakes on Bridges: Lessons Learned from Chi-Chi Earthquake
   Chin-Hsiung Loh, National Taiwan University, Wen-I Liao and Jun-Fu Chai, National Center for Research on Earthquake Engineering, Taiwan
4. Seismic Safety Evaluation of Large Scale Interchange System in Shanghai
   Lichu Fan, Jian Zhong Li, Shide Hu, Guiping Bi and Liying Nie, Tongji University, Shanghai, China.

LUNCH (12:00 Noon - 1:30 p.m.)

SESSION 7 (1:30 p.m. - 3:15 p.m. – Session Organizer: Ian Friedland)
Session Chair: Bruce Johnson
Seismic Practices for Transportation Structures and Systems

1. Seismic Vulnerability Assessment of the Seattle-Tacoma Highway Corridor Using HAZUS
   Donald Ballantyne, and Mark Pierepiekarz, ABS Consulting; and Stephanie Chang, University of Washington
2. Ground Motions, Design Criteria, and Seismic Retrofit Strategies for the Bay Area Rapid Transit District Bridge and Other Structures
   Tom Horton, Eric Fok, Ed Matsuda, William Hughes, Wen S. Tseng, Chip Mallare and Kang Chen, Bay Area Rapid Transit District Seismic Retrofit Capital Program
3. Pushover Analysis of Masonry Piers
   Ruben Gajer, Adam Hapij and Mohammed Ettouney, Weidlinger Associates, Inc.
4. Innovative Designs of Seismic Retrofitting the Posey and Webster Street Tubes, Oakland/Alameda, California
   Thomas S. Lee and Thomas Jackson, Parsons Brinckerhoff Quade & Douglas, Inc.; and Randy R. Anderson, Caltrans
5. Seismic Rehabilitation Design and Construction for the Port Mann Bridge, Vancouver, B.C.
   Keith Kirkwood, Steve Zhu and Peter Taylor, Buckland & Taylor Ltd., Canada

BREAK (3:15 p.m. - 3:45 p.m.)

SESSION 8 (3:45 p.m. - 5:30 p.m.)
Session Chair: Phil Yen
Displacement Based Design

1. Rocking of Bridge Piers Under Earthquake Loading
   Fadel Alameddine, California Department of Transportation; and Roy Imbsen, Imbsen & Associates Inc.
2. Legacy Parkway Seismic Design
   Thomas R. Cooper and Joseph I. Showers, Parsons Brinckerhoff
3. Plastic Hinge Length of Reinforced Concrete Bridge Columns
   Robert K. Dowell, Dowell-Holombo Engineering, Inc. and Eric M. Hines, University of California, San Diego
4. Applicability of the Pushover Based Procedures for Bridges
   Matej Fischinger and Tatjana Isakovic, University of Ljubljana, Slovenia
5. Seismic Performance of Reinforced Bridge Columns
   David Sanders, Patrick Laplace and M. Saiidi, University of Nevada, Reno; and Saad El-Azazy, Caltrans

RECEPTION (5:30 p.m. - 7:00 p.m.)

BANQUET (7:00 p.m. – 10:30 p.m.)
Banquet Speaker – Dr. Ian G. Buckle, University of Nevada at Reno

WEDNESDAY, May 1, 2002

SESSION 9 (8:00 a.m. - 9:45 a.m.)
Session Chair: Mark Reno
Emerging Seismic Design and Retrofit Technologies

1. Seismic Design of Concrete Towers of the New Carquinez Bridge
   Ravi Mathur and Greg Orsolini, Parsons Transportation Group; Mark Ketchum, OPAC Consulting Engineers
2. Precast Segmental Bridge Superstructures: Seismic Performance of Segment-to-Segment Joints
   Sami Megally and Frieder Seible, University of California, San Diego
3. In-Situ Tests of As-is and Retrofitted RC Bridges with FRP Composites
   C.P. Pantelides, J. Duffin, J. Ward, C. Delahanty and L.D. Reaveley, University of Utah
4. Calibration of Strain Wedge Model Predicted Response for Piles/Shafts in Liquefied Sand at Treasure Island and Cooper River Bridge
   Mohamed Ashour and Gary Norris, University of Nevada, Reno; and J.P. Singh, J.P. Singh & Associates
5. Seismic Performance of a Concrete Column/Steel Cap/Steel Girder Integral Bridge System
   Sri Sritharan, Robert E. Abendroth, Lowell F. Greimann, and Justin Vander Werff, Iowa State University; and Wagdy G. Wassef, Modjeski and Maters, Inc.

BREAK (9:45 a.m. - 10:15 a.m.)

SESSION 10 (10:15 a.m. - 12:00 Noon)
Session Chair: Ian Friedland
Development and Testing of the New LRFD Seismic Design Specifications for Highway Bridges

1. Recommended LRFD Guidelines for the Seismic Design of Highway Bridges
   Ronald L. Mayes, Simpson, Gumpertz and Heger; Ian M. Friedland, Applied Technology Council; and ATC Project Team
2. Recommended Design Approach for Liquefaction Induced Lateral Spreads
   Geoffrey R. Martin, University of Southern California; Lee M. Marsh, BERGER/ABAM; Donald G. Anderson, CH2M Hill; Ronald L. Mayes, Simpson Gumpertz & Heger; and Maurice S. Power, Geomatrix Consultants, Inc.
3. Application of the New LRFD Guidelines for the Seismic Design of Highway Bridges
   Derrell A. Manceaux, Federal Highway Administration
4. Cost Impact Study for a Typical Highway Bridge Using Different Return Period Seismic Design Maps
   Jeffrey Ger, David Straatmann, Suresh Patel and Shyam Gupta, Missouri Department of Transportation
5. Testing of the LRFD Bridge Seismic Design Provisions through a Comprehensive Trial Design Process
   M. Lee Marsh, BERGER/ABAM Engineers, Inc., Richard V. Nutt, Consultant; Ronald Mayes, Simpson Gumpertz & Heger; and Ian Friedland, Applied Technology Council
6. Panel Discussion: Presenters to discuss results and answer questions from audience.

Closing Remarks: Roland Nimis

Author Index

A

Abbas, S., 107
Abendroth, R.E., 411
Abrahams, M.J., 85
Akbas, B., 31
Alameddine, F., 299, 557
Amini, M., 491
Anderson, D.G., 437
Anderson, R.R., 271
Andrawes, B., 43
Aschheim, M.A., 527
Ashour, M., 397
Azuma, T., 53

B

Ballantyne, D., 237
Bi, G., 223
Boulanger, R.W., 521
Brown, G.V., 163
Bruneau, M., 479, 581
Bryson, J.A., 85

C

Capron, M.R., 509
Cercone, L., 557
Chai, J-F., 211
Chai, Y.H., 521
Chang, S., 237
Chen, K., 249
Chiou, B.S.J., 177
Coffman, H., 5
Comstock, G., 5
Cooper, J.D., 3
Cooper, T.R., 313
Correal, J., 539
Curras, C.J., 521

D

Delahanty, C., 383
Delis, E., 545
DesRoches, R., 43
Dowell, R.K., 323
Duan, X., 123
Duffin, J., 383

E

El Azazy, S., 3, 345, 539
Ettouney, M., 261

F

Fan, L., 223
Fares, R., 149
Fischinger, M., 335
Fok, E., 249
Friedland, I.M., 425, 475

G

Gajer, R., 261
Ger, J., 463
Ghasemi, H., 3, 175
Gloyd, S., 149
Greimann, L.F., 411
Gupta, S., 463

H

Hapij, A., 261
Hines, E.M., 323
Hipley, P., 485
Ho, L-H., 33
Horton, T., 249
Houlahan, G., 107
Hu, S., 223
Huang, M., 485
Hughes, W., 249
Hutchinson, T.C., 521

I

Idriss, I.M., 521
Imbsen, R.A., 3, 65, 299, 491, 557
Inel, M., 527
Ingham, T., 107
Isakovic, T., 335

J

Jackson, T., 271

K

Karim, K.R., 551
Ketchum, M.A., 359
Khaleghi, B., 17
Kirkwood, K.,285
Kobayashi, H., 53
Kulicki, J.M., 95

L

Laplace, P., 345
Lee, K., 479
Lee, T.S., 271
Li, J., 223
Liao, W-I., 211
Loh, C-H., 211
Lopez-Jara, J., 109
Low, S.S., 575
Lubkowski, Z., 123

M

Mackie, K., 515
Mallare, C., 249
Manceaux, D.A., 451
Mander, J., 479
Manzanarez, R., 503
Maroney, B., 41, 107
Marsh, M.L., 437, 475
Martin, G.R., 437
Mathur, R., 359
Matsuda, E., 249
Mavroeidis, G.P., 533
Mayes, R.L., 425, 437, 475
McMullin Bobb, N., 41
Megally, S., 371
Mesa, L.E., 65
Mibelli, C., 109
Mokha, A.S., 575
Murphy, T.P., 95

N

Nader, M., 109, 503
Nie, L., 223
Norris, G., 17, 397
Nutt, R.V., 475

O

O'Fallon, J., 563
Oldham, M., 123
Orsolini, G., 359

P

Pantelides, C., 383, 557
Papageorgiou, A.S., 533
Park, S.W., 175
Patel, S., 463
Pierepiekarz, M., 237
Policelli, F., 557
Power, M.S., 437

R

Reaveley, L., 383
Riemer, M., 177
Roblee, C.J., 177

S

Sah, M., 107
Saiidi, M.S., 345, 539
Sanchez, A., 149
Sanders, D., 345, 539
Sardo, T, 557
Sarraf, M., 581
Sato, N., 53
Seible, F., 371
Shakal, T., 485
Shen, J., 31
Shen, J.D., 175, 563
Showers, J.I., 313
Singh, J.P., 397
Somerville, P., 137
Sritharan, S., 411
Stojadinovic, B., 515
Straatmann, D., 463
Sturt, R., 123
Sun, J., 503

T

Tamura, K., 53, 191
Taylor, P., 285
Teyssandier, J-P., 203
Trinh, V., 149
Tseng, W.S., 249

V

Vander Werff, J., 411

W

Wahl, P.M., 85
Wang, J-N., 85
Ward, J., 383
Wassef, W.G., 411
Wesolowsky, M., 569
Wilson, J.C., 569

Y

Yamazaki, F., 551
Yashinsky, M., 175
Yeh, J., 33
Yen, W.P., 3, 33, 175, 563

Z

Zayas, V.A., 575
Zhang, H., 73
Zhu, T-J., 285

Notes

Notes

Notes

Notes

Notes

Notes

Notes

Notes

Notes

Notes